europhysics
conference
abstracts

10th EUROPEAN CONFERENCE ON CONTROLLED FUSION AND PLASMA PHYSICS

Moscow, 14 – 19 September 1981

INVITED PAPERS

Published by: European Physical Society

Volume
5H

es Editor: Dr. W. J. Merz, Zurich

aging Editor: G. Thomas, Geneva

x-Planck-Institut für Plasmaphysik
8046 Garching bei München
Po (1) 30

MTESZ — egyesületi használatra!
Kiadja: Eötvös Loránd Fizikai Társulat
Készült: 160 példányban
82/2212 MTESZ Házinyomda, Bp.
Felelős vezető: Deli Sándor

TENTH EUROPEAN CONFERENCE ON

CONTROLLED FUSION AND PLASMA PHYSICS



INVITED PAPERS

*

SUPPLEMENTS TO CONTRIBUTED PAPERS

*

POST-DEADLINE PAPERS

Max-Planck-Institut für Plasmaphysik

24. FEB 1983

Bibliothek

Moscow, September 14–19, 1981

9138-83

EUROPHYSICS CONFERENCE ABSTRACTS is published by The European Physical Society.© 1982
Reproduction rights reserved

This volume is published under the copyright of the European Physical Society. We want to inform the authors that the transfer of the copyright to EPS should not prevent an author to publish an article in a journal quoting the original first publication or to use the same abstract for another conference. This copyright is just to protect EPS against using the same material in similar publications.

The redaction works of this EPS edition of the Invited Papers and other documents of the Conference was prepared by Dr. I. Abonyi and Dr. K. Lelkes, Roland Eötvös Physical Society, Budapest.

CONTENTS

INVITED PAPERS

V.V. Alikaev, Electron-Cyclotron Plasma Heating 1

M. Bell et al., Recent PDX Results 21

H.A.B. Bodin, Reversed-Field Pinch Experiments 41

G.I. Dimov, Production of Intense Negative Hydrogen Ion Beams 81

R.R.Borchers - T.K. Fowler et al., Progress in the Tandem Mirror Program 107

G. Grieger, INTOR Physics 131

A.V. Gaponov et al., Achievements and Problems of Relativistic High-Frequency Electronics 153

M.S. Ioffe et al., Magnetoelectrostatic Plasma Confinement 177

P.L. Kapitza, The Study of Thermonuclear Problems Conducted at the Institute for Physical Problems of the USSR Academy of Sciences 197

L.I. Ponomarev, Muon Catalysis of Nuclear Fusion in Deuterium-Tritium Mixture 223

J.P. Rager, Progresses on Plasma Focus Research at Frascati 243

V.D. Shafranov, Equilibrium and Stability of Toroidal Plasma 269

N. Suzuki et al., JFT-2 Heating Experiments 307

V.S. Strelkov, Tokamak Research in the Soviet Union 327

P. Sunka, Plasma Heating by High-Power Relativistic Electron Beams 343

N.A. Uckan, Status of the Elmo Bumpy Torus Research 363

E.P. Velikhov, Controlled Thermonuclear Fusion in the USSR 383

H. Wolff, Plasma-Wall Interaction 445

C. Yamanaka, Inertial Fusion Research at Ile Osaka 469

G. Yonas, Inertial Fusion Research Using Pulsed Power Drivers 501

CONTRIBUTED PAPERS NOT INCLUDED IN VOL.I

L.J. Pan et al., The Analytical Solution and Maximum β for the Equilibrium of a Fat Tokamak with Circular Cross-Section B-6 523

Xu Fu et al., Kelvin-Helmholtz Instability in Tokamaks B-10 527

I.K. Konkashbayev et al., Open Trap with min B and $\beta = 1$ C-11 531

I.P. Afonin et al., Current Channel Forming Processes and Energy Release in the Diode of the 'Angara-I' High-Current Accelerator F-2a 535

J.L. Montanes et al., Light-Pressure Effects on Ion Spectra in Two-Ion Laser Plasmas F-8 539

W. Hintze, One-Dimensional Simulation of Collective Ion Acceleration by a Relativistic Electron Beam F-13 543

M. Lisak et al., Effects of Velocity Space Loss--Regions on the Alpha Particle Distribution Function and Collisional Alpha Particle Losses in Tokamak Reactors G-2a 547

R.R. Bartsch et al., Los Alamos Compact Toroid /CT/ Research on the Field-Reversed Configuration /FRC/ and Spheromak-type Magnetized-Gun-Generated CTs L-4 551

J.N. Mohanty, Electrostatic Waves in a Plasma Stream Instability: Modified Landau Damping and Streaming Ion Accoustic Mode M-5 555

SUPPLEMENTS TO CONTRIBUTED PAPERS IN VOL.I

D.G. Bulyginsky et al., Electron Cyclotron Heating in FT-1 Tokamak above Critical Plasma Density ...belonging to H-8 561

S.G. Goncharov et al., Post-Compression Period Investigation in Tuman-2A: A Tokamak with Magnetic Compression ..belonging to A-3 563

POST-DEADLINE PAPERS

A.A. Bagdasarov et al., Plasma Experiments on T-7 Superconducting Tokamak AP-1 567

A.V. Gorshkov et al., Plasma Potential and its Variation with ECRH on the TM-4 Tokamak AP-2 571

M.Yu.Cherkashin et al., Tearing Mode Time Evolution in T-7 Tokamak AP-3 575

V.V. Parail et al., Anomalous Plasma Diffusion in Tokamak BP-1 579

Yu.N. Dnestrovskii, Losses of Hot Injected Ions through Multiple Charge Exchange in Tokamak BP-2 583

V.V. Gavrilov et al., Compression of Plasma Jets /β =1/ in a Conic Liner and their Collision CP-2 587

V.I. Krauz et al., Plasma Focus Studies at Energies up to 250 KJ DP-1 591

V.H. Brownell et al., Ultra-High Plasma Experiments: MHD Simulations DP-5 595

.A. Batyuk et al., First Experiments on Ion--Cyclotron Plasma Heating on L-2 Stellarator EP-1 599

. Ohkawa et al., Preliminary Results from the OHTE Experiment EP-4 603

.G. Basov et al., Preliminary Experiments in the Heating Spherical Targets at 'Delfin-1' FP-1 607

.M. Zakharov et al., Pinching of a Laser Plasma in a High-Current Accelerator Diode FP-3 611

.B. Baksht et al., Generation of a Dense Hot Plasma by Fast Compression of Shells FP-5 615

.A. Andreev et al., Absorption Efficiency of Powerful Laser Radiation of Varied Duration at Wavelengths 350 nm - 1 μm in Plasma with Different z FP-6 619

G. Leira et al., Analysis of Fusion Performance by Inertial Confinement: Effects of Pressure Ionization and Electron Conduction on the Ignition of DT Fusion in Hollow-Shells by Isentropic Implosions FP-15 623

A.A. Filyukov et al., Effective Multistage Ablation FP-17 627

Yu.A. Bondarenko et al., Ablative Acceleration of Double-Layer Targets FP-19 631

A.I. Zaretski et al., Irradiation of Microspheres with the 2 Tw Iodine Laser FP-20 635

M.G. Kuznetsov, Tandem Mirror Reactor Calculations with Respect to Axial Nonuniformity of Electron Temperature GP-2 639

M.F.A. Harrison et al., Modelling of the Single--Null Divertor of INTOR: Plasma Exhaust and Gas Pumping GP-3 643

O.M. Shvets et al., ICRF Heating of a Two-Ion Currentless Plasma in the Uragan-2 Stellarator HP-1 647

A.G. Elfimov et al., Drag Currents Profiles Formation and Diffusion Control by HF Fields in a Steady-State Tokamak HP-2 651

A.V. Longinov et al., Main Features of the 'Kedr' RF Device and First Results on ICRF Heating in T-10 Tokamak HP-4 655

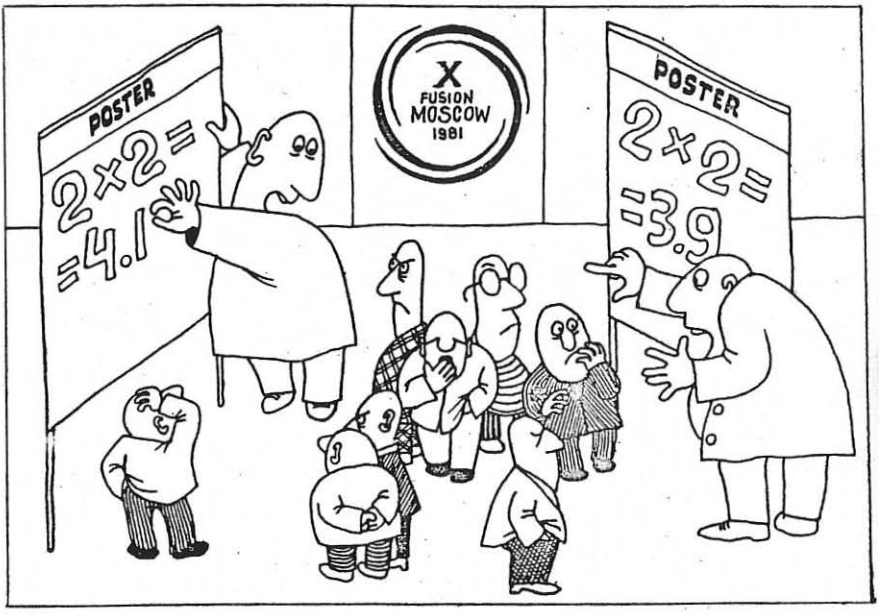
A. Buffa et al., Optimization of the Joule Heating in RFP Plasma LP-1 659

A. Buffa et al., RFP Formation and Volt Consumption with Various Current Rise Times LP-2 663

S.N. Voronkov et al., Experimental Investigation of Simulated Cyclotron Millimeter Wavelength Emission of Relativistic High-Current Electron Beam MP-2 667

A.N. Didenko et al., Experimental Investigation of Simulated Microwave Radiation of High-Power Relativistic Electron Beams MP-6 671

AUTHOR INDEX 675


POSTER
2×2=
=4.1
X
FUSION
MOSCOW
1981
POSTER
2×2=
=3.9

XI

INVITED PAPERS

PLASMA ELECTRON-CYCLOTRON RESONANCE HEATING

V.V.Alikaev

I.V.Kurchatov Institute of Atomic Energy

Moscow, USSR

Nowadays plasma electron-cyclotron resonance heating (ECRH) becomes rather widespread in tokamaks, stellarators and mirror traps. This is determined by the efficiency of the ECRH application in tokamaks as it has been demonstrated both in the USSR [1], [2], [3], and in the USA [4].

Besides, the progress in the development of millimeter-range generators (gyrotrons) during the last 10 years [5], [6], [7] provided with the possibility of application of this heating method in tokamaks like the T-10 (USSR). Numerical calculations performed for tokamaks like JET, INTOR [8], [9] demonstrate the advantages of the ECRH over the injection of neutrals to create the regime of "ignition". We discuss the latest results of the experimental ECRH studies in tokamaks in this paper.

Two types of waves may exist in plasma in the electron-cyclotron frequency range: an ordinary and an extraordinary wave. Both waves can be used for plasma heating. The refractory factor of the extraordinary wave becomes infinite in the region of the upper hybrid resonance $\omega=(\omega_{pe}^2+\omega_{ce}^2)^{1/2}$ and is equal to zero in the cut-off region $\omega=\omega_{ce}/2+(\omega_{pe}^2+\omega_{ce}^2/4)^{1/2}$ in cold plasma. The refractory factor of the ordinary wave is equal to zero at $\omega=\omega_{pe}$. The cross-section of the tokamak

plasma with the lines where the upper hybrid resonance is observed and the cut-off region is given in Fig.1 considering the ununiformity because off the toroidicity of the magnetic field and the parabolic density profile.

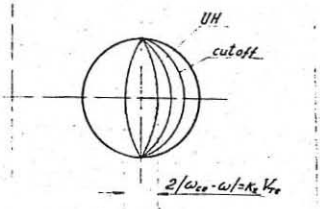


Fig. 1

Effective linear absorbtion of the HF-energy is possible in the upper hybrid resonance region, connected with the transformation of the electromagnetic wave into the plasma wave. However, such dissipation mechanism may be only used at launching of the extraordinary wave from the inner side of the torus, because the zone of intransparency is absent up to plasma densities $n = 2n_{cr}$ in such case, where n_{cr} is the density corresponding to the equation $\omega = \omega_{pe}(n_{cr})$. The ordinary wave may be launched from the outer side of the torus and propagate in plasma up to densities $n \leq n_{cr}$. The efficiency of absorbtion of both ordinary and extraordinary waves in the cyclotron resonance region is closely connected with the plasma density, temperature and the angle between the direction of the wave propagation and the

direction of the toroidal magnetic field. In standard terms, the extraordinary wave has a circular polarization with the direction of rotation similar to that of electrons in the magnetic field.

However it appears that for cold plasma with $\omega_{ce} \sim \omega_{pe}$ the polarization of the extraordinary wave in the region of the cyclotron resonance does not provide with the large efficiency of interaction with electrons. The efficiency of interaction increases with the increase of the electron temperature. The following questions should be answered to estimate the perspectives of the ECRH in large tokamaks:

1. What type of wave polarization is the most effective in such tokamaks?

2. What angle relative to the toroidal magnetic field must be used for the wave propagation in plasma?

An analysis of the trajectories and wave absorbtion in a toroidal plasma pinch must be performed to answer these questions. This aspect was thoroughly studied in [10], [11], [12], [13], [14], [15]. The extraordinary wave can propagate in plasma only from the inner side of the torus because off the existence of the non-propagation region.

The ordinary wave is also rather effectively absorbed when using such a launch. Thus there are no strict limitations on the formation of wave polarization. However, the studies of absorbtion of the extraordinary wave along its trajectory show in the T-10 [12], that even at

$\theta \approx 80^\circ$ the absorption is so strong that the wave loses its dominant power at fast electrons not reaching the electron-cyclotron region. Besides, the technical realization of such wave launch is much more complicated than that of the systems located in the outer side of the torus. An ordinary wave with $\theta = 90^\circ$ has an interesting peculiarity. The absorbtion of its energy occurs due to relativistic Doppler effect. When this wave propagates from the outer side of the torus it has a resonance with the subthermal electrons firstly. The calculations show that this wave looses almost all its energy at these electrons in the T-10.

The performed calculations also showed that the ordinary wave with $\theta = 90^\circ$ was capable to heat plasma core even at $n_{e_{max}} \approx n_{cr}$. Quasilinear theory of such heating was considered in [11], [16]. It was showed that when the ordinary wave propagated from the outer side of the torus, the bulk of electrons is heated. The extraordinary wave supplies with its energy only a small portion of overthermal electrons at plasma temperatures $T_e > 1$ keV, which proves the states of the linear theory.

Assuming the obtained experimental experience, and also the results of theoretical works it is possible to formulate the tasks where the ECRH may be applied:

1. Heating both electron and ion components of plasma.

2. Study of the variation of transport factors (thermal conductivity and diffusion) with temperature.

3. Current profile formation.

4. The creation of a stationary current.

5. Preionization.

Local energy deposit in the cyclotron region, and also the focusing of the RF radiation in the meridional cross-section of the plasma column make it possible to change the profile of the electron temperature, and, hence, the current profile [17] . It is probably possible to suppress instabilities, for example internal disruptions, by simple passing of the cyclotron region along the plasma column radius.

The ECRH of plasma may be also used to obtain a stationary current [18]. It is necessary to form the presumable heating of electrons passing along the toroidal magnetic field in one direction to obtain the stationary current. This condition may be easily fulfilled if the RF radiation is launched at an angle to the magnetic field. Although the ECRH-method efficiency to acquire the current $I(A) = P_{kW} \frac{T_e(keV)}{R \cdot n_e} 10^2$ is lower than that of the low hybrid waves, it is possible to control the profile of current in this case.

The ECR - preionization of plasma may make it possible to form the initial stage of the discharge more optimate, obtain the current breake in the chamber centre, decrease plasma-wall interaction and decrease the loop voltage. In this case, it is more convenient to use the extraordinary wave which is launched from the inner side of the torus, because the absorbtion of the ordinary wave is not enough because off low initial values of

plasma temperature and density.

The first ECRH experiments were performed in the USSR in tokamaks FT-1 in the Physical Technical Institute of the Academy of Sciences and in the TM-3 in I.V.Kurchatov Institute of Atomic Energy [1], [2], [19], [20], [21], [22]. Gyrotrons with wavelengths from 1 cm to 5 mm, power up to 100 kW and pulse duration ~ 1 ms were used in the abovementioned experiments. These generators were developed in the USSR mainly in the Institute of Applied Physics of the Academy of Sciences [5], [6].

The TM-3 experimental results made it possible to conclude the following:

1. The maximum increase of the electron temperature corresponds to the cyclotron region of heating.

2. The main part of the electron energy distribution function is heated when the resonance conditions are fulfilled ($\omega = \omega_{ce}$ or $\omega = 2\omega_{ce}$).

3. No auxiliary impurity influx was observed in plasma. Energy confinement time increased with the growth of the electron temperature.

4. The efficiency of the additional heating methods of plasma is an important parameter, the prior being determined by the ratio of the power absorbed by the long-living component of plasma to the total applied power.

It was showed that in the TM-3 experiments the efficiency of heating was not less than 50% both in the first and second harmonics of the ECR.

It should be noticed that the wave power is absorbed

during several passes through the cyclotron region because off the small size of this tokamak. The comparison of the obtained experimental value with the theoretical calculated value of the heating efficiency is hard to be performed.

Interesting experiments were settled in the FT-1 tokamak in the Physcial Technical Institute of the USSR Academy of Sciences [23], [24]. When the ordinary wave is used for heating, plasma density is limited by its maximum value (n_{cr}). If the extraordinary wave is launched from the inner side of the torus, it can propagate in plasma up to $n_o \approx 2 n_{cr}$. In this case the absorbtion of energy can occur due to two mechanisms, namely, cyclotron absorbtion in the resonant region and linear transformation in the region of the upper hybrid resonance. The HF energy was launched in these experiments both from the outer side of the torus as the ordinary wave, and from the inner side as the extraordinary wave. The system of the UHF energy input is given in Fig.2.

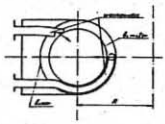


Fig.2

Electron-cyclotron heating was observed at $0.5n_{cr}<n_o<2.5n_{cr}$ in the experiments at the first harmonic. But at the inner launching of the UHF-energy the efficiency of heating was twice higher.

The efficiency of heating is determined as $\eta = \frac{P_{OH}}{P_{HF}}\left(\frac{\Delta n\overline{T}}{n\overline{T}} + \frac{\Delta U}{U}\right)$ and is equal to 0.6, where U is the loop voltage. The supply of the additional plasma energy calculated from the diamagnetic measurements as the function of density is given in Fig.3 for both types of the HF-wave launching.

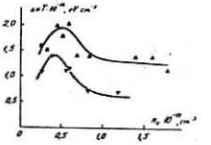


Fig.3

Laser profiles of the electron temperature and density were recently obtained in this tokamak. The energy supply of plasma and the average value of the electron diamagnetism were calculated using these data. The absolute value $\Delta\overline{nT}$ is $(1.7\div3)\ 10^{14}$ eV/cm^3 remaining at a high level in all the range of densities, which proves the results of diamagnetic measurements. However the average value $\frac{\Delta\overline{nT}}{n\overline{T}}$ decreases insufficiently at the increase of n_e from 0.43 at $n_o \approx n_{cr}$ to 0.3 at $n_o \approx 2.4n_{cr}$.

The system of the HF-energy launching from the inner side of the torus has also been applied in the ISX-B experiments (USA) [4] . A 100 kW gyrotron with 35 GHz frequency and up to 10 ms pulse duration was used in these experiments. Unpolarized radiation was launched at 45° to the direction of the main magnetic field. The electron temperature increase was equal to~400 eV in the plasma core. The decrease of plasma density was observed for the first time at heating in these experiments. Radial profiles of T_e and n_e are given in Fig.4 taken before and to the end of the gyrotron pulse.

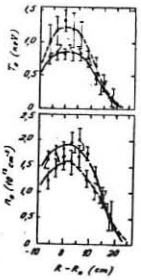


Fig.4

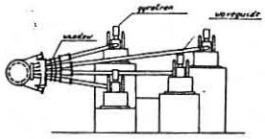


Fig.5

It is possible to see that the central density decreases from $1.8 \cdot 10^{13} cm^{-3}$ to $1.5 \cdot 10^{13} cm^{-3}$ in the process of heating. The authors point out that similar phenomenon was also observed in this tokamak during neutrals' injection.

Preionization with the ECR was also studied at this tokamak [25].

The maximum plasma density reached $4.10^{13} cm^{-3}$ in the region of the upper hybrid resonance. The loop voltage

decreased in 40% and the rate of the current rise sufficiently increased due to preionization. Similar results were also obtained in WT-1 tokamak (Kyoto, Japan) [26].

First ECRH plasma experiments were performed in the T-10 (IAE, USSR) in 1979 [3]. The experiments were performed with the power level of heating ~ 100-200 kW.

A new gyrotron array has been created in this tokamak in 1980, which consisted of four gyrotrons, cryomagnetic systems, oversize transport lines of the HF-energy and a system of antenna. Each gyrotron has the output power up to 200 kW at the pulse duration up to 150 ms. The system of antenna consists of four supersize circular waveguides, which axes are aimed at the plasma column centre which supplies with the focusing of the HF-energy to decrease the refraction effects. The main aim of the array is plasma heating in the first harmonics of the ECR with the power launched from the outer side of the torus. Thus, the array is the model of the constructed T-15 HF heating system [22].

The limit value of density when effective plasma heating can be obtained is determined by the degree of polarization and the angular divergence of the wave beam on the mounts of the antenna. Almost 70% of the output power of the array have the ordinary wave polarization ~6° which can supply with the effective plasma heating up to the central density values 7÷8 $10^{13}cm^{-3}$ according to theoretical calculations. The gyrotrons' wavelength corresponds to the value of the first harmonic of

the ECR at the magnetic field 30 kOe. The experiments were performed in two stages: on the second, and than on the first harmonic of the ECR.

It was hoped to obtain full of 30% power absorbtion of the polarized extraordinary wave on the second harmonic of ECR.

The experiments on plasma heating on the second harmonic of ECR were performed with the plasma current ~ 210 kA, magnetic field 15 kOe. The HF power absorbed by plasma during the ECRH may be found from the integral energy balance using the diamagnetic measurements' data, Joule heating power and the radiation losses power.

$$P_{Pe}^{HF} = 3/2 \left(\frac{\Delta nT}{\tau_E^o} + \frac{dnT}{dt} \right) + \Delta P_{OH} + \Delta P_{rad}$$

The main results are listed in Table I

Regime	$\bar{n}_e$ cm^{-3}	$T_e(0)$ keV	ΔT_e keV	Δt ms	P_{ew} kW	P_{ow} kW	η_{ew}	η_{full}	$3/2 nTV$ kJ	τ_E^o ms	τ_E' ms
I	$1.5 \cdot 10^{13}$	0.98	0.5	50	160	330	160%	54%	2	25	25
II	$3 \cdot 10^{13}$	0.8	0.2	80	100	200	170%	57%	1	30	28

Here $T_e(0)$ is the electron temperature calculated from the bremsstrahlung spectrum before the HF-array operation, T_e - the variation of temperature during heating, P_{ew} - the power of the extraordinary wave launched into plasma, P_{ow} - the same of the ordinary wave.

$$\eta_{ew} = \frac{P_{Pe}}{P_{ew}}, \quad \eta_{full} = \frac{P_{Pe}}{P_{ow} + P_{ew}}, \quad \tau_E^o = \frac{3/2\, nTV}{P_{OH}}$$

- the energy confinement time measured before heating,

$$\tau_E' = \frac{3/2\, nTV}{P_{OH} - 3/2 \frac{dnT}{dt}}$$ - the value measured just after the switch off of the HF array.

It is possible to make the following conclusions

having observed the abovementioned table:

1. The efficiency of heating is rather high. The extraordinary wave power is totally absorbed in the plasma core, where the energy confinement time is rather large. A notable portion of the ordinary wave power is also absorbed in this region.

2. The total energy confinement time measured before and just after the HF array operation is constant within the accurasy of measurements. Plasma heating was determined by the increase of radiation losses and impurity influx in this regime, obviously, due to the fact that the dominant portion of power delivered by the ordinary wave is partly absorbed in the plasma column periphery due to many passes of the wave through the plasma column chamber walls.

The plasma heating experiments on the first harmonic of ECR were performed at $J_p \approx 230 \div 250$ kA, $\overline{n_e} \approx 3 \div 4.5 \cdot 10^{13} cm^{-3}$ and the magnetic field 30 kOe. As it has been mentioned above, the gyrotron array is the model of the T-15 array.

Thus the following questions should be answered in the course of the experiments.

1. Is the ordinary wave absorbtion effective in the first harmonic of the ECR?

2. Will ion heating be observed?

3. What is the influence of the thermal insulation and diffusion from the electron temperature?

Time vatiations of total plasma energy (diamagnetic measurements), average density and loop voltage are

given in Fig.6.

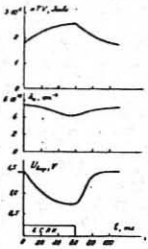


Fig. 6

The electron temperature profile variation obtained from the soft X-Ray radiation spectra and the density profile (multichannel HF-measurements) are given in Fig.7.

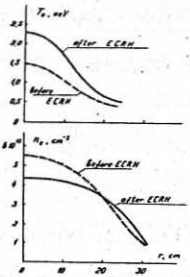


Fig. 7

The evolution of the electron temperature profile is given in Fig.8 as obtained from Thomson scattering. Good agreement should be noticed in the comparison of

the laser and the soft X-Ray measurements.

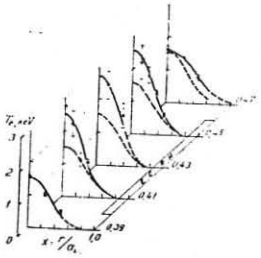


Fig.8

The main data obtained from the integral energy balance analysis of one of the regimes is given in Table II.

$\bar{n}_e$ cm^{-3}	$T_e(0)$ keV	ΔT_e keV	Δt ms	P_{ew} kW	P_{ow} kW	η_{ow}	η_{full}	$\frac{3}{2}\Delta nTV$ kJ	τ_E^0 ms	τ_E' ms
$3.63 \cdot 10^{13}$	1.3	0.6-0.8	60	160	350	128%	90%	7	42	36

where $\eta_{ow} = \frac{P_{re}}{P_{ow}}$

The energy balance equation should be given to illustrate these statements in the end of the heating pulse: $P_{Pe} = \Delta P_{OH} + \Delta P_{rad} + \frac{3/2\,\Delta nT}{\tau_E^0} + 3/2\,\frac{dnT}{dt} =$

$$= 230\,kW + 40\,kW + 140\,kW + 40\,kW = 450\,kW$$

In the regime with 3.10^{13} the increase of the central T_e was equal to 1 keV.

The following conclusions can be made from the analysis of the given data:

1. As the theory predicts, one-pass absorbtion of

the ordinary wave is rather high, the efficiency of heating reaches 90%, which may also be explained by many passes of the extraordinary wave during its absorbtion.

2. Impurity income is also observed in this regime, but radiation losses increase insignificantly (in less than 10% comparing with the input power).

3. A notable portion of power is spared to compensate Joule heating. The relative yield of this effect will decrease with the increase of the input HF power.

The supplied additional plasma energy increased at the density rise. However the maximum value of the T-10 plasma density obtained in the experiments was 4.10^{13} cm^{-3} because off the peculiarities of the chamber. The increase of ion temperature was in an agreement with the classical calculations in such conditions.

The variations of the neutron radiation and ion temperature are given in Fig.9 during the process of heating.

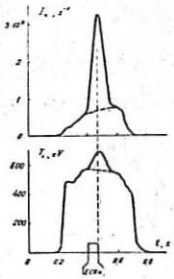


Fig.9

Ion temperature has a linear increase with the rise of the heating pulse. Its maximum increase was equal to $\Delta T_i =$ = 130 eV. The same value δT_i was obtained from the neutrals' spectra analyses.

Plasma density behaviour is notably dependent from the chamber wall conditions during the process of heating. It was possible to obserbe the decrease of the electron density in the plasma core during the ECRH in those experiments when the impurity influx from the walls was low (Fig.7).

This phenomenon is mostly evident in the latter ECRH TM-4 experiments where the walls' outgassing is very low and $n_e(0)$ decreases in 30-35%.

There is no experimental data enough now to explain this phenomenon.

The increase of the electron temperature must cause the classical Vare pinching, moreover, if the diffusion in the plasma core is neoclassical, $D \sim T_e^{3/2}$, which also causes the decrease of density. The supression of LHD-instability was observed in the experiments with plasma heating in the first harmonic of ECR at regimes with $q \approx 5$. The magnetic probe signal and the electron temperature time variation are given in Fig.10.

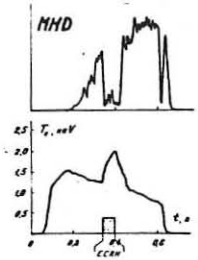


Fig.10

The electron temperature was measured from the soft X-Ray radiation analysis using the method of filters. MHD oscillations' intensity drops during the gyrotrons' operation.

ECRH of plasma becomes more and more applicable in tokamaks within last several years. The experiments are being prepared and are settled on tokamaks such as PDX, ISX-B, and Versator (USA), THOR (Italy), JET-2 (Japan) and Tosca (Great Britain) [27]. The analysis of the experimental results and theoretical calculations makes it possible to stress that the ECRH can be successfully applied for plasma heating in large thermonuclear reactors considering the physical aspects.

The main problem in this field is the possibility of powerful gyrotrons' construction in the short wave region of the millimeter wave range in the frequency range up to 150 GHz.

References

1. V.V.Alikaev et al., JETP Lett., 15, 1, 41, 1972.
2. V.E.Golant et al., Proc. III Int.Symp. on Toroidal Plasma Confenement, Garching, 1973, E-5.
3. V.S.Strelkov 9th European Conf. on Controlled Fusion and Plasma Physics, Oxford, Sept. p.387 (1979).
4. R.H.Gildenbach et al., Phys. Rev. Lett., 44, 647 (1980).
5. Gaponov A.V., Petelin M.J., Gulpatov V.K., "Izvestiya vysch. uch. zavedemi Radiofizika", 1976, 10, 9-10.
6. A.V.Gaponov et al., 4th Int.Conf. on Infrared and Nearmillimeter Waves, Miami, 9-14 Dec. (1979).
7. A.V.Gaponov et al., Int. Journal on Infrared and Millimeter Waves, v.1, N 3, p.351.
8. R.Cano, A.Carallo, H.Capes, Bull. Am. Phys. Soc. 24, 969 (1979).
9. S.M.Wolfe et al., Nucl. Fusion 19, 389 (1979).
10. Litvak A.G. et al., JETP Lett., 1975, 1, N 18, 838.
11. Alikaev V.V. et al., Paper IAE-2610, M., 1976, I.V.Kurchatov Institute of Atomic Energy.
12. Alikaev V.V. et al., Fizika Plasmy, 1977, 2, N 2, 230.
13. Fidone et al., Fontenay-aux-Roses Rapport, France, EUR-CEA-FC-912, August 1977.
14. A.C.England et al., Oak-Ridge Nat. Lab.Report, USA, ORNL/TM-6011, 1977.
15. Eldridge et al., Oak-Ridge Nat. Lab. Report, USA,

ORNL/TM-6052, 1977.

16. I.Fidone, G.Granata, R.L.Meyer, Report EUR-CEA-FC-1053 (1980), Fontenay-Aux-Roses

17. R.Cano, A.Cavallo, Report EUR-CEA-FC-1006 (1979) Foutenay-Aux-Roses.

18. N.J.Fisch, A.H.Boozer, Phys.Rev.Lett., 45 (1980) 720.

19. V.E.Golant et al., Proc.VI PCCFPP Moscow, 1973, v.1, p.587.

20. V.V.Alikaev et al., Fizika Plasmy, 2, 3, 390, 1976.

21. V.V.Alikaev et al., Fizika Plasmy, 3, 230, 1977.

22. V.V.Alikaev Proc. of Joint Varenne-Grenoble Int.Symp. on Heating Toroidal Plasmas, Grenoble, July 3-7, p.339, 1978.

23. Baranov Yu.F., Bulyginskii D.G., V.E.Golant et al., "UHF Heating of Plasma in the FT-1 Tokamak at Densities higher than the critical value", X Eur.Conf. on CTR and PP, Moscow, 1981.

24. Bulyginskii D.G. et al., Proc. II Int. Symp. on Toroidal Plasma Heating, Como, (Italy), 1981.

25. R.C.Isler et al., 8th Int.Conf. on Plasma Physics and Controlled Nuclear Fusion Research, Brussels, 1-10 July, Paper CN-38/A-5 (1980).

26. S.Tanaka et al., Proc. 2nd Grenoble-Varenna Int. Symp. on Heating in Toroidal Plasmas, Como(Italy) 1980.

27. R.Cano, Proc.2nd Grenoble-Varenna Int.Symp.on Heating in Toroidal Plasmas, Como (Italy), 1980.

RECENT PDX RESULTS

M. Bell, V. Arunasalam, M. Bitter, W. Blanchard, K. Bol, K. Brau, S. Davis, F. Dylla, H. Eubank, M. Finkenthal, R. Fonck, R. Goldston, B. Grek, R. Hawryluk, J. Hirschberg[1], J. Hugill[2], D. Johnson, R. Kaita, S. Kaye, C. Keane, T. Kozub, H. Kugel, D. Manos, D. Mansfield, T. McBride, R. McCann, D. McCune, K. McGuire, D. McNeill, S. Milora[3], D. Mueller, M. Okabayashi, K. Owens, M. Reusch, N. Sauthoff, G. Schilling, G. Schmidt, J. Strachan, S. Suckewer, H. Takahashi, F. Tenney, A. von Halle, M. Williams, K. Yamazaki[4]

Princeton University, Plasma Physics Laboratory
Princeton, New Jersey 08544, USA

ABSTRACT

Studies of high power, perpendicular neutral beam injection into limiter and divertor discharges have been performed in the PDX tokamak. With 6 MW of injected power, central ion temperatures of 5.8 keV have been achieved in hydrogen plasmas with carbon limiters at a line-average density of 4×10^{13} cm^{-3}. The experiments have shown that the heating efficiency is dependent on plasma current. At low plasma currents, values of the poloidal beta up to 1.7 have been obtained.

Using the divertor to control the density, the heating has been investigated in plasmas with line-average densities in the range $2 - 6 \times 10^{13}$ cm^{-3}. Data on the energy and particle flow in the divertor are presented. The divertor receives about 60% of the energy input to the plasma in both ohmically heated and beam heated discharges.

[1] Physics Department, University of Miami, USA.
[2] UKAEA Culham Laboratory, England.
[3] Oak Ridge National Laboratory, USA.
[4] Institute of Plasma Physics, Nagoya University, Japan.

Overview of the PDX Experimental Program

Following the report of PDX results at the IAEA meeting in July 1980 [1], experiments continued through October 1980 in the areas of both divertor physics and neutral beam heating using the two injectors then installed. In November 1980, the machine was opened for installation of the remaining two beamlines and for internal modifications, including the replacement of the titanium limiters with graphite rail limiters and installation of titanium carbide coated graphite tiles on the inner wall to receive beam power not absorbed in the plasma.

Experiments recommenced in March 1981, and have since concentrated mainly on investigating the effectiveness of high power perpendicular injection in achieving high temperature and high beta plasmas. Initially, limiter discharges of circular cross-section were run to enable a comparison to be made with tangential injection under similar conditions in PLT [2], and with previous investigations of perpendicular injection at lower powers [3]. In June, divertor operation was resumed and the investigations of neutral beam heating were continued in various divertor configurations, but predominantly in the inside-Dee configuration. During the period since March, the machine has been routinely operated at fields and currents between 80% and 100% of their design values.

The four neutral beam injectors of the joint PPL-ORNL Heating Project have been reliably operated at powers of up to 7 MW total with deuterium beams, 5 MW with hydrogen, for pulse lengths up to 300 ms. The beams operate at an energy of 50 keV and are oriented to inject at a tangency radius of 0.35 m, giving an angle of 14° from perpendicular at the center of the vacuum vessel.

Beam Heating in Limiter Discharges

To investigate the effectiveness of perpendicular injection in producing high temperature, low collisionality plasmas, PDX was operated in conditions overlapping with those of PLT [2] as far as possible. Typical parameters for the circular cross-section discharges in these experiments were: major radius R = 1.43 m, minor radius a = 0.44 m, toroidal magnetic field B_T = 2.2 T, plasma current I_p = 450 - 500 kA, limiter q-value $q_a \approx 3.0$, and line-average density $\bar{n}_e \approx 2 - 3 \times 10^{13}$ cm^{-3} at the start of injection. In order to maximize the absorbed power at modest densities, deuterium was injected. Hydrogen target plasmas were normally used to minimize the neutron production and for species discrimination in the charge-exchange measurements.

Typical results are shown in Figure 1 for discharges with ohmic heating and 1 - 4 beams injecting. The injected powers are calculated from the power inputs to the beam acceleration stages using measured beam transmission factors and an estimate of 12% for losses due to reionization in the beam ducts. The transmission factors were measured with the beam-line calorimeters and on the test stand at ORNL. The calculation of the injected power has been confirmed by preliminary measurements using the inner wall armor as a calorimeter.

In these experiments, the feedback system controlling the plasma current was turned off during the beam injection and the current was allowed to rise as the loop voltage dropped. The gas feed to the discharge was also stopped just prior to the beam pulse. Titanium gettering was applied only in the remote divertor chamber regions, so that, without injection, the density decayed relatively slowly, on a timescale of about 150 ms. The density decay was overcome by the beam

injection and at the highest powers the density rose substantially during the heating pulse. Detailed measurements of the particle balance under these conditions have not been completed at this stage.

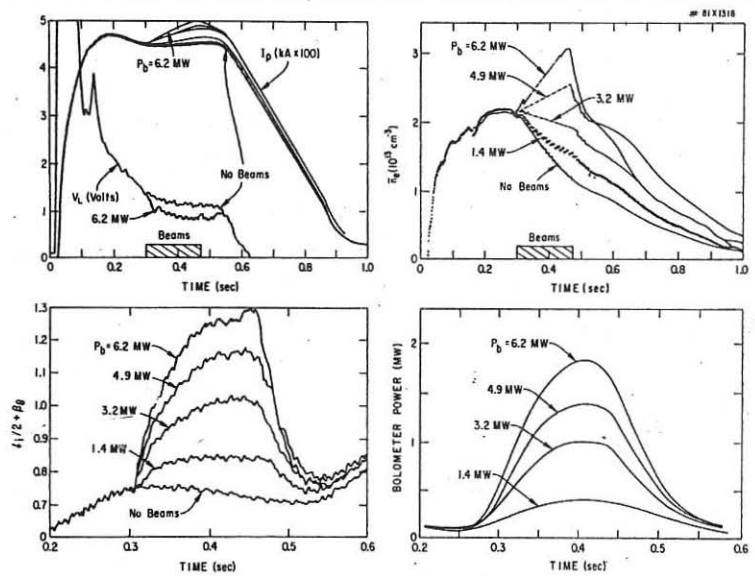


Figure 1 Typical waveforms for carbon limiter discharges during neutral beam heating: R = 1.43 m, a = 0.44 m, B_T = 2.24 T, $D^0 \rightarrow H^+$. As seen in the density trace for 1.4 MW injected power, strong sawtooth oscillations develop during the injection. The operation of the microwave interferometer became erratic during higher power beam injection. The density at the end of injection was then determined from the fringe count to the end of the discharge.

The quantity $\ell_i/2 + \beta_\theta$ shown in Figure 1 has been derived from the current in the windings maintaining the plasma equilibrium using the expressions given in reference [4]; corrections for the effects of eddy currents and leakage fields from other windings are included. The value of $\ell_i/2 + \beta_\theta$ has been found to be consistent with measurements of the external field pattern and full calculations of the MHD equilibrium configuration based on external flux measurements.

The bolometer array shows a large increase in radiated power during injection but, as a fraction of the input power, the level remains roughly constant. The bolometers are sensitive to the charge-exchange energy flux from the plasma, and as a result of their radial orientation and the perpendicular injection in PDX, charge-exchange from circulating beam ions may produce a significant component of the bolometer signal. The intensities of lines of highly ionized carbon and titanium impurities increase during injection, but typically by a factor about one half of that seen in the total radiation detected by the bolometers. The peak in the volume emissivity derived from the bolometer array, shifts inwards in minor radius slightly with increasing input power but the profile of the radiation remains hollow. The central radiation level remains below 0.1 Wcm^{-3} even at the highest injected powers.

The evolution of the ion temperature during beam heating is shown in Figure 2. A localized beam of 15 keV neutral hydrogen atoms can be fired into the plasma during the discharge to enhance the charge-exchange signal and discriminate against edge neutrals: the measurements made with this diagnostic beam are designated "active". There is good agreement between the results of the passive and active charge-exchange measurements and the Doppler broadening of the Titanium XXI K_α soft x-ray line at 2.6 Å.

There is also substantial electron heating during injection: profiles of the electron temperature and density obtained from the multiple-point Thomson scattering system are shown in Figure 3 before and during injection. The density profile remains relatively broad compared to the PLT discharges [2].

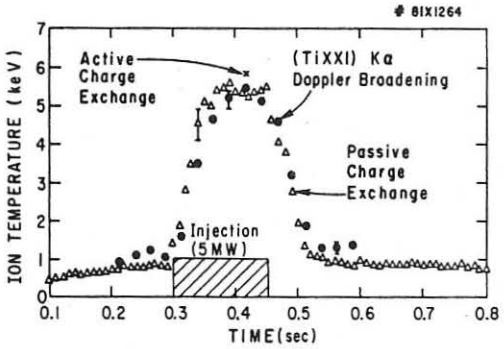


Figure 2 Evolution of the ion temperature during neutral beam heating: B_T = 2.24 T, I_p = 500 kA, $D^o \rightarrow H^+$, $\bar{n}_e = 3.8 \times 10^{13}$ cm^{-3} injected power P_b = 5.8 MW, absorbed power P_{abs} = 5.0 MW.

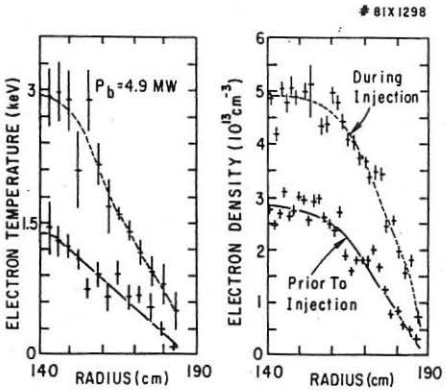


Figure 3 Thomson scattering measurements of the electron temperature and density profiles along a major radius. B_T = 2.24 T, I_p = 490 kA, P_b = 5.7 MW, P_{abs} = 4.9 MW.

The heating of circular discharges has been investigated as a function of plasma current for 200 < I_p < 500 kA. At the lowest plasma currents, large values of $\ell_i/2 + \beta_\theta$, up to 2.5, have been produced: the shift of the magnetic axis from the geometric center of the plasma column has reached 0.17 m in the equilibria computed for such plasmas. The poloidal beta, inferred from the equilibrium magnetic

data by subtracting the value of $\ell_i/2$ calculated from the temperature profile, has reached a value of 1.7. At the densities used in these investigations the contribution from suprathermal beam particles is a significant part of the total energy content, reaching as much as 60% in cases which were run at lower densities, $\bar{n}_e \sim 2 \times 10^{13}$ cm^{-3}. Since the pressure of the beam component is anisotropic with $p_\perp > p_\parallel$, the magnetic analysis, which yields the quantity $\beta_\theta = \beta_\parallel + \beta_\perp/2$, may slightly underestimate the total energy content of the plasma.

The ion temperature increases with the average power input per plasma particle, as shown in Figure 4: the charge-exchange temperatures are plotted against the power absorbed from the beams divided by the line-average electron density. The absorbed power is calculated by subtracting from the power delivered to the vacuum vessel, the loss due to shine-through of the beams, which can amount to 40% at the lowest densities involved in these experiments.

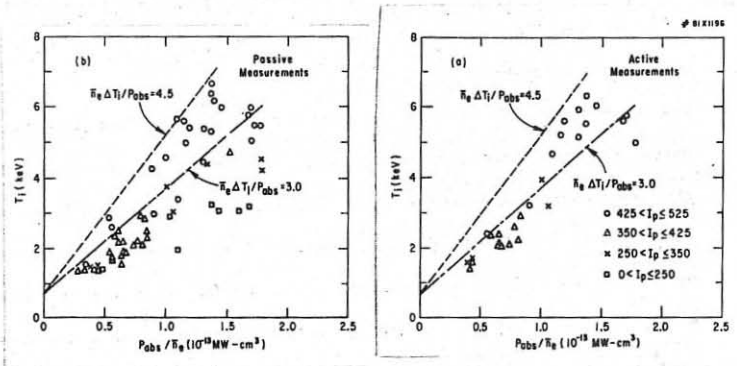


Figure 4 Variation in charge-exchange central ion temperature with absorbed beam power normalized to line-average plasma density. B_T = 2.24 T. Points are distinguished by plasma current range.

The heating efficiency as measured by the parameter $\bar{n}_e \cdot \Delta T_i / P_{abs}$ shows an improvement with increasing plasma current, as seen in Figure 5. At the highest currents, the ion heating efficiency approaches the best values observed in PLT [2] with tangential beam injection.

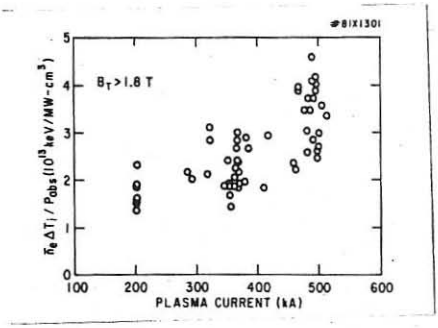


Figure 5 Variation in the central ion heating efficiency $\bar{n}_e \cdot \Delta T_i / P_{abs}$ with plasma current.

Figure 6 shows the variation in $\ell_i/2 + \beta_\theta$ with beam power for I_p = 200, 300 and 500 kA. No evidence is seen of a saturation in the energy content with increasing beam power up to the available limits. If, for a fixed beam power, the increase in stored energy remained constant, we would expect $\Delta(\ell_i/2 + \beta_\theta) \propto I_p^{-2}$. While there is an increase in slope as I_p is decreased, the variation is closer to I_p^{-1}, as seen in Figure 7, indicating a deterioration of confinement with lower currents.

The dependence of heating on the toroidal field has not been as extensively studied, but preliminary results have been obtained for the low current discharges where the toroidal field could be varied most widely. In these discharges, which were not necessarily optimized for heating and, at the lowest fields (B_T < 1.3 T) exhibited m = 2 activity before and during injection, there was a substantial degradation in the heating efficiency as the field was reduced. However, for a fixed plasma current, the highest volume-average toroidal beta was still achieved at the lowest toroidal field.

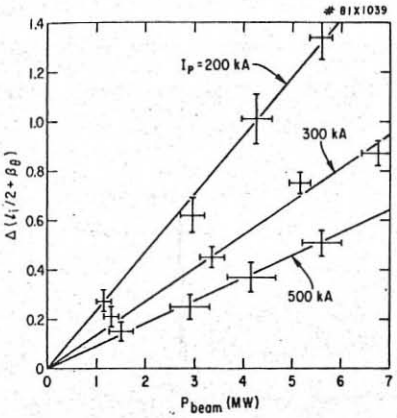


Figure 6 Increase in magnetically determined $\ell_i/2 + \beta_\theta$ with injected power for different plasma currents: $B_T = 2.24$ T. Points are averages for 5-25 discharges grouped by number (1 - 4) of beams injecting.

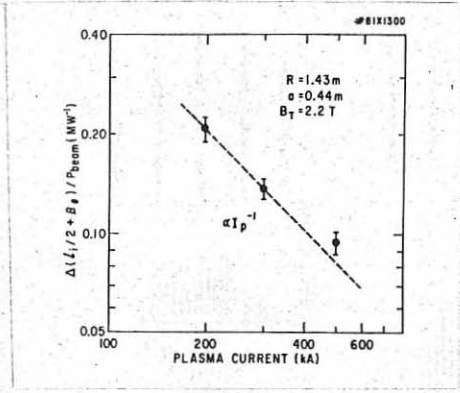


Figure 7 Variation in the slope $\Delta(\ell_i/2 + \beta_\theta)/P_b$ with plasma current.

As the current and toroidal field are changed, there are substantial changes in the MHD activity of the discharge during the heating pulse. The level of activity increases with beam power and with decreasing toroidal field. It does not appear that MHD activity is, in itself, responsible for the reduced heating observed at lower currents since discharges have been obtained at low current and high toroidal field which show very little activity, but in which there was no improvement in the overall confinement. The dominant activity has

been identified with a soft x-ray detector array as an m = 1 mode near the center of the discharge; higher m-number modes which show strong coupling to the m = 1 activity are observed with Mirnov coils. The coupling of these modes is illustrated in Figure 8.

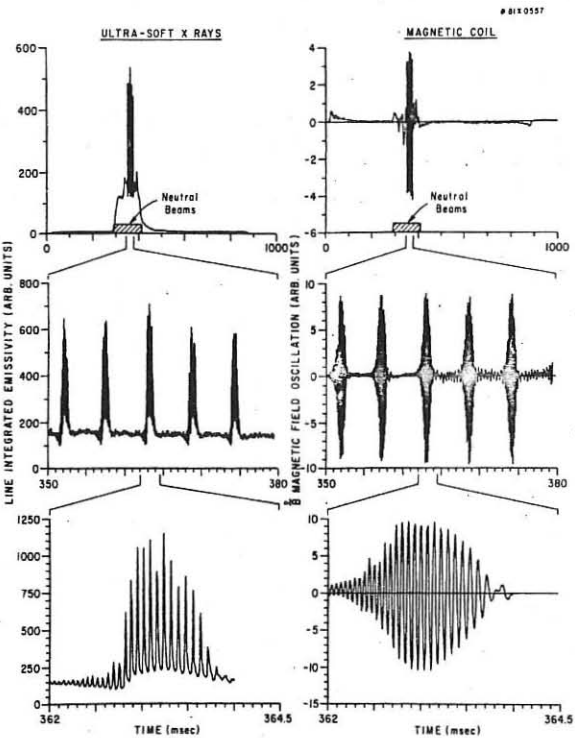


Figure 8 Coupled MHD activity recorded by a soft x-ray detector (m = 1 mode) and by Mirnov coils (m > 2 modes) during beam injection. B_T = 1.7 T, I_p = 310 kA, P_b = 6.8 MW. The frequency of oscillations increases from 2 kHz before injection to 14 kHz during injection.

A preliminary analysis of the differences between the transport properties of the low and high current limiter discharges has been undertaken. The analysis [5] uses the measured electron temperature

and density profiles in a Monte-Carlo calculation of the beam particle slowing down and energy deposition. The ion transport is then modelled by choosing both a factor α by which the neoclassical ion conductivity is enhanced and a global particle confinement time τ_p, in order to match the calculated central ion temperature with the measured value. The value of τ_p is chosen to obtain consistency with the observed H_α emission level and the decay rate of the density when gas puffing is terminated. With the appropriate values of α and τ_p, it is then possible to calculate the ion and electron energy balances and the power fluxes.

The results of these analyses show that in the 500 kA discharges, an enhancement α = 1 - 2 of the Hazeltine-Hinton value for the ion conductivity [6] and a global particle confinement time τ_p = 30 ms satisfactorily account for the observed central ion temperature. These values are similar to those which adequately model the ion transport in the best beam heating cases in PLT. The ion collisionality of these plasmas is very low: $\nu_i^* < 0.1$ over more than half of the profile, reaching a minimum $\nu_i^* \approx 0.02$ at r $\approx$ 12 cm. The central particle diffusivity in the PDX discharges tends to be 2 - 3 times the PLT value and is comparable to the INTOR scaling value [7]. This result reflects the difference in the width of the density profile between the PDX and PLT cases.

For the comparison of heating at high and low currents, the energy confinement times associated with anomalous transport processes in the core of the discharges, r < a/2, have been calculated in the analysis code. These confinement times are calculated by subtracting neoclassical transport, radiation and charge-exchange losses from the

total energy outflow from the core. The values for the 500 and 300 kA discharges are 21 ms and 14 ms respectively. This indicates that the reduced heating at lower currents is due to an increase in anomalous transport; the increase in neoclassical ion conduction and the reduction in beam power input due to the larger beam ion orbits are not sufficient to account for the reduced heating at lower currents.

In the high current, high field discharges, central values of beta, including the pressure of the fast ion component, approaching 5% have been achieved; the volume-average beta has reached 0.8% in these discharges.

Divertor Studies in Ohmic and Beam Heated Discharges

For divertor discharges, the energy deposition on the neutralizer plates is derived from a thermocouple array mounted on one pair of the inner neutralizer plates [8] and monitors of the integrated energy flux on all neutralizers. The monitors have confirmed that the energy flow to the divertors is toroidally and vertically symmetric for vertically centered discharges.

Examples of the energy deposition profiles on the outer neutralizer plate for ohmically heated and beam heated discharges are shown in Figure 9. At high neutral injection powers, the width of the energy deposition profile on the outer neutralizer plate increases, so that the peak power density on the plate does not increase linearly with injection power. Nevertheless, with 7 MW of neutral injection, peak power fluxes above 1 $kWcm^{-2}$ are being recorded at the plates.

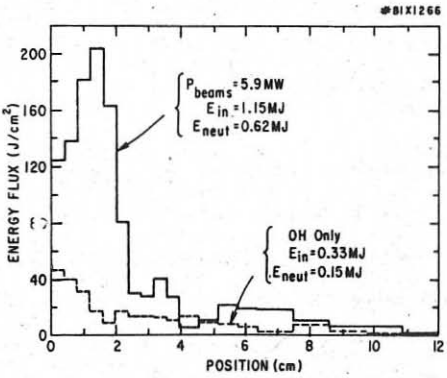


Figure 9 Energy deposition on the outer neutralizer plate of the inner divertor for ohmic and beam heated inside-Dee divertor discharges. The outer plates receive over 90% of the total energy to the divertor for vertically symmetric inside-Dee discharges.

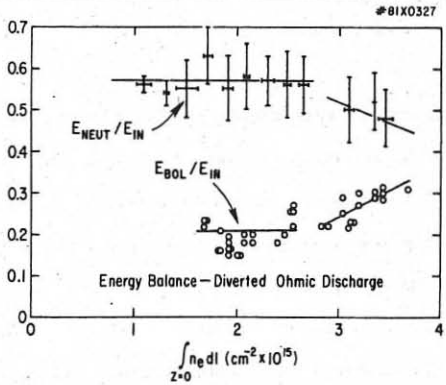


Figure 10 Variation in the energy balance of inside-Dee divertor discharges with plasma line-density. R = 1.38 m, a_{sep} = 0.38 m, B_T = 1.7 T, I_p = 300 kA. E_{neut} is the energy deposited on the inner divertor neutralizers, E_{bol} is the bolometrically measured energy from the main plasma region.

For ohmically heated inside-Dee discharges, the global energy balance has been studied as a function of the plasma density. The results, shown in Figure 10, indicate that the neutralizers receive about 60%

of the power at low densities; this fraction decreases at higher densities as the bolometer power rises. About 80% of the input power is accounted for in these measurements.

The flow of plasma onto the neutralizer for the inside-Dee discharges has been measured from the Doppler shift of a visible line of singly-ionized carbon. The region near the separatrix on the neutralizer plate was observed along two lines of sight, one parallel and one perpendicular to the local magnetic field. Data recorded from similar ohmically heated discharges in hydrogen and deuterium show that the ratio of the flow velocities is approximately 1.4:1. The measured velocities are of the order of the ion sound velocity for a plasma with $T_e \approx 20$ eV: probe measurements have yielded $T_e \approx 10 - 15$ eV close to the neutralizer plate.

In divertor discharges, the recycling coefficient for particles leaving the plasma is significantly less than unity, so that constant fueling is required to maintain the plasma density. Gas feed rates of $2 - 8 \times 10^{21}$ atoms/s are needed to sustain line-average densities of $2 - 4 \times 10^{13}$ cm^{-3} in ohmically heated hydrogen and deuterium discharges with gettering of the divertor chambers. During neutral beam injection, the required gas feed increases dramatically. For some experiments in which the density was raised substantially during injection, gas feed rates up to 3×10^{22} atoms/s ($\sim$ 500 Torr ℓ/s) have been used. This contrasts with the behavior observed in the discharges with carbon limiters where the density increased during injection without additional gas feed. Fueling of limiter and divertor discharges is compared in Figure 11 which shows the toroidal distribution of H_α emission before and during beam injection for the

two cases. While not absolutely calibrated, the intensities are directly comparable. Strong localization of the emission at the limiter and the gas feed valves is evident. The limiters in this experiment were titanium. In the limiter discharges, some increase in gas feed during injection was required to maintain the density, but the increase in emission at the gas valve was not as great as that seen in the divertor discharges.

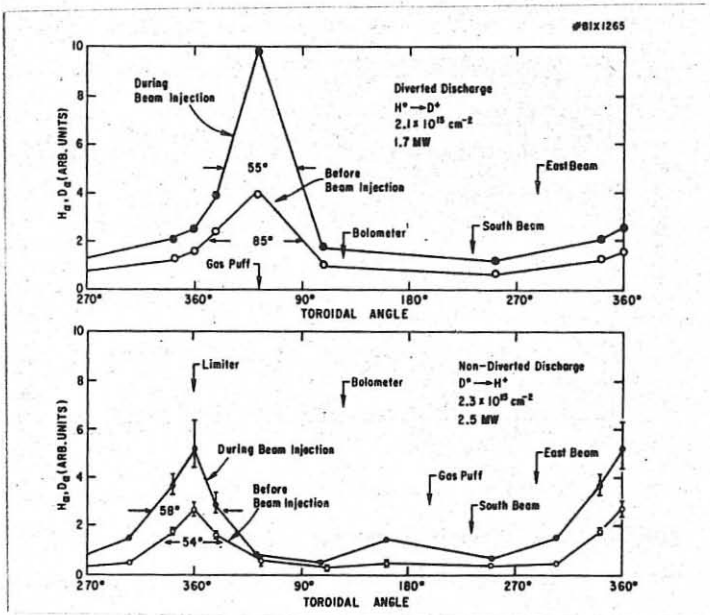


Figure 11 Toroidal distribution of H_α emission for divertor and titanium limiter discharges with and without beam injection.

As an alternative to gas puffing, injection of solid hydrogen pellets has been investigated on PDX in a series of collaborative experiments with the Oak Ridge National Laboratory Technology Group. Following initial experiments with injection of 0.9 mm diameter pellets, the injector was modified to produce 1.4 mm pellets containing typically

1.2×10^{20} hydrogen atoms. The evolution of the density profile following injection of such a pellet into a beam heated discharge is shown in Figure 12. In contrast to the relatively broad density profile which persists as the density is raised by gas puffing, the pellet leads to a highly peaked density profile. Following the pellet injection, the density profile relaxes to its original state on a timescale of about 75 ms.

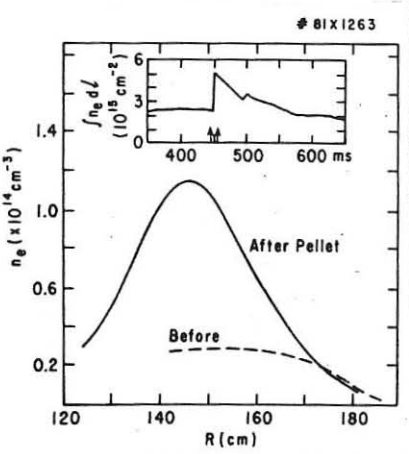


Figure 12 Radial profiles of the electron density before and just after injection of a 1.2 mm diameter solid hydrogen pellet. The inset shows the time decay of the density following pellet injection with 2 MW of neutral beam injection during the period 450 - 600 ms.

Beam Heating of Divertor Discharges

For the heating experiments, divertor operation of PDX has also been extended to higher values of the plasma current and toroidal field than previously reported. The heating efficiency in the divertor discharges appears to depend on the plasma current, as it does in the limiter discharges. The highest ion and electron temperatures have been achieved at the highest plasma currents, ~ 400 kA, in these experiments. For a constant density, the changes in the central ion temperature and in $\ell_i/2 + \beta_\theta$ also scale linearly with beam power up to the highest powers used. The ion heating efficiency, as measured by

the parameter $\bar{n}_e \cdot \Delta T_i / P_{abs}$, is the same within experimental uncertainty as in comparable limiter discharges.

The rapid decay of the density when fueling is terminated in divertor discharges provides the advantage that it is possible to raise the density substantially during neutral injection and yet avoid plasma disruption after the heating by terminating the gas feed before the end of the beam pulse. Scans of the density over a wide range were not made for the carbon limiter discharges because at high density the plasma tended to disrupt after injection. Using just two of the neutral beam injectors, values of the parameter $\bar{n}_e \cdot R/B_T$ [9] up to 9×10^{19} m^2 T^{-1} have been achieved with intense gas puffing into divertor discharges for $q_a = 3.0$.

At modest densities, $\bar{n}_e \sim 2 - 3 \times 10^{13}$ cm^{-3}, the recent divertor plasmas appear to have a higher impurity content, particularly of metals, and radiate more power during injection than earlier divertor plasmas. Whether this is a result of changes in plasma transport or in the impurity sources is being investigated. Divertor discharges at higher density, $\bar{n}_e \sim 5 \times 10^{13}$ cm^{-3}, have lower radiation levels and the radiation profile is hollow.

The first results of scanning the density are shown in Figure 13. Although the thermal component of the energy content increases slightly, the reduction in the calculated stored energy of the fast beam particles reduces the total energy content as the density rises. The causes of this apparent departure in the scaling of confinement with density from that being used in the INTOR design are now under active investigation.

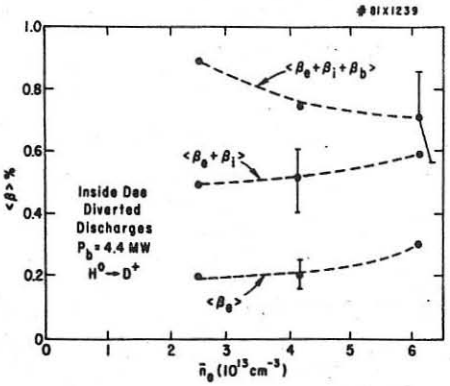


Figure 13 Variation in volume-average toroidal beta for electrons $\langle\beta_e\rangle$, total thermal component $\langle\beta_e + \beta_i\rangle$, and thermal plus fast beam component $\langle\beta_e + \beta_i + \beta_b\rangle$, with plasma density for a constant injected beam power of 4.4 MW. The beam component is calculated from the beam slowing down model. Magnetic data indicate values of $\langle\beta_e + \beta_i + \beta_b\rangle$ about 10% lower than these calculations.

ACKNOWLEDGEMENTS

The authors wish to acknowledge the major contribution of H. Haselton, W. Gardner and the Neutral Beam Development Group at Oak Ridge National Laboratory in the development of the PDX ion sources and in the fabrication of the beam systems. We wish also to thank all staff of the Princeton Physics Laboratory who have contributed to the construction and operation of the PDX tokamak.

This work was performed under the U.S. Department of Energy Contract No. DE-AC02-76-CHO-3073.

REFERENCES

[1] D. Meade, V. Arunasalam, C. Barnes, M. Bell, K. Bol et al., in Plasma Physics and Controlled Thermonuclear Fusion Research, Proc. 8th Intl. Conf., Brussels, July 1980 (IAEA, Vienna, 1981) Vol. I, p. 665.

[2] W. Stodiek, R. Goldston, N. Sauthoff, V. Arunasalam, C. Barnes et al., ibid., Vol. I, p. 9.

[3] Equipe TFR, ibid., Vol. II, p. 547.

[4] V.S. Mukhovatov, V.D. Shafranov, Nuclear Fusion, 11 (1971) 605.

[5] R.J. Hawryluk, in Physics of Plasmas Close to Thermonuclear Conditions, Proc. of the Varenna Course, August 1979 (Commission of the E.E.C., Brussels, 1980) Vol. 1, p. 19;

R.J. Goldston, D.C. McCune, H.H. Towner, S.L. Davis, R.J. Hawryluk, G.L. Schmidt, to appear in Journal of Computational Physics.

[6] R.D. Hazeltine, F.L. Hinton, Reviews of Modern Physics, 48 (1976) 239.

[7] Report on the International Tokamak Reactor Workshop, Vienna, June 1979 (IAEA, Vienna, 1980).

[8] D.K. Owens, V. Arunasalam, C. Barnes, M. Bell, K. Bol et al., Journal of Nuclear Materials, 93/94 (1980) 213.

[9] M. Murakami, J.D. Callen, L.A. Berry, Nuclear Fusion, 16 (1976) 347.

REVERSED-FIELD PINCH EXPERIMENTS

H. A. B. Bodin
Culham Laboratory, Abingdon, Oxfordshire OX14 3DB
England

(EURATOM/UKAEA Fusion Association)

Abstract

In this paper research on the reversed field pinch (RFP) is reviewed. In this system $B_\theta \sim B_\phi$, $q < 1$ and in the outer regions of the plasma B_ϕ has the opposite direction (i.e. is reversed) with respect to the axis. Since the current is not restricted to values below the Kruskal-Shafranov limit it can be large, giving powerful ohmic heating. The RFP has high shear and so confinement at high β may be possible, and an important feature is that the equilibrium is "self-generated" - the plasma itself generates and can sustain the equilibrium by a process known as self reversal.

Following a brief account of the different modes of operation of the RFP the basic theoretical properties are summarised including equilibrium and relaxed states, self reversal, stability and ohmic heating. Fusion reactor applications are mentioned briefly. The remainder of the paper discusses a new generation of RFP machines (Eta Beta II, TPE-1R(M), ZT-40(M), HBTX1A) which became operational during the last two years with currents up to 500 kiloamps and pulse lengths up to 5 - 10msec. Toroidal vessels of metal bellows construction with minor radii $\sim$ 9 - 26cms are used. The configuration is set up slowly (rise time 0.1 - 4msec) using self reversal usually assisted by B_ϕ field control. Temperatures up to several hundred eV are obtained with low fluctuations ($\delta B/B \sim 10^{-2} - 10^{-3}$). The reversed B_ϕ is sustained during the current pulse. This behaviour can be compared with so called "quiescence" on ZETA. The heating and confinement depend on I/N (peak current/filling line density) and there is an optimum value $\sim 10^{-14}$ A.m.; this leads to a simple scaling law $T \propto \beta_\theta I$ for pinches. The density rises quickly to a peak value typically $\sim 5 \times 10^{14} cm^{-3}$ and then decreases sharply; a slow phase with an e-folding time up to a few milliseconds reaching a few x $10^{13} cm^{-3}$ or more is often seen. The current pulse duration is determined by "current termination" (the current falls to zero in a few tens of microseconds) which occurs for example if field reversal is lost or the density becomes too small. Because of the density decay the streaming parameter can reach 10 - 30% and $I/N \rightarrow 10^{-13}$ A.m. at late times; experiments using gas puffing have begun. Preliminary estimates of the energy confinement time give $\tau_E \sim 0.1 - 0.4$msec. Studies are underway to determine experimental scaling laws for τ_E and T; data obtained so far shows an improvement as the current increases with $T \gtrsim I^n$ with $n \lesssim 1$ in some experiments.

1. INTRODUCTION

In this paper research on the reversed field pinch (RFP)[1] is reviewed. The RFP, like the tokamak, is a member of the toroidal pinch class of systems in which the plasma is confined by a combination of a poloidal magnetic field (B_θ) due to a toroidal current flowing within the plasma and a toroidal magnetic field (B_ϕ) generated by external coils. Both the RFP and the tokamak derive from the first scheme proposed for plasma confinement - the pinch effect[2] - as does the spheromak[3].

The difference between these systems lies in the variation of B_θ and B_ϕ with minor radius. The two main features of the RFP are, firstly, that the field components are both of the same magnitude, i.e. $B_\theta \sim |B_\phi|$, that is to say the safety factor $q = aB_\phi/RB_\theta << 1$ (a and R are the minor and major radii of the torus). The second feature is that the toroidal field reverses on the outside of the plasma with respect to its value on the axis, as shown in Fig. 1. This distinguishes the RFP from the so-called "stabilized pinch" widely studied in the early days of Fusion Research which has $B_\theta \sim B_\phi$ but no reversal and very limited regimes of stable operation. The RFP has high shear so that stability at relatively high-β (10-30%) may be possible. Because the current is not restricted to values less than the Kruskal-Shafranov limit, high currents and powerful ohmic heating can be obtained. The most important feature of the RFP is that the equilibrium is "self generated" - the plasma itself generates and can sustain the reversed field configuration by the process known as 'self-reversal'. This contrasts strongly with systems such as the stellarator where the configuration is produced by external currents or the EBT where electron rings are used.

In this paper, following a brief account of the different regimes in which RFP experiments can operate, the basic theoretical properties - equilibrium and relaxed states, the self -reversal mechanism, stability and ohmic heating are summarised. Fusion reactor applications are mentioned in Section 4. In Section 5, the main results from the small bore fast experiments carried outduring the 1970's are summarised, followed in Section 6 by a more detailed account of slow experiments with emphasis

on the four new machines now in operation, where temperatures up to several hundred eV and pulse lengths up to ∿ 10msec are reached. The parameters of these machines and the planned large RFX device are given in Table 1.

2. REGIMES OF OPERATION OF RFP EXPERIMENTS

Studies of the RFP can be divided into the 'setting-up phase' when the plasma/magnetic field system is established and the 'sustainment phase' where the current decays slowly or is held constant. RFP distributions can be set up by: (a) Fast programming, in which the external reversed field is applied rapidly (from a capacitor bank) before instabilities develop. This approach minimizes energy losses during setting up. (b) by means of the self-reversal process (c) Using a combination of self-reversal together with slow-field control; this approach is favoured for present future experiments. During the sustainment phase, the RFP can operate: (a) In the classical mode, in which the configuration decays by field diffusion ultimately leading to instability. Note that a pulsed reactor can operate in this mode since burn times can be shorter than the decay time. (b) Using external field control to extend the lifetime of the configuration in the presence of diffusion. (c) The sustained RFP where the self-reversal mechanism continues to operate after the configuration is set up, counteracting the tendency of the reversed field to decay by field diffusion. In this mode a quasi steady state can, in principle, be sustained as long as the current is maintained and experimentally field reversal lasts as long as the current pulse.

Experimentally an important parameter is the ratio $\tau_i/\tau_{A\theta}$ where τ_i is the current rise-time and $\tau_{A\theta}$ the poloidal Alfvén time; experiments are known as "fast" or "slow" according to whether this ratio is $\lesssim 1$ or $\gg 1$. The value of $\tau_i/\tau_{A\theta}$ determines whether or not the configuration is close to a relaxed state (Section 3) while it is set up. Fast rise-time experiments include most of the RFP devices operational in the 1970's such as HBTX1 at Culham,[4] ETA-BETA 1 at Padua,[5] the ZT series at Los Alamos,[6] and experiments at Tanashi[7] in which the current rises in 1 - 10 μs to ∿ 50 - 300kA. These all have provision for fast-field

programming to establish the configuration, although self-reversal has also been used. The tori had minor radii of 5 - 10 cm and were made from quartz, ceramic or glass.

In experiments with slow rise-times, the peak currents ranging from 50 - 600 kA (2MA is planned) are reached in ∿0.1 - 10 ms. Metal walled tori, minor radius typically 10 - 50 cm are usually used. These include ZETA,[8] on which in 1965 - 68 the first results on the relatively stable confinement of RFP plasma for several milliseconds was observed, the present generation of RFP machines, ETA-BETA II,[9-11] TPE-1R(M),[12,13] ZT-40(M)[14] and HBTX1A,[15] and planned future devices such as RFX (Table 1) Many other slow Pinch experiments (reviewed in Ref. 1) such as Sceptre, Perhapsatron and Alpha operated in the early days of pinch research, but these did not perform well as reversed field pinches.

3. BASIC PROPERTIES OF RFP

3.1 Theoretical pinch equilibria - relaxed states

The basic pinch equilibrium in a flux conserving cylinder is the $\beta = 0$ fully relaxed minimum-energy state given by Taylor [16] which has Bessel function (BFM) fields. According to this theory, all pinch configurations will, given some small but finite dissipation, relax to a state defined by:

$$\nabla \times \vec{B} = \mu \vec{B}$$

where $\mu \sim 2\theta/a$ and $\theta = B_{\theta wall}/B_{\phi average} \sim 2I/aB_{\phi o}$ is the pinch parameter. Solution of this equation gives the magnetic field components in terms of the Bessel functions: $B_\phi = B_o J_o(\mu r)$, $B_\theta = B_o J_1(\mu r)$ which has a reversed toroidal field when $\mu r > 2.405$ ($\theta > 1.2$). The minimum energy state becomes helical when $\theta \gtrsim 1.6$. Toroidal effects are small. The locus of stable, minimum energy states is given by the F - θ curve, where $F = B_{\theta wall}/B_{\phi average}$ is the field reversal ratio shown schematically in Fig. 2a. Although all states on this line are stable, it can be shown on MHD Theory that high-β and a vacuum region between the plasma and conducting wall are only possible with field reversal.

A BFM distribution has $|j| / |B|$ = constant with radius (Fig. 2b) and does not exist in experiment where j falls smoothly in the outer regions of the plasma to zero at the wall. There is a second class of stable equilibria, which are not fully relaxed and occur at slightly larger values of θ and higher energy, in which $|j| / |B| \neq$ constant close to the walls and j falls smoothly (Fig. 2b); these can, in principle, also exist as stationary states. These pressureless equilibria have high magnetic shear and, with slightly modified fields, can confine finite pressure. They can be stable to all MHD and tearing-mode instabilities with β up to some 20 - 30% (see Fig. 1). If they are also stable to pressure driven resistive instabilities - g-modes (Section 3.3) they can exist as stationary finite-β equilibria. If they are unstable to g-modes then whether or not they will relax to the BFM or one of the other stable zero-β equilibria is a critical but unanswered question.

When the time scale is long enough to allow relaxation, experimental field configurations are best represented by the finite - β variant of the second class equilibria and are similar in almost all experiments (both fast and slow). They depend only on the pinch parameter, θ and are insensitive to the other machine conditions. This conclusion is supported by the existence of an experimental "universal" F - θ curve (Fig. 3), which is displaced a little to higher θ compared with that for the BFM. Many of the properties of the observed relaxed states agree with the predictions of Taylor's theory. If the configuration tends to become unstable by field diffusion, the self-reversal mechanism is excited and counteracts the diffusion so that stability is maintained, which explains the observation of quasi-stationary behaviour in many experiments.[14][15][17]

3.2 The mechanism of relaxation and self-reversal

The mechanism of relaxation by which RFP equilibria are formed or sustained involves instability or turbulence which leads to the breaking and rejoining of field lines that can occur in a slightly resistive plasma. The relaxation process is dissipative and depends

on plasma conditions, in particular on the ratio of τ_i/τ_A* and on the magnetic Reynolds number, S. A mechanism involving a single helical m = 1 kink instability has been identified in compressed plasma;[18,19] another with many successively growing small amplitude m = 1 modes can explain the reversed-field generation in weakly compressed plasma.[17] It is probable that there are also fully turbulent mechanisms.[20,21] The relaxation process and instabilities which drive it are much less well understood than the properties of the final state, especially in "slow" high-S experiments. In particular, the associated fluctuations and energy losses which are expected to decrease as S rises (a scaling $\delta B/B \propto S^{-\frac{1}{2}}$ has been suggested)[17] and determine the confinement time and β are not well known at high temperatures.

3.3 Stability

The stability of the RFP has been extensively analysed,[22,23,24] mostly for the second class of equilibria. Many of the results have been confirmed by experiments in low-temperature plasmas.[18] Marginal and growth-rate analysis have been carried out both on ideal-MHD theory[25] and using the full dissipative equations[26]. On ideal theory, stability at β up to about 50% is possible; for the m = 1 tearing (kink) mode, the limiting β for stability lies between 10% and 30%. (Fig. 1 shows an example). Stability to gross kinks at relatively high- β is important because although (as explained above) an instability tends to drive the relaxation processes so that stability is recovered, in the case of a gross m = 1 instability, most of the plasma energy is lost in the process.

Theoretically, the resistive pressure-driven interchange mode[24,27] (the resistive g-mode) is important and difficult to suppress; finite Larmor-radius effects are weak in a cylinder and the high shear is of little advantage although the effect of parallel viscosity is stabilizing.[27] It can lead to magnetic island formation, non closure of magmagnetic surfaces, enhanced heat loss and limit β to 10% or less. Its properties depend on the magnetic Reynolds number and it has been

* τ_i is the current rise time and τ_A the poloidal Alfvén time.

tentatively identified experimentally[4] at low values of S (10 - 1000) it is thought to account for energy losses in a number of experiments and to play a role in the self-reversal process.

Both m = 1 modes and, particularly the m = 0 mode near the $B_\phi = 0$ surface are important. A single mode becomes more localised as S increases (Fig. 4). However, because of the multiplicity of singular surfaces in a pinch with q < 1 although individual modes become weaker, there are more of them as S rises and the simple picture must be modified when non-linear mode-mode coupling is considered. The non-linear behaviour of the g-mode and its saturation level are being studied using 2D and 3D [24, 28] codes. In a paper at this conference [29] an RFP equilibrium stable to ideal MHD and tearing modes is examined using 2D and 3D codes and although saturation effects are found for m = 1 and m = 0, the coupling between these modes gives ergodic field line behaviour. Effects of this kind might limit β to values well below 10% but much further analysis and experimental checks of the theory are needed.

3.4 Ohmic Heating

Ohmic heating [30] in pinches and tokamaks is similar and the main reason that higher ohmic powers are obtainable in pinches is that since q < 1, the current is higher for a given B_ϕ. In addition, there is a small enhancement by a factor of 2 - 4 in the RFP due to the current distribution and the aspect ratio can be optimised for ohmic heating. The value of total beta obtainable by ohmic heating in a pinch is high because

$$\beta_{tot} \approx \beta_\theta B_\theta^2 / B_\phi^2 \sim \beta_\theta \text{ when } B_\phi \sim B_\theta$$

On the other hand, the equilibrium temperature in a pinch is considerably lower at the same current than that in a small tokamak, since $T \propto \beta_\theta I^2/N$ and β_θ is smaller and N is larger in the former (see also pinch-tokamak scaling in Section 6.8).

In O-D [31, 32] and I-D calculations [33] the ohmic power is balanced against losses due to (a) impurity radiation (b) turbulent convection using a term of the form $D_\perp \sim \gamma/K_\perp^2$ giving

$$\tau_e \propto a^2/[\delta B/B(B^2/\mu_o\rho)^{\frac{1}{2}} \Lambda]$$

where γ is the growth rate, $K_\perp$ the perpendicular wave number and Λ the transverse correlation length (the other symbols are as usual) and

(c) electron heat induction assuming classical, tokamak or other scalings. Examples of the results obtained are given in Figs 5 and 6 which show reasonable agreement for ZETA and for ETA-BETA II at peak current; important differences are found however, for HBTX1A and ZT-40(M) at later times when the density becomes low due to particle losses. These calculations indicate temperatures $\gtrsim$ 100eV at a few hundred KA and that an RFP with the potential to reach temperatures extending to the KeV range requires currents $\gtrsim$ 2MA.

[34]

4. APPLICATION TO FUSION REACTOR

The main potential advantage of the RFP is that the magnetic field at and forces acting on external conductors are considerably smaller than for other toroidal systems. The use of an open structure, since the aspect ratio can be freely chosen, and the possibility of ohmic heating to ignition are other possible advantages. However, in order to have a suitable duty cycle with ohmic ignition in a few seconds, the losses must be small, $\sim$ 2 - 5x hydrogenous bremsstrahlung. Although this is a severe requirement, the advantages in reduced complexity and cost of avoiding the need for large additional heating power are very great. The reactor designs achieve these conditions at I $\sim$ 20MA with a $\sim$ 1.5m and a relatively small unit size is possible. The disadvantages include problems of the conducting shell (probably needed for high- β tokamaks also) and the size and power rating of the poloidal field power supply. Present designs are for pulsed systems (which will probably be built first). However, by operating in the "sustained mode" (Section 2) in which the configuration is sustained by the plasma as long as the toroidal current flows, quasi steady state operation is possible in principle and the pulse length is then determined by the transformer volt seconds just as in the Tokamak reactor. Parameters of superconducting reactor designs carried out by the Los Alamos and by Culham-Padua Groups are summarised in Table 2.

5. EXPERIMENTS WITH FAST RISE-TIMES

Stable distributions were set up without wall contact by fast programming with $\beta \gtrsim 50\%$ in the "fast" experiments with small bore insulating tubes.[4-7] Many theoretical predictions on relaxed states and instabilities were tested on these devices and much important information obtained, but high temperatures and good confinement were not realised. In low current conditions where no unstable fluctuations were detected, classical confinement was observed at temperatures of about 10eV. As the current was raised, although the instantaneous peak temperature increased and values of more than 100 eV were recorded,[18] there were large fluctuations and the temperature fell rapidly to about 10 or 20 eV with a fluctuation level of $\delta B/B \sim 10\%$ and confinement times of a few microseconds. The plasma decay time at currents $\sim$ 40 - 80 kA was independent of the current and neither the electron temperature nor the confinement time increased as the current was raised; the resistance did not decrease. The reasons for this behaviour are not completely understood, but it is thought that unstable fluctuations driven because β was too high were important and both ideal and resistive pressure-driven modes were tentatively identified; also, radiation losses[5] were believed to play a role.

6. NEW GENERATION OF RFP EXPERIMENTS

6.1 General

Four new intermediate sized RFP experiments are now in operation. (see Table 1). They have metal bellows liners and operate in the slow mode using self-reversal, usually assisted by field control, to establish the configuration. Peak currents used so far lie in the range $\sim$ 80 - 500 kA with rise times of a few $\times 10^{-1}$ msec up to 4 msec and pulse lengths extending to $\lesssim$ 10ms. The first two to operate, ETA-BETA II[9,10,11] in 1979 and TPE-1R(M)[12,13] in 1980 have minor radii of 12.5 and 10cm respectively, whereas ZT-40(M)[14] and HBTX1A,[15] which first operated early in 1981, have minor radii of 20 and 26cm and both are designed to operate at currents of up to 500 - 600 KA.

These devices all perform substantially better than the small

fast experiments (Section 5) and yield temperatures of $\gtrsim$ 100eV with confinement times of $\gtrsim$ 100μs compared with 10eV and a few μs at similar currents. After the distribution is set up $\delta B/B \lesssim 1\%$ compared with $\gtrsim$ 10% in the fast experiments and the density fluctuations are lower. It was shown on TPE-1R(M) and then, strikingly, on ZT-40(M) that the behaviour with metal bellows liners was much better than with insulating tori with which these two machines were first equipped. The behaviour in these new machines can be compared with that in the so called "quiescent operation" in ZETA[8] where the temperature increased after peak current to ∿ 150 - 200eV (Fig. 7) with $\tau_E \sim$ 3ms, $\beta \sim 5 - 10\%$ at I ∿ 400KA. In particular, in the new machines the temperature continues to rise due to ohmic heating after peak current and the plasma resistance falls to give long decay times. The highest temperatures published so far are on ZT-40(M) and extend up to about 200eV at (values comparable to those on ZETA); the temperature time variation is shown in Fig.8 with, for comparison, data from the ceramic torus. Recently ∿ 300 eV has been observed.

Much new information has come from these machines with studies on ETA-BETA II on the effect of varying the initial pressure which show that the confinement and heating depend on the ratio of I/N where I is the current and N the line density. This leads to a proposed ιFP scaling law (Section 6.8). In TPE-1R(M), which has a relatively high value of current density, the density-time behaviour has been studied and preliminary unpublished data indicate temperatures up to 400 - 600eV. In ZT-40(M), following a comparison between operating with ceramic and metal tori, the temperature, density fluctuation level and resistivity have been studied using Thomson scattering and a multi-channel CO_2 laser interferometer at currents between 120 and 250kA. Operation with and without power crowbar have been compared and preliminary studies of the effect of using a material limiter have been carried out. On HBTX1A, the most recent machine to operate, studies of different modes of field control with passive and active crowbar have been carried out and a detailed investigation made of magnetic field fluctuations using arrays of pick up coils inside the liner. The density behaviour has been studied using single channel CO_2 (λ = 10.6μm) and HCN (λ = 337μm) interferometers. Preliminary experiments on gas puffing have been

carried out. In the remainder of Section 6, we present and discuss some of the results obtained on these experiments.

6.2 Field Control Studies

In Fig. 9 current and magnetic field wave forms from HBTX1A are shown for three commonly used modes of setting up the configuration both with and without power crowbar. In all cases, the current pulse ends rapidly with current termination (Section 6.5). In Fig. 9(a) self-reversal on its own is used, the toroidal field circuit being crowbarred so that it behaves as an effective flux conserver. In Fig. 9(b) is for the so called "matched mode" where the reversed field within the liner is provided by the plasma self-reversal effect and that outside by the external circuit which is adjusted so that approximately no flux crosses the liner, which behaves as a virtual flux conserver with $V_\theta = 0$. The matched mode, which gives smaller flux consumption, is the most commonly used on ZT-40(M) and TPE-1R(M). Fig. 9(c) shows "aided reversal" in which the reversed field provided externally by the circuit is driven harder than in case (b) to give higher reversal ratios In this mode, which is similar to that initially used on ETA-BETA II, the current decreases sharply after the peak when the B_ϕ field is driven negative, followed by a slow decay. The pulse shapes observed on ZT-40(M) are similar to those in Fig 9(b) with the maximum pulse lengths $\sim$8ms. The plasma response to various applied fields agree satisfactorily with predictions based on coupled circuit / plasma model calculations.[35] The use of B_ϕ field control allows θ, on which the configuration depends, to be varied independently of I. In Fig 3 experimental F - θ curves from HBTX1A with rise times of 1 and 4 msec are shown, with the Taylor curve and representative points from HBTX1A and ZETA for comparison. All the experimental data lies in the neighbourhood of the so called "Universal F - θ" curve[1]

6.3 Effect of initial pressure and I/N

On ETA-BETA II[10] $\delta B/B$ increases as the filling pressure is lowered and the radiated power increases as it is raised (Fig. 10). This data is replotted in Fig. 11 as a function of I/N together with the current

decay time τ_I which depends on plasma resistance and gives an indication of the temperature. It is seen that τ_I peaks (maximum temperature) at $I/N \sim 1 - 1.5 \times 10^{14}$ Am when both the radiated power and $\delta B/B$ are small; scattering data confirms this optimum.[11] It should be noted that on ETA-BETA II, because I(t) and N(t) have similar shapes in this work, I/N can be evaluated using peak current, $\hat{I}$, and filling line density N_o; this is not so on HBTX1A and ZT-40(M).

The behaviour on ZT-40(M) and HBTX1A was slightly different in that the low pressure regime with increasing $\delta B/B$ is not reached, probably because the gas will not break down. Nevertheless, the optimum heating and confinement on all these machines occurs approximately at $\hat{I}/N_o \sim 1 - 2 \times 10^{-14}$ A.m. In HBTX1A and ZT-40(M) with active crowbar, the current remains constant but the density decays steadily throughout the pulse (Section 6.4) and so the value I/N increases continuously from its initial value by a factor $\lesssim 10$. Thus during most of the sustainment phase I/N in these larger devices exceeds the ETA-BETA II optimum and corresponds to the regime where the confinement is strongly limited by MHD fluctuations, and the streaming parameter can reach 10% or more.

Further studies on ETA-BETA II[11] show (Fig. 12) that whereas the radiation limitation is independent of the current, the high I/N limit shows a weak current dependence which can be linked with the streaming parameter ζ and the peaks of these curves occur at $\zeta \sim 3\%$.

6.4 Density-time variation

The form of density-time behaviour is similar in all machines and shows a rapid rise in n_e to a value corresponding to the filling density due to ionisation; thereafter it falls. Sometimes a rapid fall (pump-out) followed by a more gradual decay, until current termination, is found. HBTX1A data is shown in Fig. 13. The density after pump-out tends to be independent of the filling value with a possible trend to increase with current; TPE-1R(M) data is shown in Fig. 14. The steady decay contrasts with ZETA where during the 1 - 3msec quiescent period the density remained approximately constant.

The density decay time in ZT-40(M) and HBTX1A during the slow decay phase was $\sim$ 1 - 3 ms and during the discharge the density fell approximately from 10^{14} to 10^{13} cm^{-3}. The decay time increased using active crowbar, but this is probably due at least in part to recycling which has not yet been measured.

On HBTX1A periods of slow or zero density decay, which correlate in time with reduced magnetic field fluctuations, but not with density fluctuations, have been observed in discharges without power crowbar. Further studies are required to explain these and other features of the density-time behaviour.

Density fluctuations have been studied on ZT-40(M) and HBTX1A They are large during setting up, relatively small ($\sim$ 1%) during the slow decay phase and rise again just about current termination; they do not show a strong correlation with the magnetic field fluctuations.

6.5 Current termination

The current pulse usually ends with a rapid termination when the current falls to zero in a few tens of μs or less (see for example Fig. 9). Termination occurs, for example on ETA-BETA II, if the reversed field falls to zero. On HBTX1A and TPE-1R(M) and sometimes on ETA-BETA II, termination also occurs in conditions when the reversed field is maintained, although when the current terminates the reversal is also lost. In these cases, density measurements (on HBTX1A) suggest that termination is associated with a critical density value possibly $\sim$ 10^{13} cm^{-3}.

Preliminary experiments on HBTX1A with gas puffing give a 2 - 3 fold increase in density during the decay with no observable change in plasma resistance and current termination is delayed somewhat. In HBTX1A and ZT-40(M), the pulse length appears to be limited by current termination and not the poloidal circuit to 5 - 10msec.

6.6 Temperature and Energy confinement time measurements on ZT-40(M)

The time variation of the temperature on axis in ZT-40(M) determined by Thomson scattering, was shown in Fig. 8; T_e increases rapidly as the current rises to its peak value and thereafter

increase more slowly and probably saturates at later times (the measurements do not as yet extend beyond about 3ms). The temperature increases as the filling pressure is reduced and at the same pressure it increases with the current (Fig.15). Further analysis of this data is required before scaling information can be obtained particularly because of the weak dependence of the plasma density on the filling pressure.

Reliable measurements of the energy confinement time, τ_e, have not been made yet in any of these experiments. On ETA-BETA II, a value of about 100 μs is reported at this conference. In ZT-40(M) τ_e was estimated by comparing the temperature-time variation, calculated from a zero dimensional code using different values of τ_e, and experiment. It is seen (Fig.16) that τ_e exceeds 0.2ms at early times but falls thereafter; during this time, the temperature rises steadily (reaching almost 200 eV), the density decays from about 5×10^{13} to 10^{13} cm^{-3}, and the streaming parameter rises. The highest value quoted is 0.4msec on ZT-40(M).

6.7 Magnetic Field fluctuations

These have been studied on all devices, in particular on HBTXIA which has pick up coils fitted inside the liner. Fig 17 gives an example from this machine of a period of reduced fluctuations ($\delta B_\theta/dt$) corresponding to a reduction in the rate of current decay; although this is characteristic of the QP in ZETA, on HBTXIA no marked change in τ_E was generally evident. On HBTX1A and TPE-1R(M) the fluctuation level during the decay phase is smaller by a factor ~ 2 when E_ϕ is negative. We note that in ZETA there was a marked reduction in the dI/dt fluctuations when $E_\phi < 0$. It is not yet clear if the new machines are reproducing ZETA QP conditions. Typically the RMS value of $\delta b_\theta/dt$ on HBTXIA and ZT-40(M) is less than 1%, with $\delta b_\phi/dt \sim 2 - 3\ \delta b_\theta/dt$; these values are consistent with the losses using the expression given in Section 3.4.

6.8 RFP Scaling

A simple scaling law for temperature versus current has been proposed,[36] based on the observations of an optimum I/N. Pressure balance can be written, when I/N = constant, as

$$T \propto \beta_\theta \left(\frac{I}{N}\right) I = \beta_\theta I$$

This is plotted in Fig. 18 which also shows the temperature - current variation for Alcator ($\tau_E \propto na^2$) and Coppi Mazzucato ($\tau_E \propto na^3T/I$) scalings, which give, respectively, $T \propto \left(\frac{I}{a}\right)^{4/5}$ and $T \propto \left(\frac{I}{a}\right)^{2/3}$. Experimental points for ETA BETA II, ZETA and ZT-40(M) agree within experimental error with pinch scaling. Points are also plotted which show the temperature expected for some pinch machines according to tokamak scaling, which is higher, as expected, since it is well known that small low current RFP's give much lower temperatures than the corresponding tokamaks. The main reason for this difference is that small ohmically heated tokamaks have much larger values of β_θ than pinches; they can also operate at lower N. However, for large, high current machines such as RFX (also shown in Fig. 18) the temperature obtained according to pinch and tokamak scaling is similar. It may be concluded that in order to make a meaningful comparison between pinches and tokamaks a large high current ($\sim$ 2 MA) pinch device must be built. It has been assumed that β_θ is independent of current, whereas theoretically it probably falls slowly as the current is increased, but this tends to be offset because I/N increases with I (Section 6.3).

7 CONCLUSIONS AND DISCUSSION

A wealth of new data has been obtained from the intermediate experiments and many important phenomena identified which have yet to be explained. The main conclusion is that RFP devices at 100 - 300 kA now routinely yield $T \sim 100 - 200$eV (values up to 300 - 600eV have been reported) with pulse lengths of 5 - 10msec, during which the reversed field is sustained. The fluctuation levels are relatively low ($\delta B/B \lesssim 1\%$). This contrasts with 10eV, $\sim$ 10μsec and $\delta B/B \sim 10\%$ on the previous generation of small bore fast machines at similar currents. Optimum heating and confinement occurs at $I/N \sim 1 - 2 \times 10^{-14}$ A.m. and this leads to a pinch scaling law $T \propto \beta_\theta I$. On this law small pinches yield lower temperatures (at the same current) than if they operate as tokamaks with Alcator scaling, but large high current devices give similar temperatures on both scalings.

The density-time behaviour shows a rapid rise due to ionization, following which n_e decays (with an e-folding time $\sim$ 1 - 3msec on ZT-40(M) and HBTX1A) until the current pulse ends with rapid "current termination". Sometimes there is a sharp fall to a value only weakly dependent on the filling pressure, but which increases with current, followed by a slower decay. The duration of the discharge is limited by current termination in the discharge rather than the poloidal circuit. Whereas O-D calculations of T_e (Section 3.4) give satisfactory agreement at peak current, thereafter the ohmic power balance changes as N falls.

There is as yet no clear picture of the energy confinement but preliminary measurements indicate $\tau_E \lesssim$ 0.1 - 0.4msec. In HBTX1A and ZT-40(M) in sustained discharges both I/N and the streaming parameter increases with time, ζ reaching 10 - 30%.

The main thrust of future RFP work should on the one hand be to extend studies to currents of 1-2 MA or more and on the other to understand phenomena such as the density time and I/N behaviour (with further gas puffing studies to maintain N), current termination, fluctuations and confinement properties, especially as I is increased to 500-600 kA, on the intermediate experiments.

REFERENCES

[1] H A B BODIN and A A NEWTON, Nuclear Fusion 20, 1255 (1980)

[2] W H BENNETT, Phys. Rev. 45, 890 (1934)

[3] M N ROSENBLUTH and M BUSSAC, Nuclear Fusion 19, 489 (1979)

[4] P G CAROLAN et al, in Plasma Physics and Controlled Nuclear Fusion Research (Proc 7th Int Conf Innsbruck 1978) 2, 23 (1979) IAEA Vienna

[5] A A BUFFA et al, in Plasma Physics and Controlled Fusion Research (Proc 6th Int Conf Berchtesgaden 1976) 2, 447 (1977) IAEA Vienna

[6] D A BAKER et al, in Plasma Physics and Controlled Nuclear Fusion Research (Proc 6th Int Conf Berchtesgaden 1976) 1, 419 (1977) IAEA Vienna

[7] K HIRANO et al, in Plasma Physics and Controlled Nuclear Fusion Research (Proc 7th Int Conf Innsbruck 1978) 2, 55 (1979) IAEA Vienna

[8] D C ROBINSON and R E KING, in Plasma Physics and Controlled Nuclear Fusion Research (Proc 3rd Int Conf Novosibirsk 1968) 1, 263 (1969) IAEA Vienna

[9] A BUFFA et al, in Controlled Fusion and Plasma Physics (Proc 9th Europ Conf Oxford 1979) 2, 544 (1979) Culham Laboratory

[10] A BUFFA et al, in Plasma Physics and Controlled Nuclear Fusion Research (Proc 8th Int Conf Brussels 1980) 2, 275 (1981) IAEA Vienna

[11] A BUFFA et al, this Conference

[12] Y HIRANO et al, in Plasma Physics and Controlled Nuclear Fusion Research (Proc 8th Int Conf Brussels 1980) 2, 301 (1981) IAEA Vienna

[13] Y HIRANO et al, submitted to Nuclear Fusion

[14] D A BAKER et al, this Conference

[15] P G CAROLAN et al, this Conference

[16] J B TAYLOR, in Pulsed High Beta Plasmas (Proc 3rd Top Conf Abingdon 1975) Pergamon Press London 59 (1976)

[17] C A BUNTING et al, in Controlled Fusion and Plasma Physics (Proc 8th Europ Conf Prague 1977) Czechoslovak Academy of Sciences 1, 79 (1977)

[18] C W GOWERS et al, in Plasma Physics and Controlled Nuclear Fusion Research (Proc 6th Int Conf Berchtesgaden 1976) 1, 429 (1977) IAEA Vienna

[19] J A WESSON and A SYKES, Phys Rev Lett 37, 140 (1976)

[20] M G RUSBRIDGE, Plasma Phys 22, 331 (1980)

[21] C G GIMBLETT and M W WATKINS, in Controlled Fusion and Plasma Physics (Proc 7th Europ Conf Lausanne 1975) 1, 103 (1975)

[22] D C ROBINSON, Plasma Phys. 13, 439 (1971)

[23] D C ROBINSON, Nucl. Fusion 18, 939 (1978)

[24] T C HENDER and D C ROBINSON, Culham Laboratory Preprint CLM-P628 (1981)

[25] J E CROW and D C ROBINSON, in Pulsed High Beta Plasmas (Proc 2nd Topical Conf Garching 1972) Max-Planck-Institut für Plasmaphysik, Garching Report IPP 1/127, C1 (1972)

[26] J E CROW, J KILLEEN and D C ROBINSON, in Controlled Fusion and Plasma Physics (Proc 6th Europ Conf Moscow 1973) Moscow 1, 269 (1973)

[27] R J HOSKING and D C ROBINSON, in Controlled Fusion and Plasma Physics (Proc 9th Europ Conf Oxford 1979) Culham Laboratory 61 (1976)

[28] D D SCHNACK, J KILLEEN and R A GERWIN, UCRL Preprint 84301 (1980)

[29] T C HENDER and D C ROBINSON, this Conference

[30] H A B BODIN, 2nd Joint Grenoble-Varenna International Symposium, Como (1980), to be published in the proceedings

[31] P G CAROLAN Private communication 1980.
(See also reference 4).

[32] M BAGATIN et al, in Plasma Physics and Controlled Nuclear Fusion Research (Proc 7th Int Conf Innsbruck 1978) 2, 37 (1979) IAEA Vienna

[33] J P CHRISTIANSEN and K V ROBERTS, Nuclear Fusion 18, 181 (1978)

[34] R HANCOX, R A KRAKOWSKI and W R SPEARS, Nuclear Engineering and Design 63, 251 (1981)

[35] J W JOHNSTON, Plasma Physics 23, 187 (1981)

[36] S ORTOLANI, Private Communication (1981)

TABLE 1

ZETA, MACHINES NOW OPERATING AND RFX

	ZETA Harwell/Culham	TPE-1R(M) Sakura-Mura	ETA BETA II Padua	ZT-40(M) Los Alamos	HBTV1A Culham	RFX International
major radius(cm)	150	50	65	114	80	180
minor radius (cm)	48	10	12.5	20	26	60
peak current(MA)	$\sim$ 0.4	0.15	0.3	0.25	0.3	2
rise time(ms)	1.5	0.45	0.1 - 0.5	0.25	0.4 - 4	15 - 50
pulse length (ms)	3 - 5	0.8	1.0 - 2.0	5 - 10	5 - 10	0.25 sec
						TARGET VALUES
temperature(eV)	150 - 200	200 - ? $\neq$	80 - 100	150 - 300	100 - 200	$\gtrsim$ 1keV
density (cm^{-3})	5×10^{13}	$10^{13} - 10^{14}$	few $\times 10^{14}$	$10^{13} - 10^{14}$	$10^{13} - 10^{14}$	$\sim 10^{14}$
beta	$\lesssim$ 0.1	$\gtrsim$ 0.1	0.1 - 0.2			$\sim$ 0.1 - 0.2

$\neq$ Unpublished data indicate temperature $\sim$ 400-600eV

TABLE 2

PARAMETERS FOR RFP REACTORS WITH SUPERCONDUCTING MAGNETIC-FIELD WINDINGS

	LASL	Culham/Padova
Net output power [MW(e)]	1000	600
Gross thermal power [MW(th)]	3000	1900
First wall radius (M)	1.5	1.5
Major radius (m)	12.7	14.5
Toroidal plasma current (MA)	20.0	15.0
Duration of burn (s)	22.0	25.0
Duration of full cycle (s)	27.0	37.0
Energy multiplication factor, Q	15.0	11.8
Recirculation power fraction, ε (%)	16.0	21.0

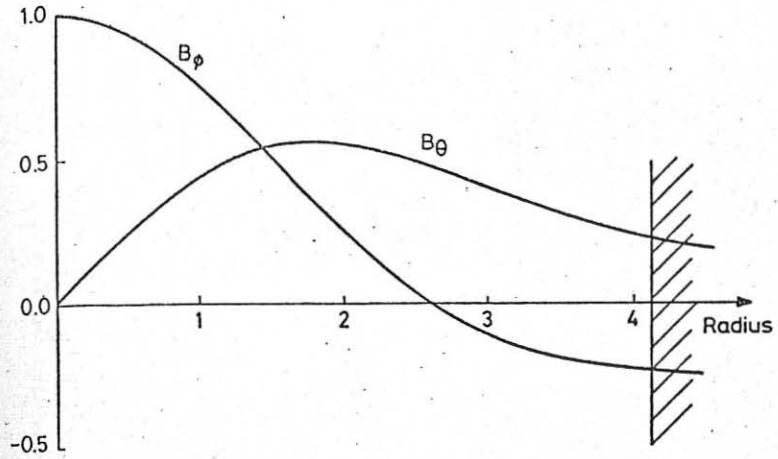


Fig 1 Radial distributions of magnetic field components of RFP across the minor radius. This configuration is tearing-mode-stable and the maximum radial position for a conducting wall to give stability is indicated by the vertical hatched line.

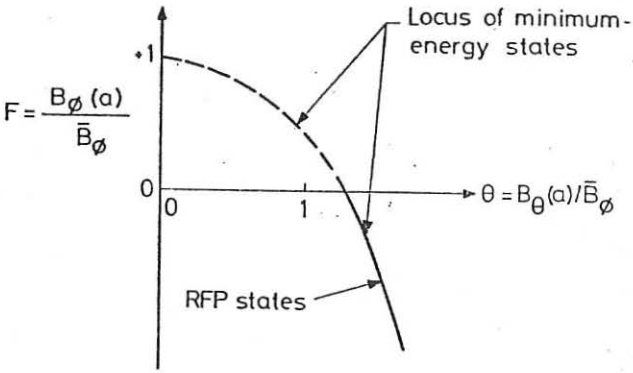


Fig 2(a) Schematic F - θ diagram

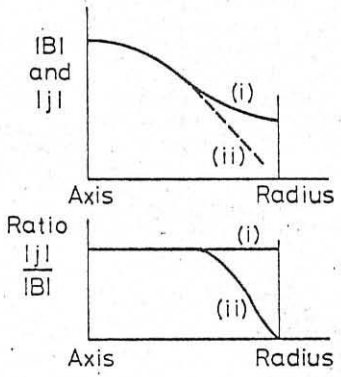


Fig 2(b) Illustrative radial distributions of magnetic field $|B|$ and current density $|j|$ (above) and the ratio $|j|/|B|$ (below) for the minimum-energy (BFM) state (case i) and a practical near-minimum-energy state where $|j|$ falls smoothly to zero at the walls (case ii).

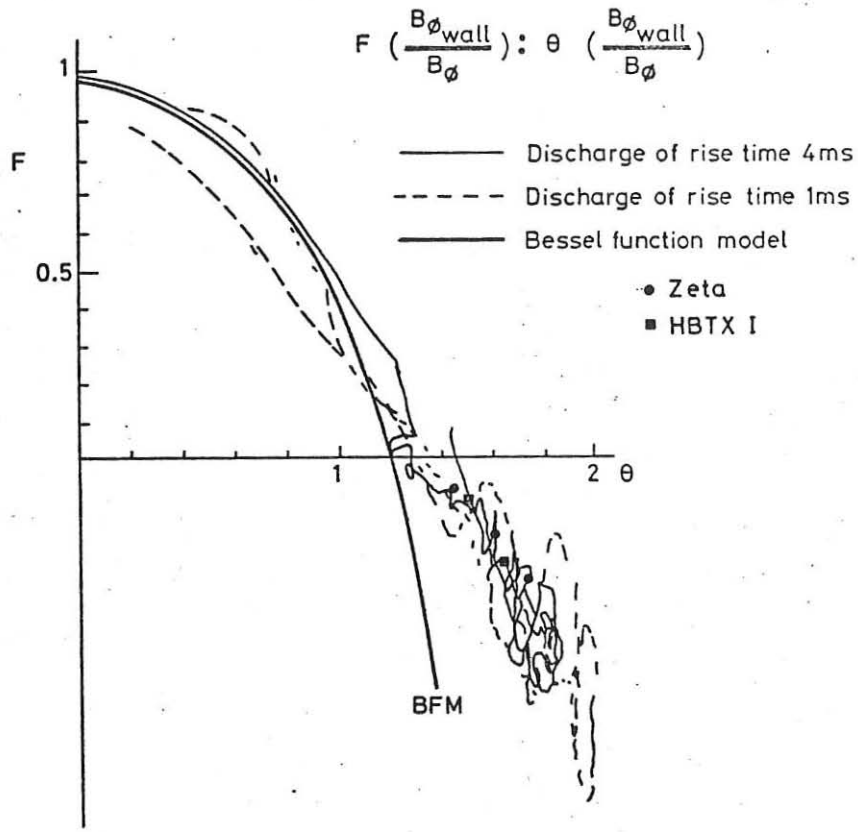


Fig 3 F-θ diagram showing lines obtained using the automatic data processing system for HBTXIA with current rise times of 1 and 4 ms, with representative points from Zeta and HBTXI and the F-θ curve for the Bessel function model for comparison.

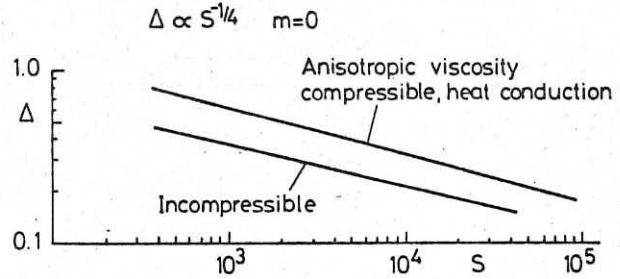


Fig 4 Resistive-layer thickness Δ as a function of S for an m = 0 instability from a calculation assuming incompressibility and from a calculation including anisotropic viscosity, compressibility and heat conduction for the resistive interchange (resistive-g) mode. (S is the magnetic Reynolds number)

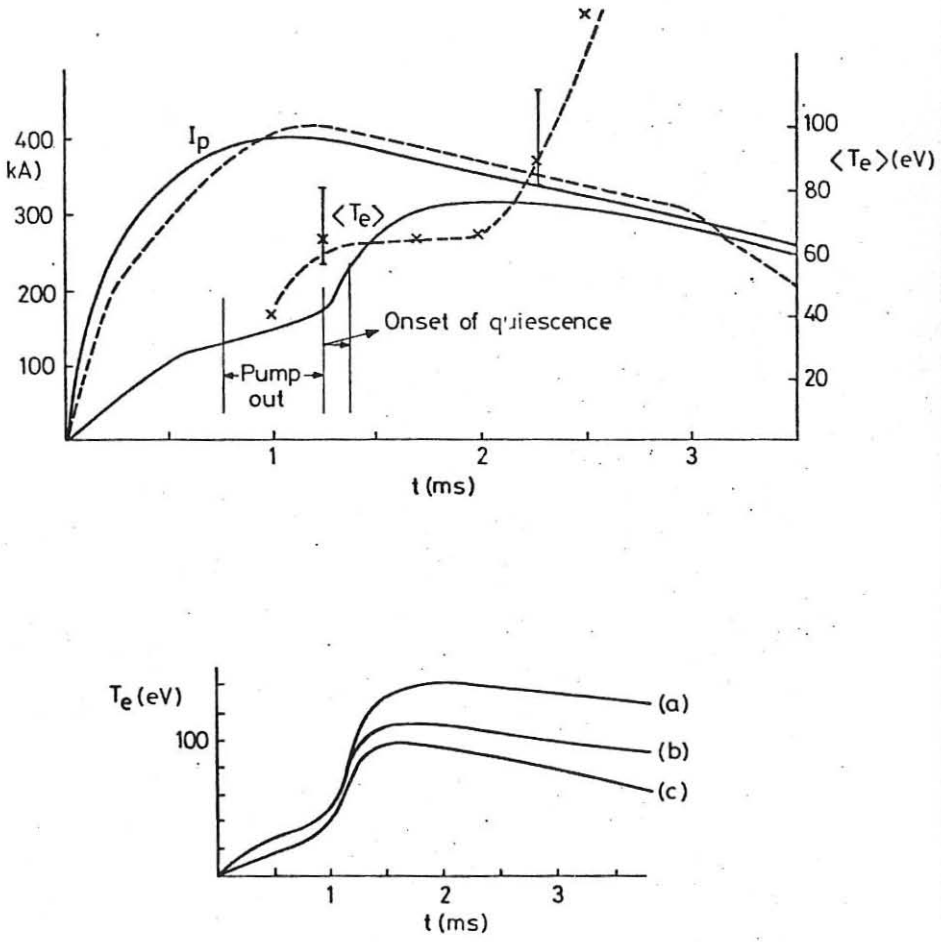


Fig 5 Results of 0-D calculations of the current and electron temperature in Zeta, with experimental data for comparison, (above) and predicted temperature-time variations for HBTXIA (below).

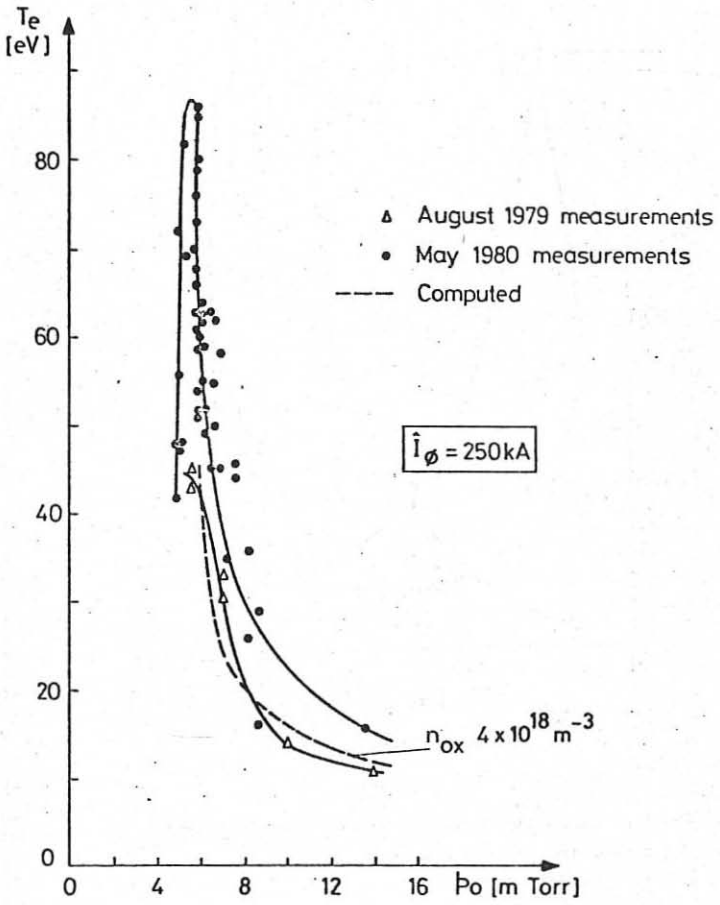


Fig 6 Electron temperature at peak current on Eta Beta II versus filling pressure - Thomson scattering measurement and O-D computations.

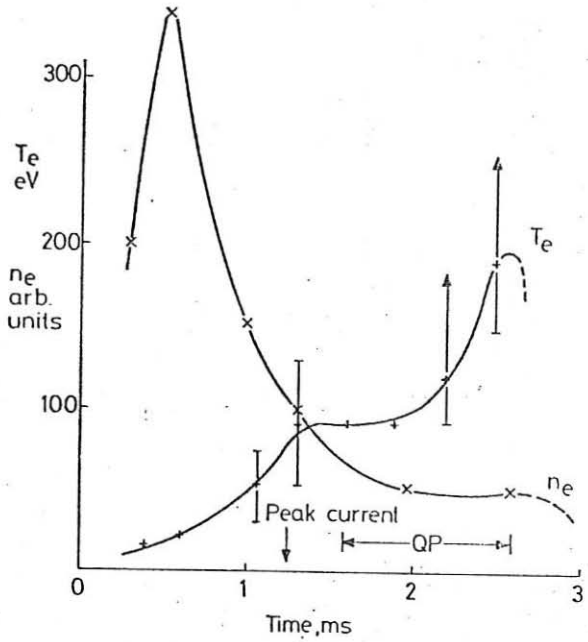


Fig 7 Electron temperature and density on axis as functions of time obtained by Thomson scattering on Zeta during the quiescent period.

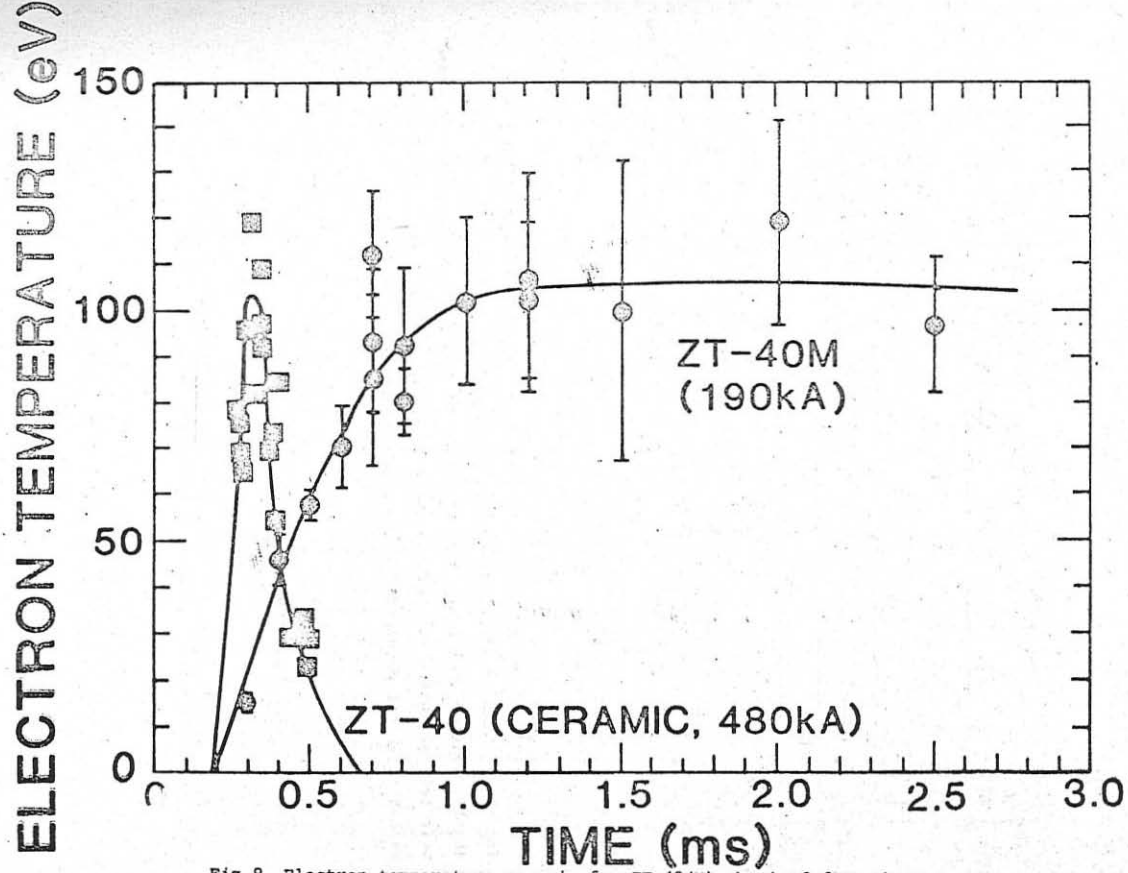


Fig 8 Electron temperature on axis for ZT-40(M) obtained from Thomson scattering as a function of time; I = 190 kA. Also shown are results for ZT-40 with a ceramic torus operating at 480 kA.

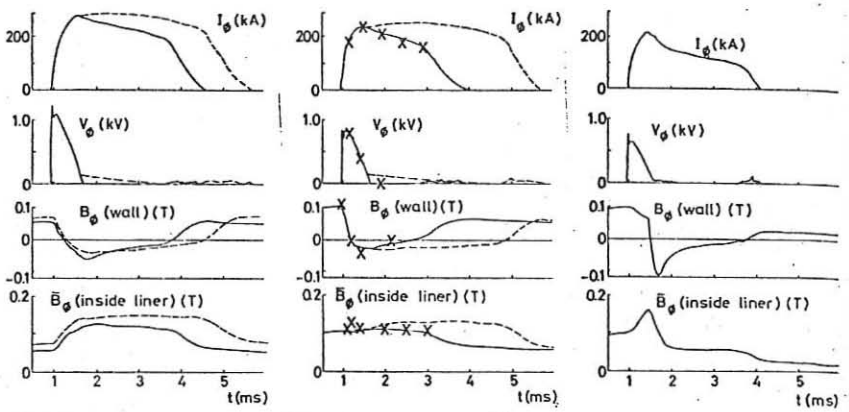


Fig 9 Waveforms of the current, voltage, B_ϕ and average B_ϕ inside the liner for HBTXIA using 3 different setting up modes. (a) self reversal on its own. (b) the matched mode where the liner acts as virtual flux conserver (c) aided self reversal where the reverse field is driven by the circuit to a value higher than that produced by the plasma self reversal effect.

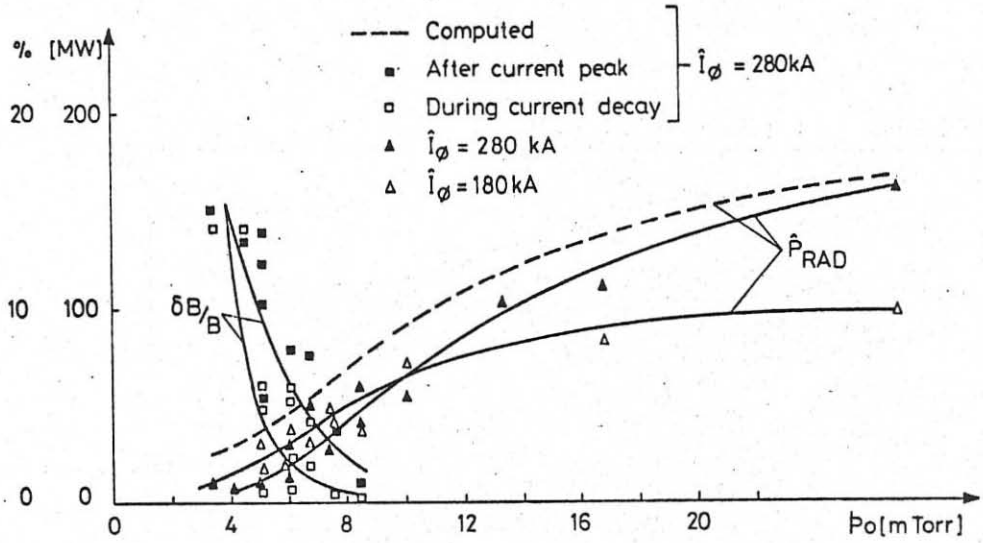


Fig 10 The magnetic field fluctuation level $\frac{\delta B}{B}$ and total radiated power as a function of filling pressure on Eta-Beta II. The computed radiated power is shown for comparison. The figure includes data before and after current peak and at different peak current values.

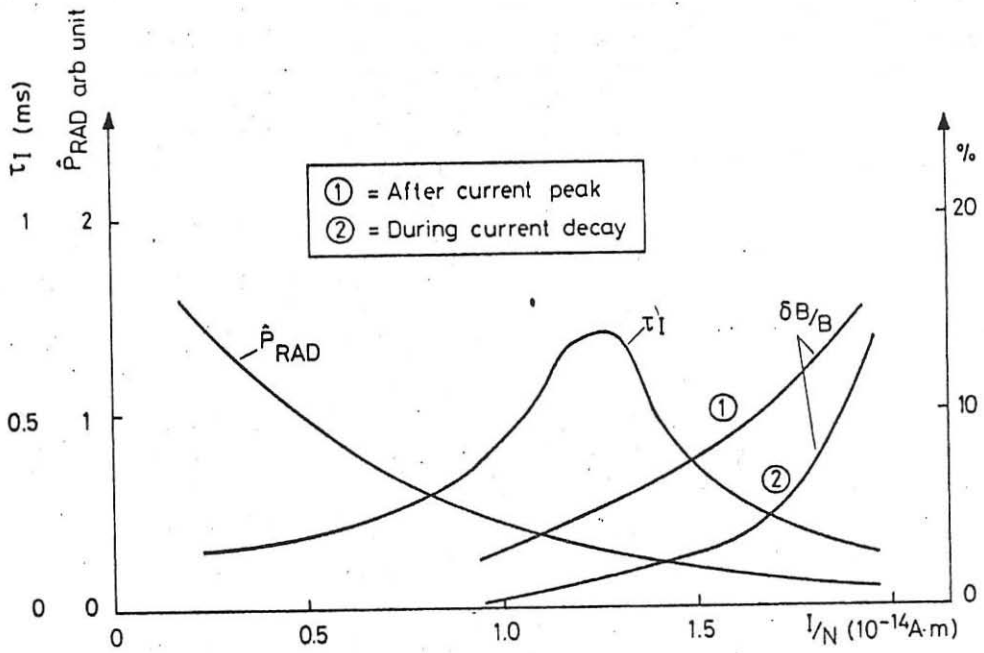


Fig 11 Total radiated power, magnetic field fluctuation level, $\frac{\delta B}{B}$, and current decay time versus I/N evaluated using the peak current and initial line density. (On ETA-BETA; I/N varies little with time in this machine).

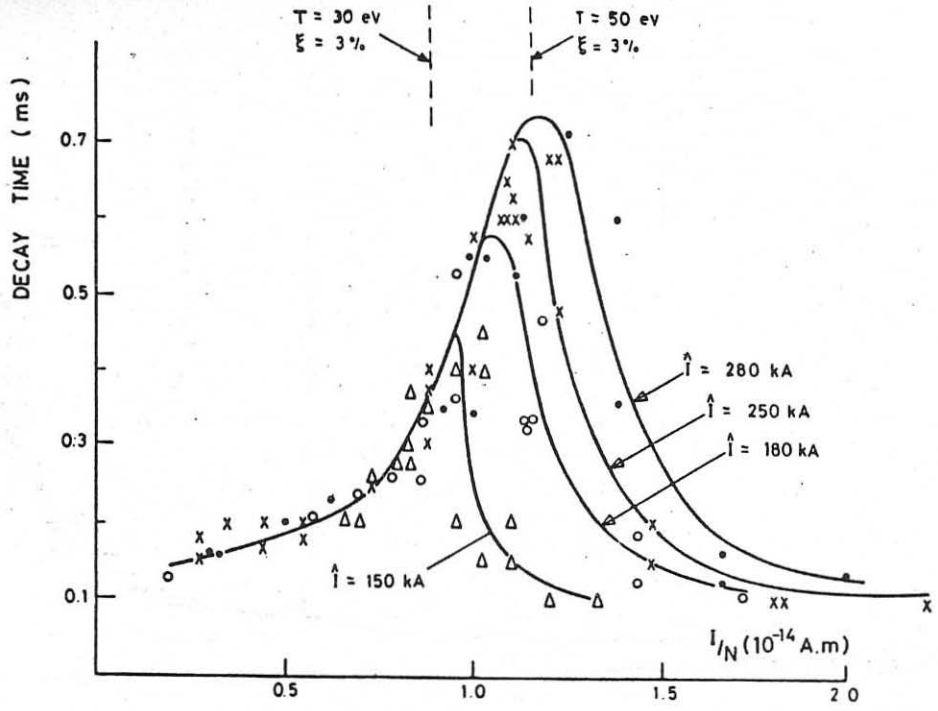


Fig 12 The current decay time on Eta-Beta II versus I/N at different values of peak current.

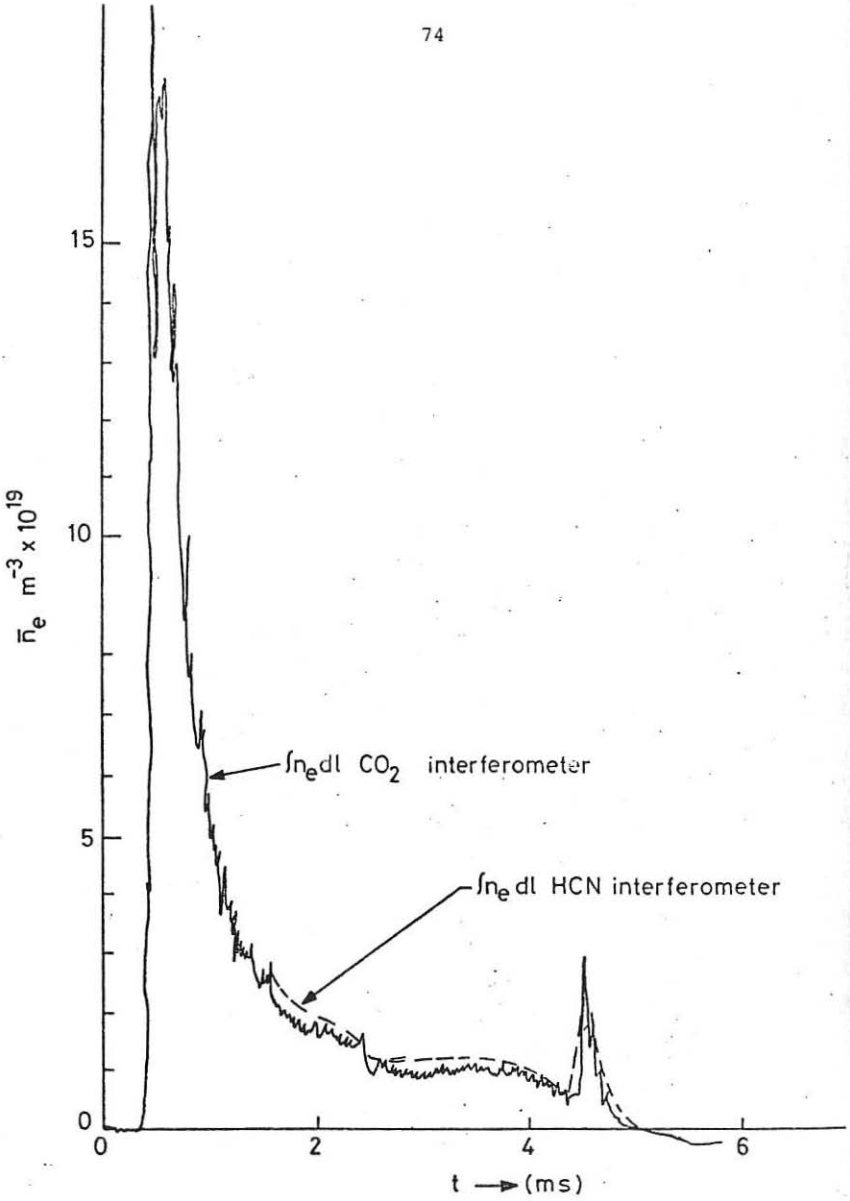


Fig 13 The line of site average electron density on HBTXIA as a function of time determined by CO_2 and HCN interferometers. Peak current ∿ 200kA with power crowbar.

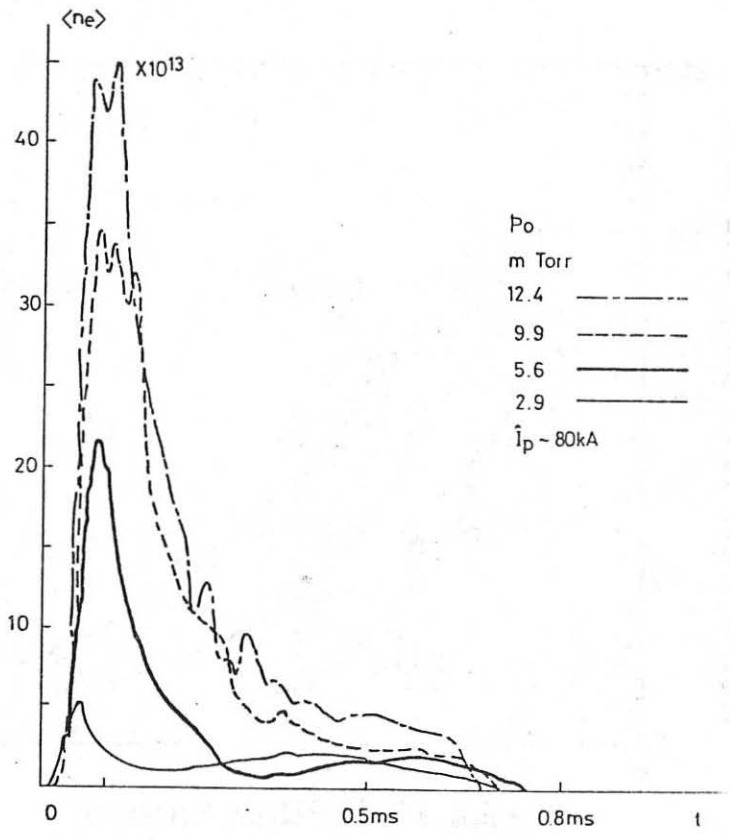


Fig 14 Electron density versus time on TPE-1R(M) at 4 different values of filling pressure, obtained from a CO_2 interferometer.

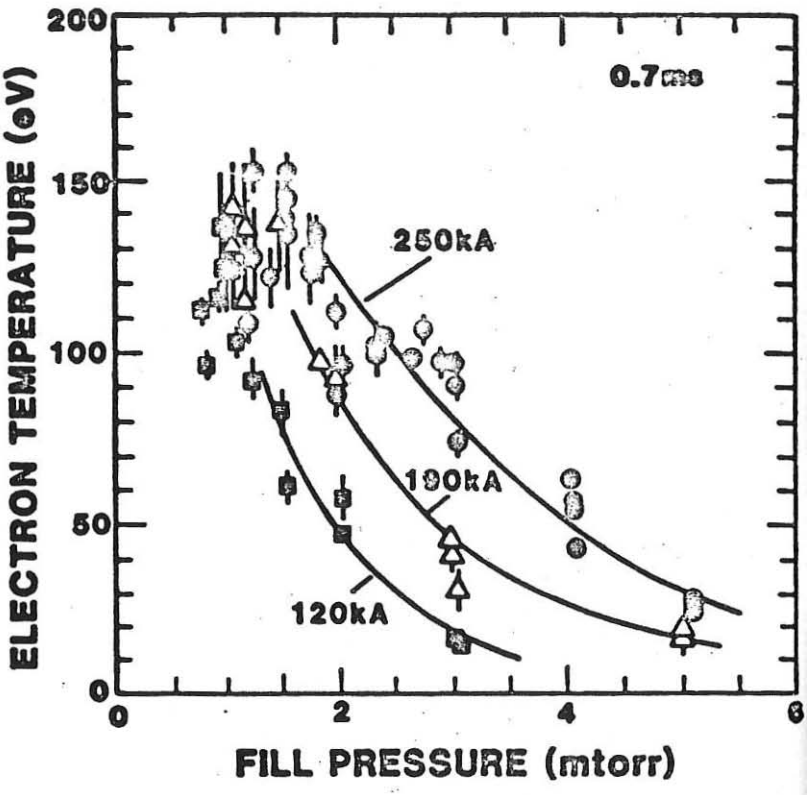


Fig 15 The electron temperature on axis in ZT-40(M) determined by Thomson scattering as a function of filling pressure at three different currents.

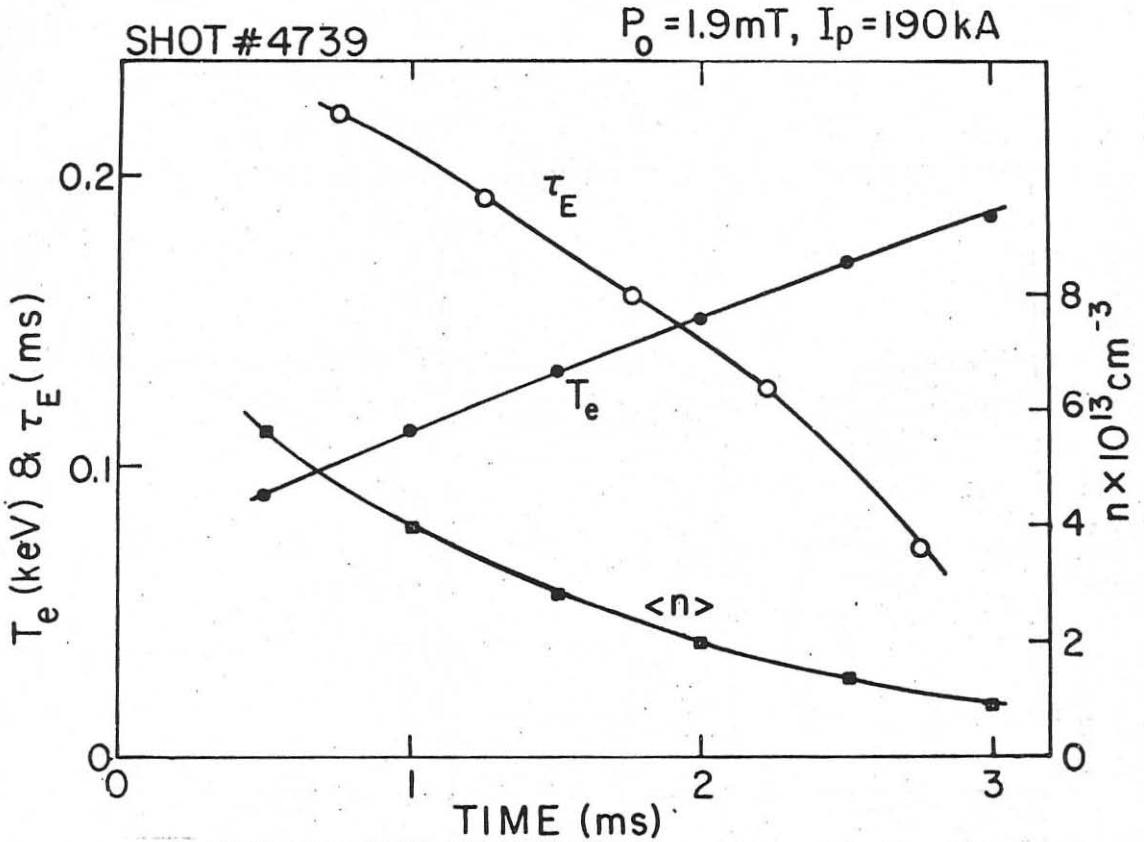


Fig 16 The estimated value of energy confinement time as a function of time on ZT-40(M); the electron temperature and average density are also shown for comparison.

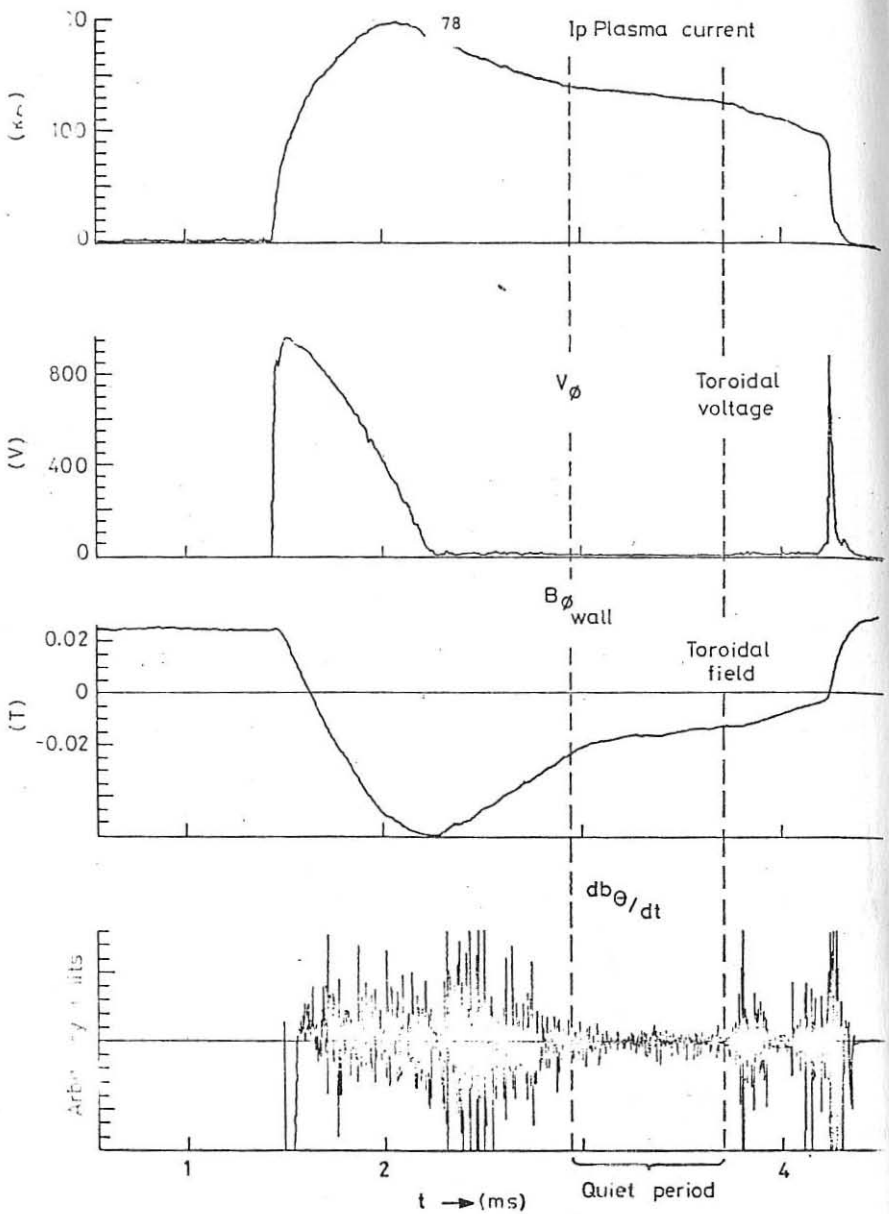


Fig 17 Wave forms of the current, voltage, toroidal field at the wall and poloidal magnetic field fluctuation signal for HBTX1A measured inside the liner showing periods of reduced fluctuations.

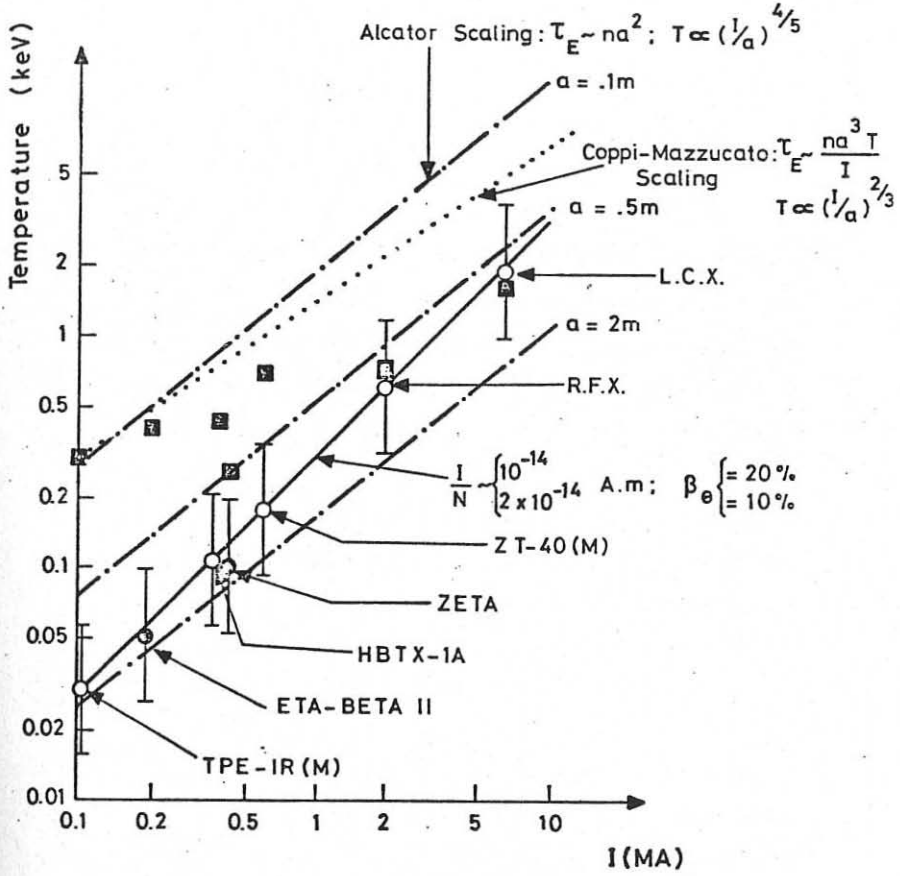


Fig 18 The electron temperature versus current for RFP scaling (solid line) and two tokamak scalings (dashed and dotted lines). The temperature on tokamak scaling depends on minor radius a and is shown for a = .1, .5 and 2 metres. Experimental values of temperature for RFP machines are indicated where available and predicted values for other machines are shown. The error bars on the predicted points indicate the uncertainty in β_θ and I/N. The squares show the temperatures which would be obtained in some RFP machines if they operated as tokamaks with Alcator scaling.

PRODUCTION OF INTENSE NEGATIVE HYDROGEN ION BEAMS

G.I.Dimov

Institute of Nuclear Physics,
Novosibirsk 630090, USSR

In two last decades the charge exchange method,which is based upon a purposeful change of the charge states of particles /1/, has found wide application in accelerators and controlled fusion researches. This method opens up principally new possibilities. The latter are mainly connected with that the charge exchange eliminates the limitations on particle motion in electromagnetic fields,which are determinated by the classic Liuville and reciprocal Poincaré theorems.

In controlled fusion researches the most application has got the capture of particles into magnetic fields due to ionization of fast hydrogen atoms in a plasma. This process makes it possible to accumulate and sustain a hot plasma in magnetic traps, to heat it and to control the particle distribution.

The necessary, in this case, powerful atomic hydrogen beams can be obtained from the accelerated positive and negative ions. Fig.1 shows the energy dependence of the conversion coefficient of different ions to the atoms normalized over a nucleon in the most preferable targets. The use of high-energy negative ions has an obvious advantage: the $H^- \rightarrow H^0$ conversion coefficient in the plasma target is as high as 84%.

To produce negative ions, it seems perspective to

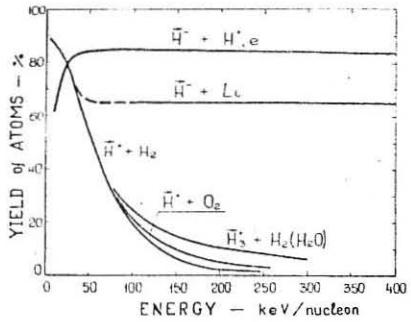


Fig. 1.

use their creation as a result of the interaction of fast particles with the gas, low-temperature plasma with the gas and the interaction of particles with the surface of a solid body. According to this, three main methods of producing intense beams of negative hydrogen ions are under development: charge exchange, plasma and surface ones. The surface method has a few modifications: thermoemission, secondary emission, surface-conversion and surface-plasma ones. Among the surface methods of producing intense beams the surface-plasma one still remains most promising.

Charge Exchange Method

This method consists in the charge exchange of the formed beams of fast positive ions to a beam of negative ions in a gas (vapour) target. When the fast hydrogen atomic particles pass through the gas, their states are changed as follows:

$$H^+ \rightarrow H, H^{**} \qquad H^+ \rightarrow H^- \qquad H^- \rightarrow H$$
$$H \rightarrow H^+ \qquad H \rightarrow H^- \qquad H^- \rightarrow H^+$$
$$H^{**} \rightarrow H, H^+ \qquad H^{**} \rightarrow H^-$$

In the energy range of maximum H^- ion yield ($\sim$1÷10 keV) the following relations between the charge exchange cross sections of ions and atoms in the ground state hold (with

few exceptions): $\sigma_{-o} \gtrsim \sigma_{+o} > \sigma_{o+} > \sigma_{-+} > \sigma_{o-} > \sigma_{+-}$.

At low velocities, in the gases with low ionization potential the capture of an electron into the metastable state by a proton is significant, but it is not likely that the electron is captured by a metastable atom; on the contrary, in the gases with high ionization potential the first process is scarcely probable and the second is significant. At high velocities the probability of both these processes decreases. At the equilibrium thickness of a gas target the capture of an electron by excited atoms does not play an essential role. This is due to the processes mentioned above and to the fact that the equilibrium fraction of excited atoms cannot be significant because of a relatively large total probability of their de-excitation and de-ionization. After the passage of the beam through the equilibrium target, the H^- ion yield is determined, in the first approximation, by two processes:

$$H \rightarrow H^- \qquad \text{and} \qquad H^- \rightarrow H.$$

Approximately the equilibrium yield of H^- ions is

$$F^- = \frac{I(H^-)}{I_0(H^+)} \sim \frac{\sigma_{o-}}{\sigma_{-o}+\sigma_{o-}}.$$

During the passage through the gas the molecular H_2^+ and H_3^+ ions are decayed into atoms and protons, the length of their path being not large. For this reason, if the thickness of a gas target is sufficiently large, the equilibrium composition of atomic hydrogen particles with the energy decreased by a factor of 2 or 3, respectively, sets up at the target exit. The characteristics of the charge exchange processes remain the same if fast hydrogen parti-

cles are replaced by deuteron ones with the same velocity.

The yield of H^- ions in gas targets, which were investigated at the beginning of the development of the charge exchange method (prior to 1965), was a few percents only. The maximum equilibrium yield of H^- ions (at optimum energy) is 2% (13 keV), 1.4% (12 keV), 1.8% (6 keV), 1%(30 keV), 2.2% (9 keV), 5.5% (2 keV), 3.3% (14.5 keV), 4.6% (8 keV), 2% (6 keV) in H_2, N_2, O_2, He, Ne, Ar, Hg, H_2O and CO_2, respectively.

The first charge exchange sources of H^- ions (the current from 2 to 30 mkA/2-4/) were constructed in Kharkov, Los Alamos and Visconsin in 1956. (The first H^- ion source, which was developed by Tuck in 1951 and based upon proton conversion on the foils, was a surface one in fact.) By the beginning of the 1970's a large number of charge exchange sources were constructed, mainly for accelerators, with the use of single-aperture proton sources of the Koller-Kistemaker type, a high-frequency source and a duoplasmatron with charge exchange in hydrogen and mercury vapours. The maximum current in these sources, about 1.2 mA, was achieved by the group of the HVEC firm in 1964, mainly due to the use of molecular H_3^+ ions as primary ones /6/.

The next step in an increase of the intensity of H^- ion beams obtained by the charge exchange method was the use of multi-aperture sources of positive ions. Such sources generate high-current H^+ beams at a low energy optimum for their recharging into H^- beams. With the use of a specially developed, multi-aperture high-current

source of positive ions we have succeeded in increasing the intensity of H^- beams obtained by the charge exchange method /7-9/. This source of positive ions is featured by the plasma production method and the multi-slit extraction geometry. It is shown schematically in Fig.2. The arc discharge in the diafragm-shaped channel generates a plasma jet incident upon the extraction system. The proton beam generated by this source was up to 3 A at an energy of 13 keV (the emission beam diameter was 2.2 cm). The attained,

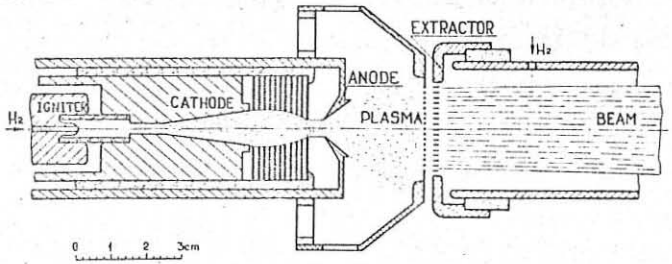


Fig.2.

normalized over electron mass, perveance of the proton beam, 87 $A \cdot V^{-3/2}$, corresponded to the increase of the proton current, compared to the current of a single-aperture ion source, by two orders of magnitude. The low content of admixtures in the ion beam (the proton content in the beam achieves 95%, the admixtures of heavy elements does not exceed 1%), low emission temperature of the plasma (0.25 eV), good homogeneity and the stability of the plasma on the emission surface, all this provided a relatively high quality of the high-intensity beam.

The H^- ion beam was obtained by recharging of protons on hydrogen in the charge exchange pipe installed directly behind the slit extraction system. The achieved compensa-

tion of the space charge of the ions was good. By 1968 the beam of H^- ions with a current of up to 15 mA /10/ was obtained; later on the current in the beam was increased up to 54 mA /9/.

In 1965-66 Donnally, Drake and Kratkov found a high yield of D^- ions if deuterons are recharged in Cs vapours: 25% at an energy of 1 keV /11,12/. Numerous experiments on charge exchange of hydrogen particles in the vapours of alkaline metals have been carried out. Fig.3 shows the energy dependences of negative ion yield for most promising alkaline metals. The high yield of H^- ions in these metals is connected with the relatively large cross section of the $H \rightarrow H^-$ process because of the large radius of the valent electron and the insignificant energy defect in this process.

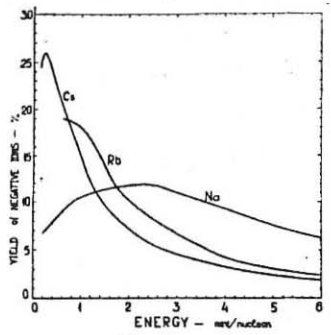


Fig.3.

All this led to the arise of new possibilities of increasing the intensity of negative ion beams. But realisation of these possibilities has been delayed because of the difficulties connected with a low energy of the effective charge exchange. It was necessary to create the sources of positive ions with extremely large perveance.

A source of positive ions with an energy of 1 keV and a current of up to 1 A has been created in Livermore (the perveance is $1.5 \cdot 10^3$ $A/V^{3/2}$) /13/. The high perveance of

this source has been achieved due to the multi-aperture extraction system of large diameter (6.3 cm) and ion deceleration after their extraction from the plasma. In 1972 Osher et al. /14/ succeeded in obtaining the D^- ion beam with the 50 mA current and a mean density of about 1.5 mA/cm^2 by charge exchange of the ions from this source in Cs vapours.

Because of the difficulties of obtaining many-ampere beams and a considerable angular spread of hydrogen particles in Cs at low energy, it seems to be reasonable to use the Rb and Na vapours for the charge exchange in spite of a lower yield of H^- ions. This circumstance has stimulated the development of negative ion sources based upon the charge exchange in Na.

In 1973, in Novosibirsk, the beam of D^- ions with a current of 104 mA and a mean density of about 6 mA/cm^2 has been obtained by recharging the deuterons at an energy of about 8 keV in a vapour-jet Na target /15/. In 1977 Semashko et al. /16/ obtained the H^- ion beam with a current of up to 1.4 A and a peak density of several mA/cm^2 by charge exchange of the 10 keV hydrogen ions with a high content of molecular ions (in Na). In 1980, in Livermore, Hooper et al. /17/ obtained the beam of D^- ions with a 2.2 A current and a peak density of 13 mA/cm^2 by charge exchange in Na vapours at an energy of 12 keV.

The analysis of experimental data /17/ has shown that there is a possibility of creating, on the basis of many-ampere high-perveance sources of positive ions, the charge

exchange D^- ion injectors with an energy of hundreds of keV, current of tens of ampers, mean current density of tens of mA/cm^2. In this case, Rb vapours as a charge exchange target seem to be more advantageroue. The expected gas efficiency of such injectors is not high: 3÷5%. However, for the injectors of negative ions a high gas efficiency is not so important since a gas source, a source of primary ions, is separated from the chamber to which the atomic beam is introduced, by charge exchange targets with low gas transmittivity.

In our opinion, the most adequate method of producing primary low-energy ions for charge exchange D^- sources is ion acceleration in a plasma. Of interest are also the experiments in Karlsruhe on production of primary particles for the charge exchange in Cs vapours in the form of a beam of accelerated clusters.

Plasma Method

This method consists in creating a low-temperature plasma with a relatively high concentration of negative ions and in extracting them from the plasma surface with subsequent formation of the beam.

For intensive production of negative ions a sufficintly high concentration of the neutral gas is required. In the hydrogen plasma the H^- ions are produced, mainly, in pair collisions of electrons with hydrogen particles:

$e + H_2 \rightarrow H^- + H$ ($\max \sigma = 1.7 \cdot 10^{-21}$ cm^2 at $E = 3.75$ eV);

$e + H_2 \rightarrow H^- + H^*$ ($\max \sigma \sim 2 \cdot 10^{-20}$ cm^2 at $E = 14$ eV);

$e + H_2 \rightarrow H^- + H^+ + e$ ($\sigma \sim 10^{-20} \div 10^{-19}$ cm^2 at $E \sim 20 \div 60$ eV);

$e + H_2^+ \rightarrow H^- + H^+$ ($\sigma \sim 5 \div 1 \cdot 10^{-18}$ cm^2 at E = 0.4÷4 eV);

$e + H_3^+ \rightarrow H^- + H_2^+$ ($\max \sigma \sim 1.6 \cdot 10^{-18}$ cm^2 at E~8 eV);

$e + H \rightarrow H^- + \gamma$ ($\max \sigma \sim 2.6 \cdot 10^{-22}$ cm^2 at E = 0.7 eV).

In collisions of electrons with excited particles the cross sections of the processes indicated above usually increase. In the first process a strong isotopic effect is observed. The dissociative attachment cross section decreases by a factor of $1.9 \cdot 10^3$.

Concentration of H^- ions is limited by the destruction processes. Such main processes in the hydrogen plasma are:

$H^- + e \rightarrow H + 2e$ ($\max \sigma \sim 3.5 \cdot 10^{-15}$ cm^2 at E~10÷30 eV);

$H^- + H^+ \rightarrow H + H$ ($\sigma \sim 1.8 \cdot 10^{-14}$ cm^2 at E~20÷200 eV, $\sigma \sim 5 \cdot 10^{-14}/E$ [eV] cm^2 at $E \ll 10$ eV);

$H^- + H_2^+ \rightarrow H + H_2$ ($\sigma \geq 10^{-13}$ cm^2 at $E < 0.5$ eV);

$H^- + H \rightarrow \begin{cases} H_2 + e \\ 2H + e \end{cases}$ ($\sigma \sim 1.5 \cdot 10^{-15}$ cm^2 at $E \sim 1 \div 10^3$ eV).

The current density of H^- ions extracted from the plasma and then accelerated, can be limited by their destruction, mainly in the process

$H^- + H_2 \rightarrow H + H_2 + e$ ($\sigma \sim 10^{-15}$ cm^2 at E = 0.3÷20 keV, $\sigma < 10^{-16}$ cm^2 at E<30 eV).

The beams of H^- ions can be obtained not only from the hydrogen plasma. For example, ionized gases and vapours from the hybrids of some metals are quite a good source of H^- ions.

In 1959, in Oak Ridge, the beam of H^- ions with a current of 11 mkA was obtained by the plasma method for the

first time (from the dioplasmatron) /18/. In 1963-65 large contribution to the development of plasma sources was made in Berkeley. Ehlers used the Penning plasma source, the design of which is shown in Fig.4. The D^- and H^- ions were extracted from the plasma through the slit in the cylindrical cathode, elongated along the magnetic field. The length of the slit was 12 mm. The D^- and H^- beams with the currents of 2 and 5.3 mA, respectively, have been obtained /19,20/. The emission current density of H^- ions was about 40 mA/cm^2.

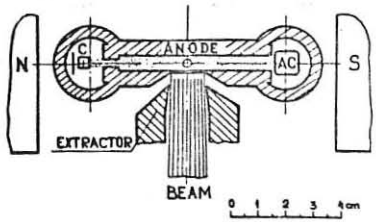


Fig.4.

In 1972, in Novosibirsk, a magnetron (planotron) plasma source schematically shown in Fig.5, was developed. The H^- ions were extracted from the plasma through the slit in the anode, elongated perpendicularly to the magnetic field. The length of the slit was 10 mm. The pulsed beam of H^- ions with a current of up to 22 mA and a high emission density of 220 mA/cm^2 was obtained /21/.

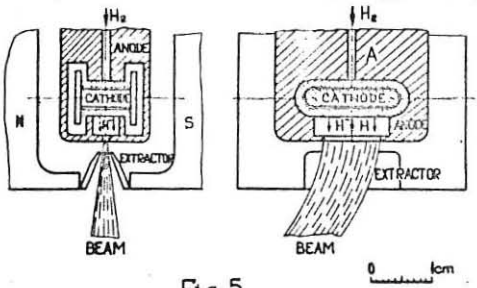


Fig.5.

The attained current density of the extracted H^- ions exceeded substantially the expected one, which has been calculated on the basis of the known, by that time, formation and destruction processes of H^- ions in the plasma.

In 1978-80, in Kiev, Gabovich et al. /22,23/ obtained the continuous H^- ion beam with a direct current of up to 20 mA from the H^- ion source of the Ehlers type (the emission slit was elongated to 40 mm). The emission current density of H^- ions was increased to 85 mA/cm^2 due to narrowing of the slit.

In 1977, in Palaiseau, Bacal et al. /24/ obtained the hydrogen plasma with unexpectedly high concentration of H^- ions. This plasma was created in a relatively large volume of about 20 l via ionization of hydrogen by a flow of electrons with an energy of up to 60 eV. The plasma density is low, $\sim 10^{10}$ cm^{-3}, at a hydrogen density of about 10^{14} cm^{-3}. According to the recent measurements, a maximum density of H^- ions is achieved at $\sim$ 1 eV electron temperature and is 35% from the electron density /25/. The obtained concentration of H^- ions is almost 100 times higher than the equilibrium value calculated without taking into account the collisions with excited particles.

As early as 1965 Demkov predicted an increase of the cross section of the formation of negative ions during dissociation of vibrationally excited molecules (by electron impact). In 1978 Allan and Wang showed experimentally that the cross section of the dissociative attachment of an electron in the process

$$e + H_2(\nu) \rightarrow H_2^- \rightarrow H^- + H$$

drastically grows with vibrational quanta. For vibrational levels $\nu = 1,2,3,4$ (E_{thr} = 3.23; 2.75; 2.29; 1.8 eV), the dissociative attachment cross section near the threshold increases, compared to a similar cross section for the

ground state $\nu = 0$ ($E_{thr} = 3.75$ eV), by a factor of 30, 500, $5 \cdot 10^3$ and $3 \cdot 10^4$, respectively /26/. The increase of the dissociative attachment cross section is connected with the larger probability of surviving the intermediate state of H_2^- because of its formation with the longer internuclear separation from vibrationally excited molecules.

The most important process in the formation of molecules excited to the lowest vibrational levels is likely to be the electron excitation

$$e + H_2(\nu) \rightarrow H_2(\nu \pm 1) + e.$$

Formation of the molecules at high-excited vibrational levels is mainly connected with the exchange of vibrations in collisions of excited molecules:

$$H_2(\nu) + H_2(\kappa) \longrightarrow H_2(\nu \pm 1) + H_2(k \pm 1).$$

In this case, at fairly low temperature the nonlinear pumping of high-excited levels can take place: at $\nu > \kappa$ the exchange $\nu \rightarrow \nu + 1$, $\kappa \rightarrow \kappa - 1$ dominates.

In limitation of the concentration of vibrationally excited molecules a large role is played by the collisions of these molecules with atoms and molecules with transition of the vibrational energy to the translational one, their dissociation and, especially, de-excitation in collisions with the walls. The role of these processes decreases with increasing the gas density and decreasing electron temperature.

At present a search for the scheme of producing intense beams of H^- ions with the use of the formation process of these ions via dissociation of vibrationally excited molecules is being carried out. The basic problems are: an increase of the absolute density of negative ions formed in

the plasma and their extraction from it. The first problem can be, probably, solved by obtaining an ionized weakly-dissociated gas with sufficiently high density in the non-equilibrium state in a weak electric field when the temperature of translational motion of molecules is ~200°K and the mean electron energy is ~1 eV. To solve the second problem, it is necessary to find the way of decreasing the neutral gas density in front of the emission hole without a significant decrease in the density of negative ions. Otherwise the beam of extracted H^- ions will be destructed on the effluent gas.

Surface-Plasma Method

This method consists in extracting and forming into the beam of the negative ions formed on the electrode surface in gas discharge. This method was developed in 1972-74 in Novosibirsk /27/. The initial experiments were directed to obtaining a high secondary emission coefficient of H^- ions from the W-surface, up to 80%, during its bombardment by Cs ions in hydrogen atmosphere with a current density of up to 10 mA/cm^2 /28/ and in discovering an increase in the output of H^- ions (from 5 to 20 mA) from a planotron plasma source similar to that shown in Fig.5, with an addition of Cs vapours to hydrogen /29/. The latter was successful due to the closeness of the cathode to the emission slit in the planotron. Moreover, we have observed the increase in the H^- ion output with decreasing the thickness of the plasma layer between the cathode and the emission slit and with decreasing the hydrogen density, as well as the saturation

of this output as the plasma density increases /30/. All this allowed to assume that intense flows of H^- ions from the plasma are caused by the emission of these ions from the cathode surface into discharge. The discharge geometry and regime, which were optimized on the basis of this assumption, led to increasing the current density of H^- ions up to 3.7 A/cm^2 (from the emission slit) at the total current of several hundreds of mA /30/. The study of the energy spectra of H^- ions produced and a number of other experiments /31,32/, as well as the calculations of the output of H^- ions from the surface /33,34/ have made it possible to determine the following surface-plasma mechanism of formation of intense flows of H^- ions from the hydrogen plasma with Cs admixture.

The electrodes in the gas-discharge plasma are bombarded by fast ions and atoms formed as a result of gas ionization, ion acceleration in electric fields, dissociation of molecular ions and charge exchange of particles. Reflection of fast particles and sputtering of hydrogen sorbing on the electrodes result in the appearance of hydrogen particles which leave the electrode surface at high velocities. Due to exchange by electrons between the electrode and the removing atoms, a part of these atoms captures the electrons on the electron affinity levels and escapes beyond the surface barrier in the form of negative ions. At a quite small thickness of the plasma above the electrode the negative ions escaping from its surface can pass, without large losses, through a plasma layer to the extraction system. Most favourable is the emission of ne-

gative ions from the cathode: the density of the bombarding ions and atoms is higher, the negative ions removing from the surface are accelerated in the cathode drop. Sorbtion of cesium provides a decrease of the work function of the electrode surface. However, in gas discharge it seems impossible to reduce the surface work function below 1.5 eV, that is still much higher than the electron affinity of hydrogen atoms. The unexpectedly large yield of H^- ions from the surface in these conditions is accounted for by a long-range action of the electron image forces and by a high velocity of the majority of the reflected and sputtered hydrogen particles.

By 1974 the beam of H^- ions with a current of about 900 mA at the 3 A/cm^2 emission density was obtained by the surface-plasma method in Novosibirsk /35/. In 1974 the same results were obtained in Brookhaven: with the help of a surface-plasma planotron source the beam of H^- ions with a current of up to 150 mA at an emission density of up to 1.5 A/cm^2 was obtained /36/. The works on the development of surface-plasma sources have been started in Leningrad, Berkeley, Oak Ridge, Amsterdam, Nagoya and Culham.

In Berkeley the secondary emission coefficient of H^- and D^- ions with bombardment of alkaline metals by positive hydrogen ions of small energy have been measured /37/. In Amsterdam, Los et al. /38/ have measured the efficiency of the formation of H^- and D^- ions at a skew escape of hydrogen particles from a cesiated tungsten surface. The maximum fraction of escaping particles in the form of H^- and D^- ions is 38% with a normal component of energy of 2.5 eV per

nucleon. From the calculations on particle reflection from a solid surface, which have been carried out by a number of authors since the middle of the 1970's, it follows that at the energy of H^- ions normally incident upon Mo, 100÷50 eV, the reflection coefficient is equal to 55-60% and continues to grow with decreasing energy. In this case, a part of the particle energy remaining after the reflection, is, in average, ~65% and it increases as the energy decreases. From comparison of the calculational data on reflection with the results by Los it follows that the secondary emission coefficient should grow, without taking into account the desorption, up to 30-35% with increasing the energy down to a few eV per nucleon. In Novosibirsk, on the basis of the separately measured ratios of the current density of H^- ions and that of positive ions to the cathode to the current density in discharge, the H^- ion yield per one positive ion incident upon the cathode in surface-plasma sources has been found. The maximum value of this magnitude is ~ 80% at a discharge voltage of about 100 eV /39/. With the composition of fast hydrogen particles in discharge taken into account, the secondary emission coefficient of H^- ions per one atomic particle can be several times lower than 80%.

In 1978, in Novosibirsk, the one-dimensional focusing of H^- ions from the cylindrical cathode surface to the emission slit was experimentally tested. In the focusing plane the compression of the flow of H^- ions from the cathode approximately by a factor of 3 was observed /40/.

Similar results were obtained in Brookhaven and Berkeley in 1980 /41,42/. These experiments have opened the way for creating multi-aperture sources with nearly total collection of H^- ions from a cathode surface and good gas efficiency.

In Novosibirsk a multi-slit H^- ion source with one-dimensional focusing has been designed /40,43/. Its schematical section is shown in Fig.6 and the geometry of emission slits in Fig.7a. By 1980 the pulsed beam of H^- ions with a current of up to 4 A at a mean density in the extraction gap of up to 440 mA/cm^2 was obtained from this source. In 1981, in Novosibirsk, Bel'chenko developed a honeycomb multi-aperture source with focusing of H^- ions from spherical dimples on a cathode surface to the circular emission holes in the anode. The geometry of the emission

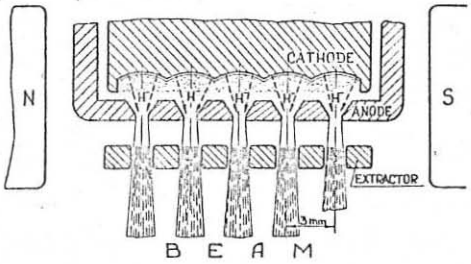


Fig. 6.

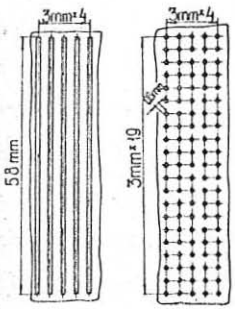


Fig. 7.

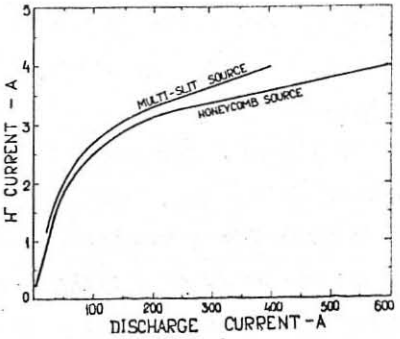


Fig. 8.

holes is shown in Fig.7b. The beam of H^- ions with the same current and density as from the multi-slit source has been produced. In Fig.8 the current dependences against the discharge current in the produced beam of H^- ions at an extraction voltage of 20-25 keV are plotted. Table 1 lists the geometrical parameters of the sources.

Table 1

Type of a source	Multi-slit	Honeycomb
Beam emission section	9 cm^2	9 cm^2
Total emission area	2.3 cm^2	0.5 cm^2
Usefull cathode surface	12 cm^2	10.6 cm^2
Total cathode surface	17.7 cm^2	15.3 cm^2

Table 2 presents the main characteristics of the sources for different current densities. The discharge voltage is $\sim$150 V. At a sufficiently high current density of H^- ions of 200÷300 mA/cm^2 the discharge current density is 3÷8 A/cm^2, current density of the ions on the cathode $\sim$0.5÷1.5 A/cm^2 /39/, discharge power per unit cathode area 0.5÷1 kW/cm^2, gas efficiency $\sim$5% in the multi-slit source and 20% in the honeycomb one. Now the honeycomb source with the 54 cm^2 emission section of the beam is being tested. The pulsed beam of negative ions with a current of 4 A at a discharge current of 200 A has been produced.

In 1980 Ehlers and Leung (Berkeley) published the results of the study of a single-aperture surface-plasma H^- source of large dimensions /42/. The scheme of the source is shown in Fig.9. In the multi-cusp chamber of 6 l vol-

Table 2

Type of a source	Multi-slit			Honeycomb		
Mean emission current density of H^- ions	$445\frac{mA}{cm^2}$	$300\frac{mA}{cm^2}$	$200\frac{mA}{cm^2}$	$445\frac{mA}{cm^2}$	$300\frac{mA}{cm^2}$	$200\frac{mA}{cm^2}$
H^- ion current	4 A	2.7 A	1.8 A	4 A	2.7 A	1.8 A
Emission current density of H^- ions	$1.73\frac{A}{cm^2}$	$1.17\frac{A}{cm^2}$	$0.78\frac{A}{cm^2}$	$8\frac{A}{cm^2}$	$5.35\frac{A}{cm^2}$	$3.6\frac{A}{cm^2}$
Discharge current	400 A	100 A	43 A	600 A	126 A	47 A
Mean current density in discharge on the cathode	$22.6\frac{A}{cm^2}$	$5.7\frac{A}{cm^2}$	$2.43\frac{A}{cm^2}$	$39\frac{A}{cm^2}$	$8.2\frac{A}{cm^2}$	$3.07\frac{A}{cm^2}$
Discharge power per unit cathode area	$3.4\frac{kW}{cm^2}$	$0.85\frac{kW}{cm^2}$	$0.37\frac{kW}{cm^2}$	$5.9\frac{kW}{cm^2}$	$1.2\frac{kW}{cm^2}$	$0.46\frac{kW}{cm^2}$
Gas efficiency	15%	5÷7%	3÷5%	25÷30%	20%	15÷20%

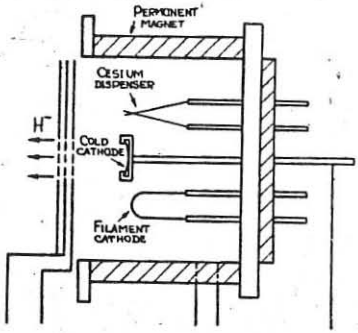


Fig. 9.

ume the non-self-sustaining discharge, up to 70 A, is maintained by a flow of electrons from thermocathodes. An additional cold cathode with the 62 cm^2 cylindrical emitting Cs-coated surface, the focal distance is about 8 cm, is installed in front of the emission slit. This source has produced a stable flow of H^- ions of up to 0.7 A at an energy of 300 eV, that corresponds to the potential on the cold cathode.

Comparison of the recent results obtained in Berkeley and Novosibirsk shows that multi-aperture surface-plasma sources of H^- ions with ion focusing onto the emission holes are subject to the simple scaling law following from the condition of passing H^- ions through the plasma: with a similar increase of the dimensions of a source the current density of the extracted H^- ions reduces inversely proportionally to the linear dimensions (the gas efficiency should remain constant). The linear dimensions in Berkeley is 30 times larger than the corresponding ones in Novosibirsk, the inverse relation between the currents of H^- ions per 1 cm^2 of a cathode surface is approximately the same: $\sim$11 mA in Berkeley and $\sim$350 mA in Novosibirsk.

This scaling law allows a decrease of the heating and sputtering of electrodes by decreasing the current density of negative ions. In the stationary regime there is no difficulty in realising the heat removal from the

electrodes up to ~1 kW/cm^2. From this point of view, it is admissible to produce the beams of H^- ions with a density of up to 300 mA/cm^2 (see Table 2). Perhaps, the limitation on electrode sputtering will be stronger. To relax it, it is expedient to lower the voltage between the cathode-emitter and the plasma down to the threshold energy for sputtering.

It is not excluded that the sputtering coefficient of about 10^{-4} is achievable and one can produce the beams of H^- ions with a density of about 100 mA/cm^2 with the year-long resource of cathode operation. The current density of H^- ions, which is attainable in stationary sources, can be reliably determined only after testings of such sources. The current density of D^- ions obtained from surface-plasma sources under the same conditions is 1.5÷2 times lower than that of H^- ions.

One can affirm that the experimental solution is found out for production of the stationary many-ampere surface-plasma sources of H^- and D^- ions. First of all, these are honeycomb sources with focusing. These sources have technological construction, good gas efficiency and allow to produce the beams with the current of tens of amperes at a current density of up to ~100 mA/cm^2. Moreover, one can construct a single-aperture source with a single spherical focusing cathode-emitter. But the current density, when producing the beam with a current of about 10 A from such a source, will be not high, ~ 20 mA/cm^2.

It deserves attention a ring surface-plasma source developed in Leningrad by Komarov and his colleagues (see

Fig.10). In the ring chamber of this source the discharge with the closed Hall current is maintained, just as in the magnetron. It is easy to achieve the use of the whole cathode surface. The one-dimensional focusing of ions onto the emission slit has been used. The ring-shaped beam of H^- ions is extracted from the ring emission slit. In 1980 this source produced the beam of H^- ions with a current of up to 2.4 A and emission diameter of 10 cm /14/.

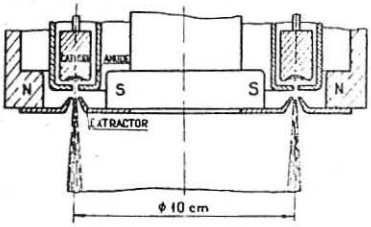


Fig.10.

Of large interest are the works initiated by Tsai, in Oak-Ridge, and concerning the production of negative ions from the existing many-ampere sources of positive ions by the surface-plasma method. The scheme of such a solution is presented in Fig.11. A surface Cs-coated converter is installed in front of the extraction multi-aperture system of the source. The geometry of this converter provides the output of the negative ions formed on its surface to the extraction system. Separation of these ions from the electrons is carried out with the help of the transverse magnetic and electric fields in the converter region. In 1980 one succeeded in obtaining, from the 5-ampere duopigatron, the beam of H^- ions whose current was about 0.5 A, current density about 20 mA/cm^2 and the energy 1 keV /45/. The

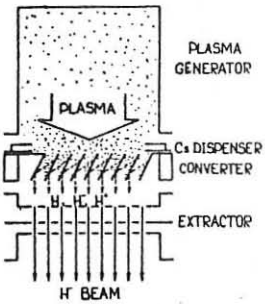


Fig.11.

achieved filtration of electrons was quite good, the electron current was by a factor of 10 less than the ion one. The gas efficiency was 3÷5%. It is planned to produce the 10 A beam of negative ions from the 100-ampere duopigatron.

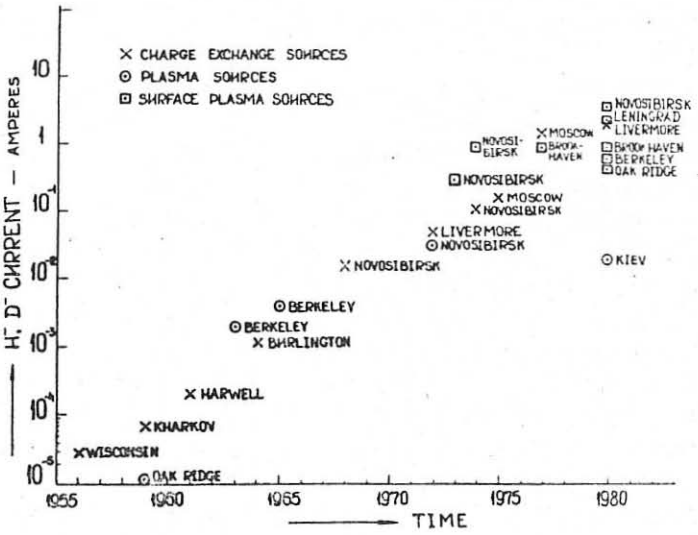


Fig.12.

In conclusion, Fig.12 illustrates the evolution of the H^- and D^- ion sources of three classes considered above. In the nearest future it is expected an increase in the intensity up to 10 A and higher. And then the main efforts will be directed to increasing the duration of operation and resource of such sources.

References

1. G.I.Dimov, V.G.Dudnikov, Plasma Physics, 4 (1978),692.
2. Ya.M.Fogel', L.I.Krupnik, V.A.Ankudinov, ZhETF, 26 (1956), 1208.
3. J.A.Phillips, J.L.Tuck, Rev.Sci.Instrum., 27 (1956),97.
4. J.A.Weinman, I.K.Cameron, Rev.Sci.Instrum., 27 (1956), 288.
5. L.W.Alwarez, Rev.Sci.Instrum., 22 (1951), 705.
6. N.B.Brooks, P.H.Pose, A.B.Wittkower, R.P.Bastide, Nucl. Instrum.and Meth., 28 (1964), 315.
7. G.I.Budker, G.I.Dimov, Proc. of the Intern. Accelerator Conf., Dubna, 1963. Atomizdat, Moscow, 1964,p.933.
8. G.I.Dimov, Yu.G,Kononenko, O.Ya.Savchenko, V.G.Shamovsky, ZhETF 38 (1968), 997.
9. G.I.Dimov, G.V.Roslyakov, PTE, 1974, N°1, 29.
10. G.I.Dimov, O.Ya.Savchenko, ZhETF 38 (1968), 2002.
11. B.L.Donnally, Patent of the United States, cl.250-84, N° 342904, Application of 3.V.1965, published 28.1. 1969.
12. C.W.Drake, R.Kratkov, Phys.Rev.Lett., 16 (1966),848.
13. J.E.Osher, G.W.Hamilton, "Proc. Symposium on Sources and Formation of Ion Beams", Brookhaven, 1971, p.157.
14. J.E.Osher, F.J.Gordon, G.W.Hamilton, Proc. II Intern. Conference on Ion Sources, Vienne, 1972, p.876.
15. G.I.Dimov, G.V.Roslyakov, Preprint INP 75-73, Novosibirsk, 1973; BNL-TR-570, Brookhaven, 1973; PTE, 1974, N°2, 33.
16. N.N.Semashko, V.V.Kuznetsov, A.I.Krylov, "Proc. Symp. on Production and Neutralization of Negative Hydrogen Ions and Beams", Brookhaven, 1977, p.170.
17. E.B.Hooper Jr., P.Poulsen, Proc. II Intern. Symposium on Production and Neutralization of Negative Hydrogen Ions and Beams, Brookhaven 1980, p.247.
18. C.D.Moak, H.E.Banta, J.N.Thurstan, J.W.Johnson, R.F.King, Rev.Sci.Instrum., 30 (1959), 694.
19. K.W.Ehlers, B.F.Gavin, E.-L.Hubbard, Nucl. Instrum. and Meth., 22 (1963), 91.

20. K.W.Ehlers, Nucl.Instrum and Meth., 32 (1965), 309.
21. Yu.I.Bel'chenko, G.I.Dimov, V.G.Dudnikov, Preprint INP 66-72, Novosibirsk, 1973; ZhETF 43 (1973), 1720.
22. M.D.Gabovich, Yu.N.Kozyrev, A.P.Naida, L.S.Simonenko, N.A.Soloshenko, Pis'ma ZhETF, 4 (1978), 378.
23. M.D.Gabovich, Yu.N.Kozyrev, A.P.Naida, PTE, 1980, N°2, 45.
24. M.Bacal, E.Nicolopulou, H.J.Doucet, "Proc. Symposium on Production and Neutralization of Negative Hydrogen Ions and Beams", Brookhaven, 1977, p.26.
25. M.Bacal, A.M.Bruneteau, H.J.Doucet, W.G.Graham, G.W.Hamilton, "Proc. II Intern. Symposium on Production and Neutralization of Negative Hydrogen Ions and Beams", Brookhaven, 1980, p.95.
26. M.Allan, S.F.Wong, Phys.Rev.Lett., 41 (1978), 1791.
27. G.I.Dimov, "Surface-Plasma Hydrogen Ion Sources", Report at"II Symposium on Ion Sources and Formation of Ion Beams", Berkeley, 1974.
28. E.D.Bender, G.I.Dimov, M.E.Kishinevsky, "Proc. of the National Seminar on Secondary Ion-Ion Emission", Kharkov, 1975; VINITI, N° 2783-75, 1975, p.119.
29. V.G.Dudnikov, Author Certificate, Cl. H0I 3/04, N°411542, Application 3.III.1972, Bul. N°2, 1974.
30. Yu.I.Bel'chenko, G.I.Dimov, V.G.Dudnikov, Preprint INP 81-72, Novosibirsk, 1972.
31. Yu.I.Bel'chenko, G.I.Dimov, V.G.Dudnikov, Izvestiya Akad. Nauk SSSR, Ser.Fiz. 37 (1973), 2573.
32. Yu.I.Bel'chenko, G.I.Dimov, V.G.Dudnikov,"Proc. II Symposium on Ion Sources and Formation of Ion Beams", Berkeley, 1974, p.VIII-1.
33. M.E.Kishinevsky, Preprint INP 116-73, Novosibirsk,1973.
34. M.E.Kishinevsky, ZhETF 48 (1978), 773.
35. Yu.I.Bel'chenko, G.I.Dimov, V.G.Dudnikov, Nucl.Fusion, 14 (1974), 113.
36. K.Prelek, Th.Sluyters,"Proc. II Symposium on Ion Sources and Formation of Ion Beams", Berkeley, 1974, p.VIII-6.
37. P.J.Schneider, K.H.Berkner, W.G.Graham, R.V.Pyle, J.W.Stearns,"Proc. Symposium on Production and Neutral-

ization of Negative Hydrogen Ions and Beams", Brookhaven, 1977, p. 63.

38. J.Los, E.A.Oberbosch, J. van Wunnik, "Proc. II Intern. Symposium on Production and Neutralization of Negative Hydrogen Ions and Beams", Brookhaven, 1980, 23.
39. V.G.Dudnikov, E.G.Obrazovsky, G.I.Fiksel, Plasma Physics, 4 (1978), 662.
40. Yu.I.Bel'chenko, V.G.Dudnikov, Preprint INP 78-95, Novosibirsk, 1978; Journal de Physique, Colloque C7, supplementau N°7, 40 (1979), p.C7-501.
41. J.G.Alessi, Th.Sluyters, Rev.Sci.Instrum., 51 (1980), 1630.
42. K.W.Ehlers, K.N.Leung, Rev.Sci.Instrum., 51 (1980),721.
43. Yu.I.Bel'chenko, V.G.Dudnikov, Preprint INP 80-34, Novosibirsk, 1980;"Proc. of the XVth Intern. Conf. on Phenomena in Ionized Gases", Minsk, 1981,part II,p.P-1504.
44. V.L.Komarov, A.P.Strokach, Preprint NIIEFA II-K-0488, Leningrad, 1980.
45. C.C.Tsai, R.R.Feerelli, H.H.Hoselton, P.M.Ryan, D.E.Schechter, W.L.Stirling, J.H.Whealton,"Proc. II Intern. Symposium on Production and Neutralization of Negative Hydrogen Ions and Beams", Brookhaven, 1980, p. 225.

PROGRESS IN THE TANDEM MIRROR PROGRAM

R. R. BORCHERS and T. K. FOWLER
Lawrence Livermore National Laboratory,
University of California,
Livermore, California
United States of America

ABSTRACT

Experimental results in TMX have confirmed the basic principles of the tandem-mirror concept. A center-cell particle confinement parameter $n\tau \sim 10^{11}$ $cm^{-3}\cdot s$ has been obtained at ion temperatures around 100 eV, which is a hundred-fold improvement over single mirrors at the same temperatures. For TMX these results have been obtained at peak beta values in the center cell in the range 10 to 40%, not yet limited by MHD activity; and ion-cyclotron resonant heating (ICRH) in the Phaedrus tandem-mirror experiment has produced beta values ~25%, which is several times the ideal MHD limit for that device. In addition, it has been demonstrated that the end fan chambers of TMX simultaneously isolate the hot electrons from the end walls, provide adequate pumping and conveniently dispose of the exhaust plasma energy either by thermal deposition on the end wall or by direct conversion to electricity (at 48% efficiency in agreement with calculations). Also, evidence was obtained for inherent "divertor" action in TMX, presumably in part responsible for the observed low impurity level (<0.5% low-Z ions in the center cell). Future work will concentrate on understanding and controlling radial transport, already in evidence in TMX, and on improved end-plug designs including the thermal barrier concept soon to be tested in TMX Upgrade. Other

tandem-mirror facilities under construction include the Gamma 10 (Tsukuba, Japan), Ambal (Novosibirsk, USSR), and the MFTF-B (Livermore, USA). The TARA (MIT, USA) experiment has been proposed and construction recommended.

1. INTRODUCTION

When this meeting was last held at Oxford in 1979, the first tandem-mirror facility with neutral-beam heating (the TMX at Livermore) was just coming into operation with positive, but preliminary results.[1] That was three years after the tandem-mirror concept was first presented at the IAEA Conference in Berchtesgaden,[2] followed by the successful demonstration of a tandem-mirror ambipolar-potential profile in the Gamma 6 (Tsukuba University, Japan) reported at Innsbruck.[3] After extensive measurements in TMX, the principle of tandem-mirror confinement appears to be well established.[4] Meanwhile, the Phaedrus tandem mirror is beginning to produce data with ion-cyclotron resonance heating at the University of Wisconsin Madison; construction of the Ambal tandem mirror at Novosibirsk is nearing completion; TMX is in the process of a major upgrade (TMX-U); completion of the Gamma 10 in Japan is about a year away; and the U.S. has embarked on the large Tandem Mirror Fusion Test Facility (MFTF-B) at Livermore, with the goal of demonstrating T_i = 15 keV and $n\tau = 5 \times 10^{13}$ cm^{-3}•s by 1985. The history leading up to these events has recently been summarized by Ryutov.[5]

The main point of the tandem mirror, and the feature best understood thus far, is the control of the end losses that have long been the primary concern in all kinds of open-ended confinement schemes. Evidence that tandem mirrors do control end losses will be the main subject of this paper. As end losses are reduced, radial transport in the central cell of the tandem mirror will

become more important, and already there is some evidence of this in TMX. This evidence will be discussed in another paper at this meeting.[6]

2. REDUCED END LOSSES

The main features of the tandem mirror are shown in Fig. 1, which is a sketch of the TMX at Livermore together with plots of the magnetic field, density, and plasma potential along the axis of the device. The tandem mirror can be thought of as two single-mirror machines (similar to the 2XIIB and earlier experiments) joined by a long solenoid. In a reactor, most of the fusion power would be produced in the solenoid. The two mirror machines serve as "end plugs" that prevent leakage of the plasma out of the ends of the solenoid. This is accomplished by continuously injecting neutral beams into each mirror cell to create a hot, dense plasma. As in any mirror machine, the lighter electrons tend to leak away faster than the ions, leaving behind a plasma whose net positive charge increases until the overall electron and ion loss rates become equal. It is the electrostatic potential difference ϕ_c between these positively charged end plugs and the solenoid that confines ions in the solenoid. The bulk of the electrons are confined by a potential drop, ϕ_e, relative to the end wall. The result is a greatly increased confinement time, ultimately to the point that, in a reactor, the solenoid can ignite.

Direct evidence that the end plugs work is shown in Fig. 2, which plots the leakage current out of the two ends of the machine as a function of time. At the left in the figure, the initial large current due to the plasma guns used for startup decreases to a low, steady level as the plasma builds up in the end plugs. Then, when only the east end plug is turned off by turning off the east neutral beams, leakage out of the east end increases sharply while

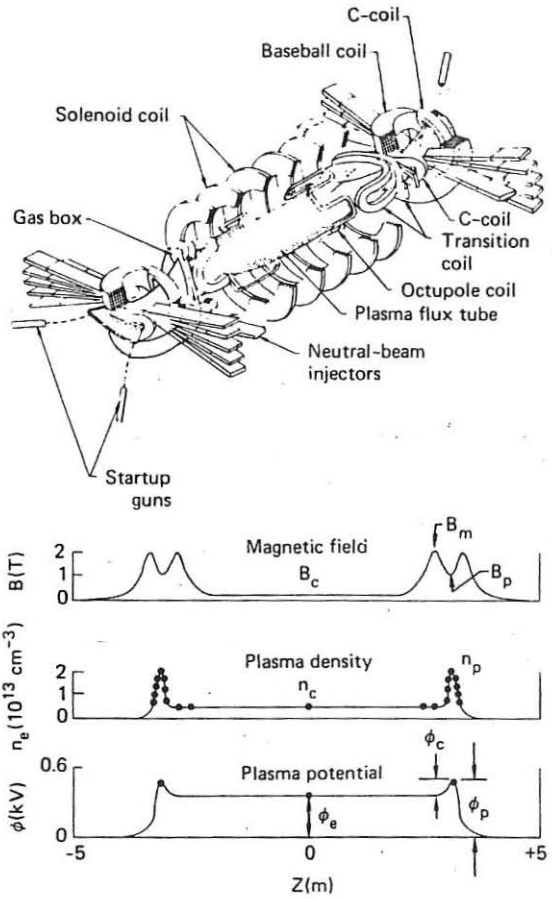


FIG. 1. Tandem-mirror experiment (TMX) coil geometry and measured axial plasma profiles: magnetic field, plasma density, and plasma potential profiles along the axis of the machine.

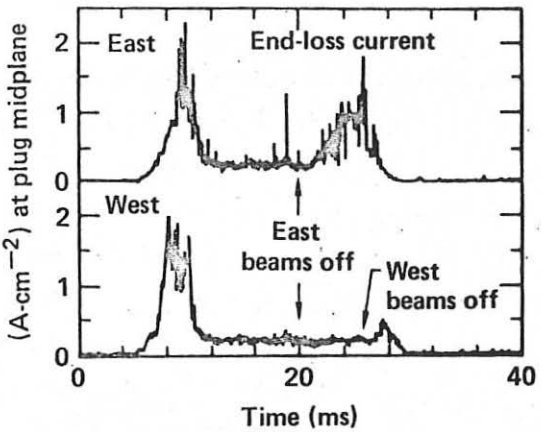


FIG. 2. Evidence for end plugging in TMX: the upper trace shows a sharp rise in current leakage from the east end of the device when neutral beams in the east end are turned off, while the west end is still plugged.

leakage out of the still-plugged west end remains small. If, instead the west beams are turned off first, it is the west end that leaks.

The density and potential profiles plotted in Fig. 1 are those actually measured in TMX under typical conditions. According to theory, for Maxwellian electrons the potential difference ϕ_c is given by

$$\phi_c = T_e \, \ell n \, \frac{n_p}{n_c} \quad , \tag{1}$$

where n_p and n_c are the densities in the plug and solenoid, respectively. The 130-V potential well, shown in Fig. 2, is in agreement with this formula for the measured electron temperature (T_e = 90 eV) and measured density ratio (n_p/n_c = 4) for the case shown.[7] Ions are confined in the solenoid for a time τ_c required for them to diffuse by Coulomb collisions over the potential barrier; for hydrogen,

$$n\tau_c = \left\{ 5 \times 10^{10} \, \frac{\phi_c}{T_i} \cdot T_i^{3/2} + 2 \times 10^{-8} \, n_c L_c R_c \, T_i^{-1/2} \right\} \exp \phi_c/T_i \quad , \tag{2}$$

where T_i is the ion temperature in the solenoid in keV, R_c is the mirror ratio between the end plugs and the solenoid, and L_c is the length of the solenoid (all lengths in cm). The second term is the flow-limited rate when the ion mean-free-path is less than $L_c R_c$. Only the first term, proportional to $T_i^{3/2}$, matters at high temperatures.

In the high-temperature regime, tandem-mirror confinement is enhanced by a large factor, $5(\phi_c/T_i)\exp(\phi_c/T_i)$, in comparison with single mirrors. This amounts to a 100-fold improvement for ϕ_c/T_i = 2.2. Indeed, the best results for TMX exhibit such improvement, as shown in Fig. 3.[7] As extraneous factors such as charge exchange, electron cooling

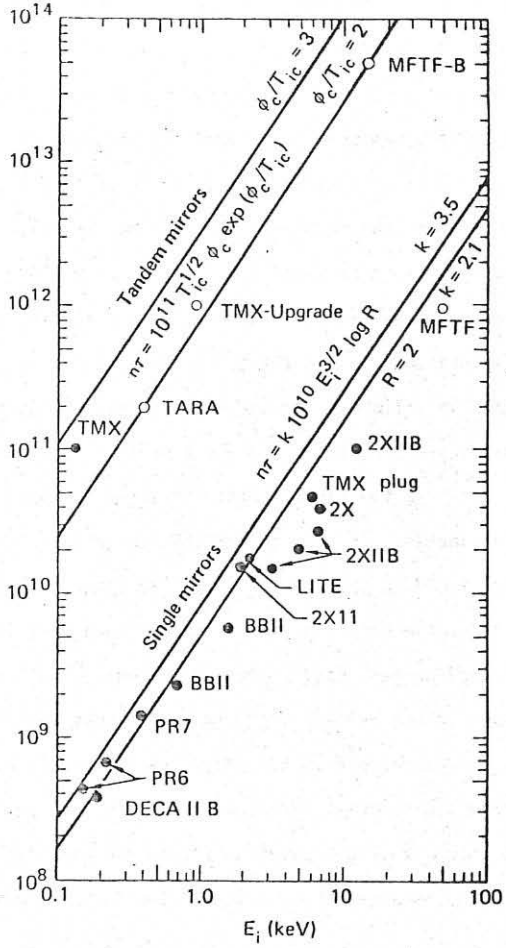


FIG. 3. Particle confinement parameter $n\tau$ versus ion energy E_i for single mirrors and tandem mirrors. Points for TARA, TMX Upgrade, and MFTF-B are projections from T. C. Simonen, Ref. 7.

and loss-cone instabilities have been brought under control over the years, single-mirror experiments have shown a steady improvement in which $n\tau$ increases proportional to $T_i^{3/2}$, up to 10 keV and more in 2XIIB (and the end plugs of TMX). Yet, because of the enhanced confinement in tandem mirrors, even at modest temperatures around 100 eV, the ion confinement in the central solenoid of TMX is already as good as the best obtained in 2XIIB. As indicated in the figure, the tandem-mirror scaling law will be further tested in the TMX Upgrade, soon to be completed, and in the MFTF-B.

Electron heat confinement is dramatically improved in TMX compared to earlier mirror experiments, again about 100-fold. As shown in Fig. 4, T_e is higher in TMX than in 2XIIB even though there is less input power to the electrons in TMX. Electron heat confinement will be discussed in the paper by Hooper et al.[6] Briefly, two factors contribute to the improvement in the electron heat confinement. First, in TMX the vacuum vessel extends well into the mirror fringe field so that the field has decreased 300-fold at the end wall. Consequently, the escaping plasma expands to a very low density, too low to ionize recycling gas; hence, there is a negligible buildup of cold plasma at the ends of the machine (10^9 cm^{-3}) and thus the hot electrons are well isolated from the ends. Secondly, whereas 2XIIB required external cold plasma streams to suppress loss cone instabilities, in TMX the outflow of plasma from the solenoid is by itself sufficient to maintain stability without the need for external sources that drain additional heat from the electrons.

3. IMPURITY CONTROL, DIRECT CONVERSION

The encouraging progress in reducing plasma leakage out of the ends of tandem mirrors permits us to focus on other features of linear systems that

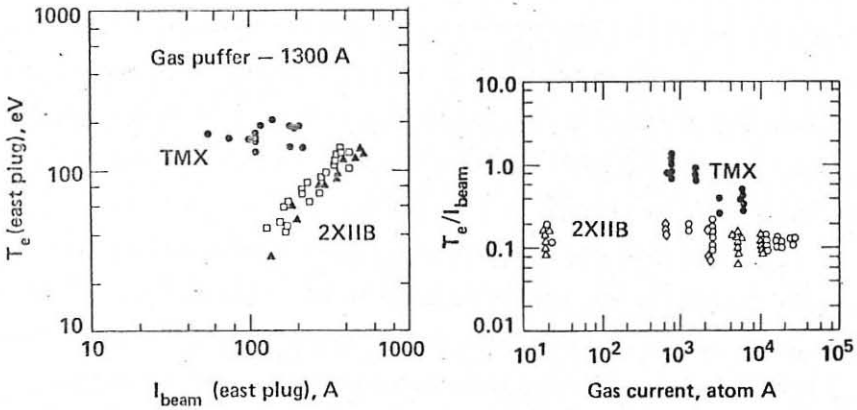


FIG. 4. Evidence that electron temperatures in TMX exceed those in the single mirror 2XIIB even though the input power to the electrons was greater in 2XIIB.

ıffer unique means of disposing of excess power, excess gas and impurities not ·eadily available in toroidal devices.

Historically, impurity radiation has not been a severe problem in mirror experiments. The TMX follows in this tradition despite the fact that, once captured in the center cell, a stripped impurity ion would be even better confined by the potential barrier than the hydrogenic ions. An extreme ultraviolet (EUV) study of the emissions from intrinsic and injected impurities has been carried out in TMX. The general characteristics of impurity emission in the TMX end plug were similar to those observed in the 2XIIB device; in particular, the results were consistent with beam-injected oxygen. The impurity level in the TMX central cell is <0.5%, mainly oxygen (0.3%) and nitrogen (0.2%).[8]

Two factors unique to mirror devices probably contribute to the low impurity content in TMX. One factor is the positive potential that expels low energy ions returning along magnetic lines from the end wall. This effect has been observed in single mirrors such as 2XIIB. The other factor is the built-in "divertor" action of magnetic lines outside of the plasma radius. It has long been known that the radius of the plasma produced by neutral injection into a mirror container is controlled by aiming the beams; typically the radial extent of the plasma stops well short of the wall with no physical limiter. In TMX, since axial confinement of solenoidal ions by the end plugs exists only out to radii within the plug plasma, in the central cell good confinement extends only out to magnetic lines in the solenoid that skim the edge of the plug plasmas as the lines pass through the plugs. Again, the plasma is isolated from the radial wall, and the magnetic lines at the edge of the hot plasma serve as a divertor, or path of escape, of ions created in the cold surface region. Experimental evidence for this effect in TMX includes a measurement of the radial potential profile, reported in Ref. 6, and the data

in Fig. 5 which shows that, for a fixed plug radius and field, the plasma radius in the center decreases as the central magnetic field is increased (so that magnetic lines skimming the plug pass through the solenoid at a smaller radius).[9]

Turning to the disposal of power and gas, we have already noted that the expanding magnetic lines at the ends of TMX serve to expand the escaping plasma density to a very low value, around 10^9 cm^{-3}. At such low densities the Debye length is large enough so that physical grids can be utilized to stop the electrons and extract energy from the ions electrostatically, a process known as "direct conversion." Previous experiments have demonstrated the concept using ion beams.[10] In TMX, the first tests of direct conversion have been carried out with plasmas. Using a device subtending only a small portion of the flux at the end wall, we were able to recover 67 watts at a potential of 565 V and an efficiency of 48% in good agreement with theoretical calculations.

Thus, the same end design that successfully isolates the hot electrons away from the end wall also expands the plasma to a density sufficiently low to carry out direct conversion. It also follows that the thermal heat flux on the end wall is acceptable; and there is adequate room for cryopanels to pump the entire machine. Moreover, this design, (merely a cylindrical vessel large enough to encompass the fringe field) is relatively inexpensive and easy to construct. The MFTF-B utilizes this design.

4. HIGH BETA

In tandem mirrors, MHD stability is provided by the end-plug plasmas that are themselves confined in stable magnetic wells and serve as anchors electrically tied to the solenoidal plasma through the plasma conduction along

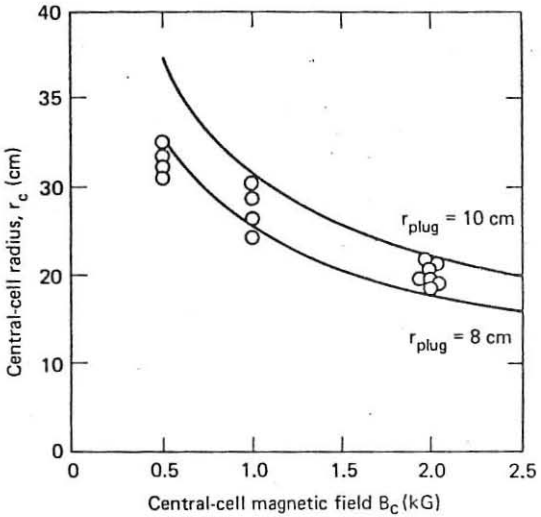


FIG. 5. Evidence of inherent divertor action in TMX; for a fixed plug radius, the central-cell plasma radius decreases as the field increases, showing that the radial extent is terminated by outflow along the magnetic lines to the ends of the device, Ref. text.

field lines. According to theory, the limit on beta in the solenoid, β_c, is set by the ballooning mode. The ideal MHD calculation gives a limit around β_c = 25% (peak value on axis) for typical circumstances, but finite Larmor radius (FLR) corrections will increase this. FLR effects are greatly enhanced in tandem mirrors by the fact that the bad magnetic curvature is isolated to a small portion of the machine (the transitions between the solenoid and the plugs). Estimates suggest a factor of 2 or more improvement in β_c, but calculations are still in progress.

Experimentally, peak β_c values in the range 10 to 40% have been obtained under various circumstances. Results from TMX are shown in Fig. 6. On the left are results with heating by the end-plugs only. For this case $\beta_c \leq$ 10%, limited by end losses rather than by MHD activity (in the figure, measured values are compared with the TAMRAC code in which all losses are "classical" end losses). The right side of the figure shows results with auxiliary neutral-beam injection into the solenoid. In this case β_c reaches values as high as 40% locally, mainly due to mirror-trapped energetic ions. Again there is no evidence of an MHD limit, though this is not necessarily in disagreement with theory and occasional plasma "dumps" were observed.* Recent results with ICRH in the Phaedrus tandem mirror at the University of Wisconsin give β_c values (up to 25%) that do appear to be several times the theoretical prediction for the ideal MHD interchange mode in that device.[11]

---

*Ref. TMX Final Report. Note that the dumps were preceded by growing m = 1 oscillations at a frequency of 5 kHZ.

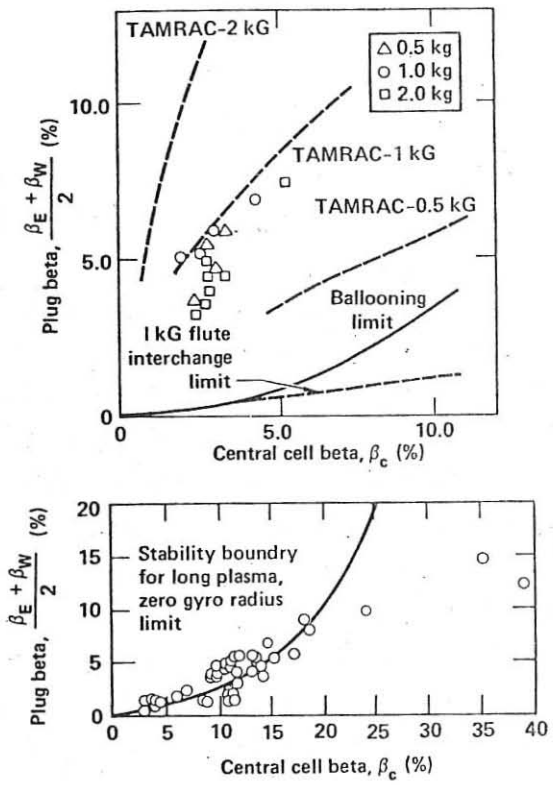


FIG. 6. TMX peak beta values in the end plug and central cell versus theoretical expectations, with and without auxiliary neutral-beam heating in the central cell.

5. LOSS CONE INSTABILITIES

Loss cone instability in the end plugs remains a problem that must be overcome more thoroughly than is possible using the technique of "stream stabilization" by the outflowing plasma in TMX. Besides causing loss of particles in the end plugs themselves, the electrostatic waves generated by loss cone modes propagate from the plugs to the solenoid where they are absorbed by the ions. Absorption occurs in the high-field transition region where the ion cyclotron frequency again matches that at the center of the end plugs. The effect is the same as if strong ICRH were applied there; namely, overheating causes enhanced end losses as ions diffuse in energy over the potential barriers.[12] This is illustrated in Fig. 7, taken from Ref. 13. The instability rf fluctuations were increased by increasing the neutral beam current fueling the end plugs without increasing the gas fuel that provided the "stream stabilization." The figure shows the observed decrease in $n\tau_c$ as the fluctuation amplitude increased, and also shows (open circles) a theoretical calculation of $n\tau_c$ based on the measured changes in fluctuation amplitude.

Much improvement is expected in end plugs with thermal barrier designs discussed in the next section. In the original TMX, loss cone instability is controlled because the outflowing plasma fills in the loss cone. Instability is only partly suppressed because the RF itself must heat the flowing ions to the energies necessary to fill in the empty portion of the velocity distribution. In the thermal barrier design, soon to be tested in the TMX Upgrade, confined plasma heated by collisions fills in the distribution where theory says it counts most, namely, at the center of the plug near the field minimum.

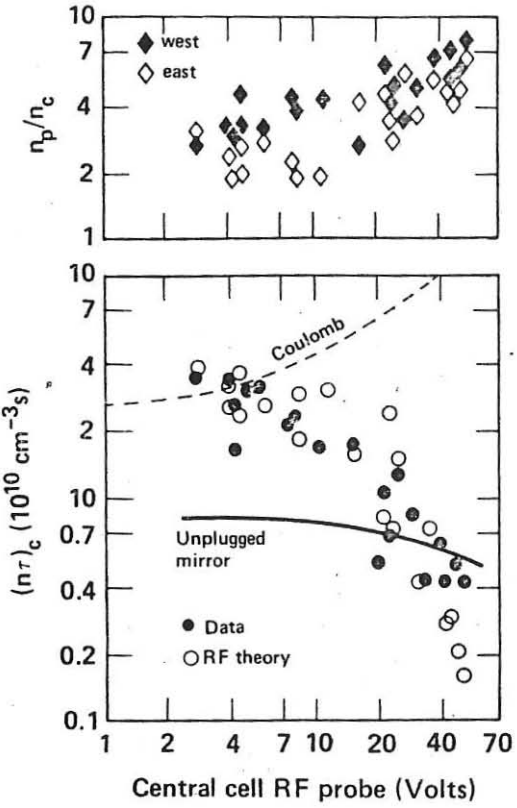


FIG. 7. Evidence for degraded central-cell confinement with increasing amplitude of rf fluctuations generated by loss-cone instabilities in the end plugs.

6. IMPROVEMENTS

In 1979, Baldwin and Logan introduced a new approach called the thermal barrier that creates end plug potentials more efficiently with less demanding beam and magnet technology.[14] In this concept the potential, given in Eq. (1), is enhanced by heating electrons in the plug to a high temperature, for example by electron-cyclotron resonant heating (ECRH). The thermal barrier isolates the hot electrons from those in the solenoid.

There are several ways to create thermal barriers in practice. Figure 8 shows the design employed in MFTF-B, which consists of two cells in series. The yin-yang cell merely provides MHD stability. All of the end-plugging takes place in the outer A-cell. The thermal barrier is created by mirror-trapped electrons (heated by ECRH at the midplane) that create a deep depression in the plasma potential. In effect these mirror-trapped electrons confine most of the thermal electrons escaping from the solenoid. The thermal ions are confined by mirror-trapped ions injected by neutral beams at an angle with respect to the field line in order to create two peaks as they "slosh" back and forth in the mirror. Applying ECRH to the outer density peak establishes the high potential peak that confines the thermal ions, all at a relatively low ECRH power because these electrons are largely isolated by the thermal barrier. Finally, to maintain low densities in the A-cell (and hence low-power requirements to sustain them), a means is provided to "pump" out thermal ions that become trapped between the mirrors in the A-cell. In the MFTF-B, pumping is accomplished by additional neutral beams aimed along the axis so that a charge-exchange collision with a trapped thermal ion converts it to an energetic ion that escapes. As noted in the previous section, and as can be seen in the figure, in this design thermal ions penetrate past the

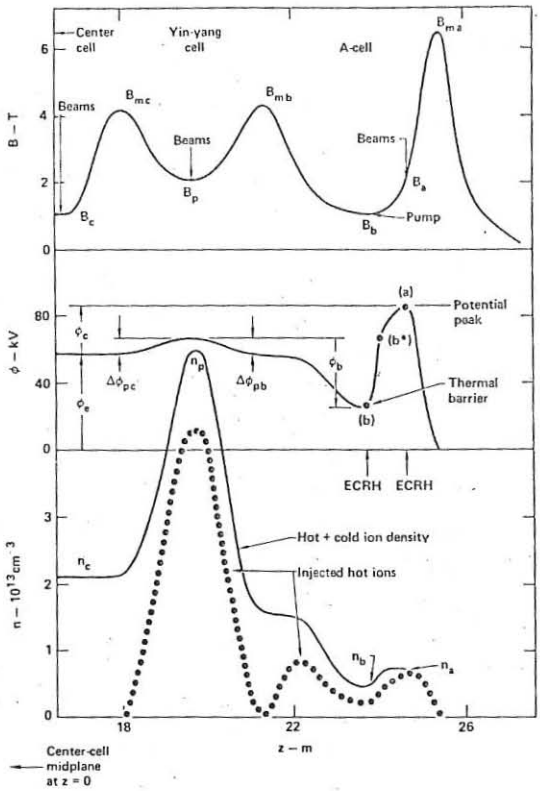


FIG. 8. Axial profiles of the magnetic field, plasma potential, and plasma densities for thermal-barrier operation in the MFTF-B tandem-mirror device.

midplane of the A-cell and thus are available to fill in the sloshing-ion loss cone and thereby prevent loss-cone instabilities.

The main elements of the thermal-barrier design described here (the sloshing ions, pump beams and ECRH) will be tested in the TMX-Upgrade beginning in 1982. Also, theoretical work continues on improved pumping schemes.

In addition to seeking improved ways to generate potentials, we are also studying simpler end plug magnet designs, especially those that provide a higher degree of axisymmetry. According to theory, the quadrupolar components of the plug and transition coils in present designs cause enhanced collisional radial transport when the bounce frequency of ions in the solenoid resonates with their azimuthal drift frequency. In a linear device, this can enhance transport of the ions radially and electrons axially (by an adjustment of ϕ so that the electrons leakage out the ends is equally enhanced). Such nonambipolar transport occurs in TMX, but it should not occur in an axisymmetric device. Evidence of radial transport in TMX will be discussed at this conference in the paper by Hooper et al.[6]

Magnet designs under consideration include an improved version of the cusp design discussed at Brussels,[15] and an "axi-cell" design that has been proposed for the TARA experiment at MIT.[16] In the axi-cell design, the thermal barrier and potentials are created in a simple mirror (two circular coils), while MHD stability is provided by yin yangs at each end.

7. NEW FACILITIES

Both at Tsukuba in Japan and at Livermore, improved tandem-mirror experiments are under construction. Gamma 10 at Tsukuba and TMX-Upgrade at Livermore will both be thermal-barrier tandem-mirror machines of similar

size. In the Soviet Union the Ambal tandem mirror is under construction. The parameters for all these facilities as well as those of TMX are shown in Table 1.

Table 1 also gives the parameters of the Tandem-Mirror Fusion-Test Facility MFTF-B currently under construction at Livermore. A layout of the facility is shown in Fig. 9. MFTF-B will demonstrate tandem-mirror confinement of a plasma at or near equivalent energy breakeven conditions. In addition, MFTF-B will demonstrate operation of a fusion device with fully superconducting magnets, under computer control, with multiple high-energy (80 keV) neutral beams, and for a sufficiently long pulse that vacuum must be maintained in the presence of equlibrium plasma-wall interactions.

MFTF-B will be a flexible facility whose physics program will include radial-transport studies, microstability studies, and exploration of the beta limits imposed by magnetohydrodynamic effects. Future upgrades of MFTF-B could include more axisymmetric configurations similar to the TARA experiment at MIT.[16]

ACKNOWLEDGMENT

This work was performed under auspices of the U.S. Department of Energy by Lawrence Livermore National Laboratory under Contract W-7405-ENG-48.

ERRATUM, UCRL-86588

In the text, p. 13, the two graphs in Fig. 6 are referred to as "left-side" and "right-side". Instead, for "left-side" read "upper" and for "right-side" read "lower". In the figure caption for Fig. 6, the "lower" graph corresponds to data "with" auxiliary neutral beam heating and the "upper" graph is the case without this heating.

TABLE I. COMPARISON OF TANDEM-MIRROR MACHINES

Parameters	TMX	TMX-U	GAMMA-10	AMBAL	MFTF-B
End plug					
Field at center, kG	10	5	6	10 to 15	20
Field at plug, kG	20	10	33	20 to 30	40
Length, cm	150	300	480	100	360
Plasma radius, cm	10	15		12	40
Injected energy, keV	13	11		25	60
Startup current, A	2 x 150	2 x 240		2 x 200	5 x 80 (0.5 s)
Sust. current, A				2 x 50	3 x 50 (30 s)
Pulse length, ms	25	75		100 to 500	30 s
Plasma density, cm^{-3}	4×10^{13}	7×10^{12}	5×10^{12}	3×10^{13}	6×10^{12}
Ion energy, keV	13	10	30/15	20	60
Electron temp., keV	0.260	0.600	1.0	1.0	1.0
Central cell					
Field, kG	0.5 to 2	3	4	1.5 to 2.25	5 to 10
Length, cm	640	800	640	350	3000
Plasma radius, cm	30	20		30	56
Plasma volume, ℓ	800	600		300	3×10^4
Injected energy, keV		11 k			60
Injected current, A		180		20	50
Plasma density, cm^{-3}	3×10^{13}	2×10^{13}	10^{13}	10^{13}	2×10^{13}
Ion trap, keV	0.25	0.9	1.0	0.5	15
Confining pot., keV	0.300	2.2	2.5	1.1	28
Confinement par $cm^{-3} \cdot s$	10^{11}	10^{12}	10^{12}	3×10^{13}	5×10^{13}

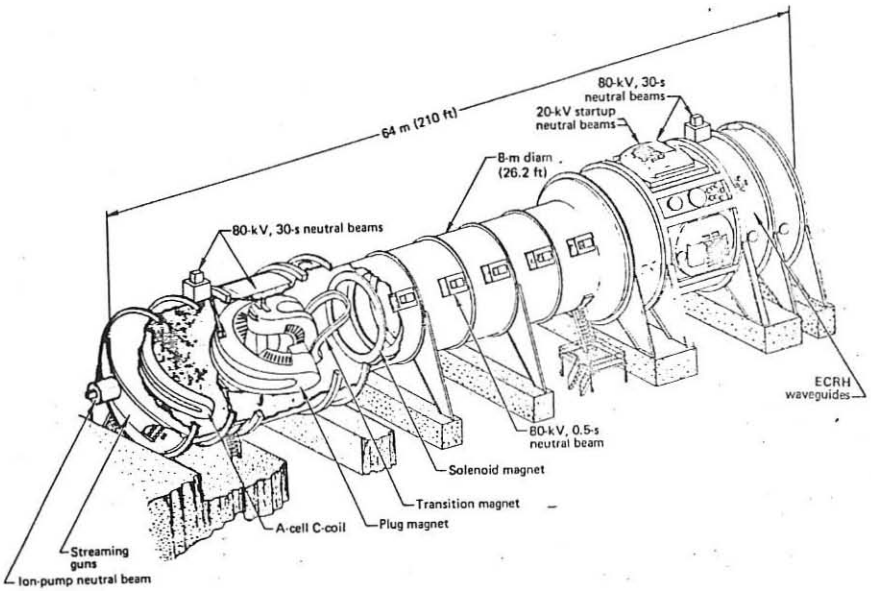


FIG. 9. MFTF-B facility.

REFERENCES

1. T.K. Fowler and F. H. Coensgen, "Progress in Mirror Machine Research," in Proceedings of the Ninth European Conference on Controlled Fusion and Plasma Physics (Oxford, UK, 1979); Lawrence Livermore National Laboratory, Report UCRL-83305 (1979).

2. G. I. Dimov, V. V. Zakajdakov, and M. E. Kishinevskii, in Proceedings of the Sixth International Conference on Plasma Physics and Controlled Nuclear Fusion Research (Berchstesgaden, 1976), IAEA, Vienna (1977) Vol. III, p. 177; G. I. Dimov, V. V. Zakaidakuv, and M. E. Kishinevskii, Fiz. Plazmy 2, 597 (1976); and T. K. Fowler and B. G. Logan, Comments on Plasma Physics and Controlled Fusion, 2, 167 (1977).

3. S. Miyoshi, K. Yatsu, T. Kawabe, K. Ishii, A. Itakura, H. Ishizuka, and S. Hagiwara, in Proceedings of the Seventh International Conference on Plasma Physics and Controlled Nuclear Fusion Research (Innsbruck, 1978), IAEA, Vienna (1979) Vol. II, p. 437.

4. T. C, Simonen et al., in Proceedings of the Eighth International Conference on Plasma Physics and Controlled Nuclear Fusion Research (Brussels, 1980), IAEA, Vienna (1981); Lawrence Livermore National Laboratory, Preprint UCRL-83515 (1980).

5. D. D. Ryutov, Nucl. Fusion 20, 1068 (1980).

6. E. B. Hooper et al., in Proceedings of the Tenth European Conference on Controlled Fusion and Plasma Physics (Moscow, USSR, 1981); Lawrence Livermore National Laboratory, Report UCRL-85883 (1981).

7. T. C. Simonen, Lawrence Livermore National Laboratory, Preprint UCRL-85834 (1981); submitted to Nuclear Fusion.

8. S. L. Allen, O. T. Strand, H. W. MOOS, R. J. Fortner, T. J. Nash, and D. P. Dietrich, Lawrence Livermore National Laboratory, Report UCID-18883 (1981); submitted to Nuclear Fusion.

9. R. P. Drake, "Control of Plasma-Wall Interactions in Tandem Mirrors," Lawrence Livermore National Laboratory, Abstract UCRL-86253 (1981).

10. W. L. Barr and R. W. Moir, Lawrence Livermore National Laboratory, Report UCRL-86331 (1981) (to be published).

11. A. W. Molvik et al., "MHD Stability Experiments in the Phaedrus Tandem Mirror," American Physical Society, Division of Plasma Physics, Twenty-third Annual Meeting, New York, October 12-16, 1981, to be published in Bull. Am. Phys. Soc.

12. T. D. Rognlien and Y. Matsuda, Nucl. Fusion 21 345 (1981).

13. R. P. Drake et. al., Nucl. Fusion, 21, 359 (1981).

14. D. E. Baldwin and B. G. Logan, Phys. Rev. Lett. 43, 1318 (1979).

15. B. G. Logan et. al., in Proceedings of the Eighth International Conference on Plasma Physics and Controlled Nuclear Fusion Research (Brussels, 1980), IAEA-EN-38/E2.

16. J. Kesner, Nucl. Fusion, 20, 557 (1980).

DISCLAIMER

This document was prepared as an account of work sponsored by an agency of the United States Government. Neither the United States Government nor the University of California nor any of their employees, makes any warranty, express or implied, or assumes any legal liability or responsibility for the accuracy, completeness, or usefulness of any information, apparatus, product, or process disclosed, or represents that its use would not infringe privately owned rights. Reference herein to any specific commercial products, process, or service by trade name, trademark, manufacturer, or otherwise, does not necessarily constitute or imply its endorsement, recommendation, or favoring by the United States Government or the University of California. The views and opinions of authors expressed herein do not necessarily state or reflect those of the United States Government thereof, and shall not be used for advertising or product endorsement purposes.

INTOR PHYSICS

G. Grieger

Max-Planck-Institut für Plasmaphysik
EURATOM-Association, D-8046 Garching

ABSTRACT

INTOR is a cooperative project running under the auspices of the IAEA, with the EC, Japan, USA, and USSR as partners. INTOR will have the task to demonstrate the physics needed for a tokamak demonstration reactor (DEMO) and to be a test bed for the development of DEMO technology. The "Data Base Assessment" phase of the INTOR workshop has shown that the data base is sufficient for initiating the INTOR project provided the simultaneously identified research and development (R and D) programme will be initiated and produce results at the required rate. Recently, the "Definition" phase of INTOR was concluded with a conceptual design and the definition of a number of short-term R and D projects, the results of which will be needed for improving the reliability of the data base.

The conceptual design of INTOR is strongly determined by requirements of engineering, remote maintainability and reliability of operation, i.e. physics has to provide solutions compatible with these requirements. This led to the introduction of a single null poloidal divertor and the request to produce a configuration with high enough plasma beta by a coil system having all the poloidal field coils outside the toroidal field ones. This problem could be solved. The properties of the plasma confined in this configuration and the implications arising from the above requirements are discussed in this paper.

INTRODUCTION

INTOR (INTERNATIONAL TOKAMAK REACTOR) is a cooperative project between EURATOM, Japan, the USA, and the USSR. It is running under the auspices of the IAEA. Its task is the definition, the design, the construction,

Max-Planck-Institut für Plasmaphysik

and, finally, the operation of the next step fusion device after the JET, JT-60, TFTR, and T-15 generation. In this project, the main work is done by the home bases of the four partners which are groups of engineers and physicists of considerable strength. About six to eight scientists per partner form a workshop which holds regular sessions at the IAEA headquarters in Vienna, typically four per year, and of 2 - 3 weeks duration each. The workshop defines the tasks for the home bases.Afterwards, it collects the incoming information, and after intense and critical discussions selects the optimum solution of the problems studied. On this basis, it then defines the home task for the next session.

This way of working has proved to be extremely successful, because it draws upon the knowledge and creativity of the world fusion programme, and the critical discussions in Vienna give the highest possible chance for arriving at optimal solutions.

The INTOR project is subdivided into phases. Phase 0 was running the full year 1979 and was devoted to a "Data Base Assessment". During this phase, the existing data base was studied component-wise and compared with the needs for the construction of an INTOR-like device. This phase finished with a comprehensive report and the conclusion that the existing data base is sufficient for starting the definition of INTOR, but a number of R and D programmes were identified which have to be initiated at the same time. Their results are needed before the construction of INTOR can start. A first set of major parameters of INTOR was also produced as input to the definition phase.

The "Definition" phase started in January 1980 and was finished in time in July 1981 with a new INTOR report on the INTOR conceptual design. During this phase, also the interdependences of all components of the device were studied and the internal consistency of the conceptual design largely, though not fully achieved. For the time being, the state of consistency reached, however, is considered sufficient in that it allowed the identification of all major critical points. The INTOR

workshop concluded that the conceptual design is workable and a number of short term R and D needs were defined to put some elements of the data base on safer grounds and to allow the inclusion of some advanced technologies for which the feasibility demonstration is still missing.

INTOR - PHYSICS

This paper deals with the physics aspects of INTOR as they are described in the phase-I report. Technology will only be delt with to the extent it sets requirements to physics. This follows from the programmatic objectives of INTOR:

- INTOR should be the maximum reasonable step beyond the next generation of large tokamaks (TFTR, JET, JT-60, T-15) in the world fusion programme.
- INTOR should demonstrate the plasma performance required for tokamak DEMOs.
- INTOR should test the development and integration into a reactor system of those technologies required for the DEMOs.
- INTOR should serve as a test facility for the blanket, tritium production, materials and plasma engineering technology development.
- INTOR should test fusion reactor component reliability.
- INTOR should test the maintainability of a fusion reactor.
- INTOR should test the factors affecting the reliability, safety and environmental acceptability of a fusion reactor.

or in short: Apart from a demonstration of plasma physics, the main task of INTOR is to serve as a test bed for the development of DEMO technology.

This is a new situation for physicists. They have to provide conditions acceptable to engineering where reliability determines the solutions. The plea for greater safety factors, margins, redundancy very rapidly becomes expensive and unacceptable.

In this sense physics has to provide (i) a plasma burning for more than 100 seconds, (ii) a sufficient neutron wall loading of about 1.3 MW m^{-2}, (iii) a sufficient neutron fluence which calls for a high duty cycle ($\geq$ 70 %) and a high availability in turn (up to 0.4 - 0.5), (iv) reliable operation for up to 10^6 discharges, and (v) not to come up with requirements too complicated for allowing "economic" engineering solutions. These considerations are setting the frame for the discussion of INTOR physics.

Two of the major design decisions taken were of great and far reaching influence:

(i) The inclusion of a divertor. It was felt that only this way the wall bombardment and the plasma impurity content could be kept low enough for a reliable INTOR operation. The ash exhaust would be achieved the same way. A single-null poloidal divertor was considered optimal under the overall INTOR conditions.

(ii) That there should be no poloidal field coils arranged inside the toroidal field coils because a credible remote maintenance procedure would hardly be compatible with interlinked coils.

The major INTOR parameters are listed in Tab. I. The arrows indicate the changes made from phase 0 to phase I. They mainly result from the inclusion of the single null poloidal divertor. As will be seen later, its physics leads to a scrape-off layer thickness which at the inside is three times as large as at the outside. This made it necessary to shift the major radius of the plasma by 10 cm to the outside, for "centering" the plasma again in an unchanged vacuum vessel. By this measure, however, the plasma radius became smaller by 10 cm.

TABLE I

Major INTOR Parameters

	Phase 0		Phase I	
Major radius	5.2	→	5.3	m
Plasma radius	1.3	→	1.2	m
Elongation	1.6		1.6	
Triangularity	-		≈ 0.25	
Tor. Magn. Field	5.5		5.5	T
Plasma current	6.4		6.4	MA
Safety factor q_I	2.5	→	2.1	
DT power	620		620	MW
Average ß (burn)	5	→	5.6	%
Average DT density	$1.3 \cdot 10^{20}$	→	$1.4 \cdot 10^{20}$	m^{-3}
Average DT temperature	10		10	keV
Neutron wall load	1.3(1.6)		1.3	MW/m^2
Burn time	> 100	→	100 → 200	s
Duty cycle	≥ 0.7		up to 0.8	
Neutral beam energy	175		175	keV
Neutral beam power	75		75	MW

(Evolutions from Phase 0 to Phase I are indicated by arrows)

In order to maintain the wall loading at the required level, the beta value had to be increased. This could only be done in a credible fashion if the q-value was decreased simultaneously, leaving the poloidal beta unchanged.

1) Equilibrium configuration - poloidal coils

Before the poloidal field coil distribution could be determined, it was necessary to fix the size and number fo the TF-coils. There, the driving requirements were easy access to plasma, blanket, and shield which would

favour a low number of coils of large size. Low ripple, on the other hand, requires a high number of coils also of large size whereas compactness drives the design to smaller coil sizes. 12 coils with 7.7 x 10.7 m^2 bore were considered the optimum.

The poloidal field coils had to generate the required ellipticity and triangularity of the plasma together with an active null point in the lower part of the configuration to form the single null divertor (see Fig. 1). Both conditions had to be maintained to an acceptable degree also during plasma start-up. In addition, the inactive null point at the top of the configuration had to be away far enough in order not to broaden too much the scrape-off layer in this regime. Coil positions were only available where they did not interfere with the straight and horizontal access to both the inner shield and the divertor chambers.

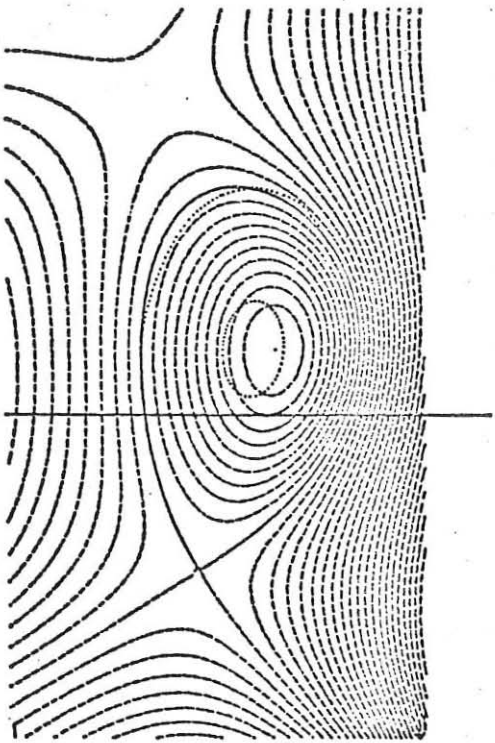


Fig.1. INTOR poloidal field configuration for $\beta_p = 2.6$. Dotted lines: $\beta_p = 0$.

An optimized configuration is shown in Fig. 1. For the operational value of $\beta_p = 2.6$ it has the required ellipticity and sufficient triangularity. The $\beta = 0$ case is also indicated. It shows that by varying the poloidal currents, the configuration can practically by maintained, except for the ß-shift of the plasma center. The somewhat

reduced triangularity for ß = 0 should not have a major effect since this property only becomes important when approaching the ß-limit.

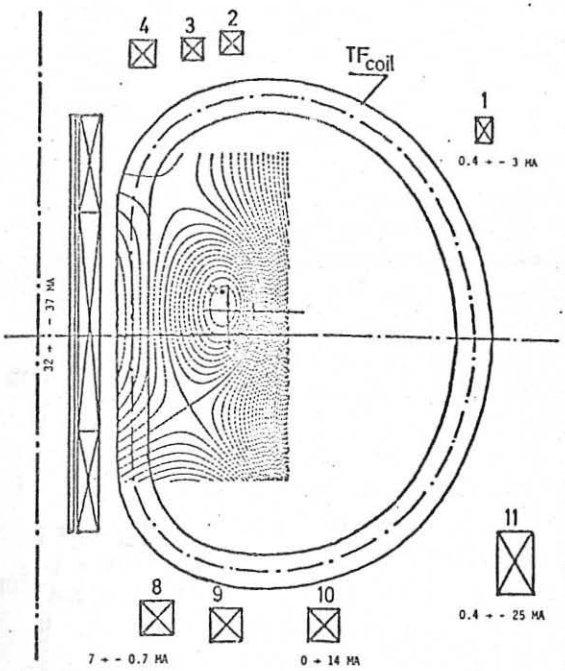


Fig.2. INTOR PF coil arrangement. For some coils, the required currents for plasma current start and for the final configuration are shown.

Fig. 2 shows the INTOR configuration together with the field producing coils. It is immediately apparent from this figure that the advantage of increased maintainability by choosing large TF-coils has its price in large PF-coil currents which add up to 100 MA turns in magnitude for a 6.4 MA plasma current. The plasma has been shifted slightly upward for effective use of the space within the main field coils. Also for reasons of economy, all coils contribute to the OH flux swing of 110 Vs.

To illustrate the situation, for some of the coils their currents at ß = 0 and at full beta are indicated. Except for the centre OH coil, coil 11 carries by far the largest load. Its radius has to be large enough for lifting the coil out of the machine for maintenance but, nonetheless, this coil has to give the main dipole contribution to the lower

null-point. It should be noted that the large PF-coil currents also lead to respectable forces between the TF- and PF-coil systems.

The following sections now will discuss the physics of a plasma confined in this configuration.

2) Energy confinement

During phase O ALCATOR scaling with $\tau_E \approx 0.5\, n_e a^2$ was the best choice. In the meantime, a much more refined data base exists for clean OH-plasmas with medium q-values and densities ranging from $2 \cdot 10^{19}$ to $2 \cdot 10^{20}\ m^{-3}$. The large scattering of the data points (see INTOR report) is still a matter of great concern but it can be extracted from the data that, for the density range of INTOR operation, a factor of two improvement might be adequate. The present INTOR parameters include this factor in the safety margin although the uncertainty might be slightly greater than this factor.

The large scattering of the data also led to the proposal of alternative scaling laws. In this connection, the importance of the major radius experienced new attention. Indications came from divertor experiments and T-11 proposed $\tau_E \sim \sqrt{a} \cdot n_e \cdot R^{2.8}$ which, however, for the range of INTOR operation leads to about the same result. Certainty on the confinement properties under INTOR conditions will probably not come before the next generation of tokamaks will produce reliable results. Two indications, however, seem to follow from the present data base: There seems to be at least a weakly positive temperature dependence for τ_E and a steep but soft increase of transport seems to occur when approaching the ß-limit. This supports the hope for an automatic burn control at $ß = ß_{max}$.

For the ion heat conduction, the INTOR design basis of $\chi_i \approx 3\chi_{iNC}$ is confirmed.

3) Magnetic field ripple

An essential improvement was obtained for the effect of the magnetic field ripple. Introduction of the proper geometry into the calculations led to a reduction of the ripple induced heat losses by orders of magnitude, particularly in the high temperature regime. Fig. 3 compares the earlier (dotted) with the present results for half the plasma radius. Neutral injection losses are still localized and leading to a loss of less than 5 % of power with 0.25 MW/m^2 at the wall during start-up. Burn control, on the other hand, has become much more difficult by this method since it requires a much larger ripple variation than originally estimated. In addition, an even further reduction of the ripple induced heat losses is not excluded since effects of radial electric fields are not yet included in the calculations. Experiments in WENDELSTEIN VII-A point in this direction.

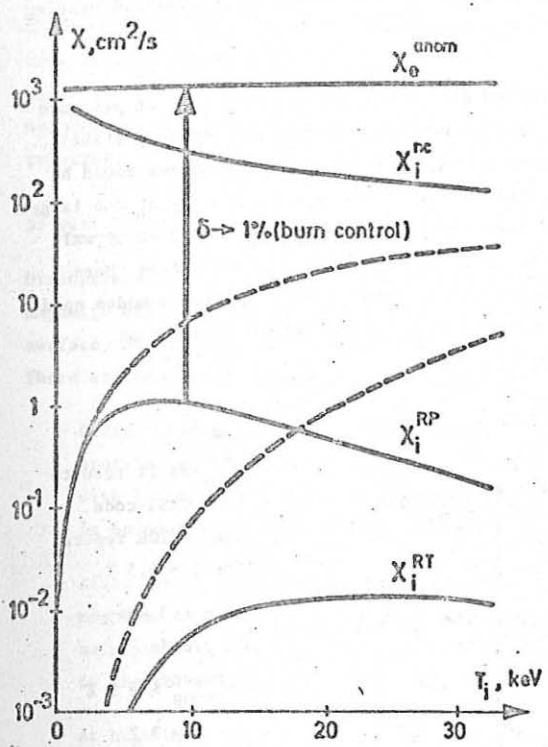


Fig.3. Heat conduction and magnetic field ripple. RP: ripple-plateau, RT: ripple-trapped.

4) Stability limits

In INTOR $\beta \geq 4$ % is required for reaching ignition. The operating value of $\beta = 5.6$ % was chosen for achieving sufficient reactivity and wall loading and to allow some margin for impurities including helium. The increase in the loss rates when approaching the beta limit should carefully be determined by experiments in order to avoid the initial heating power foreseen for INTOR to be too small.

According to theory, attention has to be paid to the growth of pressure driven modes, namely (i) to free boundary kinks which could be stabilized if the distance between a conducting wall and the plasma could be kept smaller than 0.2 a; (ii) to ballooning modes occurring at the large radius side at regions of high ∇n, which are nearly unaffected by wall stabilization, and (iii) to internal dissipative instabilities. Here the high m modes are probably not critical whereas the low m modes need further studies also for their connection with disruptions. Most critical are cases (i) and (ii).

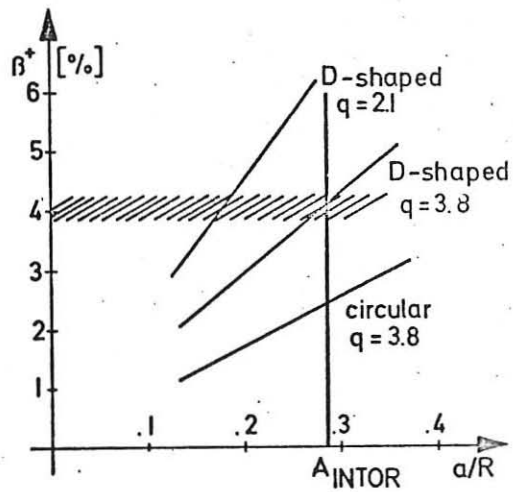


Fig.4.

β^+_{max} as it results from PEST-code (see INTOR report) for B = 5.5 T.

$\beta^+ \simeq 1.3 \langle\beta\rangle$

It yields

$\langle\beta^{theory}_{INTOR}\rangle \simeq 3$ %

for q = 3.2.

Fig. 4 shows the results obtained with the PEST code. Probably, the essential results are not the absolute values achieved for ß, but the gain when going from circular to D-shaped cross-sections or from high- to low-q-operation. INTOR is using these factors and aims at D-shape, low-q operation.

Experiments in T-11, ISX-B, JFT-2, TOSCA have reached ß-values of 2.5 % for circular plasmas. If the transition to D-shaped plasmas and low-q operation hold their promise, then $ß_{INTOR}$ = 5.6 % is a reasonable assumption. But experimental verification of these trends is urgently required.

5) Disruptions

Disruptions are potentially dangerous to the device for their electromagnetic effects, their thermal effects causing a melting of the wall surface, and the large forces exerted to the structure of the device. There are several cases which have to be considered in this connection:

- During the plasma current rise resonances are moving through the profile leading to bursts of kink-like perturbations connected with losses of bits of plasma energy. These losses can be kept in bounds if the current rise is not too fast.

- After having reached the current plateau, internal relaxations might occur, connected with fluctuations of all plasma parameters, mainly of T_e. These fluctuations typically contribute with 10-20 % to the energy losses which is considered acceptable.

- At high density, tearing modes might lead to the formation of islands causing short-circuits of part of the confinement space.

- Minor disruptions with bursts of perturbations of the poloidal field were observed to cause energy losses of up to 30 % in T-11 and 10-20 % in TFR. Particularly if the higher figure were true, measures would have to be taken against these modes, perhaps by feed-back heating.

- Major disruptions lead to sudden losses of 50-70 % of the plasma energy so that plasma current and equilibrium are difficult to maintain. They occur when q(a) gets too low or n_e too high with the threshold depending on the impurity concentration. The density limit could be increased during the last years from $5 \cdot 10^{19} \frac{B_o}{R}$ to $9 \cdot 10^{19} \frac{B_o}{R}$ in PDX with neutral injection (N.I.). This value is still a factor of two short with respect to the INTOR needs.

The particular hazard to the machine made it necessary to develop a characterization of major disruptions for engineering purposes. After long and deep study of all the available information, the following characterization was formulated: 30 % of the plasma energy will go uniformly to the first wall and the other 70 % to 30 % of the wall surface, mainly the inboard part of the wall, with a peaking factor of two. The total energy dissipated is 220 MJ for β = 5.6 % and the decay times for both current and energy are 20 ms. The disruption occurrence will not exceed $5 \cdot 10^{-3}$ during stage I (less than every 200th discharge) and 10^{-3} during stages II and III. Such disruptions still lead to a melting of the wall surface and can have decisive influence on the lifetime of the machine. It is therefore clear that experiments on disruptions are urgent. These should include the investigation of the disruption scenario and its dependence on the discharge parameters.

6) Vertical position control

Stability of the vertical plasma position would require a conductive shell at a distance of not more than 30 cm from the plasma surface. Active feed-back control, on the other hand, should not aim at time constants less than 50 ms if the power required should not become excessive because of the fields having to penetrate through the massive blanket and structure. A full conducting wall is certainly not possible because maintenance and assembly conditions require easy access to the interior. Also the breeding efficiency would be unduly reduced by additional neutron absorption in such a wall. The solution selected is a 12 section loop system built into the first wall as shown in Fig. 5.

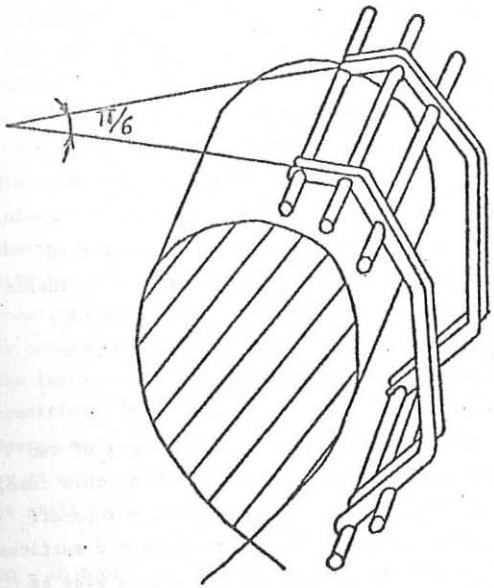


Fig.5. Vertical position control unit.

This should give the required short term stability, should not unduly interfere with the maintenance system and yield an acceptable time constant for the active feed-back system. But further, more detailed studies are necessary on the efficiency of this system.

7) Plasma edge and divertor

Plasma edge and divertor are setting an essential part of the boundary conditions to the plasma. Transport of heat and particles, extraction of thermal power and ashes occurs via the plasma edge. The reactions of the wall in providing recombination, in getting eroded by sputtering and, hence, becoming a source of impurities, in getting hot, requiring cooling and experiencing stresses from temperature gradients are all determined by the plasma edge conditions. High power densities at not too high edge plasma densities lead to high erosion rates. The only choices one has are either to provide for large areas - and there are limits to that - or to consider a frequent exchange of heavily loaded surfaces. From these thoughts preference was given to a divertor.

Local divertor schemes like the bundle divertor were studied first, but it was found very difficult to achieve compatibility with the other

reactor requirements. The poloidal divertor, on the other hand, just allowed the creation of conditions for the lifetime of the first wall to approach the projected lifetime of INTOR.

Single and double null divertors have distinct differences. In a double null divertor, both null points lie on the same separatrix thus completely disconnecting the inner and outer scrape-off layers. Since the main loss flux is in the outward direction, it can be assumed for the inside scrape-off layer to be rather thin which would allow the location of the plasma rather close to the inside wall in the high field region. All this is positive. A disadvantage connected with this system is that it needs twice as many divertor modules which makes their handling more difficult.

For a single null divertor it is probably again the outer part of the scrape-off layer which is determined by the loss flux. But in this case, the poloidal magnetic flux has to be the same in the whole scrape-off layer, and as a result of the finite beta shift of the magnetic surfaces, the inner part of the scrape-off layer becomes three times as wide as its outer part and is thus occupying expensive space in the high-field region. Nevertheless, this arrangement was chosen for INTOR since it allows the usage of the upper region for a tritium breeding blanket for reducing the request for tritium supply and since it promises an easier maintenance with only one set of divertor modules.

The special requirements for INTOR to have all PF coils arranged outside the TF coils allows only small curvatures of the magnetic lines and thus leads to a relatively open configuration so that practically the divertor plates are part of the discharge chamber. At first glance, this looks disadvantageous but, at second glance, this reveals rather interesting properties.

There are three rather stringent input conditions to the plasma edge and the divertor physics: (i) The α-power to be removed from the plasma is P_α = 124 MW leading to an average power flux across the separatrix

of $\langle Q_{th} \rangle = 0.37\ MW/m^2$. (ii) The helium production rate connected with this power flux and thus the helium exhaust flux is $\Gamma_{\alpha,ex} = 2.2 \cdot 10^{20} s^{-1}$. (iii) The average density in the discharge for producing this power is $\langle n \rangle = 1.4 \cdot 10^{20} m^{-3}$. The conditions in the scrape-off layer and the divertor have to be compatible with these numbers.

Since the INTOR Phase-Zero Report was written, a great amount of new information came up from ASDEX, PDX, and T-12 for separate divertor chambers, from DOUBLET III for a relatively open geometry, and from DITE for a bundle divertor. For edge densities of $0.2 < n_{edge} < 5 \cdot 10^{19} m^{-3}$ these results yield a width of the scrape-off layer of about 2 cm which is compatible with a Bohm diffusion coefficient of $D \approx 1\ cm^2 s^{-1}$ within the layer. The edge temperatures were between 10 and 50 eV under these conditions, but the full parameter dependencies are still unknown. Operation of the divertor as a magnetic limiter reduces metal impurities by an order of magnitude but the divertor action on low-Z impurities is still open.

20 - 40 % of the power is usually found to be radiated to the first wall, the rest going to the divertor chamber. There, 30 - 70 % of it is deposited on the divertor plates, with the remaining part carried to the chamber walls by radiation and charge exchange. Also, a high recycling rate is observed within the scrape-off layer with recycling factors of up to 2 - 4.

There is a strong increase of the neutral density in the divertor chamber and factors of 50 have been observed for the ratio of the neutral densities in the divertor chamber and at the limiter. This factor increases with increasing plasma density, indicating that the plasma is very efficient in plugging the divertor throat and that the back flux of neutrals is small. Further, an impurity accumulation is found near the divertor plates, with the ratio between divertor gas density and plasma ion density increasing with atomic number.

Comparisons between single and double null divertor operation in ASDEX and PDX have shown that the loss flux is mainly going in outside direction, yielding a ratio of the fluxes to the outer and the inner divertor plates of 4:1 in double null operation and about 1:1 in single null operation where the tendency towards pressure balance along the lines of force drives part of the flux via the inner part of the scrape-off layer to the divertor plates.

These experimental results, although obtained for power fluxes and plasma densities much smaller than conceived for INTOR, now allow a rather realistic modelling of the plasma edge to be started. Physics arguments clearly favour the double null divertor, but the strong engineering arguments, like having to deal with only half of the divertor modules, achieving easier maintenance conditions, having more space

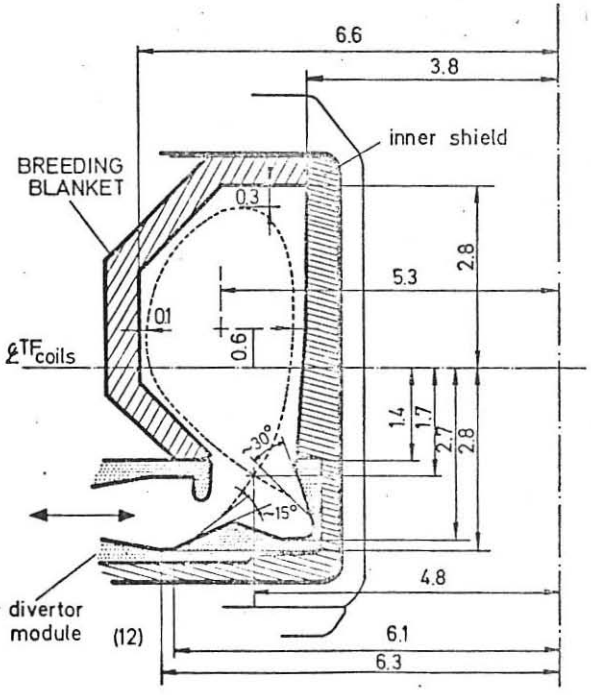


Fig.6. Removable divertor module, the dotted line indicating the separatrix which is the inner limitation of the scrape-off layer.

available for tritium breeding thus also achieving a higher reactor relevance as a whole, were rated higher than the physics arguments and led to the selection of a single null poloidal divertor for INTOR.

Fig. 6 shows a sketch of the INTOR divertor module with a divertor plate surface of 75 m^2 designed for "easy" replacement and carefully shaped to keep the power flux densities in acceptable limits.

As standard case for INTOR operation, a high edge density of $5 \cdot 19^{-19}_{m}{}^{-3}$ and an edge temperature of about 100 eV were selected which should be achieved by shallow fuelling. This should lead to a power load to the divertor of 80 MW, composed of 70 MW carried to the divertor plates by ions and electrons with an equal share, 5 MW charge exchange occurring in the divertor chamber and 5 MW radiation. Under such conditions, both the penetration depth of neutrals and the diffusion length across the scrape-off layer are about 3 cm in length so that an outboard distance between separatrix and wall of 10 cm should be sufficient for forming a cool protective layer.

Fig. 7 shows results of plasma edge modelling. Ionization processes in regions of still high enough plasma temperature lead to a sheath of rather constant plasma density thick enough to shield the plasma core from a large fraction of the impurities originating from the chamber wall. The resulting DT flux to the outboard di-

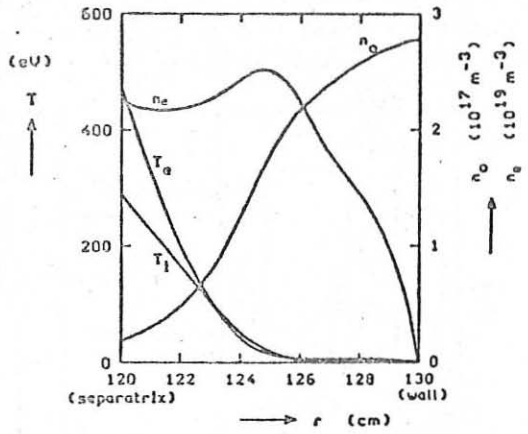


Fig.7. Plasma edge conditions.

vertor plates is about $5 \cdot 10^{23} s^{-1}$ and the He flux about $2.5 \cdot 10^{22} s^{-1}$ for a relative He concentration of about 5 %. Comparing the latter figure with a plasma He production rate of $2.2 \cdot 10^{20} s^{-1}$ leads to a pumping speed of $2 \cdot 10^5$ 1/s for a divertor density of about $10^{19} m^{-3}$, which sounds very acceptable.

For arriving at an acceptable plasma-wall interaction, it is very important to meet such operating conditions. They would allow a stable burn and a sufficient lifetime of the first wall, long enough maintenance periods for the divertor and thus a higher availability of the machine as a whole. Large efforts went already into modelling of the plasma edge and resulted in the good prospects described. But this vigorous research effort must continue in order to put the predictions on a more reliable basis.

8) INTOR operating scenario

Fig. 8 shows the envisaged INTOR operating scenario and the time dependence of the loop voltage, the average density, the plasma current, and the electron temperature, in particular. The scenario can be broken down into four phases, start-up, burn, shut-down, and dwell, each of which will be delt with separately.

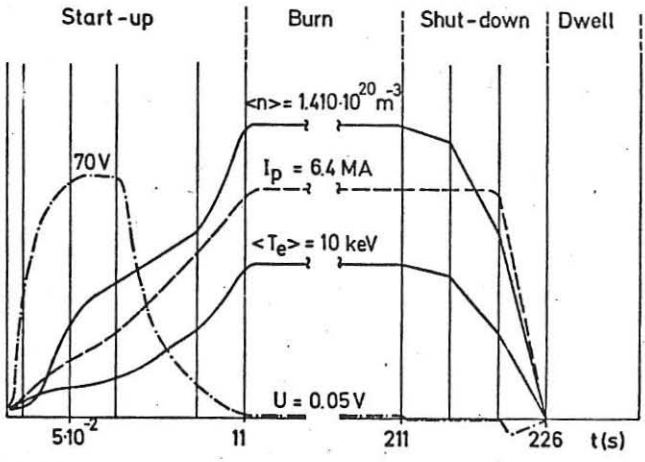


Fig.8. INTOR operating scenario.

a) Start-up

Plasma break-down will take about 140 ms. In order to be compatible with the superconducting coils, it is essential to limit the flux variation in the OH-transformer, and thus the loop voltage. Experiments have shown that an electric field of $1 - 2.5 \frac{V}{m}$ is sufficient for break-down if the initial gas pressure is between 1 and $3 \cdot 10^{-4}$ torr and the stray magnetic field smaller than 0.2 % of the toroidal field. 70 V maximum loop voltage is therefore selected for INTOR. The initial power losses are mainly via radiation (70 %) and charge exchange (20 %). The inclusion of 5 - 10 MW ECRH is proposed for assisting the fast penetration through the radiation barrier. ECRH was selected for this purpose because of its localized power deposition with bulk heating of the electrons and the prospect of no extra generation of impurities.

The current rise from zero to 5.4 MA is estimated to take about 5 s. In order to avoid minor disruptions and the connected energy losses during this phase, and to allow the proper current profile to develop, $\dot{I}$ has to be kept smaller than I/τ_{skin} or at $6 \cdot 10^6$ A/s for $I \leq 0.6$ MA and at $1 \cdot 10^6$ A/s for $I > 0.6$ MA. In order to meet the power balance, $\langle n \rangle$ has to be risen linearly to $5 \cdot 10^{19} m^{-3}$. An impurity density of $n_{ox} = 2 \cdot 10^{17} m^{-3}$ and $n_{Fe} = 5 \cdot 10^{16} m^{-3}$ is tolerable and sufficient for plasma edge cooling. There is no divertor action during the early start-up phase. During this phase, limiter strips of 1 m width at the upper and lower outboard side have to take up the loss power of 10 MW with a power density of 0.3 MW/m^2 and a peaking factor of 1.5.

The heating to ignition will then be done during the next 6 s by 75 MW, 175 keV neutral injection. Neutral injection is still considered to be the method of highest predictability. $\langle n \rangle$ will further rise during this phase from $5 \cdot 10^{19}$ to $1 \cdot 10^{20} m^{-3}$ and β from ≈ 0 to 4 %. By flux conservation, this increase in β simultaneously leads to a rise of the plasma current to its final value of 6.4 MA which, at the same time, is a method least sensitive to skin currents. At the start of neutral injection, beam shine through will lead to a bombardment of the opposite wall by about 1 MW/m^2. As the density rises, shine through will disappear but beam ripple losses will start to occur. These have been delt with already under 3).

b) Burn phase

A controlled plasma burn at a temperature of 10 keV is intended for 100 to 200 s. Burn control by variation of the toroidal ripple might be too difficult to achieve since a fast response with seconds time constant would be required. Also, a selfstabilizing by the plasma-ß shift into regions of higher ripple is considered too weak or too space consuming. The same might be true also for feed-back stabilization by compression and decompression in combination with additional heating. On the one hand, this would have been a method well understood and applicable by using existing components, perhaps with some upgrading. But on the other hand, it might turn out to be too expensive to provide the additional 10 cm space around the plasma and too difficult to keep the separatrix in space according to the divertor requirements. Therefore, finite-ß control, if feasible, will still be the optimum burn control.

The INTOR operating scenario makes the essential assumption that a plasma current profile optimal for stability can be created during start-up and then will persist during the full burn time because the skin time under INTOR conditions will be 1000 s, i.e. five times longer than the anticipated burn time. Experimental confirmation of such slow current diffusion at high plasma temperature is urgently needed.

c) Shut-down

The shut-down phase should be as fast as possible but without increase of the heat flux to the wall and without triggering disruptions which, perhaps, can only be avoided by the inclusion of a proper control scheme. The burn termination could be initiated by a stop of the fuelling and a step-back to the OH-regime during 10 s. Injection of impurities is an additional idea but probably not wanted because it requires a fast cleaning process afterwards and might rise the probability for the occurrence of disruptions.

The current ramp-down is intended in 5 s by applying a reversed loop voltage. Although the L/R-time is 15 s under these conditions, a reduction of this time to 5 s seems to be feasible. Sufficient current

penetration is still expected and no excessive generation of run-away electrons.

d) Dwell phase

20 s are reserved for this phase. During this time, the chamber has to be pumped down to about $3 \cdot 10^{-5}$ torr ($\hat{=} 2 \cdot 10^{18}$ m^{-3}) so that the proper gas composition can be reestablished for the next pulse. At the end of the dwell phase, the gas release from the walls, from traps, and from large remote surfaces through perhaps narrow gaps has to be down to 1/30 from the burn value, i.e. to $\approx 10^{18}$ $m^{-2}s$. This is so because with D coming from neutral injection, a 50 % DT mixture just at the ignition time could only be reached if one started from a pure T gas and had no other D sources. Computer models indicate that a dwell time of 20 s should be reasonable if the wall temperature is kept above 200 C.

CONCLUSIONS

It was the main task of the INTOR physics group to work out plasma confinement conditions which allow the selection of reasonable engineering solutions for the construction of the device, and also lead to acceptable operating scenarios coupled with the achievement of a sufficiently high reliability. During phase I of the INTOR workshop, a workable conceptual design for INTOR could be developed with positive answers to all these points. There are, however, some items where better solutions could be applied if their feasibility were demonstrated. This led to the definition of a number of short-term R & D topics which should allow essential improvements of the INTOR concept if sufficiently positive results occur in time. Important examples in the field of physics are the following:

- Beta limit scaling with triangularity and asymmetry
- High density divertor operation
- Atomic data for the plasma edge
- Ripple induced hot ion and thermal ion transport model tests

- Characterization of disruptions
- Low voltage start-up
- Vertical position control theory
- Pellet fuelling studies
- RF heating modelling and tests.

In the meantime, INTOR was moved into phase IIa which will deal with the analysis of critical issues. In this connection, it is of particular importance that the above topics will be picked up immediately by those experiments which are particularly suited for tackling them. If this will happen and if the support by the home bases will remain as strong as it was, then the INTOR team is convinced that also phase IIa will be finished in time with an INTOR reference design developed on the bases of results coming from the worldwide fusion programme.

REFERENCES

INTOR Group, "International Tokamak Reactor - Phase I", IAEA, Vienna, to be published. (See there for further references).

ACHIEVEMENTS AND PROBLEMS OF RELATIVISTIC HIGH FREQUENCY ELECTRONICS

A.V.Gaponov, M.I.Petelin, V.A.Flyagin
Institute of Applied Physics, Academy of Sciences of the USSR, Gorky, USSR

Let us begin with explanations, why this report on the high-power high-frequency electronics is included in the program of the conference on controlled fusion and plasma physics. There are two reasons: first, the electronics is the nearest relative to the plasma physics and these two sciences always interchange ideas; second, the electronics supplies the plasma physics with sources for heating and diagnostics.

Now, why is this report restricted to the relativistic branch of electronics? As a matter of fact, increasing the electron energy up to relativistic magnitudes, the HF electronics can both escalate the radiation power and broaden the frequency diapason [1].

Practical attempts to use relativistic effects for producing the coherent (stimulated) radiation of electron beams began in the late fifties, when some theoreticians [2-6] (mostly plasma physicists) noticed, that nonequilibrium ensembles of electrons gyrating in the magnetic field can amplify electromagnetic waves due to relativistic dependence of the gyrofrequency (cyclotron frequency) on the electron energy. Among numerous versions of devices based on this effect (cyclotron resonance masers), the most viable at weak-relativistic electron energies

proved to be the gyrotron [7] . Now it delivers the highest output radiation powers in cw and long pulse regimes at mm and sbmm waves.

A new impact to the relativistic electronics was given in the late sixties by the advent of high-current electron accelerators. Now various types of HF generators driven by such accelerators provide the highest short pulse powers at cm, mm and sbmm waves [1,8-11] .

And, at last, in the middle seventies, using an "ordinary" linear accelerator with a very high repetition rate, it became possible to create a generator of infrared waves - the free electron laser [12] .

This survey deals with HF generators driven by both mildly- and strong-relativistic beams+).

The (mildly-relativistic) gyrotron

The simplest theoretical model of the cyclotron resonance maser is the LC-circuit, where the capacitor contains a beam of electrons gyrating in the homogeneous sta-

+) Though the survey is devoted to the stimulated collective radiation of intense electron beams, it is worth noting that the individual radiation of ultrarelativistic particles under certain conditions can be narrow directed and concentrated in a narrow frequency band as well. The latter is valid, in particular, for ultrarelativistic electrons and positrons channeled in crystals [13] . This method realized at 1-10 GeV accelerators has already allowed to produce X-rays with 10^{-2} - 10^{-3} A° wavelengths [14-16] .

tic magnetic field and forming, in the initial state, a stationary ring (Fig. 1a). Let the electron gyrofrequency

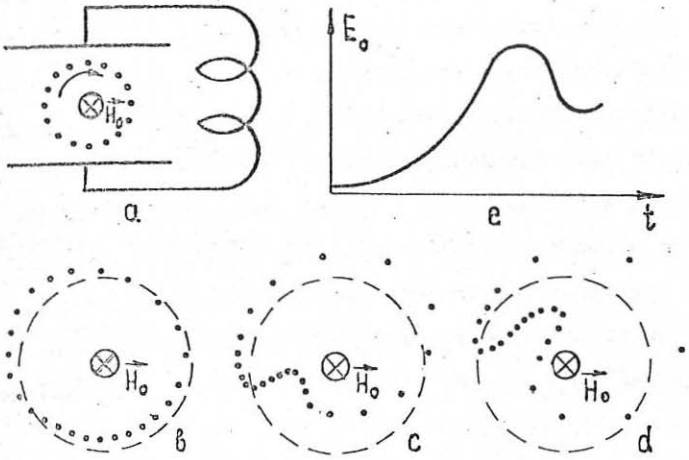


Fig. 1. Cyclotron resonance maser: a - scheme, b,c,d- - modulation, bunching and deceleration of electron ring by HF field, e - HF field vs time.

$\omega_H = e H_0/mc$ be close to the eigenfrequency of the LC-circuit $\omega_0 = c/\sqrt{Lc}$. Evolution of the electron ring under this resonance condition is shown in Fig. 1, b,c,d. The primary electromagnetic "fluctuation" disturbs the electron energy so, that the latter increases for electrons situated in accelerating phase and decreases for electrons situated in decelerating phase. The variation of electron energies results in the change of their masses and gyrofrequencies (the relativistic effect !). Due

to the difference in gyrofrequencies, electrons begin to gather in a bunch. This bunching of inertial type is similar to that in the ordinary travelling wave amplifier. As the bunch arises in the decelerating phase, the electron energy is transferred to the HF field and the latter increases (Fig. 1e). According to numerical calculations (the electron-HF field interaction in the model is described by the same equations as in the cyclotron resonance travelling wave amplifier [17]), the efficiency of the "device" shown in Fig. 1a amounts up to 70%.

A practical version of cyclotron resonance masers, most popular at present, namely the gyrotron is shown schematically in Fig. 2. Electrons leave the axisymmetric

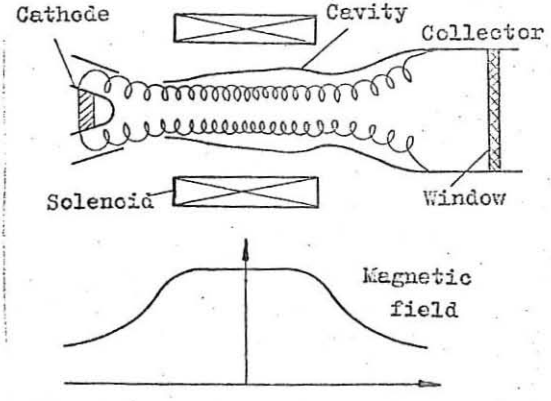


Fig. 2. Gyrotron

magnetron-injection gun and enter the magnetic field increasing in the direction of the interaction space. In the increasing field the electron flow undergoes compres-

sion and the electron gyration momentum grows according to the adiabatic invariant $P_\perp^2/H = \text{const}$ (compare with motion of particles in plasma magnetic traps). Then electrons enter the open quasi-optical cavity resonator, where the static magnetic field is uniform (or slightly nonuniform) and so the cyclotron resonance interaction between the particles and the HF field takes place. Escaping the cavity, the electrons move in decreasing (decompressing) magnetic field and settle on walls of the output waveguide. Such devices using high voltage electron guns with high compression and cavities with dimensions greatly exceeding the radiation wavelength, are able to gain high powers at all frequencies, at which the cyclotron resonance condition (1) can be satisfied by magnetic fields available.

The power of mildly-relativistic gyrotrons in the cw regime

wavelength(mm)	power(kW)	origin
0.92	1.5	[7]
2	22	[7]
10	200	[18]

and in the long pulse regime

wavelength(mm)	power(MW)	pulse duration(s)	origin
3.0	1.1	10^{-4}	[7]
6.7	1.25	$3\ 10^{-5}$	[7]

is 10 - 1000 times greater than that achieved by other

HF sources at the same wavelengths.

For the mm wave gyrotrons 30-40% efficiencies are ordinary. At cm wavelengths efficiencies are higher (the highest efficiency obtained in a gyroklystron amplifier was 70% [7]), but the output power of the cm gyrotrons is lower than that of conventional HF generators in the same range.

Recently, at "T-10" tokamak, for plasma heating, a complex of gyrotrons was mounted, each of them delivering 200 kW in a 0.1 s pulse at 3.5 mm wavelength, the radiation being linearly polarized and concentrated in 4°angle.

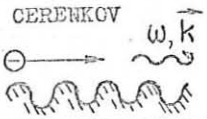
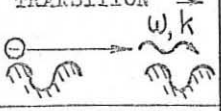
For the sake of plasma diagnostics, a 0.6 mm 20 kW gyrotron with pulsed magnetic field is elaborated with pulse duration equal to 10^{-4}s.

HF generators driven by high-current accelerators

The high-current accelerators suggest to the high-frequency electronics 10^4 - 10^6A beams of electrons with 10^6 - 10^7 eV energies in 10^{-8}s pulses. The theory [1] seems to have analyzed all possible methods to convert the energy of such beams into microwave radiation. All synchronisms (Cerenkov, transition bremsstrahlung, wave scattering - Table I) between electrons and electromagnetic waves, all mechanisms of electron beam bunching and all kinds of the feedback have been considered using the simplest theoretical models.

Of course, each HF generator with relativistic e-beam has its more or less close analog among devices with non-relativistic electron energies (so it is reasonable to

Table I

TYPE OF STIMULATED RADIATION	HF DEVICES
CERENKOV 	TWA, BWO OROTRON MAGNETRON
TRANSITION 	MONOTRON KLYSTRON TWYSTRON
BREMSSTRAHLUNG 	CYCLOTR. MASER SYNCHROTR. GEN. UBITRON
SCATTERING 	PARAMETRIC DEVICES (SCATTRON)

call relativistic HF generators mostly by "old" nonrelativistic names - Table I). However, for all relativistic HF generators, laws governing the choice of optimal parameters are, naturally, quite different from those for nonrelativistic ones [1]. For instance, in the Cerenkov devices, the optimum magnitude of the synchronous (longitudinal) wave field component increases proportionally to the root of electron energy, if the latter is nonrelativistic, and decreases inversely to the electron energy, if the latter is ultrarelativistic.

If parameters of a HF generator are optimum, its efficiency, in principle, can be tens per cent at any high electron energy (see the following Table concerning the simplest theoretical models [19,1]). Of course, if the optimum parameters are not accessible, the efficiency decreases. Among the unfavourable factors are the electron ve-

Table II. Theoretical efficiency for HF devices at ultra-relativistic electron energies

Type of stimulated radiation	Synchronism	Type of generator (amplifier)	Efficiency %
Cerenkov	$\omega = k_{\parallel} v$	TWA	30
		BWO	15(45)
		orotron	23,5
		magnetron	100(asympt)
transition	$\omega \approx k_{\parallel} v$	monotron	22
		twystron	58
bremsstrahlung	$\omega \approx k_{\parallel} v$	synchrotron generator	10
	$\omega = k_{\parallel} v \pm \omega_H$	cyclotron autoresonance maser	20
	$\omega = (k_{\parallel} + \bar{k}) v$	ubitron	25
wave scattering	$\omega - \omega_i = (k_{\parallel} + k_i) v$	scattron	10

locity scatter, the HF discharge and, at short waves, difficulties of obtaining electron beams of sufficient density.

Now the output powers of HF generators driven by HC accelerators (Fig. 3) are 10-100 times above the level obtained by the "conventional" ("thermocathode") electronics. At dm and cm waves dominate Cerenkov generators, namely,

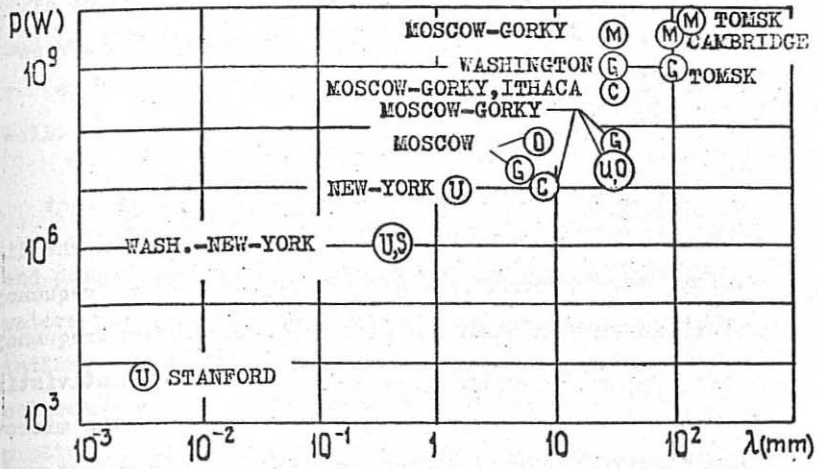


Fig. 3. Pulse powers of HF generators driven by high-current and high-repetition-rate accelerators: C - carcinotron, M - magnetron, O - orotron, G - gyrotron, U - ubitron, S - scattron.

the BWO and the magnetron with powers of 10^8 - 10^{10}W and efficiencies of tens (up to 30 - 40) per cent [1,9,20]. At mm waves Cerenkov devices share records with bremsstrahlung ones: the maximum efficiency obtained with a gyrotron at 7.5 mm is 7% [10], the maximum power obtained with an orotron at 9 mm is 70 MW [11]. At sbmm waves the bremsstrahlung and wave scattering generators (the ubitron and the scattron) deliver 1 Mw with 0.1% efficiency [21,22].

Most generators produce 10^{-8}s single pulses. At the same time, some generators driven by HC accelerators operate with 10^{-6}s duration pulses (namely, a magnetron [23]

and a BWO described in the report by N.I.Zaitsev et al. at this conference) and one (BWO) does with 100 Hz repetition rate [20].

Free electron lasers

One of relativistic effects consists in the fact that relativistic electron oscillator radiates in the direction of its translational velocity wave with frequency $\sim\gamma^2$ times greater than the electron oscillation frequency (here γ is the Lorentz factor); it is the relativistic Doppler effect, which was suggested for use in the microwave electronics by V.L.Ginzburg [24]. This effect was successfully exploited in an ubitron (Fig. 4), which was

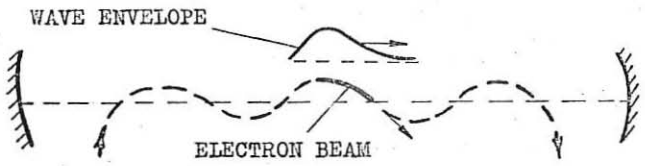


Fig. 4. Free electron laser - ubitron generating IR radiation.

driven by a linear accelerator delivering 2,6 A, 4 10^{-12}s pulses of 43 MeV electrons with 120 MHz tact frequency. The ubitron produced 7 kw peak power with 0.006% efficiency at 3.4μ m wavelength [12]. The latter belongs to the infrared band, so the device is called laser. As far as this laser is based on the stimulated radiation of classical particles, it is called the free electron laser (FEL).

Let us note that since the 0.4 mm wavelength obtained in [21,22] (see above) also belongs to the infrared range, corresponding generators may be called lasers as well.

Problems of increase in power and frequency

The tendency for future increase in frequency, power and pulse duration of the relativistic electron HF generators meets problems of intense electron beam transportation, high frequency discharge elimination, cathode and collector plasma drift suppression, etc. Most of these problems loosen, if space-developed quasi-optical electrodynamic systems are used. This possibility was discussed in [19,25,1] and has already been realized in some experiments [7,10,11,12,26].

Progress in the field strongly depends on development of methods which would provide steady (reproducible) generation of a single monochromatic mode or, at any rate, generation of a set of modes with characteristics steady in the statistical sense. Accordingly, the problem has two aspects: 1) linear selection of modes, 2) nonlinear interaction (including competition and cooperation) of modes.

Linear selection of modes. To provide the single mode operation with high efficiency, it is sufficient (though not necessary) that the optimum current of the working mode is less than start currents of all other ("parasitic") modes. Let us mention the main approaches to the problem.

In HF generators electron beams of high intensity are usually transported along metallic surfaces (in most cases within metallic tubes) playing role of waveguides. If the cross-section of such a waveguide is much larger than the intended wavelength, waves able to be in synchronism (resonance) with electrons

$$\omega - k_{\parallel} v_{\parallel} = s\Omega \qquad (s = 0, \pm 1, \pm 2 \ldots) \qquad (1)$$

compose spectrum of high density. Let us note, however, that in the general case these waves, even having close frequencies ω and propagation constants $k_{\parallel}$ (at a fixed s-th harmonic of electron oscillation frequency Ω), differ in group velocity $d\omega/dk$ and transverse structure. These factors discriminate competing modes and can be used to provide the single mode generation.

The lower is the group velocity, the higher is the wave radiation resistance with respect to the electron current. Besides, the low group velocity waves reflect from very small irregularities of the waveguide. So, the electron beam prefers to interact with modes close to the cut-off.

As the simplest example of the sort we may consider the gyrotron [7,17] (Fig. 5). In this case the near-cut-off modes of a cylindrical waveguide, according to the Brillouin concept, are composed of rays almost perpendicular to metallic walls. So the electrodynamic system is equivalent to the two-mirror resonator, where any mode composed of rays steeply inclined to the mirrors is of poorer quality than the operating (near-cut-off) mode.

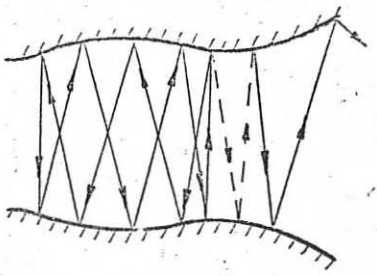


Fig. 5. Side view of rays composing operating mode of gyrotron.

Resonators of the sort are used both in weak-relativistic [7,17,18] and relativistic [10,26] gyrotrons and can be used in all generators based on the stimulated bremsstrahlung radiation when $S > 0$ in (1) and on the wave scattering.

To realize the described regime in the Cerenkov generators, one should add to the near-cut-off wave a slow space harmonic synchronous to electrons. This can be done by corrugation of metallic walls. Azimuthal corrugation is used in relativistic magnetrons with diffraction output of power [9], longitudinal one in orotrons at both nonrelativistic [27,28] and relativistic [11] electron energies.

Let us note that as a result of longitudinal corrugation, each mode in addition to "usual" (lowest) attenuation band acquires higher attenuation bands caused by the Bragg reflection and by the Bragg scattering in other

modes of the "initially" smooth waveguide (Fig. 6). At

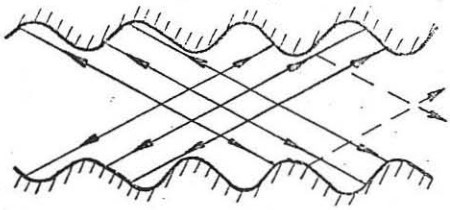


Fig. 6. Rays composing high-quality mode of corrugated resonator under Bragg reflection regime.

cut-off frequencies separating pass and attenuation bands, the group velocity of eigenmodes of the corrugated waveguide is zero. A section of such a waveguide has resonant modes with eigenfrequencies close to the cut-off frequencies (If the corrugation is slightly nonregular, the eigenfrequencies may occur within the attenuation band).

The phase velocities of partial waves composing the eigenmodes in the Bragg reflection resonators can be close to and even less than the light velocity (the latter is possible, if the corrugation is deep enough). So such resonators are attractive for use in mm and sbmm wave generators, nemely in dopplertrons (free electron masers and lasers) and in Cerenkov devices.

In the extended interaction space generators, along with discrimination between modes differing in longitudinal field distribution, one ought to discriminate modes differing in transverse structure. Owing to the latter difference, the coupling of modes with electron beam is

not equal.

For example, in the axisymmetric gyrotron (Fig. 7)

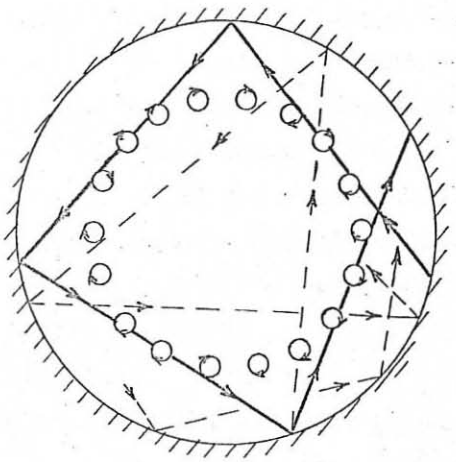


Fig. 7. Electron flow and rays composing operating (solid lines) and "parasitic" (dotted lines) modes in cross-section of gyrotron.

the coupling is strongest for a mode composed of rays tangent to the electron flow. For other modes either rays are out of the flow (so the electrons move in a relatively weak field) or the effective volume of the HF field is too large (so the normalized electron density is relatively low). This consideration agrees with dependence of the coupling coefficient [17]

$$L = \frac{J^2_{m-s}(\nu_{mp} R_б / R_р)}{\nu^2_{mp} - m^2} \qquad (2)$$

on the flow radius $R_б$, the resonator radius $R_р$, mode azimuthal index m and ν_{mp}, which is p-th root of

equation $J'_m(\nu)=0$, $J_m(\nu)$ is the Bessel function.

If the radius of the electron flow is close to that of the resonator and the both are large enough compared with the wavelength, the mode of the strongest coupling is a mode of whispering gallery $(m>>p)$. Of course, the same is valid for axisymmetric generators of all types. Note, that in the axisymmetric orotron [29] electrons interact not with the "main" field, but with the slow harmonic pressed to walls; the electron-wave coupling is determined by expression [30]

$$\frac{|E_{\parallel}|^2}{P}=K\frac{2\ell^2}{k_{\parallel}cR_r^2}\frac{I^2_{m-s}(\varkappa R_e)}{I_{m-s}(\varkappa R_r)}, \qquad (3)$$

where for E-modes $K=(k_{\perp}^2+\bar{k}k_{\parallel})^2/k$, for H-modes $K=\bar{k}^2km^2/(\nu^2_{mp}-m^2)$; $E_{\parallel}$ is longitudinal electric field, P is wave power, $I_\ell(x)$ is modified Bessel function, $\varkappa=k/\gamma\beta$, $\beta=v/c$, $k_{\perp}$ is o-th space harmonic transverse wave number, d, ℓ and S are (helical) corrugation period, amplitude and azimuthal index.

The whispering gallery regime is used in high-power mildly-relativistic gyrotrons, where the single mode operation is provided, using resonators with diameters up to 15λ, the modes possessing azimuthal indexes up to 30. Of course, breaking the axial symmetry of a gyrotron, one can provide excitation of a bulk mode. By this method, in relativistic gyrotrons described in [10,26], TE_{13} mode was obtained.

Cerenkov excitation of a whispering gallery mode, namely TE_{51} (with rotating structure), by a relativistic

electron flow in a section of corrugated axisymmetric waveguide was observed under the near-cut-off regime in the Institute of Applied Physics, the wavelength being 3 cm, the output power some tens megawatts. As for the experiment with mm wave axisymmetric relativistic orotron [11], where excitation of E_{07} mode was reported, it seems likely, that the nature made an exception from her rules.

In some cases effective mode selection can be achieved using absorption of parasitic modes by the electron beam itself. For instance, N.F.Kovaljov noticed that in the Cerenkov generators, where the electron beam is directed by the homogeneous magnetic field, the absorption owing to cyclotron resonance between electrons and the main (o-th) space harmonic of the wave

$$\omega - k_{\parallel}^{\circ} v = \omega_H$$

depends on transverse structure of modes.

It is worthy of remark that the near-cut-off HF generators saturate at relatively low electron currents. Therefore, possessing high-current electron beams, it is expedient to use their interaction with waves of high group velocity. In generators of the kind, to provide the mode selection, most attractive are diffraction methods [1,19].

A simple illustration of the methods was suggested by N.F.Kovaljov (Fig. 8): a band stream of ultrarelativistic $\gamma >> 1$ electrons penetrating the space between two close parallel corrugated metallic bands (corrugation

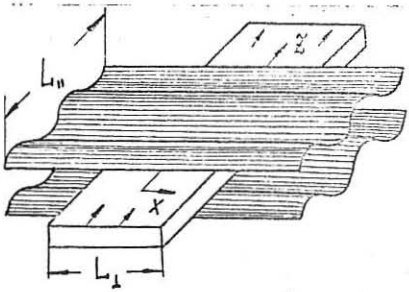


Fig. 8. Backward wave oscillator with diffraction selection of modes.

of the walls can be changed for that of the stream). The complex envelopes of wave field (F) and alternating current (J) obey equations

$$i\frac{\partial^2 F}{\partial \xi^2} + \frac{\partial F}{\partial \zeta} - i\delta F = iI(\xi)f(\zeta)J, \qquad \frac{\partial^2 J}{\partial \zeta^2} = -f(\zeta)F, \tag{4}$$

$F(\xi,\zeta_K) = 0$, $J(\xi,0) = 0$, $\partial J/\partial\zeta\big|_{\zeta=0} = 0$ and radiation condition for F at $\xi \to \pm\infty$. Here $\zeta = (\omega/2\gamma^2 c)z$, $\xi = (\omega/e\gamma)x$, $I(\xi)$ is normalized stationary current, $f(\zeta)$ is normalized radiation resistance, δ is proportional to difference of electron and light velocities. Taking $f(\zeta)$ in the "klystron" form $f = \delta(0) + \delta(L_{\parallel})$ one easily obtains dependence of start currents of various modes on the Fresnel parameter $C = 4L_{\perp}^2/\lambda L_{\parallel}$. If the parameter does not exceed 1, the start current of mode with single x-variation is at least 1.81 times lower than that of the mode with two x-

variations.

Nonlinear competition and cooperation of modes. It is convenient to begin the analysis of this problem with investigation of stability of the stationary single-mode generation with respect to excitation of other modes situated in the same synchronism band. In the generator with high-Q resonator this process can be reduced to superposition of binary interactions of rival modes via the primary (saturated) mode. The elementary interaction may be classified as the four-photon decay, when the energy conservation law allows the primary ("o") mode and the rival ones (" +" and " -") to be connected, if their eigenfrequencies are equidistant

$$\omega_+ + \omega_- \approx 2\omega_0 . \qquad (5)$$

As for the momentum conservation law, in the axisymmetric system, it allows to connect only modes with equidistant azimuthal indexes

$$m_+ + m_- = 2m_0 . \qquad (6)$$

In particular, for the gyrotron (Fig.7) with "klystron" approximation of longitudinal HF field structure $f(z) = \varepsilon\delta(z) + \Delta\delta(z-L)$, where $\varepsilon << A$, the increment p of the perturbation obeys equation

$$\left[p + \sigma_+ - i\delta_+ + i\cos\psi_0 - i\beta_+\frac{R+1}{2}e^{-i\psi_+}\right] \times$$
$$\times \left[p + \sigma_- - i\delta_- - i\cos\psi_0 + i\beta_-\frac{R+1}{2}e^{i\psi_-}\right] = \beta_+\beta_-(R-1)^2 e^{i\psi_- - i\psi_+}, \qquad (7)$$

where δ_i is proportional to $\omega_i - \omega_0$, σ_i is parameter determined by "cold" losses and by losses owing to

the force bunching of electrons, β_i is electron-mode coupling parameter, $R = XJ_1'(X)/J_1(X)$ is the electron bunching parameter proportional to amplitude of the primary mode, $J_1(X)$ is the 1-st order Bessel function, $\psi_i = (\omega_i - \omega_H)L/v_{||}$ +)

If $\mathrm{Re}\, p > 0$, the single mode regime is unstable. In this case, to describe the process in its development, the nonlinear theory is necessary. An adequate method is suggested in [32] and a report by N.S.Ginzburg et al at this conference.

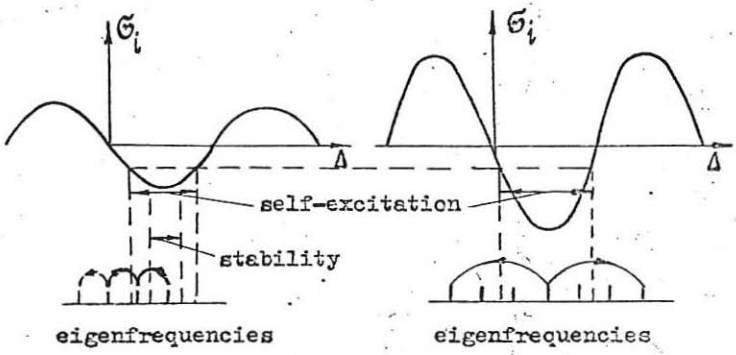


Fig. 9. Effective conductivity due to the inertial bunching of electrons $\sigma_i(\Delta)$ and decay of modes at small (a) and large (b) excesses over threshold; Δ is mismatch from strict resonance (synchronism).

+) In an asymptotic case, when the rival modes strongly differ in the frequency mismatch relative to the primary one, in coupling with electron beam or in the quality, Eq.(7) reduces to that for the single mode perturbation examined in [31].

Briefly, results obtained with Eq.(7) and the nonlinear theory are the following. If excess of electron current over the start value is not very large (Fig. 9a, 10a), competition of modes ends in establishment of a single mode, which eigenfrequency belongs to a stability band. If the excess is large enough (Fig.9b,10b,10c),

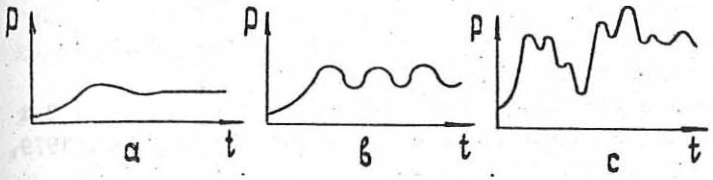


Fig. 10. Output power vs time at small (a), moderate (b) and large (c) excess over threshold.

nonlinear interaction of modes results in automodulation. The latter at moderate excesses over the threshold is periodic (the phase locking of modes - Fig.10b) and at very large excesses stochastic (Fig.10c).

In our report we have discussed only a part of problems being solved by the HF relativistic electronics. Among other problems of great interest in the field is, in particular, utilization of plasma electrodynamic systems [33] . However, we hope, that the deficiencies of our survey will be filled up by original reports presented at the conference.

REFERENCES

1. Relativistic high-frequency electronics, ed. by A.V.Gaponov, Inst.Appl.Phys., Gorky, 1979.
2. Twiss R.G., Austral.J.Phys., 1958, 11, No.4, p.567.
3. Schneider J., Phys.Rev.Lett., 1959, 2, No.12, p.504.
4. Gaponov A.V., Izv.VUZ. - Radiofizika, 1959, 2, No.3; p.450; No.5, p.836.
5. Pantell R.H., Proc. IRE, 1959, 47, No.6, p.1146.
6. Zheleznyakov V.V., Izv.VUZ. - Radiofizika, 1960, 3, No.1, p.57.
7. Andronov A.A., Flyagin V.A., Gaponov A.V. et al., Infrared Physics, 1978, 18, p.385.
8. Granatstein V.L., Parker R.K., Sprangle P., Proc. 3-d Int.Conf. on Electr. and Ion Beams, Novosibirsk, 1979, vol.2, p.715.
9. Kovaljov N.F., Krastelev E.G., Kuznetsov M.I. et al., Pis'ma ZhTF, 1980, 6, No.8, p.459.
10. Voronkov S.N., Krementsov V.I., Shelkov P.S., 4th Int.Conf. on Electr. and Ion Beams, Paris, 1981, abstract 5 p.14.
11. Alexandrov A.F., Galuzo S.Yu., Kanavets V.I. et al., Pis'ma ZhTF, 1981, 7, No.10, p.587.
12. Deacon D.A.G., Elias L.R., Madey J.M.J. et al., Phys. Rev.Lett., 1977, 38, No.16, p.892.
13. Kumakhov M.A., Phys.Lett., 1976, A57, p.17; Terhune R.W., Pantell R.H., Appl.Phys.Lett., 1977, 30, No.6, p.265; Wedell R., Phys.Stat.Sol.(b), 1980, 99, p.11.
14. Aganyants A.O., Vartanov Yu.A., Vartapetyan et al., Pis'ma ZhETF, 1979, 29, p.554.
15. Miroshnichenko I.I., Murray J., Awakyan R.O. et al., Pis'ma ZhETF, 1979, 29, p.786.
16. Kalinin B.N., Kaplin V.V., Potylitsin A.P. et al., Phys.Lett., 1979, A70, p.447.
17. Gaponov A.V., Petelin M.I., Yulpatov V.K., Radiophysics and Quantum Electronics, 1967, 10, p.794.
18. Jory H.R., Report to II Int.Symp. on Heating in Toroidal Plasmas (Como, Italy, Sept. 1980).

19. Petelin M.I., Lectures on Microwave Electronics, Izd.Saratov Univers., 1974, B.IV, p.179.
20. Belousov V.I., Bunkin B.V., Gaponov A.V. et al., Pis'ma ZhTF, 1979, 4, No.23, p.1443.
21. McDermott D .B ., Marshall T.C., Schlesinger S.P. et al., Phys.Rev.Lett., 1978, 41, No.20, p.1368.
22. Granatstein V.L., Schlesinger S.P., Herdon M. et al., Appl.Phys.Lett., 1977, 30, No.9, p.384.
23. Didenko A.N., Sulakshin A.S., Fomenko G.P. et al., Pis'ma ZhTF, 1978, 4, No.14, p.823.
24. Ginzburg V.L., Izv. AN SSSR, ser.fiz., 1947,11,p.165.
25. Providakes G., Nation J.A., Read M.E., IEEE Trans., 1977, MTT-25, No.6, p.563.
26. Ginzburg N.S., Krementsov V.I., Petelin M.I. et al., Pis'ma ZhTF, 1977, 4, No.3, p.149.
27. Rusin F.S., Bogomolov G.D., High power electronics, ed. by P.L.Kapiza, M., Izd. "Nauka", No.5, 1968, p. 45.
28. Shestopalov V.P., Diffraction electronics, Izd.KhGU, 1976.
29. Nefyodov E.I., Izv.VUZ. - Radiofizika, 1977, 20, No. 11, p.1740.
30. Kovaljov N.F., Elektronnaya Tekhnika, ser.1, Elecktr. SVCh, 1978, No.3, p.102.
31. Zarnitsyna I.G., Nusinovich G.S., Izv.VUZ. - Radiofizika, 1974, 17, N.12, p.1858.
32. Bratman V.L., Ginzburg N.S., Petelin M.I., Izv.AN SSSR, ser.fiz., 1980, 44, p.1595.
33. Rabinovich M.S., Rukhadze A.A., Plasma physics (in Russian), 1976, 2, No.5, p.715.

MAGNETOELECTROSTATIC PLASMA CONFINEMENT

M.S.Ioffe, B.I.Kanaev, V.P.Pastukhov,
V.V.Pitersky, R.R.Chistjakov, E.E.Yushmanov

I.V.Kurchatov Institute of Atomic Energy,
Moscow, USSR

ABSTRACT

Results in the studies of plasma behaviour in the traps with a cusped magnetic field and with electrostatic suppression of plasma losses through the magnetic gaps are given in the presentation. The main attention is paid to the experiments in the "Atoll" circular trap. The main purposes of these experiments:

1) to develop the methods of filling the trap with plasma,
2) to study the confining properties of the trap.

I. INTRODUCTION

The idea of magnetoelectrostatic confinement, in a wide interpretation of these words, can be referred to all the systems in which the plasma confinement is provided by the combined effect of a magnetic field and an electrostatic one, in particular, to the tandem ambipolar traps, to the traps with a rotating plasma, and even to an ordinary mirror trap with hot ions where electrons are actually confined by an electric field (not magnetic one).

In this presentation only one of such systems will be discussed, i.e. an magnetoelectrostatic trap with cusped magnetic field (MET).

Rapid plasma losses along the field lines are known to be the main deficiency of ordinary cusped magnetic traps.

In plasma with low β , the losses are provided by nonconservation of adiabatic invariancy in the magnetic moment of particles in the vicinity of the zero field points. At $\beta = 1$, when the magnetic field is practically completely excluded from the plasma volume and plasma is separated from the field by a transition layer, the particles entering the layer run off along the field and, then, the losses are determined by a width of the transition layer. The width of the layer, in its turn, depends on the mechanism of transverse electron transfer.

In 1966, O.A.Lavrentiev [1] suggested to apply an external electric field to diminish the longitudinal losses. His idea was discussed in papers (see, e.g. [2,3]). Therefore, we remind here only the initial physical principles of his suggestion.

Using the cusped fields, one can let the magnetic flux to pierce plasma through rather narrow gaps. If one makes their width equal 2δ , considerably greater than the Larmor radius of electron but not exceeding a few Debye radii r_D corresponding to the density and temperature of electrons in the gaps, the longitudinal loss of electrons can be prevented electrostatically. For this purpose, the gaps are limited with conducting walls behind which the electrodes-reflectors, negatively charged respective to the walls, produce a high potential barrier to electrons. For the prevailing portion of electrons unable to overcome this barrier, the only loss channel remains: a diffusion transfer across the magnetic field to the walls of the gaps. Therefore, one can expect a considerable increase in the

electron confinement time. As for ions, if the time of their free outflow through the gaps τ_{io} *) is less than the diffusion electron life time $\tau_{e\perp}$, the losses will be controlled by an electrostatic barrier in front of the gaps. The barrier should be formed automatically of such a height to reduce the ion losses down to the electron ones. Plasma acquires, in this case, a negative potential respective to the gaps. Distribution of the potential set in the trap is shown in Fig.1.

In the method under discussion, the confining properties of the trap depend actually on the level of real limiting the transverse electron losses by the magnetic field.

Lavrentiev based his suggestion on the ideas of classical diffusion due to Coulomb collisions. At $\beta \approx 1$, the life time of particles in the trap is determined, in this case, by a relationship [4]:

$$\tau_{clas} = \tau_{ei} \frac{2\mathcal{N}}{\alpha} \frac{a\omega_{pe}}{c} \qquad (1)$$

where τ_{ei} is the electron-ion collisions time, $\mathcal{N} = \frac{\ell}{\rho_e}$ is the number of electron Larmor radii at the halfwidth of the gap, a is the characteristic transversal plasma dimension, α is the numerical factor dependent on the ratio T_i/T_e (at $T_i = T_e$ $\alpha \simeq 3$), ω_{pe} is the plasma electron frequency, c is the velocity of light.

A trap with reasonable reactor parameters and with the acceptable values of Q ($Q = 5 \div 10$) is shown to be

*) $\tau_{io} = 4V/\bar{v}_i S$; V is the plasma volume, $\bar{v}_i$ is an average ion velocity, S is the total area of the gaps.

feasible, in principle, by the calculations made in [5], for the case of a classical diffusion. But there are some reasonable grounds to consider that the classical diffusion will not actually take place. A strong inhomogeneity in the plasma density and the electric field in the transition layer are the factors favourable to the development of micro-instabilities which are able to cause an anomalous transverse transfer of electrons in MET. The physical mechanism of such a transfer is totally identical to the mechanism of an anomalous widening in the transition layer in the ordinary cusped traps.

In accordance with [6], at the moderate electric field corresponding to $T_i \lesssim T_e$, a long wave type of the ion-sound instability with $k\rho_e \sim 1$ and with $\omega \sim \gamma \sim \sqrt{\omega_{Bi}\,\omega_{Be}}$ is present, because the ion Landau damping has a considerably weaker effect on it in comparison with an ordinary short-wave ion-sound instability. This instability results in a widening of the layer beyond the gap where electrons are not confined more in the longitudinal direction by the electric field and can, therefore, escape relatively fast along the field lines due to scattering into the loss cone. As it is shown in [6], the longitudinal losses in the external part of the layer are determined by the Coulomb scattering, the instability role is reduced to the maintenance of the plasma density profile corresponding to the marginal stability condition. At $\beta \approx 1$, an anomalous life time of electrons dependent on this mechanism is determined by a relationship:

$$\tau_{anom} \simeq 0.5\,\tau_{ei}\,\frac{a\,\omega_{pi}}{c}\,\exp\left\{2\sqrt{2m_e/m_i}\right\} \qquad (2)$$

here ω_{pi} is the plasma ion frequency.

The mechanism of the electron transversal transfer mentioned can take place not only at $\beta \approx 1$ but at the low plasma pressure when the magnetic field configuration in MET slightly differs from that under vacuum conditions. In this case, typical for the modern experiments, the plasma volume division into the non-magnetized region and the transition layer loses its grounds, and the expressions for the classical and the anomalous life time of electrons should be modified, according to the real geometry of the trap. For the Atoll facility, which we will speak later about, these expressions look as follows:

$$\tau_{clas} \approx 2\mathcal{N}^2 \tau_{ei} \qquad (3)$$

$$\tau_{anom} \approx \tau_{ei}\left(0.4 + 0.3 \exp\left\{2\mathcal{N}\sqrt{2m_e/m_i}\right\}\right) \qquad (4)$$

Studies in MET have been carried out for some years at the Kharkov Physicotechnical Institute (USSR) as well as at the Quebec University in Canada. The main experimental results were obtained for the recent years at the facilities "Jupiter 1A" and "Jupiter 1M" [7,8]. The magnetic field in these facilities has a spindle cusp configuration. The typical plasma parameters: $n \sim 10^{12}\,cm^{-3}$, $T_e \simeq 40eV$, $T_i \approx 100eV$, plasma volume $\simeq$ $100cm^3$; the particle life time observed is a few hundred microseconds. The authors of these papers are ready to interpret the results obtained as those indicating the classical character of the plasma losses. But, nevertheless, one should note that the ab-

sence of experimental data on the plasma density and potential profiles, on the amount of impurities, as well as utilization of the simplified theoretical estimations, without plasma configuration peculiarities of the spindle cusp taken into account, can make conclusions of such type insufficiently based.

The experimental research in the Atoll facility, Kurchatov Institute of Atomic Energy, has been started in the second half of 1980. Its main goal is to study the confining properties of the magnetoelectrostatic traps, and, first, the mechanism of the electron transversal transfer. The results obtained up to now are not sufficiently completed yet. But they have manifested some interesting physical phenomena respective to the process of confinement itself and to the peculiar features of the trap filling with plasma and ion behaviour in it.

2. Short description of the Atoll facility

The view of the facility is shown in Fig.2. The magnetic field has a circular quadrupole configuration. It is produced with four pairs of coils (1); the current-carrying conductors of the coils are inserted into the metallic cases which are reinforced in pairs with supporting arms (2). The magnetic gaps, 2 mm wide, are formed by the walls of these cases. The radius of external gaps is 64 cm, that of internal ones is 32 cm, the field within the gaps can reach 15 and 30 kOe, respectively. The least distance between the plasma center (5) and the edge field lines touching the gap walls is 6 cm; the field at these points along the edge lines is a mini-

mal one and equal to 4.5% of the field in the external gaps.

The electrodes-reflectors (3) are located behind the gaps. A pair of circular electrodes is displaced between each gap and reflector. A negative potential respective to the reflector can be apllied to these electrodes to cut off the secondary electrons knocked out of it by ions. A small area of the reflector against one of the internal gaps is replaced by an electron gun (4) capable to inject a narrow electron beam with a current 300÷500mA into the trap at the gun voltage 2÷4 kV.

The magnetic system with the electrodes fastened to it is placed into a vacuum chamber (6), 180 cm in diameter, 100 cm wide. The chamber is pumped out up to the pressure of 10^{-8} torr, the hydrogen pressure 10^{-6} torr is maintained inside it in the process of experiments.

2. Methods of filling the trap with plasma

To develop the method of filling the trap with plasma within the circular region, 1 m in diameter, 50 liters in volume, was one of the important problems at the initial stage of research.

Having in mind the confinement dependences on the electron transversal transfer, where the value of β is of minor importance, we didn't aim at the production of plasma with $\beta \simeq 1$ that would be not an easy problem by itself. Instead of this, our efforts were directed onto the production of plasma not so dense and hot but with easely reproducible parameters in order to have a convenient object for research.

An easy way of filling the trap is an ignition of a Penning type discharge in it at low hydrogen pressure. The discharge is initiated with an electron beam of low intensity from the gun, then it ia developed and maintained by the secondary electrons from the reflectors. These electrons accelerated by the potential difference between the reflector and the gap pass into the central region of the trap and serve as an energy source for the plasma production and heating.

Thus, at the reflector voltage - (1,5 ÷ 2,5) kV and at hydrogen pressure $(3 \div 5).10^{-6}$ torr, it is possible to obtain a quasi-stationary plasma regime, about 10 ms duration, with an average density $(2\div3).10^{11}\,cm^{-3}$. If one cuts-off the flux of secondary electrons from the reflectors at a certain time, the discharge is interrupted and plasma transits into a free decay. A radio-interferometer signal typical for such a regime is shown in Fig.3^{a}.

Later, an interesting phenomenon was observed. It consists of the following. At the higher magnetic fields (higher than 7.5 kOe in the external gaps) a quasi-stationary state of plasma with quite the same density continues to exist even when the electron emission from the reflectors is completely cut-off; a signal from the radio-interferometer, for this case, is given in Fig.3^{b}; the instants of cutting the secondary emission off are shown in Fig.3^{a} and 3^{b} with arrows. We found that such an"emissionless" plasma discharge is maintained due to the heating of electrons at their motion in the electric field which

exists inside plasma. The origin of this field will be discussed later. Emissionless discharge is more convenient for the plasma confinement research, as a high frequency noise observed at the injection of high energy electrons from the reflectors makes the confinement slightly worse. All the subsequent results are related to the discharge of such type and correspond to the standard regime with the following external parameters: field in the external gaps is 8 kOe, hydrogen pressure in the trap is 5.10^{-6} torr, reflector voltage is -2 kV, additional voltage across the rings cutting the emission off is -1.5 kV.

4. Experimental results and discussion

The plasma density distribution along the line passing through a zero magnetic field point, perpendicular to the plasma ring, has been measured with a miniaturized Langmuir probe which does not introduce remarkable changes into the integral plasma properties.

On the distribution obtained (Fig.4) there is quite a flat central part with a radius 2 cm; beyond it, the density monotonously decreases towards the periphery. One should note, in particular, that the density is not turned to be zero near the edge field line (r = 6 cm), as one could expect in accordance with the classical diffusion of electrons, but spreads far outwards.

The electron temperature has been measured with the same probe by the method of high frequency voltage superposition near the "floating point" [9] ; the value obtained is $T_e \simeq 25$ eV.

As for ions, one should speak not about their temperature but about some average energy which is determined by the character of their motion in plasma. In order to make this problem clear, one should discuss the distribution across the gap of an ion flux leaving the trap.

As it has been mentioned in introduction, if the diffusion life time for electrons, $\tau_{e\perp}$, exceeds the time of free outflow of ions through the gaps, τ_{i0}, plasma will acquire a negative potential in order to form a potential barrier for ions in front of the gaps. This barrier equalizes the ion losses with the electron ones. One should keep in mind in this case that the barrier height is not the same across the gaps because in the gaps themselves there is a potential distribution with a deep minimum in the middle (due to non-compensated electronic charge in the gaps). Therefore, the ion losses in the trap are found to be concentrated in a narrow zone near the middle of the gap, where the barrier height is a minimal one.

Under definite conditions, when $\tau_{e\perp}$ slightly exceeds τ_{i0}, the balance of ion and electron losses can be maintained even in the complete absence of the barrier against the middles of the gaps. In this case, ions freely flow out through the narrow "open corridor" and their losses are controlled with the corridor width. In this case, the lateral regions of the gap remain closed by the barrier as usually.

In both cases, it is important that ions can leave

the trap only out of the internal plasma region which is limited by the field lines piercing the narrow loss zone through the gaps.

Out of this interpretation of the ion loss, it remains unclear how ions leave the external plasma regions. Indeed, ions formed at the periphery, outside the permitted loss region, cannot penetrate into it because, at the instant of their production in the process of gas ionization, they have almost zero energy and consequently, they are effectively magnetized. In reality, such possibility can occur due to the piling of slow ions in the external plasma regions which, in its turn, is responsible for an increase in the potential there. As a result, in plasma such an electric field is set, $E_\perp$, which is able to "pull" the periphery ions into the internal region due to their quasi-cycloidal motion in the crossed fields $E_\perp$ and B. In this motion, ions pass many times through the region of a weak magnetic field where they acquire the necessary longitudinal momentum, due to nonadiabaticity, and leave the trap.*)

The electric field presence in plasma has been found in the measurements of the plasma potential and its distribution along the radius. The potential distribution has been measured in the same direction as the plasma density distribution (see, above). The potential has been

---

*) Emissionless discharge mentioned in chapter 3 is maintained due to this field $E_\perp$.

determined by the method of a floating probe*). The results of such measurements are given in Fig.5. One can see that there is a considerable electric field at the distances greater than 3 cm from the centre; at the periphery ($\tau > 5$ cm) it reaches 80 V/cm.

One can estimate an average ion energy in their cycloidal motion by the known electric and magnetic fields when the radial density distribution is taken into account; for ions at the periphery, it equals to 50 eV. The energy of ions produced in the central region ($\tau < 3$ cm) is probably lower than this value because the electric field there is low or absent.

An useful experimental information on the ion energy distribution was obtained with the charge-exchange fast neutral energy analyzer with 100 eV as a lower energy threshold [10]. Having in mind an anisotropic distribution dependent on the cycloidal ion motion, the analyzer has been set so that only those particles enter it which are formed in the ion charge-exchange near the top of their cycloidal trajectories. The ion energy distribution obtained is given in Fig.6. It is plotted in assumption that the main mass of ions in plasma consists of protons and their charge-exchange occurs due to atomic hydrogen. For qualitative consideration on the character of this distribution, the possible inaccuracy dependent on this

*) It is known that the difference between the floating probe potential and the plasma potential is about 3 Te/e; under our operating conditions it is comparatively low, because the plasma potential is considerably greater than Te/e.

assumption has no principal importance. It is important to note two features in the distribution. First, in the energy range studied ($E > 100$ eV), the main portion of ions has an energy no greater, than a few hundreds eV. It does not contradict with the data on the average ion energy obtained in the periphery (one should remember that the ion energy on the cycloid top is 4 times greater than its average energy). Another feature is the presence of ions with energies higher than 600-700 eV in the spectrum. This value is the upper energy limit which ions can acquire in the existing transversal potential well (see Fig.5). Therefore, it is evident that the high energy tail in the distribution has another origin. With sufficient grounds, one can explain it by the ion acceleration due to microinstabilities.

Looking again at Fig.5, one can find some additional information which can be obtained from the radial potential distribution. From this figure, it follows that the longitudinal losses of electrons through the gaps are suppressed by a very high barrier in front of the reflectors ($e\varphi_e / T_e \approx 50$) and electrons are forced to leave only across the magnetic field. These conditions completely satisfy the main idea of confinement on which MET is based. Indeed, the life time of electrons in the trap has raised in comparison with the case when the longitudinal suppression is absent. The fact that the plasma potential is a negative one speaks for it; it should be so when $\tau_{e\perp}$ exceeds τ_{io} . But in the experiments described, this excess is not so high to require high ion barrier in front

of the gaps.*) Such conclusion follows from independent potential measurements at the centre of the gap. They show that this potential is rather close to the potential in the central plasma region. Thus, in our case, one has an "open corridor" realized.

Now, compare the experimental data on the plasma confinement with the calculated ones two cases: classical diffusion at electron-ion collisions and anomalous transfer under long-wave ion-sound instability.

The data on the particle confinement time, τ_{conf}, can be obtained from the quasi-steady-state discharge when the plasma parameters remain unchanged for milliseconds. At this stage, the losses of particles and the rate of their production are equal to each other and hence $\tau_{conf} = \tau_{ion} \equiv \frac{1}{n_0 \langle \sigma_i v \rangle_e}$, where n_0 is the density of neutral hydrogen, $\langle \sigma_i v \rangle_e$ is a factor of ionization rate by electrons dependent on T_e. The values n_0 and T_e are known from the experiment: $n_0 = 1.8 \cdot 10^{11} cm^{-3}$, $T_e = 25$ eV; this value of T_e corresponds to $\langle \sigma_i v \rangle_e = 3 \cdot 10^{-8} cm^{-3}$; $\tau_{conf} = 1.8 \cdot 10^{-4}$ s, respectively.

Classical and anomalous diffusion life-times, calculated by the formulae (3) and (4) (See introduction) are: $\tau_{clas} = 5 \cdot 10^{-2}$ s ($\mathcal{N} = 65$, $\tau_{ei} = 6.5 \cdot 10^{-6}$ s for $n = 3 \cdot 10^{11} cm^{-3}$, $T_e = 25$ eV) and $\tau_{anom} = 1.2 \cdot 10^{-4}$ s. Thus, $\frac{\tau_{conf}}{\tau_{clas}} = 3.6 \cdot 10^{-3}$ and $\frac{\tau_{conf}}{\tau_{anom}} = 1.5$.

*) The ion barrier height under optimal conditions $\approx 7 T_i/e$ at transversal electron transfer due to the Coulomb collisions.

Comparison of only these values shows that we deal with transversal electron transfer which greatly differs from the classical one (in the Atoll experiments under study, this difference is about 300 times). Comparison between the experimental curves of radial density distribution and the calculated ones bring us to the same conclusion. These curves are given in Fig.7. Here: curve 1 - experiment, 2 - classical diffusion, 3 - ion - sound instability (all the curves are normalized to the same value $\int n dl$). The curve 3 has been calculated in assumption that the established density profile keeps plasma near the stability threshold; the characteristic value of the density gradient is of an order of the ion-sound Larmor radius.

The data on plasma confinement in Atoll are in a good agreement with the ideas developed in 6 on the mechnism of transversal electron losses dependent on the long-wave ion-sound instability excitation. At the same time, one should emphasize that the more definite conclusions can be made only on the basis of the experimental data related to the detailed study of the instability, i.e., in particular, the frequency spectrum of oscillations and the structure of the driven waves. To obtain these data is an aim of further research.

In conclusion, one should note that the mechanism of losses in Atoll, in its main features, seems to be specific one not only for MET. As it has been mentioned in introduction, the similar mechanism should be found in the ordinary casped traps because the pronounced plasma

edge there, corresponding to the classical diffusion, should be smeared by an instability of the similar type as in MET.

Conclusion

Let's enumerate the results of research in Atoll in that order which allows to give a notion on some pecularities in the behaviour of plasma in the magnetoelectrostatic traps.

1. Electrostatic suppression of the longitudinal electron losses increases life-time of electrons to such a degree that this time becomes longer than the time of free outflow of ions through the gaps. As a result, plasma acquires a negative potential respective to the walls of the gaps.

2. The flow of escaping ions is found to be concentrated in a narrow zone in the middle of the gaps; dimensions of the zone determine the boundary of the internal plasma region out of which ions can leave the trap.

3. Localization of the ion escape region serves as a ground for the transversal electric field origin. The field is such that ions produced at the plasma periphery can penetrate into this region.

4. This electric field:

a) accelerates ions up to considerable energies in their cycloidal motion in the trap,

b) provides heating of electrons and the conditions for the plasma selfmaintenance in the absence of the external energy inflow due to the secondary-emission electrons from the reflectors (emissionless discharge).

5. Plasma confinement in the trap does not correspond to the laws of classical electron diffusion across the magnetic field; the confinement time is a few hundred times smaller than the classical one.

6. The characteristic density gradient length along the plasma edge (or the size of the transition layer) is of an order of the ion-sound Laromor radius.

7. An anomalous transversal electron transfer seems to be induced by a microinstability. Existence of this microinstability is proved by the fact that the ion energy spectrum has a long high energy tail.

8. The experimental results on plasma confinement seems to show the determinant role of a long-wave ion-sound instability in the anomalous electron transfer. This statement needs an additional experimental checking by the study of microcharacteristics of the instability.

References

1. O.A.Lavrent'ev "Study in the electromagnetic trap". Thesis for a Candidate degree (Phys.-math.), Kharkov (1966). 2.
3. V.P.Pastukhov, E.E.Yushmanov "Magnetoelectrostatic trap", preprint JAE - 3042 (1978) (in Russian)
4. V.P.Pastukhov, Fisika plasmy, 4, 560 (1978)
5. E.E.Yushmanov, Nuclear Fusion, 20, 3 (1980)
6. V.P.Pastukhov, Fisika plasmy, 6, 1003 (1980)
7. O.A.Lavrentiev, V.A. Potapenko, J.A.Stepanenko Zh.Kh.Fiz., 46, 115 (1976).
8. Yu.S.Azovsky, O.A.Lavrent'ev et al. Ucranian

Fiz. Zh. 26, 429 (1981).

9. B.J.Kanaev, V.V.Pitersky, E.E.Yushmanov Zh. Tekh. Fiz., 44, 2302 (1974).

10. Yu.V.Gott, V.Y.Telkovsky, Zh.Tekh.Fiz.34, 2114 (1964).

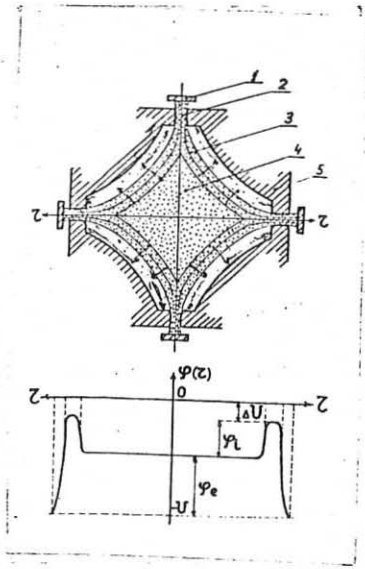


Fig.1

On top: diagram of the simplest magnetoelectrostatic trap:

1 - reflector-electrode, 2 - gap, 3 - transition layer, 4 - non-magnetized ragion, 5 - conducting wall.

Down: potential distribution along the trap axis.

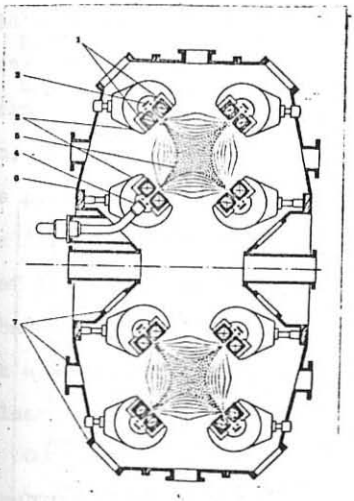


Fig.2

Atoll diagram:

1 - magnetic field coils, 2 - arms, 3 - reflector--electrodes, 4 - electron gun, 5 - plasma, 6 - vacuum chamber

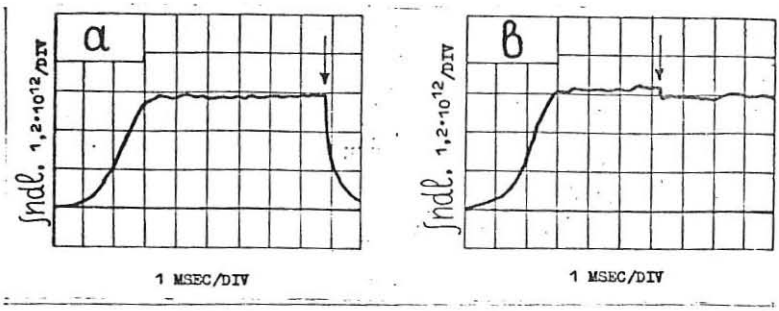


Fig.3 Oscillograms of the signal from the radiointerferometer: 3a - discharge with secondary electron injection, 3b - emissionless discharge

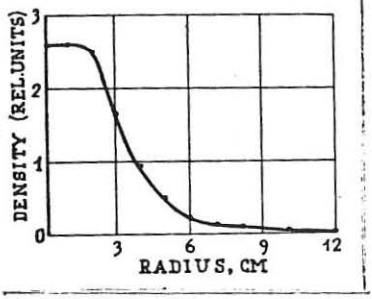


Fig.4 Plasma density radial distribution

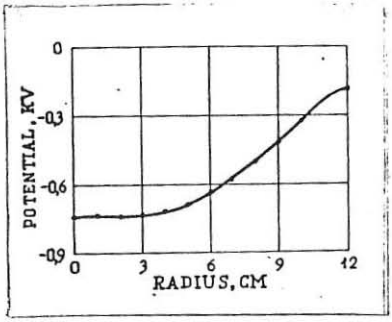


Fig.5 Plasma potential radial distribution

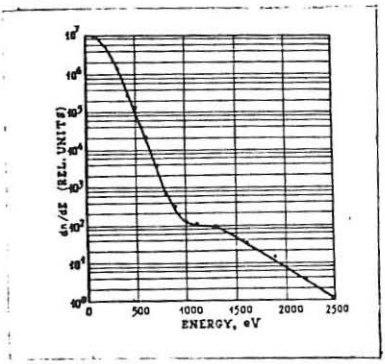


Fig.6 Ion energy spectrum

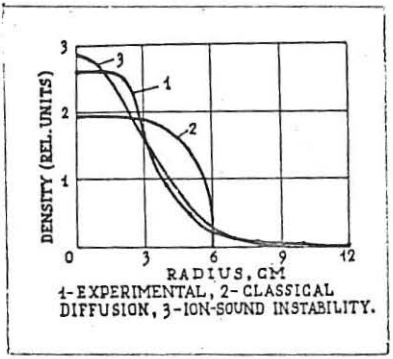


Fig.7 Experimental and calculated density distribution

THE STUDY OF THERMONUCLEAR PROBLEMS CONDUCTED AT THE INSTITUTE FOR PHYSICAL PROBLEMS OF THE USSR ACADEMY OF SCIENCES

P.L.Kapitza

Institute for Physical Problems, Academy of Sciences of the USSR,Moscow, USSR

Summary. This work presents the investigations which have been carried out during the last few years by the staff of the Institute for Physical Problems. Important scientific problems which still require investigation are indicated. Further efforts towards their solution are considered.

In the nineteen fifties I started to work in the field of electronics. In time this work led me to the creation of a high power continuously operating microwave generator which we called the "Nigotron". This, in its turn, suggested the possibility of creating high temperature plasma. During the last few years we, at the Institute for Physical Problems, have concentrated on the study of the physical properties of this type of plasma and we have become more and more convinced that these researches are opening up new possibilities for attaining thermonuclear synthesis on a large scale.

Our basic work on the physical properties of plasma is published in papers [1] and [2] where a possible way to construct a thermonuclear reactor which works on these principles is described. The advantages of this

method for obtaining thermonuclear energy compared with the pulsed mode have been studied in [3] . Lately progress has been made in this work at the Institute for Physical Problems with the participation of a considerable number of scientists working in the Physical Laboratory. Now this work is at the stage when we can, with greater certainty, evaluate the emerging possibilities.

Last year sufficient progress was made to realize clearly the difficulties of applying the properties of our plasma to thermonuclear synthesis. The main difficulties of high temperature plasma creation by our method are the supply of high power continuous microwave radiation to feed the plasma discharge and the stabilization of this discharge when freely floating in a gaseous medium.

The scheme of the experimental apparatus is shown in Fig.1 ([1] , Fig. 5.1). E_{01} - mode of UHF oscillations is excited in a cylindrical resonator of diameter $2A$ and length L . The freely floating cord-like plasma discharge of length $2l$ is created in one of the electrical field maximums along z -axis. Stabilization of this discharge in radial direction is obtained by means of gas rotation around the axis z . The UHF electrical field keeps the discharge at its maximum amd provides plasma stability along z -axis. In the experiments with hydrogen or deuterium at several atmospheres (wavelength λ = 19 cm) the maximum power absorbed by the plasma was 15 kw. In these conditions the length of the cord reached 12 cm and its diameter approached 1 cm (see [1]), Fig. 2.4 and 2.5).

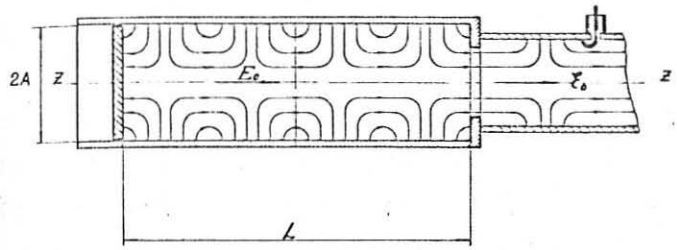


Fig. 1. End feed of the discharge

It was most interesting that at sufficiently high pressure and microwave power the plasma discharge in both hydrogen and deuterium was eggshaped with a luminous centre and diffuse boundaries called by us "fur-coat". In the well defined central region of the cord-like plasma the white luminiscence was very bright which showed the presence of two types of plasma.

While studying the properties of the cord discharge [1] we come to the conclusion that the brighter luminosity appears when the power and pressure are very high. Under these conditions the plasma is completely ionized and reaches a temperature of millions of degrees. At the same time the temperature and the size of the cord increased with the increase of power. But the experiment shows that the absorbed power in our installation is limited by the conditions which insure the stability of the discharge. When the length of the cord $2l$ exceeds $\lambda/2$

the cord discharge may jump independently along the axis z. The simple explanation of this effect is that the frequency of the cord oscillations is near the frequency of the oscillations of the generator. The oscillation phase changes near the resonance and the electric field no longer maintains the cord at the maximum microwave field, so the discharge is thrown out of equilibrium.

It was possible to increase the stability of the plasma discharge along the axis z by blowing the cooling gas, but we did not manage to increase the length of the plasma discharge sufficiently and the supplied power was limited to 15 kilowatts. Therefore, to increase the length of the discharge we increased the wavelength λ of microwave radiation. For this purpose we have built an installation three times larger in which the wavelength of microwave oscillations was equal to 55 cm, the absorbed power was about 40 kw, and the length and diameter of the cord were also three times larger. The temperature of the electrons in the plasma then reached $7 \cdot 10^6$K. To further increase the supplied power without increasing the size of the installation we decided to use magnetoacoustic waves. The advantage of this method is that these oscillations provide effective ion heating in the plasma [1] § 8, [4].

In order to heat the ions of the plasma to thermonuclear temperature by this method we drew up a new project for the reactor ([2], Fig. 1). Its construction turned out more complicated. Therefore we decided to increase the power supplied to the plasma cord without increasing the length of the wave. Here our main difficulty was to con-

struct a resonator in which a discharge with a length of the order of $\lambda/2$ was prevented from jumping along the z -axis to the adjacent regions of cavity, that is the resonator must provide axial stability of the plasma. This problem can be solved if the central part of the resonator is below cutoff for E_{01} -mode:

$$2a < 0{,}76\lambda \qquad (1)$$

In this case power may be supplied to the middle of the discharge (see Fig. 2) instead of the usual end supply, shown in Fig. 1.

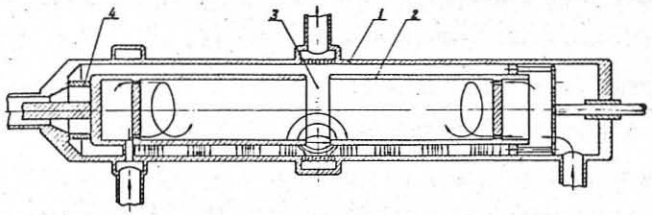


Fig. 2. One-slit resonator

As we see from Fig. 2 the main oscillation system is the resonator which has a narrow slit between two coaxial cylinders (1), (2). The wavelength in such a system is approximately equal to the wavelength in free space. The power from the nigotron is transmitted through a ceramic window (4). The cord discharge is formed inside the cylinder (2) of the diameter $2a$ which is below cutoff for this wavelength. The coupling between this volume and the main

oscillating system is obtained through a coaxial narrow slit (3). The oscillations passing through this slit into the cutoff region exponentially decrease along the axis z. For an approximate description of the oscillating processes in such a system we can use Lagrange functions technique (see [1]). The calculations of the field in such a system do not present much difficulty when the cord discharge is very small or entirely absent. When the conductive plasma discharge is long the UHF field easily penetrates into the cutoff region and calculations become more complicated.

We assume that to stabilize such an oscillating system the oscillation energy in the coaxial part (1) must be significantly greater than in the region of the plasma cord discharge. Therefore the volume of the resonator (1) must be significantly larger than that in the region of the plasma cord discharge, so the external volume of the resonator (1)-(2) must be as large as possible. This system was found to be very effective in practice. We were able to increase the power supplied to the cord by an order of magnitude, that is up to 100 kilowatts. The length of the plasma discharge was increased three times and its diameter was increased to 5 cm, when the deuterium pressure was about 7-8 at. The electron temperature was higher than $5 \cdot 10^7$K.

Before describing the properties of a high power plasma cord I want to consider the possibilities which are opened by the use of our slit resonator for increasing the size and power of the cord discharge without change of wavelength. It is obvious that this can be done by in-

creasing the number of coaxial slits. If they are (as shown in Fig.3) at a distance of a free-space wavelength from each other the electrical field in the inside cylinder will keep its sign and the plasma discharge will increase in length. We experimented with a two-slit system.

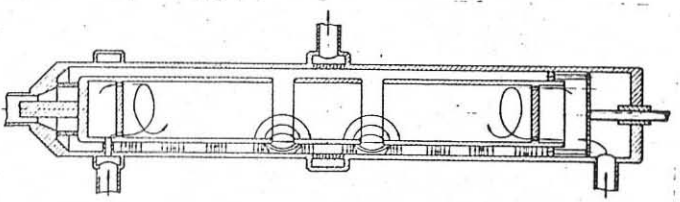


Fig. 3. Two-slit resonator

In this way one can construct a toroidal resonator, as shown in Fig. 4, giving us the opportunity to create a circular cord discharge. But this method demands work on a larger scale far beyond the possibilities of our laboratory.

In all this work S.I.Filimonov, A.I.Degal'tsev, A.B. Manenkov, V.I.Chekin took part.

The existence in the plasma of electrons at a temperature $T_e \sim 10^8$-10^9K is possible, as has already been shown, because at the boundary of the hot discharge a double layer is formed which reflects hot electrons without significant losses. In Fig. 5 this layer is between radii a and b. The processes taking place in this layer are quantitatively described in [1]§5, §6. The existence of this double layer is now established. The energy

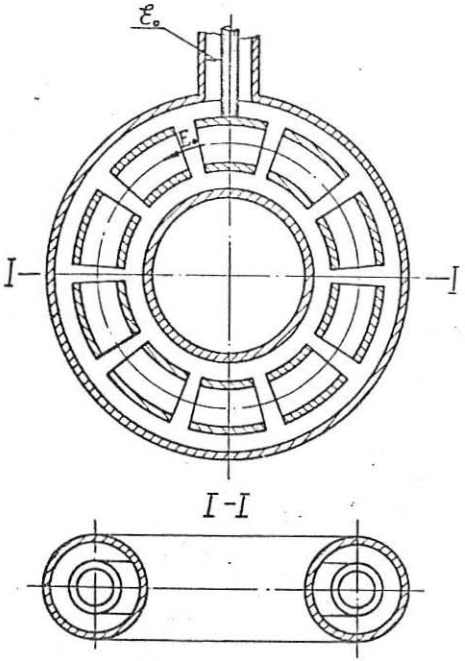


Fig. 4. Toroidal cavity

is transferred from UHF electric field to electrons in the skin-layer which practically coincides with the double layer. Owing to the high heat conductivity of the electrons, their temperature T_e has a small gradient inside the plasma. We assume that beyond the skin-layer in the region of $r = 0$ up to $r = b$ the temperature T_e is constant (Fig. 5). In the presence of the magnetic field([1], eq. 7.5) heat conductivity decreases with the square of the field and when the field intensity reaches several kilogauss, the heat conductivity practically vanishes. If the heat is to be distributed in the centre of the plasma dis-

charge in the presence of a strong magnetic field we must assume that the heat conductivity in the centre of the plasma arises owing to the turbulence.

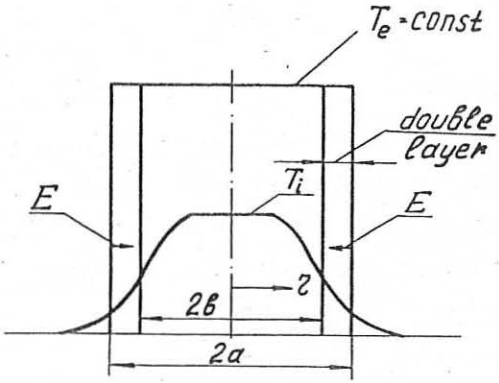


Fig. 5. Radial distributions of plasma temperatures

Heat transfer from the plasma to the surrounding gas ([1] , § 6) takes place owing to the interaction of ions and electrons with the atoms of hydrogen or deuterium. Energy transport from the hot electrons to the ions occurs in two ways. The first and the most effective one is a collective interaction in the double layer (see[1] , §6). In this process the ions which enter the electric field of the double layer gain energy according to the formula (4.10) [1].

The remaining heat is transferred not collectively but by individual collisions which take place inside the

volume of the plasma cord in a region of $r = 0$ to $r = b$. This quantity per unit lenth of the cord we shall call Q_e (see eq. (4.20) in [1]).

$$Q_e = \pi b^2 \frac{n(T_e - T_i)}{\tau_{eq}} \frac{\text{erg}}{\text{s} \cdot \text{cm}} . \qquad (2)$$

In this equation n is the electron density which we assume to be equal to the density of the ions. τ_{eq} is the time required to equalize the temperature when the energy is diffused by collisions between the ions and electrons. This value has already been calculated by Landau and is given in [1] (eq. 4.19). Let us calculate Q_e for deuterium ions ($m = 3{,}3 \cdot 10^{-24}$g):

$$Q_e = 2{,}75 \cdot 10^{-19} \pi b^2 \frac{(1-a)\Lambda n^2}{T_e^{1/2}} \frac{\text{erg}}{\text{s} \cdot \text{cm}} , \qquad (3)$$

where $a = \frac{T_i}{T_e}$ is the ratio of the ion temperature to the temperature of the electrons, and Λ is the logarithmic term. We simplify our calculations by assuming that this heat conductivity from the electrons to the ions in the region of $r = 0$ to $r = b$ takes place homogeniously and is determined by the temperature difference $T_e - T_i$. Then we have

$$2\pi r K_{i\perp} \frac{\partial T_i}{\partial r} = \frac{r^2}{b^2} Q_e \; ; \; Q_e = \text{const.} \qquad (4)$$

The coefficient of the heat conductivity which takes place perpendicularly to the magnetic field $K_{i\perp}$ is determined by Eq. 7.5 in [1]:

$$K_{i\perp} = 1{,}3 \frac{k^2 T_i n}{m_i \omega_i^2 \tau_i} , \qquad (5)$$

where Larmor's frequency for deuterium ions is:

$$\omega_i = \frac{e Z}{m_i c} H = 4{,}85 \cdot 10^3 H \frac{1}{\text{sec}} , \qquad (6)$$

and τ_i is the ion relaxation time. Then the coefficient of the heat conductivity of deuterium in a magnetic field is:

$$K_{i\perp} = 1{,}38 \cdot 10^{-17} \frac{\Lambda n^2}{T_i^{1/2} H^2} . \qquad (7)$$

We have already assumed that Q_e is constant and now we consider that the temperature of ions on the periphery of the cord can be ignored when $r = b$ as compared to the temperature T_i of ions in the centre of the discharge. Then by solving the equation (4) we get the temperature of ions at the centre of the plasma cord:

$$T_i = 8{,}67 \cdot 10^{30} \frac{H^4 Q_e^2}{\Lambda^2 n^4} \; ; \; r = 0 \; ; \; Q_e = \text{const.} \qquad (8)$$

By substituting the value of Q_e from (2) we obtain

$$\eta = \frac{\sqrt{a}}{1-a} = 8{,}1 \cdot 10^{-4} n b^2 \frac{H^2}{T_e} \; ; \; a = \frac{T_i}{T_e} < 1 , \qquad (9)$$

From this equation we can determine the ratio α of ion temperature T_i to the electron temperature T_e. Note that in (4) T_i is independent of the plasma density. The dependence of (9) is shown in Fig. 6.

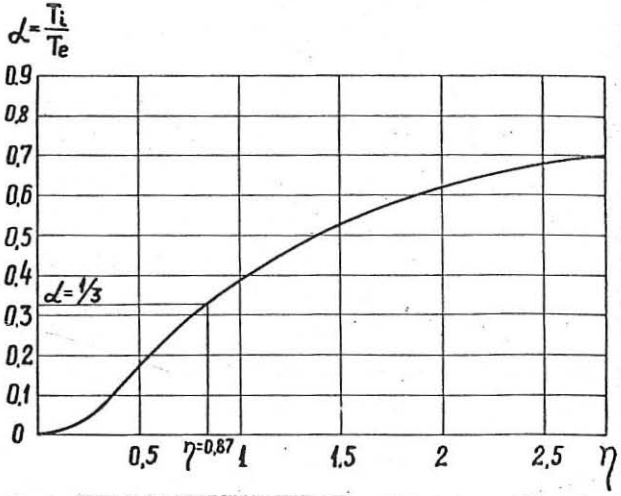


Fig. 6. Ion temperature dependence on electron temperature, plasma radius b and magnetic field $\left(\eta = \frac{\sqrt{\alpha}}{1-\alpha}\right)$

From the diagram it is obvious that the temperature of the ions cannot be higher than the temperature of the electrons and therefore $\alpha < 1$. For a weak magnetic field the ion temperature increases with the 4th power of the magnetic field. In stronger magnetic fields when α is close to 1/3 the ion temperature increases in proportion to the square of the magnetic field.

The influence of the magnetic field on the ion heat conductivity is caused by circular bending of ion trajectories. Owing to this, the free path of the ions decreases

and is limited by the diameter of the orbit as shown in [1], §7. Therefore the heat conductivity will be determined by the coefficient (5) only when it is less than the heat conductivity in the absence of a magnetic field (see[1], Eq. 4.26)

$$K_{i\perp} = 4{,}7 \cdot 10^{-32} \frac{n T_i \tau_i}{m_i} \qquad (10)$$

By comparing this expression with (5) we have:

$$\frac{K_{i\perp}}{K_i} = \left(\frac{0{,}73}{\omega_i \tau_i} \right)^2 . \qquad (11)$$

From this expression we get the value of the magnetic field. In stronger magnetic fields the heat transfer in a plasma will be determined only by the heat conductivity in a magnetic field. τ_i (the time of relaxation) there is a well known expression [1] (4.27):

$$\tau_i = 1{,}3 \cdot 10^{13} \frac{T_i^{3/2} \sqrt{m_i}}{\Lambda n} \text{ s} \; ; \; Z = 1 \qquad (12)$$

Then from the expression (6) and (11) we get:

$$H_K = 6{,}4 \cdot 10^{-6} \frac{\Lambda n}{T_i^{3/2}} \qquad (13)$$

For the plasma in our cord this magnetic field equals 5 kGs. Now we have all the necessary relations to estimate the temperature to which the ions can be heated by the electrons, and also to estimate the size of the installa-

tion necessary to insure a measurable continuous flux of neutrons.

The most direct method for determining the electron temperature of the plasma is to measure the density n and the pressure p, which are connected by the following classical relation

$$p = n_i k T_i + n_e k T_e + n_0 k T_0 . \qquad (14)$$

This expression is the basic one for determining the temperature as it is true for any velocity distribution function of particles. For hot and completely ionized hydrogen or deuterium plasma the density of the electrons n_e equals the density of the ions n_i and the density of the neutrals n_0 can be ignored. In our experiments we could also ignore the temperature T_i when compared with the temperature of electrons T_e.

Pressure p of the plasma can be taken as equal to the pressure of the surrounding gas [1] (4.16) as the surface tension of the double layer can be ignored. Therefore the temperature of electrons can be obtained simply by determining their density n_e:

$$n = n_i = n_e = \frac{7{,}3 \cdot 10^{21}}{T_e} p ; \; n_0 = 0 ; \; n_i = n ; \; T_e >> T_i . \qquad (15)$$

So far there are only two reliable methods to determine n. The first one was to measure the cutoff frequency of probing radiation. This frequency equalled the

plasma frequency of the electrons along the axis of the plasma cord. Then the density n could be determined from Langmuir's expression for plasma frequency. This method for determining the cutoff frequency has the advantage of being direct. But in real experimental conditions the transverse size of the probing beam was not too small compared to the diameter of the plasma cord. This resulted in a strong refraction which led to the overestimation of the cutoff frequency and measured values of electron density.

The second method is based on the measurement of the phase shift of the probing wave which occurs when it is propagating through the plasma cord. These measurements were made by means of an interferometer at a wavelength of 119 μm (water vapour laser). From these measurements we were able to find the profile of the electron density at a cross section of the cord and the absolute value of the density to an accuracy of about 10%. The results of the measurements of plasma diameter, the density n_e and the corresponding temperature T_e in deuterium plasma at a pressure of up to 8 at and power of up to 100 kw are given in Fig. 7-9. In these figures dashed lines indicate the regions of the experimentally measured plasma parameters.

So far we have said nothing about the length of the plasma discharge. To measure this length we had to build a special apparatus. Our results are shown in Fig. 10. The length of the plasma cord was up to 30 cm and its diameter was up to 5 cm. These sufficiently large dimensions enabled us to study the space distribution of the

parameters of the plasma electronic component by means of submillimeter waves. In all these measurements were used a number of original tec niques elaborated by our research workers E.A.Tishchenko, V.G.Zatsepin and V.B.Lazarev [5].

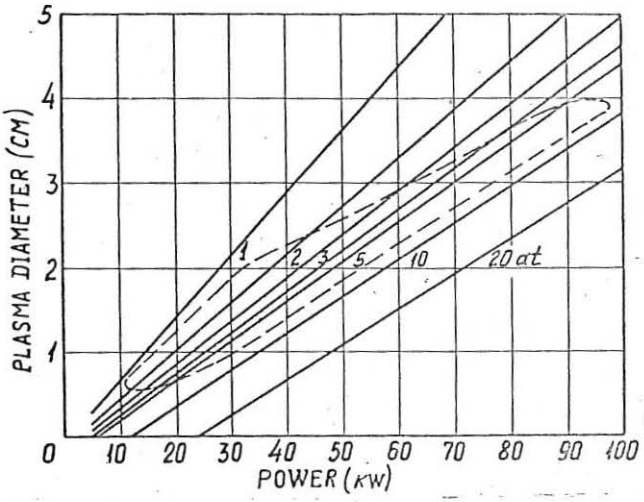


Fig. 7. Dependence of plasma diameter on power at different pressures in deuterium

An original type of laser on water vapours was constructed by G.D.Bogomolov and V.V.Zav'yalov [6].

Now we can be quite sure that the exceptionally high electron temperature of several million degrees was really reached. The physical possibility of the existence of hot plasma may be explained by effective thermal insulation at the boundary of the discharge (see [1], § 4). The electron temperature jump at the plasma boundary we connect with the existence of a double electrical layer

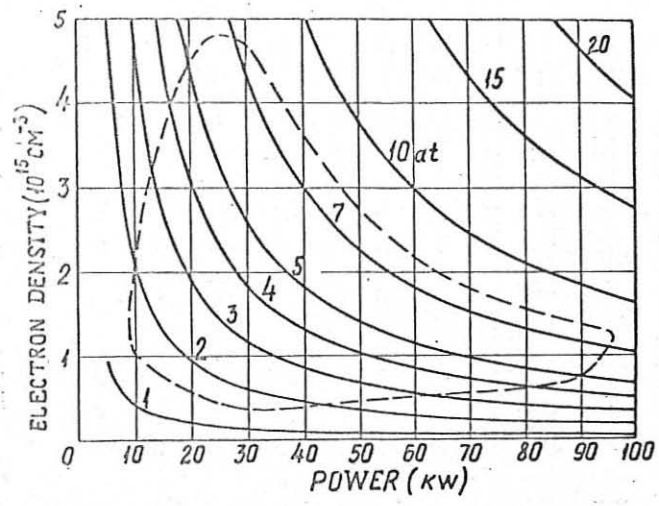


Fig. 8. Power dependence of electron density in deuterium plasma

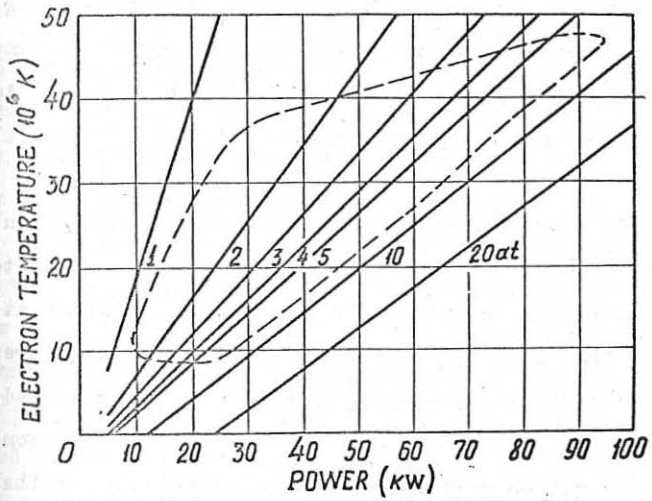


Fig. 9. Dependence of electron temperature on power

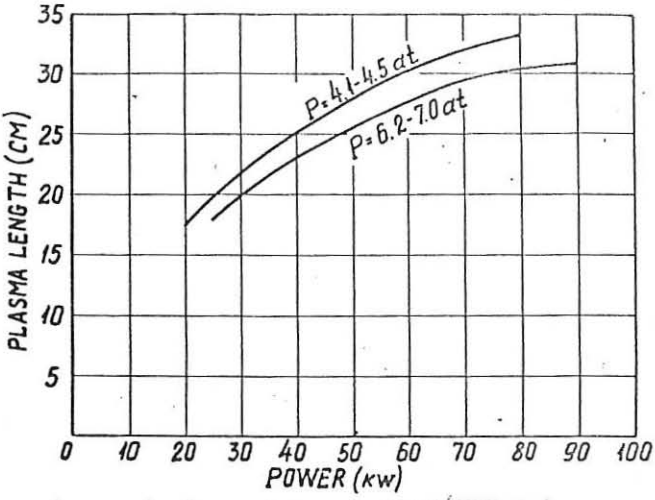


Fig. 10. Dependence of plasma length on supplied power

which reflects electrons without thermal losses. This explanation corresponds to that given by Langmuir a long time ago when describing an analogous temperature jump in a high pressure gas discharge tube. Such a double layer is formed at a dielectric boundary and makes it possible to raise the temperature of the electrons to tens of thousands of degrees. We assume by analogy that a double electric layer is formed in the cord discharge owing to the jump in its density. This is supported by the fact that a cord discharge can only be formed at a high pressure. At these pressures up to 25 at the plasma cord had clearly outlined boundaries. Under more favourable conditions the plasma cord had a radial distribution of the electron density almost of the rectangular shape.

Still other investigations were made which proved that our plasma was really hot. Let us enumerate them: from curves in Fig. ° which present the density of the electrons we see that with the increase of the applied power and the increase of the plasma temperature the density of the electrons correspondingly decreases. In a cold plasma just the opposite would have taken place.

There are certain other factors which confirm that the brightness of the radiation at the centre of the cord discharge decreases when the power is increased. A most significant fact is that the radiation at the lines of impurity atoms diminishes and at the same time the bremsstrahlung increases. This has a very natural explanation (see [1]). In such a case the temperature of the plasma increases.

Investigations of the skin-resistance of the plasma cord in a hot plasma were described in[1, 7]. These experiments showed without exception that the resistance was many times less than in a cold plasma and so proved the high temperature of our plasma once again.

Particular attention should be paid to the influence of the magnetic field on the plasma cord. This question was discussed in § 7 of [1]. It is characteristic that when the gas pressure is less than 2 at and the intensity of the longitudinal magnetic field reaches 24 kGs, the cord is slightly lengthened and radially compressed. At the same time the electron density along the cord axis is slightly increased and, as shown by the formula (15) the temperature of the electrons falls. At high pressure

Max-Planck-Institut für Plasmaphysik

this effect practically disappears. We explain this effect (see [1] , § 7) by the fact that at low pressures, less than 2 at, the double layer is not yet fully formed and the magnetic field influences the anomalous skin-resistance causing it to decrease.

For several years we made experiments for measuring the diamagnetic moment of the plasma cord using a diamagnetic probing coil. We used two methods - the modulation technique for a stationary discharge and quenching of the plasma. They both revealed that plasma magnetization did not exceed 1 Gs in the external field up to 24 kGs. This effect shows that the plasma of the cord discharge is probably in a near-equilibrium state.

K.A.Zhdanov, V.G.Zatsepin and E.A.Tishchenko took part in the experiments to measure the diamagnetism of the cord.

Now we must again pay very particular attention to the spectral radiation of the plasma in a wide range of wavelengths. Application of this technique in visible range was described in [1] ,§ 3. Generally the parameters of the plasma are determined by measuring the Doppler and Stark broadening of the spectrum lines.

This investigation led us into unexpected difficulties, simply because in the hot region of the cord discharge there were no spectrum lines and the spectrum consisted entirely of bremsstrahlung. The presence of bremsstrahlung at the far-ultraviolet region (1000 Å) also gives us the value of the electron temperature. There-

fore we paid particular attention to the spectral method in this region.

The main difficulty is the strong absorption of the photons at these energies in the hydrogen surrounding the cord discharge. This absorption greatly increases in the presence of even small amounts of impurities. Therefore the photons could not be found for a long time. At first we tried to detect these photons of high energy with a photomultiplier registering the filtered light radiation. In the end we managed to find the photons by using the gas-flow counter instead of the photomultiplier. This counter is sensitive only to photons with energies of more than 90 eV but is insensitive to ultraviolet radiation. In this way we managed to discover photons of up to 300 eV in the plasma cord. This corresponds to a temperature of $T_e > 3 \cdot 10^6$K. These counters were suggested and constructed by V.D.Peskov.

Now the investigations of this radiation and the determination of its spectrum is conducted by V.D.Peskov and E.R.Podolyak.

An investigation of the scattering of a laser beam in the plasma cord threw some light on the processes taking place in the plasma.

By measuring the profile of the line of the scattered laser radiation one can, theoretically, determine not only the mean velocity of the electrons but also the electron velocity distribution function. It is well known that these measurements can be accomplished by means of the

radiation from a powerful laser. This method is used to investigate only rare plasma.

The investigation of our plasma cord by this method presents great difficulties as the scattering which has an intensity proportional to n_e has to be detected at the background of a powerful continuous plasma radiation which is proportional to the square of the electron density n_e^2 along the whole spectrum.

This research work is in the hands of G.D.Bogomolov and V.V.Zavyalov but so far we cannot be sure that the difficulties will be overcome.

From this short summary of our investigations we see that there are no factors which contradict the existence in our cord of a plasma with an electron temperature of tens of millions of degrees. Therefore all we need to obtain thermonuclear fusion is that the temperature of the ions and that of the electrons in our plasma cord should be of the same order.

The main difficulty in achieving a thermonuclear reaction by our method is to obtain this equilibrium.

The heating of our plasma is achieved by means of the action of the microwave field on the electrons which absorb the supplied energy. Owing to the confining double layer in practice we can assume that all this energy goes to heating of the ions. This energy is then transferred to the surrounding medium by the usual collision process. It is obvious that the ion temperature will be lower than the electron temperature as the amount of heat transferred will be small owing to the great difference in the mass

of the electrons and ions.

Our problem is to provide the conditions under which the electron and ion temperature will be equal.

The amount of heat transferred from the electrons to the ions in the plasma is proportional to the volume of the plasma cord. Ions lose part of this heat when penetrating the boundary (of the cord) into the surrounding medium. Therefore for a given heat conductivity of the ion gas the temperature of the ions grows with an increase in the radius of the cord. From this we see that for a given heat conductivity of the ion gas there will be a critical cross section of the plasma cord at which the temperature of the ions reaches a value close to the electron temperature - the condition necessary for a thermonuclear reaction. However an estimation of the known ion heat conductivity of the plasma showed that the critical values of the cord's diameters would have to be of the order of several kilometers. This cross section could be decreased by decreasing the heat conductivity of the ion gas. This latter could be achieved by placing the cord in a magnetic field. From the aforementioned formulas we find that the diameter of the critical cross section of a plasma cord in a strong magnetic field of some tens of kilogauss is about 10 cm. We have hopes of achieving this in the near future.

These estimations have not taken into account the possible appearance of heat conductivity by convection. According to Maxwell's formula when the length of the

mean free path of the electrons and ions in the plasma is of the order of centimeters and the temperature gradient is very large the inner stresses can be very strong - ten orders of magnitude greater than in gases. This could lead to convectional currents and turbulence in plasma.

The presence of a magnetic field could influence the character of these phenomena and with additional effect of an electric field on convection, could make a theoretical approach exceedingly complicated even with a very rough estimation of the convection.

Undoubtedly, convectional conductivity will lessen the effectiveness of the heating of the ions and then the critical cross section of the plasma cord will increase, and with it the size of the reactor for producing useful energy. If these sizes reach an impracticable value we will have to find a way to decrease the convectional heat conductivity.

Another problem which has to be solved is the heat loss at the end of the cord. This heat loss is due to the following factors. The first factor is the fast particles in the plasma which may exist at the "tail" of the velocity distribution function. The second is the ordinary thermal particles. Both these losses can be compensated by exchanging the linear plasma cord discharge for a circular plasma cord discharge. For this we must have a toroidal multi-slit resonator.

There are many interesting problems demanding a solution and in conclusion I would like to mention one of them as an

example. Let us take the transformation of the microwave discharge from a diffuse state into a cord-like one. Here we are immediately faced with much of interest. Apparently, the phenomenon strongly depends on the type of gas, its pressure and the amount of power supplied to the plasma. For instance, this transformation in helium presented many difficulties. We succeeded only after a very careful cleansing of the resonator of all the impurities (especially hydrogen) having an ionization potential less than helium. Only after this processing the helium took on a cord-like shape at a pressure of about 18 at and power of about 10 kw. This is only one example to underline the absolute necessity of carrying out all experiments with the greatest care and accuracy.

Without a deep understanding of the processes taking place in the plasma we shall never be able to understand the mechanism of the cord formation. The study of these processes is now at the stage when experiment is in advance of theory.

References

1. P.L.Kapitza, ZETF, V.57, p.1801 (1969); Sov.Phys.JETP, v. 30, p. 973 (1970).
2. P.L.Kapitza, ZETF, v.58, p.377 (1970); Sov.Phys.JETP , v. 31, p.199 (1970).
3. P.L.Kapitza, Pis'ma v ZETF, v.22, p.20 (1975); JETP Letters, v.22, p.9 (1975).
4. P.L.Kapitza, L.P.Pitaévskii, ZETF, v.67, p.1411 (1974);

Sov.Phys.JETP, v.40, p. 701 (1975).

5. V.B.Lazarev, E.A.Tishchenko, V.G.Zatsepin, ZTF, v.50, p. 186 (1980).
6. V.V.Zav'yalov, G.D.Bogomolov, Pis'ma v ZETF, v. 20, p. 393 (1974); JETP Letters, v.20, p.176 (1974).
7. P.L.Kapitza, S.I.Filimonov, ZETF, v. 61, p.1016 (1971); Sov.Phys.JETP, v.34,p.542 (1972).

MUON CATALYSIS OF NUCLEAR FUSION IN DEUTERIUM-TRITIUM MIXTURE

L.I.Ponomarev
Joint Institute for Nuclear Research
Dubna, USSR

1. Introduction

The early history of the muon catalysis was reviewed in detail in papers [1,2]. It originated in 1947 from the hypothesis by Frank [3], he came to while interpreting the experiments by Lattes, Occhialini and Powell [4] where decay of pion into muon $\pi^- \to \mu^-$ had been identified. In 1954 Zel'dovich [5] considered some of μ-catalysis stages and estimated their rates. In 1957 the experiment by Alvarez et al. [6] where the μ-catalysed fusion was observed in H_2+D_2 mixture completed this first period.

From 1957 to 1963 the most part of both experimental (L.Lederman et al., V.P.Dzhelepov et al., A.Ashmore et al., J.Doede et al.) and theoretical (Ya.B.Zel'dovich, S.S.Gerstein, J.Jackson, S.Cohen et al., etc) works were performed (see surveys [1,2]) where the μ-catalysis stages had been studied in detail mainly in H_2+D_2 mixture and pure deuterium D_2 . In these studies the idea to use muon catalysis as a way of nuclear energy production was found unreal [1,7,8] .

The interest to this idea revived in 1977 when the high efficiency of muon catalysis in deuterium-tritium mixture was predicted [9], the statement having been supported experimentally by V.P.Dzhelepov, V.G.Zinov et al.[10] in 1979. The present survey covers this latter period of muon catalysis investigations as well as the studies by Yu.V.Petrov [11] who showed that the muon catalysed dt - fusion combined with the fissile nuclides blanket can provide a positive energy gain.

In the following we do not concern any technical or engineering aspects of this problem, because they can become of actual interest only after the muon catalysis phenomenon as itself be examined rather well.

First of all three main questions should be answered:

how many dt -reactions one muon can catalyse?

what is the energy necessary to produce one muon?

what is the net energy output per one muon, the multiplication of fusion neutrons in the uranium blanket being taken into account?

The main idea of the muon catalysis is well known: μ^- of mass $m_\mu = 206.8 m_e$ forms a mesic molecule $dt\mu$ [x] with nuclei d and t, the distance between them being diminished down to $\sim 5.10^{-11}$ cm and

---

[x] Following the tradition we use the term "mesic molecule" for the mesic molecular ions $(dt\mu)^+$, $(dd\mu)^+$, etc, i.e., the systems of a muon and two hydrogen isotope nuclei.

hence the probability of nuclei penetration through the Coulomb repulsion barrier increasing to such an extent that the nuclear fusion

$$d + t \longrightarrow {}^4He + n + 17.6\ MeV \qquad (1)$$

occurs during 10^{-12} s, i.e. practically instantly compared to the μ^--lifetime $\tau_0 = 2.2\ 10^{-6}$ s. With 0.99 probability the μ^- is released and can catalyse the next fusion. The number of cycles which a muon has time to catalyse depends on all the mesic atomic and mesic molecular processes which occur in the deuterium-tritium mixture.

Note that contrary to the thermonuclear synthesis where reaction (1) should take place at high temperature $\sim 10^8$ °K and small density $\sim 10^{14}$ cm^{-3} of D_2+T_2 mixture, the most favourable conditions for μ-catalysed fusion are fulfilled at temperatures 10^2–10^3 °K and density $\sim 4 \cdot 10^{22}$ cm^{-3}, i.e. practically at the room temperature and the pressure of D_2+T_2 mixture about 10^3 atm.

2. Kinetics of the Muon Catalysis Processes

The muons are produced from the decay of pions generated in the collisions of accelerated protons (deuterons, tritons, etc) with a nuclear target. At projectile energy about 1 GeV/nucleon the decay muons have the average energy $\sim$ 200 MeV. In the dense D_2+T_2 mixture they slow down to energies 2 keV during $\sim 10^{-8}$ s /12,13/ and then during $\sim 10^{-11}$ s cascade down to K-orbits of $d\mu$ and $t\mu$-mesic atoms /14/ .

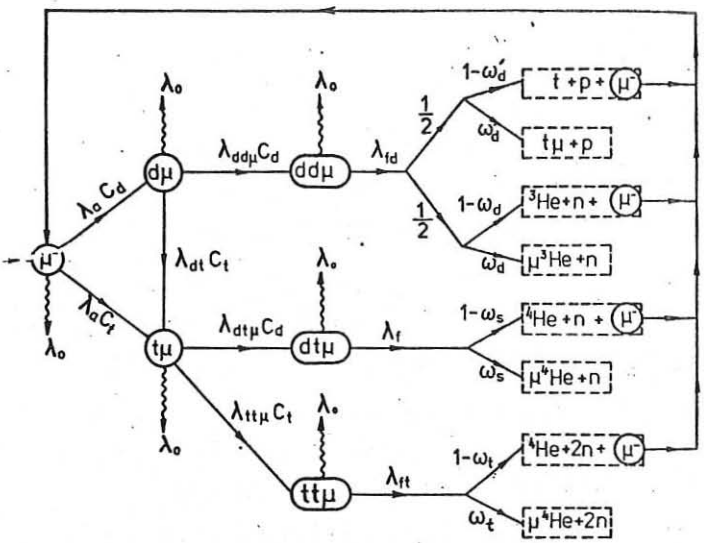


Fig.1. The scheme of the muon catalysis processes in deuterium-tritium mixture.

The general scheme of the subsequent processes of muon catalysis is pictured in Fig.1. Mesic atoms $d\mu$ and $t\mu$ with initial energy ~ 1 eV [12] colliding with nuclei of D_2 and T_2 molecules form mesic molecules $dt\mu$, $dd\mu$ and $tt\mu$, the rates being $\lambda_{dt\mu}$, $\lambda_{dd\mu}$ and $\lambda_{tt\mu}$, respectively. Besides, since the ground state of $t\mu$-atom is by 48 eV deeper than that of $d\mu$-atom, the irreversible isotopic exchange process

$$d\mu + t \longrightarrow t\mu + d \qquad (2)$$

takes place with the rate λ_{dt}.

In the mesic molecules $dt\mu$, $dd\mu$ and $tt\mu$ the nuclear fusion occurs with rates λ_f, λ_{fd} and

λ_{ft} , respectively.

The number of cycles X_c catalysed by one muon during its life-time $\tau_o = \lambda_o^{-1}$ is /15/:

$$X_c^{-1} = \omega_s + \frac{\lambda_o C_d}{\lambda_{dt} C_t} + \frac{\lambda_o}{\lambda_{dt\mu} C_d} + \frac{\omega_d}{2} \cdot \frac{\lambda_{dd\mu}}{\lambda_{dt\mu}} + \omega_t \cdot \frac{\lambda_{tt\mu} C_t}{\lambda_{dt\mu} C_d} \qquad (3)$$

Here C_d and C_t are relative concentrations of deuterium and tritium ($C_d + C_t = 1$); all the rates correspond to the given temperature and density of D_2+T_2 mixture, ω_s , ω_d and ω_t are the probabilities of muon sticking to helium in the reactions:

$$dt\mu \longrightarrow \mu\,^4\mathrm{He} + n \qquad (4a)$$

$$dd\mu \longrightarrow \mu\,^3\mathrm{He} + n \qquad (4b)$$

$$tt\mu \longrightarrow \mu\,^4\mathrm{He} + 2n \qquad (4c)$$

The number of cycles X_c depends mainly on the values of ω_s , λ_{dt} and $\lambda_{dt\mu}$. It is evident that even at infinitely high rates λ_{dt} and $\lambda_{dt\mu}$ the quantity $X_c = \omega_s^{-1}$ is limited by the relative probability ω_s of processes (4a) and $dt\mu \longrightarrow {}^4\mathrm{He} + n + \mu^-$. For a long time the theoretical estimates of the $dt\mu$-molecule formation rate gave $\lambda_{dt\mu} \sim 10^4\ s^{-1}$ /1/ which in accordance with (3) lead to $X_c < 1$ and, hence, to the conclusion about μ - catalysis inefficiency.

The situation altered in 1977 when the existence of a loosely bound state of $dt\mu$-mesic molecule was established /9/ and the high rate of $dt\mu$ resonant formation ($\lambda_{dt\mu} \gg \lambda_o$) was predicted. This enabled one to

Table 1

The main characteristics of the muon catalysis processes

Process	Theory	Experiment	References
Atomic capture, λ°_{a}, s^{-1} $\mu^- + D_2 \longrightarrow d\mu + D + e$	$\sim 10^{11}$	$> 10^{10}$	Markushin /14/ Anderhub et al. /16/
Isotopic exchange, λ°_{dt}, s^{-1} $d\mu + t \longrightarrow t\mu + d$	$2 \cdot 10^{8}$	$(2.9 \pm 0.4) \cdot 10^{8}$	Ponomarev /17/ Bystritsky et al. /10/
$dd\mu$-molecule formation, $\lambda_{dd\mu}$, s^{-1} $d\mu + D_2 \longrightarrow [(dd\mu)^+ d2e]^*_{\nu}$	$0.8 \cdot 10^{6}$ x)	$(0.85 \pm 0.11) \cdot 10^{6}$	Vinitsky et al. /9/ Bystritsky et al. /18/
$dt\mu$-molecule formation, $\lambda_{dt\mu}$, s^{-1} $t\mu + D_2 \longrightarrow [(dt\mu)^+ d2e]^*_{\nu}$	$\gtrsim 10^{8}$ x)	$> 10^{8}$	Vinitsky et al. /9/ Bystritsky et al. /10/
$tt\mu$-molecule formation, $\lambda_{tt\mu}$, s^{-1} $t\mu + T_2 \longrightarrow [(tt\mu)^+ te]^+ + e$	$3.0\,10^{6}$	–	Ponomarev and Faifman /19/
Spin-flip process, λ°_{d}, s^{-1} $d\mu(\uparrow\uparrow) + d \longrightarrow d\mu(\uparrow\downarrow) + d$	$4.6 \cdot 10^{7}$	$> 4 \cdot 10^{7}$	Ponomarev et al. /20/ Bystritsky et al. /34/
Spin-flip process, λ°_{t}, s^{-1} $t\mu(\uparrow\uparrow) + t \longrightarrow t\mu(\uparrow\downarrow) + t$	$0.9 \cdot 10^{9}$	–	Matveenko et al. /21/

Sticking probability, ω_s $dt\mu \rightarrow \mu^4He + n$	$0.86 \cdot 10^{-2}$ $0.91 \cdot 10^{-2}$	-	Gerstein et al. /22/ Bracci and Fiorentini /23/
Sticking probability, ω_d $dd\mu \rightarrow \mu^3He + n$	0.15	< 0.13	Gerstein et al. /22/ Dzhelepov et al. /33/
Sticking probability, ω_t $tt\mu \rightarrow \mu^4He + 2n$	~0.1	-	Gerstein et al. /22/
Nuclear reaction, λ_f, s^{-1} $dt\mu \rightarrow {}^4He + n + \mu^-$	$1.1 \cdot 10^{12}$	-	Bogdanova et al. /24/
Nuclear reaction, λ_{fd}, s^{-1} $dd\mu \rightarrow {}^3He + n + \mu^-$	$5 \cdot 10^{10}$	-	Vesman /25/
Nuclear reaction, λ_{ft}, s^{-1} $tt\mu \rightarrow {}^4He + 2n + \mu^-$	-	-	
Molecular isotopic exchange, λ_m, s^{-1} $t\mu + {}^3He \rightarrow t\mu^3He \rightarrow \mu^3He + t$	$5 \cdot 10^8$	-	Aristov et al. /26/

x) The values of $\lambda^{\circ}_{dd\mu}$ and $\lambda^{\circ}_{dt\mu}$ are given at the resonant collision energy.

revise the idea of μ -catalysis and to reconsider the possibility of its practical use.

3. The Rates of Muon Catalyses Processes

As a rule the rates of mesic atomic and mesic molecular processes are proportional to the density of the mixture: $\lambda_{dt}=\lambda^{\circ}_{dt}\varphi$, $\lambda_{dt\mu}=\lambda^{\circ}_{dt\mu}\varphi$, etc., where $\varphi = \rho/\rho_{\circ}$ is the density of the mixture, $\rho_{\circ} = 4.25\cdot10^{22}$ cm^{-3} is the density of the liquid hydrogen, λ°_{dt} , $\lambda^{\circ}_{dt\mu}$, etc. are the rates of the corresponding processes reduced to the density $\rho_{\circ}$. Their theoretical and experimental values are listed in Table 1.

Mesic molecules $dt\mu$ and $dd\mu$ can be formed in five, and $tt\mu$ in six states of rotational (J) and vibrational (v) motions, their binding energies ε_{Jv} being limited between 360 eV and 0.7 eV. (See Table 2).

Table 2

The binding energies ε_{Jv} (eV) of (Jv) states of mesic molecules x)

(Jv)	(00)	(01)	(10)	(11)	(20)	(30)
$dd\mu$	325.0	35.8	226.6	1.91	86.3	-
$dt\mu$	319.2	34.9	232.4	0.64	102.5	-
$tt\mu$	363.0	83.9	289.2	45.2	172.7	48.7

x) The results of paper /27/ . For the mesic molecule $dt\mu$ the binding energy is reckoned from the ground state of $t\mu$ mesic atom.

Mesic molecule $tt\mu$ is formed predominantly in the state (J=1, v=1) with the binding energy $\varepsilon_{11} = 45.2$ eV by the dipole E1-transition with the conversion of the electron of T_2 molecule, according to the scheme

$$t\mu + T_2 \longrightarrow [(tt\mu)^+ t\, e]^+ + e$$

Mesic molecular ion $(tt\mu)^+$ stands for the heavy "nucleus" of a usual molecular ion, the released binding energy ε_{11} being carried away by the emitted electron. The rate of this nonresonant process is comparatively low: $\lambda^{\circ}_{tt\mu} = 3\cdot 10^6$ s^{-1} /19/.

The formation of $dd\mu$ and $dt\mu$ molecules due to the existence of loosely bound states (J=1, v=1) with binding energies $\varepsilon_{11}(dd\mu) = 1.91$ eV and $\varepsilon_{11}(dt\mu) = 0.64$ eV /27/ occurs according to the resonant mechanism suggested by Vesman /28/ for the formation of $dd\mu$ molecule:

$$d\mu + D_2 \longrightarrow [(dd\mu)^+ d\, 2e]^*_\nu \qquad (5)$$

In such a process there is no electron emission, the binding energy $\varepsilon_{11}(dd\mu)$ being transferred to the excitation of the vibrational state ν of the molecular complex with the mesic molecular ion $(dd\mu)^+$ as the specific "nucleus". After experiments /18/ and theoretical calculations /9, 27, 28/ the existence of such a resonant mechanism can be confidently trusted.

The rate $\lambda^{\circ}_{dt\mu} \gtrsim 10^8$ s^{-1} of the analogous reaction of the $dt\mu$ -molecule resonant formation (see Fig.2)

$$t\mu + D_2 \longrightarrow [(dt\mu)^+ d\, 2e]^*_\nu \qquad (6)$$

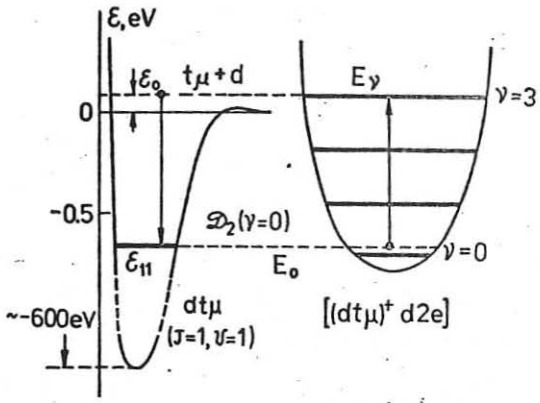


Fig.2. The scheme of the $dt\mu$ -molecule resonant formation: the process takes place provided the resonance condition $\varepsilon_o + |\varepsilon_{11}| = |E_o - E_\nu|$ is fulfilled, where ε_o is the $t\mu$ -atom kinetic energy, ε_{11} the $dt\mu$-molecule (J=1, ν=1) state binding energy, E_o the D_2 molecule ground state energy, E_ν the energy of the molecular complex $[(dt\mu)^+ d2e]$ vibrational state ν .

was calculated in paper /9/ . It turned out to exceed significantly the previous estimates ($\lambda^\circ_{dt\mu} \sim 10^4$ s^{-1}) /1/ and the rate $\lambda^\circ_{dd\mu}$. The experimental lower limit $\lambda^\circ_{dt\mu} > 10^8 s^{-1}$ has been recently obtained at the Laboratory of Nuclear Problems of JINR and is in fair agreement with the theoretical predictions.

The muon sticking probabilities ω_s, ω_d and ω_t (see Fig.1) were calculated in papers /7,8,22,23/. Their values are listed in Table 1, the probability of μ^- - stripping while μHe atoms slowing down

$$(\mu He)^+ + d \longrightarrow \begin{cases} He^{++} + d\mu \\ He^{++} + d + \mu^- \end{cases} \qquad (7)$$

being taken into account. According to /22,23/ the stripping process diminishes the initial magnitude of ω_s by 20-25%.

4. The Number of Muon Catalysed Cycles

As it is seen from Table 1, the most of muon catalysis processes have not been studied experimentally. Hence, the number of cycles X_c can be only estimated.

It follows from expression (3), that the maximum number of cycles X_c is achieved at the tritium concentration $C_t \approx (1+\gamma)^{-1}$ in $D_2 + T_2$ mixture /15/, where

$$\gamma = \left(\lambda_{dt} / \lambda_{dt\mu} \right)^{1/2} \qquad (8a)$$

$$X_c^{-1} = \omega_s + \frac{\lambda_0}{\lambda^0_{dt}\varphi} \gamma \left(2 + \gamma + 0.7\varphi\right) \qquad (8b)$$

Using the data from Table I we obtain the lower limit for X_c at the density of liquid hydrogen $\varphi = 1$

$$X_c > 50 \qquad (9)$$

This estimate is rather sensitive to the rate $\lambda^0_{dt\mu}$. Estimate (9) was obtained with the rate $\lambda^0_{dt\mu} = 10^8\ s^{-1}$ corresponding to the binding energy $\varepsilon_{11}(dt\mu) = 1.09$ eV. The subsequent refined calculations /27/ give for the binding energy $\varepsilon_{11}(dt\mu) = 0.64$ eV, and hence, essentially

higher rate $\lambda^{\circ}_{dt\mu}$ is expected: $\lambda^{\circ}_{dt\mu} = 3 \cdot 10^{8}$ s^{-1} giving $X_c \approx 70$, $\lambda^{\circ}_{dt\mu} = 10^{9}$ s^{-1} giving $X_c \approx 100$.

The current value $\omega_s \approx 0.9 \cdot 10^{-2}$ is valid provided reaction (4a) occurs from the ground state (J=0, v=0) of mesic molecule $dt\mu$. However, the $dt\mu$-molecule is resonantly formed not in the ground state but in the fifth excited one (J=1, v=1; see Table 2). During the cascade transitions from the latter to the (J=0, v=0) state, fusion can occur in the intermediate state (Jv) of the $dt\mu$-molecule, the muon sticking probability being suppresses for the fusion in the rotational J=1 states. It should lead effectively to some additional decrease of ω_s compared to that from Table 1.

There are many additional effects which can influence the details of muon catalysis: relativistic corrections to the energy levels of mesic molecules /29-32/, the molecular charge-exchange process /26/, the kinetics of thermalization of muonic atoms, etc.

Refined values of $\lambda^{\circ}_{dt\mu}$ and ω_s are being calculated at present, but still to determine the number of cycles X_c conclusively, of utmost importance is experimental measurement of $\lambda^{\circ}_{dt\mu}$ and ω_s as well as "the integral experiment", i.e. direct measurement of X_c in a wide range of φ and C_t.

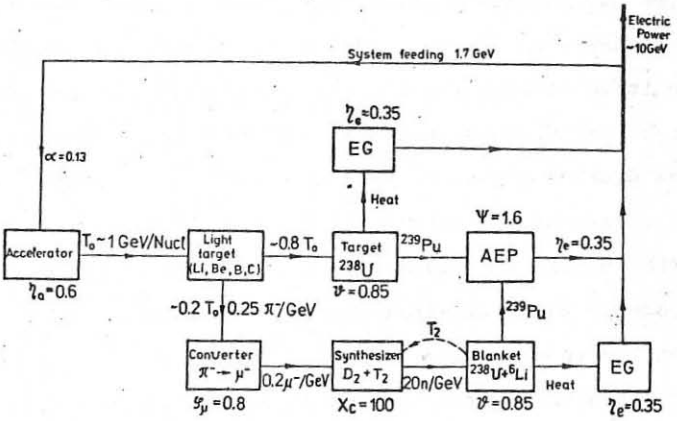


Fig.3. The scheme of the muon catalysis hybrid fusion–fission breeder.

5. The Energy Balance of Muon Catalysis

One of the conceivable schemes of muon catalytic hybrid fusion–fission breeder (MC–Hybreeder) /35/ is presented in Fig.3. The deuteron beam with the energy T_o ~1 GeV/nucleon produces 0.25 π^-/GeV in the light target (Li, Be, B, C), spending ~20% of the projectile initial energy /36/ x). It is known /37/ that fast nucleons cause

x) Since at intermediate energies π^- are preferably generated in neutron–neutron collisions, the maximum yield ~ 0.5 π^-/GeV should be expected for the tritium as both projectile and target /36/. Light elements are preferred as a target because for them both the nuclear absorption of pions produced and radiative losses are minimal.

about 20 fissions per 1 GeV in ^{238}U -target and produce 60 ^{239}Pu nuclei, their yield increasing linearly with the nucleon energy in the range 0.5÷2 GeV. Hence, the deuterons of the incident beam, having about 0.8 GeV/nucleon after the light target cause 0.8×20 =16 fissions in ^{238}U and produce 0.8×60×0.85 = 41 ^{239}Pu nuclei /11/ ($\vartheta = 0.85$ is the slow neutron utilization factor). These latter can give 41×1.6 =65 additional fissions in a thermal reactor (Ψ =1.6 is the multiplication factor, which takes into account the Pu breeding in a thermal reactor /11/). Thus, in the scheme considered the electronuclear breeding channel (EN-channel) can produce in all 16+65=81 fissions, i.e. 81×0.2 ≈ 16 GeV of thermal or 16×0.35 =5.6 GeV of electric energy ($\eta_e = 0.35$ is the efficiency of nuclear power plants).

In the muon catalytic channel (MC-channel) the pions generated in the light target decay to μ^- and antineutrino with probability φ_μ . Accepting rather an optimistic value of the conversion coefficient $\varphi_\mu = 0.8$, we find that 0.25×0.8=0.2 μ^- /GeV are produced, which after catalysing X_c = 100 fusions (1) in D_2+T_2 mixture release 0.2×100× ×17,6 MeV = 0.35 GeV energy and 20 neutrons.

In a thick ^{239}U blanket each fusion neutron with energy 14.1 MeV produces 1 fission and 4 additional slow neutrons /11/ . Taking into account the slow neutrons utilization factor ϑ , and spending one neutron for tritium regeneration, we find that 4 fusion neutrons produce in the blanket 4×0,85-1 =2.4 commercial ones and

consequently 2.4 ^{239}Pu nuclei. Thus, there in the MC-channel 20 fissions plus 20×2.4×1.6 =77 fissions of ^{239}Pu, i.e. altogether 97 fissions occur which produce 97×0.2≈19 GeV of thermal or 6.8 GeV of electric energy.

The total energy output in EN-and MC- channels is 35 GeV of thermal or 12 GeV of electric energy per 1 GeV of beam energy, 45% of which being due to EN-channel and 55% to MC-channel. The analogue of the plasma energy gain factor equals Q=0.35 for MC-channel, and with the EN-channel taken into account, i.e. for MC-Hybreeder system as a whole Q=0.6. The blanket provides the additional energy gain by a factor of 60.

Believing the efficiency of the accelerator to be $\eta_a = 0.6$ /38/ for MC-Hybreeder we obtain 12 GeV electric energy output per 1/0.6=1.7 GeV input energy, i.e. the fraction of energy spent for the system feeding is $\alpha = 0.13$.

6. Summary

Serious studies of μ-catalysis in the deuterium-tritium mixture have in fact just begun. Till now even its main characteristics have not been measured: the total number of μ-catalysis cycles X_c, the sticking probability ω_s; only the lower limit of the $dt\mu$-molecule formation rate $\lambda_{dt\mu}$ has been measured. Besides, the π^--mesons yield from the deuteron (or triton) collisions with a light nuclear target has not been measured and the $\pi^- \to \mu^-$ conversion coefficient φ_μ is unknown for the realistic facilities.

It is also necessary to know some other properties of the process in question: the rate $\lambda^{o}_{tt\mu}$, the values ω_d and ω_t, the rates λ_{fd} and λ_{ft}, etc.

Nevertheless, even today one can conclude that μ-catalysis of nuclear fusion reaction $d + t \longrightarrow {}^4He + n$ combined with Uranium-238 blanket can provude the positive energy output. The economical efficiency of such means of nuclear energy production and its technical realization depend, actually, on successful solution of many engineering problems.

In any case, there is no doubt that the muon catalysys phenomenon is worth to be investigated thoroughly.

References

1. Ja.B.Zel'dovich and S.S.Gerstein, Uspekhi Fiz.Nauk 71, 581 (1960); English transl. Sov.Phys.-Uspekhi 3, 593 (1961).
2. S.S.Gerstein and L.I.Ponomarev, "Mesomolecular Processes Induces by μ^- and π^- Mesons", in "Muon Physics", v. III, p.141, Eds. V.Hughes and C.S.Wu, Academic Press, N.Y., 1975.
3. F.C.Frank, Nature 160, 525 (1947).
4. C.M.G.Lattes, G.P.S.Occhialini and C.F.Powell, Nature 160, 453 (1947); 160, 486 (1947).

5. Ya.B.Zel'dovich, Doklady Akad.Nauk USSR 95, 493 (1954);
6. L.W.Alvarez, H.Brander, F.S.Crawford, Jr., J.A.Crawford, P.Falk-Vairant, M.L.Good, J.D.Gow, A.H.Rosenfeld, F.Solmitz, M.L.Stevenson, H.K.Ticho and R.D.Tripp, Phys.Rev. 105, 1127 (1957).
7. Ya.B.Zel'dovich, Zh.Eksper.Teor.Fiz. 33, 310 (1957); English transl. Sov.Phys.- JETP 6, 242 (1958).
8. J.D.Jackson, Phys.Rev. 106, 330 (1957).
9. L.I.Ponomarev, Proc. VII Int.Conf.High Energy Phys. and Nucl.Structure, p.403, Zurich, 28 Aug.-2 Sept., 1977. S.S.Gerstein and L.I.Ponomarev, Phys.Lett. 72B, 80 (1977).
S.I.Vinitsky, L.I.Ponomarev, I.V.Puzynin, T.P.Puzynina, L.N.Somov and M.P.Faifman, Zh.Eksper.Teor.Fiz. 74, 849 (1978); English transl. Sov.Phys.-JETP 47, 444 (1979).
10. V.M.Bystritsky, V.D.Dzhelepov, Z.V.Ershova, V.G.Zinov, V.K.Kapyshev, S.M.Mukhamet - Galeeva, V.S.Nadezhdin, L.A.Rivkis, A.I.Rudenko, V.I.Satarov, N.V.Sergeeva, L.N.Somov, V.A.Stolupin, V.V.Fil'chenkov, Zh.Eksper. Teor.Fiz. - Pisma, 31, 249 (1980); English transl. Sov. Phys.-JETP, Letters, 31, 228 (1980). Zh.Eksper.Teor.Fiz. 80, 1700 (1981).
11. Yu.V.Petrov, Nature 285, 466 (1980);
Yu.V.Petrov, Proc. 14th LNPI Winter School, p.139, Leningrad, 1979.

12. M.Leon, H.Bethe, Phys.Rev. 127, 636 (1962).

13. G.Ya.Korenman, Yadern. Fiz. 32, 916 (1980).

14. V.E.Markushin, Zh.Eksper.Teor.Fiz. 80, 35 (1981).

15. S.S.Gerstein, Yu.V.Petrov, L.I.Ponomarev, L.N.Somov and M.P.Faifman, Zh.Eksp.Teor.Fiz. 78, 2099 (1980); English transl. Sov.Phys. - JETP 51, 1053 (1981).

16. H.Anderhub, J.Böcklin, M.Devereux, F.Dittus, R.Ferreira Marques, H.Hofer, Hein Hofer, F.Kottmann, O.Pitzurra, P.G.Seiler, D.Taqqu, Ch.Tschallär, J.Unternährer, M.Wälchli, SIN Newsletter No.12, 32 (1979).

17. L.I.Ponomarev, Proc. VI Int.Conf. on Atomic Physics, Riga, 17-22 Aug., 1978, p.182, Zinante-Riga, Plenum Press - New York.

18. V.P.Dzhelepov, P.F.Ermolov, V.I.Moskalev and V.V. Fil'chenkov, Zh.Eksper.Teor.Fiz. 50, 1235 (1966); English transl. Sov.Phys.-JETP 23, 820 (1966).
V.M.Bystritsky, V.P.Dzhelepov, K.O.Oganesyan, M.N.Omel'janenko, S.Yu.Porokhovoj, A.I.Rudenko, V.V.Fil'chenkov, Zh.Eksper.Teor.Fiz. 66, 61 (1974); English transl. Sov.Phys. - JETP, 39, 19 (1974).
V.M.Bystritsky, V.P.Dzhelepov, V.I.Petrukhin, A.I.Rudenko, L.N.Somov, V.M.Suvorov, V.V.Fil'chenkov, G.Hemnitz, N.N.Khovansky, B.A.Khomenko and D.Horvath, Zh. Exper.Teor.Fiz. 76, 460 (1979); English transl. Sov. Phys.- JETP, 49, 232 (1979).

19. L.I.Ponomarev and M.P.Faifman, Zh.Eksper.Teor.Fiz. 71, 1689 (1976); English transl. Sov.Phys. - JETP, 44, 886 (1976).

20. L.I.Ponomarev, L.N.Somov and M.P.Faifman, Yadern.Fiz. 29, 133 (1979);English transl. Sov.Phys.- J.Nucl.Phys. 29, 67 (1980).

21. A.V.Matveenko and L.I.Ponomarev, Zh.Eksper.Teor.Fiz. 59, 1593 (1970); English transl. Sov.Phys. -JETP, 32, 871 (1971).

22. S.S.Gerstein, Yu.V.Petrov, L.I.Ponomarev, N.P.Popov, L.P.Presnyakov and L.N.Somov, Zh.Eksper.Teor.Fiz. 80, 1690 (1981).

23. L.Bracci and G.Fiorentini, Nucl.Phys. A364, 383 (1981).

24. L.N.Bogdanova, V.E.Markushin, V.S.Melezhik, L.I.Ponomarev, Preprint JINR E4-80-819, Dubna (1980).
L.N.Bogdanova, V.E.Markushin, V.S.Melezhik, Zh.Eksper.Teor.Fiz. 81, 829 (1981).

25. E.A.Vesman, Eesti NSV Teaduste Acad. Fuusika Astron.- Inst. Uurimused (ESSR), 18, 429 (1969).

26. Yu.A.Aristov, A.V.Kravtsov, N.P.Popov, G.E.Solyakin, N.F.Truskova and M.P. Faifman, Yadern.Fiz. 33, 1066 (1981).
A.V.Kravtsov, N.P.Popov, G.E.Solyakin, Yu.A.Aristov, M.P.Faifman and N.F.Truskova, Phys.Lett. 83A, 379 (1981).

27. S.I.Vinitsky, V.S.Melezhik, L.I.Ponomarev, I.V.Puzynin, T.P.Puzynina, L.N.Somov and N.F.Truskova, Zh.Eksper. Teor.Fiz. 79, 698 (1980);English transl. Sov.Phys.- JETP, 52, 353 (1980).

28. E.A.Vesman, Zh.Eksper.Teor.Fiz. Pisma, 5, 113 (1967); English transl. Sov.Phys. - JETP, Letters, 5, 91 (1967).

29. D.Bakalov, Phys.Lett. 93B, 265 (1980).

30. D.Bakalov, Zh.Eksper.Teor.Fiz. 79, 1149 (1980); English transl.Sov.Phys. - JETP, 52, No.4 (1980).

31. V.S.Melezhik, and L.I.Ponomarev, Phys.Lett. 77B, 217 (1978).

32. D.Bakalov, S.I.Vinitsky and V.S.Melezhik, Zh.Eksper. Teor.Fiz. 79, 1629 (1980); English transl. Sov.Phys.- JETP, 52, No.5 (1980).

33. V.P.Dzhelepov, P.F.Ermolov, Yu.V.Katyshev, V.I.Moskalev, V.V.Fil'chenkov, M.Friml, Zh.Eksper.Teor.Fiz. 46, 2042 (1964); English transl. Sov.Phys.- JETP, 19, 1376(1964); Nuovo Cim. 33, 40 (1964).

34. V.M.Bystritsky, V.P.Dzhelepov, V.G.Zinov, A.I.Rudenko, L.N.Somov and V.V.Fil'chenkov, Zh.Eksper.Teor.Fiz. 80, 839 (1981).

35. S.S.Gerstein, Yu.V.Petrov, L.I.Ponomarev, Yu.M.Shabel'sky, Soviet patent document No.713373, Int.Cl.G21G1/00 (1981).

36. Yu.V.Petrov and Yu.M.Shabel'sky, Yad.Fiz. 30, 129 (1979); English transl. Sov.J.Nucl.Phys. 30, 66 (1979).

37. R.G.Vasil'kov, V.I.Goldanski, B.A.Pimenov, Yu.N.Pokotilovski, L.V.Chistyakov, Atomnaja Energija 44,329 (1978).

38. S.O.Shriber, J.S.Fraser and P.R.Tunnicliffe, Proc. X Int.Conf. High Energy Accelerators, p.408, Protvino, 1977.

PROGRESSES ON PLASMA FOCUS RESEARCH AT FRASCATI

J.P. Rager

Associazione EURATOM-CNEN sulla Fusione, Centro di Frascati,
C.P. 65 - 00044 Frascati, Rome, Italy

1. INTRODUCTION

The name Plasma Focus (PF) has been bestowed upon a development of the fast dynamic Z-pinch characterized by a new type of electrode configuration which lends itself to the production of a non-cylindrical implosion of the current sheath. It produces a short lived, rather dense plasma, whose properties are dominated by the occurrence of macroscopic and microscopic instabilities.

In most cases, the plasma is created by the discharge of a capacitor bank and the dynamics of the current sheath has two successive fundamentally different phases: a long time scale phase (several microseconds) from breakdown to maximum compression, during which the energy initially stored in the condenser bank is transferred to the load as magnetic energy in cables, in the collector and in the inductance, as kinetic energy in the moving sheath; a short time phase (in the 100 ns time scale) during which part of the magnetic energy available in the load is converted with a high efficiency into useful kinetic and thermal energy of reacting particles.

For the past five years research on Plasma Focus (PF) has been dealing with two main problems:

(a) how to optimize plasma focus design in order to achieve the maximal nuclear reactivity for a given level of stored energy,

(b) which basic physical mechanisms determine the extraordinary efficiency of neutron production for such a configuration.

The former point touches the problem of engineering the current sheath, the latter embraces the plasma dynamics of the compressed phase. An issue clearly related to both is, how far can a PF be extrapolated for application to controlled nuclear fusion. Time limitation does not allow me to treat both aspects, therefore, I shall concentrate on aspects of PF research essentially related with the physics of the neutron production. For the last five years, experimental results gathered at Frascati, on the large 1 MJ facility, prompted a drastic reexamination of the PF modelling, as it was established and confirmed that when the energy level is scaled up[1,2]:

- the role of fast particles creating neutrons in the neutral gas laying in front of the gun is but a secondary effect of limited interest,
- most neutrons are produced in the pinch, and the neutron production is associated with local plasma dynamics
- the plasma density values remain essentially the same and the energy distribution function of reacting particles is substantially maintained,
- but, the duration of the neutron emission and the plasma size increase. Furthermore, a clear distinction is introduced between the beam optimized and the neutron optimized regimes[2].

The scope of this paper is to demonstrate further that the PF is a magnetized, turbulent plasma in which a substantial fraction of the content forms a stream of particles of moderate energy ($\sim$ 100 keV) eventually trapped when relaxation occurs following a strong macroscopic disruptive instability. Up to the time of the 1980 IAEA Conference, the idea of an eventual relaxation of the plasma into a long lasting force-free configuration was essentially based on the necessity that, in order to justify the large neutron yields found on large plasma focus with acceptable particle and energy contents, the best use should be made of the accelerated particles which could not fly freely across the pinch. Furthermore, the neutron production time scale exceeds by an order of magnitude the transit time of a 100 keV

d^+. Trapping is a necessity but is not achievable in an ideal Z-pinch magnetic field configuration. We demonstrate in this paper that, as far as macroscopic and microscopic activities are concerned, the characters of the plasma are very different during these two successive phases and we document two new fundamental properties:

- the plasma focus prossesses a self generated B_z field of comparatively high intensity (comparable to B_θ), a consequence of the current sheath structure presumably inherited from the former break-down and run-down phases,
- the plasma focus neutron production is mostly related to the properties of a stream of trapped ions turbulently produced. Physical conditions are met to assume the existence of a relaxed plasma state, as first proposed in Ref. 3.

2. CHARACTERS OF THE PLASMA DYNAMICS DURING NEUTRON PRODUCTION

Large, long living, reproducible plasma configurations produced in large energy PF devices permit to take full advantages of the application of optical diagnostic technique, such a shadowgraphy, Mach-Zehnder interferometry and light scattering. They tell us that there exist two different phases of the pinch.

2.1 Cylindrical Column Phase Following the End of the Implosion and Occurrence of Microscopic Instabilities

For neutron optimized regimes, the implosion phase is fully macroscopically stable.

An S_k-light scattering experiment similar to that reported by the Heidelberg University Plasma Focus group in a paper of this Conference[4], show the existence of two successive phases of anomalous density fluctuations of different physical natures. The first microscopic turbulence occur in a low density plasma which preceeds the main current sheath. This confirms observation reported earlier[4,5], on PFs of much lower energy levels. The frequency inegrated diffused light intensity can only be detected in the 15° forward de-

tection channel. The intensity is then two orders of magnitude larger than the thermal level (assuming that the latter is determined by the threshold detection level of the system which is set at 10^{17} cm^{-3}). After maximum compression, the pinch reexpands cylindrically, while the current sheath continues its vertical motion at a moderate velocity ($v_z \sim$ $\sim 5\ 10^6$ $cm\ s^{-1}$). It must be pointed out that the vertical mass motion in the pinch, related to a non cylindrical implosion of the current sheath is a phenomenon which constantly accompanies the pinch dynamics of the column and the macroscopically unstable phases, and is responsible for delays in the occurrence of typical phenomena at different axial positions.

Informations deduced from the thermal part of the S_k spectra, are in absolute agreement with density values derived from Mach-Zehnder interferometry. Electron temperatures reach maxima clearly larger than values derived from 2D-mhd codes, which should be situated in the range of 300-500 eV. We find 1.5-2 keV! T_e presents a rather hollow profile, while n_e peaks on axis. Again this finding is similar to an observation reported in[6], for a PF of much lower energy level. In[6], the electron temperature was measured by the two filter-technique using a soft X-ray pinhole camera and a gated image converter.

As documented in more details later, the B_z component of the magnetic field, localized at the end of the implosion phase in a circular ring of limited extension at the plasma boundary, diffuses toward the center on a time scale clearly requiring anomalous resistivity. A space scale of $0.5 < L < 1$ cm, and a time scale of $\tau_{diff} = 10\text{-}20$ ns, require $150 < \sigma < 10^3$ $moh \cdot m^{-1}$, while Spitzer's conductivity reaches $3\ 10^7$ at $T_e = 1$ keV. The microscopic turbulence cited above is probably responsible for both the anomalous high diffusion rate of B_z and the too high electronic temperature. Conductivities such as evaluated above agree well with the energy needed to heat the electrons assuming Joule heating with a plamsa current equal to the pinch current of 1 MA.

Events which follow maximum compression, related to the onset of the neutron emission show two different kinds of characters. Macroscopically speaking, the configuration is stable against the outwardly directed acceleration, related to the radial cylindrical reexpansion of the pinch. Short wavelength instabilities are observed in the lower part of the column, wriggling the outerboundary. Microscopic anomalous fluctuations set in again, this time at the plasma boundary, while n_e and T_e decrease locally. S_k-scattering provides an interesting possibility to follow both thermal and turbulent properties during this time; Fig. 1 illustrates the results. At the very start of the neutron emission, the plasma is thermal with a peak (axial) density of 6 - 8 10^{18} cm^{-3} and a peak temperature of 1.5 - 2 keV (boundary). The electron temperatures is slightly lower at higher z values where dynamics appear delayed by 30 ns. Anomalous density fluctuations mostly occur at the plasma boundary. Density gradients along the z axis smooth out.

The neutron production during the whole rise time (lasting 50 ns) amounts to 30% of the total pinch production. Radial profiles peak on axis (as n_e)[1]. Few neutrons are produced in the zone above the pinch. The anomalous density fluctuations which accompany neutron emission rise time have a clearly different character from those measured previously. In fact, we do observe both light scattering in the forward ($\alpha \gg 1$) and the perpendicular ($\alpha < 1$) direction simultaneously; this allows us to situate the ratio of anomalously scattered light to thermal scattered level at 15°, at 6 to 10. This is not accompanied or followed by any electronic temperature rise. It must be assumed that the turbulent wave spectrum acts directly upon the ions, as by the way, suggested by the simultaneous observations of a rise in nuclear reactivity.

A fast growth rate ($\tau \sim 20$ ns) Rayleigh Taylor type instability develops there after creating locally a strong necking. This happens at different places and times while the microscopic activity is observed to be still active. For

shot conditions reported here, a total disruption of the plasma column follows. The plasma can reach tiny transverse dimensions of the order of 1 mm or so. If we assume B_z to be frozen in, it then can locally rise to large value, probably close to 1 MG.

This phase marks the maximum nuclear reaction rate in the plasma. A vertical pushing still persists at that moment in the upper part of the plasma column, creating shells of plasma of rather large external dimensions.

2.2 The Quiescent Blob Phase and the Decay of the Neutron Emission

The plasma reconfigures after the instability phase creating rather large plasma blobs, characterized by a long life time (100 - 150 ns), slow expansion, reduced particle density (a few 10^{17} cm^{-3}). The plasma in the blob is microscopically quiescent. During this phase neutrons are produced following a rather flat radial profile. It is during the blob phase that we observe the most intense secondary neutron emission, extending over a domain defined by $5 < z < 12$, $-6 < r < +6$ cm^{1}. This effect is attributed to the runaway of some of the fast deuterons existing in the blob which are imperfectly trapped, or diffuse from a region of closed field lines to a region of open field lines and then escape. The relative intensity of the secondary emission varies shot to shot and can even be almost undetectable in some instances.

3. EVIDENCE OF A LONGITUDINAL COMPONENT OF THE MAGNETIC FIELD

Temptative interpretations of the PF physics based on plasma relaxation involve foundamentally the existence of an axial component of the magnetic field; its flux, related to the azimuthal flux, is a scale parameter for the definition of the relaxed state configuration[3]. Also, the shear it causes is an important aspect of the magnetic confinemt .

An experiment of Faraday rotation has been performed at Frascati, in order to put into evidence the existence of

such a component and to determine its magnitude and finally its dynamics. The necessity to individuate the effect beyond doubt dictated the used of a Wollaston analyzer and the observations of the light intensities of the two emerging beams simulataneously. Indeed, setting the Wollaston at 45° with respect to the direction of the incident plane of polarization, any rotation of the plane results in conjugated changes in the light intensity, with create a darker image on one of the two beams and a correspondingly brighter image on the other one. Experiments confirm the existence of such an effect, of far greater extent than the 2° threshold imposed by the optical set up. Shadow effect on the Faraday rotation imaging frame has been minimized by depth of field control (depth of field is 18 mm, centered 11 mm above anode level). In this situation the shadow effect introduces a relative change in illumination of less than 10% provided $\nabla^2 n_e < < 10^{21}$ cm^{-5}. Faraday effect is shown on Fig. 2.

At the end of the implosion phase the Faraday effect is localized at the pinch periphery where density peaks at 2 10^{18} cm^{-3}. B_z appears to quickly diffuses toward the center where it reaches a value of 400 kG when the density reaches its peak value of 6 - 8 10^{18}. During the instability phase, conjugated filament resp. black/white may appear in the images possessing no azimuthal symmetry. Features can be locally very bright.

One of the many problems related to the interpretation of the Faraday effect is the practical impossibility to derive a realistic dispersion relation including non uniform non steady plasma properties, boundary conditions and the propagation of the wave at an arbitrary angle with respect to the magnetic field.

However the observation of a maximum of light modulation peaking on axis at the time of the maximum density phase of the cylindrical plasma column is surely attributable to the only longitudinal component as the azimuthal magnetic field must be zero at that point. For the derivation of the quantitative value of the magnetic field, the

question of determining the spatial extension on which the magnetic field exists is an important but open question. We assume a 3 cm longitudinal path to be compared with the 4 - 5 cm of the pinch extension. Such an assumption is not critical to the scope pursuied here as the lowest B_z value is still large. It is critical for the dirsuptive phase were a strong break in the space scale occurs, requiring either very high local plasma densities or large magnetic field modules, to provoke a detectable event.

To be noted that we never observe a change in the sign of the B_z magnetic field component, which would be easily detectable as it inverts black/white occurrence on the two images respectively.

4. MAIN CHARACTERS OF THE DEUTERON ENERGY DISTRIBUTION FUNCTION

The high emissivity of a large PF device is particularly appropriate for single shot investigations of the characters of the deuteron energy distribution function with a coarse space and time resolution. We know since[7], that two neutron sources have been identified. The main source coincides with the pinch, producing 70 - 80% of the emission. Its radial profile follows pretty well the changes of the plasma distribution with time, from column to blob. The second neutron source produces the remaining 20 - 30%. It can be suppressed (for instance using a solid obstacle), without influencing the emission in the lower part.

4.1 Evidences of a Closely Grouped, 100 keV Mean Energy Stream of Orbiting Deuterons

Since the early studies on neutron spectroscopy carried out on low energy PF, it has been known that the so called end-on spectrum was characterized by the existence of an energy shift of the maximum of the histogramm, of the order of 400 keV. It has been demonstrated since that this line shift does not vary at all when PF energy level is scaled up[1]. But the interpretation of such a simple feature involved a num-

ber of free parameters such as, the actual energy distribution of the d^+ and their angular spread. In the past it has been postulated that the angular distribution could be a hollow one with maximal intensity peaking at some 60°, and that a power law spectrum of the form

$$\frac{dN}{dE} \propto AE^{-\gamma}, \quad 3 < \gamma < 4$$

extends over a range of energies of say 30 - 300 keV.[8]

It is fundamental to carry out a number of spectral investigations with time and space resolutions to determine wether this line shift corresponds to an actual 100 keV energy of axially streaming deuterons and to know further where and when they are formed. A second paradox to deal with is that related to the existence of a large FWHM neutron spectrum as seen side-on. In fact a 400 keV FWHM spectrum can neither be explained by an axial beam target which produces a very slim broadening side-on, nor by a thermal spectrum which would have had a 20 - 30 keV temperature. Again neither forward scattering nor absolute neutron yield derived independently from plasma density profiles and time of production could agree with such a hypothesis. We need therefore a side-on component of the ion motion of a rather high magnitude. It is fundamental to discern whether this component is related to the existence of a conical beam target involving the presence of large energy deuterons or whether it is due to a single group of particle of a more moderate energy which circulate in one or the other direction following trapped orbits.

□ Experimental Results

Using a solid obstacle placed at z = 6 cm down stream, it has been possible to suppress most of the neutron of the secondary production. It has been shown that the line shift is a feature already existing in the pinch neutron spectrum[1]. Using a shadow bar technique, it has been possible to measure the FWHM of the side on neutron spectrum of the secon-

dary source. This FWHM is clearly smaller than that related to both the whole neutron spectrum or the pinch neutron spectrum.

Using a set of nuclear emulsion plates located at 0°, 20°, 40° and 90° respectively it is confirmed that the changes in energy shift of the neutron emission vs angle follow that predicted by a 100 keV deuteron energy component flying axially, Fig. 3.[9]

The most astonishing results is the evidence of a 100 keV d^+ stream orbiting in a plane perpendicular to the experiment main axis, on a space scale corresponding to the pinch main geometrical measurement of the neutron emitted in a plane perpendicular to the axis using an array of 4 collimators viewing the source, let us say, on its lhs and rhs as well as in both forward and backward direction, see Fig.3. Results show that non of the four, single shot measured spectra look like the usual volume integrated one. Irregular patterns of lines have main features centered around 2.2, 2.45 and 2.8 MeV obeying a scheme of deuteron motion circling around the experiment axis. It must therefore be concluded that the large FWHM of the side on spectrum is related to the existence of spectral structures due to particles streaming in a plane perpendicular to the axis.

Neutrons produced in the corona above the pinch confirm these findings. As seen previously, the secondary source has a depth ranging from 8 to 10 cm above the pinch. It can be shown easily that such a depth cannot be related to the slowing down of fast d^+ in a neutral gaz. At 100 keV, d^+ stopping power is maximal ($6.5\ 10^{-15}$ eV $atom^{-1}$ cm^{-2}) and particle energy loss is only 1.2 keV $\cdot$ cm^{-1} in average for a gaz density of $2\ 10^{17}$ cm^{-3}. Hence, as already proposed in Ref. 8, we must assume the existence of a cold plasma in which momentum slowing down is more effective. For a $T_e = 25$ eV electron temperature, it can be shown that a 100 keV d^+ travels 17 cm in 80 ns; it then has reached 22 keV and has released all its yield. However already 90% of the yield has been released while the deuteron has travelled 9 cm and

reached 50 keV in 35 ns. Neutron production time by free streaming 100 keV ions is much less than the actual neutron production time in that place. It means that: *Deuterons are lost in a continuous manner from the pinch zone.*

□ Energy and Particle Contents

If we now evaluate which energy is necessary to produce the 30% average of the total neutron yield following the assumptions formulated above and how many particles have been consumed we find respectively:

$$W_B = 23 \text{ kJ} \qquad N_B = 1.5\ 10^{18}$$

If we now make the assumption that instead of a monochromatic beam, we have an energy distribution following a power law, such as reported previously, these numbers jump to, (still considering interaction at gaz filling density):

$$W_B = 40 \text{ kJ} \qquad N_B = 6\ 10^{18}.$$

Remember that the total pinch content at the start of the phenomenon was only 10^{19} and that net pinch current for the same conditions never exceed 1 MA. Clearly the second proposition is to be rejected. *Most particles producing these neutrons have energies closely groupped around 100 keV.* Higher energies must be discarded on the ground that exposing a Li D target to the stream do not produce either Li-D or d-d neutrons.[10] The question of wether or not all these deuterons partecipate in the neutron production of the main source remains obviously open.

4.2 Possible Existence of Particle Momentum Slowing Down and Trapping

It has been stressed for sometime that discrepancies noted between neutron spectra measured by time of flight (TOF) or by nuclear emulsion plates (NEP) result from an ap-

parently over abundant relative concentration of fast neutrons in the TOF-spectra.[11] Such a feature can be attributed to a change vs time of the d^+-energy distribution function. Assuming that fast neutrons are emitted earlier in time (cumulated with the effect of a long neutron production time) results in an apparently broader FWHM. It has been shown since then by the Los Alamos PF group[12], that harder neutrons are emitted earlier and that the effect is clearly visible if one follows the TOF signal deformations using several TOF stations at different distances.

As a 100 keV d^+ has a time of flight of 5 - 10 ns across or along the pinch, to be efficiently slowed down it must remain in the rather cold ($\sim$ 400 eV electron temperature) moderatly dense plasma (plasma density evolves from a peak 6-8 10^{18} to a low 1-3 10^{17} cm^{-3}) for most of the neutron production time. Indeed 100 keV ion slowing down time is of the order of 300 ns for $T_e = 400$ eV, $n_e = 2\ 10^{18}$! which is comparable to the total neutron production time.

A change in the orientation in space of the particle trajectories from a mainly equational motion to a mainly vertical motion in the late phase would also produce an apparent time dependant change in the side on neutron energy spectrum. The fact that the FWHM of the side on neutron spectrum of the corona is clearly less than the corresponding spectrum of the main source is coherent with the fact that escaping deuterons might have less equatorial momentum than when they are in the blob.

Alternatively, if we allow the deuterons to fly freely across the pinch and be lost, we must find a mechanism which steadily refurnished the energy to a new deuteron. It leads to large particle content and energy requirements. As blobs are seen microscopically quiescent the origin of the energy transfer must be found in a macroscopic effect such as a local anhilation of magnetic flux.

A second fundamental data supporting the ideal of ion trapping and momentum slowing down come from the observation of fast 14 MeV range neutron produced by the secondary $t(d,n)\alpha$

reactions. Measurements of such neutrons have been performed using nuclear emulsion plates, side-on and end-on, for three successive shots producing 10^{12} neutrons in the 2.5 MeV range.

Scanning the plates yield a relative neutron production at 14.3 MeV compared to 2.45 MeV of $Y_{DT}/Y_{DD} = 2 \pm 0.6 \cdot 10^{-3}$. However some anomalous spectral feature observed at the end-on plate makes that such a high relative yield cannot be considered as certain.[13] A more conservative evaluation situate this ratio at $6 \cdot 10^{-4}$. This is still two orders of magnitude larger than fast neutron yield produce in the neutral gaz by free flying 1 MeV tritons.

We want to stress the point that slowing down of triton is an absolute physical necessity to justify such a relative yield, as a 1 MeV triton has a 0.4 b nuclear cross section, compared to 5 b at 200 keV. Slowing down being completly inexistant in a cold neutral gaz, the triton must interact with a cold plasma. It can be shown easily that

$$Y_{DT}/Y_{DD} = n\tau_s \int_{W}^{W_o} \frac{\sigma_{D\tau} v_T}{2W} \, dW$$

where $n\tau_s$, the product of density per slowing down time of triton, is a function of T_e essentially. Hence we don't need to know the time dependence of n_e to calculate the yield.

The integral, is a function of the triton energy only and can be calculated parametrically vs $\alpha = \tau/\tau_s$, where τ is the actual trapping time. Calculations show that 90% of the yield is released when $\alpha = 1.1$. As 14 MeV neutrons should be produced in the decay phase rather than in plasma column for $T_e = 100$ eV, confinement time ranges from 0.3 to 3 μs for $n_e = 2 \cdot 10^{18}$ to $2 \cdot 10^{17}$ cm^{-3}.

4.3 Which Fraction of the Neutron Emission is Isotropic in Energy

Both the end-on neutron spectrum of the pinch, and the spectrum of the whole emission measured at 40° exibit a marked emission of neutron of 2.5 MeV. Assuming that the line

shifted forward is essentially due to deuterons travelling axially, it is possible to evaluate which fraction of the emission is emitted around 2.5 MeV. From the line intensity ratio of 1.5 at 40°, it turns out that 50% of the whole neutron emission is emitted isotropically in energy. Deducing the contribution of the corona above the pinch, it turns out that deuterons spent 70% of their time in the perpendicular direction in average. We check further that with the same hypothesis the line ratio should be 2 at 0° and 1.88 at 20°. We find experimentally $1.8 < I_{(0°)} < 2.8$ and $1.5 < I_{(20°)} < 1.9$. $I_{(0°)}$ and $I_{(20°)}$ are respectively the relative intensities of the shifted line at 2.8 Mev compared to the 2.45 MeV line on the same spectrum. The correspondingly calculated anisotropy is however a bit high at 1.5 as compared to the 1.1 - 1.2 experimentally observed. This can be attributed to our assumption that the line centered around 2.5 MeV has no fluence anisotropy, which is not true considering that deuterons are orbiting in a plane perpendicular to the axis. The existence of a well detached line of emission at 2.5 MeV in the forward direction has already been observed on a 12 kJ PF[14], stressing again the similarities between low and high energy PF devices.

5. WHICH MECHANISMS CAN ACCOUNT FOR d^+ ACCELERATION?

It is possible to delineate a robot portrait of the acceleration mechanisms based on the following features:

- physical occurence timed with neutron emission either partial (rise time) or total
- it must be able to transfer large energy content to the deuteron stream
- it must explained the existence of a privileged energy of the ions ($\sim$ 100 keV).

Three basically different mechanisms have been proposed to give account of d^+ acceleration: a plasma diode effect, an inductive acceleration, microscopic turbulences.

- diode type acceleration. The idea is based on the observation that e^- and d^+ beams escaping from the PF have image

spectra and that the disruptive instabilities which severe the plasma column can interrupt the current flow and build large accelerating electrostatic fields in the gap. We observe on this experiment that such a phenomena happens too late as compared to the onset of the neutron emission (40-60 ns).

□ Inductive acceleration. Inductive acceleration can happens when the magnetic field, initially localized at the boundary and outside of the pinch column, diffuse rapidly toward the center because of the onset of anomalous resistive effect. Indeed the Faraday rotation experiment shows such an effect happening at the end of the radial collapse phase. But such a phenomenon occur before neutron production onset and lasts for a short period of time.

It is sometime arbitrary to separate the two fore mentioned phenomena as a fast diffusion of the magnetic field, on a fast implosion of the plasma current in a necked zone cause both a change of inductance vs time finally building up an electrostatic electric field. It can be shown simply that the associated flux variation corresponds to a low magnetic energy dissipation as $\Delta(LI) = V,\Delta t = 210^{-3}$ V.s with $I \sim 10^6$ A give a magnetic energy variation of the order of 1 kJ which is an order of magnitude smaller than the energy content necessary to justify the observed neutron yield.

□ Why microscopic effects are probable. Microscopic effects are observed during neutron emission rise time. The individuation of the type of turbulence as a very uncertain issue. Empiric considerations based on energy requirement fix the effective collision frequency around 30 ωp_i. We observe furthermore that the flux is destroyed far from the pinch zone as it should be, has a resistance been put in series with the gun inductance. Closely grouped particle energies in the ion spectrum let us think to the ion energy being gained mostly in a saturation regime of wave amplitude. Energy gained by the ion stream is typically 10 times the energy in the thermal plasma.

It is clear from timing and time-scale properties that this mechanism would act directly and essentially upon the ions.

□ Now we can also consider *Flare type* acceleration. The substantial and rapid steepening of the B field gradients lead to particle acceleration. Such explosions relax the force free field into a partially open field and can explain why the neutron production in the corona is related to the occurrence of the macroscopic activity. This mechanism provides accelerated particles with energies[15]

$$E = \frac{1}{2} e_B L_{Acc} \frac{L_{\parallel}}{t_{expl.}} \zeta^{-3/4}$$

$t_{expl.}$ is the explosion time, L_{Acc} is the distance over which the particle experience acceleration and ζ is the reduced time (in units of t_{expl}), $L_{\parallel}$ is the gradient space scale. To be noted that the energy picked up by the particles do not depend on mass and, therefore, e^- and d^+ have image spectra. Introducing values taken from experimental observations to justify 100 keV particle energy, we need a MG field. However, most ions produced in such a way are runaway ions as they are accelerated in the open field part and are produced when the nuclear reactivity is already reaching its maximum. They cannot substantially play a role in the main neutron production. Furthermore the mechanism cannot provide large amount at energy.

It is clear that there can also be a superposition of events with a fraction of the population being emitted by a macroscopic kind of particle acceleration mechanisms. We must bear in mind the fact that on some plasma focus[16] neutrons are observed being emitted without any kind of macroscopic instabilities and that the main virtue of macroscopic instability might be of being one possible driver for plasma relaxation.

6. CONCLUSIONS

Some important progresses have been achieved on the understanding of PF basic physics.

Most models proposed up to now give account of the plasma focus behaviour on a space time integrated basis and

fail to explain satisfactorily the phenomenological succession of events. Especially time and space resolved information on the evolution of the d^+ energy distribution were hard to get as they needed the large neutron fluence achievable only on large PF devices. From a pure experimental point of view, we confirm in this paper that most of the characters defining the dynamics of anomalous density fluctuations measured on low energy plasma focus are also observed on large energy plasma focus. This proposition bolsters further the conclusion reached earlier at Frascati[3] that neutron yield scaling is achieved maintaining essentially unaltered the properties of the distribution function of the reacting deuterons.

We establish experimentally the existence of a vertical component of the magnetic field and the existence of a stream of trapped deuterons of moderate energy.

We demonstrate the necessity of trapping ions based on both particle and energy content requirements c. the evidence that neutrons are still being produced on an extended period of time when no macroscopic or microscopic activities can be detected, on the evidence that charged particles are lossing momentum which they can do only if they spent an extensive period of time in a moderately low temperature plasma.

We demonstrate the existence of a turbulence when 100 keV d^+ are generated which act directly upon the ion.

Not all aspects of the problem are yet cleared. All the ions involved in the acceleration process are not produced at the same place and at the same time. A quantitative cross--check of the neutron production during the rise time remain, therefore, rather ambiguous. Paradoxically we observe on a time integrated basis that the ion stream produces an effect on a space scale close to the blob radius. We must suppose strong inhomogeneities in the B field module distribution and plasma density during the blob phase.

In[1,3] we speculate on the possibility that some of the observations could be related to the formation of a relaxed plasma state evolving toward a minimum energy, quasiforce free situation. A first relaxation might occur already during

the column phase, dominated by magnetic field diffusion due to microscopic anomalous effects. This situation is unstable against fast convective motion, when anomalous dissipation can no longer smooth out strong B field gradient created during the convective motion.[17] A second relaxation sets up explosively with plasma tongues flaring out, finally forming the large plasma blobs, microscopically and macroscopically quiescent observed during the decay phase of the neutron emission.

All indications gathered so far show that a true scaling occurs when the energy is increased, conserving the main properties of the deuteron energy distribution of the reacting particles, and increasing particle content and burn time.

The problem of how n and τ participate in the scaling of $n\tau \propto I_p^{2.1}$ is a fundamental aspect related to the basic physical properties of relaxed plasma state and is not known. When $n\tau$ increases, electrons which under present physical conditions remain cold, will be heated up and might cause unsuspected losses in the energy content of the pinch. As well, large increase in time could lead to a reversal of time scale hierarchy with catastrophic effects on energy and particle confinements, not predictable from present-day knowledge. If the energy is delivered to the reacting ions in a single burst of short duration compared to the total neutron production time, time scale increase vs energy level will meet a practical limit when fast ions are slowed down to such an extent that they do not contribute any more to the yield, unless another mechanism, not yet put in evidence, is able to replace the lost reacting particle in the energy distribution function.

ACKNOWLEDGEMENTS

The author wishes to thank C. Gourlan, H. Kroegler and B.V. Robouch and the whole technical staff of the Plasma Focus Group at Frascati for their continuous participation in the Plasma Focus Research activities. Also the author is indebted toward the numerous visiting scientists who contributed so marvelously to the experimental efforts and in particular to J. Ehrhardt and P. Kirchesch who performed the scattering measurements and K. Steinmetz for neutron measurements from Heidelberg University. G. Fischfeld (from Rosario University, Argentina) is acknowledged for his achievement of the Faraday rotation experiment. Special thanks go to Prof. K. Hübner of Heidelberg University for his continuous cooperative effort and for many stimulating scientific discussions.

REFERENCES

1. J.P. Rager, L. Bilbao, H. Bruzzone, C. Gourlan, U. Guidoni, H. Kroegler, S. Podda, B.V. Robouch, K. Steinmetz, Proc. of the 8th Int. Conf. on Plasma Phys. and Controlled Nuclear Research, Bruxelles 1980, IAEA (Vienna 1981), Vol. II, p. 209
2. R.L. Gullickson, A. Gentilini, J.P. Rager, K. Steinmetz, Report 80.5, Associazione EURATOM-CNEN sulla Fusione, Centro di Frascati, Frascati, Rome, Italy (1980)
3. B.V. Robouch, A. Sestero, S. Podda, Plasma Phys. 22, 1039 (1980)
4. J. Ehrhardt, P. Kirchesch, R. Bätzner, H. Behler, G. Böckle H. Bruhns, K. Hübner, K. Steinmetz, N. Wenzel, Proc. at 10th European Conf. on Controlled Fusion and Plasma Phys., Moscow 1981, Vol. I, D3
5. A. Bernard, J.P. Garçonnet, A. Jolas, J.P. Lebreton, J. de Mascureau, Proc. at the 7th Int. Conf. on Plasma Phys. and Controlled Thermonuclear Research, Innsbruck 1978, IAEA (Vienna 1979) Vol. II, p. 159
6. L. Bertalot, R. Deutsch, H. Herold, U. Rückle, M. Sadowski, P. Schilling, M. Schmidt, Proc. of the 8th Int. Conf. on Plasma Phys. and Controlled Nuclear Research, Bruxelles 1980, IAEA (Vienna 1981), Vol. II, p. 177
7. J.P. Rager, B.V. Robouch, K. Hübner, K. Steinmetz, Report 81.25, Associazione EURATOM-CNEN sulla Fusione, Centro di Frascati, Frascati, Rome, Italy (1981)
8. A. Bernard, Proc. of the 3rd Topical Conf. on Pulsed High β Plasma, Ed. D.E. Evans, Pergamon Press (1976) p. 69
9. K. Hübner, J.P. Rager, K. Steinmetz, Proc. at the 10th European Conf. on Controlled Fusion and Plasma Phys. Moscow 1981, Vol. I, D2
10. H. Conrads, J.P. Rager, B.V. Robouch, K. Steinmetz, 1980 IEEE Conference record, 2D6, Madison Wisconsin USA (May 19-21, 1980)

11. C. Gourlan, H. Kroegler, Ch. Maisonnier, J.P. Rager, B.V. Robouch, L. Bertalot, A. Gentilini, B. Arcipiani, E. Pedretti, K. Steinmetz, Proc. 2nd Int. Conf. on Energy Storage, Compression and Switching, Venice 1978; and Report 79.23/cc, Associazione EURATOM-CNEN sulla Fusione, Centro di Frascati, Frascati, Rome, Italy (1979)
12. H.W. Kruse, G.N. Minerbo, 1981 IEEE Conference record, Paper 3C4, Santa Fé, New Mexico, USA (May 18-20, 1981)
13. K. Hübner, J.P. Rager, K. Steinmetz, Report 2/81, Institut für Angewandte Physik, Heidelberg University (1981)
14. K. Steinmetz, H. Bruhns, J. Ehrhardt, K. Hübner, P. Kirchesch, G. Mechler, Proc. at the 7th Int. Conf. on Plasma Phys. and Controlled Thermonuclear Research, Innsbruck 1978, IAEA (Vienna 1979) Part B, Vol. II, p. 135
15. B.C. Low, Astrophysics J. 189, 353 (1974)
16. T. Kobata, communication at the 1st Int. Plasma Focus Workshop, Brussels 1980, Ed. by J.P. Rager and B.V. Robouch, Report 80.56, p. 38, Associazione EURATOM-CNEN sulla Fusione, Centro di Frascati, Frascati, Rome, Italy (1980)
17. C.W. Barnes and P.A. Sturrock, Astrophys. J. 174, 659 (1972)

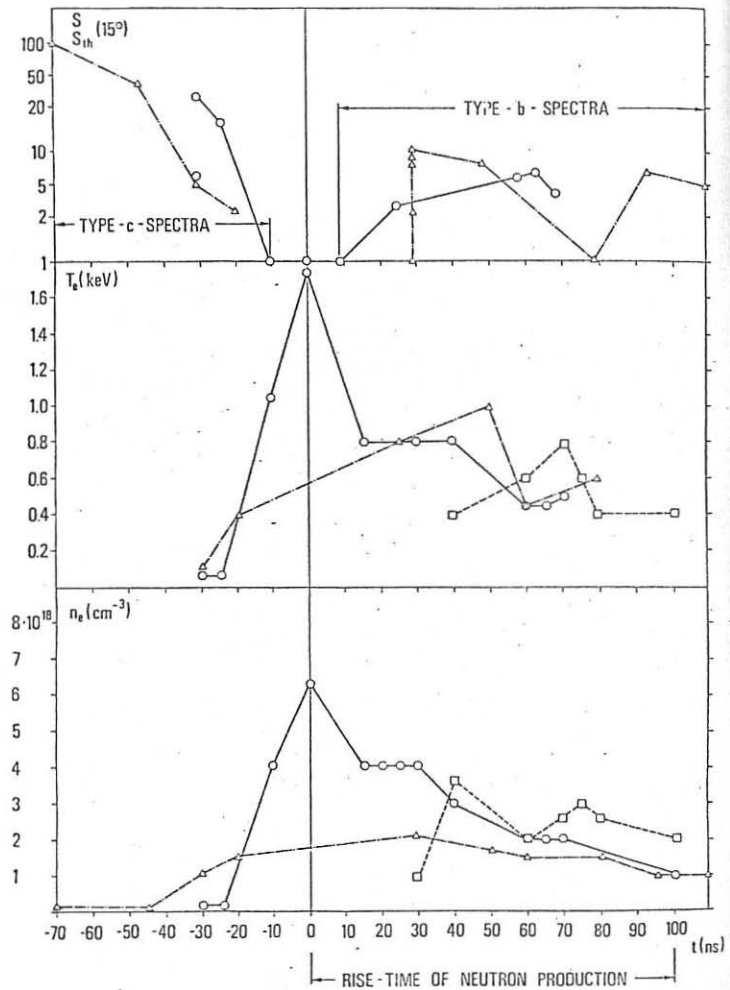
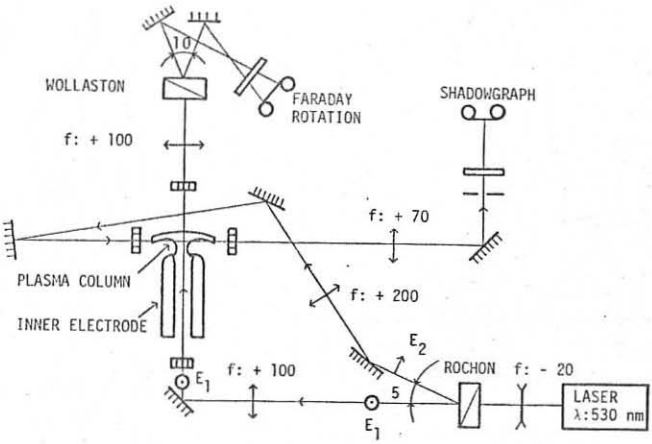


Fig. 1

S_k scattering measurements: (a) light intensity ratio scattered at 15° forward, reported to thermal level measured when $\alpha < 1$ and electronic temperature (b) and density (c) for three points of measurements: ○ z = 7, R = 5; △ z = 17, R = 6; □ z = 17, R = 0.



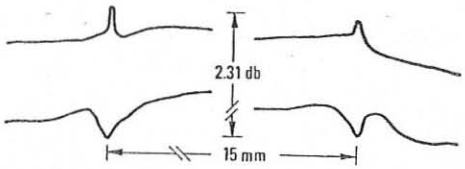
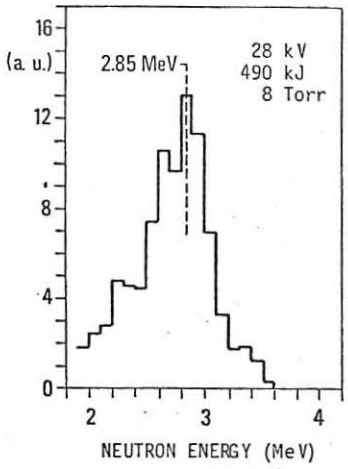
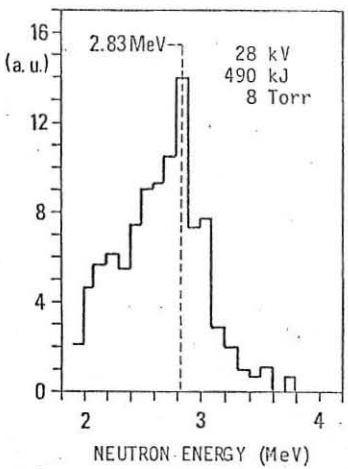


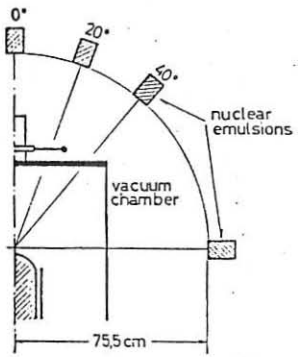
Fig. 2

a) Optical set up for Faraday rotation

b) Densitometer traces showing Faraday effect at the end of the implosion







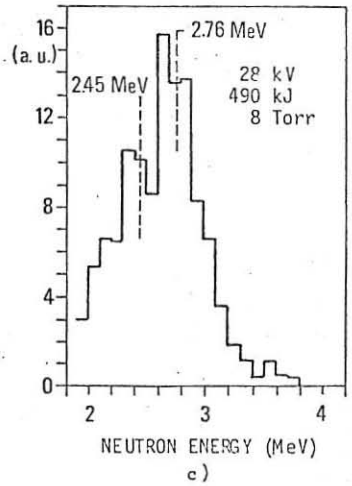


Fig. 3

Time and space integrated neutron spectra (NEP) measured at (a) 0°, (b) 20°, (c) 40°. In the insert is shown the geometrical disposition around the PF

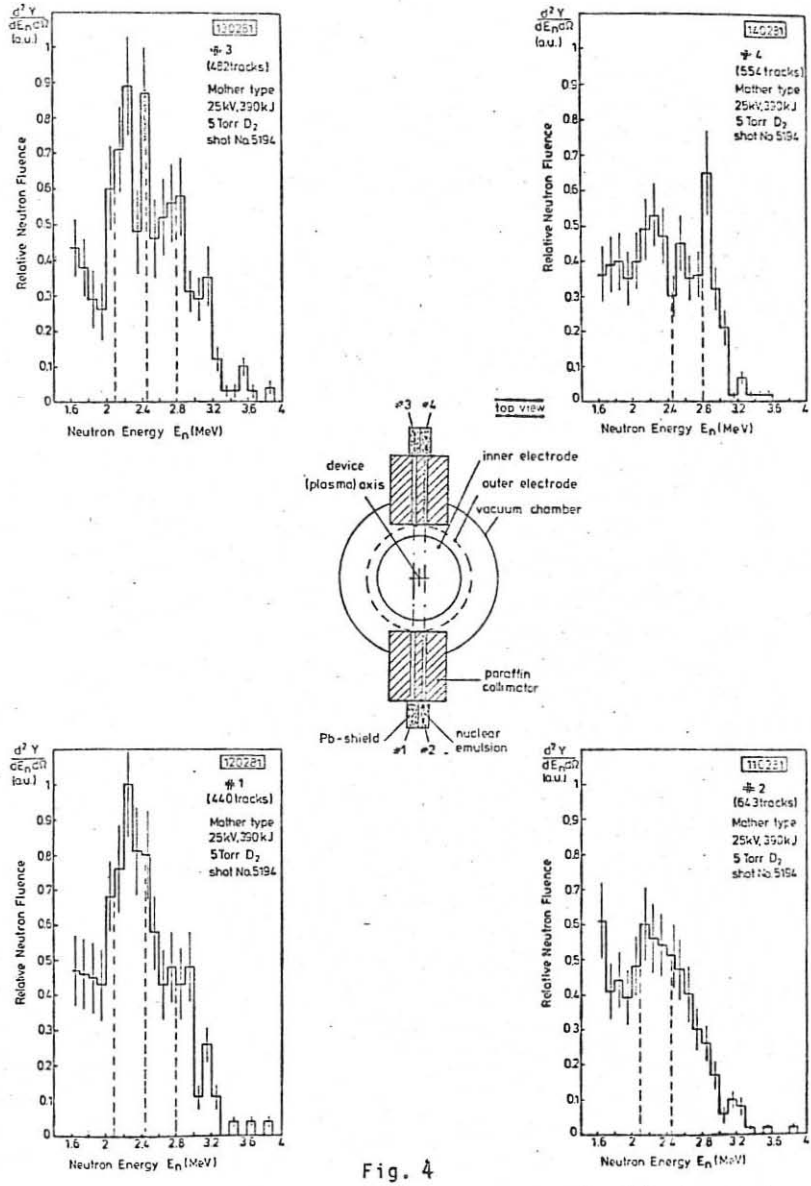


Fig. 4

Neutron spectra measured side-on through a four-channel collimator viewing as indicated in central insert.

EQUILIBRIUN AND STABILITY OF TOROIDAL PLASMA

V.D.Shafranov
I.V.Kurchatov Institute of Atomic Energy

At present the following closed (toroidal) systems for the magnetic plasma confinement are considered, first of all, as a possible basis of the fusion reactor:

a) tokamaks, b) stellarators,
c) stabilized pinches, d) bumpy tori ,
e) compact tori .

To maintain equilibrium, the toroidal current should be induced in the systems (a,c,e), while the systems (b,d) are stationary magnetic plasma traps.

The equilibrium should be stable in the toroidal systems for their steady or quasi-steady functioning.

Initially, the theory of equilibrium and stability elucidated the basic physics of the plasma confinement and operated with the simplified models rather than with the real systems. In many cases it resulted in pessimistic conclusions. For example, the cylindrical plasma model with flat current distribution used at the first steps of the tokamak studies didn't leave any opportunity of obtaining the stable plasma confinement. Only later consideration of the bell-shaped profiles revealed the stability zones in the parameters of a toroidal disharge thus explaining the stable tokamak operation. Furthermore, long ago the pressure-driven instability seemed to be inevitable because of the convexity of the magnetic field lines. But later, it has become clear that an average curvature of the field line in a torus can be negative, as if it corresponded to a concave, in the average, magnetic surface. In combination with the magnetic field shear it stabilizes a number of MHD modes and allows to expect rather high plasma pressure in the system. Then, the plasma self-stabilization effects of the same origin with a rise in its pressure have been found. All this shows an importance of taking into account the real geometry of a system for the proper estimation of its possibilities. It is

especially important for the reactor designe. Here the error in estimation of ß (ratio of the plasma pressure to that of the magnetic field), say by 30%, can have fatal consequences.

Therefore, up-to-date theory of equilibrium and stability aiming an optimization of the toroidal systems operates with a complicated 2-D and 3-D computational codes.

In this review, the relevant results in the tokamak theory, and the calculations related to a helical stabilized pinch will be presented. A substantional part of the paper will be devoted to the recent remarkable achievements in the stellarator theory. I shall not go into the systems of the bumpy torus type - a special paper is presented to this conference. As for the compact tori , I restrict myself only by the following remarks.

The compact tori are topological toroidal plasma configurations produced in a singly connected region, i.e. they don't need a toroidal chamber and the toroidal magnetic field coils. They have arisen as a result of the external magnetic field reversal in the theta-pinch or of the internal magnetic field reversal in the mirror trap with high plasma pressure. The macroscopic stability of the compact torii have been observed by R.Kh.Kurtmullaev and his colleages who gave the compact tori their title. Later a concept of the compact tori stabilized by a toroidal field was also introduced as an extreme case of a fat tokamak. The theoretical studies performed have shown that the optimized stable systems of this kind remind more the stabilized toroidal pinches. The compact tori are attractive because, being closed, they have rather high ß and simple geometry of a chamber. This makes them suitable for designing the fusion reactor modules of moderate power. Nevertheless, until now, they remain to be rather exotic systems with a lot of problems.

I. Tokamaks

a) The main parameters.

Tokamak - an axially-symmetric system, in principle - is characterized by a shape of the magnetic surface cross-sections $a(r,z) = \text{Const}$, which can be expressed as follows:

$$r = R + \Delta + a\cos\theta + \delta\cos^2\theta$$
$$z = \lambda a \sin\theta \qquad (1)$$

(here $\Delta(a)$ is the shift; $\lambda(a)$, $\delta(a)$ are the ellipticity and triangularity parameters), and by the next important parameters: the aspect ratio $A = R/a_p$ ($a = a_p$ is the edge magnetic surface of the plasma), the toroidal and poloidal "beta"

$$\beta_T = \frac{2\mu_0 p_{max}}{B_T^2(R)} , \qquad \beta_J = \frac{8\pi \int p\, ds}{\mu_0 J^2} , \qquad (2)$$

the rotation number or the safety factor

$$q(a) = \oint \frac{B_T\, dl_p}{2\pi r B_p} . \qquad (3)$$

Here $B_T = B_0 R/r$ and B_p are the toroidal and poloidal magnetic fields, p,J are the plasma pressure and the current; the integrals are taken over magnetic surface cross-section square in formula (2), and over cross-section arc length in formula (3). The International system of units is used, $\mu_0 = 4\pi\cdot 10^{-7}$. For the tokamak of circular cross-section

$$q(a) \approx 5\cdot 10^6 \frac{B_0 a^2}{J(a) R} \left\{ 1 + \frac{a^2}{R^2}\left[1 + \frac{1}{2}\left(\beta_J + \frac{l_i}{2}\right)^2 \right] \right\} . \qquad (4)$$

The parameter l_i is determined in the similar manner as β_J with substitution of p by $B_p^2/2\mu_0$. The toroidicity corrections become important at $A \lesssim 3$ and, especially, when β_J is close to its extreme value $\beta_J \approx R/a$.

b) Equilibrium. The plasma pressure in the toroidal systems is usually considered to be isotropic, and the following equilibrium equations are used:

$$\vec{p} = \vec{j} \times \vec{B}, \qquad \nabla \times \vec{B} = \vec{j}, \qquad \nabla \cdot \vec{B} = 0 . \qquad (5)$$

From the first vector equation it follows that $\vec{B}\cdot\nabla p = 0$, i.e.

the pressure is constant on the magnetic surfaces. Nowdays, attention is attracted to the cases when, e.g. as a result of neutral injection, one needs to discern the longitudinal and transversal plasma pressures, $p_{\parallel} \neq p_{\perp}$. In this case, instead of the equation $\vec{B}\cdot\nabla p = 0$, one obtains the condition for $p_{\parallel}$ /1/:

$$\vec{B}\cdot\nabla p = \frac{p_{\parallel} - p_{\perp}}{2|\vec{B}|^2}\,\vec{B}\cdot\nabla|\vec{B}|^2 , \qquad (6)$$

and only for $p_{\parallel}$, one approximately obtains $p_{\parallel} \approx p_{\parallel}(a)$, $p_{\parallel}$ variation along the field line being of the order of $\delta p_{\parallel} \approx \frac{a}{R}(p_{\parallel} - p_{\perp})$. As for the transversal pressure, the equilibrium equation doesn't impose any restrictions to its distribution along the field lines. Thus, e.g., an observation of maximum pressure shift different from that of the magnetic surfaces will be an explicit indication of the pressure anisotropy.

In the axially symmetric case, the equation for the poloidal function Ψ, obtained at $p_{\parallel} \neq p_{\perp}$ by H.Grad /2/, is expressed as

$$r^2 \mathrm{div}\frac{\nabla\Psi}{r^2} = -4\pi r^2 \frac{\partial p_{\parallel}}{\partial \Psi} - \frac{G(\Psi)G'(\Psi)}{1-(p_{\parallel}-p_{\perp})/B^2} + 2\pi r^2 \frac{(p_{\parallel}-p_{\perp})\partial B^2}{B^2 \cdot \partial \Psi} -$$

$$- \nabla\Psi\cdot\nabla\left(\frac{p_{\parallel}-p_{\perp}}{B^2}\right) - \sum_k J_k \frac{\delta(r-r_k)}{r}\delta(z-z_k) , \qquad (7)$$

$$\vec{B} = \frac{1}{2\pi r}\nabla\Psi\times\vec{e}_{\varphi} + \frac{G(\Psi)/2\pi r}{1-(p_{\parallel}-p_{\perp})/B^2}\,\vec{e}_{\varphi} . \qquad (8)$$

Computations (e.g. see /3/) and an analysis of the equation show that the pressure anisotropy doesn't have a strong effect on the magnetic configuration. All is reduced mainly to the fact that the diamagnetic effect now depends on $p_{\perp}$, while the toroidicity effects depend on $p_{\parallel}$.

A typical problem in the equilibrium theory is the calculation of the system of external currents J_k, providing maintenance of the equilibrium with the prescribed shape of the plasma cross-section and stable plasma pressure and current density profiles. At present, rather effective methods of solving the equation (7) with isotropic pressure, $p_{\parallel}=p_{\perp}=p$,

have been developed /4-7/. As an example, the results of the computation for the plasma shape accepted for international design INTOR, with the poloidal divertor at the bottom, are given in Fig.1. The necessary form is provided by the poloidal field windings located rather far from the toroidal magnetic field coils. The calculations made independently by the US, European, Soviet and Japanese teams are in good agreement with each other. The total current through the windings is about 100 MA at the plasma current 6 MA /7a/.

The solution of the 2-D equilibrium equation is necessary not only for design work but also for the stability studies and for the general simulation of a disharge in the process of its evolution. Here, the equilibrium should be computed, in principle, for each time step. Therefore, a development of the simplified methods of describing the equilibrium is of importance. Among them the moment method /8,9/ and its upgrade version - a variational method developed recently by V,D.Khait et al./10/ seem to be promising. V.D.Khait has shown that the ordinary differential equations for the parameters Δ, λ, δ etc. can be obtained as the Euler-Ostrogradsky equation of the functional $\int(B^2/2 + p)dV$. The similar development of the moment method is also suggested in /11/.

c) Stability. In tokamaks as in any other toroidal system, a concept of resonance perturbation is of great importance. It is a helical perturbation $\exp i(m\theta - n\zeta)$, the pitch of which coincides with an average pitch of the magnetic field line. The condition of this is

$$mq(a) = n \qquad (9)$$

A rational magnetic surface a = Const, for which this condition is satisfied is called the resonance one. At the resonance perturbation the field lines are minimally curved. Therefore, only a small store of energy dependent on the pressure is needed to excite them. The non-local unstable kink modes are also typical for the current-carrying plasma. They are developed in the ideally conducting plasma, if the profile q(a) is not monotonous one, i.e. there are two re-

sonance surfaces with the same q in the system. Nonlinear development of these very instabilities at the initial stage of the tokamak disharge results in a bell-shaped (not skinned) current profile corresponding to a monotonous profile of q(a) /12/. For monotonous profiles only those instabilities can manifest themselves for which the constraints imposed by the ideal MHD fluid equations are removed. First of all, this is a tearing-mode and its extreme appearence as a free boundary kink mode when the resonance magnetic surface occurs in vacuum region. The most dangerous large-scale resonance perturbations, mq = n, with low m and n, can be avoided in the system at the special profiles of q(a). One can say that the elaborated experimental methods of preparing the stable disharges are reduced to the obtaining of the parameters related to this stability zone.

Some news in the disruptive instability. Inspite of the considerable progress in organizing stable disharges including those with low q at the boundary /$q(a_p) \approx 2$/, the problem of current-driven instabilities is far from it solving yet. Experimentally found disruptive instability greatly restrict the range of stable regimes in a tokamak.

Many papers were devoted to the explanation and search for the ways of stabilizing the disruptive instability. The widely spread viewpoint is that the disruption is a development of a few interacting tearing modes. This interaction occurs due to the toroidal coupling of the harmonics with azimuthal numbers m and $m \pm 1$ /13/ and due to nonlinearity of the harmonics with different m/n (e.g. m/n=2/1 and 3/2), as well. In the development of a tearing mode, the resonance surface is splitted and the magnetic islands are formed. Their size is proportional to the square root of the resonance harmonic amplitude. Therefore, even weak interaction of different modes can result in overlaping of the islands and stochasticity of the magnetic field structure. As the numerical computations /14/ have shown, such interaction between different helical modes accelerates the growth of initial perturbation, generates a series of new helical modes of approximately the equal amplitudes. This can be in-

terpreted as the disruption instability.

A clear criterion of the disruption appearance was recently given by L.E.Zakharov /15/. It is based on the analisis of the forces emerged at a helical deformation. It was found that the kink instabilities are caused by the disruptive force of interaction between the plasma current and the toroidal magnetic field $\vec{j}_{pl} \times \vec{B}_T$. The self-contractive force $\vec{j}_{pl} \times \vec{B}_{pl}$ prevents the disruption. In the case of uniform current, the disruptive force becomes more than contractive one at a sufficiently low current density, when the condition

$$nq < m - 1 \qquad (10)$$

is violated at the left boundary of the kink unstable zone. If the current density is sufficiently high so that the condition (10) is fulfilled, the disruptive force will not be able to deform the plasma column. The stability criterion for a bell-shaped current profile is expressed as

$$nq(0) < m - 1 \ . \qquad (11)$$

This condition being violated, the disruptive force $\vec{j}_{pl} \times \vec{B}_T$ undoubtedly exceeds the self- contractive one. At the nonlinear stage, this inequality of forces is retained. Hence, it follows that the unstable kink mode has no stationary stabilizing mechanisms and should result in a considerable rearrangement of the configuration (i.e. in disruption). Sykes and Wesson /16/ also associate the disruption with the absence of a new statinary (helical) equilibrium at the parameters corresponding to the kink instability zone.In a stable regime, the current profile satisfies the necessary requirements of the linear theory of stability. A current density drop in the core results in the unstable current profile and, as a consequence, in a disruption.

According to Zakharov, the results of the kink mode development considerably depend on the current density on the axis. If the criterion (11) is satisfied, the kink mode will not be able to rearrange the core where the contractive force is greater than the disruptive one. As a result, only the periphery of the plasma column will be rearranged.

This is a minor disruption. If the criterion (11) is violated, the unstable helical mode (m,n) will completely turn out the plasma column. In this case, according to the theory of reconnection /17/, the value nq(0) becomes equal m and, in accordance with (11), the mode m+1 becomes unstable and turns plasma out again, etc. This is the major disruption. Three possible regimes in a tokamak are presented in Fig.3. A means of preventing disruption, in accordance with this consideration, is the maintenance of high current density at the centre of the discharge to satisfy the requirements of the linear theory of stability. One important conclusion follows from this: at least in the disharge with low $q(a) \approx 2$, the current profiles with q(0) appreciably less than 1 (criterion (11) for m=2) should be realized.

On the ß-limit in a tokamak. If one is lucky to get in a stable zone of the current-driven kink modes, the problem of the pressure-driven local modes remines yet. The instabilities of these modes are believed to impose a restriction on a local pressure gradient and, finally, on the permissible ß. The system is natural to be chosen so that this limit would be a maximal one.

Optimization of the parameters in a tokamak is, roughly speaking, done in the following way. Proceeding from the theoretical evaluation of stability and equilibrium ß-limit as $ß \approx a/Rq^2$, one choses the minimal aspect ratio A=R/a compatible with the engineering requirements. Then, varying the parameters $q(a), \lambda(a), \delta(a)$ one studies numerically a) a large-scale kink instability, b) small-scale local instability (ideal ballooning modes).

The methods of solving the second of these problems, reduced to finding the eigenvalues of the second-order differntial equation (Connor,Hastie,Taylor equation /17/), are the most advanced ones. Instead of the more complicated problem of studying the kink instability, the "reasonable" profile q(a) is often chosen at which, in accordance with the experience, the instability is not expected. The results of the locally stable plasma pressure limit calculations

made in different laboratories differ slightly that indicates some subtlety of the problem. We present here the data by Degtyarev et al. (M.V.Keldysh Institute of Applied Mathematics). These data seem to be reliable due to the high accuracy in the description of equilibrium owing to application of the inverse variable method. Here, instead of the values of $\psi(r,z)$ in the fixed pointh of the nest, the coordinates r,z of the magnetic surfaces are directly calculated. This allows to increase significantly the accuracy of computing the averaged coefficients inherent the problem. The calculated limit pressure profiles for the configuration in Fig.1, at q changing from 1 on the axis to 2 on the plasma edge, are given in Fig.4. The limit value of a parameter $\beta=2\mu_0\int p ds/\int B^2 ds$ is equal 4.5% in this case.

At present, there is no common opinion on what would be q on the disharge axis. Until now, there is no reliable methods of finding q(0) in stable disharges. From a widely spread interpretation of the relaxation oscillations near the axis (observed as soft X-ray radiation dependent on the electron temperature) as the development of an internal kink instability, it follows that q(0) cannot be appreciably lower than 1. A few years ago, when the stable disharges have $q(a)\approx 3\div 4$, the drop in q from 1 to 3 over the radius seemed to be quite reasonable. It corresponds to an appreciable current peaking which provides the stability to the kink modes, $m>2$. A considerable progress in a decrease of q on the plasma edge down to $q\approx 2$ is reached at present in some tokamaks. If $q(0)\approx 1$, the profile will be rather smooth that will make the disharge unstable to the kink modes. As it has been alredy said, out of the analysis of forces which arise at the helical distortion of the plasma column, L.E.Zakharov has made a conclusion on inevitable distruction of the plasma column when the disharge parameters enter the zone of linear kink instability. Hence, one can conclude that in stable discharges with $q(a)\approx 2$, the value of q on the axis should be noticeably less than 1. According to the criteria by Bussac et al./18/, the internal ideal helical

modes allow the values of $q(0) \geq 1/2$. Therefore, it is natural to consider the profiles q(a), corresponding to q(0)=1/2, q(a)=2. The marginal pressure profile respective to the local modes, which corresponds to this case, is given in Fig.4. Here ß = 4 ÷ 6 %.

At present, it is not known whether the theoretical pressure limit could be exceeded or not. It is natural to consider that an excess over the limit pressure gradient results in an increase of transport so, that at high heating power, the anomalous transport will be established for sustaining the marginal profile. In this connection, the experiments on additional plasma heating up to the critical pressure are of great importance. The first experiments of such kind with neutral injection were done in a tokamak with circular cross-section. The result $ß \approx 3\%$ was published /19/, while the theoretical limit was evaluated as 2% /20/. This should not be considered as a discreapancy. The point is that the theoretical value $ß \gtrsim 2\%$ has been calculated at some given profiles $q(\psi)$, $p(\psi)$ which can differ from the experimental ones. The calculations of the marginal pressure profile, when only $q(\psi)$ is prescribed, made by Degtyarev et al. give the higher values of ß, namely, ß=2.2% at q changing from 1 up to 2 and ß=4% at q changing from 0.5 up to 2 (Fig.5).

Formally even these values of ß don't represent the limit. With an increase in pressure, plasma first enters the instability zone. Then the self-stabilizing effect occurs. This effect, recently widely discussed (see e.g. /21/), is illustrated in Fig.6. For the circular cross-section with A=4 and $1 < q < 3$, there is stability at $ß < 2.13\%$ (the first stable equilibrium) and at $ß < 8.5\%$ (the second stable equilibrium).

2. Helical stabilized pinch.

Recently, the physical vocabulary was enriched by a new term - translational transform. It has been introduced by T.Ohkawa to designate the effect of transforming the poloidal flux generated by the plasma column current into the toroidal one. In essence, this effect was discovered earlier by O.I.

Fedyanin and E.D.Andryukhina /22/ in L-2 stellarator with OH current. It manifested itself in the high shear stellarator as the dependence of a diamagnetic signal on the OH current direction.

The origin of the translational transform can be explained in electrotechnical language. In difference from a case of axial symmetry when the poloidal and toroidal electric circuits are independent, in the system of a stellarator type, the poloidal and toroidal circuits are electrcally coupled, i.e. their mutual inductance differs from zero. Let Ψ, F be the poloidal magnetic flux and current, external relative to the given magnetic surface, and Φ, J be the toroidal flux and current counted off the magnetic axis. Then, from the general equilibrium equation (see below, eq. (20)) it follows

$$\begin{aligned} J &= -\alpha_{22}\Psi'(a) + \alpha_{23}\Phi'(a) \\ F &= -\alpha_{23}\Psi'(a) + \alpha_{33}\Phi'(a) \end{aligned} \qquad (12)$$

Here the magnetic surfaces are labelled by the coordinate a (later, it is an average cross-section radius), α_{ik} are the geometric factors determined only by the magnetic surface shape. They can be calculated as the metric coefficients $g_{ik} = \frac{\partial \vec{r}}{\partial x^i}\frac{\partial \vec{r}}{\partial x^k}$ of the flux coordinate system $x^1=a$, $x^2=\theta$, $x^3=\zeta$ with "stright" field lines, averaged over the angular variables, $\alpha_{ik} = \langle g_{ik}/\sqrt{g}\rangle_{\theta,\zeta}$, $g=\mathrm{Det}\, g_{ik}$. It is easy to see that the term α_{23}/α_{22} expresses the rotational transform for the stellarator with the same shape of the magnetic surfaces as those produced in a pinch:

$$\iota_o = -(\Psi'/\Phi')_{J=0} = \alpha_{23}/\alpha_{22} . \qquad (13)$$

At $\iota_o \neq 0$, Φ' is explicitly dependent on the longitudinal current J,

$$\Phi' = \frac{1}{\alpha_{33}}(F + \iota_o J)/(1 - \frac{\alpha_{22}}{\alpha_{33}}\iota_o^2), \qquad (14)$$

that is a manifestation of translational transform.

This effect explains the suggestion by Ohkawa et al. /23/ to use the external helical fields for a stationary

maintenance of the reversed field pinch with monotonous profile of q(a) necessary for stability (Fig.7). Usually, the field reversal outside the stabilized pinch is established spontaneously. J.B.Taylor explained it as a process of transition into a stable state with a minimum energy. However, the turbulent mechanism of generating the required poloidal currents (which is manifested by the strong fluctuations observed in plasma) seems to be undesirable because it makes the thermal insulation worse. The reversed field configuration is desirable to satisfy the ordinary "laminar" transport equations.

The stationary cylindrically-symmetric plasma configuration is compatible with the Ohm's law

$$\vec{j} = \sigma_{\parallel} \frac{(\vec{E}\vec{B})\vec{B}}{|\vec{B}|^2} + \frac{\vec{B}\times\nabla p}{|\vec{B}|^2} \qquad (15)$$

without reversal of the B_z field. But B_z close to zero can be realized. Therefore, only a small negative addition to B_z is sufficient to sustain the reversed field profile. To estimate the reversed field effect in the helical pinch, let us consider the relationship (14) outside plasma, where F and J are constant, $F=F_e, J=J_p$. Let's choose the total poloidal current through the toroidal field coils, F_e, so, that Φ' would be reduced to zero at a certain external magnetic surface $a=a_o$: $F_e = -\iota_o(a_o)J_p$. Taking into account an estimations $\alpha_{22} \sim 2\pi a/L$, $\alpha_{33} \sim L/2\pi a$, $\iota_o \ll L/2\pi a$, one obtains for an average external longitudinal field $\bar{B}_z = \Phi'/2\pi a$:

$$\bar{B}_z = \frac{J}{L}\left[\iota_o(a) - \iota_o(a_o)\right] . \qquad (16)$$

One can see that for the average field reversal it is important that the geometrical rotational transform would be changed with radius, $\iota_o'(a) \neq 0$.

The equilibrium code developed at the Institute of Applied Mathematics has allowed to study the translational transform in its pure form, in the absence of the plasma poloidal current ($\beta_J=1$). A stright helically-symmetric column equivalent to a torus with aspect ratio R/a=10 has been considered. The plasma pressure has been taken as a linear function ψ

(approximately, a parabolic distribution). The second function $F_h(\psi)$ (current through the helicoidal strip), which occurs in the equation, similar to (8), for $\psi = \psi(r, \omega - \alpha z)$,

$$\operatorname{div} \frac{\nabla\psi}{1+\alpha^2 r^2} = \frac{2\alpha F_h}{(1+\alpha^2 r^2)^2} - \frac{F_h F_h'(\psi)}{1+\alpha^2 r^2} - 4\pi^2 R^2 p'(\psi) \ , \qquad (17)$$

as a source, is calculated under the condition of a zero poloidal current I. An average longitudinal magnetic field B_z, which emerges as a result of the translational transform, is calculated by the formula

$$B_z = \frac{F_h(0) - I(\psi) + \alpha R(\frac{r}{R}\frac{\partial\psi}{\partial r} - J)}{2\pi R(1+\alpha^2 r^2)} \ . \qquad (18)$$

Both, B_z and $q(\psi)$ are equal zero on the axis and are maximal ones on the plasma edge (Fig.8). An addition of the external field displaces the curves up. The maximum q versus the helical field-periods-number $N=\alpha R$ at the different ratio of the elliptical cross-section semiaxes, b/a, is given in Fig.9. The calculation of a stationary distribution corresponding to Ohm's law has been also done. A stationary profile q, at $\sigma_{\parallel}$= Const inside plasma, and $\sigma_{\parallel}=0$ outside it at $\beta_J=0.2$, with the q reversal on the plasma edge, is demonstrated in Fig.10. This profile will be expected to be stable if one applies the cylindrical pinch stability results. Actually, the stability of the helical pinch has not been studied yet, this problem remines to be solved.

Thus, the direct computations confirm the idea of T.Ohkawa et al. on the possibility of the stationary (as far as the current is sustained) maintenance of the reversed profile.

3. Stellarators.

From the theoretical viewpoint the stellarator, as a stationary magnetic plasma trap, is the most appropriate basis for a fusion reactor. But the configuration of stellarator which includes the helical magnetic fields is more complicated than that of the symmetric systems considered above. Eventually, this results in a delay - both experimental and theoretical - in the stellarator studies in comparison with

the tokamak. At present, the time of failures in the stellarator studies which took place in the sixties, has come to the end. The experiments on ohmic heating performed initially in small stellarators and then in second-generation-stellarators with plasma radius up to 20 cm and magnetic field up to 30 kGs, have shown that the helical field improves the confinement of ohmically-sustained plasma. Then, in Wandelstein YII A with neutral injection and in a new device Heliotron E with RF heating /24/, the currentless hot plasma with the temperature of a few hundred eV was sustained well. At the same time the theoretical estimations of a danger from the trapped particles were decreased. Engeneering consideration have shown the possibility of the modular design of the stellarator windings. It was found out that the stellarator design can be not much more complicated than the tokamak one.

All this induced an interest to the stellarators as a basis for a stationary fusion reactor. In this connection, the problem of the plasma pressure limit in stellarator acquires importance. It includes an answer to such problems as 1) what is better: large aspect ratio or small one like that in a tokamak, 2) should one tend to provide a large shear, or it is better to arrange an average magnetic well, etc.

In difference from the systems with axial and helical symmetry, there is no equation, similar to the two-dimensional equation for ψ, to describe the closed stellarator. The main approaches here are 1) expansion in terms of the helical field amplitude, 2) expansion in terms of the ratio of a distance from the axis to the period of helical field. In the seventies, at a time of the violent attack by tokamaks, the attention to the stellarator theory decreased noticeably. Recently, the theoretical studies in stellarator became more active. Besides 3-D numerical codes, the improved analytical methods, more universal than previously, are being developed now.

L.M.Kovrizhnykh and S.V.Shepetov at the Lebedev Institute /27/ and H.R.Strauss at the Princeton University /28/

used an averaging along the system to obtain a simplified 2-D system of equations for average values. In the usual stellarator ordering worked out by the Princeton theoreticians (small helical field amplitude) the equilibrium equations by Kovrizhnykh and Shepetov have the form:

$$\begin{aligned} \nabla p &= \vec{j}\times\vec{B} + \vec{B}\times\vec{B}\times\nabla\lambda \\ \nabla\times\vec{B} &= \vec{j} + \nabla\times\vec{B}^{*} \\ \nabla\cdot\vec{B} &= 0 \end{aligned} \qquad (19)$$

Here, $\vec{B},\vec{j}$ are the averaged field and current density, $\lambda = -A\vec{j}\vec{B}/|\vec{B}|^2$, while A function and $\vec{B}^{*}$, an effective two-dimensional magnetic field, are calculated at a given helical field. This system gives wide opportunities for solving a number of problems and it has already given some interesting results /29,30/.

Another approach has been developed by M.I.Mikhailov /31/. He has shown that the method of inverse variables applied previously for the long period systems is applicable also to the "ordinary" many-periods stellarators. The advantage of this method is that there is no procedure of averaging in which a part of information is naturally lost. Here the problem is reduced to finding the metric coefficients $g_{ik}=\frac{\partial\vec{r}}{\partial x^i}\frac{\partial\vec{r}}{\partial x^k}$ of the special flux coordinate system $x^1=a$, $x^2=\theta$, $x^3=\zeta$, satisfying the equations (g = Det g_{ik}):

$$\begin{aligned} p'V' &= I'\Phi' - J'\chi' \\ \frac{\partial\nu}{\partial\zeta} + \iota\frac{\partial\nu}{\partial\theta} &= \frac{4\pi^2 p'}{\Phi'}\left[\langle\sqrt{g}\rangle_{\theta,\zeta} - \sqrt{g}\right] \\ -\nu + \frac{\partial\varphi}{\partial a} &= \frac{g_{12}}{\sqrt{g}}\chi' + \frac{g_{13}}{\sqrt{g}}\Phi' \\ J + \frac{\partial\varphi}{\partial\theta} &= \frac{g_{22}}{\sqrt{g}}\chi' + \frac{g_{23}}{\sqrt{g}}\Phi' \\ F_0 - I + \frac{\partial\varphi}{\partial\zeta} &= \frac{g_{23}}{\sqrt{g}}\chi' + \frac{g_{33}}{\sqrt{g}}\Phi' \end{aligned} \qquad (20)$$

Here $I(a), J(a), \chi(a), \Phi(a)$ are the poloidal and toroidal currents and magnetic fluxes, $p(a)$ is the pressure, $V(a)$ is the volume enclosed with the magnetic surface $a(r)$ = Const,

two singlevalued functions ν, φ are the characteristics of the plasma current and magnetic field.

It is important that the independent investigations have lead to the same results. They clarify some peculiar features of the stellarator, described below.

a) Pecularities in the equilibrium.

Elasticity of the magnetic surfaces at positive shear. One feels intuitively that the stellarator magnetic system is more stiff than that of the tokamak. Indeed, the magnetic surfaces in a tokamak are produced by a current which flows in plasma. Thus a plasma shift does not change a relative position of the magnetic surfaces. Their distortion arises only at high ß approaching the equilibrium limit. As for the stellarators, the magnetic surfaces are preset by the external currents, and if the rotational transform is not uniform (i.e. there is a shear), the shift of the plasma column, even at low ß will deform the system of magnetic surfaces. The difference between the tokamak and the stellarator is well seen from the Greene, Johnson, Weimer equation for the shift $\Delta(a)$ /32/, which can be written in the form *)

$$\left[(\iota_0\Delta)'a^3\right]' + \frac{1}{\iota_J}\left(\iota_J a^3\Delta'\right)' = -\frac{2p'(a)Ra^2}{(\iota_0+\iota_J)B_0^2} + \frac{p'a^2RV_0''(\Phi)}{(\iota_0+\iota_J)}\Delta \,. \qquad (21)$$

Here, ι_0 is a vacuum rotational transform, ι_J is that induced by OH current. One can see that in a tokamak ($\iota_0=0$) the homogeneous equation ($p'=0$) has a solution $\Delta'=0$. It means that e.g. an application of the transversal homogeneous magnetic field displaces the surfaces as a whole. In the stellarator with a shear ($\iota_J=0$, $\iota_0'(a)\neq 0$) the solution of homogeneous equation,

$$\Delta = \mathrm{Const}/\iota_0(a) \qquad (22)$$

explicitly shows a change in the relative shift of the magnetic surfaces. In the ordinary case of a positive shear, $\iota_0'(a)\neq 0$, the internal surfaces will be displaced more than the external ones, i.e. a tokamak-like condition, with

*) I am obliged to V.D.Pustovitov as he attracted my attention to this form.

the casing at the pressure rise, is provided. In this case, plasma is known to be stable respective to its shift as if the magnetic surfaces would be elastic ones. If the axis is shifted towards the reduced toroidal field, then at $\iota_0' > 0$ an average magnetic well will arise. This method of the well creation in l=3 stellarator was known to be suggested by J,B.Taylor /33/.

The loss of elasticity at high aspect ratio. At the fixed pitch of helical windings with an increase in the system length and, correspondingly, in the number of its periods, the rotational transform rises, and shift decreases at given plasma pressure. But in this case, a magnetic hill ($V_0'' > 0$), which occurs as a stiffness coefficient before Δ in a sum with $(a^3 \iota_0')'$, rises, Therefore, at a high number of periods (strong rippling), the sign of the stiffness coefficient is changed and, with an increase in the plasma pressure, an instability arises which is similar to the mode m=1, n=0 in the ordinary mirror trap. This is the reason why the multiperiodic systems with large aspect ratio, like Scyllac, are not suitable without feed-back stabilization.

This conclusion can be referred only to the systems with planar axis. If the axis of a system has a form of the helical line around the torus, its local curvature, which provides the well production, will not be dependent on the axis length. Thus, no limitation to the number of periods arises in this case.

b) Pecularity in the stability against the local modes. The stellarators are free of the main tokamak current-driven instabilities. Thus, only pressure-driven instabilities remain. One of them is positional instability - mentioned above - developed in the multiperiodic systems with planar axis at rather high plasma pressure. Another one is a local qasi-flute-like mode. It can be stabilized by a shear or by a magnetic well. The question, what is more important - shear or well - is a standard topic for discussion by the members of the stellarator community. At dawn of the fusion research, more than 20 years ago, the Princeton theoreticians showed that, in the l=3 stellarator the shear stabilization provides

stable plasma confinement with ß≈10%. In l=2 stellarator, which is preffered due to the higher topological stability of the internal magnetic surfaces, the large shear is also possible provided short-period-helical-windings are used. But in this case, the ß-limit decreases essentially due to an increase in the mean curvature of the magnetic field lines. For L-2 device parameters, where the rotation transform changes from ι=0.2 on the axis to ι=0.7 on the edge, stable ß will be no greater than 1%, if the curvature of the system is not taken into account /34/. Thus, the stabilization by the shear itself doe's not work in l=2 stellarator, and one should rely on the magnetic well.

As is known /35,36/ in the l=2 stellarator with a sufficiently low aspect ratio and small number of periods (e.g. as in Wandelstein YII-A, where R/a=15, N=5) there is a magnetic well. It can be increased using a combination of the 2nd and 3d harmonics of the magnetic field $B = \nabla(\varphi_2 + \varphi_3)$ with the same period:

$$\varphi_2 = \varepsilon_2 \frac{2R}{N} B_0 \frac{1}{2} \left(\frac{Na}{R}\right)^2 \sin(2\theta - N\zeta) + \ldots$$
$$\varphi_3 = \varepsilon_3 \frac{2R}{N} B_0 \frac{1}{8} \left(\frac{Na}{R}\right)^3 \sin(3\theta - N\zeta) + \ldots \qquad (23)$$

In this case, there is no limitations imposed by the MHD instability, but the equilibrium ß is small. Thus, this extreme case of the low-shear-stellarator is not suitable also. One should recur to the systems with shear.

Let consider stability criterion for a stellarator with shear. In the stellarator there is no danger of ballooning modes which impose a pressure limit in the tokamaks. This phenomenon can be explained by the same stiffnes of the system at $\iota_0' > 0$ described above. Therefore an estimation of the pressure limit is done on the basis of the general well-known Mercier criterion. The detailed analysis of stability is given in papers /27,38/. We present here some simple relationships from paper /37/, where some nonessential toroidal corrections are omitted but the coupling of the 2nd and 3d harmonics (23) is taken into account. In this case, an

additional term $N^2a^2\mathcal{E}_2\mathcal{E}_3/2R$ should be added to the right-hand side of the equation (21). A magnetic well, $V''(\Phi)<0$, is described as follows

$$V''(\Phi) = \frac{1}{B_0^2}\left(\frac{N^2\mathcal{E}_2^2}{2R} - \frac{3\Delta'}{a} - \Delta''\right). \qquad (24)$$

Using the eq. (21), one can eliminate the combination $3\Delta' + a\Delta''$, and Mercier criterion, containing $V''(\Phi)$, takes the form ($s=\iota_0'a/\iota_0$):

$$\frac{s^2}{4} - \frac{2p'a}{B_0^2\iota_0^2}\cdot W > 0, \qquad (25)$$

where W is a noncompencated part of the $V''(\Phi)$:

$$W = -\frac{N^2}{4}\left(\mathcal{E}_2^2 - \frac{\mathcal{E}_2\mathcal{E}_3}{\iota_0^2}\right) - \frac{R(\iota_0'a^3)'}{2\iota_0 a^3}\Delta . \qquad (26)$$

The first term with $\mathcal{E}_2^2$ is a destabilizing one, the second term with $\mathcal{E}_2\mathcal{E}_3$ describes the stabilization by a mixture of the 2nd and 3d helical harmonics. The last term is related with the mentioned above magnetic well deepening at $(a3\iota_0')>0$, $\Delta<0$ (outwards shift). In papers /27,29,38/ Kovrizhnykh and Shepetov pay attention to the fact that at the pressure pumping this term gives selfstabilization of plasma due to its natural expansion along the major radius. The Kovrizhnykh and Shepetov effect differs from the effect of selfstabilization in the tokamaks and low-shear stellarators , discovered previously by A.B.Mikhailovsky et al. (see /39/ and the references there), by the fact that it is linear one in Δ , and consequently, appears already at rather low value of ß. If the vacuum magnetic surfaces even doesn't posses a well, the latter can arise at $ß \gtrsim \iota_0(0)\iota_0^2(a)/N$, that gives, e.g. for L-2 device, $ß \gtrsim 0.1\%$. This self-stabilization effect is the most remarkable feature of the ordinary high-shear stellarators with moderate aspect ratio.

One should note that the theoretical limit to a relative depth of the magnetic well is equal $2a/R$. Therefore, with an increase in the aspect ratio the depth of the well, no matter how it is produced, inevitably decreases, and the stability ß-limit drops. Meanwhile, the equilibrium ß rises

(Fig.11). The intersection of the curves β_{st} and β_{eq} determines an optimum which was estimated by M.I.Mikhailov as a β_{eq}-value at the maximum aspect ratio providing a compensation of the magnetic hill by a shift of the magnetic surfaces. For l=2 stellarator, $(R/a)_{max} \approx 2N\Delta/a\epsilon$, $\epsilon \approx N\varepsilon_2^2/8$, so that /40/

$$\beta = \left(\frac{\Delta}{a}\right)^2 \left(\frac{Na}{R}\right)^2 \varepsilon_2^2 \quad . \tag{27}$$

A modest estimation at $\Delta/a = 1/2$, $aN/R = 1$, $\varepsilon_2 = 1/2$ shows that $\beta \approx 6\%$ is achieved, at $R/a = 16$.

Thus, one can now answer the question, what is better for stellarator - shear or the magnetic well,- in the following way: the shear is better, when it provides creation of the magnetic well necessary for stability. It causes an option of the optimal (not very large) aspect ratio $R/a \lesssim N/\epsilon$.

As it has been noted above, the conclusion respective to the optimal aspect ratio for stellarators does not spread on the stellarators with spatial (nonplanar) axis. In the latter case the pressure limit is determined by the local curvature of the axis, which does not depend on the total axis length. Such systems with D-shaped magnetic surface cross-section differ from the tokamaks by the fact that the pressure here seems to be noticeably higher than 6% due to the absence of ballooning mode instability.

c) Stellarator with rectilinear sections. Although the stellarator has the advantages discussed, the reactor on its base seems to be rather complicated in operation because of the stellarator windings. Is it possible to separate the confining windings with their complex design from the main reactor part by designing the latter as a rectilinear section with the stright field lines? The stellarator with rectilinear sections is not a news. The C stellarator was designed as a racetrack one. Uragan-2 also has the rectilinear parts. But the insertion of the rectilinear sections without helical windings is not harmless for the plasma equilibrium. The current arising due to the charge separation in the curvilinear sections, at $\epsilon \sim 1$ should pass through the

whole system to be closed in plasma. This Pfirsch-Schlüter current of a dipole type produces a transversal magnetic field which the stronger distorts the magnetic surfaces, the longer the section on which this field affects. Hence, a decrease in the equilibrium β , when the sections with straight field lines are introduced. To have no effect of the straight sections on plasma equilibrium and stability, the charge separation current should be closed within a curvilinear section. In paper /41/ it is shown that this can be realized with a special connector of the rectilinear elements (CREL).

Let's explain the idea of CREL by a simple example. Out of the plasma equilibrium equation

$$\frac{dp}{dx} = j_{\perp} B \tag{28}$$

it follows that the poloidal current through the strip, between two adjacent magnetic surfaces, $p = \text{Const}$, $p + dp = \text{Const}$, along the magnetic field line, is equal

$$dI = \int j_{\perp} dx\, dl = dp \int \frac{dl}{B} , \tag{29}$$

where the integral is taken over the length of the field line. If for all the field lines on the surface $p = \text{Const}$, the current between two end sections of the CREL is the same, there will be no longitudinal current passing to the rectilinear sections. Thus, the CREL should satisfy the condition

$$U = \int \frac{dl}{B} = \text{Const} \tag{30}$$

for all the field line pieces between the end sections. For the curved solenoid the integrand is proportional to the square of the field line curvature radius, $U = Cr^2$. Let the solenoid be composed of three semitori with an angle α between their planes. Introducing the polar coordinates in the solenoids cross-section, one obtains $U_o = Cr^2 =$

$C\,(R_o + \rho\cos\theta)^2$ for the central solenoid, and $U_1 = C\left[R_o + \rho\cos(\theta+\alpha)\right]^2$, $U_{-1} = C\left[R_o + \rho\cos(\theta-\alpha)\right]^2$ for two end ones. In the linear, relative to the curvature, approximations the terms with $\sin\theta$ are cancelled out in the sum $U = U_o + U_1 + U_{-1}$ and one obtains

$$U = 3CR_o^2 + 2CR_o(1 + 2\cos\alpha)\,\rho\cos\theta. \qquad (31)$$

We see, that U does not depend on the initial field line azimuth, θ, when $\alpha = 120^\circ$. The CREL with the planar axis should have a variable curvature. The closed traps with such CREL's are shown in fig.12,13. They are rather long and are called by us "DRACON" (russian abbreviation for a "long equilibrium configuration"). In the DRACON the magnetic field can be reduced in linear sections without any effect on the plasma pressure. This increases β averaged along the system, as shown in Fig.14. It means that one can have $\beta \simeq 20 \div 30\%$ in the trap in comparison with $\beta \simeq 5 \div 10\%$ for the ordinary stellarators. This is an advantage of the new systems.

In the DRACON-traps the CREL has the same functions as the plugs in the ambipolar traps. Stabilization can be provided either like that in stellarators (average magnetic well due to the CREL curvature) or by means of quadrupole lenses at the CREL outlet into the rectilinear sections.

4. Conclusion. Recently, an appreciable progress has been reached in the development of a theory of toroidal plasma systems.

By independent calculation in different laboratories, it has been shown that the β-limit is close to a value acceptable for the reactor design ($\beta \simeq 4\%$) in a tokamak with a moderately peaked current. If one takes into account that, according to the analysis of the kink instability made by Zakharov, the real peaking is greater than the accepted one in the majority of calculations, the limit β-value will actually have a 1.5-fold rise.

The idea of stationary maintenance of the reversed field in a helical stabilized pinch, suggested by T.Ohkawa is confirmed by the direct calculations.

The analitical studies have manifested a strong stabilizing mechanism in the stellarators with shear at the moderate aspect ratio. There is no calculations here similar to those for tokamaks, but estimations demonstrate the possible stable equilibrium in stellarators with ß-values not less than those in tokamaks.

An opportunity of inserting the rectilinear sections preferable in operating, without any loss in the confining properties of the closed stellarators is proved.

References.

1 В.Д.Шафранов. В кн. Вопросы теории плазмы. Под ред. Леонтовича М.А. М.:Атомиздат,1963, вып.2,с.129.

2.H.Grad.Phys.Fluids, 10,137(1967).

3.W.A.Cooper,G.Bateman,D.B.Nelson.Nucl.Fusion, 20,985(1980).

4.K.Lackner. Computer Physics Communications, 12,33(1976).

5.J.L.Johnson,H.E.Dalned et al., Journal of Computational Physics, 32,212(1979).

6.R.Gruber,F.Troyon,D.Berger et al., Computer Physics Communications, 21,323(1981).

7.П.Н.Вабищевич,Л.М.Дегтярёв,В.В.Дроздов. Препринт ИПМ им.М.В.Келдыша АН СССР, №5, 1980.

7a.P.N.Vabishchevich,L.M.Degtyarev et al., Proc. 10th Europ.Conf.Moscow(1981) G-4.

8.Л.Е.Захаров,В.Д.Шафранов. ЖТФ, 43, 225 1973.

9.Л.Е.Захаров,В.Д.Шафранов. Препринт ИАЭ-3075,Москва 1978.

10.В.Д.Хаит. Физика плазмы, 6, 871 1980.
V.D.Khait,V.K.Kolesnikov.Proc. 10th Europ. Conf., Moscow (1981) B-8

11.L.L.Lao, S.P.Hiershman,R.M.Wieland.Preprint ORNL/TM-7616 (1981).

12.В.В.Параил,Г.В.Переверзев. Физика плазмы,6, 27 1980.

13.D.Edery,J.L.Soule,R.Pellat et al., Plasma Phys. and Contr.Nucl.Fus.Res.,1980, Eighth Conf.Proc., Brussels, IAEA,Vienna,1,269(1981).

14.H.R.Hicks,J.A.Holmes,B.A.Carreras et al.,ibid,1,259(1981).
15.Л.Е.Захаров.Физика плазмы,7,18(1981).
L.E.Zakharov.Proc. 10th Europ.Conf.,Moscow (1981), B-2.
16.A.Sykes,J.A.Wesson. Plasma Phys. and Contr.Nucl.Fus. Res.,1980, Eighth Conf.Proc.Brussels,IAEA,1,237(1981).
17.J.M.Connor,R.J.Hastie,J.B.Taylor.Phys.Rev.Lett.,40,396 (1978).
18.E.N.Bussac,R,Pellat,D.Edery,J.L.Soule,ibid,35,1633(1975).
19.K.Murakami,D.W.Swain,S.C.Bates et al.,Plasma Phys. and Contr.Nucl.Fus.Res.,1980,Eighth Conf.Proc.,Brussels, Iaea,Vienna,1,377(1981).
20.A.M.M-Todd,J.Manickam,M.Okabayashi et al.,Nucl.Fusion, 19,743(1979).
21.H.R.Strauss,W.Park,D.A.Monticello et al.,Nucl.Fusion, 20, 638(1981).
22. Э.Д.Андрюхина,О.И.Федянин.Физика плазмы,3,792(1977).
23.T.Ohkawa,M.Chu,C.Chu,M.Scaffer.Nucl.Fusion,20,1464(1980).
24.K.Uo,A.Iiyoshi,T.Obiki et al.,Proc. 10th Europ.Conf., Moscow (1981) E-1.
25.R.Chodura, W.Dommasck,W.Lotz,J.Nührenberg,A.Schlütter. Plasma Phys.and Contr.Nucl.Fus.Res.,1980,Eighth Conf. Proc.Brussels,Iaea,Vienna,1,807(1981).
26.D.C.Barnes,J.U.Brackbill,W.O.Schneider.Nucl.Fusion,21, 537(1981).
27. Л.М.Ковржных,С.В.Щепетов.Физика плазмы,6,976(1980).
28.H.R.Strauss.Plasma Physics,22,733(1980).
29.L.M.Kovrizhnykh,S.V.Shchepetov.Proc. 10th Europ.Conf., Moscow (1981), E-11.
30. I.S.Danilkin,L.M.Kovrizhnykh,S.V.Shchepetov,ibid,E-10.
3. М.И.Михайлов.Физика плазмы,6,45(1980).
32.J.M.Greene,J.L.Johnson,K.E.Weimer.Plasma Phys.,8,145(1966).
33.J.B.Taylor.Phys.Fluids, 8,1203(1965).
34.И.С.Данилкин.Физика плазмы,4,1033(1978).
35.V.D.Shafranov,E.I.Yurchenko.Nucl.Fusion, 8,329(1968); Л.С.Соловьёв,В.Д.Шафранов,Э.И.Юрченко. Plasma Phys. and Contr.Nucl.Fus.Res.,IAEA,Vienna,1,175(1969).
36.D.Lortz,J.Nührenberg.Nucl.Fusion,18,807(1978).

37.L.E.Zakharov, M.I.Mikhailov, V.I.Pistunovich et al., Plasma Phys. and Contr.Nucl.Fus.Res.,1980,Eighth Conf. Proc.Brussels,IAEA,Vienna,1,313(1981).

38.Л.М.Ковриженых,С.В.Шепетов.Физика плазмы,7,419 1981 .

39.A.B.Mikhailovsiy,V.V.Demchenko.Proc. 10th Europ.Conf. Moscow (1981),B-11.

40.V.D.Shafranov.Nucl.Fusion, 20,1075(1980).

41.V.M.Glagolev,B.B.Kadomtsev,V.D.Shafranov,B.A.Trubnikov. Proc. 10th Europ.Conf.,Moscow.(1981),B-11.

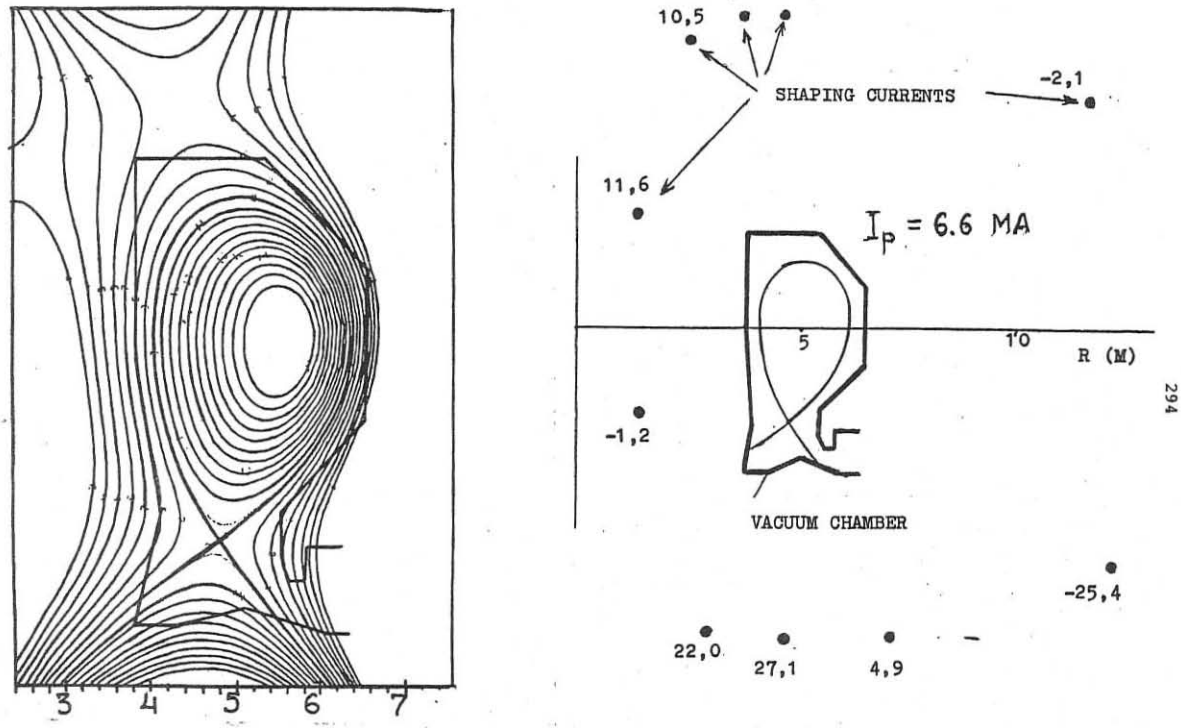
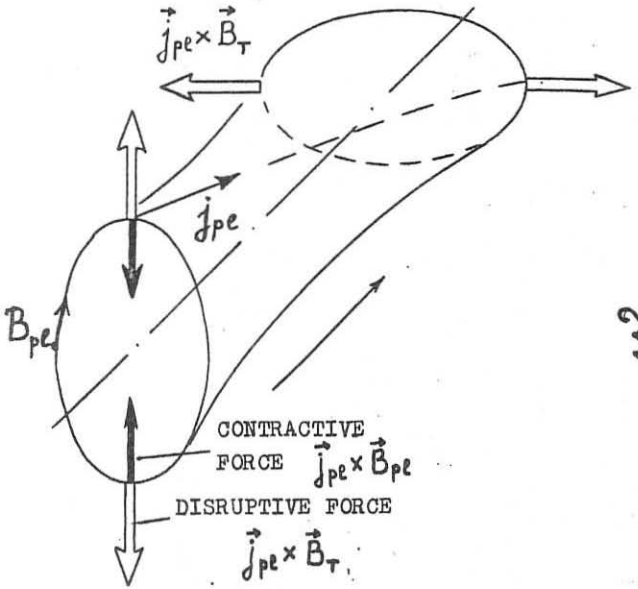


FIG.1. INTOR: FLUX SURFACES AND SHAPING CURRENTS

(according to P.N.Vabishchevich, L.M.Degtyarev, V.V.Drosdov et.al., see Report G-4, This Conference)



CONTRACTIVE AND DISRUPTIVE FORCES

IN A HELICALLY DEFORMED CURRENT CHANNEL

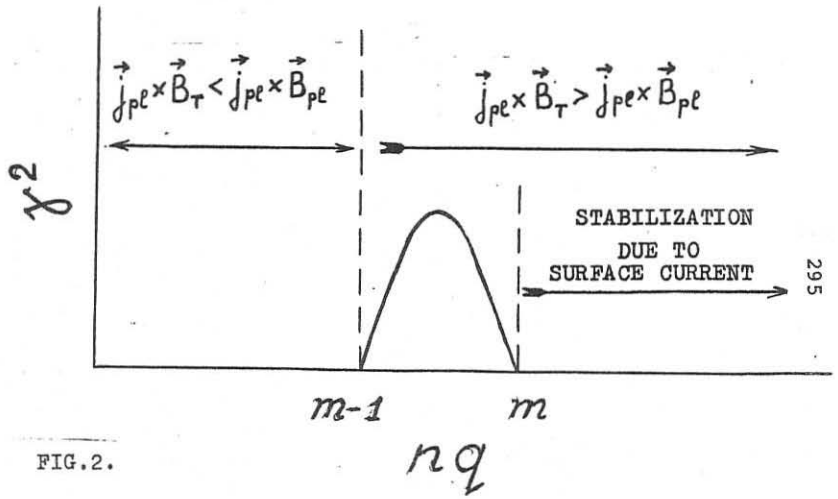


FIG.2.

KINK MODE STABILITY DIAGRAM

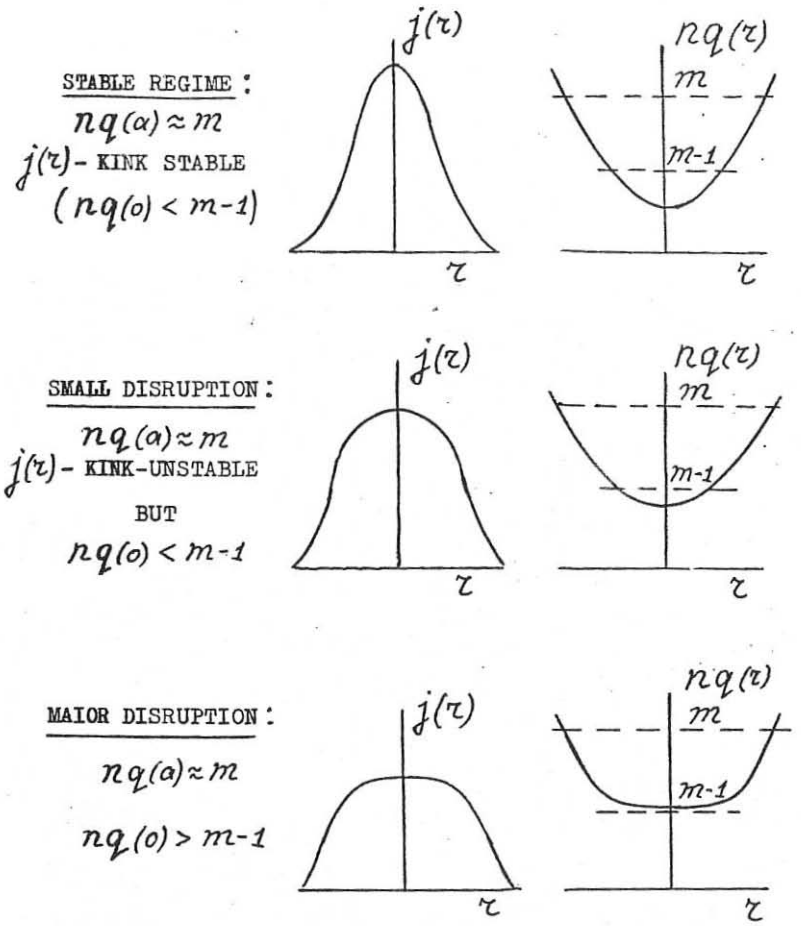


FIG.3. THREE SPECIFIC REGIMES IN TOKAMAK

(according to L.E.Zakharov)

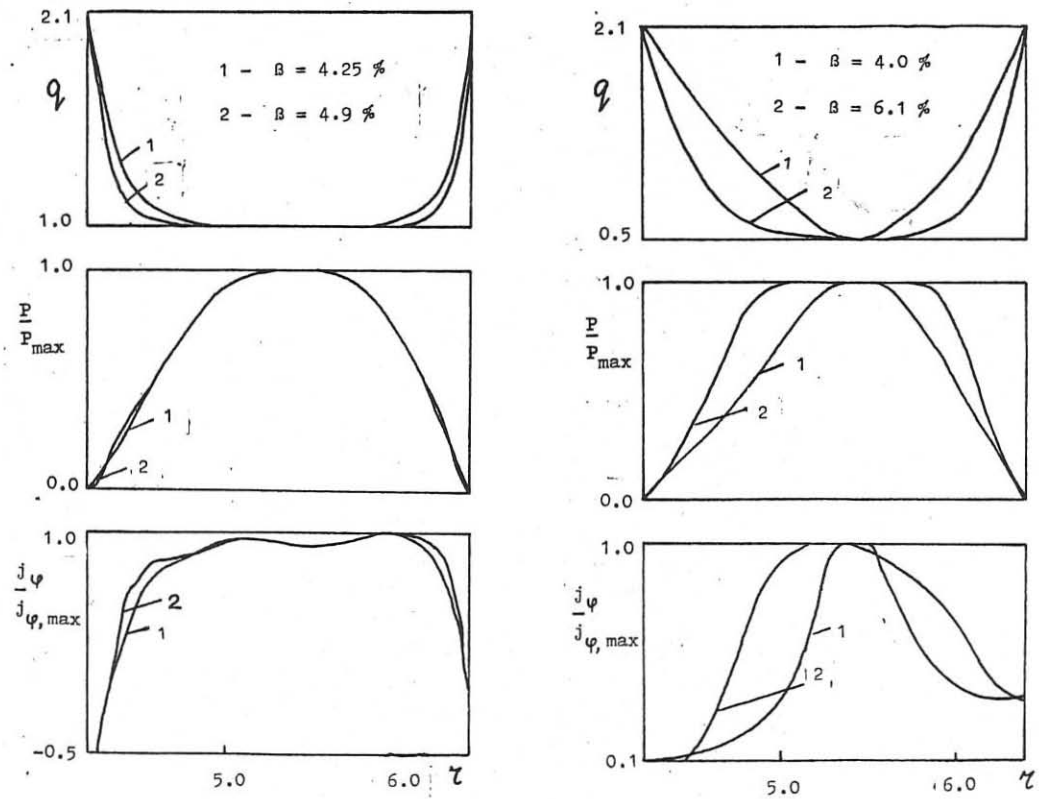
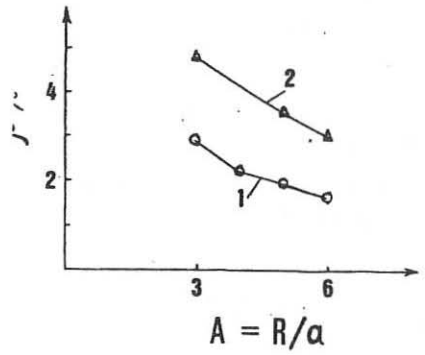


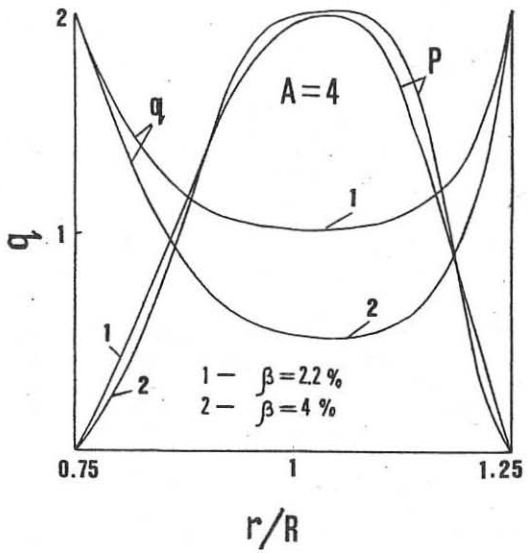
FIG.4. MARGINAL STABLE PROFILES FOR INTOR

Max-Planck-Institut für Plasmaphysik
8046 Garching bei München



β – LIMIT VERSUS ASPECT RATIO

$q(\psi)$ IS PRESCRIBED
$p(\psi)$ IS MARGINAL



MARGINAL PLASMA PRESSURE PROFILE AT A PRESCRIBED $q(\psi)$ – PROFILE

FIG.5. BALLOONING STABLE β IN THE FIRST ZONE OF STABILITY FOR CIRCULAR CROSS-SECTION TOKAMAK

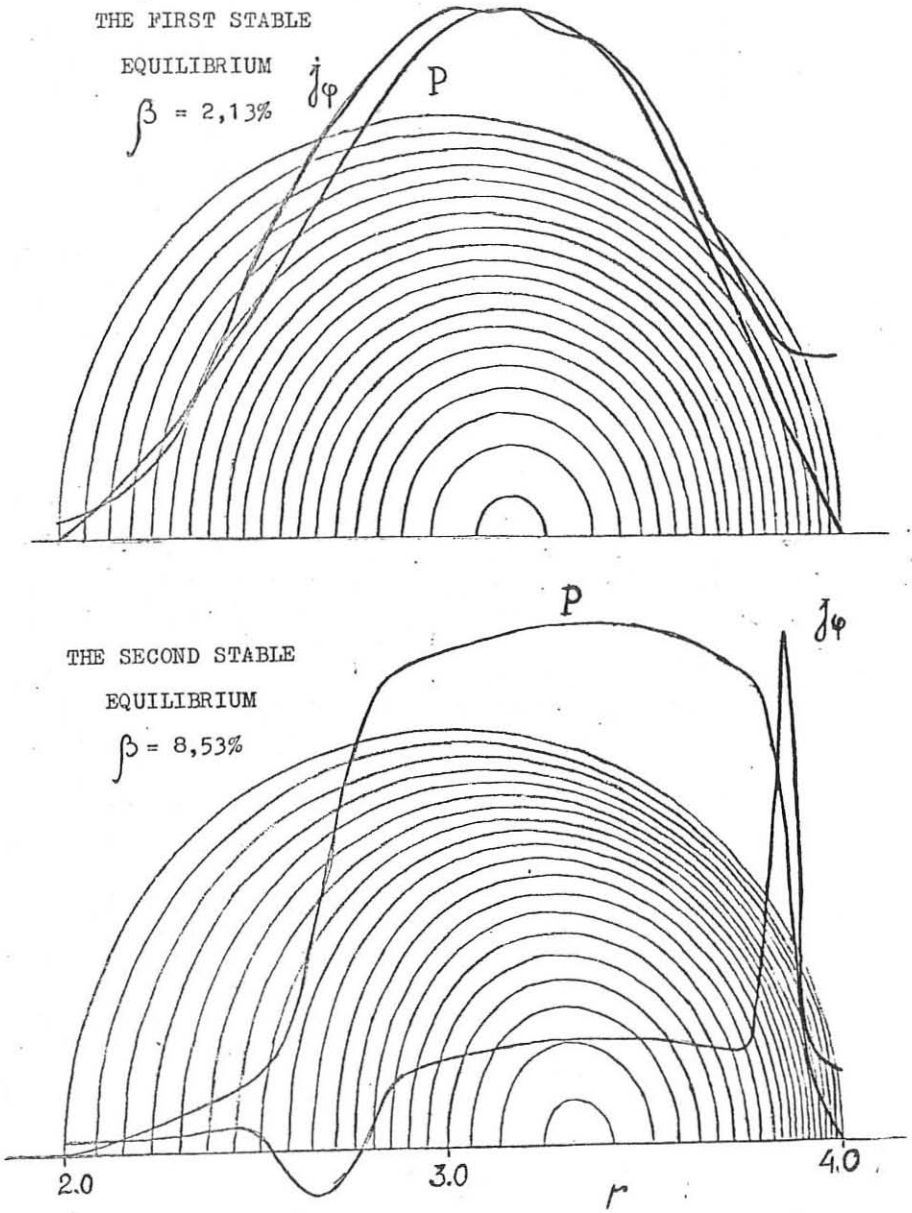


FIG.6. TWO MARGINALLY STABLE EQUILIBRIA IN THE TOKAMAK WITH CIRCULAR CROSS-SECTION

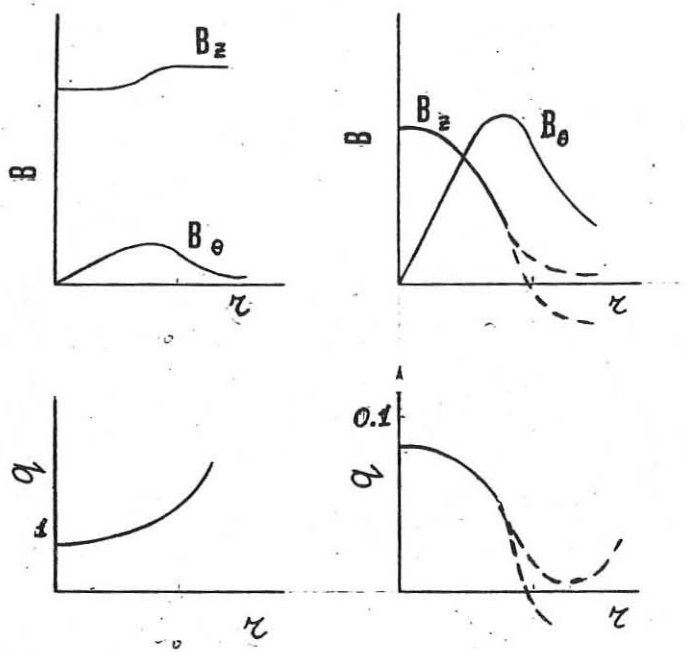


FIG.7. PROFILES B_ϕ, B_z AND q IN A TOKAMAK (on the left) AND IN THE STABILIZED PINCH (on the right)

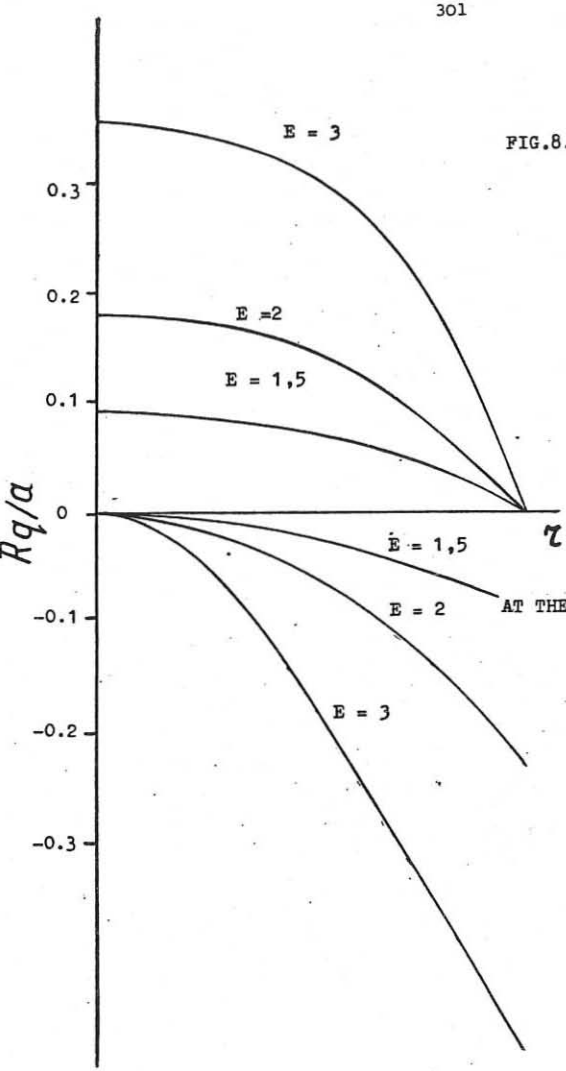


FIG.8. EFFECT OF THE EXTERNAL LONGITUDINAL FIELD, B_0, ON THE PROFILE $q(\tau)$ IN THE 1-2 HELICAL PINCH, WITH ZERO POLOIDAL CURRENT ($\beta_J \approx 1$)

E is the ratio of cross-section semi-axes on the edge

The equivalent aspect ratio R /a =10, number of periods N=9,

AT THE BOTTOM: External longitudinal field $B_0=0$

ON TOP: B_0 is chosen out of the condition, $q=0$, on the edge

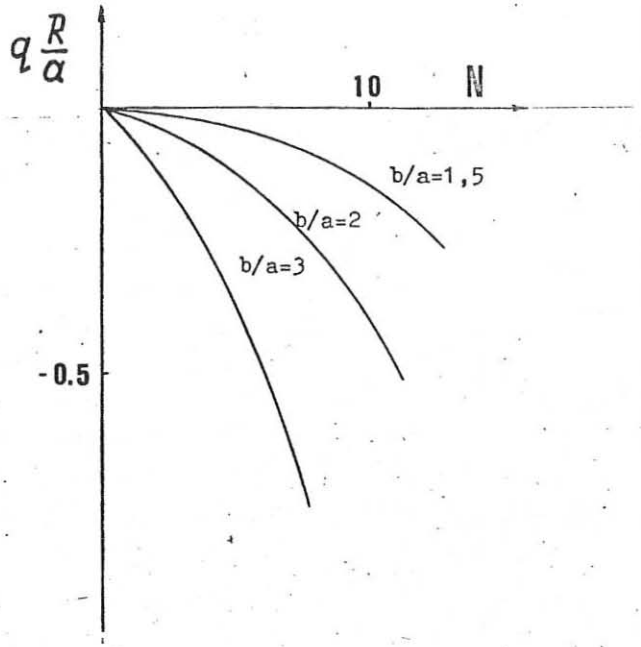


FIG.9. ROTATIONAL TRANSFORM ON THE EDGE OF A PLASMA COLUMN WITH ROTATING ELLIPTIC CROSS-SECTION (zero azimuthal current, $(\beta_J \simeq 1)$. Equivalent R/a=10

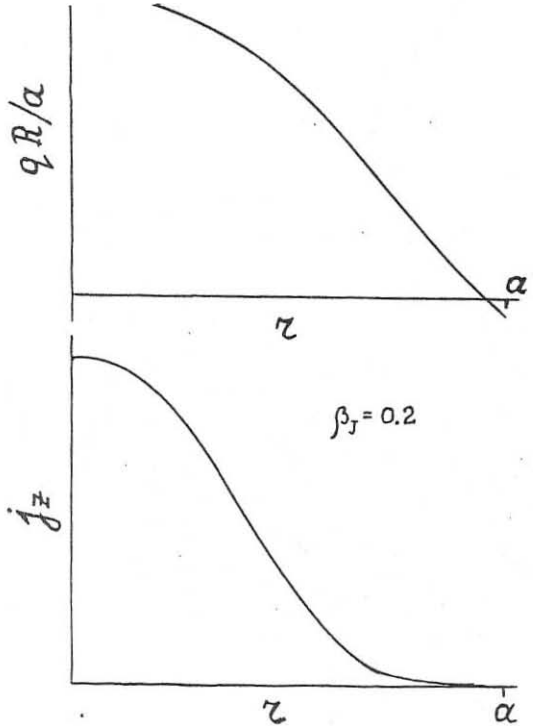


FIG.10. 1-2 STABILIZED HELICAL PINCH; STATIONARY STATE

σ = const, r<a ;

σ = 0, r>a.

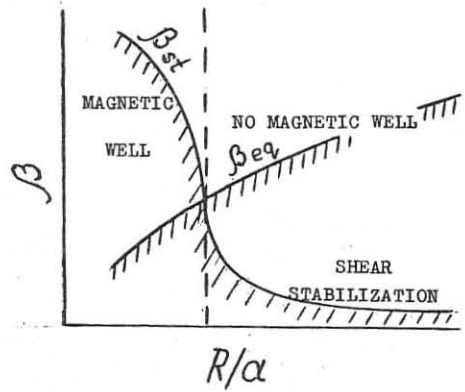


FIG.11. EQUILIBRIUM AND STABILITY DIAGRAMM FOR ℓ - 2 STELLARATOR

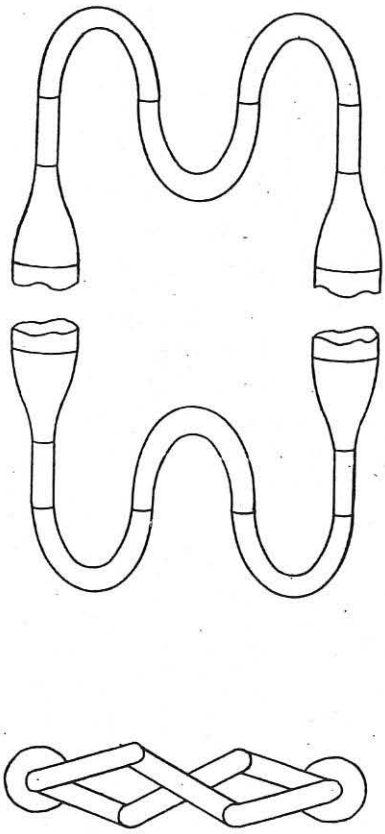


FIG.12. SPACE AXIS STELLARATOR
WITH RECTILINEAR SECTIONS

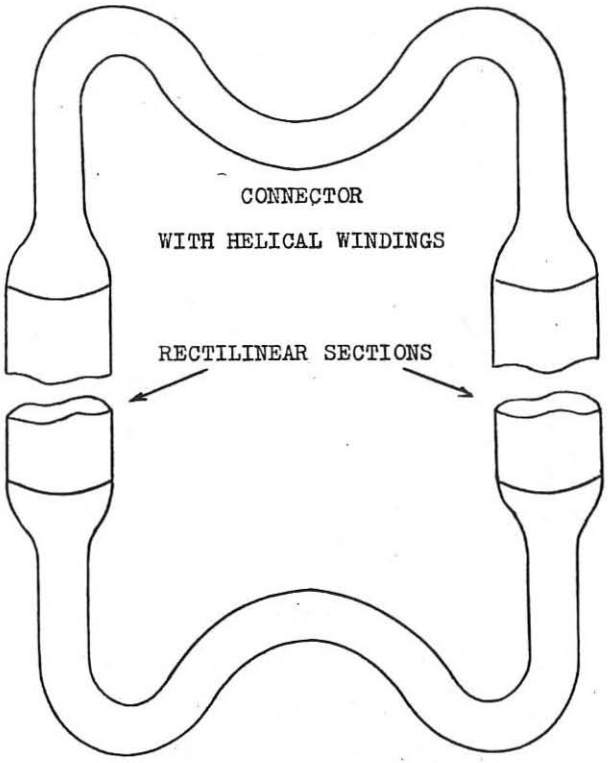


FIG.13. PLANAR AXIS STELLARATOR
WITH RECTILINEAR SECTIONS

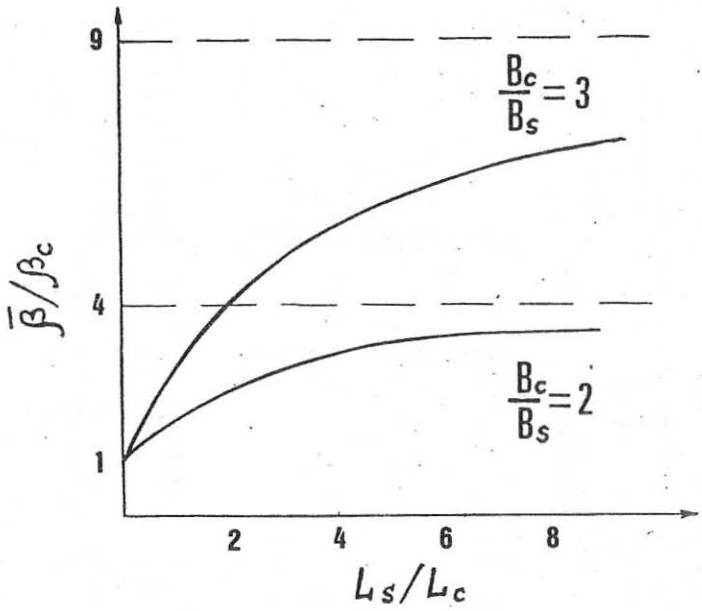


FIG.14. INCREASE IN $\bar{\beta}$ AVERAGED ALONG THE TRAP RESPECTIVE TO β_c IN THE CONNECTOR, VS. THE RATIO OF THE RECTILINEAR SECTION LENGTH, L_s, TO THE CONNECTOR LENGTH L_c

JFT-2 HEATING EXPERIMENTS

JFT-2 Group presented by N. Suzuki

Japan Atomic Energy Research Institute, Tokai, Naka, Ibaraki, Japan

Abstract

Additional heating experiments carried out on JFT-2 tokamak are summarized. NBI heating (2 MW) produced a high β plasma of the volume average β, $\langle\beta\rangle \simeq 3\%$ at $\bar{n}_e \simeq 10^{14}$ cm^{-3}. ICRF heating (0.5 MW) in a two ion hybrid regime showed a high efficient ion heating of $4.5\text{-}6.0 \times 10^{13}$ eV·cm^{-3}/kW at $\bar{n}_e \simeq 3 \times 10^{13}$ cm^{-3}. LHRF heating (0.3 MW) showed a bulk ion heating of $2\text{-}3 \times 10^{13}$ eV·cm^{-3}/kW at $\bar{n}_e \simeq 2 \times 10^{13}$ cm^{-3}, an electron heating of 1×10^{13} eV·cm^{-3}/kW at $\bar{n}_e \simeq 1 \times 10^{13}$ cm^{-3} and a rf current drive of 20 kA at $\bar{n}_e \simeq 5 \times 10^{12}$ cm^{-3}. ECH (0.2 MW) confirmed a good electron heating of 7 eV/kW for an X-mode and 5 eV/kW for an O-mode at $\bar{n}_e = 7 \times 10^{12}$ cm^{-3}, and also showed the reduction of the breakdown voltage down to 12 V.

1. Introduction

The additional heating methods, NBI,[1)2)3)] ICRF,[4)] LHRF[1)5)6)] and ECH[7)8)] have been applied to JFT-2 tokamak and each heating capability was investigated. Adding to the heating experiment, other important researches which will improve the tokamak were done on obtaining the high-β plasma, driving the plasma current by rf and saving the volt second during the current build-up phase. In this paper, the major results of these studies are summarized.

JFT-2 is a shell-less tokamak with a feedback control system of

plasma position. Machine parameters are: R = 90 cm, a ≤ 28 cm, B ≤ 1.6 T and time constant of control vertical field $\tau_r \simeq 5$ ms. Plasma parameters with joule heating are $I_p \leq 170$ kA, $\bar{n}_e \leq 6 \times 10^{13}$ cm^{-3}, duration time $\tau_d \leq 200$ ms, $T_{eo} = 0.5$–1.0 keV, $T_{io} = 0.25$–0.5 keV, $V_L \simeq 1.0$–2.5 V and $Z_{eff} = 1$–2. Low current discharge cleaning and titanium coating are employed to reduce both light and heavy impurities.

Diagnostics was described in ref.(1) and some diagnostics such as a mass-sensitive cx analyser, a neutron counter and a multi PIN array are added. The arrangement of diagnostic instruments and heating apparatus is shown in Fig. 1.

2. NBI Heating

In order to study a high-β tokamak plasma, a NBI system was installed to JFT-2 in March 1980. The system consists of a coinjector and a counter injector with the injection angle of 40° to the plasma axis. Each beam line has an ion source of 40kV/65A and the maximum power of each neutral beam measured at the injection port is 1 MW. An almost circular plasma is investigated under a wide range of parameters, i.e. NBI of 0.8–2.0 MW, R/a = 3.5–4.75, $q_a = 2.0$–4.2, $n_{eo} = (2.5$–$16.0) \times 10^{13}$ cm^{-3} and $B_T = 0.95$–1.4 T.

Typical time behaviors of plasma characteristics are shown in Fig. 2. After starting NBI, loop voltage decreases, ion and electron temperatures increase and also plasma density increases because of an intense gas puffing (Fig. 2-c). The radiation loss power is mainly due to oxygen and is about 20% of the total input power during NBI heating.

The observed maximum β at ∿2 MW experiment is as follows: the peak β-value $\beta_o = 8\%$ due to the thermal component and 11% including the beam

component and the volume average β-value is 3.0% due to the thermal component and 3.3% including the beam component. The calculated β_p from the average β values is 2.6 due to the thermal component and 3.2 including the beam component but the β_p from magnetic measurements, i.e. poloidal field and vertical field measurement, is 1.8-2.3. If we consider uncertainties of the temperature and the density profile, especially the ion density, the calculated β_p from the density and temperature should be 2.0-2.7 due to the thermal component.

In Fig. 3, observed β-values are compared with the critical β-values obtained from the ballooning analysis.[10] In the analysis, the critical values are obtained with an optimized pressure profile and with a reasonable current profile. The observed total β values including the beam component are higher than the critical β values from the analysis, e.g. the maximum β_o and the maximum $\langle\beta\rangle$ are 1.7 and 1.3 times higher than those theoretical values, respectively. The thermal β values, however, are similar to the theoretical values. The experimental results shown in Fig. 3 were obtained with the injection power of 1.2-2.0 MW.(*) With increasing the power up to 1.8-2 MW, the obtainable β value does not strongly increase but a β limitation was not clearly found.

The observed plasma parameters are analyzed by using a tokamak code including NBI heating, neutral particle transport and sawtooth effect. The results suggest that the transport in the high-β plasma is about the same in a low-β plasma within a factor of 2, i.e. $\chi_e = 3\text{-}4 \times 10^{17}/n_e$ cm^2s^{-1}, $D_p \simeq 0.3\chi_e$ and $\chi_i = 3\text{-}4\chi_{neo}$ where n_e is plasma density in cm^{-3} and χ_{neo} the neoclassical value.(**)

---

*) In the previous papers[1)-3)], the injection power was not correct, i.e. 1-1.5 MW instead of 0.8-1.2-MW. **) These values are larger than the provious values shown in refs. (1) and (2).

The density clamping is observed as shown in Fig. 4. In order to clarify this phenomenon, the particle confinement time τ_p and the recycling rate R are investigated by measuring the total particle loss flux as shown in Fig. 4.[11] The particle confinement time is not strongly affected by the injection but the trapping coefficient (1-R) is increased by a factor of 2 with the injection. This reduction in the recycling rate can explain the observed density clamping.

Impurities are also investigated with the high power heating. In usual cases, the metal impurities such as Ti, Fe and Mo increase with a high power heating, however, arcing is not observed on a limiter surface. In a helium operation, the increments of the metal impurities are larger than those in a hydrogen operation. These results suggest that the ion sputtering is also the dominant metal impurity source as in an ohmic plasma. With the intense gas puffing, the increment of the edge temperature is suppressed and thus impurity production is reduced even with NBI.

3. ICRF Heating

ICRF heating experiment at JAERI has restarted with 0.5MW/18-20MH_z after the successful ICRF experiment with a high heating efficiency.[12)13)] The objective of the present experiment in JFT-2 is to clarify ICRF heating mechanisms by using both inside and outside antennas. In this paper, results with the inside antenna are summarized.

In the two-ion hybrid regime, the minority to majority ion density ratio is a key factor in the fast wave damping and the associated heating especially for the higher field incidence with the inside antenna. In the experiment, the proton-to-deuteron density ratio n_H/n_D determined spectroscopically was varied from the very dilute minority case of $n_H/n_D \lesssim 3\%$ to the mode conversion dominant case of $n_H/n_D \sim 30\%$, and the majority deuteron

and minority proton energy spectra were investigated by using a mass sensitive neutral energy analyser as shown in Fig.5.

For $n_H/n_D \lesssim 3\%$, prominent non-Maxwellian spectrum appears for hydrogen and it weakens with increasing n_H/n_D and is almost in accordance with that of deuteron for $n_H/n_D \sim 20\%$. The local heating power to protons is derived from fitting the proton energy spectra to the Fokker-Planck theory.[16] The result shows that the fundamental proton damping has the maximum at $n_H/n_D \sim 10\%$. On the contrary, the increases of the deuteron temperture were almost constant at least up to $n_H/n_D \sim 20\%$.

Using the measured ion and electron temperatures, the rf power densities depositted to deuterons and protons are calculated from a local power balance equation including the collisional power transfer between each species and the neoclassical thermal conduction loss. Figure 6-a shows the result. In spite of relatively large error bars, it is clearly demonstrated that the wave damping changes with changing n_H/n_D in this experiment with the high field incidence. Second harmonic deuteron heating is dominat for the dilute minority case of $n_H/n_D \lesssim 3\%$ and decreases gradually with increasing n_H/n_D. Fundamental proton heating efficiency has the maximum value at $n_H/n_D \sim 10\%$.

For $n_H/n_D \gtrsim 20\%$, the rf power to ions decreases and the electron heating is observed. For example, we observed comparable electron and ion heating in the plasma core, i.e. $\Delta T_e \sim 200$ eV, $\Delta T_i \sim 300$ eV with $\bar{n}_e \sim 3\times10^{13}$ cm^{-3}, $n_H/n_D \sim 30$ %, B_T =1.3 T and net RF power P_{net}= 260 kW.

Figure 5 shows an example of the deuterium and hydrogen energy spectra during the heating for $n_H/n_D \sim 10$ % and net RF power of 260 kW. In addition to energetic protons, significant high energy components appear in the deuteron energy spectrum. This indicates that the second harmonic deuteron heating actually occurs in this experiment with the higher field incidence, which was not observed in other experiments with the lower

field incidence.[14] Theory including the ion Bernstein wave suggests such difference of the wave absorption between the higher and lower field incidence.[15]

The toroidal field does not change the wave damping mechanism but decides the spatial deposition profile of the rf power. Figure 6-b shows the central ion heating efficiency as a function of the troidal magnetic field B_T and the position of a proton cyclotron resonance layer R_H for $n_H/n_D \sim 10$ %. The sharp and asymmetric curve with respect to the plasma center can be explained by the localized wave absorption between the hybrid and cyclotron resonance layers. The effective width of the rf power deposition is estimated to be 9 cm for the case of B_T =1.2 T by using the 1-D code assuming a rectangular power deposition profile, which is comparable to a distance of 7 cm between the two-ion hybrid and cyclotron resonance layers. The abrupt drop of the heating efficiency below 1.15 T and above 1.3T is explained by the decrease of rf power density due to the deviation of the wave damping zone from the plasma center. This result confirms that the rf power deposits to the plasma in the region between the two-ion hybrid and cyclotron resonance layers.

4. LHRF Heating

The 750 MHz rf system is composed of four 80 kW klystron and a phased array of four wave guides. Width of each waveguide is 33 mm and 15 mm for ion and electron heatings, respectively. A net rf power of more than 200 kW was injected to the plasma with a good coupling efficiency of 70 to 90%. An optimized launcher for ion heating has a Ti-coated surface and the irradiated rf power has a sharp N_z spectrum, where N_z is parallel refractive index (peak N_z= 5, half width ΔN_z= 3 at a phase difference of adjacent wave guides $\Delta\phi$ = 180°).

Results of the ion heating experiment are as follows. Ion tempera-

tures obtained from parallel and perpendicular charge exchange and with Dopplar broadning (Ti XIV, O VII, C V) show an increase of ion temperature all over the radius. At centre the increase of T_{io} from 400 eV to 700 eV at $\bar{n}_e = 1.9 \times 10^{13}$ cm^{-3} is observed. Ion heating rate is 2-3 $\times$ 10^{13} eV·cm^{-3} /kW at $\bar{n}_e = (1\text{-}3) \times 10^{13}$ cm^{-3} as shown in Fig. 7. $\Delta\phi$ dependence of ion heating rate is well explained with the depositted power simply calculated from the Brambilla's theory. This implies the accessibility condition and the N_z spectrum do take an important role in the ion heating for LHRF. Density dependence of ion heating rate indicates that the observed low density limit is consistent with the linear theory, but the high heating rate at a higher density can not be explained without some non-linear effects. However this wide range of density window is a favorable feature for future application.

In these experiments I_p, V_L and $\bar{n}_e$ remain almost constant during the rf pulse and T_{e0} increases a little, the increment of which may not be attributed to the direct electron heating but to the change of electron-ion energy transfer.

Power balance consideration assuming the neoclassical transport shows that the depositted power to ions is about 110 kW at P_{net} = 200 kW, so the ion heating efficiency is about 50%. The residual power should be lost near the boundary. For example, two types of high energy ions were observed on the cx spectrum. One with a reasonable long decay time of 2-3 ms suggests the high energy ion production near the plasma center but another with a short decay time of 0.2 ms suggests the high energy ion production near the plasma edge. It is also abserved that the boundary electron temperature affects the ion heating efficiency. The rather high heating efficiency shown in Fig. 7 obtained with a rather high edge temperature. These results suggest that the residual power is

lost rapidly via the parametric decay instability and a suppression of the instability leads the higher heating efficiency.

In the electron heating experiment, narrow width launcher (15 mm) was used to obtain the larger N_z spectrum. Experimental parameters are; deutrium plasma, $\bar{n}_e = 1.0 \times 10^{13}$ cm^{-3}, $P_{RF} = 200$ kW, $\Delta\phi = 180°$, peak $N_z = 12$ and half width $\Delta N_z = 7$. In this condition, the LH wave has not the turning point in a plasma, that is, $\omega_o/\omega_{LH}(0) > 1.7$ (ω_o; pump frequency and $\omega_{LH}(0)$; lower hybrid frequency at the plasma centre). Measured increase of electron temperature is 200 eV from laser scattering, while soft x-ray spectrum suggests the production of energetic electrons. The lower hybrid wave couples with energetic electrons as expected from the Landau damping.

Experimental conditions for the rf current drive are; $B_T = 1.0$ T, $I_p = 60$-70 kA, $\bar{n}_e = 0.4$-0.6×10^{13} cm^{-3}, $T_{e0} = 0.5$-0.7 keV, $Z_{eff} = 1.5$-2 and deutrium plasma. In this condition ($\omega_o/\omega_{LH}(0) > 2$), collisions become less and the electron current can be driven by the LH wave propagating unidirectionally via the electron Landau damping. RF power of 150 kW was launched into the plasma at $\Delta\phi = 90°$, here the N_z spectrum has a gentle peak near $N_z = 5$ with the half width of $\Delta N_z = 7$. Typical time behaviour of plasma parameters are shown in Fig. 8 together with no rf case (dotted line). The loop voltage V_L falls smoothly and reaches a quasi-steady state 10 ms after the rf turned on. Central electron temperatures are also shown in Fig. 8. Soft x-ray spectrum was measured with an intrinsic Ge detector covering a wide energy range up to 200 keV. At the no rf phase s.x. spectrum showed a bi-Maxwellian feature indicating the existance of runaway electrons. During the rf pulse, however, the runaway electrons were suppressed and the s.x. emission in the energy range of 3-15 keV was enhanced remarkably (Fig. 9). In this phase,

central electron temperatures decreased a little rather than increased and the second harmonic electron cycrotron radiation decreased remarkably. These results confirm that the relative drop of loop voltage $\Delta V_L/V_L$ during the rf pulse dose not come from excitation of runaway electrons but from the rf-induced current. The rf induced current of 20 kA can be estimated from the relation of $I_{RF} = I_p \cdot \Delta V_L/V_L$ and is given as 20kA/150kW in this experiment.

Soft x-ray spectrum during the rf pulse was analyzed and is shown in Fig. 9. In this figure, solid circles indicate the measured points and solid line shows calculated s.x. spectrum from the electron distribution function which satisfies a coupled quasi-linear Fokker-Planck equation[9] (dotted line). The distribution function thus obtained shows the quasi-linear plateau in the energy range of 3-18 keV, which corresponds to N_z = 8.5-3.7. This range of N_z spectrum agrees well with calculated one from the Brambilla's theory. The modified distribution function gives the equivalent rf-driven current density of 15 A/cm^2 at the plasma centre, while the average current density is 10 A/cm^2 from the above value of 20 kA. These results show the LH could produce the current of broad profile.

5. ECR Heating (Japan-US collaboration program)

A high power rf source is a Varian 28 GHz gyrotron with 200 kW capability for up to 40 ms. RF power was fed into the plasma through three types of launch system :

1) Ordinary mode (E//B) launch system with 8 conical horn antennas located at the low field side. The angle between the horn axis and the plasma axis is at $\theta_z = \pm 80°$, then the wave propagates nearly perpen-

dicularly to B_T (n_z = ±0.17).

2) Extraordinary mode ($E \perp B$) launch system with slotted array antenna located at the high field side. The wave vector is steerable in the horizontal phane over a range of ±45° (n_z = 0-±0.86).

3) TE_{02} mode launch system with open-ended circular waveguide at the top of the vacuum chamber. The TE_{02} output of the gyrotron is transferred directly to the plasma.

Base plasma parameters in the ECH experiment are as follows; B_T = 0.6-1.2 T, $\bar{n}_e$ = 5-15 × 10^{12} cm^{-3}, I_p = 70-75 kA, T_{e0} = 500-700 eV, V_L = 1.0-1.6 V, $Z_{eff} \leq 2.0$ and a = 25 cm. Net rf power of 45-110 kW was applied for 14-20 ms typically.

Time evolution of plasma parameters with and without rf power is shown in Fig. 10 for X-mode heating at B_T = 1.0 T, θ_z = 48° and P_{RF} = 85 kW. Central electron temperature T_{e0} measured with laser scattering and soft x-ray spectrum increased from 600 eV to 1200 eV and one turn voltage V_L dropped from 1.4 to 1.1 V. The line averaged density $\bar{n}_e$ decreased from 7 × 10^{12} cm^{-3} to 5 × 10^{12} cm^{-3} during rf pulse. These features of plasma parameters in X-mode heating are almost the same as in O-mode heating.

RF power dependence of ΔT_{e0}, ΔV_L and $\Delta \bar{n}_e$ are shown in Fig. 11 for $\bar{n}_e$ = 7 × 10^{12} cm^{-3}. The increase of T_{e0} and the drop of ΔV_L are almost linear with the rf power up to 110 kW. Heating rates obtained are 7.0 eV/kW for X-mode; 4.7 eV/kW for O-mode and 1.5 eV/kW for TE_{02} mode. These results are consistent with the expected features from calculations of wave damping for O-mode and X-mode heating. The density drop during rf heating may be resulted from the edge heating as that observed in other heating experiments.

Pre-ionization with ECH was investigated and satisfactory reduction

of the breakdown voltage was obtained.[17] Typical data with and without ECH pre-ionization are shown in Fig. 12. The breakdown voltage is reduced from 25 V to 12 V and about 30% of the transformer flux is saved in the first 5 ms. Plasma current and electron density is built up smoothly. Electron density of initial plasma produced by ECH is about 8×10^{11} cm^{-3}. Necessary conditions for effective pre-ionization have been investigated and following parameters were found out; $P_{RF} \geq 30kW$, pulse length $T_p \geq 3ms$ and the position of the resonance layer $X_r \leq a/2$.

6. Summary

Each heating method was compared with others from various viewpoints, as shown in Table 1.

Ion heating rates observed in JFT-2 experiments are $4.5\text{-}6 \times 10^{13}$ $eV \cdot cm^{-3}/kW$ for ICRF, $2\text{-}3 \times 10^{13}$ $eV \cdot cm^{-3}/kW$ for LHRF and $2\text{-}3 \times 10^{13}$ $eV \cdot cm^{-3}/kW$ for NBI. However, ion heating mechanisms of rf heatings are not well established in comparison with NBI.

Electron heatings are demonstrated in every method. Among them ECRH is most efficient as expected. Other rf's may be effective at optimized conditions. Of course, ECRH is required to develop a high power generator.

Accompanyng problems with high power heating are effect on the transport and the impurity problem. Density clamping is observed in all cases, although measurements of particle flux to the wall and limiter indicates that loss flux increases only a little. The density clamping can be well explained by the increase of trapping coefficient on the wall resulted from the edge temperature increase.

Metal impurity release by the ion sputtering was successfully

reduced to an acceptable level with a Ti-gettering and an intense gas puffing, especially in NBI. However, it seems more serious in much higher power level and might not depend on a heating method.

Another subject investigated is the current sustaining. One possible way was shown in the LHRF heating. In this experiment, superthermal electrons play a key role for efficient current drive.

Finally, schedules of additional heatings in JAERI are as follows; hybrid heating of NBI (2 MW) and ICRF (1 MW) and then 0.6-0.8 MW LHRF heating experiments will be carried out in JFT-2. Then 4 MW ICRF will be applied to JFT-2M which will start in 1982 after the shutdown of JFT-2. Moreover, 7.2 MW NBI experiment is just beginning in Doublet-III. For JT-60, 20 MW NBI and 10 MW LHRF are now being prepared.

7. Acknowledgments

This paper represents the all additional heating experiments on JFT-2. Key persons for individual heating method are; S. Yamamoto and Y. Shimomura for NBI, H. Kimura for ICRF, T. Imai and T. Yamamoto for LHRF and T. Yamamoto and C.P. Moeller of GA for ECRH. The anthors are grateful to the JFT-2 and NBI operation groups for their reliable operations and to the members of Japan-US collaboration for the ECH experiment. We also appreciate Drs. S. Mori, Y. Iso, Y. Obata, M. Tanaka and Y. Tanak for their continuous encouragements.

References

1) Suzuki N., Imai T., Fujisawa N., et al., IAEA-CN-38/t-2-3 (1980).

2) Shimomura Y., Suzuki N., Naeno M., et al., Japan Atomic Energy Research Institute Report JAERI-M 9065 (1980).

3) Yamamoto S., Maeno N., Suzuki N., et al., "Magnetohydrodynamic Activity in the JFT-2 Tokamak with High Power Neutral Beam Injection Heating", to be published in Nuclear Fusion.

4) Kimura H., et al., "First Results on the JFT-2 ICRF Heating Experiment (Higher Field Side Excitation)", to be published in Japan Atomic Energy Research Institute Report.

5) Imai T., Yamamoto T., Suzuki N., et al., "LHRF Heating Experiment in JFT-2", Proceedings of the 4th Topical Conference on RF-Plasma Heating, Austin, Texas, Feb. 1981.

6) Yamamoto T., Imai T., Shimada M., et al., Phys. Rev. Lett. 44 (1980) 716.

7) La Haye R.J., Moeller C.P., Funahashi A., et al., "Electron Cyclotron Resonant Heating with an Ordinary Mode Antenna in the JFT-2 Tokamak", General Atomic Report GA-A 16109, October 1980, Proceedings of the 4th Topical Conference on Radio Frequency Plasma Heating, Texas, (1981) D4-1 and submitted to Nuclear Fusion.

8) Moeller C.P., Yamamoto T., et al., "Electron Cyclotron Heating Experiments on the JFT-2 Tokamak Using an Inside Launch Antenna", to be published.

9) Karney C.F.F. and Fisch N.J., Phys. Fluids 22 (1979) 1817.

10) Azumi M., Tsunematsu T., Itoh K., et al., IAEA-CN-38/K-1-1 (1980).

11) Matsumoto H., Kimura H., Sengoku S., et al., "Particle Confinement during High Power Neutral Beam Injection in JFT-2 Tokamak", submitted to Nuclear Fusion.

12) Kimura H., Odajima K., Iizuka S., et al., IAEA-CN-38/D-5-2.

13) Iizuka S., Odajima K., Kimura H., et al., Phys. Rev. Lett. 45 (1980) 1256.

14) Hosea J., Boyd D., Bretz N., et al., IAEA-CN-38/D-5-1.

15) Colestock P.L., Davis S.L., Hosea J.C., Princeton Plasma Physics Laboratory Report PPPL-1754 (1980).

16) Stix T.H., Nucl. Fusion 15 (1975) 737.

17) Matsuzaki Y., private communication.

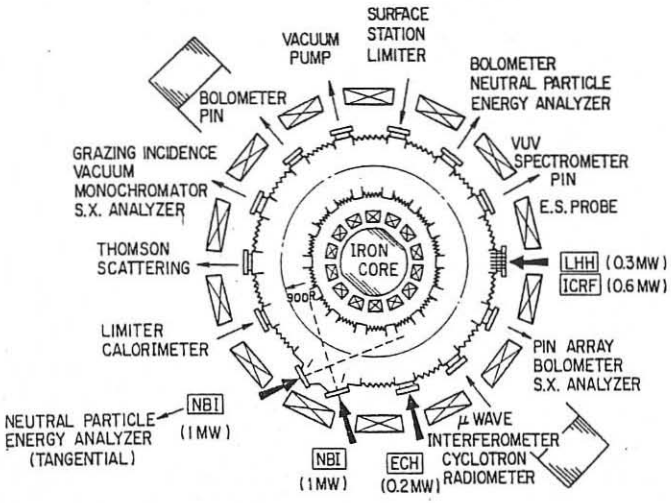


Fig. 1 JFT-2 tokamak. Top view with diagnostic instruments and heating apparatus.

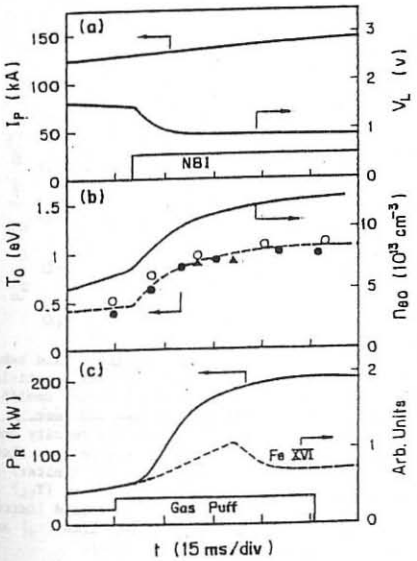


Fig. 2 Time behaviours of plasma current I_p, loop voltage V_L, central density n_{e0}, ion temperature, electron temperature, radiation loss power P_R, line intensity of Fe XVI 361.0 Å and gas influx. B_T=1.1 T and a_p=21 cm. The plasma radius is defined by the rail limiters. Injection power is 1.2-1.5 MW.

- ● : Ion temperature measured by a cx analyser.
- ▲ : Ion temperature measured by doppler broadening of titanium line emitted from a central part of the plasma column.
- ○ : Electron temperature measured by Thomson scattering and a soft x-ray energy analysis.

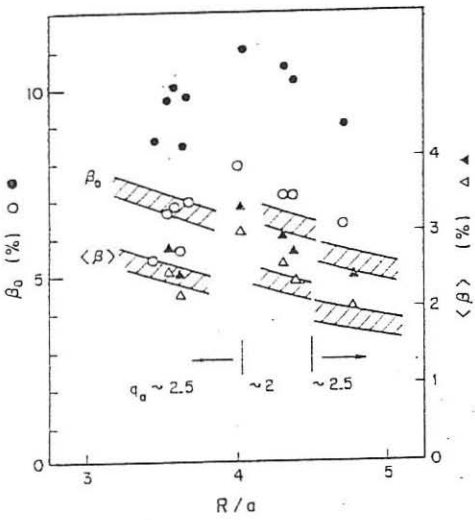


Fig. 3 Critical β values obtained from the ballooning analysis and observed β values. R/a: aspect ratio, q_a: safety factor, β_0: peak β and <β>: average β. ○ △ due to thermal component and ● ▲ : including the beam component in experiment with power of 1.2-2 MW. ////// : critical peak β value from the analysis and ////// : critical average β value. The lower lines indicate the critical values for q_0=1 and the upper lines for q_0=0.9.

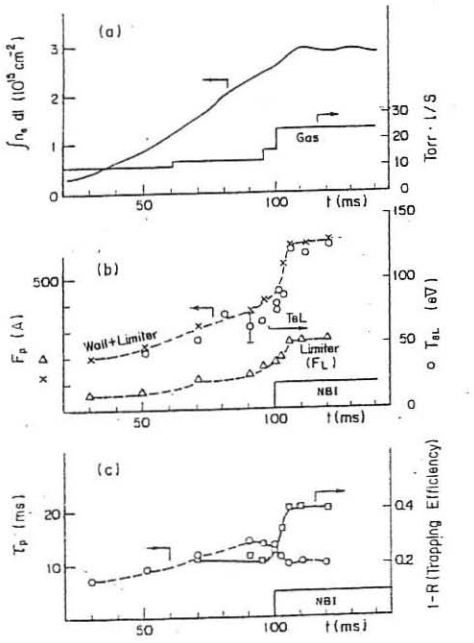


Fig. 4 Density clamping. Time behaviours of particle loss flux, particle confinement time and trapping coefficient. NBI starts from 100 msec. (a) Electron line average density and gas puffing rate. (b) Particle loss flux (△; limiter, ×; wall and limiter) and boundary electron temperature (T_{eL}) measured by a electrically biased limiter. (c) Particle confinement time (τ_p) and trapping coefficient (1-R).

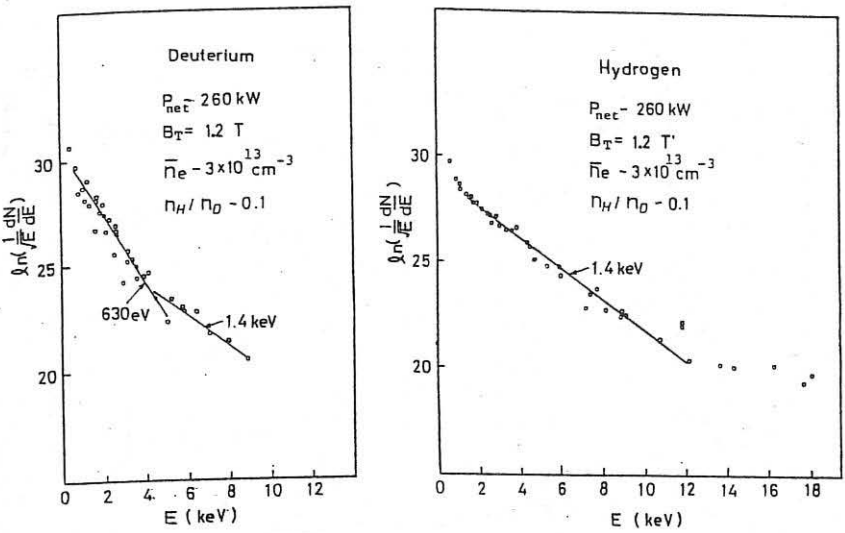


Fig. 5 (a) Deuterium and (b) hydrogen energy spectra during the heating of the higher field incidence measured with a mass-sensitive charge exchange neutral analyzer. Net rf power P_{net} = 260 kW, frequency f= 18MHz, B_T=1.2 T, $n_H/n_D \sim 0.1$, base elctron temperature $T_{eo} \sim 600$eV, ion temperature $T_{io} \sim 330$ eV, and electron density $\bar{n}_e \sim 3x10^{13}$ cm^{-3}.

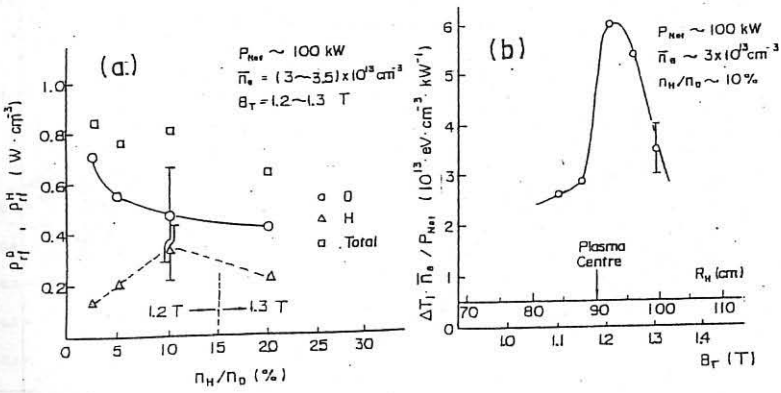


Fig. 6 (a) Heating power density to deuterons P_{rf}^D(○), protons P_{rf}^H(△), and total heating power density $P_{rf}^D + P_{rf}^H$(□) at the plasma center vs. n_H/n_D. They are derived from a local power balance equation, using measured ion and electron temperature and electron density.
(b) B_T-dependence of the central deuteron tempefature increase normalized by the rf net power and the average electron density. The proton-to-deuteron density ratio $n_H/n_D \sim 10\%$, frequency f= 18 MHz.

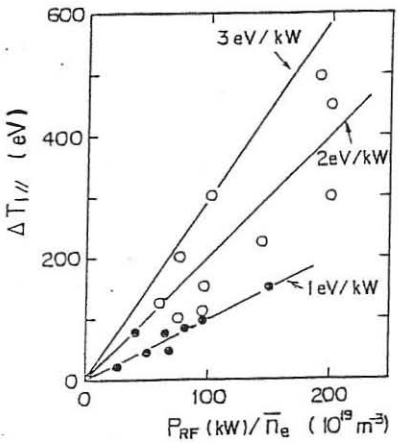


Fig. 7 Ion heating efficiency of LHRF heating. Increase of ion temperature ($\Delta T_{i\parallel}$) measured with parallel charge exchange as a function of rf input power normalized by averaged density ($P_{RF}/\bar{n}_e$). Open and closed circles correspond to 33 mm width launcher and 15 mm width launcher, respectively.

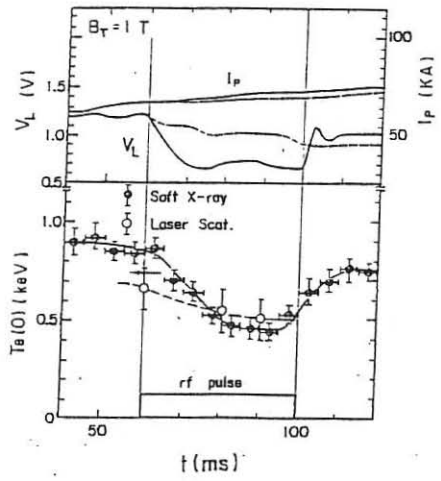


Fig. 8 Time behaviour of plasma parameters during current drive experiment. Plasma current (I_p), one turn loop voltage (V_L) and electron temperature measured by soft x-ray (●) and laser scattering (○). Solid and dotted lines correspond to with and without rf, respectively.

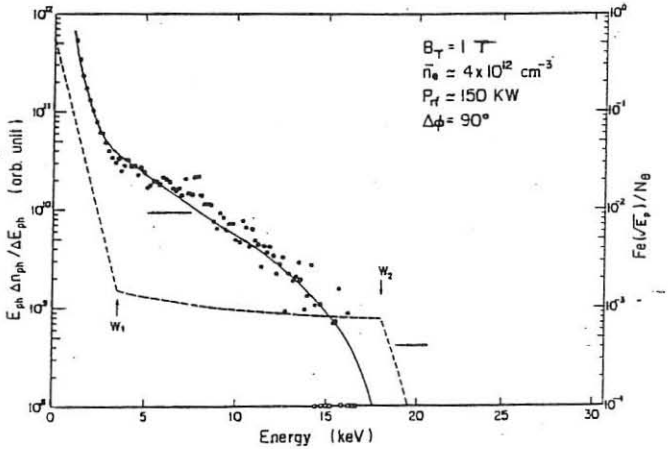


Fig. 9 Soft x-ray spectrum during rf pulse of the current drive experiment. Closed circles (●) correspond to the measured points. Calculated sx spectrum (solid line) and fitted electron distribution function (dotted line).

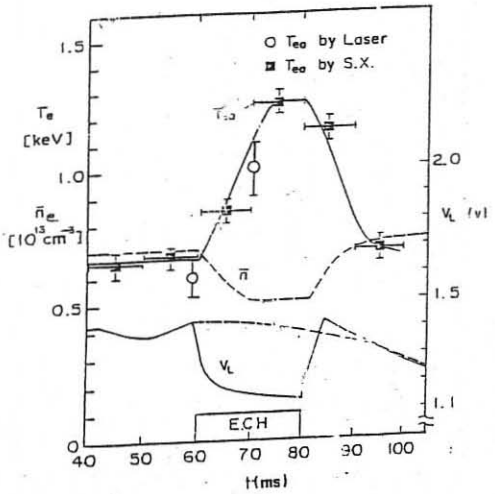


Fig. 10 Typical time evolution of plasma parameters for X-mode launching. B_T=1 T, I_p=70 kA, $\bar{n}_e$=7×10^{12} cm^{-3}, P_{RF}=85 kW, n_z=0.66.

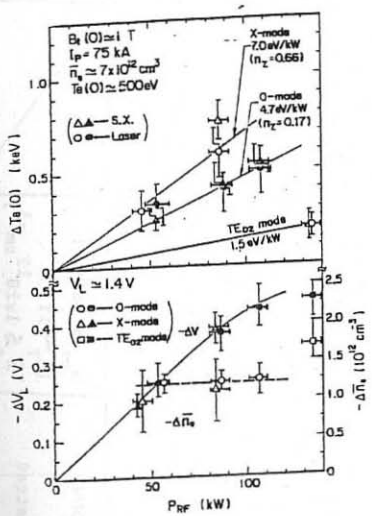


Fig. 11 RF power dependence of ΔT_{e0}, ΔV_L and $\Delta\bar{n}_e$. Heating rates are 7.0 eV/kW for X-mode, 4.7 eV/kW for O-mode and 1.5 eV/kW for TE_{02} mode, respectively. B_T=1 T, I_p=75 kA and $\bar{n}_e$=7×10^{12} cm^{-3}.

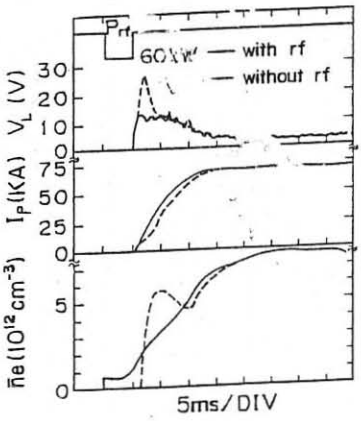


Fig. 12 Start-up phase of plasma with the ECH pre-ionization. Solid line with rf and broken line without rf. B_T=1 T, P_{RF}=60 kW and T_p=5 msec.

Table 1. JFT-2 Heating Experiment

	Max. Power/Net Power & Structure	Restrictions for Target Plasma	Ion Heating Rate $\Delta T_i \bar{n}_e / P_{in}$ ($\times 10^{13}$ eVcm^{-3}/kW)	Electron Heating Rate $\Delta T_e / P_{in}$ (eV/kW)	Impurity Radiation Loss P_R/P_{in} & Metal Increase	Comments
NBI	2MW/1.6MW (40kVx65Ax2) & Co+Counter	$\bar{n}_e > 3\times10^{13}$ cm^{-3}	2-3 at $\bar{n}_e = 6\times10^{13}$ cm^{-3}	0.5-1 at $\bar{n}_e = 6\times10^{13}$ cm^{-3}	$P_R/P_{in} < 0.3$ & $\Delta I/I = 2$-3	Increased density limit (Murakami factor of 9) Clear heating mechanism Intense gas puffing
ICRF	0.5MW/0.35MW (18-20MHz) & Inside (or outside) all metal antenna	Two ion hybrid layer and ω_{ci} (n_H/n_D & B_T)	4.5-6 at $\bar{n}_e = 3\times10^{13}$ cm^{-3}	~ 1 at $\bar{n}_e = 3\times10^{13}$ cm^{-3}	$P_R/P_{in} \sim 0.2$ & $\Delta I/I \sim 5$	Electrical noise Ti-gettering to Antenna Breakdown of Transmission line
LHRF	0.32MW/0.25MW (760 MHz) & 4 grill launcher	Accessibility & turning point ($\bar{n}_e$ & B_T)	2-3 at $\bar{n}_e = 2\times10^{13}$ cm^{-3}	~ 1 at $\bar{n}_e = 1\times10^{13}$ cm^{-3}	$P_R/P_{in} < 0.25$ & $\Delta I/I = 2$-3	Current drive Launcher aging
ECH	0.2MW/0.15MW (28 GHz) & Horn & slotted antenna	ω_{ce} & cut-off ($B_T \sim 1$T & $\bar{n}_e \lesssim 1\times10^{13}$ cm^{-3})		7 with X-mode & 4.7 with O-mode at $\bar{n}_e = 7\times10^{12}$ cm^{-3}	$P_R/P_{in} < 0.2$ & $\Delta I/I \sim 0$	Reduced breakdown voltage High frequency ?

TOKAMAK RESEARCH IN THE SOVIET UNION

V.S.Strelkov
I.V.Kurchatov Institute of Atomic Energy,
Moscow, USSR

Experimental research and engineering development carried out in the Soviet Union according to the Tokamak Program have a goal to provide the necessary basis in science and technology for the fusion reactor design. Construction of the T-15 tokamak is considered as a near-term problem, then the machines of the next generation - INTOR or TFR (Test Fusion Reactor) - are considered to be built (Fig.1).

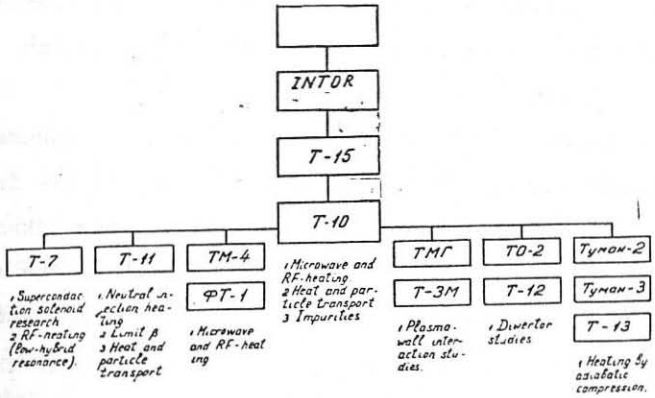


Fig.1 Tokamak - program development

Tokamak research is carried out at three Institutes: mainly it is concentrated at the Kurchatov Institute of Atomic Energy, where there are eight functioning tokamaks, and T-15 is under construction now. The following studies have been intensively developed in the last few years: different methods of additional plasma heating, heat and particle transport, impurity control.

Studies in the additional plasma heating by adiabatic compression as well as microwave and RF-heating are carried out at the Ioffe Physical - Technical Institute in Leningrad.

Heating by the Alfven waves is studied in the tokamaks of relatively small size at the Physical Technical Institute in Sukhumi; the possibility of maintaining the stationary current in a torus by RF-fields is also studied there.

A successful operation of T-7 - the first tokamak with a superconducting winding of the toroidal field - is an important advanced step in technology. At this tokamak the necessary experience to design T-15, where the superconductors will be also used, has been obtained. Another important engineering solution is a gyrotron set for the microwave heating in T-10 which is the T-15 full-scale model in many parameters and 1/6 in the number of gyrotrons.

Methods of additional plasma heating

Studies in additional plasma heating are carried out in three directions: neutral injection, different methods of RF and microwave heating and adiabatic compression.

Neutral injection is the most advanced method now-

days. The injection power exceeds the power of Ohmic heating in many experiments. Regimes with the values of β close to the theoretical limit ($\beta_{experim.}$ = = 2.5%) have been obtained in T-11 with the additional heating by neutrals. The limit β is expected to be realized due to increase in the power of injection.

The parameters of an injector are easely extrapolated up to those of a reactor. But some difficulties arise because of a decrease in the injector efficiency with an increase in the beam energy besides the technological problems of providing the injector operation in a zone of high activity, near the reactor. RF and microwave heating lack these deficiencies. The efficiency of generators is not changed when one applies them to the reactor parameters, the set of generators can be displaced beyond the shield as the RF-energy can be introduced through the labyrinths in it.

Adiabatic compression is an effective method of plasma heating. In all the experiments in which the magnetic field rise occurs faster than the skin-time, the adiabatic heating takes place. An increase in the energy confinement has been observed. But at present, application of this method to the reactor seems to be problematic.

Heating at Electron-Cyclotron Frequency. Use of the electron-cyclotron waves is mainly limited by the difficulties in the development of microwave power generators.

The works on construction of these generators are being developed at the Institute of Applied Physics (Academy of Sciences, USSR). When the electron-cyclotron resonance (ECR) is used the heating occurs in the local plasma region of the resonance magnetic field. It allows, in principle, to control over the current profile in a tokamak by a change in the electron temperature.

This opportunity of changing the temperature profile is realized in the ФТ-1 tokamak experiments /1/. At the electron-cyclotron resonance heating, electrons receive the energy from the wave and then transfer it to ions. For the reactor parameters, the energy confinement time should be considerably greater than the temperature equalization time.

The ECRH-efficiency at the higher plasma density is limited by refraction and reflection of microwaves when the generator frequency approaches the plasma electron one. In the experiments in the ФТ-1 tokamak ECRH power was launched from the side of a large magnetic field - in difference from other experiments - that allows to penetrate into the region of densities 2-3 times higher than the critical one.

Microwave-set at T-10 includes four gyrotrons. The output power of each gyrotron is 200 kW. The pulse duration for heating is up to 150 ms. The wave-length is 3.5 mm. It corresponds to the resonance field B=3T. The experiments were carried out at the magnetic fields equal 1.5 T and 3 T, i.e. the plasma heating at the second har-

monic and at the first one of the electron cyclotron frequency was studied /2/. As a rule, 500 kW were introduced additionally into plasma in the T-10 experiments : 2/3 of the total amount were an ordinary wave, 1/3 of it was an extraordinary one. The efficiency of heating at the second harmonic is determined as the ratio of the plasma energy change rate to the input power. It was higher than 50%.

If one takes into account the power of an extraordinary wave only, the efficiency will be found higher than 100%. It allows to make a conclusion that an appreciable absorption of an ordinary wave also was observed at the fields $B = 1.5$ T.

The efficiency of heating at the first harmonic was about 90%. Oscillograms of voltage at the microwave heating are shown in Fig.2. Due to a rise in the electron temperature, the power of Joule heating has an approximately two-fold drop and equals 160÷180 kW in this case, i.e. the power of microwave heating exceeds the power of ohmic heating more than two times. A change in the electron temperature profile at the microwave heating is shown in Fig.3.

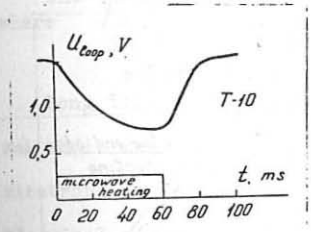


Fig.2 T-10 Loop voltage oscillogram at ECRH

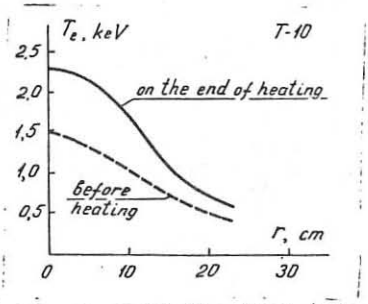


Fig.3. T-10 Electron temperature profile befor ECRH and in the end of it

An increase in the electron temperature at the centre of the plasma column is equal 0,8 keV. The maximal increase observed in temperature is somewhat higher than 1 keV. The temperature of deuterons is also rises at the heating. A neutron flux intensity in time is shown in Fig.4.

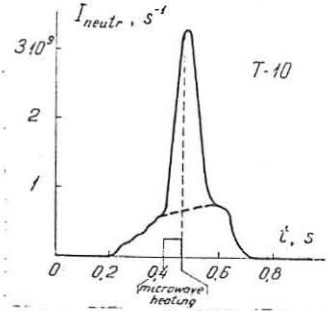


Fig.4 T-10 Neutron flux intensity vs . time

A rise in the deuteron temperature equal 130 eV occurs in accordance with the electron-ion energy exchange due to the Coulomb collisions (Fig.5)

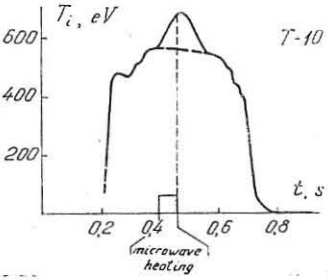


Fig.5 T-10 Deuteron temperature calculated from the neutron flux intensity vs . time

Behaviour of the plasma density at the microwave heating is interesting. If the chamber wall conditions are good enough, a drop in density will be observed at the heating (Fig.6).

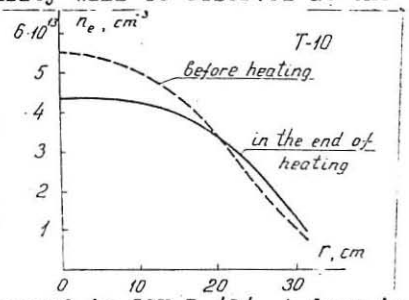


Fig.6 T-10 Change in the plasma density distribution at ECRH

First this effect was observed in JSX-B /3/. A drop in

density at the centre reaches 20% in T-10 and 30% in TM-4.

It is impossible to explain a decrease in the plasma density by a decrease in the influx of electrons which appear as a result of ionization. On the contrary, the spectral and bolometric measurements show that an influx of hydrogen and impurities rises at the heating. A drop in density can occur as a result of the increased diffusion from the plasma core at the heating or a decrease in the drift fluxes towards the core at this time.

Application of the additional heating gives an opportunity to investigate the dependence of the heat conduction coefficient on the electron temperature. It is known that such a dependence cannot be studied separately because of unavoidable correlation between the temperature and the current in plasma with the Joule heating only. The electron heat conduction coefficients obtained in the experiments on the second harmonic at the time of heating and after it are found to be close to each other. Although the accuracy of these experiments does not allow one to make a statement on the independence of χ on T_e, the results obtained allow one to speak about absence of the strong dependence, i.e. $\chi \sim T_e^{\alpha}$ where $|\alpha| \leq 0.5$.

Heat conduction and diffusion

Long term studies on heat conduction in the tokamak ohmic regime reveal two main facts: heat conduction of electrons is anomalously great in comparison with the neoclassical value and the anomalous electron heat conduction drops with a rise in the plasma density. A rise in the energy confinement time with density was recently confirmed

in the experiments in T-7 (Fig.7).

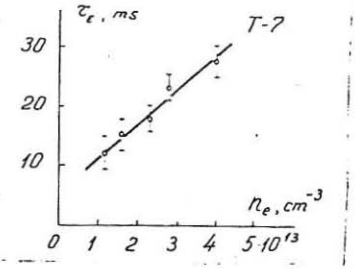


Fig. 7 T-7 Energy confinement time vs.plasma density

It was experimentally found that $n_e \chi_e = 5.10^{17} cm^{-1} s^{-1}$ (what is known as the Alcator scaling). The studies on heat conduction in the regimes with low q in T-10 have given the two - fold lower values of χ_e in comparison with those which correspond to the Alcator scaling [4]. In the regimes with high q, in which the relaxation oscillations with m=1 in the plasma core are absent, the values of χ_e are low.

Studies on the energy balance in T-11 at different positions of the limiter and comparison between the results obtained at T-11 and at T-10 allow to find a dependence of the heat conduction on the geometry [5]. The analysis carried out by Merezhkin and by Mukhovatov shows that $\chi_e = 10^{20} \frac{T_e}{n_e q R} \left(\frac{r}{R}\right)^{1,25}$. The dependence $\chi_e \sim \frac{1}{R}$ in this relationship is important. It shows that $\tau_e \sim a^2 R \sim R^3$ when the main heat losses are due to the electron heat conduction.

One should note that the dependence $\chi_e \sim \sqrt{T_e}$ does not contradict the data on the microwave heating. But this problem needs a more precise solution.

Diffusion of charged particles has been studied by different methods. The detailed study on the particle balance with regard to the ionization flux due to hydro-

gen atoms coming from the pulse valve, limiter and from the walls, has been carried out recently for T-11.

The dependence of the diffusion coefficient and heat conduction on the value $\frac{\sqrt{T_e}}{qR}\left(\frac{r}{R}\right)^{1,75}$ found in T-11 is given in Fig.8.

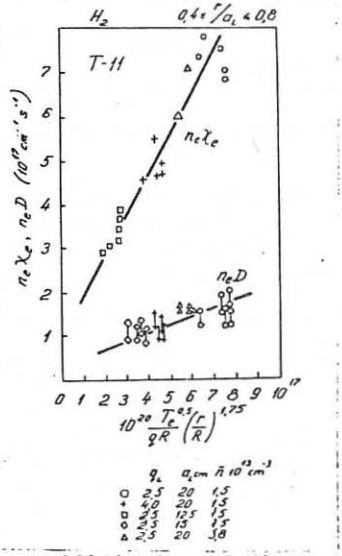


Fig.8 T-11 Heat conduction and diffusion coefficients vs. $\sqrt{\frac{T_e}{qR}}\left(\frac{r}{R}\right)^{1,75}$

One can see that the diffusion coefficients and those of thermal conduction have only 4 - 5 - fold difference [6].

A periodic gas puffing and the measurements of phase and amplitude in the density oscillations allow to determine the diffusion coefficient. Study on the saw-tooth oscillations in density in T-10 and in Tuman-3 - when an internal disruption occurs - reveals an importance of the drift particle fluxes towards the centre of the plasma column. One should assume that the plasma inward flow exceeds the diffusion flow outwards to explain a rise in the plasma density in the core at the time between the internal disruptions. Simulation of the process shows that the

flux in its absolute value is close to the flux provided by a neoclassical pinching of the trapped particles. But the observed dependence of the experimental flux on the parameters seems not to be neoclassical one. In particular, one does not succeed in explaining the density decrease during ECRH in TM-4 on a basis of the neoclassical pinch effect. In the same tokomak, the space potential was measured by a heavy-ion beam probe (Fig.9).

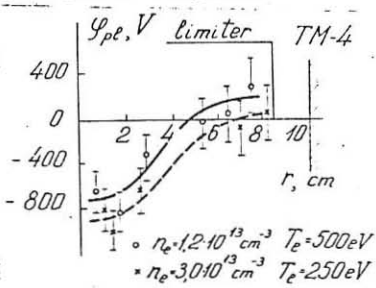


Fig.9 TM-4 Plasma potential distribution along the radius

The space potential of plasma in the core is negative and equal to a few hundred eV. A sign of the potential is an indication of the determinant role of the ion component in the diffusion losses. A rise in the electron temperature from 500 eV to 900 eV at ECRH does not result in a noticeable change in the potential. Thus, the density decrease at ECRH depends on the electron losses only.

Asymmetry of distributions along the minor radius

The study on heat transport and diffusion needs to know the distribution of different parameters across the plasma column. Under close examination it has been found that the electron temperature and density profiles are asymmetric ones in the regimes with low density in T-10 /7/. The maximum distribution of electron temperatu-

re along the major radius is found to be shifted respective to the magnetic axis determined with the magnetic probes and with the radius r_s found from a change in the phase of saw-tooth oscillations (Fig.10).

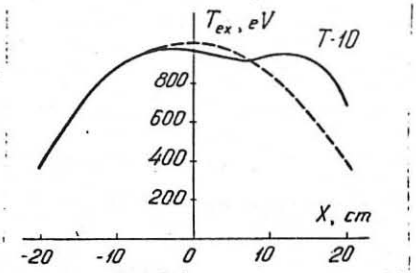


Fig.10 T-10 Electron temperature distribution asymmetry along the radius

The asymmetry observed is associated with a sufficiently large amount of trapped particles under the conditions of low density and high ripples of the magnetic field in T-10. Under these conditions, the transversal plasma pressure determined by the transversal energy of untrapped and trapped particles is not the same across the magnetic surface, as well as the surfaces of equal pressure cannot coincide with the magnetic ones.

Study of impurities

Study of impurities is important in the modern experiments. Effective methods of the wall cleaning have been developed in recent years. These methods allow to have plasma with a low amount of impurities. The effective plasma charge is found to be close to unity.

The impurity and cold hydrogen fluxes profoundly effect on the electron temperature profile and that of the current in a tokamak. This explains the influence of the chamber wall conditions on the reproducibity of

of stable discharges with low q in T-10. Two regimes of the discharge in T-10 are possible: with a dominance of light or heavy impurity dependent on the preliminary treatment of the wall. The presence of light impurities like carbon seems to cool the periphery of the discharge. Thus the spectrum of the particles bombarding the wall is changed and the atomic flux of a metal into the discharge decreases. One can assume that the light impurities can serve as a gaseous blanket protecting the wall.

Three main aspects of the impurity problem should be named: study of dynamics and impurity confinement in the plasma column, study of a divertor and different materials for the wall of a discharge chamber.

The impurity confinement has been investigated in T-10 in accordance with the so-called Argon Program [4]. The main result of these experiments: ions of argon, which imitate the ions of heavy impurity, are confined in plasma like the ions of the plasma bulk deuterium, the impurity ion accumulation does not occur. Study on a one-null and two-null poloidal divertors were carried out in T-12 [8]. Efficiency of the divertor was demonstrated. The particles beyond the separatrix are transported into the divertor volume with the efficiency close to unity. The radiation losses have a two-fold drop due to a decrease in the impurity flux into plasma.

The first experiments with a toroidal divertor have been begun in TO-2.

The experiments on the wall temperature effect on

the influx of hydrogen and impurities into the plasma column were carried out in the TM-4 chamber of stainless steel /9/. It is shown that with a rise in the wall temperature from 20° to 300°C the influx of impurities into the plasma column also rises. An increase in the plasma electron temperature from 8 to 12 eV in the scrape-off layer is observed. The recycling coefficient for hydrogen rises from 0.6÷0.7 for a cold wall up to 0.9 for a hot one.

The graphite as a material for the discharge chamber wall was studied in the TMT -tokamak.

The same discharges as in the similar facilities with the chambers of stainless steel can be obtained in the graphite chamber. But it is not possible to obtain the same discharges in different shots because of high absorption of graphite. The stationary conditions of the discharge are possible at the temperature of graphite equal 300°C.

The first experiments on the limiter wall erosion have been started in the T-3 M tokamak /10/.

Conclusions

1. The efficiency of the microwave plasma heating at the electron-cyclotron resonance has been demonstrated. This method will be used in the T-15 tokamak as well as the neutral injection.

2. Heat conduction and diffusion studies have been continued. The plasma diffusion as well as the electron heat conduction is anomalously great. The diffusion coefficient is 4÷5 times less than the electron heat conduction.

3. The particle balance in plasma is determined by diffusion from the centre outwards and by the drift flux from outside to the centre.

References

1. Yu.F.Baranov, D.G.Bulyginsky - Paper H-21 at this Conference.

2. V.V.Alikaev,Yu.J, Arseniev et al. Paper H-3 to this Conference.

3. R.M.Gilgenbach et al.Phys.Rev.Lett.44 647(I980).

4.A.B.Berlizov,V.I.Bugarya et al.in Plasma Phys.and Cont.Nucl.Fusion Res.Vol.I,IAEA,Vienna(I98I) 23.

5. V.S.Mukhovatov, V.G.Merezhkin et al. Pis'ma Zh.Ehksp.Teor. Fiz. issue 9, p.463-467, 1981.

6. V.M.Leonov, V.G.Merezhkin et al. Paper A-17 to this Conference.

7. G.A.Bobrovsky, N.L.Vasin. Paper to this Conference.

8. N.N.Brevnov, A.N.Vertiporokh. Paper J-2 to this Conference.

9. V.J.Bugarya, A.V.Gorshkov et al. Paper A-15 to this Conference.

10.D.G.Baratov, V.N.Demchenko et al. Paper J-11 to this Conference.

Figure captions

Fig.1 Tokamak-program development

Fig.2 T-10 Loop voltage oscillogram at ECRH.

Fig.3 T-10 Electron temperature profile before ECRH and in the end of it.

Fig.4 T-10 Neutron flux intensity time.

Fig.5 T-10 Deuteron temperature calculated from the neutron flux intensity time.

Fig.6 T-10 Change in the plasma density distribution at ECRH

Fig.7 T-7 Energy confinement time plasma density

Fig.8 T-11 Heat conduction and diffusion coeffi-cients

Fig.9 TM-4 Plasma potential distribution along the radius

Fig.10 T-10 Electron temperature distribution asymmetry along the radius.

PLASMA HEATING BY HIGH-POWER RELATIVISTIC ELECTRON BEAMS

P. Šunka

Institute of Plasma Physics, Prague, Czechoslovakia

1. Introduction

Advances in high-power electrical technology and successful generation of intense relativistic electron beams at multiterawatt power level has stimulated enhanced interest in application of such beams in controlled fusion research. The very direct application of intense E-beams is the heating of a plasma to thermonuclear temperatures. Systems with both inertially confined solid-density D-T targets and relatively low-density ($10^{13} - 10^{17}$ cm^{-3}) magnetically confined plasmas are intensively studied now. In the case of inertial confinement, major effort is directed towards the development of accelerators capable of producing the required high-power (100 TW) short-pulse (30 ns) electron (or light ion) beams, and to the focusing of the beams onto small pellets.

The principal roles for E-beams in magnetic confinement schemes are the following:

a) Plasma heating in open traps /1 - 3/.

b) Generation and sustaining of toroidal current and additional plasma heating in Tokamaks /4 - 6/.

c) Creation of the magnetic field with geometry suitable for long-time plasma confinement (compact toroids) /7/.

As for the open systems, the major problem is an efficient energy transfer from the beam to a plasma, the energy deposition

length having to be comparable with the system length. On the other hand, in the case of toroidal systems, the main difficulties are connected with injection and trapping of the beam into closed line geometry. The energy deposition length can be much longer than the system dimensions (however, the beam energy has to be deposited before it is lost by other processes).

In this talk we briefly summarize main results achieved in plasma heating in linear open traps. This topic is closely related to the concept of long solenoid fusion systems, proposed by Budker /1/, Benford /2/, and Ryutov /3/. In such systems plasma column of about 100 m long with a density of $10^{17}cm^{-3}$ immersed in a magnetic field of 10 T is heated up to the thermonuclear temperature (5 – 10 keV) by the high-power REB injected along the magnetic field lines. Recently, Thode /4/ proposed to use a dense ($10^{17} - 10^{20}cm^{-3}$) multikilovolt plasma (volume $3 - 50\,cm^3$), rapidly heated by a high voltage REB as an inertial confinement fusion driver. Since the heating by classical binary collisions of beam and plasma electrons is inefficient even in the above mentioned range of plasma parameteres, collective energy coupling processes have to be exploited.

2. Plasma heating by a propagating electron beam.

Typical arrangement of an experiment on plasma heating by intense REB is shown schematically in Fig. 1. The beam is injected axially through a thin foil into the interaction chamber filled by a preformed plasma or by a neutral gas. External magnetic field (homogeneous, mirror, multimirror or other geometry) prevents free radial motion of plasma and beam electrons and, to some ex-

tent, it confines the plasma axially. The space charge of the injected beam is neutralized by plasma ions and the beam current I_b is partially or fully compensated by the "return" current I_{rc} driven in a plasma by the electric field induced at the beam front due to the rising beam current ($n_b \ll n_p$ is assumed; n_b, n_p being the beam and plasma electron density, respectively).

Theory of the interaction of an intense REB with a plasma predicts two strong instabilities:

a) Return current instability (Buneman and ion acoustic modes) driven by the relative drift between plasma electrons and ions. This instability is excited if the electron drift velocity v_d exceeds some threshold value v_{Te} /8 - 10/. Assuming full compensation of the beam current by the return current ($v_d n_p \approx c \cdot n_b$), the return current instability starts at

$$n_b > \alpha \frac{v_{Te}}{c} \cdot n_p \qquad (1)$$

where v_{Te} is the thermal velocity of plasma electrons and α is a numerical factor ranging from $(m_e/m_i)^{\frac{1}{2}}$ (for a plasma with $T_e \gg T_i$) to unity (for plasma with $T_e \simeq T_i$). Thus, heating of a plasma with $n_p = 10^{17}\,cm^{-3}$ up to 10 keV tmperature would require beam current densities exceeding 1 MA cm^{-2}, even for the lowest value of α ($\alpha \sim 10^{-2}$ for deuterium plasma). In present day experiments beam current densities of 1 - 10 kA cm^{-2} are usually used and, therefore, an efficient return current heating can be expected only at low plasma densities ($n_p \lesssim 10^{13}\,cm^{-3}$).

b) The electron-electron two-stream instability (e-e mode) driven by the relative drift between beam and plasma electrons. Theory of the two-stream instability has been extensively studied by

many authors /9-15/. Generally, two different regimes of instability are distinguished, the hydrodynamic and the kinetic. Which regime will be established depends strongly on the spread in longitudinal velocities of the beam electrons

$$\Delta v_z = c\,\frac{\Delta E}{\gamma_0^3 E} + c\,\bar{\theta}^2 \qquad (2)$$

which is due to the beam energy spread ΔE and or to the spread in angle of the beam velocity vector relative to the beam propagation direction, represented here by the mean angle $\bar{\theta}$. In the real beam generators all beam electrons are accelerated almost to the same energy and only the spread in $\bar{\theta}$ (caused mainly by elastic scattering of beam electrons passing through the anode foil) is important ($\bar{\theta}^2 \gg \frac{\Delta E}{\gamma_0^3 E}$).

The hydrodynamic instability is excited by a "cold" beam with $\bar{\theta}^2 < \frac{1}{\gamma_0}\left(\frac{n_b}{n_p}\right)^{\frac{1}{3}}$. The linear growth rate in this limit is given by /11/

$$\delta_k = \sqrt{\frac{3}{2}}\,\frac{\omega_p}{\gamma_0}\left(\frac{n_b}{n_p}\right)^{\frac{1}{3}}\left(\cos^2\phi + \gamma^2 \sin^2\phi\right)^{\frac{1}{3}} \qquad (3)$$

where ω_p is the electron plasma frequency and ϕ is the angle of the wave vector $\vec{k}$ with respect to the beam propagation direction. Spectrum of the excited Langmuir waves is sufficiently narrow and it may be approximated by a single wave. The wave growth is saturated by trapping of the beam electrons into the potential well of the wave. When the angular spread of the beam is large enough ($\bar{\theta}^2 \gg \frac{1}{\gamma}\left(\frac{n_b}{n_p}\right)^{\frac{1}{3}}$), the kinetic instability with the growth rate /11/.

$$\delta_k = \omega_p \frac{n_b}{\gamma_0 n_p}\,\frac{1}{\bar{\theta}^2}\,\frac{\omega_p^2}{\omega_p^2 + k^2 c^2} \qquad (4)$$

is excited. The wave spectrum is broad and and quasilinear or nonli-

near wave-wave scattering processes should stabilize the wave growth.

An intermediate regime, in which neither hydrodynamic nor kinetic limit applies strongly, has been studied by Thode / 17, 18 /. On the base of extensive computer simulations he finds that when $\bar{\theta} < \gamma^{-1}$ and/or $\Delta n/n_b > 0{,}15$ the instability is quasihydrodynamic in character and the wave growth saturation is primarily governed by trapping of the beam. The growth of the most unstable wave is approximated by the following formula / 18 /

$$\delta_{2h} = 0{,}866\,\omega_p \frac{(1+\beta^2\gamma\bar{\theta}^2)^{\frac{1}{2}}}{\gamma} \left(\frac{n_b}{n_p}\right)^{\frac{1}{3}} \frac{\Delta n}{n_b} \qquad (5)$$

$\Delta n/n_b$ is the fraction of electrons in the scattered beam which interacts with the wave in a hydrodynamic fashion. This fraction is given by

$$\frac{\Delta n}{n_b} = 1 - e^{-\frac{S}{F}} \qquad (6)$$

where F is the foil scattering function ($F \approx \beta^4\gamma^2\bar{\theta}^2$) and $S = \beta^2\gamma\,(n_b/n_p)^{\frac{1}{3}}$ is the strength parameter. Thus, the expression (5) represents a connection between the hydrodynamic and kinetic interactions.

Although the linear theory predicts sufficiently high growth rate of the Langmuir waves, it is the nonlinear evolution of the instability and the wave energy density at saturation which determines how much of the beam energy can be deposited in a plasma. Nonlinear stage of the two-stream instability has been extensively analysed / 11-14, 16 / assuming the quasilinear beam relaxation, beam trapping and nonlinear wave-wave interactions as the saturation mechanisms limitting the wave growth. As the results of each nonlinear model are applicable for very different values of beam-plasma

system parameters, we look first over the parameters of the present-day experiments and the achieved experimental results.

We consider experiments in which a relativistic electron beam is injected into a straight, partially or fully ionized plasma immersed in an external magnetic field. A summary of eight recently published experiments is given in Table 1. These experiments cover a broad range of plasma and beam densities ($n_p = 10^{12} cm^{-3} - 10^{17} cm^{-3}$, $n_b = 5 \cdot 10^{10} - 10^{14} cm^{-3}$, $10^{-5} < \frac{n_b}{n_p} < 1$, interaction lengths ($L = 0{,}2 - 7{,}5$ m), and angular spreads of the beams ($\bar{\varphi} = 0{,}01 - 1$ rad). Solid beams with diameters of 2 – 10 cm are injected, except the Los Alamos divece, where a hollow beam of diameter 2 cm and 0,3 mm thick is used. Preformed plasma diameters (3 – 20 cm) exceed that of the beam in all experiments. In the case of Imperial college the beam is injected into a neutral hydrogen at pressures of 0,1 – 1 Torr.

In all experiments diamagnetic loop measurements were used as the main method to determine the plasma energy density $W_p = n_p T_p$ (T_p is the average gain in perpendicular energy per electron-ion pair). In most of the experiments /19 – 28/ the local electron distribution function (perpendicular to the beam direction) was determined by Thomson scattering of ruby laser light. Faraday cups, calorimeters and energy analysers were used for measurements of the beam characteristics after the interaction. Besides the mentioned methods, various other diagnostics (optical spectral lines, X-rays, fast neutrals, microwave radiation, magnetic probes) were employed to get more detailed information on the beam-plasma interaction.

The typical experimental procedure is to fix the beam ener-

gy E_b, particle density n_b (beam current) and the mean angle $\bar{\Theta}$ (anode foil) and to vary the plasma particle density n_p. The observed maximum plasma energy densities W_p as measured by diamagnetic loops at the end of the beam injection are also indicated in the Table 1. The measured values ($10^{16} - 10^{19}$ ev cm^{-3}) are by several orders of magnitude higher than those corresponding to the classical binary collisions of beam and plasma electrons. The maximum heating efficiencies $\gamma_{max} = Q_p/LQ_b$ expressed in per cents of the total beam energy Q_b deposited in 1m long plasma column are given in the last column of the table.

Results of the detailed diamagnetic loop measurements are plotted in Fig. 2. Here the energy coupling efficiency expressed in ratio $\frac{W_p}{W_b}$ of the plasma to the beam energy density is plotted versus the ratio $\frac{n_b}{n_p}$ of the beam to plasma particle density. The mean angular spreads calculated for the applied anode foils are also indicated in the Fig. 2. Systematic measurements were performed on the INAR, TRITON and Cornell University devices. Other experiments are represented only by single points. No attempt to take into account energy losses during the heating pulse has been done. In spite of very different experimental conditions and of the inaccuracy in determining the value of $\frac{W_p}{W_b}$, some general tendencies in behaviour of the energy coupling efficiency are apparent.

a) For fix beam parameters the value of $\frac{W_p}{W_b}$ fals rapidly at $\frac{n_b}{n_p} < 10^{-3}$ (suggesting transition into a weaker instability regime).

b) For all values of $\frac{n_b}{n_p}$ the coupling efficiency $\frac{W_p}{W_b}$ decreases with the increasing angular spread of the beam (thicker

anode foils) suggesting thus that the two-stream instability is responsible for the observed plasma heating (return current instability should not be affected by the beam angular spread).

c) Diverse values of $\frac{W_p}{W_b}$ measured for similar system parameters ($\frac{n_b}{n_p}$, $\bar{\Theta}$) in the experiments can be attributed to an energy loss during the heating pulse. One can expect that the loss would be higher in short devices (Los Alamos, Imperial College) or in weakly ionized plasmas (BP-II-6, TRITON) if compared with long machines with well ionized plasmas (INAR, GOL, Cornell University).

Several special measurements were performed to demonstrate the decisive role of the two-stream instability in process of plasma heating by intense F-beams. Variation of the heating efficiency with angular spread of the beam has been already mentioned. Results of such measurements (as obtained on the INAR device) are shown in Fig. 3. Here, the beam energy loss (calorimetric measurements) and the total energy transferred to the plasma (diamagnetic loop data), both normalized to the initial beam energy, are plotted versus the anode foil thickness. By decreasing the foil thickness from 50 μm to 6 μm the heating efficiency increases five to seven times. For very thin foils (6, 10 μm) the calorimetric data give higher efficiencies than the diamagnetic ones indicating thus some plasma energy loss during the heating process. Effect of the beam divergence on the interaction is even more evident from longitudinal profiles of the energy deposited in a plasma (Fig. 4/21/). For thin foils the energy deposition is highly non-uniform with the strongest interaction occurring near the beam entrance into the plasma. Measurements of angular distribution of

the interacting beam at various distances from the anode foil performed by means of a miniature Faraday cup with a collimator / 22/ confirme that the beam distribution broadens out at first 10 – 20 cm remaining almost unchanged at the following 100 cm of the interaction length.

Direct evidence of activity of the two-stream instability is the presence of microwave radiation in the frequency band corresponding to the second harmonic of the electron plasma frequency $2\omega_p$. This radiation originates either in nonlinear interaction of Langmuir oscillations or in bunching of the beam electrons due to their trapping in the strong Langmuir wave. Results of measurements of the microwave radiation near $2\omega_p$ are plotted in Fig. 5 /20/. Microwave power in frequency band 100 – 180 GHz is detected near the beam entrance ($z = 40$ cm) for various thicknesses of the anode foil. Comparing the Fig. 5 and Fig. 3 it is apparent that the radiated power varies in the same way as the heating efficiency.

All the above mentioned results clearly demonstrate that the beam energy is released in plasma via the two-stream instability and, therefore, preferential heating of the electron component is to be expected. In several experiments / 19 – 28/ the electron temperature was measured by means of Thomson scattering of ruby laser light. Although the electron temperature measured by Thomson scattering exhibits the same scalling as the total perpendicular energy measured by diamagnetic loops (see Fig. 6), in various experiments the Thomson scattering gives values of T_e of 4 to 30 times lower. This discrepancy is a result of the contribution of a high-energy overthermal plasma electron component (not seen

by Thomson scattering) and of heated ions to the total plasma perpendicular energy. Both the ion heating and the overthermal plasma electrons were observed in experiments but it is still not enough data to account them to the overall energy balance.

3. Enhanced plasma heating by reflexing high-power E-beams.

Formation of a dense cloud of relativistic electrons oscillating between real and virtual cathodes has been proposed to be used for accumulation of the REB energy in a plasma /37, 38/ and for collective ion acceleration / 39, 40/. Such an oscillating electron cloud is created by injection of a high-current beam into either a vacuum space or a short plasma column with a free vacuum boundary. Simultaneously, strong axial magnetic field is used to prevent radial motion of the oscillating beam electrons.

In our experiments / 33 - 35 / the oscillating high-current relativistic electron beam is used for heating of a dense plasma. Experimental investigation of the role of a virtual cathode in the beam energy transfer processes has been performed in REBEX device, schematically shown in Fig. 7. The beam (500 keV, 10 - 40 kA, 70 - 120 ns) is injected into a conducting vacuum chamber (L = = 2,1 m, D = 150 mm) containing a hydrogen plasma from a double conical plasma gun which is located near the beam entrance. The gun generated plasma expands along the external magnetic field (mirror ratio 1,5; B_{max} = 0,7 T) with the front velocity of $(2-4).10^4$ $m\,s^{-1}$, reaching the downstream end plate 50 - 100 us after the gun firing. The maximum plasma density of a short cluster (0,6 m) exceeds $10^{15}\,cm^{-3}$ and it decreases to $10^{14}\,cm^{-3}$ for the full-length plasma column. By varying the time delay t_d between firing the gun

and the beam we were able to compare the plasma heating efficiency in both the propagating and the oscillating beam regimes.

On the base of diamagnetic loop measurements we found that the propagating beam deposits about 10 per cent of its energy in 2m long plasma of the density $10^{14}cm^{-3}$. This energy transfer rate is comparable with other experiments listed in the Table 1. However, in the oscillating beam regime the heating efficiency increases up to 30 per cent regardless the higher plasma density ($n_p = 2 \cdot 10^{15}cm^{-3}$) and the shorter interaction length ($L_p \lesssim 1$ m). In regimes with the maximum heating the plasma energy density reaches such a high value that the external magnetic field is almost displaced on the axis. Thomson scattering and X-ray measurements indicate that appreciable fraction of the plasma energy is carried by overthermal electrons.

The decisive role of the reflected beam electrons in enhancement of the plasma heating was demonstrated clearly in experiments with a movable collector which enabled us to realize the transition from the oscillating to the propagating beam regime at fixed plasma parameters. In Fig. 8, the electron current to a movable collector (dashed lines) and the plasma diamagnetism near the beam entrance (solid lines) are plotted versus the collector position. Each couple of curves corresponds to a different location of the plasma boundary. As the collector approaches the plasma boundary the current to it increases from the vacuum value to the full one while the plasma diamagnetism falls by an order of magnitude.

To get an insight into the complex oscillating beam dynamics, a $1\frac{1}{2}$ dimensional PIC computer code simulating the reflex E-beam system coupled to an external electric circuit (pulse forming line)

was developed /41/. Electrons emitted from the cathode surface and accelerated within the cathode-anode gap are scattered in the anode according the foil scattering model. After some time delay ions ($\frac{m_i}{m_e} = 100$) are emitted from the anode in both directions. Typical results of the numerical run are shown in Fig. 9 where the normalized diode current and voltage pulses are plotted (ion emission starts at $\tau = 20$). Fast periodical changes of the virtual cathode position and of its potential depth result in strong bunching of the oscillating electrons and in modulation of the diode voltage U_b. Slow changes in U_b have a time scale of ion breakdown processes in the diode. Strong electron bunches moving in both directions are formed also in numerical runs in which the virtual cathode region is separated from the high-voltage diode by a plasma column. This bunching of the oscillating beam electrons is likely the cause of the enhanced plasma heating observed in the experiment.

4. Discussion

Considering the experimental data it can be hold as well established that the two-stream instability is responsible for the plasma heating in the reported experiments. Nevertheless, the direct comparison of the experimental and theoretical results is difficult to make. Since the spectrum of excited wave is not a known quantity for the time being, only the macroscopic beam and plasma parameters can be compared with theoretical models.

The ranges of validity of different beam relaxation models are shown in Fig. 10 /16/ (the kinetic regime of the two-stream instability is assumed). The regions I, II, III correspond successively to the applicability of the quasilinear theory, the weak

turbulence theory accountig for induced scattering on ions, and to the strong turbulence theory of modulational (oscillating two-stream) instability. The parameters of all present-day experiments fall into the last region III. The modulational instability heating mechanism is supported also by the anomalous heating of an overthermal plasma electron component observed in most of the experiments. Moreover, the detailed calculations of the heating rate due to the modulational instability (kinetic regime) performed for the TRITON experiment are consistent with the experimental results /26/.

On the other hand the heating efficiency measured in the Cornell University experiment scales according to the quasihydrodynamic theory /17/. However, this experiment was performed at relatively high values of $\frac{n_b}{n_p}$ for which the transition to fully kinetic regime occurs for values of $\bar{\theta}$ considerably larger than the approximate analytic solution suggests /15/. On can thus expect that in the experiments with high-quality beams the wave growth is limited by the beam dynamics, the energy of the excited waves being transferred to plasma particles via the modulational instability.

References:

/ 1/ G.I.Budker, Proc. of VI the European Conf. on Contr.Fusion and Plasma Physics Vol. II, p. 136, Moscow (1973)

/ 2/ J.Benford, T.S.T. Young, B.Ecker, D.Dakin, I.Smith, S.Putnam, V.Bailey, Proc. of International Topical Conf. on Electron and Ion Beam Res. and Tech. Vol. II, p. 477, Albuquergue (1975)

/ 3/ D.D.Ryutov, Uspekhi Fiz. Nauk 116 (1975) 341

/ 4/ A.Mohri, K.Narihara, Y.Tomita, T.Tsuzuki, M.Hasegawa, K.Ikuta, Nuclear Fusion, Supplement 1981, Vol. 1, p. 511

/ 5/ V.Bailey, J.Creedon, B.Ecker, H.Helava, G.A.Proulx, International Topical Conf. on El. and Ion Beam Res. and Tech. Palaiseau, France 1981, paper 3P, 3 (will be published)

/ 6/ B.R.Kusse, G.A.Proulx, ibid, paper 3P1 (will be published)

/ 7/ J.D.Sethian, K.A.Gerber, D.N.Spector, A.E.Robson, ibid, paper 3P2 (will be published)

/ 8/ L.E.Thode, Report of LASL, LA-7715-MS (1980)

/ 9/ L.I.Rudakov, Zh. Eksp. Teor. Fiz. 59 (1970) 2091

/10/ R.V.Lovelace, R.N.Sudan, Phys. Rev. Lett. 27 (1971) 1256

/11/ B.N.Brejzman, D.D.Ryutov, Nuclear Fusion 14 (1974) 873

/12/ Ya.B.Fainberg, V.D.Shapiro, V.I.Shevchenko, Zh. Eksp. Teor. Fiz. 57 (1969) 966

/13/ L.E.Thode, B.B.Godfrey, Phys. Fluids 19 (1976) 316

/14/ L.E.Thode, R.N.Sudan, Phys. Fluids 18 (1975) 1552

/15/ R.L.Ferch, R.N.Sudan, Plasma Physics 17 (1975) 905

/16/ A.A.Galeev, R.Z.Sagdeev, V.D.Shapiro, V.I.Shevchenko, Zh. Eksp. Teor. Fiz. 72 (1977) 507

/17/ L.E.Thode, Phys. Fluids 19 (1976) 305

/18/ A.V.Arzhannikov, A.V.Burdakov, B.N.Brejzman, A.S.Burmasov, L.N.Vyacheslavov, V.S.Koidan, V.V.Konyukhov, V.A.Kornilov, Eh.P.Kruglyakov, V.N.Lukyanov, K.I.Melker, A.A.Podyminogin, A.I.Rogozin, D.D.Ryutov, Nuclear Fusion, Suppl. 1979 Vol.II, p.623

/20/ A.V.Arzhannikov, A.V.Burdakov, V.S.Burmasov, V.S.Koidan, V.V.Konyukhov, K.I.Melker, A.I.Rogozin, L.N.Vyacheslavov, Proc. of the 3rd Top. Conf. on High Power El. and Ion Beam Res. and Tech. Novosibirsk 1979, Vol. 1, p. 29

/21/ A.V.Arzhannikov, A.V.Burdakov, V.S.Koidan, V.V.Konyukhov, K.I.Melker, A.I.Rogozin, Pisma Zh. Eksp. Teor. Fiz. 17 (1978) 173

/22/ M.A.Greenspan, C.Ekdahl, J.D.Sethian, C.B.Wharton, Phys. Fluids 23 (1980) 205

/23/ J.D.Sethian, C.A.Ekdahl, Phys. Rev. Lett. 42 (1979) 711

/24/ C.B.Wharton, Proc. of the 2nd Int. Topical Conf. on El. and Ion Beam Res. and Tech. Ithaca, N.Y.1977, Vol. 1, p. 407

/25/ A.K.L.Dymoke-Bradshaw, A.E.Dangor, D.A.Hammer, J.D.Kilkenny, ibid, Vol. 1, p. 343

/26/ D.A.Hammer, K.A.Gerber, W.F.Dove, G.C.Goldenbaum, B.G.Logan, K.Papadopoulos, A.W.Ali, Phys. Fluids 21 (1978) 483

/27/ D.A.Hammer, K.A.Gerber, A.W.Ali, IEEE Transactions on Plasma Science, PS-7 (1979) 83

/28/ V.S.Burmasov, A.D.Khilchenko, V.A.Kornilov, E.P.Kruglyakov, V.N.Lukyanov, A.A.Podyminogin, Yu.A.Tsidulko, L.N.Vyacheslavov, Plasma heating by REB in long solenoid (this conf.)

/29/ B.Jurgens, P.H.de Haan, E.H.A.Granneman, H.J.Hopman, Proc. of the 2nd Int. Topical Conf. on High Power El. and Ion Beam Res. and Tech., Ithaca, N.Y. 1977, Vol. 1, p. 369

/30/ G.C.A.M.Jansen, P.H. de Haan, H.J.Hopman, 4th Int. Topical Conf. on High Power El. and Ion Beam Res. and Tech., Palaiseau, France 1981, paper 3P6 (will be published)

/31/ P.H. de Haan, H.J.Hopman, G.C.A.M. Jansen, E.H.P. Granneman, P.S.Strelkov, Proc. 3rd Int. Topical Conf. on High Power El. and Ion Beam Res. and Tech., Novosibirsk 1979, Vol. 1, p. 123

/32/ M.D.Montgomery, J.V. Parker, K.B. Riepe, R.L. Sheffield, Proc. 4th Int. Topical Conf. on High Power El. and Ion Beam Res. and Tech., Palaiseau, France 1981, paper 3C2 (will be published)

/33/ P. Šunka, V. Babický, M. Člupek, K. Jungwirth, K. Koláček, I. Kováč, V. Piffl, J. Ullschmied, M. Řípa, ibid, paper 3P7 (will be published)

/34/ P. Šunka, K. Jungwirth, I. Kováč, J. Stöckel, V. Piffl, J. Ullschmied, Proc. of the 3rd Int. Top. Conf. on High Power El. and Ion Beam Res. and Tech. Novosibirsk 1979 Vol. 1, p. 103

/35/ P.Šunka, K. Jungwirth, I. Kováč, V. Piffl, J.Stöckel, J.Ullschmied, Nucl. Fussion, Supplement, 1977, Vol.II, p.535

/36/ S. Robertson, A. Fisher, C.W. Roberson, Phys. Fluids 23 (1980) 318

/37/ D.D. Ryutov, G.V. Stupakov, Fiz. Plazmy 2 (1976) 566

/38/ A.V. Arzhannikov, A.V. Burdakov, V.S. Koidan, D.D. Ryutov Zh. Eksp. Teor. Fiz. Lett. 24 (1976) 19

/39/ D.D. Ryutov, G.V. Stupakov, Fiz. Plazmy 2 (1976) 767

/40/ A.V. Burdakov, V.S. Koidan, A.I. Rogozin, V.V. Tschikunov, Zh. Eksp. Teor. Phys. 80 (1981) 1391

/41/ K. Jungwirth, Res. Report IPP 2/79, Inst. of Plasma Phys. Prague

Table 1

DEVICE		INAR Novosib. /19 – 21/	Cornell Univ. /22 – 24/	Imperial College /25/	TRITON NRL /26, 27/	GOL Novosib. /19, 28/	BP-II-6 Amsterdam /29 – 31/	Los Alamos /32/	REBEX Prague /33, 34/
BEAM	E_b /MeV/	1	0,35	0,35	0,5 – 1	0,5	0,6	3	0,5
	I_b / kA /	25	2 – 20	50	25 – 100	55	5	70	10 – 50
	τ / ns /	50	60	100	60	35	50 – 220	50	70; 120
	n_b /cm^{-3}/	(0,2 – 1) x 10^{12}	(0,2 – 2) x 10^{11}	4 . 10^{12}	(3 – 5) x 10^{11}	3,5 . 10^{11}	2 . 10^{11}	1 . 10^{14}	(0,3 – 1) x 10^{12}
	Anode foil	Ti: 6; 10; 25; 50 μm	Ti: 12,5 ; 25; 50 μm	Myl: 12,5 μm Al: 25 μm	Ti: 25 μm	$\bar{\Theta}$ = 23°	Ti: 30 μm	Ti: 30 μm Myl: 7,6 μm	Al: 20 μm Myl: 6 μm
PLASMA	n_p /cm^{-3}/	(0,08 – 7) x 10^{15}	(0,05 – 2) x 10^{13}	5 . 10^{15}	(0,05 – 4) x 10^{15}	(3 – 5) x 10^{14}	(0,001–2) x 10^{14}	10^{17}	(0,01–2) x 10^{15}
	B_0 / T /	2,5 / 4,2	0,26/0,47	1,2 – 1,8	0,5	1,4 / 2,4	0,2 / 0,3	9	0,45/0,6
	L / m /	2,4	1,5	0,3	4	7,5	2,5	0,2	2,1
	n_b / n_p	10^{-4}–10^{-2}	0,004–0,05	8 . 10^{-4}	10^{-4}–10^{-2}	10^{-3}	10^{-3}– 1	10^{-3}	10^{-4}–10^{-2}
	$\bar{W}^m_p$ /eVcm^{-3}/	3 . 10^{17}	3 . 10^{17}	2,5 . 10^{18}	5 . 10^{16}	10^{17}	10^{16}	10^{19}	2 . 10^{18}
	Q_p/LQ_b /m^{-1}/	10 %	20 %	6 %	7 %	5 %	1 %	5 %	(3 – 30)%

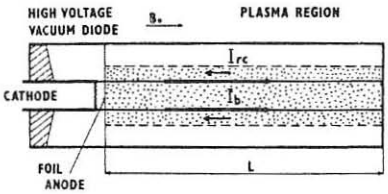


Fig. 1 Scheme of a typical experiment on plasma heating by a high-power relativistic electron beam

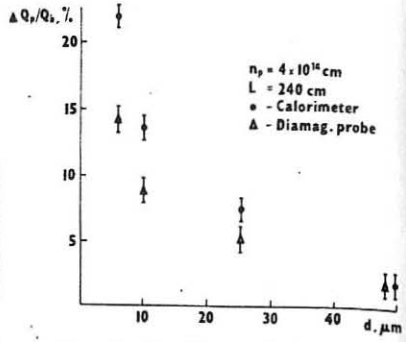


Fig. 3 Heating efficiency versus the anode foil thickness /21/

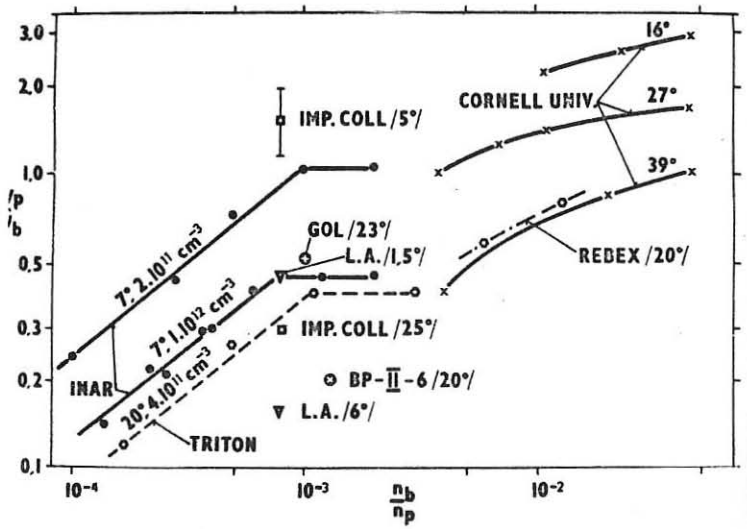


Fig. 2 Ratio $\frac{W_p}{W_b}$ of the plasma to beam energy density as measured in various experiments versus the beam to plasma density ratio

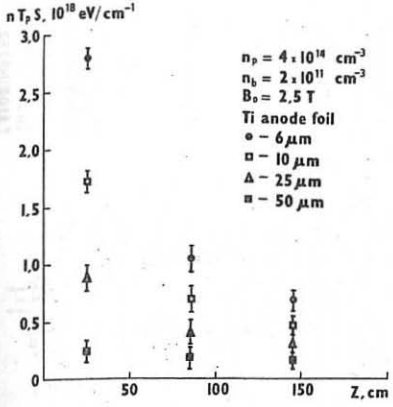


Fig. 4 Longitudinal profiles of plasma energy content for different anode foil thickness /21/

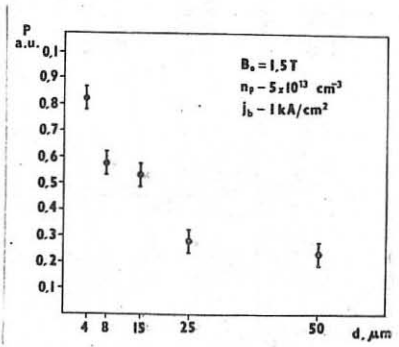


Fig. 5 Microwave radiation near $2\omega_p$ versus the anode foil thickness/20/

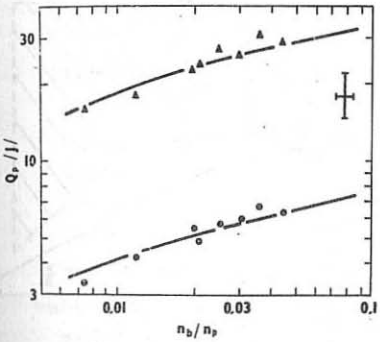


Fig. 6 Scalling of plasma heating as determined by diamagnetic loop measurements (triangles) and Thomson scattering (circles) with beam-to-plasma density ratio

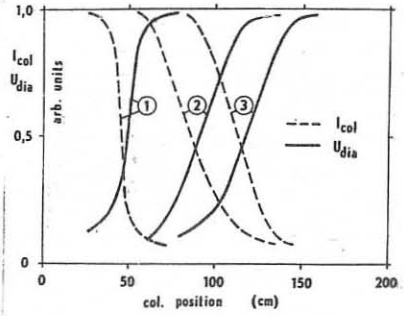


Fig. 8 Plasma diamagnetism and electron collector current versus the collector position ① neutral gas only
② t_d = 25 μs
③ t_d = 40 μs

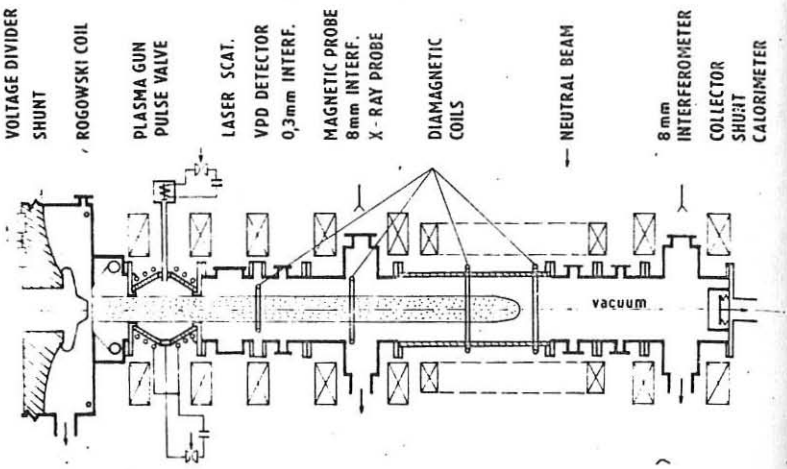


Fig. 7 Scheme of the interaction part of the REBEX device

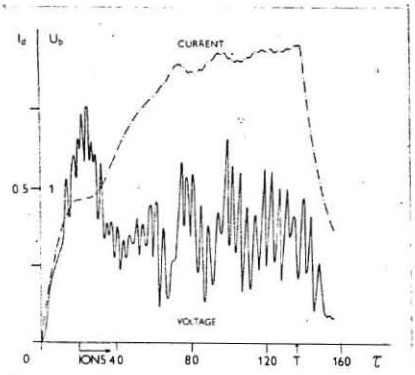


Fig. 7 Current and voltage pulses of a reflex diode with ions ($\gamma = 2$, $m_i/m_e = 100$)

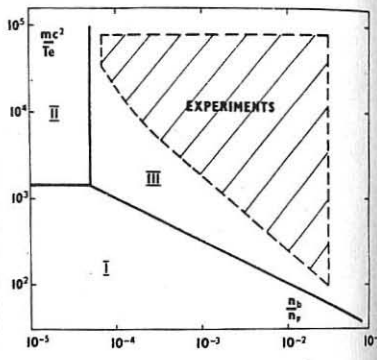


Fig. 10 Ranges of validity of
I–quasilinear theory
II–weak turbulence theory
III–strong turbulence theory
($m_i/m_e = 2 \cdot 10^3$, $\bar{\mathcal{E}}^2 = \gamma^{-1}$)

y acceptance of this article, the
ublisher or recipient acknowledges
e U.S. Government's right to
tain a nonexclusive, royalty-free
ense in and to any copyright
vering the article.

STATUS OF THE ELMO BUMPY TORUS RESEARCH*

N. A. Uckan

Oak Ridge National Laboratory
Oak Ridge, Tennessee, U.S.A.

Recent developments in the ELMO Bumpy Torus (EBT) program of experiment, theory, technology development, and reactor studies are reviewed. The 28-GHz gyrotron is routinely operated at 200 kW (cw) on EBT-S. Operation through 200 kW shows that the EBT-S experiments now cover a broader parameter range and the electron transport continues to scale neoclassically. The ring power losses scale classically, and in all electron cyclotron heated devices ring temperatures scale with ρ_{eR}/L (where ρ_{eR} is the ring electron gyroradius and L is the magnetic field scale length). The initial steady-state fast-wave ion cyclotron heating experiment has been successful and shows a several fold increase in energetic ion population. Analyses of a large number of modes and ring core coupling in stability calculations indicate that a substantial, stable, finite-beta operating window is available with $\beta_{core} \gtrsim 10\%$. The coupling of the ring power balance to the core plasma beta limits, based on the present theories, raises a concern for a reactor, and parametric studies indicate possible operating windows and optimization paths. The technology development for the next device, EBT Proof-of-Principle (EBT-P) experiment, is progressing well with the operation of the 60-GHz development gyrotron at 125 kW for 60 ms and operation of the two superconducting development magnets (7.4 T, 10,000 A/cm^2) over the design field.

1. INTRODUCTION

The plasma in a bumpy torus is confined in steady state in a bumpy magnetic field produced by joining a number of simple magnetic mirrors in a large aspect ratio torus. However, the simple bumpy torus is MHD unstable. In the ELMO Bumpy Torus (EBT),[1] the stability is achieved by the high-beta, hot electron rings[2,3] that are formed as a natural consequence of electron cyclotron heating (ECH) in the midplane of each mirror section. If the ring beta is sufficiently high, the local magnetic wells produced by these rings stabilize the toroidally confined plasma[4] (an average minimum-B stabilization). Bumpy torus plasmas employing ECH are currently being studied in the EBT[5,6] at the Oak Ridge National Laboratory (ORNL) and in the Nagoya Bumpy Torus[7] (NBT) at Nagoya University. Since the first EBT experiment EBT-I began operating, work has progressed from demonstrating macrostability[1] to an increasingly detailed understanding of confinement scaling,[5-11] stability,[12] heating,[13] and ring power balance.[3,14-17]

---

*Research sponsored by the Office of Fusion Energy, U.S. Department of Energy, under contract W-7405-eng-26 with the Union Carbide Corporation.

The observed confinement properties of toroidal core[5-11] (especially those of electrons) and ring plasmas[15,16] agree well with the classical and neoclassical theoretical models.[3,8,18-20] The experiments, with the exception of toroidal core beta, have been operating in the dimensionless parameters regime remarkably close to a reactor[6,21] with observed[5,6,10] scaling of $n\tau \sim T^{3/2}$, both of which give promising reactor projections. As a reactor, EBT offers several specific advantages; they are:[21] truly steady-state operation, the potential for moderate-to-high beta, a large aspect ratio, a simple magnetic field system, modularity, favorable geometry (for ease of maintenance), modest technology requirements, and good economics.

Many years of steady progress in EBT research as well as its reactor potential have led to the selection of the EBT concept as the leading alternative to tokamaks and mirrors in the U.S. magnetic fusion program. A large-scale EBT, the EBT Proof-of-Principle (EBT-P) experiment,[22] is now under construction and expected to be completed in mid-1985. The task of this device will be to study confinement scaling, power balance, and stability boundaries of both core and ring plasmas while increasing the important physical quantities (n, T, τ, etc.) to a level that could test whether the EBT concept has the capability to lead to a viable D-T burning device. The EBT-P will also represent a significant step toward establishing a technology base.

In what follows, we review the characteristics of the EBT plasma, discuss the experimental results from EBT-S, and summarize the theoretical studies. Some of the scaling results are presented, and reactor projections and technology development areas are highlighted.

2. CHARACTERISTICS OF EBT PLASMA

In the present EBTs, the plasma is produced and heated in steady state by ECH. Heating power is provided by microwaves at several frequencies ranging from 8.5 GHz in NBT to 18 GHz in EBT-I and to 28 GHz in EBT-S. (EBT also uses 10.6 GHz.) Ion cyclotron resonance heating (ICRH) has recently been used in EBT-S (and in NBT as well).

There are two principal plasma components: a relatively low density, mirror-trapped, high-beta, hot electron ring and a higher density warm toroidal core plasma (see Fig. 1). There is also a cold edge (surface) plasma outside the hot electron rings. The parameters of these components vary widely with operating conditions. Three

distinct operating (C, T, and M) modes are observed which are distinguished by the background neutral pressure and the fluctuation levels for a given microwave power.[1] In the C-mode, the plasma is cold and noisy and there is no hot electron ring. In the T-mode, the hot electron ring forms with sufficient beta, the plasma is quiescent, the ambipolar potential well is established, and confinement of the core plasma improves with temperature. The stable, well-confined mode of operation of EBT is the T-mode in which all the basic premises of the concept are at work. The physical dimensions and typical range of measured plasma parameters of EBT-I/S are listed in Table 1. Finally, in the M-mode, the plasma is unstable and acts like disconnected, mirror-like sectors.

By forming a magnetic well of sufficient depth [the threshold value of ring beta is $(\beta_{ring})_{crit} \simeq .2\Delta/\langle R_c \rangle \sim 5\text{-}10\%$, where $\Delta \simeq$ ring scale length and $\langle R_c \rangle \simeq$ average magnetic radius of curvature] at the plasma edge, the hot electron rings provide stabilization for the toroidal core plasma.[4] Ring stability requires a sufficient level of cold plasma[3,23] (provided by the toroidal core). The T-M transition might be related to insufficient cold plasma density. The rings form at the location of second harmonic ($\omega \sim 2\omega_{ce}$) resonance with a radial half-width Δ of a few hot electron gyroradii (ρ_{eR}) and an axial length comparable to the plasma radius.[3,15] In the T-mode the potential is peaked in the region of the rings[24] and negative at the center such that the ambipolar electric field is radially inward ($E_r < 0$) inside the ring and outward ($E_r > 0$) outside the ring.

Since EBTs are closed field line devices, field errors can cause enhanced fluctuations, increased particle diffusion, deterioration of plasma parameters, etc.[25,26] In the experiments, the optimization of plasma parameters occurs when magnetic error fields are globally cancelled (by superimposed, weak, quadrupole magnetic fields).

Collisionless scaling ($\nu/\Omega < 1$, where ν is the collision frequency and Ω is the poloidal precessional drift frequency) has been observed in experiments[6-10] where the electron energy confinement time increases with temperature ($\tau_E \sim T_e^{3/2}$). Theoretical calculations[8,20] compare favorably with experimental results and confirm that the gross behavior of the core density and temperature is dominated by neoclassical electron transport[18] (while ion transport determines the electric field to maintain ambipolarity).[20] This leads to EBT scaling[6]

$$n\tau \sim A^2 T_e^{3/2} \left(1 + \frac{R_c}{R_E}\frac{e\phi}{T_e}\right)^2 \quad \text{for } \nu/\Omega < 1 \ , \tag{1}$$

where $\nu/\Omega \sim nBR_c a/T_e^{5/2}$; a is the mean plasma radius; A is the magnetic aspect ratio defined as R/R_c; and R, R_c, and R_E are the major radius of the torus, the magnetic radius of curvature, and the electric field scale length, respectively. The potential $e\phi$ is approximately proportional to electron temperature[8] ($e\phi/T_e \sim 0.6$). The dominant ring losses are drag cooling, scattering, and synchrotron radiation.[14,15] In the present experiments, the ring temperatures were observed to obey $\rho_{eR}/L \sim 5\text{-}6 \times 10^{-2}$ scaling[17] (where L is the characteristic magnetic field scale length). The required ring sustaining power is modest,[3,15] primarily determined by drag cooling and scattering. However, in future experiments radiation losses will play an important role in determining the ring temperatures and power balance.[8,17]

In EBT, there is a natural divertor action for the wall-generated impurities at the plasma edge (outside the rings) where most of the drift orbits intersect the wall.[5,6] Also, the potential barrier that peaks near the ring effectively screens the toroidal plasma from incident impurities; i.e., $E_r > 0$ outside the ring and, hence, strongly repels impurities coming from the wall.

A comparison of the observed ring and core plasma parameters in past and present experiments suggests that most of the dimensionless parameters are constant or that they vary in the direction of improvements.[3,6,15,21] When the dimensionless parameters required for an EBT reactor (as well as for EBT-P) are examined,[21] one finds that with the exception of core beta, the EBT-I/S experiments are already operating in the correct regimes.[6]

In the present experiments, the losses limit the core beta to $\beta_{core} \leq 0.5\%$ whereas $\beta_{ring} \sim 10\text{-}40\%$ is routinely attained. Theoretical studies indicate a stable finite-beta operating window[12] of $\beta_{core} \gtrsim 10\%$. Although the present experiments cannot investigate this beta range, the EBT-P experiment is expected to have β_{core} values on the order of a few percent that enable testing of some of the predictions.

Table 1. Machine and plasma parameters of EBT-I/S and EBT-P.

	EBT-I	EBT-S	EBT-P[a]
MACHINE			
MAJOR RADIUS (m)		1.5	4.5
MEAN PLASMA RADIUS (m)		~0.1	~0.17
MEAN COIL RADIUS (m)		~0.16	~0.28
ASPECT RATIO		~9	~16
NUMBER OF SECTORS		24	36
MIRROR RATIO		~2	~2.2
MIDPLANE FIELD ON AXIS (T)	0.5	~0.72	1.5 (2.3 max)[b]
RESONANCE (ECH) FIELD (T)	~0.64	1.0	~2.1 (3 max)[b]
HEATING (cw)			
ECH (FREQUENCY/POWER, max)			
–CORE HEATING	18 GHz/60 kW	28 GHz/200 kW	60 GHz/1.2 MW[b]
–PROFILE HEATING	10.6 GHz/30 kW	18 GHz/50 kW	28 GHz/400 kW
ICH (FREQUENCY/POWER, max)		3-30 MHz/20 kW	60 MHz/1 MW
HOT ELECTRON RING[a,c]			
n_{ring} (m^{-3})	~1-2.5 x 10^{17}	~2-4 x 10^{17}	~0.4-1 x 10^{18}
T_{ring} (keV)	~180-250	~450-560	~1000-1500
β_{ring}	~10-30%	~10-35%	~10-40%
TOROIDAL CORE PLASMA[a,c]			
n_e (m^{-3})	~0.5-1.5 x 10^{18}	~0.5-2.5 x 10^{18}	~1-2 x 10^{19}
T_e (keV)	~0.2-0.5	~0.2-1.1	~1-4
T_i (BULK) (keV)	~0.02-0.04	~0.02-0.04	~0.5-3
T_i (TAIL) (keV)	~0.1-0.3	~0.1-0.3	~?
$\Delta\phi$ (POTENTIAL WELL)(V)	~100-300	~100-600	~500-3000
$\beta_{core,max}$	~0.1-0.3%	~0.1-0.5%	~1-5%

[a]PLASMA PARAMETERS FOR EBT-P ARE PREDICTED VALUES.

[b]EBT-P MAGNETS ARE CAPABLE OF OPERATING AT HIGHER FIELDS CORRESPONDING TO 90 GHz (3 T RESONANCE FIELD).

[c]THE RANGE OF PARAMETERS GIVEN CORRESPONDS TO A RANGE OF EXPERIMENTAL CONDITIONS AND OPERATING PARAMETERS (i.e., POWER, PRESSURE, ETC.). THEY DO NOT REPRESENT UNCERTAINTIES AND/OR ERROR BARS.

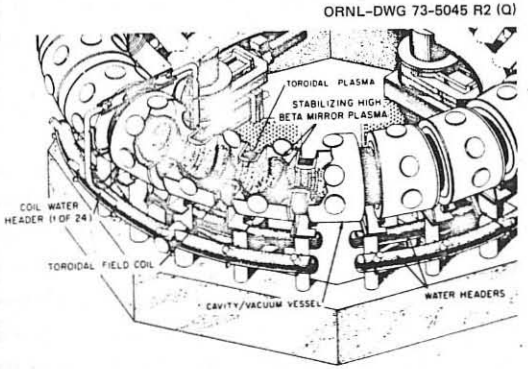


Fig. 1. ELMO Bumpy Torus experiment — cutaway drawing.

3. EXPERIMENTAL RESULTS

The plasma properties have been determined mostly in the T-mode because of the relatively long lifetimes and low fluctuation levels. The core plasma parameters are determined by a large number of standard diagnostics (similar to ones currently used on tokamaks) and specially developed diagnostics (i.e., heavy ion beam probe, etc.). Rings are energetic (temperatures are a couple of orders of magnitude higher than the core, however, and less dense), and their properties are studied by hard x-ray, synchrotron, and diamagnetic diagnostics.

3.1 Rings

The rings must form with sufficient beta (stored energy, $W_\perp$) to modify the magnetic field gradients to provide average minimum-B stabilization for toroidal core plasma. Experimentally, stabilization is evidenced by a reduction of the density fluctuations and by the appearance of a symmetric ambipolar potential well[15] (C-T transition). The experimental value of beta at the C-T transition is in the range of a few percent and is observed to be nearly constant (within a factor of 2) for large variations in microwave power and pressure as well as frequency[16] (see Fig. 2). At the C-T and T-M transitions the critical pressure varies as the square root of the microwave power[16] ($p_o \sim P_\mu^{1/2}$). Figure 2 shows both transitions and indicates that the operating window increases with power.

Significant improvements in ring parameters were observed with an increase in microwave frequency[15] (or alternatively with magnetic field, $f_\mu \sim B$), as shown in Fig. 3. These can be summarized as follows:[15] (1) distribution functions are Maxwellian (Fig. 3.a); (2) ring temperature and density increase with microwave frequency (or B) although temperature increase is more pronounced (Fig. 3.b); (3) for a given B (or frequency), ring temperature is almost constant and nearly independent of power and pressure, whereas density increases as the microwave power increases (or neutral density decreases) (Fig. 3.c).

Synchrotron emission from the ring electrons has been measured in the frequency range 80-110 GHz.[27] As expected, the radiation spectrum is monotone and the intensity levels are in reasonable agreement with the theoretical predictions.[28] Comparison of various characteristic rise and decay times from synchrotron emission and hard x-rays shows[16] that the ring temperature decays more slowly than the density.

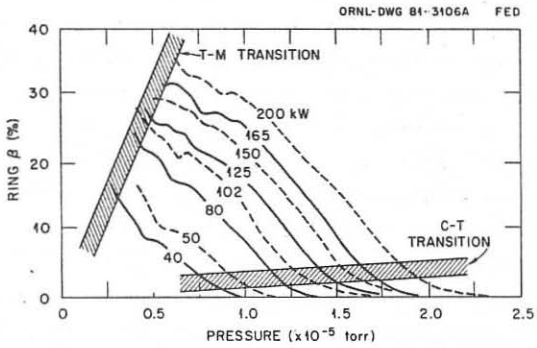
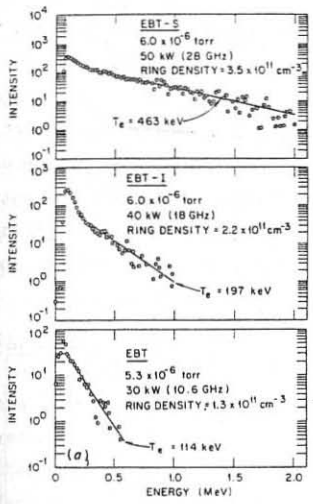


Fig. 2. Variation of the experimental values of ring beta with microwave power and operating pressure indicates the widening of the operating window with power. The C-T and T-M transitions are shown.



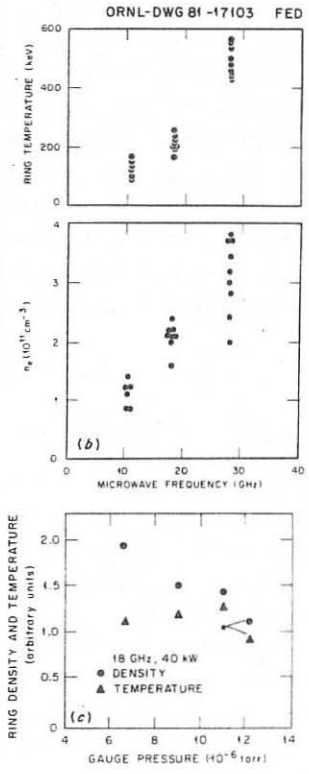


Fig. 3. Experimental observation of ring properties for various operating conditions: (a) hard x-ray spectra; (b) variation of ring temperature and density with frequency (the range of points at each frequency corresponds to a range of experimental conditions); and (c) variation of ring density and temperature with neutral density (pressure).

3.2 Toroidal Core Plasma

The data base for EBTs now covers a broader parameter range (see Table 1). Figure 4 shows the variation of electron densities and temperatures with microwave power and pressure. The electron line density $\bar{n}_e \ell$, as measured by a 9-channel microwave interferometer, increases with power and is almost constant in the T-mode. The electron temperatures, as measured by soft x-ray detectors, increase with power and decreasing pressure. At high power levels, the T-mode operating window is large (see Fig. 2) and $T_e \gtrsim 1$ keV, $n \sim 2 \times 10^{12}$ cm^{-3} have been measured. Spatial profiles of electron temperature from Thomson scattering and soft x-ray are almost flat.[9] The 9-channel microwave interferometer shows that the density profiles become more peaked as the power increases or as the pressure decreases. There exist controlled power/pressure pairs such that scale lengths can be kept constant[10] [data points with $p_o \sim P_\mu^{1/2}$ and data points at the lowest operating pressure $(p_o)_{TM}$].

The measured ion distributions are non-Maxwellian and are fit by multitemperature Maxwellian components.[5,9] The temperatures of these various components (ranging from 20-40 eV to 200-300 eV) are nearly independent of operating conditions, whereas the densities change. The density of the energetic tail component increases with power and decreasing pressure. At present, quantitative ion measurements are difficult because: (1) ions are only weakly heated through electrons, (2) the energy range is too low for good measurements, and (3) charge-exchange losses are substantial ($\tau_{cx} \sim$ few ms).

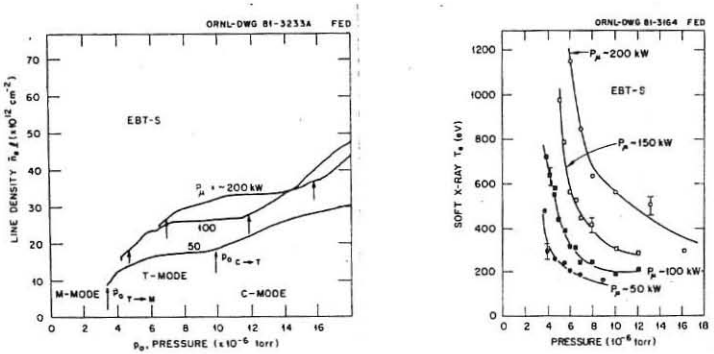


Fig. 4. Variation of electron densities and temperatures with microwave power and pressure.

Measurements of the ambipolar potential with a heavy ion beam probe[24] show that, when the field errors are minimized, there is an almost parabolic potential well in the core plasma. The potential peaks near the radial position of the hot electron rings and is positive (with respect to the wall). It is negative at the center of the plasma. The resulting electric field is radially inward inside the ring, outward outside. The magnitude of the potential well depth increases with power and with decreasing pressure and is observed to vary with the electron temperature;[10] $e\phi \sim 0.6\ T_e$.

The EBT plasma is remarkably clean. The principal impurity is aluminum (the material of the vacuum vessel). Typical $A\ell^+$ densities in the central plasma column are $\sim 10^{-3}\ n_e$. The aluminum density decreases with the charge state, but the temperature increases. $A\ell^{+3}$ temperatures have been observed[29] to be as high as ~650 eV ($\sim e\phi$). This temperature exceeds that expected from E × B motion and implies that an auxiliary method must be present for raising the aluminum ions to these high energies. Aluminum confinement times are found to be smaller than the electron confinement time by several orders of magnitude.[29] The low impurity concentrations results in negligible impurity radiation.

Plasma fluctuations have been measured, and several features have been observed:[30] (1) they are predominantly low frequencies (<200 kHz); (2) the C-T-M mode hierarchy can be correlated with the fluctuation activity, where the fluctuation amplitude decreases at the C-T transition with the formation of the rings and increases near the T-M transition; (3) high frequency fluctuations are generally found outside the rings; and (4) enhanced fluctuations near the T-M transition may have some correlation with the increased high energy ion tail and observed fast multiply ionized aluminum ions.

Steady-state, fast-wave ICRH experiments (auxiliary heating) have been performed at power levels up to 20 kW on EBT-S using an all metal, double Faraday-shielded, one-third (120°) loop antenna located in a cavity midplane.[31] (Typically, the ratio of ICRH power to ECH power $\lesssim$ 10%.) A broadband matching circuit was used covering the frequency range of 10-50 MHz. The experiments have shown:[31] (1) high antenna loading (up to 90%) for majority deuterium (~98%) and minority hydrogen (~2%) plasmas; (2) strongly damped but propagating waves around the torus for $f > 30$ MHz; and (3) production of substantial energetic ion tails. Increasing amounts of ICRH power increase the energetic ion population more than an order of magnitude.[31]

4. THEORETICAL STUDIES

4.1 Stability

The EBT has several features that make the theoretical treatment of its stability difficult because of the presence of high-beta, hot electron rings.[12] The diamagnetic drift frequency of the hot electrons (ω_{dh}) is comparable to or greater than the ion cyclotron frequency (ω_{ci}) and larger than characteristic frequencies of MHD interest. Also, the ring width is only a few hot electron or core ion gyroradii. Thus, the full problem involves multispecies, kinetic, and finite gyroradius effects in 3-D geometry.

During the past several years, stability calculations have evolved with respect to treatment of ring-core coupling effects.[12,32] At present, EBT stability calculations have indicated the existence of several modes which can limit the core beta, core density, and ring density: these are core interchange, the compressional Alfvén wave, and the hot electron interchange.[12,32] A range of models and ring-core coupling have been considered in studying these modes. Results from these studies continue to show:[12] (1) the average minimum-B stabilizes core plasma at low β_{core}, and (2) ring stability requires a sufficient core plasma density [e.g., $n_{cold}/n_{hot} > f(\omega_{dh}/\omega_{ci})$ decreases with increasing ω_{dh}/ω_{ci}]. In addition, an upper core beta stability boundary is present due to either compressional Alfvén or core interchange modes depending on the models used.[32] The plasma is stable against core interchange if[32]

$$\beta_{core} \lesssim \alpha\Delta/R_c \qquad (2)$$

where $\alpha \sim 2$-4, depending on the hot electron distribution function ($\alpha \sim 2$ for a Maxwellian and $\alpha \sim 4$ for a delta function), and R_c is the curvature at the location of the ring. The compressional Alfvén mode[32] limits the core plasma density (which in turn limits β_{core}), and ring density is limited by ring interchange instability[12] at high β_{ring}. At present, both modes (compressional Alfvén or core interchange) indicate a substantial stable finite core beta operating window[12] ($\beta_{core} > 10\%$).

4.2 Transport

The confinement of core plasma electrons in the present experiments has been satisfactorily described with the collisionless

neoclassical transport theory.[10] The neoclassical transport rates[7,18] are determined by drift orbit shift $\Delta x = v_y/\Omega$, where $v_y \sim T/eBR$, $\Omega = \Omega_{VB} + \Omega_{EXB} \sim (T/eBR_c r)(1 + eE_r R_c/T)$, and $E_r \sim \phi/R_E$. For the experimentally observed sign of the electric field, radially pointing inward, $eE_r R_c$ is negative for ions and positive for electrons, thus causing $\Omega \gtrsim 0$ for a class of ions. In the collisionless limit ($\nu_e/\Omega_e < 1$), the diffusion coefficient for electrons is given by[18]

$$D_e \sim \langle \nu_e (\Delta x)^2 \rangle \sim a^2 \frac{n}{A^2 T_e^{3/2}} \left(1 + \frac{R_c}{R_E}\frac{e\phi}{T_e}\right)^{-2} \qquad (3)$$

and this functional is part of all transport coefficients and survives with more refined analysis.[19,20]

The ambipolar electric field builds up to equalize the electron and ion particle losses so that charge conservation and quasineutrality are obtained. However, neoclassical ion transport is complicated by the resonant character of the ion drifts ($\Omega \gtrsim 0$) and by the existence of a high energy ion tail. In addition, ions are only weakly heated by Coulomb collisions and are susceptible to what would otherwise be negligibly small nonclassical effects, such as fluctuations, that can heat the ions to produce a well-confined high energy ion tail.

Within the context of neoclassical theory, transport coefficients for ions[19] (with $E_r < 0$) exhibit collisional ($\nu/\Omega_{VB} > 1$), plateau ($A^{-3/2} < \nu/\Omega_{VB} < 1$), and banana ($\nu/\Omega < A^{-3/2}$) transport regimes. The predictions of the theory (in the collisionless electron regime with plateau ion transport) obtained from the 1-1/2-D transport calculations[20] are in reasonable agreement with the experimental observations when the fluctuation levels are low. However, in cases with higher levels of fluctuations the magnitude of the electric field observed in the experiment is higher than that obtained from theory,[11] suggesting the necessity to consider additional ion losses such as contributions from the high energy ion tail and from impurities (e.g., Aℓ). Experiments[8,10] show a potential well depth ϕ on the order of T_e, but plateau neoclassical theory[20] for purely Maxwellian ions predicts ϕ on the order of T_i. Contributions of non-Maxwellian ion tail and Aℓ impurities to the potential are found to be significant.[11]

A positive electric field is also possible in that the roles of electrons and ions are interchanged. That is, the electrons, rather than the ions, are electrostatically confined in the center. The

equilibrium with $E_r > 0$ would enhance plasma confinement due to scaling with ν_i instead of ν_e.

4.3 Heating

In the present and near-term EBT devices ECH forms the primary energy source for the toroidal core plasma as well as for the hot electron ring. A statistical model for ECH has been developed which includes:[13] 3-D ray tracing and absorption, Budden tunneling for the surface plasma, and wave reflection and depolarization at the cavity walls. Estimates of power deposition in the ring, core, and surface plasma components in EBT-I/S are found to be in reasonable agreement with the experimental measurements.

The hot electron ring is observed to form at the location of second harmonic resonance, and the simple stochastic ECH theories are unable to account for the required second harmonic heating for ring formation.[15] This is because, for a low temperature core plasma (as in the C-mode in EBT-I/S, $T_e \sim 20$-30 eV), the linear second harmonic wave/particle interaction is quite weak and is reduced by a factor $J_1^2(k_\perp \rho_e) \simeq k_\perp^2 \rho_e^2 \sim 10^{-4}$ from that of the fundamental. It is shown that the second harmonic heating is highly pitch angle ($V_\perp/V_\parallel$) dependent and the motion of particles with large initial $V_\perp/V_\parallel$, which are important in ring formation, is superadiabatic rather than stochastic.[15] Detailed calculation of orbits shows periodic energy sloshing in that large energy excursions occur, taking particles initially at ~20-30 eV to almost a keV in a time comparable to one mirror bounce time. Although a small fraction of pitch angle space near $V_\parallel \simeq 0$ is affected by this process, this can be as much as ~50% of the ring electrons and suggests that coherent, long-term wave/particle interaction may be important in producing the ring. After particles scatter into the stochastic region of velocity space, the usual linear second harmonic heating serves to establish the relativistic rings.

4.4 Ring Physics

If the rings can be stabilized against drift instabilities,[3] classical losses should dominate the power requirements. The power absorbed in the ring per unit volume, $P_{\mu R}/V_R$ (where V_R = ring volume), is balanced by losses due to drag cooling of hot electrons on core electrons, pitch angle scattering of the ring electrons, and synchrotron radiation. It is given by[3,15] (in mks units with T in keV)

$$P_\mu/V_R = 5 \times 10^{-38} \frac{n_R n_c \gamma}{(\gamma^2 - 1)^{1/2}} \left(1 + \frac{0.5}{\gamma + 1}\right) + 1.6 \times 10^{-20} n_R B_R^2 (\gamma^2 - 1) \quad (4)$$

where $\gamma = 1 + T_R/511$; n_R, T_R, and B_R are the density and temperature of the ring and magnetic field at the ring location, respectively; and n_c is the toroidal core plasma density near the vicinity of the ring. For ring temperatures characteristic of past and present experiments ($T_R < 1$ MeV), drag losses dominate (decreasing as $T_R^{-1/2}$). At high ring energies ($T_R > 2$ MeV), accelerated ring cooling will occur due to synchrotron radiation. Hence, the resulting loss rate has a broad minimum (near $T_e \sim 1$ MeV) that is bounded by these loss mechanisms.

5. SCALING AND POWER BALANCE

To investigate the scaling and power balance of ring and core plasmas, specific theoretical predictions (classical and neoclassical) are examined and compared with experimental observations. It is shown that the ring power losses are essentially classical,[15,16] and core plasma confinement is dominated by neoclassical electron transport.[8,10]

5.1 Ring Scaling

During the last two decades the production of high-beta, hot electron plasmas with ECH has been amply demonstrated in open and closed geometries.[3] A wide variety of conditions were present in these experiments with an order of magnitude change in magnetic fields (~1-10 kG), ECH frequencies (~6-55 GHz), and hot electron temperatures (~50-1200 keV). An analysis of the data[17] (shown in Fig. 5) from all these experiments (that used single ECH frequency) indicates that the hot electron temperatures do increase with magnetic field strength (or equivalently ECH frequency) and scale length. In particular, they all obey $\rho_{eR}/L \simeq$ constant ($\sim 5\text{-}6 \times 10^{-2}$) scaling[17] (see Fig. 5), where ρ_{eR} and L are the hot electron gyroradius (relativistic) and magnetic field scale length, respectively. This is roughly the value at which conservation of the adiabatic invariant μ begins to break down and indicates that the hot electron temperatures are probably limited by nonadiabatic particle behavior. The ring temperature in EBT is determined by this criterion; only a small variation is observed.

The measurements of characteristic ring times, together with the measurements of the stored energy ($W_\perp$) determine the overall ring power loss. In individual measurements, synchrotron losses are predicted to

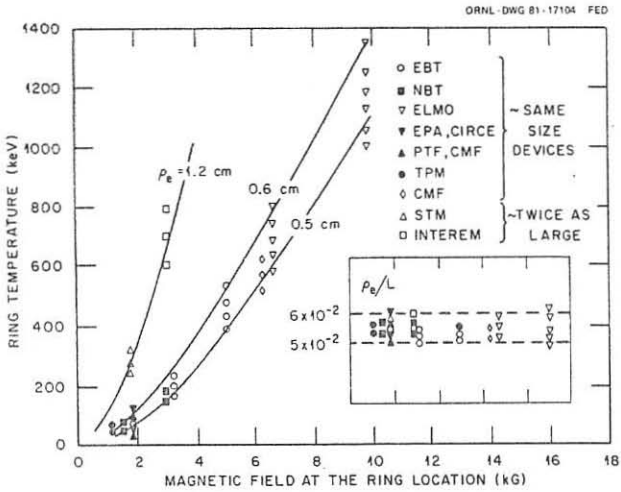


Fig. 5. Data from all ECH hot electron plasmas (ring temperature vs mangetic field) indicate that the ring temperatures fit a simple scaling; $\rho/L \approx$ constant.

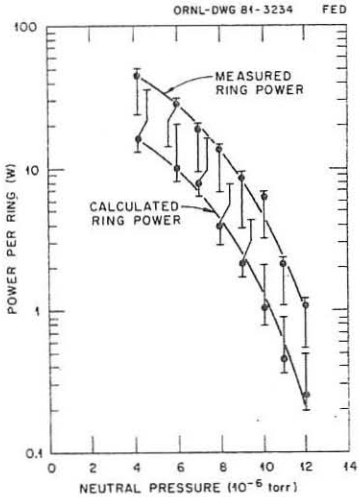


Fig. 6. Measured and calculated ring sustaining power (error bars are shown for both).

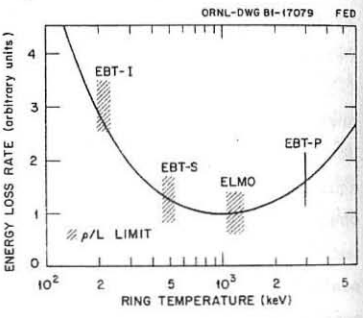


Fig. 7. Variation of ring power loss (normalization constant is $\propto V_R \beta_R B_R^4$) with ring temperature. Shown (hatched) are limits of ρ/L scaling for EBTs and ELMO. (The vertical line is the limit for EBT-P.)

be low and the measurements support this prediction.[27,28] Scattering loss measurements scale with $n_R n_c$ as expected,[16] although additional scattering losses as much as the classical value cannot be excluded.[16] Figure 6 shows the measured and calculated ring sustaining power along with associated error bars. Since the measured values are based on the shortest characteristic ring time (rise of hard x-ray signal), they represent the upper limit. Calculated values are from Eq. (4) and represent the lower limit. Agreement is within a factor of 2-4; uncertainties in the experiment and in the estimates are sufficient to account for this difference.

The ring power loss as a function of ring temperature is plotted in Fig. 7, indicating the broad minimum mentioned earlier. Also shown (hatched) are the limits of ρ_{eR}/L scaling (adiabatic energy limit) for the past (ELMO) and present EBTs; the limit for EBT-P is indicated with a vertical line. All the ECH experiments to date have been operated to the left of the minimum in the energy loss curve where drag losses dominate (only in the ELMO experiment did synchrotron radiation have a significant contribution), and ring energies are limited by the ρ_{eR}/L scaling given in Fig. 5. However, for EBT-P (and an EBT reactor), this limit is above the minimum in the energy loss curve. Thus, the ring temperature in EBT-P should be close to the minimum energy expected from classical processes and is not determined by the adiabatic limit.[17] However, if enough power is provided to overcome the synchrotron radiation losses, it may be possible to vary the ring temperature and observe scaling characteristics in this regime as well.

5.2 Core Plasma Scaling

The EBT-S experiments now cover a broader parameter range and validate, in more detail, the hypothesis of neoclassical electron confinement.[8,10] Because the power flow in EBT is through electrons, the neoclassical theory has only been validated for electrons.

An empirical finding from the experiment is that $e\phi/T_e$ (~0.6) is nearly a constant and is only weakly dependent on power. Also, the scale lengths can be kept constant for controlled $p_o(P_\mu)$, as discussed earlier. With these simplifying assumptions, expressions can be derived for a neoclassical relationship between electron density, temperature, and the microwave power. This yields[10]

$$P_\mu \sim n^{2/T_e^{1/2}} \sim (n\ell)^{2/T_e^{1/2}} \quad . \tag{5}$$

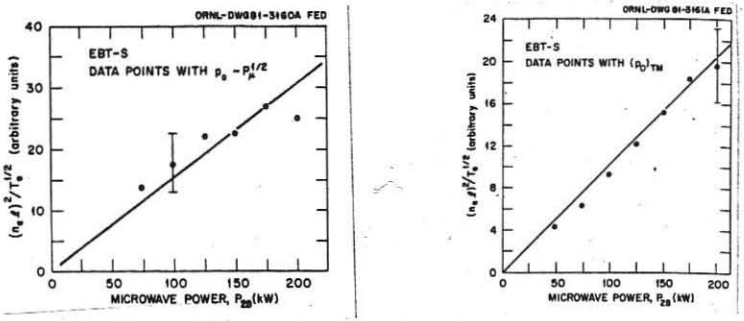


Fig. 8. Relationship between microwave power and experimentally measured electron line density ($n\ell$) and electron temperature (T_e) indicates that $P_\mu \sim (n\ell)^2/T^{1/2}$ for data points with constant scale lengths and $e\phi/T_e$.

The comparison of the experimental values of $(n\ell)^2/T_e^{1/2}$ (where $n\ell$ and T_e are the results of the direct measurements from the microwave interferometer and soft x-ray, respectively) with microwave power P_μ is shown[10] in Fig. 8. It indicates that the electron power balance is neoclassical within the experimental error bars.

Because the neoclassical transport coefficients[18] for particles and energy have the same functional dependence on plasma parameters, the ratio of the energy confinement time to the particle confinement time $\tau_E/\tau_P \sim$ constant (for constant scale lengths and $e\phi/T_e$). Experimentally this is also observed.[10] The density and electron temperature both increase with power[10] ($n \sim P_\mu^{0.6}$, $T_e \sim P_\mu^{0.4}$) and are consistent with neoclassical predictions.

6. EBT-P EXPERIMENT AND TECHNOLOGY DEVELOPMENT

The successful resolution of the key physics issues of the EBT concept is the primary objective of the EBT-P program.[22] These issues can be summarized as follows: (1) ring scaling – power balance, production and control, stability, and coupling between the ring and core plasmas; (2) transport scaling (especially those of ions) – dependence of confinement on magnetic field, density, and temperatures, ambipolar potential, aspect ratio, etc.; (3) beta limits on core plasma – dependence of core beta on operating parameters of the ring and core plasma; and (4) physics and technology of high power

heating. The expected performance of the EBT-P is scaled from the present experimental results and theoretical predictions discussed in previous sections. The physical dimensions and expected range of plasma parameters are listed in Table 1.

The two principal technology development requirements for EBT-P are the high current density superconducting magnets and 60-GHz gyrotrons. The 60-GHz gyrotron basic design is very similar to the 28-GHz gyrotron now used on EBT-S, which is now routinely operated at 200 kW, cw. The first 200-kW, 60-GHz development gyrotron has operated for 0.1 ms at over 50% efficiency. (Recently 60 ms, 125 kW has been achieved.) Two superconducting development magnets (a NbTi pool-boiling metastable magnet with design value 7.4 T and 10,000 A/cm^2) have exceeded the design criteria of 7.4 T by 6%.

7. REACTOR PROJECTIONS

Reactor studies have been made and are continuing, and they show broadly that an EBT reactor is an exciting prospect though clearly there are uncertainties and physics and technology issues to be resolved.[21] To predict the plasma properties in a reactor, experimental data discussed in previous sections require large extrapolations. However, extrapolations based on the observed dimensionless parameter scaling (with the exception of core beta) offer some plausibility.

The EBT-P experiment is expected to address most of the reactor issues in transport, stability, heating, and technology. One area of concern in a reactor, based on the present theories, is the coupling of the ring power balance to the core beta limits ($\beta_{core} \sim \Delta/R_c$), in that minimizing ring power requires thin (small Δ) rings whereas high beta (~fusion power density) requires thick (large volume) rings. Results from a parametric study[33] that include boundaries of the operating regime for a reactor indicate that the overall reactor $Q_{electric}$ value ranges from ~2 to ~50, depending on the uncertainties. Detailed studies are under way to optimize reactor performance with respect to beta, power density, wall loading, etc.

Aside from the beta issue, several techniques have been studied to enhance reactor performance. These include:[21] (1) the use of supplementary [aspect ratio enhancement (ARE), symmetrizing (SYM), etc.] coils[34] to improve confinement and/or stability and reduce

overall device size; (2) the control of ambipolar potential[11] (and its sign, i.e., the positive electric field) to enhance confinement and possibly to allow the use of alternative fuels in a reasonably sized device; (3) the possibility of "fundamental ring" mode heating[7] to reduce microwave frequency requirements by a factor of 2; and (4) the use of ion rings[3] (if proven to provide min-B stability) to reduce the ring power requirements. (See Ref. 21 for details.)

8. SUMMARY REMARKS

During the last couple of years, substantial progress has been made in the EBT program of experiments, theory, technology development, and reactor studies. The discussions in this paper have been limited to those areas which have significant new results and/or important implications. The following points summarize these discussions:

(a) Operation at power levels through 200 kW of 28-GHz microwaves shows that (1) the EBT-S experiments now cover a broader parameter range ($T_e \sim$ 100-1100 eV, $n \sim 0.5\text{-}2.5 \times 10^{12}$ cm^{-3}, $\beta_{ring} \sim$ 10-40%, etc.), (2) the electron transport continues to scale neoclassically ($P_\mu \sim n^2/T_e^{1/2}$, $\tau_E/\tau_P \sim$ constant, $n \sim P_\mu^{0.6}$, $T_e \sim P_\mu^{0.4}$, etc.), and (3) the stable operating window, the T-mode, continues to increase with increasing microwave power.

(b) The experimental and theoretical understanding of ring power balance has advanced significantly: (1) the power losses (synchrotron, scattering, and total power) scale classically, and the measurements agree with the estimated value to within a factor of 2-4 (uncertainties in the experiment and in the estimates are sufficient to account for this difference); and (2) in all ECH devices the ring temperatures obey ρ_{eR}/L scaling, and EBT-P will be the first experiment not to be constrained by this limit.

(c) The technology of coupling steady-state fast-wave ICRH into the EBT plasma has been demonstrated.

(d) The analysis of a large number of modes and ring core coupling continues to find that: (1) the $d\ell/B$ (minimum-B) stabilization criteria is appropriate, (2) a sufficient cold plasma density stabilizes the core interchange, and (3) a substantial, stable, finite-beta operating window is available ($\beta_{core} \gtrsim 10\%$).

(e) At the present, the coupling of the ring power balance to the core beta limits is a concern in a reactor.

(f) Technology development for EBT-P is progressing well; operation of a 60-GHz development gyrotron at 200 kW for 0.1 ms (at 125 kW for 60 ms) and operation of the two EBT-P development magnets at the design field of 7.4 T are considered to be significant.

ACKNOWLEDGMENT

The overview material presented in this paper covers the work of the entire EBT group at ORNL, and the author would like to thank them for their valuable input and suggestions. Most of the experimental results from the EBT-S are very recent and have not yet been published elsewhere. In this respect, inputs by F. W. Baity, L. A. Berry, G. R. Haste, D. L. Hillis, and T. Uckan are gratefully acknowledged.

REFERENCES

1. R. A. Dandl et al., ORNL/TM-3694 (1971); R. A. Dandl et al., Plasma Physics and Controlled Nuclear Fusion Research 1974, Vol. II, 141 (1975).
2. R. A. Dandl et al., Plasma Physics and Controlled Nuclear Fusion Research 1968, Vol. II, 435 (1975); R. A. Dandl et al., Plasma Physics and Controlled Nuclear Fusion Research 1971, Vol. II, 607 (1972).
3. N. A. Uckan, ed., EBT Ring Physics, Proceedings of Workshop, CONF-791228, Oak Ridge (1979).
4. D. B. Nelson and C. L. Hedrick, Nucl. Fusion 19, 283 (1979); G. E. Guest, C. L. Hedrick, and D. B. Nelson, Phys. Fluids 18, 871 (1975).
5. R. A. Dandl et al., Plasma Physics and Controlled Nuclear Fusion Research 1978, Vol. II, 365 (1979); R. A. Dandl et al., ORNL/TM-6457 (1978).
6. L. A. Berry, C. L. Hedrick, and N. A. Uckan, ORNL/TM-6743 (1979).
7. M. Fujiwara et al. (NBT Group) and F. W. Baity et al. (EBT Group), Plasma Physics and Controlled Nuclear Fusion Research 1980, Vol. I, 845 (1981).
8. N. A. Uckan et al., Status of EBT Research, ORNL/TM-8006 (to be published).
9. R. J. Colchin, Bull. Am. Phys. Soc. 26, paper 1A2 (1981); G. R. Haste, Bull. Am. Phys. Soc. 25, 921 (1980); L. Bighel and J. A. Cobble, Phys. Rev. Lett. 46, 430 (1981).
10. L. A. Berry and T. Uckan "Confinement Scaling of Core Plasma Electrons in EBT-S" (submitted for publication); T. Uckan et al., ORNL/TM-7897 (1981).
11. N. A. Uckan, ed., Ambipolar Potential Formation and Control in Bumpy Tori and Mirrors, Proceedings of Workshop, CONF-810511, Oak Ridge (1981).
12. N. A. Uckan, ed., EBT Stability Theory, Proceedings of Workshop, CONF-810512, Oak Ridge (1981).

13. D. B. Batchelor, ORNL/TM-6320 (1978); D. B. Batchelor, Plasma Phys. 22, 41 (1980); H. Weitzner and D. B. Batchelor, Phys. Fluids 23, 1359 (1980); D. B. Batchelor, ORNL/TM-7001 (1981).
14. S. K. Borowski, N. A. Uckan, E. F. Jaeger, and T. Kammash, Nucl. Fusion 20, 177 (1980).
15. N. A. Uckan et al., Plasma Physics and Controlled Nuclear Fusion Research 1980, Vol. I, 831 (1981).
16. G. R. Haste, Bull. Am. Phys. Soc. 26, paper 6G8 (1981).
17. N. A. Uckan, Bull. Am. Phys. Soc. 26, paper 6G15 (1981).
18. L. M. Kovrizhnykh, Sov. Phys. JETP 29, 475 (1969); D. A. Spong et al., Nucl. Fusion 19, 665 (1979).
19. D. A. Spong and C. L. Hedrick, Phys. Fluids 23, 1903 (1980); R. D. Hazeltine and P. J. Catto, Phys. Fluids 24, 290 (1981).
20. E. F. Jaeger and C. L. Hedrick, Nucl. Fusion 19, 433 (1979); E. F. Jaeger et al., Phys. Rev. Lett. 40, 866 (1978); E. F. Jaeger et al., Phys. Rev. Lett. 43, 443 (1979); E. F. Jaeger et al., Nucl. Fusion 19, 1627 (1979); E. F. Jaeger et al., ORNL/TM-7558 (1980).
21. N. A. Uckan, Nucl. Eng. Des. 63, 271 (1981); N. A. Uckan et al., Plasma Physics and Controlled Nuclear Fusion Research 1978, Vol. II, 343 (1979).
22. See EBT-P Proposed Reference Design Report, ORNL/TM-7191 (1980).
23. R. R. Dominguez and H. L. Berk, Phys. Fluids 21, 827 (1978).
24. F. M. Bieniosek, Study of Plasma Confinement in ELMO Bumpy Torus with a Heavy-ion Beam Probe, Ph. D. Thesis, Rensselaer Polytechnic Institute, Troy, New York (1980).
25. T. Uckan et al., in Ref. 11, p. 205 (1981).
26. B. H. Quon et al., ORNL/TM-6075 (1977).
27. T. Uckan, J. Wilgen, and L. Bighel, Bull. Am. Phys. Soc. 25, 832 (1980).
28. N. A. Uckan et al., ORNL/TM-7687 (1981).
29. R. K. Richards and E. F. Jaeger, in Ref. 11, p. 167.
30. L. Bighel, G. R. Haste, and A. Komori in Ref. 12, p. 75.
31. F. W. Baity et al., in Ref. 11, p. 441.
32. D. A. Spong, in Ref. 12, p. 33; J. W. Van Dam et al., ibid., p. 97; D. A. Spong et al., ibid., p. 115; K. T. Tsang and C. Z. Cheng, ibid., p. 141.
33. N. A. Uckan, D. A. Spong, and D. B. Nelson, ORNL/TM-7857 (1981).
34. L. W. Owen and N. A. Uckan, ORNL/TM-7729 (1981); and EBT Reactor Magnetics and Particle Confinement, J. Fusion Energy (to be published).

CONTROLLED NUCLEAR FUSION IN THE USSR

by E.P.Velikhov,
Kurchatov Institute of Atomic Energy

The USSR controlled nuclear fusion research programme is based on the following assumptions:

Today there is an approach that should enable us to develop and build a fusion reactor and to guarantee with reasonable assurance its operation and its performance parameters, relying upon up-to-date scientific and technological data. This is the "Tokamak" concept based upon several well-established experimental and theoretical principles (stability and equilibrium - Leontovich, Shafranov); neoclassical diffusion and heat conduction - (Pfirsch, Schlüter, Shafranov, Sagdeev, Galeev) and also upon some empirical relations scalable to reactor conditions (ohmic heating - regime confinement - Artsimovich et al., pressure ß limitation, impurity behaviour, magnetic thermal insulation empirical scaling laws - the so-called Alcator scaling and its revised versions, etc.
We have already gained a limited but substantial engineering experience in operating the main reactor systems (auxiliary heating techniques, long-duration DC operation superconducting magnetic systems, impurity control, etc.).

The goals of our present programme are the following:

1. Further elaboration of physical mechanisms, in particular, of those importants in reactor - close conditions (collisionless regime with unimportant ohmic heating contribution, etc.).

2. Development of experimental facilities essential for reactor - quality plasma research including conditions of essential fusion - power heat production.

3. Testing of the basic technical principles underlying the reactor concepts, i.e. those of INTOR.

We are well aware of the probability that some new, better than tokamak, concepts may arise in the course of further research progress. Nevertheless, we are confident that the up-to-date fusion state of art and its importance in the implementation of the power productinn programme justify the development and construction of an INTOR-type test fusion reactor with the objective to demonstrate the technical feasibility of controlled nuclear fusion in early 1990s. In this respect we agree with the decision of the IAEA International Controlled Nuclear Fusion Council.

On the other hand, the tokamak, regarded as a power plant, presents some limitations and disadvantages that are apparent already today. They have to do with its topology itself, with limited q and ß values, etc. Therefore, we pay considerable attention, as far as we can, to further physical research in the field of open-end systems (ambipolar and multiple-mirror) and of stellarators, although the latter may indeed be regarded, from the point of view of engineering, as a tokamak modification. The up-to-date state of these branches of research may be described as clarification of basic physical mechanisms. Simultaneously, we proceed with physical research concernig plasma confinement and heating in compact tori (Kurtmulaev), the use of pulsed injectors (Skvortsov) and DC injectors (Morozov) together with some other schemes

requiring physical proof of the basic concept involved.

In the field of the so-called inertial confinement or, in other words, microexplosion approach we consider it necessary to postpone the choice of the main approach until various drivers (i.e. lasers, super-fast condenser-bank storage, inductive storage) are well compared from the point of view of both pure physics and technical feasibility. From the point of view of physics this choice depends upon establishing the feasibility of real-size target ignition and burning as a function of power (10-1000 TW) and also of the start energy input (10^5-10^8 J). At present, along with certain physical investigations, the necessary experiemental techniques are being developed.

A. Magnetic confinement

1. The Tokamak concept

In the traditional field of quasistationary plasma state in tokamaks we are presently able to predict plasma parameters with adequate reliability only in the highest electron density ohmic heating regime which exhibits energy losses close to neoclassical theory results. With decreasing density the anomalous electron heat conduction starts prevailing in the energy losses. No theory of anomalous transport mechanisms in tokamaks has yet been developed. Therefore any up-to-date predictions concerning the main operation regime (moderate density, high-power auxiliary heating) are based upon scaling up the modern-tokamak empirical relations.

The main trend in the anomalous electron heat conduction behaviour is its decrease with growing plasma density

($\chi \sim \frac{1}{n_e}$, $\tau_{Ee} \sim \bar{n}_e$). Recent T-10 and T-11 experiments have revealed a strong dependence of the electron thermal conductivity on the torus major radius R and on the r/R ratio. The electron heat-conduction scaling law, derived from those experiments, is fairly consistent with the $\chi_e = n_e \chi_e$ experimental data at other facilities in the ohmic heating conditions (Fig. 1). The dependence of χ_e on the electron temperature is yet not clear.

The available experimental evidence seems to suggest this dependence to be weak. The T-11 data is in fair agreement with $\chi_e \sim \sqrt{T_e}$ law. According to some T-10 preliminary results on microwave plasma heating [2], $\tau_{Ee} \sim T_e^{\alpha}$ with $-0.5 < \alpha < 0.5$. One can expect further T-10 experiments, with higher heating power and longer microwave pulse duration, to provide more accurate data concerning this dependence. Note that a slow χ_e rise with increasing temperature (e.g. $\chi_e \sim \sqrt{T_e}$) would not in the least frustrate the tokamak reactor prospects.

During the last year the problem of plasma diffusion in a tokamak had become much clearer. Experiments on the T-11 device [3] have confirmed the $D_e \sim I/n_e$ dependence and have shown the χ_e/D_e ratio to remain roughly constant over a wide experimental condition range, amounting to~4-5 in hydrogen plasma. Computer simulations of the $n_e(r)$ profile time dependence in T-10 and TUMAN-3 sawtooth oscillation regimes have revealed the important role of plasma pinching in the plasma-column central part. They suggest nearly neoclassical pinch velocities at moderate densities [4]. The T-10 and

FT-1 experiments have shown that the rate of impurity ion diffusion depends but slightly on the ion mass and charge and nearly coincides with the main plasma diffusion rate [5,6]. Measurements of the direction and magnitude of the electric field in plasma were performed at the T-10 [5], FT-1 [6] and TM-4 [7] facilities. These data are important in order to develop anomalous transport models. According to the experimental results obtained the electric field sign differs in different regimes. Fig.2 presents the electric potential profile measured in the TM-4 tokamak using a 50 keV Cs^+ probing beam. Here the electric field sign in most of the plasma sheath volume corresponds to predominant ion loss.

Due to the favorable dependence of τ_{Ee} upon plasma density, namely $\tau_{Ee} \sim \bar{n}_e$, and the resulting $n_e \tau_{Ee} \sim n_e^2$ scaling, one should evidently find most efficient the reactor regime with moderate temperature and the highest possible density, the latter being defined by the plasma pressure limit

$$\beta_p = \frac{8\pi \langle n_e (T_e + T_i) \rangle}{(I_p / ca)^2} \leq \frac{R}{a}$$

Assuming β_p = const, the reactor plasma density and ultimate density would increase as I_p^2. Therefore the highest n_e and $n_e \tau_E$ values should be attainable at the lowest possible values of the safety factor $q(a) = \frac{5a^2 B_T}{R I_p}$. The T-10, T-11, T-7, TMG and TUMAN-3 experiments have shown that it was easy to achieve low MHD perturbation - level and fairly good confinement regimes at q(a) $\simeq$ 1,3-1,4. The prospects of usable ultra-low q(a) $\simeq$ 1,3-1,4 regimes are still vague. In the T-11 tokamak 1 the transition from q(a) $\simeq$ 2,5 to

$q(a) \simeq 1{,}3\text{-}1{,}4$ resulted in a considerable intensification of MHD plasma activity and a 2,5-fold reduction of τ_E . The τ_E decrease turned out to be more serious than expected from the $\tau_{Ee} \sim q(a)$ scaling resulting from q(a) = 2-4 regime data, obtained at the same facility. In T-11 fast neutral beam injection at $q(a) \simeq 2{,}5$ did not reveal any energy confinement time deterioration for $\beta_p \sim \frac{R}{2a}$ and $\langle \beta_T \rangle \simeq 2\%$ [1].

An important problem of a tokamak reactor is indeed impurity control. The use of a divertor is expected to substantially alleviate its solution. The efficient operation of a poloidal diverter with either two nulls or a single null (drop-like configuration) was demonstrated in T-12 experiments [9]. The efficieny of of heat and particle removal into the divertor volume was shown to be close to unity. The divertor switch-on reduced substantially the influx of high-Z impurities into the plasma. Tests of a toroidal convertor are underway at the TO-2 tokamak.

One can limit the impurity influx in the absence of any divertor by an appropriate choice of wall material and also by controlling the impurity ionization state, the hydrogen re-cycling and wall plasma temperature by means of discharge and heating. A substantial reduction of high-Z impurity influx due to wall plasma cooling with low-Z impurities was demonstrated in T-10 tokamak.

The risk of plasma contamination with impurities can be dimished by a proper choice of first wall material. Most present tokamaks employ stainless steel as discharge chamber material and graphite as limiter material. In the T-11 facility

both the first wall and limiter are made of molibdenium. Experiments are under way with the TMG device having a graphite discharge chamber. There is experimental evidence that rather clean plasmas ($Z_{off} \approx 1$, low radiation losses) can be obtained in modern tokamaks by means of efficiently cleaning the walls of the weakly-bound impurity and by programming rationally the discharge, without using divertors. However, one should bear in mind, that the transition from currently used tokamaks to the reactor should entail a substantial increase of the heat power flux through the plasma boundary (from 5-10 to 30-50 W/cm^2). The behaviour of materials at high thremal stresses will be studied at the material testing facility T-3M.

The next major physical problem concerns the behaviour of plasmas with auxiliary heating power much in excess of the ohmic heating power. In fact any auxiliary heating represents a substantial plasma perturbation with the appearance of additional momentum, non-equilibrium phase-space distribution, inhomogeneous heat release etc.

We have now two sets of experimental results in essential non-ohmic heating regimes, namely, the electron cyclotron resonance heating and the neutral beam injection heating data. In both cases the auxiliary heating power could considerably (3 to 10 times) exceed that of ohmic heating.

ECRH experiments are performed at the T-10, FT-1 and TM-4 tokamaks. At the T-10 facility [2] four 3.6 mm wave-length gyrotrons are used. Each gyrotron has a nominal power of 200 kW. In experiments with ECRH at the first cyclotron harmonic (30 kG resonance magnetic field) a considerable decrease

in ohmic heating power (from $\sim$300 down to $\sim$ 150 kW), an increase in ion temperature and a certain reduction in plasma density (Fig. 3,4) were observed during ECRH.

The ECRH experiment at the FT-1 facility [8] involved microwave input from the high magnetic field side (through the torus inner wall). Such a power input technique made it possible to achieve high wave absorption one way passage through the plasma. With inside placed microwave input it was possible to achieve efficient ECRH not only at lower than critical densities $n_e < n_{ec}$ with $\omega_p < \omega_{ce}$ (as was the case with the outside placed microwave input) but also at super-critical densities (up to $n_{e\,max} \simeq 3 n_{ec}$).

At the T-10 device, we have started experiments on heating plasmas with magneto-acoustic waves at frequencies close to the ion cyclotron frequency. In the well-known T-11 experiments the injection power 0.6 MW exceeded by an order of magnitude the instantaneous ohmic heating power and the plasma regime was relatively non-collisional.

In both cited groups of experiments the ion energy losses were in good agreement with neoclassical theory, while the electron energy losses were well described with Eq.1. However, several new physical phenomena emerged as described in papers presented to the conference.

An important technological development was the successful test of the T-7 device, being the first tokamak with superconducting NbTi magnetic winding. Experiments in this tokamak are underway with 20 kG toroidal field and 200 kA plasma current.

The next major step in the Soviet Union's CNF programme will involve building the T-15 facility to achieve plasma

close to breakeven. Using microwave and fast neutral beam heating in T-15 it is expected to get a plasma with $n_e \sim 10^{14}$ cm^{-3} density and $T_i(o) \sim$ 10 keV ion temperature. The ohmic heating regime is expected to provide $n_e \tau_E \sim 10^{14}$ cm^{-3}.

One can hope that the successful implementation of this step would allow to determine the reactor critical size.

In the "classical" tokamak discharge there is no thermal--insulating vacuum layer between the plasma column and the wall. Consequently we regard as very interesting attempts to create such a layer by detaching the plasma from the wall, e.g. due to minor-radius adiabatic compression. The first demonstration of a substantial (one order of magnitude) improvement in thermal insulation by this technique was achieved in TUMAN-2 facility. Further experimental results achieved at TUMAN-2A device and presented to the present conference have shown that the thermal insulation phenomenon depended to a great extent on detachment velocity. We are planning to go on with this research at the new TUMAN-3 device which has already yielded some results. Besides, adiabatic compression is a very attractive method of tokamak plasma heating, at least in experimental devices meant for physical research. Today there is no other known heating method not only entailing no unwanted effects of the impurity influx type, but also resulting in prolonged energy confinement. Therefore the widening of adiabatic compression application to include breakeven plasmas looks very attractive. Perhaps the combined detachment from walls and adiabatic heating will make it

possible to produce fusion-condition plasmas. As shown at the Kurchatov Institute of Atomic Energy [10], this could be achieved in tokamaks with fairly high magnetic field, since the energy input into a breakeven experiment should be inversely proportional to the fourth power of magnetic field intensity.

Evidently, the mechanical and thermal properties of real materials should limit this tendency, resulting in the existence of an optimal magnetic field making both the toroidal field energy and the adiabatic compression power minimal. According to calculations performed at the Kurchatov Institute of Atomic Energy, for an experiment with fusion power equal to energy loss power the optimal field ranges from 10 to 14T. This corresponds to a 70 MJ toroidal field energy and a 10^{10} W driver power. The experiment scheme, optimal in respect of minimizing both size and stored energy, comprises combined major and minor-radius compression due to the rise of both the toroidal and poloidal fields. Fig.5 presents parameters of a possible breakeven experiment in a high-field tokamak with plasma adiabatic compression. The parameters were proposed in our paper to the Brussels conference [11] using computer results. A plasma of nearly the T-10 device size (major radius of about 1 m, miner radius of 32 cm) with something around $5 \cdot 10^{13}$ cm^{-3} numerical density should be produced in a relatively low magnetic field (2 T) and heated up to about 1 keV by means of neutral injection and (or) ion-cyclotron heating (with the power of about 1 MW). After being heated the plasma must be compressed with the rising toroidal field (2.5-fold

field rise) and move inwards along the major radius. After compression the plasma parameters should be as follows: major radius-41 cm, minor radius-1 cm, density - over 10^{15} cm^{-3}, temperature - 7÷10 keV. The plasma current will be around 1 MA with 12.8 T toroidal field. The computer simulation indicates that a deuterium-tritium plasma, with such parameters, should produce fusion energy in amounts comparable with plasma energy losses. Therefore in such experiments one could expect to observe effects related to a multi-megawatt intense nuclear fusion reaction in the plasma.

After the Brussels conference the Efremov Research Institute of Electrophysical Devices together with the Kurchatov Institute of Atomic Energy have performed physical - engineering studies to explore the technical feasibility of the proposed experiment and to specify the technological-engineering schemes of all the device subsystems. The main results of this work ware reported at the Conference on Engineering Problems of Thermonuclear Reactors, held in Leningrad in mid-1981.

Fig.6 presents the device schematic. In order to reduce the voltage over the toroidal field winding during adiabatic compression this winding was made of 32 single-turn sections. The peak current in the winding is 27 MA, the peak field on the conductor being 21.2 T. The poloidal field winding is so designed that the magnetic field of the inductor is used not only for current excitation but also for plasma column compression along the major radius. The toroidal and toroidal power supply is of inductive storage type. The largest inductive store, feeding the toroidal field windings, is a torus

located right under the tokamak. It is able to supply 150 MJ to the load at $1.3 \cdot 10^{10}$ W peak power. For better understanding of the device systems engineering problems, two mock-up experiments are underway in the Kurchatov IAE.

The TM-200 facility (Fig.7) was used to test a circular cross-section copper-conductor toroidal magnetic system. An up to 17T magnetic field was achieved in this system. At present a 1:10 mock up of the toroidal magnet is being manufactured. This mock-up comprises all design features adopted for the above described high-field tokamak with plasma adiabatic compression (Fig.8). To properly scale thermal conditions the magnetic field pulse is to be shortened 100 times. The magnetic field strength and all structural material specifications will be the same as in the real-size project. The slide shows the mock-up toroidal winding bandages.

The recently launched second mock-up experimental device T-13 (Fig.9) is intended to study the physical problems involved in plasma column formation using a magnetic limiter in a sophisticated - shape discharge chamber and also in plasma displacement along the major radius.

Fig.10 presents the T-13 tokamak set-up. The elongated camera shape together with special movable poloidal field coils make it possible to prepare an either round or elongated cross-section plasma column located at wish anywhere between 40 cm and 87 cm major radii. The toroidal field at 40 cm major r-dius amounts to 17 kG. The T-13 device should also serve to solve other physical problems, in particular, to investigate the dependence of the energy confinement time on the

major radius of the plasma column.

Such is the programme of tokamak research in the USSR. Fig.11 presents a comprehensive comparison of plasma column relative size in the above mentioned tokamaks.

II. Open-end systems

In principle open-end traps possess several substantial advantages over closed ones:

$\beta \sim 1$ attainable;

DC operation possible;

less sensitive to impurities;

easier manufacture and maintenance.

All this justifies the up-to-date prevailing evaluation of open-end traps as second in priority (after the tokamaks) promising approach to the magnetic confinement fusion reactor. At the same time, unlike the situation with tokamaks, the bulk of physical information about plasma behaviour in open--end systems is far from being sufficient to guarantee the final goal achievement, making use of any one of the known trap types: ambipolar, centrifugal, multi-mirror, etc. Each of these systems has a number of undoubtable potential advantages but there are also quite a number of obscure points concerning their operation, the extrapolation scale from the existing systems to reactors often amounting to several orders of magnitude. Consequently, during the recent years several large open-end systems were and are being built in the USSR. Provided these devices reach nominal plasma parameters*,

---

* Unfortunately, this reservation is well founded there having been too many open-end systems in history, that had never attained nominal specifications

they will make it possible to simulate with fair scaling the plasma behaviour in reactor-size systems.

Let us start with ambipolar traps proposed by Dimov and his colleagues several years ago [12]. At present, the Institute of Nuclear Physics in Novosibirsk is completing the construction of the AMBAL facility. The photograph of AMBAL at the assembling stage is shown in Fig.12. The main specifications of the device are given in Table 1 (Fig.13). According to several plasma-state dimensionless parameters non-dimensional parameters characterising the plasma state the AMBAL device is close to the ambipolar thermonuclear fusion reactor. One of its particular features is a high ratio of the electron temperature T_e over ion temperature T_i in the end-on plug mirror. This ratio $(T_e/T_{i\ end}) \approx 5 \cdot 10^{-2}$ is close to the expected reactor value $(T_e/T_{i\ end}) \simeq 10^{-1}$. In current experiments the $T_e/T_{i\ end}$ ratio with satisfactory longitudinal confinement regimes have never exceeded 10^{-2} ⌘.

The important role of the $(T_e/T_{i\ end})$ ratio is due to the fact that, according to the simpliest physical considerations, high $(T_e/T_{i\ end})$ values favour the growth of cone instabilities. At the same time the admissible microfluctuation level limitations are very severe due to the fact that in a fusion reactor the microfluctuation contribution to ion scattering becomes comparable with Coulomb collisions already at $\frac{W}{nT} \sim 10^{-8}-10^{-9}$, with W representing the fluctuation energy level.

⌘ The high value of T in the AMBAL device is due to the relatively small volume of the central cell of the tandem mirror. With regard to this point AMBAL differs considerably from TMX in which the plasma volume in the central cell is 5 times larger.

Note, that up-to-date ambipolar reactor projects were based upon the assumption of purely Coulomb particle losses in the plug mirrors. Hence it would be reasonable to try to take into account the virtual microturbulence effects, at least phenomenologically. To do this one could, for instance, introduce an effective collision frequency

$$\nu = A\nu_{\text{Coulomb}}$$

instead of the Coulomb collision frequency ν_{Coulomb}, with $A > 1$[*]. A value of A = 10 seems to be critical for the reactor feasibility. However, it would be interesting to establish the upper microfluctuation level at which the reactor could still "survive".

Microfluctuation effects are also vital for the "thermal barriers" idea proposed in Livermore two years ago [13]. However, in this case the main contribution is likely to be due to streaming-type and "anisotropic"-type instabilities instead of the cone instability.

It is in order to resolve this problems experimentally that the AMBAL facility is being built.

Next in importance is a group of physical problems concerning radial plasma losses. Until recently the reactor concepts envisaged that MHD-plasma stability would be maintained due to the use of magnetic wall-type axially asymmetric magnetic fields, i.e. in the same way as in ambipolar trap mock-ups, already existing or under construction. Soon after the ambipolar trap idea was publisished it was remarked [14] that the

---

[*] In the same way as in the pseudoclassical theory of transport phenomena in tokamaks.

magnetic system asymmetry could result in considerable radial plasma losses from the central cell. The main contribution to the losses turned out to be due to the so-called "resonance particles". This term denotes particles whose leading center is turned around the magnetic axis over a $\Delta\varphi$ angle close to $(k + \frac{1}{2})$ in the course of one mirror-to-mirror transit. The rotation is due to the electric and gradient drifts, k being an integer (k = 0,1,2...). The lack of axial symmetry results in resonance-particle radial "random walks", which could greatly exceed the Larmor radius. Fig.14 illustrates the k = 0 resonance particle trajectory shape as projected to the trap equatorial plane. Resonance particle collisions result in neoclassical-type losses. Estimates show that such losses may become inadmissibly large unless special measures are taken. The special measures mean a choice of the axial-asymmetric mirror geometry which would considerably reduce radial walks. In principle, "good" mirrors do exist, but it is still not clear whether they can be constructed by means of sufficiently simple external coils.

Recently, V.V.Arsenin and A.V.Timofeev suggested a radical solution involving the use of totally axial-symmetric systems [4]. Fig.15 shows one of the "Arsenin - trap" versions, the plasma MHD stability being ensured due to a pair of Andreoletti traps provided in both end-on regions of the system. Another version (Fig.15) comprises a sufficiently long plug trap together with an additional steep no-minimum-B mirror filled with low pressure plasma. The additional trap ensures stability against shifts of the plasma column as a

whole. The higher flute modes should be suppressed due to finite Larmor radius effects. The near future will show to what extent such systems will be apt to guarantee MHD stability and how practical they are.

One should recall here another loss mechanism, which aroused considerable interest 15-20 years ago, but which for some obscure reason is almost never mentioned today in the course of parametric evaluation of open-end-trap reactors. I mean the so-called "universal" instabilities of inhomogeneous plasmas which may lead to Bohm diffusion coefficients. Such instabilities are particularly dangerous in long systems with straight field lines, which is just the case with the ambipolar trap central cell. It is not unlikely that their stabilization would require that some shear be provided. The latter may be achieved by passing an electric current along the system axis (at some risk of having to cope with a multitude of current-driven instabilities).

To make possible the experimental study of plasma MHD stability and radial transport mechanisms in reactor-like conditions we shall have to substantially extend the central cell of the AMBAL device, which will be done in 1984/85 after a new laboratory building will have been constructed at the Institute of Nuclear Physics. An important point is that the AMBAL plug mirrors have some inherent resource. Their magnetic field can be raised 1.5 times over the level which will be actually used during their first two years of operation. Since the new laboratory building will have a sufficiently powerful electric supply (a 90 Mw shock generator) this "resource" will

be utilized resulting in a device with substantially better parameters than the present-day AMBAL.

In the extended AMBAL, high electron temperatures will be maintained by using auxiliary heating techniques, including the electron-cyclotron resonance heating. Fig.16 shows the location of the extended AMBAL inside the new laboratory building.

The Institute of Nuclear Physics is constructing another big machine the multi-mirror trap GOL-3 which, as seen from Fig.16, will share the new laboratory building with the extended AMBAL facility.

Multi-mirror traps belong to a totally different open-end system branch, namely, the one oriented towards confinement of plasmas with charged particle free path λ substantially exceeding the device length L .

Longitudinal plasma confinement at $\lambda < L$ is not subject to any microinstabilities, allowing good predictions to be made of longitudinal lifetime. Thus, results of plasma confinement experiments in multi-mirror systems were found to be in close agreement with "classical" theory predictions [16]*.

In the multi-mirror reactor version being developed at the Institute of Nuclear Physics the radial plasma confinement is to be achieved by means of a corrugated metal liner leaving to the magnetic field the sole task of suppressing transverse

---

* Another representative of the $\lambda < L$ system class is the "gas dynamic" trap [17] which is an axial-symmetric mirror machine with a very high mirror ratio

heat conduction. This permits, on the one hand, to secure MHD stability of plasma in an axial-symmetrical system, and on the other hand, to soften the requirements to the magnetic field strength (achieving $\beta > 1$).

This approach is attractive because it allows to employ simple and inexpensive technologies in the future fusion reactor design. On the other hand, at the experimental device level grave difficulties arise since a proper simulation of $\beta \gg 1$ wall confinement requires energy inputs to the plasma in the 100 kJ ÷ 1 MJ range. The necessary capabilities will become available with the construction of the GOL-3 device which will employ a 1 MJ electron beam for plasma heating (the feasibility of highly efficient beam energy deposition in plasmas with $3 \cdot 10^{14}$ cm^{-3} ÷ 10^{16} cm^{-3} densities has been demonstrated in the GOL-1 and INAR experiments at the Institute of Nuclear Physics [18]). Major GOL-3 characteristics are listed in Table 2 (see Fig.17). Physical experiments on this device will be chiefly concerned with establishing the sealing laws for wall confinement of $\beta \gg 1$ plasmas.

The Soviet Union has relatively large machines representing the "classical" mirror trap (OGRA-4 at the I.V.Kurchatov Institute of Atomic Energy) and the rotating plasma trap (PSP-2 at the Institute of Nuclear Physics) families. A general view of the former is presented in Fig.18 and its parameters are listed in Table 3 (see Fig.19). The device will serve to thoroughly study three groups of physical effects of immediate relevance to the assessment of the ambipolar trap prospects. These problems comprise the mechanism of plasma oscil-

lations around the drift and cyclotron ion frequencies, the dependence of the oscillations on the stabilizing plasma jet parameters, on the number of ion gyro-radii over plasma diameter, on the electron temperature, etc.; anomalous transport across the field and into the loss cone; plasma interactions with the walls and with the residual gas.

The PSP-2 parameters are listed in Table 4 (see Fig.20) and its photograph is shown in Fig.21. The potential advantage of this type of device is the absense of cone instabilities; the key physical problem to be solved is how to secure the MHD stability of a rotating plasma.

The Soviet Union is also engaged in cusp-geometry trap research with electrostatic plugs. This area is covered in M.S.Ioffe's review paper presented at this conference and we shall not discuss it. Two representative devices of this type, namely the ATOLL and JUPITER 2M, are included in Table 5 (see Fig.22) listing the big Soviet open-end traps, both completed and under construction.

Simultaneously with experimental and theoretical research, several institutes are working on the fusion reactor conceptual design. Thus, the I.V.Kurchatov Institute of Atomic Energy together with the Institute of High Temperatures of the USSR Academy of Sciences, and the Institute of Nuclear Physics of Siberian Division of the USSR Academy of Sciences develop an ambipolar-trap reactor design. The D.V.Efremov Research Institute of Electrophysical Devices, together with the Leningrad Polytechnical Institute and the Institute of Nuclear Physics of the Siberian Division of the USSR Academy of Sciences de-

velop a multi-mirror trap reactor design.

What will be the likely future developments of the open--end trap field? In the next 4-5 years the up date generation of facilities (see Table 5 in Fig.22) will be used in attempts to demonstrate the viability of the relevant open-end system concepts and to find scaling laws which are essential for the next step. The choice of one or two candidates for this next step will depend on experimental data obtained and on the analysis of various reactor conceptual design. Of course, results obtained on open-end traps abroad will not be left unheeded. An international effort sharing in open-end system research could be particularly efficient today because this research area abounds in challenging and promising proposals that await analysis and testing.

The next step should be to construct one or two devices on a scale between T10 and T15.

III. Alternative Magnetic Confinement Schemes

Among the so-called "alternative" approaches being investigated in the USSR, I should like to single out the following:

1. Research on high-power, high-frequency discharges in high-density hydrogen being carried out by Academician P.L.Kapitsa. Particularly intriguing are his unusual results suggesting an anomalously good thermal insulation of hot electrons. The experiments are being continued with the aim of obtaining a hot-ion plasma. Details of these excellent experiments are described in a special paper presented to this conference.

2. Research into the so-called "compact tori". This work, carried out by R.Kurtmullaev's team at the Institute of

Atomic Energy, has demonstrated the feasibility of developing a compact toroidal Z-pinch. To achieve this they used the shock heating (much like the θ-pinch technique), the reversed field configuration, created due to field sign reversal and using barrier fields to prevent plasma-wall interactions, heating due to the shock axial plasma ploughing, and development of a fairly stable compact configuration. This research team has also shown that such an object can be transported via a metallic tube and subjected to further adiabatic compression by a metallic liner.

The main objective of the ongoing experiments is to use a new device with a power input of $\sim$ 1 MJ to investigate hot plasma stability and existence regime at temperatures $\gtrsim$ 1 keV under clean vacuum conditions.

3. We continue to be interested in the feasibility of using pulsed plasma accelerators (Skvortsov, Institute of Atomic Energy) and of developing powerful quasi-stationary accelerators (Morozov, Institute of Atomic Energy) for filling up open-end traps with hot plasma.

B. Microexplosions

Microexplosition feasibility studies aim primarily at finding out the minimal energy and minimal power input for igniting a thermonuclear fusion target.

We have repeated in the Soviet Union experiments on spherical D-T target compression in order to obtain quantitative estimates of the minimal required energy Q_{min}, and minimal required power input, W_{min}. Fig.29 shows theoretical data on possible initiation regions for lasers (10^5 J, 10^{14} W), electron and ion beams ($10^7 \div 10^6$ J, 10^{14} W) and for liners

using magnetic insulation (10^6 J, 10^{13} W). In view of the complexity of the process owing to its hydrodynamic instability an experimental test over the entire region must be made for which purpose the necessary base is being developed in the USSR.

1. Lasers

In the laser field, work is going on at the P.N.Lebedev Physical Institute of the USSR Academy of Sciences with neodymium lasers DELFIN and UMI-35, on MISHEN-2 (jointly with the Institute of Atomic Energy) and on several smaller devices. New results have been obtained at the I.V.Kurchatov Institute of Atomic Energy with a photodissociation iodine laser. I should like to elaborate in some detail on the early results of the latter experiment.

A single-channel 1.315 μ wavelength photodissociation iodine laser "ISKRA-IV" has been developed [19]. The experimental data obtained show that to a large extent we have successfully realized the main advantages of iodine lasers which are the following:

(a) feasibility of fairly homogeneous pumping of large cross-sections of working materials (C_3, F_7I mixed with a variety of buffer gases, CO_2, SF_6, Ar, etc.);

(b) feasibility of optimizing gain by varying the laser medium composition;

(c) relatively low superluminescence level due to the sufficiently long excited iodine lifetime ($\sim 10^{-1}$ s);

(d) significantly less critical self-focusing limitations in the laser medium, making it possible to raise radiation power output without noticeable energy losses.

Max-Planck-Institut für Plasmaphysik
8046 Garching bei München

The ISKRA IV single-channel laser was used for the irradiation of 150-170 μ diameter and I μ thick spherical glass microtargets filled with a D-T gas mixture at 10-40 atm pressure.

In early laser runs experiments the 270 mm diameter output beam was split into four beams using beam-splitter plates. The four beams were focused onto the glass target with 10-20 accuracy by means of four F = 270 mm parabolic mirrors. The four paraboloids were positioned at the apexes of a tetrahedron inscribed into the chamber diameter. The beam output divergence at the 80 per cent energy level was $(1 \div 2) \cdot 10^{-4}$ rad. To achieve a more homogeneous irradiation the target was located in the plane where the focusing spot diameter was about 200 μ.

Optical decoupling elements in the shape of glass-substrate bismuth film filters and bleaching dye solutions were provided in order to prevent self-excitation of the master oscillator-amplifier-target chain. It was found possible to achieve an energy contrast $K_E \sim 10^7$ and a power contrast $K_p \sim 2 \cdot 10^6$ in the output beam.

In the experiments the laser energy input into the target chamber was 500 J. At this energy level, the "exploding pusher" regime [20] is preferable for attaining high neutron yields. This regime is attainable in case the fast electron temperature is sufficiently high ($\geqslant$ 10 keV), which requires a $\geqslant 10^{15}$ W/cm^2 power density at the microtarget surface. To achieve such output power fluxes at the above-mentioned output energy level and target size one must have a laser pulse duration $\leq$ 0.3 ns.

The laser pulse shortening was achieved both by steepening up the master oscillator laser pulse front and by an appopriate choice of the iodine laser amplification stages. Thanks to these measures it was possible to obtain an output pulse length of $\tau_{0.5} = 0.3 \pm 0.05$ ns which fits the calculated neccessary value.

The important point is that in contrast to the neodymium lasers the device output energy was practically the same over the 1 ns to 0.25 ns pulse duration length.

Special purpose calorimeters were developed to measure the energy balance in the laser plasma. In the highest neutron yield experiment ($N \simeq 1.5 \cdot 10^5$ neutons per pulse) the total energy input to the chamber amounted to 480 J, the energy incident onto the target was 280 J and the energy absorbed in the target was 50 J. The laser radiation flux density at the target was 10^{15} W/cm^2.

The continuous X-ray spectrum measured by the foil filter method is illustrated in Fig.23. The temperatures corresponding to the soft and hard parts of the spectrum were $T_s \simeq 1$ keV and $T_h \simeq 9$ keV respectively. The corona temperature in the vicinity of the critical surface was determined from line spectrum measurements (relative intensities of the He and H-like silicon ion resonance lines). This temperature was found to be $\simeq$ 0.8 keV.

The pinhole target images in self X-ray radiation made it possible to evaluate the DT compression factor as 30 (see Fig. 24).

Fig.25 presents neutron yield data. The experimental neutron yield is plotted along the ordinate axis, with the

yield expected values being plotted in the abscissa. Expected yield values were found from a semi-empirical model [20] fitted to the results of "exploding pusher" experiments at the Livermore National Laboratory; these results are illustrated in the same figure. Our results are seen to be in good agreement with the Livermore experimental data. The hot electron temperature measured in our experiment ($\simeq$ 9 keV) suggests that, at the glass microtarget thickness mentioned above, we also worked in the "exploding pusher" regime.

Now to summarize. As a result of research in "ISKRA-IV" the laser power was raised by shortening the pulse from 1 ns to 0.3 ns with practicaly no energy loss. A 10^5 neutron yield was obtained for the first time with DT gas spherical target iodine laser irradiation, the volume compression ratio being around 30.

2. "Angara" Programme

In recent years two novel research branches have emerged in the inertial confinement CNF, both utilizing the REB generator technique, viz., high-current light-ion beams and energy concentration by means of current magnetic field driven cylindrical liners. While the US programme is fully light-ion oriented, we are in no haste to modify our own approach, feeling that the beam-driven CNF electron beams may turn out to represent the easiest route to nuclear fusion burn.
Liners accelerated to speeds in excess of 10^7 cm/sec can be used to secure the gas dynamics of the inner fusion target compression and, according to computation results, one can expect to achieve fusion burn in this way at a 20-30 TW current supply output power.

Let us dwell at some length on the merits and disadvantages of each of the two approaches. The success in self-focusing high-current relativistic electron beams directly inside the diode and the experimental discovery of an enhanced energy deposition in the anode foil plasma due to the extended time of electron transit, because of electrons being magnetized, have made it possible to perform an important experiment in IAE during 1976-77. This experiment has demonstrated the working principle of an optimal fusion target intended for charged particle beams. In the intervening five years the mechanism of the enhanced energy deposition has been corroborated and well understood. An analytical theory and a mathematical model of the effect were developed describing the REB passage as a relativistic electron gas flow through high density plasma described in the MHD approximation (Kurchatov Institute of Atomic Energy, Institute of Applied Mathematics of the USSR Academy of Sciences). Today, there is no apparent reason to doubt that we should have a megampere beam able to provide a 10^{13} W per cm^2 power flux incident at the anode foil, it will be possible to heat the foil to a temperature around 100 eV. Such an experiment would represent an important step in the electron beam programme, and we are planning to carry it out on the A-5 module in 1981/82. Having obtained data on the heat fluxes and the spectrum of the electrons and quanta behind the foil it will be possible to design and calculate the REB fusion target with higher accuracy.

The problem posed by this approach is the physics of the diode used in our experiments. Its a priori essential compo-

nent is the plasma formed during power input. It has been demonstrated that the current start in such a diode is usually delayed relative to the voltage pulse. The current is then quickly short circuited by the dense plasma emerging from the electrodes (Fig. 26). As a result, although the power flux at the anode foil is high (10^{13} W/cm^2), its time integral is just enough to heat a 10 μ thick golden foil to 30 eV. Temperature measurements at the foil front and rear sides by a photodiode are in satisfactory agreement with calculations taking into account the magnetic stopping of electrons in the foil plasma which manifests itself in the anomality factor of $-\frac{3}{2}$ I/10^4 γ. Recent research results suggest that the introduction of a controlled fast prepulse can modify the electric current delay and build up both the REB power and total energy deposition (see Fig.27).

The development of an experimentally verified theory of the plasma-filled diode represents the main task of the future programme for this approach. Should we succeed in solving the problem of effective REB self-focusing, inside the diode, the approach based upon energy concentration at the diode via magnetic self-insulation transfer lines and upon target heating, with the target shell representing the diode anode, will have evident advantages as the shortest way towards fusion burn, because it does not involve the complicated problems of transport through the gas and focusing upon the target of many beams.

As mentioned previously, a light-weight milligramm-range cylindrical liner accelerated by the pressure of the magnetic field of current driven by a REB generator is a concentrator

of energy and power. This approach is traditional in the research done at the Institute of Atomic Energy. An accelerated liner can be regarded as the first stage of a complex gas dynamic process in a multi-shell target. Indeed, in order to attain the desired ρr value it is advisable to shift from 2-D to 3-D compression of fusion fuel at the final stage. The Institute of Atomic Energy has started acceleration experiments on its "Angara" module device with a thin milligramm--weight plastic liner and a multiple-wire liner. The results repeat to some extent those obtained in the multi-wire shell acceleration studies at the Maxwell Power and Physics International laboratories in the USA. We hope to solve the problem of low-inductive power supply from the "Angara-5" first phase eight modules using a 3-D magnetical self-insulation current collector (Fig.28). This structure's assemblies have been tested at Angara I and at the "Angara" module.

Finally, some remarks on the light-ion inertial confinement fusion programme. It is with great interest that we are following the progress being made by US scientists in this field. On the other hand, both the accumulated experimental evidence and the theoretical research indicate that this path is pregnant with serious difficulties in obtaining an ion beam with a small enough angular divergence, in its focusing, in its transportation through magnetic channels in a gas, and in superposing beams on the target. We are planning to start a limited-scale ion-beam programme whith the main

emphasis on the fundamental problems of magnetically insulated diode physics and on the achievement of megampere ion fluxes. It is envisaged that the Angara 5 modules will operate with voltage polarities.

At present, in the Institute of Atomic Energy assemblage work is in progress on eight modules of the "Angara 5" device (first phase).

The magnetohydrodynamic cumulation of shell implosion driven by the current magnetic field provides an option to hope for the feasibility of igniting a spherically symmetrical fusion target.

Thus, we expect to obtain during this five-year period sufficient results on fusion reaction ignition in microtargets together with sufficiently realistic computer schemes and then to choose the most optimal type of driver and target. Alongside the above-mentioned schemes we are continuing work on assessing the feasibility of a thermonuclear reaction in a target induced by heavy ion beams using existing and novel accelerator and storage-ring technologies.

Currently very fine feasibility studies are also in progress into the cold catalysis of a fusion reaction. In spite of the limitations of the theoretical "price" of the neutrons produced, owing to the "high cost" of the muon and its attachment losses, we are not losing hope of using this technique at least for obtaining a new fissile fuel. Here Nature has given us another resonance and the recent theoretical and experimental research results are in good agreement.

Conclusion

The main emphasis of Soviet fusion research in the 11th five-year Plan period is to demonstrate the feasibility of controlled fusion in tokamak-type systems, to look for efficient alternative concepts and to explore them, above all, the open-end trap concepts; to study the physical mechanisms of microexplosion initiation using a variety of drivers so as to find the leading trend in this field.

Corroborating the main research direction, viz. the development of a tokamak reactor, the Soviet Union is carrying out extensive engineering-technological and material research which is beyond the scope of the present conference. The USSR takes an active part in the development of the next generation of thermonuclear devices - the INTOR Project. We believe that the level of international cooperation which has been reached in the twenty-five years since the first public report on controlled thermonuclear fusion, presented by I.V.Kurchatov at Harwell, is an important achievement of the scientists concerned with this problem around the world and a major factor of the final success.

References

1. V.M.Leonov et al. in "Plasma Physics and Contr. Nucl. Fusion Res." (Proc. of VIII-th Intern. Conf.; Brussels, 1980) Vol. I, IAEA, Vienna (1981) 393; A.B.Berlizov et al., ibid, 23.
2. V.V.Alikaev. Tenth European Conf. on Contr. Fusion and Plasma Physics, vol. 1, Contributed papers, H-3
3. V.M.Leonov et al. Tenth European Conf. on Contr. Fusion and Plasma Physics, vol. 1, Contributed papers, A-17
4. Yu.N.Dnestrovskij et al. Tenth European Conf. on Contr. Fusion and Plasma Physics vol. 1, Contributed papers, B-15
5. S.M.Egorov et al. "Pellet diagnostics experiments in T-10 Tokamak". Tenth European Conf. on Contr. Fusion and Plasma Physics, vol. 1, Contributed papers, A-36
6. A.P.Zhilinsky et al. "Investigation of FT-1 Tokamak plasma by means of pellet injection". Tenth European Conf. on Contr. Fusion and Plasma Physics, vol. 1, Contributed papers, A-3a.
7. V.I.Bugaria et al. The study of subwall plasma parameters in the TM-4 Tokamak with different methods of chamber wall cleaning. Tenth European Conf. on Contr. Fusion and Plasma Physics, vol. 1, Contributed paper, A-15
8. Yu.F.Baranov et al. "Electron cyclotron heating in FT-1 Tokamak above critical plasma density". Proc. of Tenth European Conf. on Contr. Fusion and Plasma Physics, vol. 1, Contributed papers, H-8
9. N.N.Brevnov et al. "Fluxes of energy and particles the T-12 Tokamak with divertor". Proc. of Tenth European Conf. on Contr. Fusion and Plasma Physics, vol.1, Contributed papers, J-2

10. V.F.Demichev, V.A.Chuyanov. Prepr. Institute of Atomic Energy 3222, 1979

11. E.A.Azizov et al. Paper V-3 presented at the 8th International Conference on Plasma Physics and Controlled Nuclear Fusion. Brussels, 1980

12. G.I.Dimov, V.V.Zakaidakov, M.E.Kishinevsky in "Fizika plazmy", 2 (1976), 597

13. D.E.Baldwin, B.G.Logan. Improved tandem mirror fusion reactor. Phys Rev Lett., 43, oct. 1979.

14. D.D.Ryutov, G.V.Stupakov. Pisma v JETPh, 26 (1977), 186

15. V.V.Arsenin. "Fizika plasmy", 6 (1980), 551

16. G.I. Budker, V.I.Danilov, E.P.Kruglyakov, D.D.Ryutov, E.V.Shun'ko. JETPh, 65 (1973), p. 562

17. V.V.Mirnov, D.D.Ryutov. "Voprosy atomnoi nauki i tekhniki" (problems of atomic energy and technique), ser. "Termoyadernyy sintez" (thermonuclear fusion) 1980, p. 57

18. V.S.Koidan, E.P.Kruglyakov, D.D.Ryutov. Paper 3C3 presented at the 4th International conference on physics and technique of powerful electron beams" Palaiseau (France), July, 1981

19. S.B.Kormer, Izv. AN SSSR, 44, 2002 (1980)

20. E.K.Storm et al., Phys. Rev. Lett., 40, 1570 (1978)

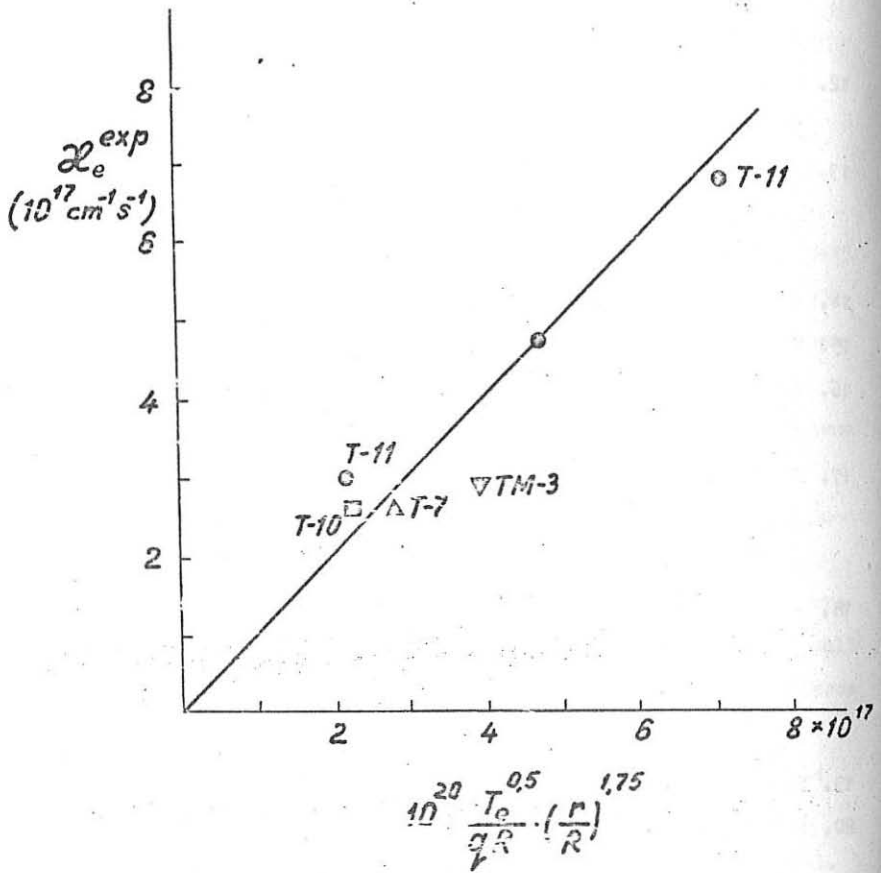

8
6
4
2
χ_e^{exp}
$(10^{17} cm^{-1} s^{-1})$
T-11
T-11
T-10
T-7
TM-3
2
4
6
8×10^{17}
$10^{20} \frac{T_e^{0.5}}{qR} \cdot \left(\frac{r}{R}\right)^{1.75}$

Fig.1

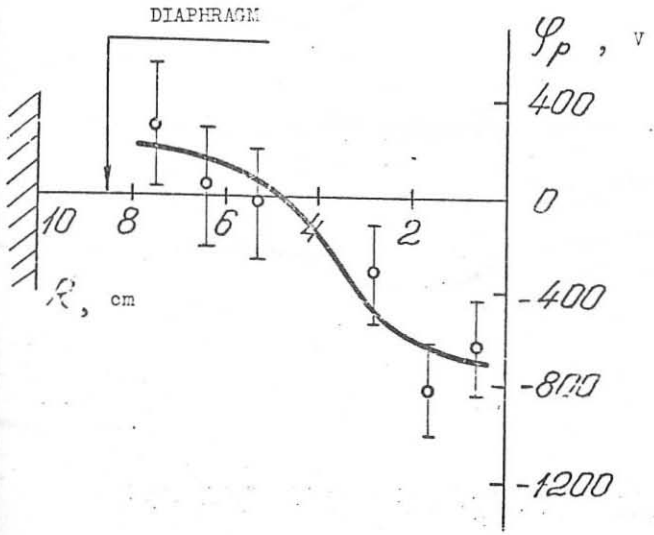


Fig.2

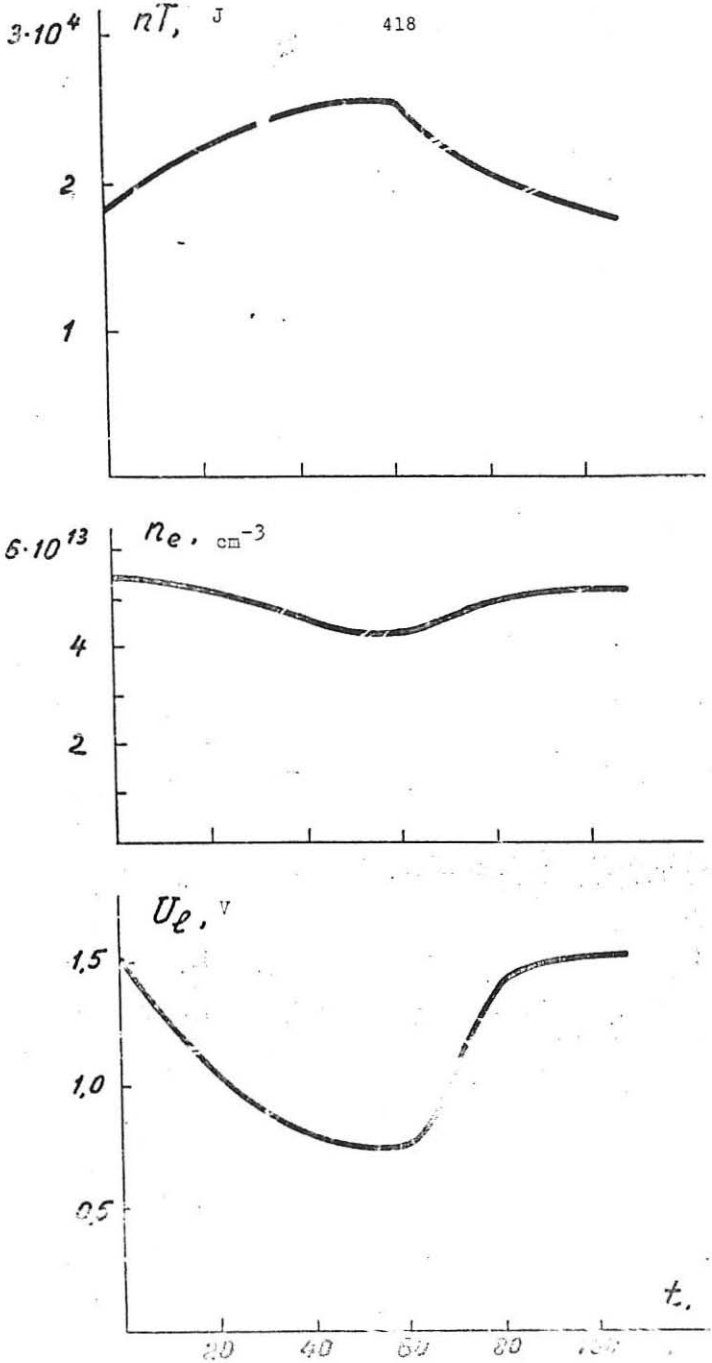


Fig.3

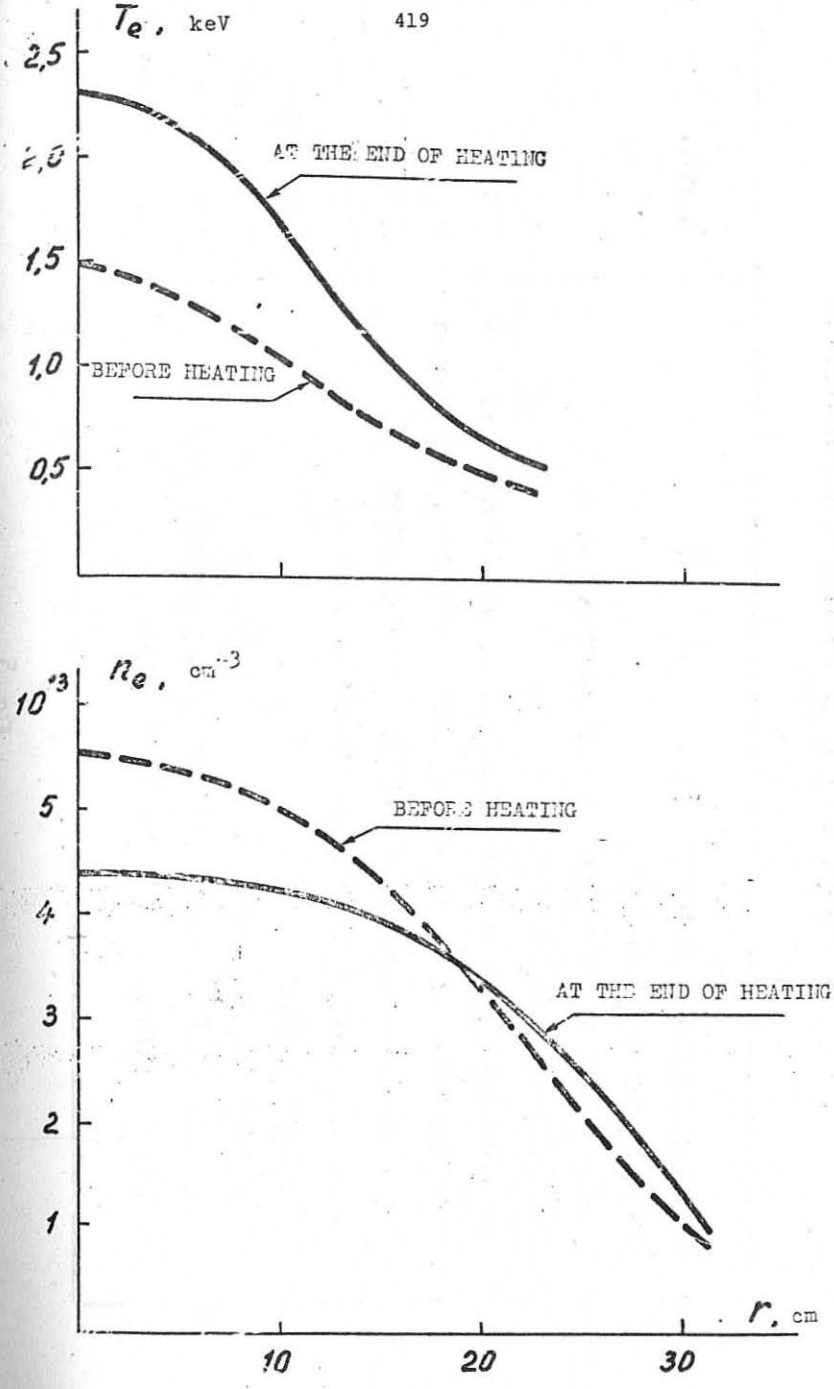

T_e, keV
2,5
2,0
1,5
1,0
0,5
AT THE END OF HEATING
BEFORE HEATING
n_e, cm^{-3}
10^{13}
5
4
3
2
1
BEFORE HEATING
AT THE END OF HEATING
r, cm
10
20
30

Fig.4

PARAMETERS OF A TOKAMAK WITH STRONG FIELD AND WITH ADIABATIC COMPRESSION

INITIAL MAJOR RADIUS, R_c	1.06 m
INITIAL MINOR RADIUS, a_c	0.32 m
INITIAL MAGNETIC FIELD AT THE RADIUS 1.06 m, B_c	2.0 T
INITIAL PLASMA CURRENT, I_c UP TO	0.48 MA
MAJOR RADIUS OF PLASMA COLUMN AFTER COMPRESSION, R	0.415 m
MINOR RADIUS OF PLASMA COLUMN AFTER COMPRESSION, a	0.125 m
FIELD AT A RADIUS 0.415 m AFTER COMPRESSION	12.9 T
PLASMA CURRENT AFTER COMPRESSION, I UP TO	1.2 MA
ADDITIONAL HEATING POWER	1 – 2 MW
AVERAGE PLASMA DENSITY AFTER COMPRESSION, N	$\sim 10^{15}$ cm^{-3}
AVERAGE PLASMA TEMPERATURE AFTER COMPRESSION, T	>7 keV
ENERGY CONFINEMENT TIME (EXPECTED)	30 – 100 ms

Fig. 5

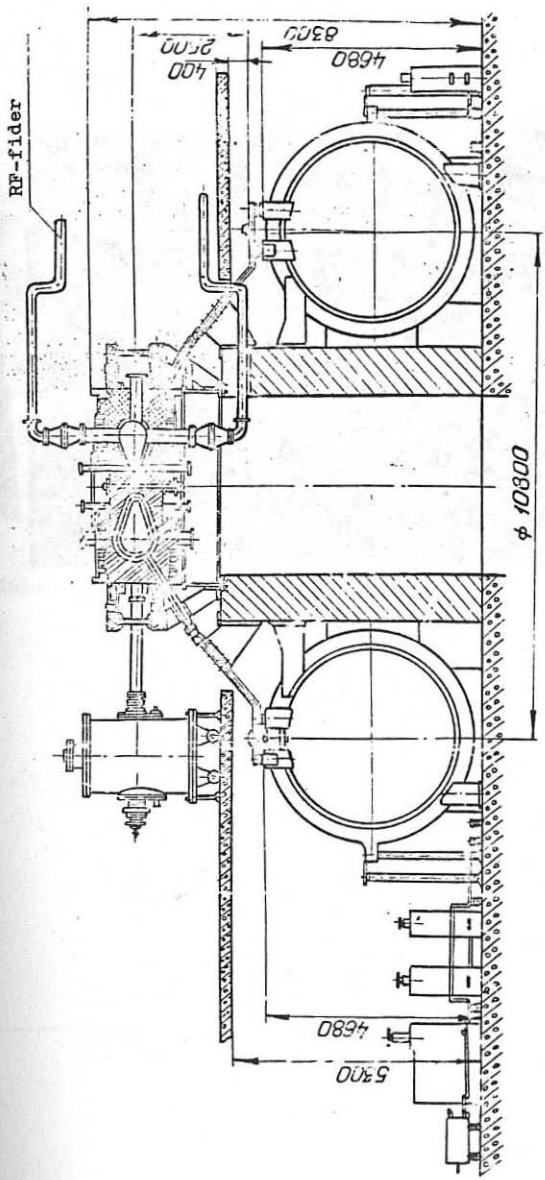


Fig.6

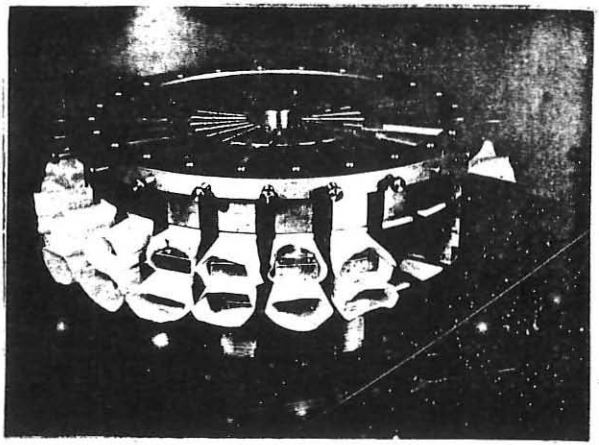


Fig.7

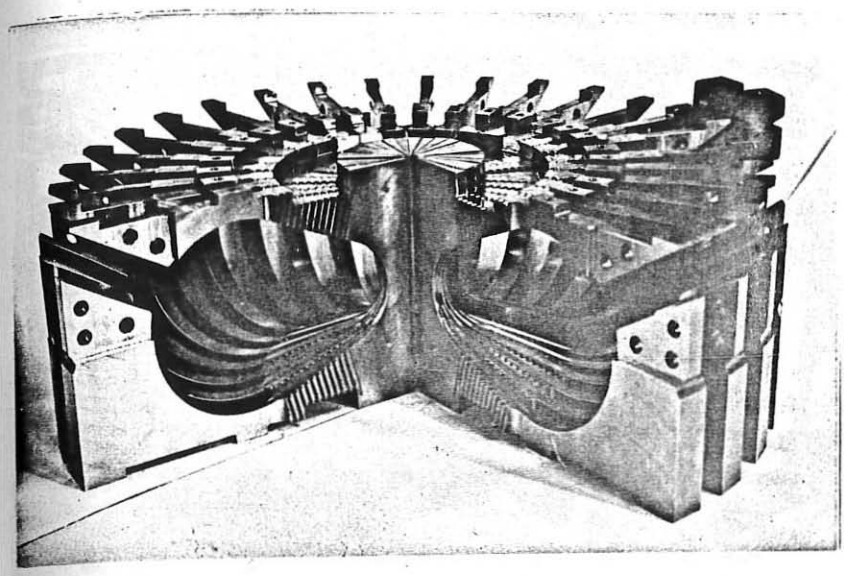


Fig.8

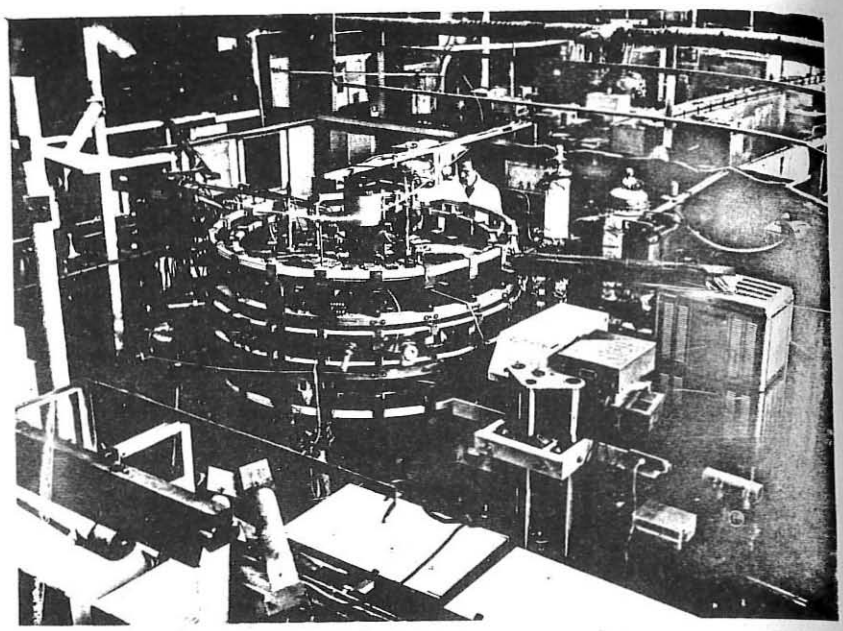


Fig.9

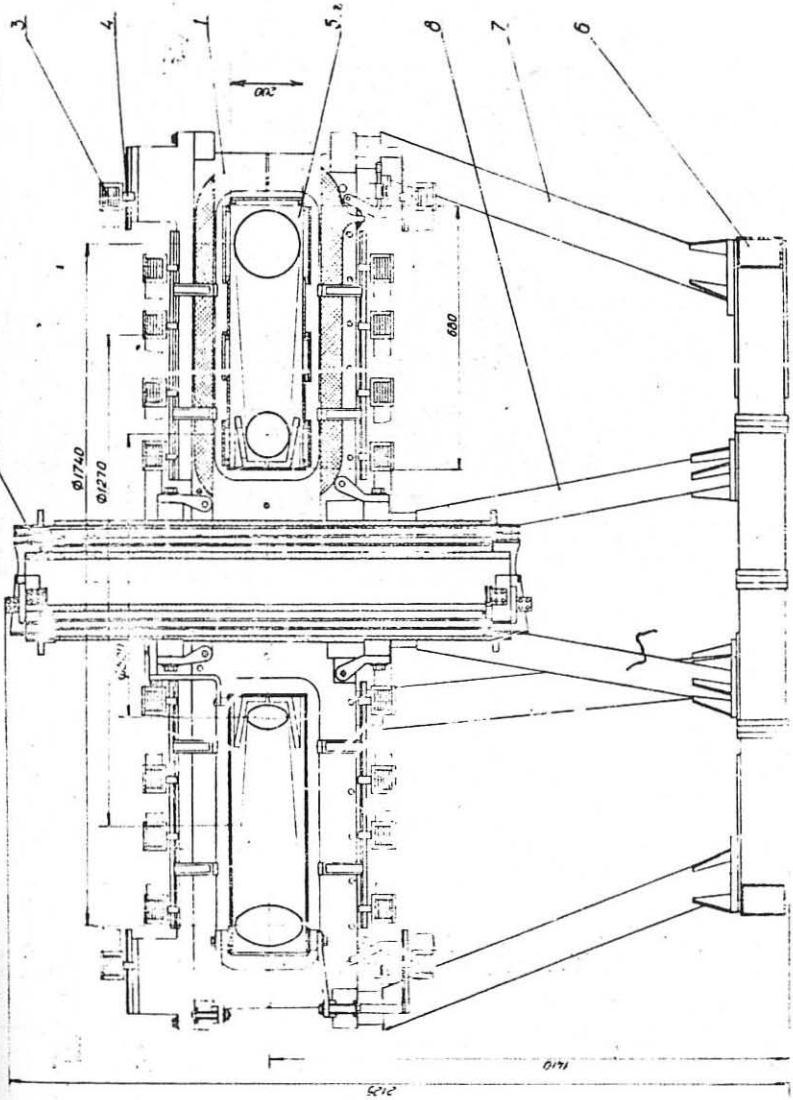


Fig. 10

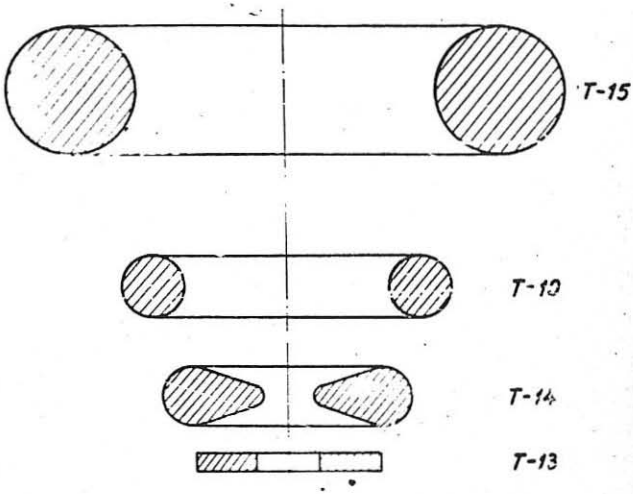


Fig.11

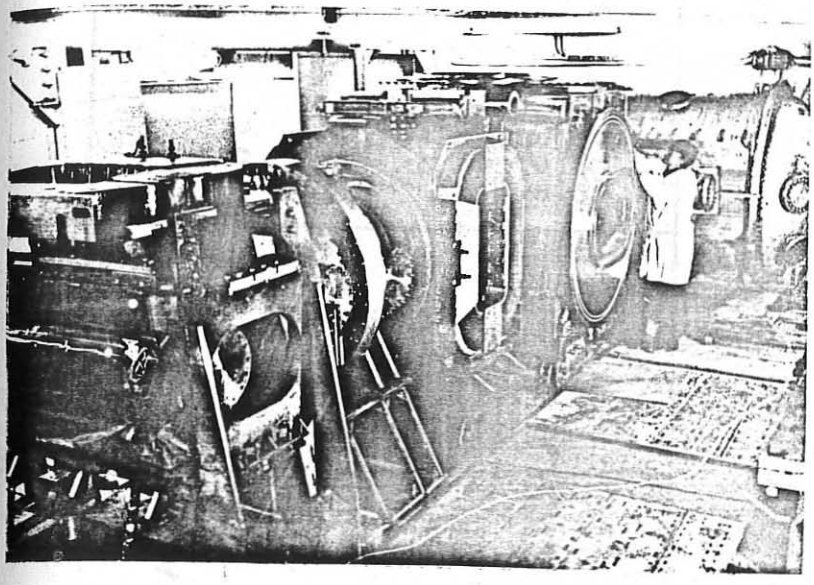


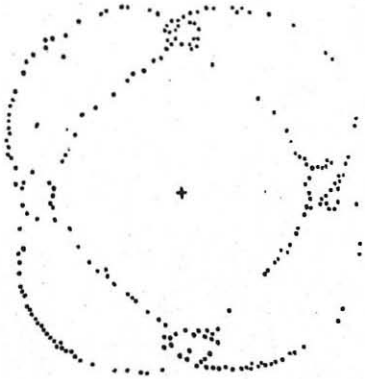
Fig.12

THE TANDEM TRAP AMBAL

	PLUGS	SOLENOID
LENGTH (m)	1,0	3,5
PLASMA DIAMETER (m)	0,24	0,60
CENTRAL FIELD (TESLA)	1	0,15
MIRROR FIELD (TESLA)	2	2
PLASMA DENSITY (cm^{-3})	3.10^{13}	1.10^{13}
ION TEMPERATURE (keV)	20	0,5
ELECTRON TEMPERATURE (keV)	1	1

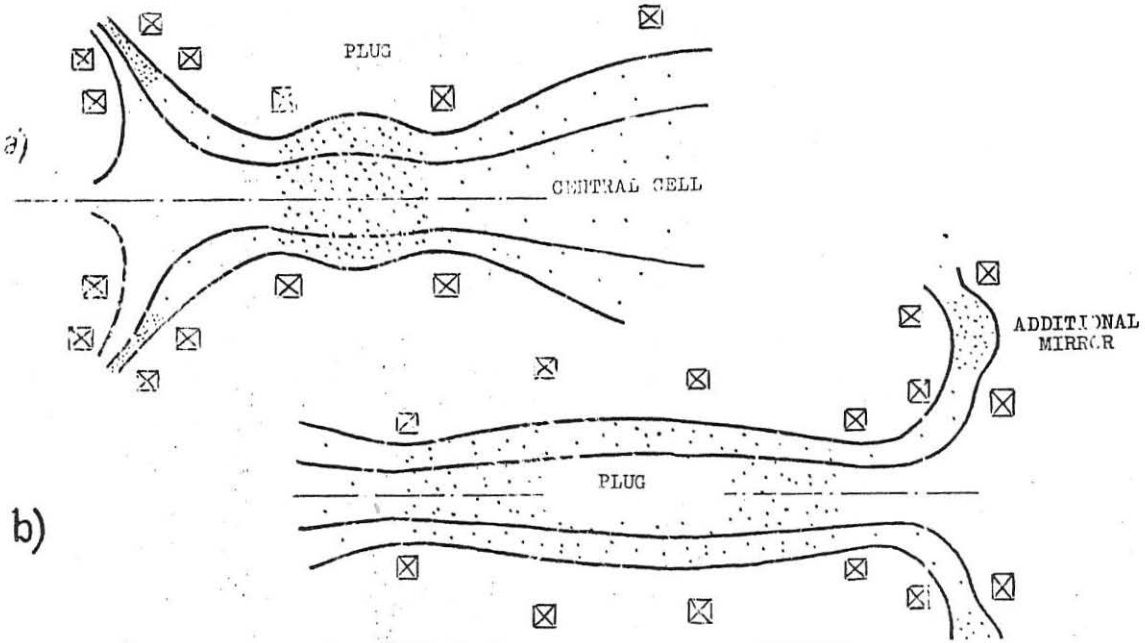
Fig. 13

RESONANT DIFFUSION



CALCULATED TRAJECTORY OF A RESONANT PARTICLE IN "SEM" DIVICE – A SMALL MODEL OF A NONAXISYMMETRIC AMBIPOLAR TRAP. SHOWN ARE THE POINTS OF SUCCESSIVE CROSSINGS OF THE PARTICLE WITH THE EQUATORIAL PLANE.

Fig. 14



MAGNETIC FIELD CONFIGURATION IN ARSENIN-TYPE AXIAL SYMMETRIC TRAPS. BY THE DOTS IS MARKED THE REGION OCCUPIED BY THE HOT PLASMA.

a) Andreoletti traps at the ends provide MHD stability of the outer plasma sheet.

b) An example of MHD stable configuration against the first flute mode.

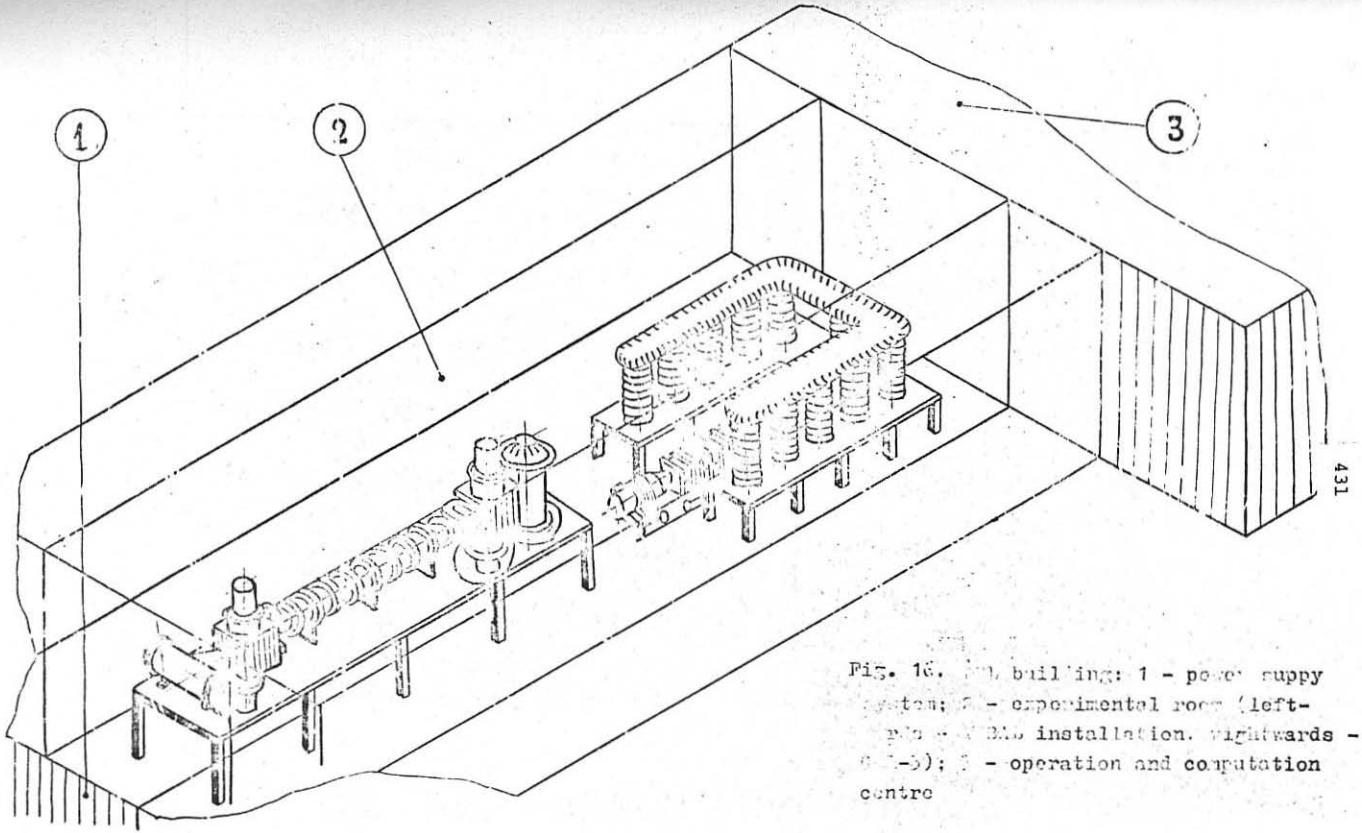


Fig. 16. [illegible] building: 1 - power supply system; 2 - experimental room (left-[illegible] installation, rightwards - [illegible]); 3 - operation and computation centre

THE MULTIMIRROR TRAP GOL–3

LENGTH	20 m
MEAN PLASMA DIAMETER	6 cm
MEAN MAGNETIC FIELD	6 Tesla
MIRROR RATIO	2
NUMBER OF TRAPS	30
PLASMA DENSITY	10^{17} cm^{-3}
PLASMA TEMPERATURE	1 keV

Fig. 17

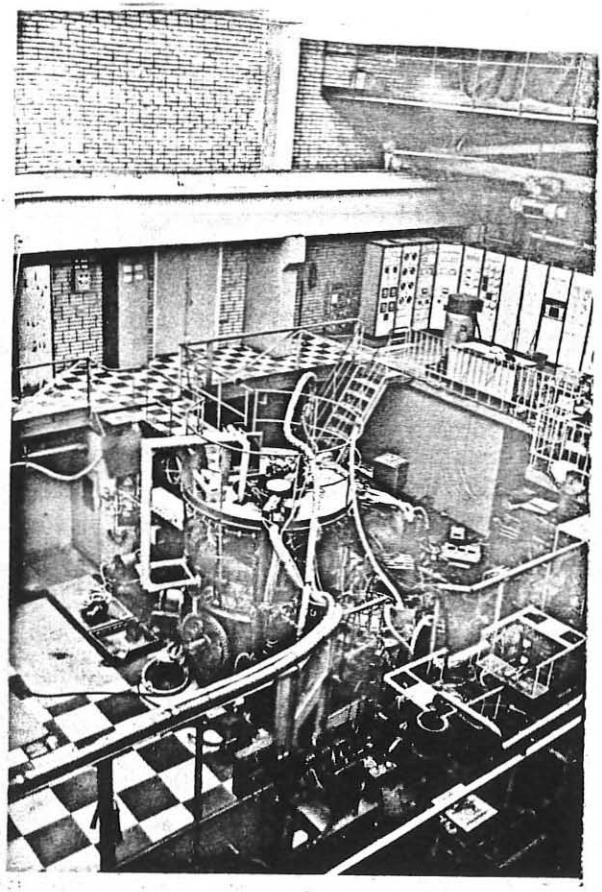


Fig. 18

OGRA–4

INSTALLATION

SUPERCONDUCTING BASEBALL: MIRROR TO MIRROR DISTANCE 70 cm;
FIELD (TESLA) 1,3/3,7 (MINIMUM/MIRRORS);
INJECTORS – 4: I_{ing} up to 100 Aeq; E_{ing} = 15 – 30 keV;

INVESTIGATION TASKS

THE STUDY OF PLASMA OSCILLATIONS NATURE,
ANOMALOUS TRANSPORT MECHANISMS IN A QUADRUPOLE
MIRROR TRAP AND THE SEARCH OF THE POSSIBILITY
TO CONTROL THEM.

Fig.19

THE ROTATING PLASMA TRAP PSP–2

ION ROTATION ENERGY	30 – 100 keV
ION ENERGY	10 – 50 keV
PLASMA DENSITY	$10^{12} - 3{,}10^{13}$ cm^{-3}
PLASMA VOLUME	0,6 m^3
ELECTRIC FIELD	20*) – 100 kV/cm
VOLTAGE	200*) – 1000 kV
FIELD MINIMUM/MIRROR	3/7,2 (Tesla)

*) EXPERIMENT 1.07.1981.

Fig. 20

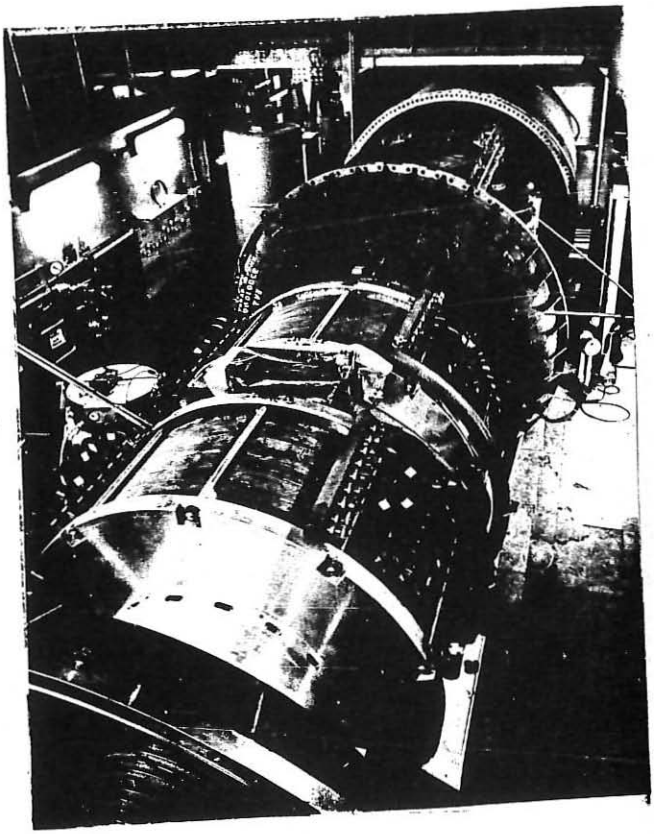


Fig.21

OPEN TRAPS OF PRESENT GENERATION

INSTALLATION	TYPE	LOCATION	FINISH OF CONSTRUCTION
OGRA–4	SUPERCONDUCTING BASEBALL	KURCHATOV INSTITUTE	1980
ATOLL	CIRCULAR QUADRUPOLE WITH ELECTROSTATIC PLUGS	–"–	1980
PSP–2	ROTATING PLASMA AXIAL SYMMETRIC MAGNETIC TRAP	NOVOSIBIRSK	1980
AMBAL	TANDEM TRAP	–"–	1981
GOL–3	MULTIMIRROR TRAP WITH DENSE PLASMA	–"–	1983

Fig.22

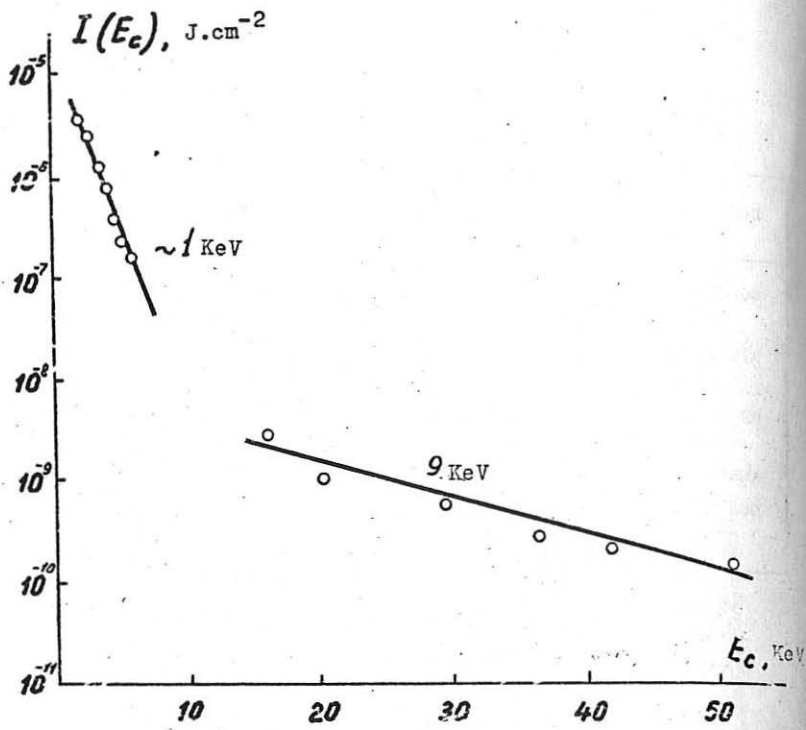


Fig.23 X-ray spectrum

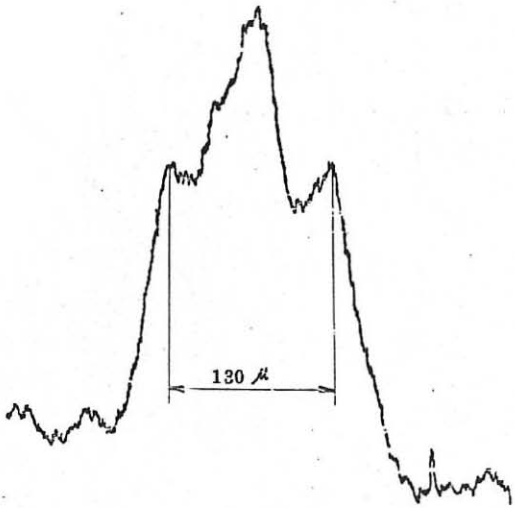
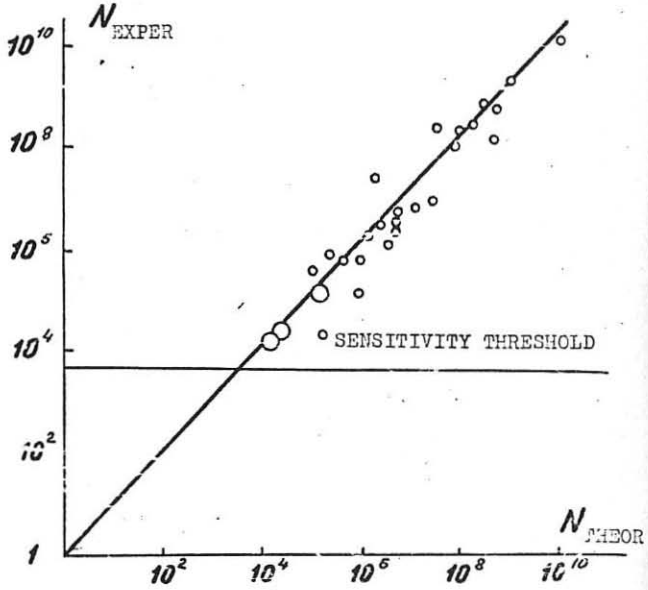


Fig.24 X – RAY DENSITY PROFILE



○ — „Iskra – IV"

○ — LIVERMORE

Fig.25 NEUTRON YIELD

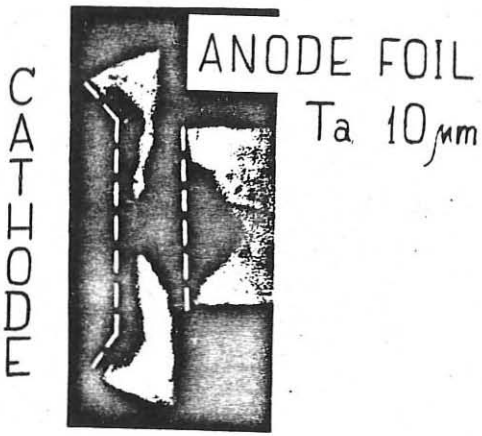


Fig. 26. The shadograph (λ = 5320 Å) of the diode gap at the moment 100 ns after the start of the current. (U = 0,8 MV, I = 200 kA). The diode gap equals to 0,28 cm.

The shadow boundary corresponds to the electron density $\sim 10^{19}$ cm^{-3}.

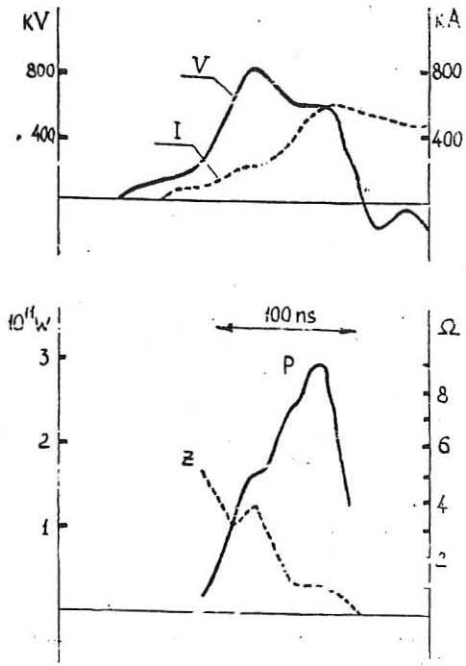


Fig. 27. Time dependence of the diode impedance and power release calculated by oseillagrams of current and voltage, in presence of prepulse.

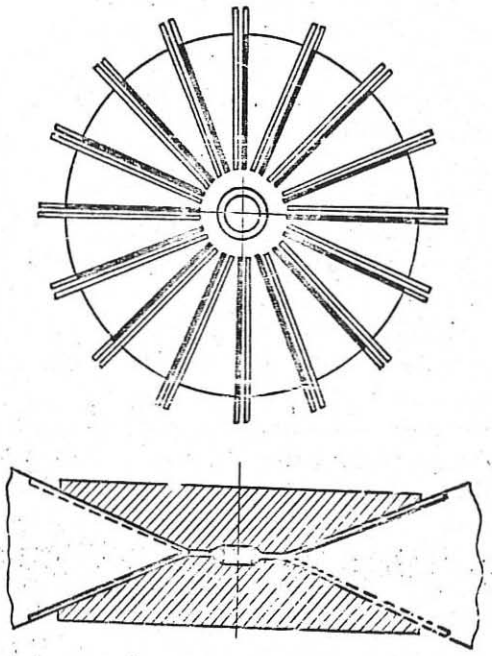


Fig. 28

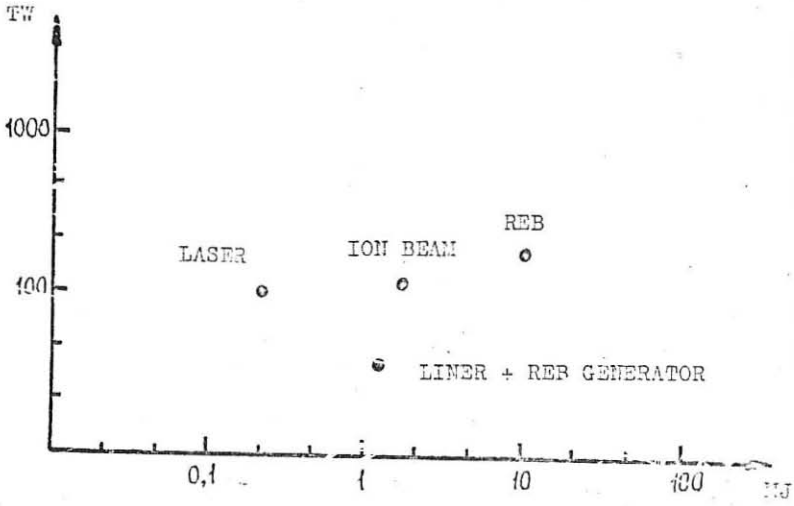

TW
1000
100
LASER
ION BEAM
REB
LINER + REB GENERATOR
0,1
1
10
100
MJ

Fig.29

PLASMA-WALL INTERACTION

H. Wolff
Zentralinstitut für Elektronenphysik
der AdW der DDR, 1080 Berlin, GDR

INTRODUCTION

Impurity control and plasma-wall interaction are among the outstanding key issues of development of magnetic confinement fusion devices. Mainly in tokamak research to which the following will be restricted was gathered considerable experience in the areas of particle control and plasma position control resulting in plasmas with extremely low impurity contents. Accidental interactions of the plasma column or fast electrons with the wall and inner structures of the tokamak can be avoided successfully. By appropriate choice of the construction materials, careful conditioning and operation of the machine the effective charge Z_{eff} in most present-day tokamaks can be brought close to unity. But there is concern that the longer pulses and higher wall loadings expected in future tokamak installations will result in significantly increased impurity generation. There is a number of research programs and special installations dealing with different aspects of plasma-wall interaction and impurity control, especially aimed to assess the feasibility of tokamak reactors.

The up-to-date state of knowledge of plasma-wall interaction is extensively reviewed by McCracken and Stott /1/. Since that a number of publications and especially the last in a series of conferences on plasma-surface interaction, which took place in 1980 /2/ have given further information in this field. But nevertheless there is still considerable need to experimentally investigate and to understand the plasma near the wall, to determine the flux of particles and energy onto the walls and to get more insight into the phenomena of impurity transport. Models are urgently needed which will bring together the complex interrelated processes such as working gas recycling, impurity production and transport.

THE ENERGY BALANCE

The particle and energy confinement is a measure for tokamak performance. A main goal of confinement experiments is to resolve the particle and energy loss processes into their constituent elements in order to distinguish between losses which are inherently coupled with the principles of magnetic confinement and others which depend on plasma impurities or instabilities and which hopefully can be reduced after proper understanding of their origin.

The walls of a tokamak are bombarded by radiation, neutral atoms and by charged particles which have diffused across the confining magnetic field. The magnitude of the outward flux of radiation and particles depends largely on the conditions of the discharge, its stability and impurity content. But it is extremely difficult to determine those fluxes, their composition and energy distribution. Most of the tokamak diagnostics is dealing with this problem but the results are still disappointing, differing widely in dependence on the individual conditions of the tokamak and the special experiment. The energy and particle balance of tokamak discharges are considered in the following.

In contemporary Ohmic heated tokamaks, depending on the impurity content and the phases of the discharge a large percentage of up to nearly 100 % of the Ohmic input power may be radiated. In the initial phase of the discharge ($T_e \leq 50$ eV) line radiation from the working gas and low Z-impurities (O, C, N) is emitted uniformly from the plasma, balancing the full Ohmic heating power. If the available voltseconds permit to "burn through" this start-up phase the quasi-steady plateau is reached, where the radial electron temperature and density profiles may be characterized by the impurity radiation. Three standard types of tokamak discharges can be discerned /3, 4/. The first two types are characterized by high values of Z_{eff}. The one type is the low Z-dominated ("dirty") discharge, in which oxygen and carbon contamination is high. Most of the Ohmic power is radiated from the cooler peripheric parts of the discharge by partially ionized low-Z impurities while the

electron temperature tends to be high in the core zone, and the radiated power there constitutes only a minor fraction of the input power. Fig. 1b demonstrates this case for PLT with graphite limiters. The radially integrated input and radiated power shown on the right hand side of this figure indicates clearly that only little power is radiated from the hot core, the rest transported outward into the colder shell by an "anomalous" transport mechanism, mainly electron convection and conduction.
In the presence of more high-Z impurities e.g. metals from walls or limiters and less amounts of light impurities a detailed balance between the input power and the radiation at all radii develops. This second type, the radiation dominated discharge shown in fig. 1a is characterized often by a hollow electron temperature profile.

Very clean discharges with $Z_{eff} \simeq 1$, obtained with graphite limiters and after special cleaning procedures allow to reach higher densities. In this case the radiation is only a fraction of the Ohmic input (fig. 1c), the rest is lost by particle transport to the walls, limiters or to divertors. The measurement of this radially resolved energy balance is suffering from several uncertainty sources, because the determination of the radial distribution of the input power depends on measured profiles of T_e (e.g. by Thomson scattering), plasma current and loop voltage, assuming a constant value of Z_{eff} over the plasma cross section, and the validity of the conductivity formula by Spitzer. The radiated power is measured by bolometer detectors which give only local information on the radiation energy (together with the neutral particle energy). Radiation anisotropies and local neutral particle concentrations cannot be detected.
In most cases of clean, high density discharges with low-Z limiters a deficit in the power balance appears which can amount to 50 % of the input power /4/, but no satisfactory explanation can be given where the missing energy went. Radiation anisotropies and local neutral particle concentrations near the limiter or gas feed ports, which produce

enhanced charge exchange could be able to carry out an extra amount of power. Also an anomalous charged particle transport across the scrape-off layer can be supposed which up to now could not be detected unequivocally. It seems that the divertor tokamaks which can be operated also with a limiter are able to shed light on this problem. Recent measurements by the ASDEX-team with very clean diverted discharges revealed that the power balance shows in this case no major deficit (cf. Table 1).
These results indicate, that the unexplained power loss in limiter discharges should be due to a parallel flow in the scrape-off layer onto the limiter coupled with the production of a cold gas blanket in the vicinity of the limiter. The build up of this blanket may be a reason why only a small part of the deficit power can be detected on the limiter itself, while the rest enhances the local power unload to the walls mostly not detected by bolometer devices for technical reasons.

More generally it can be stated, that every obstacle e.g. a probe or antenna placed in the scrape-off plasma produces a considerable pertubation in its vicinity coupled with an enhanced power unload to the walls. This conception is supported e.g. by a finding during measurements with the surface analysis station WASA on T-10. The bolometer array of T-10 located in the vicinity of the WASA-probe showed a strong increase of its readings when the probe was moved toward the plasma edge. Striking evidence of the build-up of a higher neutral particle density near the limiter gave recent results obtained from ASDEX /5/, investigating the recycling. A similar result was reported by the PDX-team /6/ which also pointed out that the missing energy in the nondiverted case may be due to asymmetries in power loss, e.g. enhanced recycling at the limiter which are not measured by the bolometer.

PARTICLE BALANCE

So, the uncertainties of the power balance may be considerable but that of the particle balance is even larger, mainly because it is very difficult to measure particle

fluxes to and from the walls and other material structures. The main processes of the particle balance are recycling of the working gas including fueling and exhaust processes and the production and dynamics of impurities. Although these processes are substantially interrelated recycling and impurity behaviour in most models are treated separately. The models vary greatly in complexity, some treating only spatial averaged quantities, others radial transport with and without time dependence /7, 8/.

Without going into details of these models it should be pointed out that there exists a considerable discrepancy of views concerning the impurity generation. It is generally accepted that sputtering is the main process of heavy impurity production, the role of unipolar arcs still being somewhat obscure. The pollution of the plasma by light impurities - mainly oxygen and carbon - depends on the degree of cleanliness of the surfaces exposed to the plasma.

The question is whether ions of the working gas and/or of impurities diffusing across the magnetic field to the walls and possibly accelerated by Langmuir sheaths are the main impurity source by sputtering or if the impurities are produced by the ion flow in the scrape-off to the limiter or any other protuberance of the vessel which acts as a limiter. We will discuss this problem more in detail, and consider therefore somewhat closer the recycling and impurity generation.

RECYCLING

The behaviour of the working gas pressure in tokamaks during and after the discharge is rather complex and governed by the recycling at the walls /1, 9/. Charge exchange neutrals and ions which have diffused across the confining field or were guided along field lines into the scrape-off layer, impinge on the walls, limiters and other internal structures. There they are partially backscattered, mostly in form of neutrals, partially they are absorbed, trapped and may be reemitted by subsequent diffusion. Besides that working gas desorption by particle bombardment and photons takes place /10/. The density behaviour of a tokamak depends very sensitively upon those mechanisms of recycling,

especially because the amount of working gas accumulated in the solid structures and walls can be several orders of magnitudes larger than that in the plasma. For tokamak operation it is usually desirable to have an effective recycling coefficient less than unity, so that the density can be controlled by external gas feed.
Very convincing is the isotope change-over technique to demonstrate the influence of the wall interaction processes on plasma density and composition used in T-2, DITE, ISX and TFR /11, 12, 13, 14/, indicating clearly the importance of the choice of suitable wall material with a low tendency of working gas accumulation, a problem of extraordinary interest in tritium fueled systems.
Direct measurements of recycling, the working gas flux to and from the walls, its charge state and energy distribution are very difficult. Detection and energy analyzing of the charge exchange neutral outflux is an important tool in understanding recycling. The widespread used gas stripping cells give information on the outflux only at energies above several hundred eV, thus probing primarily the plasma core. A time of flight method first used by Voss and Cohen /15/ is capable to measure the energy distribution of outflowing neutrals in the energy range down to 28 eV. First measurements of the energy spectrum of the neutral deuterium outflux of PLT showed a strong increase of the neutral flux with decreasing energy. The bulk of the charge exchange neutrals are emitted at energies up to 200 eV. Comparing the measured total neutral particle outflux and the corresponding power outflux due to charge exchange neutrals in the flat top phase of the discharge with the total particle loss and the Ohmic heating power the authors conclude that the power and particle loss due to charge exchange neutrals down to 28 eV are negligible small, at least away from the limiter and assuming an isotropic flux. But as already discussed the particle flux is far from being isotropic and strong local enhancements of the neutral outflux are to be expected. It should be pointed out that also neutrals below 28 eV can substantially con-

tribute to the recycling if one assumes the existence of an enhanced low energy recycling in the boundary plasma. No direct evidence for this process is available up to now.

The ions of the working gas which diffuse across the field out of the plasma core are considered free streaming in the scrape-off layer with nearly the ion sound velocity parallel to the resulting magnetic field. The perpendicular diffusion coefficient $D_\perp$ is very difficult to determine and known only by order of magnitude, depending on the models used for its calculation.
Because of the lack of a valid model for the diffusion coefficient which explains the observed tokamak behaviour, one assumes the same anomalous diffusion coefficient $D_\perp$ for all species. Experimentally $D_\perp$ is inferred from measurements of density profiles and the evaluation of source and loss terms. The whole procedure is prone to arbitrariness, e.g. the determination of the wall loss term is very problematic. Perpendicular diffusion coefficients determined this way range from the Bohm value down to less than one tenth of it. An order of magnitude estimate shows that ions reach the walls in the case when the thickness of the scrape-off layer d, defined by the limiter edge to wall distance, becomes comparable with $\sqrt{D_\perp \frac{L}{v_\parallel}}$ where L is the path length along the magnetic field lines. This sort of estimations, however, seems to be not very useful because of the large uncertainties contained. In most model calculations the ions diffusing to the walls are neglected, all ions are assumed to flow along the magnetic field lines to the limiter or into the divertor chamber.

This situation demonstrates clearly the importance of other more direct methods to determine the parallel and perpendicular components of the particle flux in the boundary plasma and the scrape-off layer.
Very useful tools for the study of working gas recycling are deposition probes exposed in the limiter shadow and their subsequent investigation by thermal desorption, nuclear reactions, damage analysis and SIMS /16, 17, 18, 19/. The evaluation of probe measurements yielded the following

results which were similar in the investigated tokamaks: 1. the integral flux parallel to $\vec{B}_T$ shows by order of magnitude, that most plasma ions flow onto the limiter; 2. the energy of these ions near the plasma edge ranges about from 50 eV to 200 eV, the different methods showing unsatisfactory agreement; 3. only very few measurements are available which compare the flux and energy parallel and perpendicular to $\vec{B}_T$ giving comparable values /19/. Recently new methods were introduced like the determination of the energy of gyrating ions by the transmission of apertures in thick shields /20/ and the $\vec{E}x\vec{B}$ drift analyzer /21/ which gives the parallel flux and energy distribution of ions in real time. These methods look very promising but further results are needed for their critical examination.

The measured densities or temperatures have an exponential decay from the radial positions of the measuring probes. The e-folding lengths found in the scrape-off layers for a variety of different plasma conditions in DITE, PLT and ISX-B /18, 19, 22/ depend on core densities or temperatures and also on the thickness of the limiter shadow region. They range from 20 to 60 mm. About the same attenuation length is found in arcing intensity and for the electron density measured by Langmuir probes /22/. But especially Langmuir probe results obtained in the strong magnetic field of a tokamak should be considered with caution. Most careful comparisons of Langmuir probes with other methods were made by Proudfoot et al. /22/ which gave a good agreement.

There are some publications which consider the existence of an universal Langmuir sheath on all surfaces which are in contact with the plasma giving an extra acceleration of the ions in direction onto the surface /23/.

The action of Langmuir sheaths in the presence of strong magnetic fields should be carefully analyzed. The existing experimental results do not allow to draw appropriate unambiguous conclusions.

The measurements of the recycling ions and neutrals near the wall which are available at present are obtained on

different tokamaks with conditions hardly to compare. The agreement is poor and it is very difficult to draw any conclusions of universal validity. Nevertheless it should be possible to make on the basis of the existing measurements the following tentative statements concerning the scrape-off plasma of a limiter operated tokamak at least for the steady state phase of the discharge: 1. charge exchange neutrals and ions diffusing across the $\vec{B}_T$-field far away from limiters constitute only a minor part of the recycling (it cannot be excluded that very low energy neutrals (<30 eV) give a notable contribution); 2. the main contribution to the recycling is produced by the ion flux onto the limiter possibly supported by the density enhancement in the vicinity of the limiter and the formation of a Langmuir sheath; 3. the formation of a Langmuir sheath parallel to the wall and its influence on wall interaction requires more detailed experimental and theoretical investigations. There considerable deviations have to be expected from the discussed behaviour of recycling during start-up and at the end of the tokamak pulse, in particular a major contribution of the walls.

This above stated conception received recently strong support by investigations of recycling in ASDEX with divertor and the comparison with limiter discharges in the same machine /5/. In the pumped divertor mode the density decay after gas feed shut off becomes equal to the particle containment time, the effective recycling coefficient in the torus being near zero. This leads to the conclusion that the main part of the plasma in the scrape-off layer is streaming into the divertor where it is neutralized and effectively pumped by Ti-gettering while the recycling at the torus walls is negligible.

These results look very promising and there is hope that investigations of that kind in divertor-tokamaks will give important information on the entire recycling problem.

THE ROLE OF IMPURITIES IN A TOKAMAK PLASMA, THEIR GENERATION AND BEHAVIOUR

The necessity for maintaining plasma purity has long been recognized as an important condition for successful toka-

mak operation. Since early experiments the plasma cleanliness in tokamak devices has been improved considerably owing to better vacuum techniques, to the choice of suitable construction materials and machine conditioning processes and last but not least by increased operating experience. Most present-day tokamaks have a wide region of stable operation thanks to the low Z_{eff} reached, as shown in the plot (fig. 2) /1/ of the normalized current 1/q over the normalized density $n_e \frac{R}{B_T}$. The contures of Z_{eff} which put a border round the regions of stability show how the range of stable operation expands as Z_{eff} is reduced.

Spectroscopic measurements show that light impurities, especially oxygen, appear early in the tokamak discharge when the ion temperature is still low. The upper density limit is despite careful cleaning procedures, still posed by disruptions preceded by an increased influx of light impurities. The most abundant low-Z impurities in tokamak discharges are oxygen and carbon and to a less extent Cl, S and N. The concentration of O and C is low in the bulk of construction materials mostly used in tokamaks like stainless steel or inconel. However, the surfaces of these materials are generally covered with layers containing large amounts of O and C, even after thorough chemical cleaning procedures (etching and treating with different solvents), baking and outgassing in ultra high vacuum. In the last years considerable progress has been achieved in developing efficient discharge conditioning procedures, reviewed by Dylla /24/. The use of surface analysis methods and residual gas analysis led to an insight into the conditioning processes, to the understanding of the physical and chemical surface process during cleaning and power pulses.

The conditioning procedures include mostly a combination of the following steps: 1. Chemical or physical pretreatment of the construction material; 2. Baking under ultra high vacuum condition; 3. Discharge cleaning; 4. Wall coating or gettering. The first step is only capable of a gross reduction of surface contaminations. It has been

shown /25/ that an effective further cleaning can be achieved by the initiation of plasma chemical reactions producing volatile compounds which can be pumped by ultra-high vacuum methods. For the demonstration of the cleaning processes it is useful to refer to a schematic representation of the near surface region e.g. of stainless steel /24/, fig. 3. The bulk material is covered with the passivation oxide layer of several ten nanometers thickness consisting of metal-oxides like FeO, Fe_2O_3, Cr_2O_3, water and other C- and O-rich compounds. This near surface layer is covered by an upmost layer of hydrocarbons, water and adsorbed residual gases like CO and CO_2. Partially these residual gases can be absorbed also by the less compact structure of the oxide layer. As a rule the surface of the bulk material is not smooth but its structure is disturbed by machining, etching etc. in a layer up to several /um, showing grain boundaries and mechanical cracks. The more coarse cracks are also covered with surface layers, the grain boundaries are the accumulation sites for S and Cl.

Low temperature ($T_e < 10$ eV) low pressure discharges in hydrogen (up to several Pascal) in combination with elevated wall temperature proved to be very effective in reducing the different surface contaminations. By the action of hydrogen ion bombardment complex hydrocarbons are partially cracked into volatile compounds, CH_4 and C_2H_6 being the most probable reaction products. It is important to use a sufficiently low plasma temperature to prevent an appreciable dissociation and ionization of the released gases. In a similar way CO and CO_2 are released by plasma chemical reactions and a nearly perfect removal of surface carbon can be attained.

The production of volatile water molecules is somewhat complicated and closely connected with the reduction of the metal oxides. As it was shown by XPS the iron-oxides are easily reduced while the chromium oxides are more stable /26/. The reduction of iron-oxides at least partially takes place via production of hydroxides and sub-

sequent liberation of water /25/.
The passivation oxide layer can be reduced only to a certain degree, while the remainder of the oxides is stable. There are considerable differences in the stability of various oxides with respect to reduction with hydrogen, e.g. Cr_2O_3 is much more stable than FeO or NiO. These oxides together with adsorbed residual gases and impurity layers in cracks establish a permanent oxygen source for tokamak discharges.
A certain reduction of oxygen generation can be achieved by titanium gettering which proved to be very successful in a number of tokamaks. The action of Ti-gettering implicates the formation of stable Ti-oxides and their burial by Ti-films. But films produced by repeated Ti-gettering tend to flaking, in particular if saturated with working gas. In future reactors gettering seems to be impracticable because of the tritium-accumulation in Ti-getter films.
Oxides can be totally removed by using sputtering processes with ion energies above the sputtering threshold. But it should be noted that a redeposition of the sputtered products inside the vessel would be the main effect which can be adverse to a proper tokamak operation. Thus the conclusion can be drawn that plasmachemical conditioning procedures in hydrogen discharges ending up in volatile reaction products are most promising for reducing the low-Z impurity sources.
Despite thorough conditioning the complete elimination of light impurities seems to be impossible. Oxygen remains the dominant impurity in all known tokamak devices at least during the start-up phase of the discharge. Spectroscopic measurements and time resolved investigations by surface analysis probes show that the oxygen density rises fast in the start-up phase, sometimes having a slight maximum there. During the plateau phase in a quiescent, not disturbed discharge the oxygen concentration remains constant. Only at the end of the discharge, especially when coupled with a disruption, a pronounced rise of the oxygen signals is observed. Qualitatively this behaviour coincides with the

conception that the surface interaction of the plasma is most intensive only in the start-up and shut-off phases when the MHD activity of the plasma is high. During the steady state phase the surface interaction should be concentrated on the limiter or inside the divertor chamber, in analogy to the main flux of the working gas, while the flux of impurity ions to the walls is low. This is one important point of discussion, especially in connection with the question of the production of heavy impurities by sputtering.

In the following the main sources of heavy impurities are discussed. In spite of a great number of different measurements and model calculation it seems impossible up to now to give clear-cut answers to the following questions:

1. What is the contribution to the impurity production by wall sputtering processes due to charge exchange neutrals and ions of the working gas and due to ions of impurities?
2. Which portion of the impurities is produced on the limiter surfaces facing B_T by working gas ion sputtering, light and heavy impurity ion sputtering?
3. What is the contribution to the impurity generation by arc discharge type erosion processes (unipolar arcs)?
4. Which is the transport behaviour of impurity ions in the tokamak plasma? Is there an impurity accumulation in the plasma core to be expected?

There is an extensive literature, a large number of measuring results is reported, but there is nearly as large a number of different interpretations. The discussion is complicated because the experimental results are mostly attained with different installations and with barely to compare conditions and in nearly all cases they are subject to considerable measuring uncertainties. This situation is an unfavourable starting point for the discussion of the questions formulated above.

SPUTTERING DUE TO PLASMA SPECIES

As already discussed the charge exchange neutrals and ions of the working gas diffusing across the $\vec{B}_T$-field far away from limiters or other internal structures protruding into

the scrape-off layer give only a minor contribution to the recycling. Accordingly the expected metal impurity generation by wall sputtering due to the working gas should be low. Voss and Cohen /15/ estimated the sputtered iron flux due to charge exchange neutrals on the basis of their measurements to 2,2 . 10^{12} atoms $cm^{-2}s^{-1}$ during the flat top portion of the PLT-discharge with peaks at start-up and at the end of the discharge. They took already into account that working gas particles at oblique angels of incidence on the wall give an enhanced contribution to sputtering due to the fact that at oblique incidence the sputtering yield, e.g. for hydrogen is up to 20 times the value at normal incidence. Even considering the additional acceleration of ions by the Langmuir-sheath, which is not very conceivable in the case of a surface parallel to $\vec{B}_T$, the metal impurity generation by working gas species at the wall away from limiters or other structures with locally enhanced density is small and does not explain the metal impurity concentrations found in clean, high density discharges. Another strong argument in favour of this statement is the fact that changes of the working gas from H to D and to He do not show a pronounced increase of wall specific metal impurities as should be expected with respect to the considerable difference of the sputtering yields for different types of plasma ions. The increase of Mo-contamination in consequence of the change from deuterium to helium observed by Suzuki et al. /27/ is no contradiction because it is related to the sputtering of the Mo-limiter.

There is, however, some strong evidence, that ions should be responsible for the impurity generation by wall sputtering. Investigations by Oren et al. /28/ have shown that the metal influx increases as the negative bias potential is increased on special isolated metal targets placed close to the inside wall. These authors observed that the metal influx is very asymmetric and correlated with the position of the plasma. As reported by the T-10 team /29/ the metal impurity generation increases with the decrease of the thickness of the scrape-off layer. It is supposed that

that these metal impurities (which are typically wall material) originate from the walls.

A more general approach given by McCracken /30/ to estimate the sputtering due to plasma ions is to consider the total energy coming out in the ion channel. Bearing in mind that the energy transferred to the ions and charge exchange neutrals must arrive at the walls or limiters and using Bohdansky's empirical formula for the sputtering yield /31/ the total sputtering rate for any material or plasma species can be estimated without knowing the energy of the ions arriving at the walls. The sputtering rates calculated will include sputtering by both ions and charge exchange neutrals since both result in energy loss from the ion channel. It will not include the effects due to sheath potentials accelerating ions since this energy will be absorbed from the electron channel. The metal impurity generation calculated this way corresponds by order of magnitude with measured values of metal impurity concentration.

Since in the foregoing was shown that wall sputtering is too small, the conclusion can be drawn that plasma ion sputtering contributes substantially to the metal impurity generation at limiters and that ions and charge exchange neutrals can give an additional share at local asymmetries and density enhancements. But there is still no firm experimental evidence that the working gas species sputtering is the determinating mechanism.

IMPURITY ION SPUTTERING

Impurity ion sputtering seems to be an important impurity generation process according to indications by a number of experiments. In JFT-2 /27/, PLT /32/, and T-10 /29/ a relation between the concentration of light impurities, above all oxygen, with the generation of metal impurities was observed. At the same time the electron temperature of the edge plasma was found to have a great influence on the impurity generation.

Most of these observations can be explained with the following conception.

Impurity ions do not, as to be expected by the neoclassical

theory, accumulate in the plasma core. It was shown experimentally that a continuous transport of impurity ions in low charge states to the axis of the discharge is balanced by an outward orientated transport of impurity ions, mostly in higher charge state. The driving mechanism for this outward directed transport of impurities is still an open question. Some experiments indicate that sawtooth oscillations may be responsible for that /29/. Like in the case of plasma particle transport the ratio of the perpendicular to the parallel components of the outward diffusing impurity ion flux could not be determined up to now. According to the cross field diffusion of working gas ions it should be expected that the major part of the impurity ions is guided onto the limiter where the main sputtering should occur. Up to now deposition probe measurements did not give unambiguous results concerning the ratio of the perpendicular to the parallel impurity flux. Only recent investigations on divertor discharges /5, 6, 33/ showed that the main impurity source was moved into the divertor chamber, demonstrating very convincing the major role of the parallel flux.

In a simple zero dimensional impurity balance model taking into consideration only one impurity species McCracken /1/ showed that at impurity sputtering rates S_i above unity the total number of impurity ions should increase indefinitely. For most impurity ions the sputtering rate can attain large values because of their high mass and charge states and possibly because they can be accelerated in a Langmuir sheath to many times the energy of singly charged atoms. The impurity ion energy at which $S_i > 1$ is well within the values to be expected with real tokamak conditions. This model, however, is an obvious oversimplification. The increased influx of light impurities cools the plasma edge by ionization and radiation losses and thus lowers the energy of the ions sputtering the wall and limiter and preventing the indefinite increase of impurities. A more complete model should take into account the plasma edge parameters and the different behaviour of light and heavy impurities. Oxygen, the most abundant im-

purity, which is generated in the very beginning of the discharge by the strong interaction of the unstable start-up plasma with all inner surfaces is considered to sputter heavy impurities by the above described mechanism, the ion energy and thus the sputtering rate being determined by the edge temperature. Correspondingly there should be an increase of metal impurities with an increase of the light impurity concentration as long as the edge temperature keeps nearly constant. When the edge plasma is heavily cooled by a stronger influx of light impurities or by an additional working gas feed a reduction of the metal sputtering should be expected. This behaviour of the metal impurity generation in dependence of the light impurity concentration and the edge temperature was calculated by Cohen et al. /34/ (fig. 4) for the system oxygen-wolfram. It explains qualitatively the apparently conflicting experimental observations that in some cases the light and heavy impurity concentrations are directly proportional /27, 32/ and in other cases e.g. /35/ a reciprocal proportionality is observed.

Estimates of the heavy impurity generation on the basis of sputtering by light impurities give the right order of magnitude which has to be expected according to experimental studies.

IMPURITY GENERATION BY ARCING PHENOMENA

Post operation investigations of structures protruding into the boundary plasma like limiters, neutralizer plates, probes, RF-antennas etc. revealed the action of arc discharge erosion phenomena in nearly all tokamaks. In most cases linear tracks can be discerned, their microstructure resembles the cathode tracks produced by metal vapour arcs in vacuum. A closer investigation shows that these tracks follow a distinct direction in the resulting magnetic field $\vec{B}$ which generally consists of two components. The first is the retrograde motion (contrary to the Amperian $\vec{j} \times \vec{B}$-rule) and the second is a drift motion (Robson-drift) which occurs only if the magnetic field is inclined to the surface /36/. If $\vec{B}$ is perpendicular to the surface arc spots move randomly similar to the case without an external magnetic

field. Arcing tracks are observed mainly on the ion drift side of the inner tokamak structures and on surfaces parallel to the magnetic field. The arcing intensity (total length of arc tracks per square cm and per tokamak-pulse) is decreasing with approximately the same e-folding length as the electron temperature of the boundary plasma.

Two different types of arc tracks occur, in dependence on surface conditions - a phenomenon well known from vacuum arc studies /37/. In the one case the arc tracks are made up of chains of partially overlapping craters with diameters of about 10 μm. This type of craters is known to develop on clean surfaces, free of sorption layers, or on weakly oxidized surfaces. In some cases craters with diameters up to 100 μm were observed which possibly develop on clean surfaces at elevated temperatures /38/. The other type of arc tracks which is due to contaminated surfaces shows a fern-like structure and moves much more randomly. It consists of groups of small craters, with diameters less than 1 μm, on surfaces with thick contamination layers sometimes not showing a dicernible crater structure. In the case of clean metal surfaces the average impurity generation by arcing may be estimated by evaluating the material removed from the tracks taking into account their local distribution. This procedure is subject to great uncertainties, giving at the best an order of magnitude estimate. No way is known which allows to register the time evolution of all arcing tracks per discharge. Therefore one depends upon extrapolations from small probe surfaces, where arc currents and the development of single tracks can be studied. Average arc durations of 5 to 50 μs are observed with arc spot velocities between 30 to 300 m/s. The arc current ranges from 10 to 100 A with a crater current density in the case of clean surfaces of the order 10^{12} A/m^2.

The approximate impurity production per track ranges from 10^{16} to 10^{17} atoms. Taking into account the average arcing intensity and its exponential decrease with the distance from the plasma a rough estimate gives an erosion of 10^{19} atoms per discharge in a medium sized tokamak. In the

case of fern-like tracks the estimate is more uncertain and depends largely on the kind and the thickness of contamination layers. It tends to give lower values of eroded impurities which are composed mainly of low-Z species. By order of magnitude this amount is comparable with or even larger than the amount of metal impurities detected in many tokamak discharges.

Time resolved probe measurements correlated with spectroscopic investigations showed that arcing phenomena occur almost exclusively during phases of unstable plasma performance e.g. during breakdown and start-up, at plasma termination coupled with instabilities or at instances of plasma pertubation by deliberate gas injection.

The most striking feature of the arcing phenomena occurring in thermonuclear devices is the absence of an easy identifiable anode while the cathode or more exactly the remnants of arc cathode processes can be detected unambiguously. The anode is considered either to be distributed over a large area of the inner walls or possibly concentrated in an isolated area in the vicinity of the cathode spot. An explanation of this so-called unipolar arc has been given already by Robson and Thonemann /39/ considering the Langmuir sheath potential $U_L = \frac{kT_e}{2e} \ln \frac{m_i}{2\pi m_e}$ to be the driving e.m.f. (in the case of a H-D plasma U_L is approximately 3 kT_e, neglecting secondary electrons).

If this potential drop exceeds the arc cathode drop of potential, typically 15-20 V, an unipolar arc may be sustained. The electrons which are emitted from the cathode spot return via the distributed anode. The energy for the circulating current is provided by hot plasma electrons.

Like a vacuum arc the unipolar arc has a minimum current of several Amperes leading to a minimum area condition for the anode zone depending on the plasma density and electron temperature in its vicinity.

The occurrence of unipolar arcs is much less a question of the arc existence conditions rather than of suitable ignition conditions /40/. Neither the field strength (10^4 ... 10^5 V/cm) nor the energy input of the stable sheath would be sufficient to initiate an arc. Supposed ignition pro-

cesses are local enhancements of the sheath potential and field strength or localized thermal electron emission produced by the contact of the hot plasma with walls during instabilities, runaway beams or by the sudden dissipation of poloidal magnetic energy accumulated in isolated plasma flux tubes, when they are interrupted by material structures (e.g. limiter) /41/. This last mechanism or the additional action of the loop voltage which can attain large values during start-up /42/ explain the prevailing ignition of arc spots on the ion drift side of limiters.

It is an open question which fraction of the material eroded by arcing actually gets into the plasma, especially because a considersble portion is ejected in form of metal droplets which are partially found in the vicinity of the eroded structures and some of which are exceptionally large due to the big (~100 /um) craters.

An important problem is whether there are possibilities to suppress arcing by certain conditioning processes. It was established that the experiences from vacuum discharges are fully transferable. By suitable choice of material, cleaning and discharge conditioning arcing can be reduced to a certain amount, especially arc tracks of the fern-like structure can be avoided this way.

Arcing seems to be no problem during the steady state phase of the discharge. During start-up no menas are known to completely avoid arcing. It seems to be useful to aim at a as short as possible start-up phase, low plasma densities and temperatures near solid surfaces and small subdivided inner structures.

CONCLUSIONS

Z_{eff} near unity has been attained in almost all present-day tokamaks by methods developed in a semi-empirical way: plasmachemical discharge cleaning and Ti-gettering to decrease the light impurities, plasma edge cooling and transfer of the impurity generation into the divertor chamber to diminish the heavy ones.

Generally the impurity sources are well known, the corresponding fundamental processes like desorption, surface melting and evaporation, plasma chemical reactions, sputter-

ing, arcing etc. are investigated in a sufficient extent to carry out model calculations. Naturally there is still lack of more refined data and synergistic effects must be taken into consideration. The main problem, however, is the incomplete knowledge of the flux of plasma and impurity species from the plasma core to the solid surfaces. The cross field diffusion coefficients, the perpendicular and parallel components of the outflux, the charge state and energy distribution of the particles arriving at the solid surfaces, the action of a Langmuir sheath are almost unknown by quantity. The problem is even more complicated because anisotropies of the fluxes seem to play a decisive role.

At this point it is very difficult to decide which of the impurity generating mechanisms is the crucial one. Sputtering by working gas ions and by impurities just as arcing produce comparable quantities of impurities (at least by order of magnitude).

Another open question is which portion of the impurity species generated at surfaces actually gets into the plasma, how deep do they penetrate and is there any recycling in the outer edge. This is important in particular to erosion phenomena such as arcing which can produce among others larger particle aggregats, droplets, chunks etc.

More refined investigations of the plasma edge and of the scrape-off layer are imperative. As to be expected, all probe methods (both deposition and real time probes) suffer from the perturbation of the plasma near the probe, from the hardly to verify action of space charge sheaths and possibly from an enhanced recycling near the probe. Improved probe measurements with better directional and time resolutionand higher sensitivity are urgently needed as well as measurements of the outflux of neutral particles down to low energies in the vicinity of places with enhanced recycling and far away from such places. Laser fluorescence spectroscopy raises great expectations because of its potential possibilities to perform local time-resolved measurements of the densities and velocity distributions of

the impurities and the plasma species without disturbing the plasma. It is hoped that the new divertor tokamaks will give more information concerning the above raised questions by comparing the performance of a limiter with that of a divertor.

ACKNOWLEDGEMENT

I have the pleasure to thank my colleagues K.F. Alexander, E. Hantzsche, B. Jüttner, J. Lingertat and P. Pech for helpful discussions.

REFERENCES

/1/ G.M.McCracken, P.E.Stott, Nucl.Fusion 19 (1979) 889

/2/ Plasma Surface Interaction in Controlled Fusion Devices, Proc. 4th Int. Conf., Garmisch-Partenkirchen FRG 1980, North-Holland Publ.Corp. 1980, Reprinted from J.Nucl.Mat. 93&94 (1980)

/3/ R.J.Bickerton, J.Nucl.Mat. 76&77 (1978) 16

/4/ E.B.Mesarvey et al., J.Nucl.Mat. 93&94 (1980) 267

/5/ G.V.Gierke, MPI Plasmaphysik Garching, Jahresbericht 1980, 49

/6/ D.K.Owens et al., J.Nucl.Mat. 93&94 (1980) 213

/7/ H.C.Howe, J.Nucl.Mat. 93&94 (1980) 17

/8/ H.Vernickel et al., Proc.Int.Symp. Plasma-Wall Interaction Jülich 1976, 207

/9/ E.S.Marmar, J.Nucl.Mat. 76&77 (1978) 59

/10/ G.M.McCracken, Proc.Int.Symp.Plasma-Wall Interaction Jülich 1976, 339

/11/ V.A.Simonov et al., Proc.IAEA Conf.Plasma Phys.Contr. Nucl.Fusion, Salzburg 1961, paper CN-10/254

/12/ G.M.McCracken et al., Nucl.Fusion 18 (1978) 35

/13/ H.Helava, Bull.A.P.S. 22 (1977) 1147 (6A4)

/14/ TFR Group, J.Nucl.Mat. 93&94 (1980) 173

/15/ D.E.Voss, S.A.Cohen, J.Nucl.Mat. 93&94 (1980) 405

/16/ S.K.Erents et al., J.Nucl.Mat. 93&94 (1980) 115

/17/ G.Staudenmaier et al., Nucl.Fusion 20 (1980) 96

/18/ S.A.Cohen et al., J.Nucl.Mat. 93&94 (1980) 109

/19/ R.A.Zuhr et al., J.Nucl.Mat. 93&94 (1980) 127; 146

/20/ G.Staudenmaier et al., J.Nucl.Mat. 93&94 (1980) 121

/21/ P.Staib, J.Nucl.Mat. 93&94 (1980) 351

/22/ G.Proudfoot, P.J.Harbour, J.Nucl.Mat. 93&94 (1980) 413

/23/ V.S.Voitsenya et al., Review Paper, Preprint KFTI 81-24, Kharkov, USSR 1981

/24/ H.F.Dylla, J.Nucl.Mat. 93&94 (1980) 61

/25/ F.Waalbroeck et al., Berichte der KFA Jülich No. 1692, Dez. 1980

/26/ P.Staib et al., J.Vac.Sci.Technol. 17 (1980) 291

/27/ N.Suzuki et al., Proc. 9th Europ.Conf.Contr.Fusion a. Plasma Physics, Oxford 1979, paper D2.3

/28/ L.Oren et al., J.Nucl.Mat. 76&77 (1978) 412

/29/ A.B.Berlizov et al., 8th IAEA Conf.Plasma Physics a. Contr.Nucl.Fusion, Brussels (1980) paper CN-38/A-2

/30/ G.M.McCracken, J.Nucl.Mat. 93&94 (1980) 3

/31/ J.Bohdansky et al., J.Appl.Phys. 51 (1980) 2861

/32/ S.Suckewer, R.J.Hawryluk, Phys.Rev.Letter 40 (1978) 16499

/33/ S.Sengoku et al., J.Nucl.Mat. 93&94 (1980) 75

/34/ S.A.Cohen et al., J. Nucl.Mat. 76&77 (1978) 459

/35/ E.Hinnov et al., Nucl.Fusion 18 (1978) 1305

/36/ W.Hintze, M.Laux, Beitr.Plasmaphys. 21 (1981) 213

/37/ B.Jüttner, Beitr.Plasmaphys. 19 (1979) 25

/38/ B.Jüttner (priv. communication)

/39/ A.E.Robson, P.C.Thonemann, Proc.Phys.Soc. 73 (1959) 508

/40/ E.Hantzsche, Proc. 15th Int.Conf.Phen.Ion.Gases, Minsk 1981, topical lecture

/41/ S.V.Mirnov, Fizika Plasmy 7 (1981) 687

/42/ A.V. Nedospasov, V.G.Petrov, J.Nucl.Mat. 93&94 (1980) 775

Table 1 (ASDEX)

	limiter mode	divertor mode
Ohmic heating	290 kW	290 kW
radiation (torus)	50 %	34 %
radiation (divertor)	-	40 %
neutralizer plates	-	21 %
power deficit	50 %	5 %

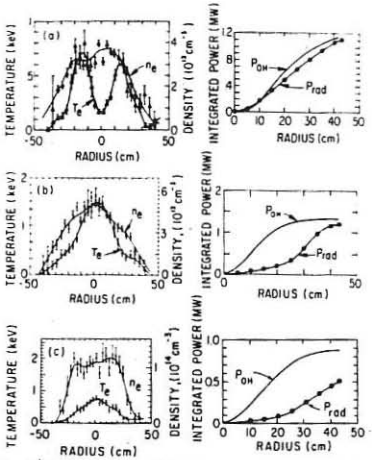


Fig. 1 | Radial profiles of electron temperature and density from Thomson scattering and bolometer measurements of radiated power for ohmically heated discharges for three different cases: (a) tungsten limiters showing the hollow temperature profile and totally radiation-limited discharges; (b) graphite limiters, peaked temperature profile, large power radiated from outside, little radiation from hot center; (c) graphite limiters, titanium evaporated on walls between discharges, low power radiated from center, power radiated from outside distinctly less than power input.

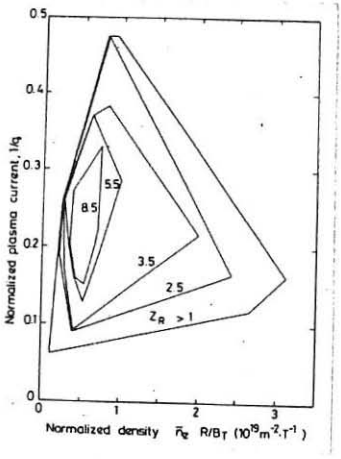


Fig. 2: Regions of stable tokamak operation /1/.

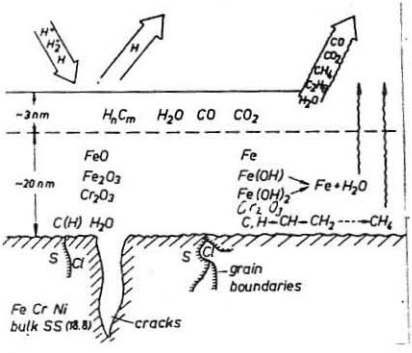


Fig.3: Schematic representation of the near surface region of stainless steel /24/.

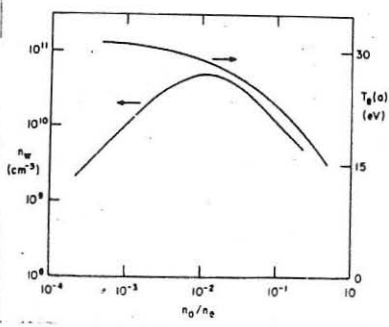


Fig. 4: Predicted steady state tungsten concentration caused by O^{6+} oxygen ions sputtering a limiter, as a function of oxygen concentration. The ions were assumed to be accelerated by the sheath potential. At high concentrations the edge cooling reduces the energy of the ions and reduces the sputtering rate /34/.

INERTIAL FUSION RESEARCH AT ILE OSAKA

C. Yamanaka

Institute of Laser Engineering
Osaka University
565
Japan

Abstract

The outline of "Project KONGOH" at ILE Osaka is presented. The four waves of lasers, output of 7 TW, 3 kJ are provided as well as light ion beam of 1 MeV, 200 kA.

The wave length scaling of ablation is discussed. Hot electron driven ablation is analized. The uniformity of compression and filamentation of the pellet surface are investigated.

Advanced target design "cannon ball pellet" is proposed. Anomalous transport "Osaka effect" is also reexamined to this scheme.

Conceptual design of ICF reactor using magnetic guided Li fall is tabulated.

INERTIAL FUSION RESEARCH AT ILE OSAKA

C. Yamanaka

Institute of Laser Engineering
Osaka University

1. Introduction

The project "KONGOH" has started to demonstrate the scientific feasibility of inertial confinement fusion since 1980 at ILE Osaka.

Inertial confinement fusion research is based on the three important items: development of powerful energy driver, pertinent design of a fuel pellet and precision diagnostics for implosion.

The driver program at ILE has made significant progress in three categories. The GEKKO program on glass laser systems has developed to provide the laser wave length of 1.06 μm, 0.53 μm and 0.32 μm. The maximum output of the laser at the moment is 7 TW 2 kJ. The GEKKO XII system will be completed in a year which can deliver 40 TW, 20 kJ in twelve beams. The LEKKO program has constructed an 8 beam CO_2 laser system of 10 kJ in 10 μm wave length. And the light ion beam system "REIDEN IV" is also completed to deliver the beam of 1 MV 200 kA.

The various kinds of drivers can supply the interesting experimental results with the comparison of different coupling data.

The pellet design and fabrication are also developed. Several simulation codes: Lagrangian, particle in cell, iced-ale etc. have been organized to estimate the process of implosion and to design the pellet.

The implosion has been investigated depending upon the fundamental data of the interaction: absorption, energy transport and ablation.

Anomalous transport called "Osaka effect" has been retreated to use for a new implosion scheme.

A concept of inertial confiment fusion reactor has been investigated. The design of ICF reactor "SENRI-I" utilizes a thick Li flow guided and controlled by a magnetic field to mitigate the wall loading of the reactor chamber. The data of concept design seem to be very interesting.

2. Energy drivers

ILE has three different kinds of drivers: GEKKO series of Nd glass lasers, LEKKO series of CO_2 lasers and REIDEN series of focused LIB generators. Table 1 shows our laser systems, details of these are reported elsewhere[1].

(1) GEKKO series glass lasers

GEKKO II(GII) is a silicate glass two-beam laser system which has been used since 1975 for the basic experiments. GII can deliver 0.4 TW/0.1 ns or 0.1 kJ/0.8 ns in 80 mm^{ϕ} beam aperture.

GEKKO IV, four beam system was developed in 1978 using Nd-phosphate laser glass, which could deliver 1 TW/0.1 ns per beam. The tetrahedral symmetric focusing optics was used for the ablative compression experiments. GEKKO MII, 200 mm^{ϕ} aperture two-beam system has been completed in 1980. Peak output power of 3.4 TW/0.1 ns per beam was recorded. This laser is a prototype for GEKKO XII system. The main efforts were concentrated fabricating the most efficient laser as well as the full automatic control system.

A block diagram of the control system is shown in Fig.1. The laser controller commands the sequential performance of various laser components and monitors and the operation data of the system.

The functions of the alignment controller consist of the optical alignment of laser beam, positioning the pinhole of the spatial filter and the beam synchronization. The accuracy of the alignment and the required time are described in Table 2. The target controller commands the target chamber selecting and positioning a target by the computer-controlled image processing.

The main console holds these controllers by a computer command so that the whole GMII system can be remotely monitored and controlled. Fig. 2 indicates the laser bay of GMII system.

GEKKO XII, 12 beam system 20 kJ, 40 TW has been started to construct which will be completed by 1983.

(2) LEKKO series CO_2 lasers

The overview of LEKKO CO_2 lasers in tabulated in Table 1. LEKKO I was completed in 1976 as the first proto-type of multistage system of short pulse CO_2 laser for fusion research, which was converted to two beam system LEKKO II.

LEKKO II, two beam 1 kJ CO_2 laser system which was completed in 1977, has been used for the investigation of laser target coupling and its wavelength scaling. It has been also utilized for getting technical data and engineering developments for the design and construction of LEKKO VIII.

The construction of LEKKO VIII, eight beam 10 kJ CO_2 laser system, has been completed by the end of 1980 with satisfactory results at full rating. The layout is shown in Fig. 3(a) with the laser beam path in Fig. 3(b). The staging of LEKKO VIIIis shown in Fig. 4 with the beam diameter and gain length at each stage, and with other components such as electrooptical shutter, Faraday rotator isolator, saturable absorber cells, beam expander and spatial filter or uni-

directional guide optics.

Laser performance test such as output power, small signal gain, pulse deformation, s/n ratio and beam uniformity are measured. The simulation results of the system performance are shown in Fig. 5 with the test results, which accords with the designed parameters. The output power of 1 TW/beam, 800 J with 0.8 ns pulse, has been achieved using a single spectral line laser pulse, which is still increasing with the optimizations of the conditions of operation. The usage of multi-line operation is adoped.

(3) REIDEN series particle beam drivers

Particle beam drivers have also been developed constructing pulse power generators REIDEN I at 1972 and then REIDEN II, III and IV at 1980. REIDEN IV, 10^{12} W and 100 kJ machine with characteristic impedance of 1 ohm, has been constructed to develop the pulse power technology for one module of MJ reactor system and to perform implosion experiments in higher power region by LIB. The details of the drivers and target experiments are described in Appendix 1.

3. Interaction processes

As the basic data, absorption, induced loss radiation, preheat due to hot electrons, x-ray and shock wave are very important items. The energy flow from the absorbed region into the denser region is an essential process for the ablative pressure of laser fusion.

The wave length dependence of laser plasma coupling is shown in Fig. 6. The classical absorption is dominant for the 0.5 μm laser at the laser intensity around $10^{14}/cm^2$. Collective processes such as resonance absorption[2] and parametric decay instability are active for the 10 μm laser[3]. For the 1 μm laser, both mechanisms are

involved for the absorption. The collective absorption produces the hot electrons which penetrate into the pellet inflicting the limitation of the ambipolar field.

For a low Z target, deposited energy by laser is mainly carried by electrons, while for a high Z target the radiation converted from the laser light carries the energy into the pellet. The radiation mean free path becomes much shorter than the plasma scale length in a high Z plasma at the electron temperature of a hundred electron volts, which infers validity of black body radiation. The radiation flux becomes larger than the thermal electron flux. As the profile of temperature and density is determined by an energy transport process, the ablation properties depends on the transport which are discussed in the next section. Here the radiation conversion data are presented. Fig. 7 shows the wave length dependence of absorption and conversion for a gold foil target. The absorption rate and the conversion efficiency decrease with increasing the laser wave length. In Fig. 8 radiation conversion efficiency by gold foil depending the laser intensity is given. The conversion[4] efficiency of 10 μm laser is much smaller than these of the shorter wave length lasers due to the long range of hoter electrons.

As for the lateral energy transport, Fig. 9 shows the temperature distribution at the rear surface of aluminium foil target irradiated by 10.6 μm CO_2 laser of 5×10^{14} w/cm^2. The hot electron can play a role to equalize the temperature for the distance of ten times of a spot diameter.

Here one should comment on the anomalous transport effect[5] (Osaka effect). This is observed on a double layer foil target of low Z and high Z materials when the laser irradiates to the high Z layer

side. Adjusting the laser intensity, the target can open a window to transport the laser light. The possible mechanisms of this effect might be follows: (1) low density channel due to the laser light filamentation (2) target heating due to high energy particles (3) x-ray heating of the target (4) formation of channel by prepulse of laser. As mentioned later, it will be applicable for a advanced targets.

4. Ablation properties

Many theoretical and experimental works have been done on the ablation processes. In Fig. 10, a pressure profile and the mach number of the ion flow velocity are shown together with the temperature profile. These are obtained by 1D Hydrodynamic simulation including hot electron dynamics described by a multi-group diffusion mode[6]. The ablation structure consists of three parts: (i) stationary deflagration, (ii) isothermal expansion and (iii) anomalous region near the cut-off point. One can apply a self-regulated flow model[7] to the ablation to estimate the Chapman-Jougeiet point density, and the ablation rate and pressure. Comparing the conventional ablation (shorter wave length and lower intensity) and the hot electron driven ablation (longer wave length and higher intensity) the latter shows the increase of mass ablation rate as well as ablation pressure due to the increase of density at Chapman-Jougeit point caused by the long mean free path of hot electrons.

Using the hot electron average energy given by Estabrook and Kruer's formula[8], the ablation mass rate $\Delta\dot{m}$ and the ablation pressure are obtained as follows[7]

$$\Delta\dot{m} = 9.6 \times 10^5 \, t^{-2/3}[(1 - f_i)\eta_{ab}]^{0.59} I_L^{0.85} \lambda_L^{1.04} (g/sec\ cm^2)$$

$$P_{ab} = 93\ t^{-1/3}[(1-f_i)\eta_{ab}]^{0.67} I_L^{0.93} \lambda_L^{0.52}\ \text{(M bar)}$$

where t is the laser pulse duration in ns, η_{ab} is the absorption efficiency, λ is the laser wave lenght in μm, I_L is the laser intensity in 10^{15} w/ cm^2 and f_i is the energy loss rate obtained by the jump condition at the cut-off point.

Setting $(1-f_i)\eta_{ab} = 0.15$, $t = 0.255$ ns, $\lambda = 1$ μm and $I_L = 6 \times 10^{15}$ w/cm^2, $P_{ab} \sim 200$ Mbar agrees with the sumulation results of Fig. 10. In Fig. 11, our laser experimental results and theoretical estimation for $1-f_i = 0.5$, $t = 1$ ns are presented. One can note, the ablation pressure is decreased at the wave length of 1.06 μm.

The stability of ablatively accelerated foil targets has been studied by x-ray shadowgraphy and x-ray spectral analysis at the rear surface of the target by using a probe laser light for emission excitation. Results show the interal layer mixing is occured. As indicated in Fig.12, the multilayered target Au/Al/Au or CH/Al/Si is irradiated by the main laser to drive the acceleration and then a probe laser hits the rear surface to excite Al atoms which penetrate the third layer by mixing[9]. The data indicate the local mixing up to a maximum level of 20 % due to microinstability at the layer interfaces.

The uniform irradiation[10] of laser beam on a pellet target is very important to ablative compression. In Fig. 13, several focusing conditions on a pellet show the different x-ray backlighting images of compressed cores. Overlapping focus can keep the uniform irradiation, but center focus produces the amplification of nonuniforminty by a free falling process after the laser pulse. The optical schlieren photogram in Fig. 13, at the early period of time, the wisker like

surface filamentation appears. A model for this feature is presented. In Fig. 14, the hot electrons expand from the cut-off point and the cold electron return current is induced. When the hot electron flux is high enough, multi-streams among hot and cold electrons and ions cause instabilities. One can set velocity distribution functions of each species being shifted Maxwellians and derive a dispersion relation for a coupled electromagnetic and electrostatic mode[11]. As the ion acoustic instability excites predominately short wavelength mode propagating against the heat flux, the transport coeffeicient is affected by the instability. While excited electromagnetic waves have longer wavelength, the order of laser spot size, the heat flux is perturbed laterally and the ablation front is distorted in a large scale by a growing magnetic filed. Linear mode analysis as well as nonlinear stages using PIC code have been studied. The magnetic field generated at the cut-off point diffuses into plasma accumulating to form filamentations[12]. The result is shown in Fig.15.

5. Advanced target design

To perform high compression of the pellet, a double shell target [13] has several advantages such as suppression of hot electron preheat in the inner shell due to vacuum insulation and increase of compression velocity of the inner shell driven by the heavy outer shell. One of the problems of double shell targets to study is stability at compression. We have investigated the compression behavior of double shell target the dimensions of which are as follows: an inner shell is a glass microballoon, 50 $\sim$ 100 μm in diameter, 1 μm thick and an outershell is parylene balloon, 140 $\sim$ 180 μm diameter, 5 $\sim$ 6 μm thick. Fig. 16 is a double shell target, the fabrication techniques of which

are given in elsewhere[14]. X-ray back lighting technique[13] using two spectrum and successive two frames is prepared. X-ray sources from Cu and Mo are used to illuminate the outer shell and the inner shell respectively. Fig. 17 shows the experimental arrangement for this scheme. Two pinhole cameras have Be filters to prevent the emitted light from the shells themselves. Gekko IV glass laser delivers four beams to the target in tetrahedral symmetry, pulse duration 100 ps, energy 40 J/beam. Fig. 18 shows the experimental results with 1D simulation data. The nonuniformity of shell structure due to finite number of beam irradiation is greatly reduced at the inner shell. A foam target 300 μm in diameter which has a glass micro balloon of 100 μm diameter in the center shows a good uniform compression results measured by the x-ray backlighting. The very light foam layer, the density of 0.12 mg/cm^3 can reduce the severe condition of non uniform irradiation of a few laser beams as well as the focusing stringency.

Ablative implosion by lasers is expected to have high absorption rate and high hydrodynamic efficiency. We have investigated an improvement of target characteristics using a double foil[15] structure which has a laser inlet hole in a heavier foil. Laser light is introduced into the space between double foils to produce plasma there and drive the ligher foil. Ablative process due to a rocket model has hydrodynamic efficiency about 10 %, while this new target of a cannon ball model can have nearly 100 % efficiency. The problems of this target are the passing efficiency of laser light through an inlet hole of the foil and outflow of plasma through this hole.

In experiments we use a gold or aluminum foil as a front sheet and a propylene foil as a rear sheet. The inlet hole is 100 ∿ 150 μm in diameter. Fig. 19 shows the shadowgram of target behaviors at 12.9

ns after the glass laser irradiation of 100 ps and 5J.

Incident, reflect and transport light are measured by micro-calorimeters. In Fig. 20 the rear foil responce is given with 1D simulation data. If we use the heavier front foil, the ablation efficiency can be expected up to 70 %. Table 3 shows the performance of these targets. The similar analysis in shell structures[16] called "canon ball pellet" has been performed. The concept is shown in Fig. 21. The 1D simulation of this scheme is given in Fig. 22. Anomalous transport effect[17](Osaka effect) might be used to this target design.

6. Reactor Concepts

The SENRI-I is a conceptual design of a laser fusion reactor driven by 1 $\sim$ 5 MJ laser pulses[18-22]. It is aimed in the SENRI-I to utilize DT reaction energy of 1000 MJ, 1 Hz to generate 426 MW net electric power and to breed tritium. The inner wall of the spherical SUS structure is covered by a thick Li layer which flows from top to bottom to form a reactor cavity (R $\sim$ 5.00 m), being guided and controlled by static magnetic field. A concept of the magnetically guided Li flow reactor SENRI-I is shown in Table 4. The inner Li flow is used not only as a protector of the SUS first wall from neutron and radiation damage, but also as a coolant and a breeder. Temperature increase per 1000 MJ DT reactions ($N = 3.55 \times 10^{20}$) and tritium breeding ratio was exmined in Ref. (18) for both 14 MeV monochromatic neutron spectrum and softened one in a high density bare DT pellet, where $\rho R = 3.0$ g/cm^2. Tritium breeding ratio η_B is $\sim$ 1.6 and the flux of 14 MeV neutrons is reduced by the 64 cm thick Li layer to be $\sim$1/23 at the inner surface of the first wall. The maximum temperature increase is $\sim$3 deg/1000 MJ reaction in the inner Li and $\sim$1.5 deg/1000

MJ DT reactions in the SUS first wall. We studied the neutron energy spectrum from the compressed pellets with various tampers and get neutronic features in the designed blanket for the SENRI-I. We also examined the effects of the thickness of the inner Li flow on tritium breeding ratio, 14 MeV neutron flux in the SUS first wall and the temperature increase.

7. Summary

Inertial confinement fusion depends on the three important issues: development of energy drivers, excellent performance of fuel pellets based on the theoretical and experimental aspects of ablation and reactor concepts.

ILE has developed four wave length lasers, 0.32 μm, 0.53 μm, 1.06 μm and 10 μm as well as light ion beam.

The coupling of beams and plasma is a fundamentally important item: absorption, transport and ablation which are determined by the wave length scaling of drivers. We have compared the different data of various drivers to find the optimal conditions.

The ablation process is divided to three categories: radiation driven compression, thermal plasma driven compression and hot electron driven compression. We proposed a self regulated flow plasma model to explain the experimental data. The wave length scaling of ablation process was clarified that a few μm wave length laser is less effective in ablation.

Uniformity of irradiation is very important. The focusing condition has strong effect for uniformity. However "foam target" as well as double shell target could have a good responce to the beams of finite numbers. The lateral heat conduction due to hot electron was

also very effective to keep uniformity.

The filamentation of the pellet surface was also investigated. A dispersion relation for a coupled electromagnetic and electrostatic mode of shifted Maxwellian plasma gave the distortion of ablation front due to magnetic field accumulation. 2D PIC simultation data was used for nonlinear stage of phenomena.

As for the ablation instability, a probe laser method was introduced to find the layer mixing during compression. The instability soon reached to saturation and showed 20 % mixing at most.

Advanced target design is proposed. "Cannon ball like pellet" can have an excellent behavior of ablation. Double plane target experiments and 1D code calculation indicate the very high hydrodynamic efficiency of compression. Shell scheme was also simulated. Anomalous transport properties "Osaka effect" might be applicable to this novel pellet design.

ICF reactor concept has been studied to clarify the several merits of this type of concepts. The data is very interesting in technological point of view.

In appendix, light ion beam fusion efforts at ILE and the world wide major drivers are summarized for references.

Appendix I: LIB Research at ILE Osaka

Current efforts of light ion beam for fusion reseach are as follows; development of pulsed power technology, ion beam generation and focusing, diagnostics of the beam, beam transport, and target interactions.

1) Development of pulsed power technology

Reiden IV light ion beam driver as shown in Fig. 23 was built. The output parameter at the diode is 1.1 MeV, 0.8 MA and pulse length 60 ns. It is composed of a Marx generator stored energy 150 kJ, output voltage 2.5 MV, an intermediate storage capacitor, a pulse forming line, a transmission line and a diode. The waveforms of each section are indicated in Fig. 24 with simulated waveforms in right.

2) Light ion beam generation and focusing

Light ion beam is generated using a pinch reflex diode and a magnetic insulated diode.

Using the pinch reflex diode the ion beam current is 200 KA with the particle energy of 1 MeV. The typical waveforms are indicated in Fig. 25. A relation of the diode voltage and current is indicated in Fig. 26. The results corresponded well to the focused flow model.

Anode temperature was estimated from the Thomson parabola analizer assuming Saha thermal equillibrium[23].

Beam was focused ballistically due to the curvature of the anode. The particle orbit was estimated by a shadow box as shown in Fig. 27. The beam was focused when the neutralizing foil 0.5 μm thick was set. The 95 % current neutralization was observed. The ion current of 200 kA with particle energy 1.1 MeV was extracted and focused to the current density of 40 kA/cm^2.

3) Diagnostics

The diagnostics are developed to determine current density in the gas and at focus spot. Using the B-N activator in the beam path the mean energy and number of particles were estimated[24].

Focused beam spot size was measured by the P("B, α)2α reaction. Fig. 28 shows the α particle images emitted from the focal spot[25]. The current density was also measured using D(D, n) He^3 reaction. When the $(CD_2)_n$ target was used, the deuterons of natural abundance in the proton beam react with deuterons in the target. From the neutron measurement the current density was estimated.

4) Transport

The guiding discharge channel was produced in ethylen gas of 20 torr by the CO_2 laser beam. The threshold of the laser initiated breakdown is shown in Fig. 29[26].

Fig. 30 shows the characteristics of proton energy and transport maximum angle of the beam which are well accorded with theoretical estimation..

5) Interactions

The ablation pressure was estimated from the response of the irradiated foil. Fig. 31 shows the relation between irradiated power density and ablation pressure. The dashed line is obtained from the free expansion model. The solid line shows the simulation results assuming the flat deposition profiles of beam energy over the range[27].

6) Summary

The technology of TW pulsed power was developed. The ion beam of 1 MV and 200 kA was focused within 1 cm in radius. The beam was transported through the plasma channel initiated by the CO_2 laser. The ablation pressure scaling to the beam power density was obtained.

Appendix II: World Major Energy Drivers for ICF Research

1. Glass Laser

Country Laboratory Name	Number of Beams	Output Power (TW)	Output Energy (kJ)	Pulse Length (ns)	Remarks (completed)
USA					
LLNL					
Argus	2	5	2	0.03-1.0	
Shiva	20	30	10	0.1-1.0	
Nova-1	10	100	100	0.1-3.0	(1983)
LLE Rochester					
GDL	1	0.7		0.1	
Omega X	24	15	5	0.03-0.1	
NRL					
Pharos II	6	0.7	1.3	0.1-1.0	
KMS					
Chroma I	2	0.6	1	0.1	
USSR					
Levedev					
Mishen	4		1	1.0	
Delfin	216	33	100	0.2-3.0	under construction
Avrora	20		50-500	0.03-10	under construction
JAPAN					
ILE Osaka					
Gekko II	2	0.4	0.12	0.1-1.0	
Gekko IV	4	2	1	0.1-1.0	
Gekko MII	2	7	3	0.1-1.0	
Gekko XII	12	40	20	0.1-1.0	(1983)
IPP Nagoya					
Halna	1	0.1		0.1	
UK					
Rutherford					
Vulcan	6	3.6	1.2	0.1-1.0	
AWR	2	1	1	0.05-1.0	
FRANCE					
Limeil					
P102	2	0.6		0.08	
Octal	8	2	1	0.1-1.0	
Ecole Polytech.					
Greco	1	0.25	0.25	0.1-2.5	
ITALY					
Frascati	2		0.25	2.0	
POLAND					
Kalisky Inst.	4		0.1	3.0	
AUSTRALIA					
LIP-4	4	1.2	0.12	0.005-0.01	

Appendix II (continued)

2. CO_2 Laser and Iodine Laser

Country Laboratory Name	Number of Beams	Output Power (TW)	Output Energy (kJ)	Pulse Length (ns)	Remarks (completed)
USA					
LANL					
DBS	2	2.5	2.5	1	
Helios	8	10	10	1	
Antares-I	2×(12)	40	40	1	(1983)
JAPAN					
ILE Osaka					
Lekko II	2	1	1	1	
Lekko VIII	8	10	10	1	
CANADA					
NRC					
Coco II	1	0.2	0.2	2	
ITALY					
Frascati					
Chimera	2	0.2	0.2	1	(1981)
POLAND					
Kalisky Inst.	8	6	6	1	
FRG					
IQO, Garching					
Asterix III	1	1.1	0.4	0.35	Iondine Laser

Appendix II (continued)

3. Particle Beam

Country Laboratory Name	Number of Beams	Output Power (TW)	Particle Energy (MeV)	Pulse Length (ns)	Remarks (completed)
USA					
Sandia					
Proto II	1	9	1.5	24	
PBFA I	36	40	2.4	24	
PBFA II	72	80	2.4	24	(1984)
NRL					
Gamble II	1	1	1.0	80	
USSR					
Kurchatov					
Angara V-M	1	1	2.0	80	
Angara V	50	50	2.0	80	(1983)
FRANCE					
Valduc					
Sidnix	1	1	1.0	80	
FRG					
Karlsruhe					
Kalif	1	2	2.0	50	
JAPAN					
ILE Osaka					
Reiden IV	1	1	1.0	60	

References

1) C. Yamanaka et al, "Glass Laser Facilities for Laser Fusion Research at ILE, Osaka" "Progress on LEKKO VIII CO_2 Gas Laser System at Osaka", IEEE J. of Quantum Electron., vol. QE-17, 1639, Sept., (1981)

2) Y. Sakagami, Phys Rev. A 21, 882 (1980)

3) H. Nishimura et al, Plasma Physics 22, 69 (1980)

4) H. Nishimura et al, Phys. Rev. A 23, 2011 (1981)

5) J. Mizui et al, Phys. Rev. Lett. 39, 619 (1977)

6) T. Yabe, K. Mima et al, Nuclear Fusion 21-7 (1981) (to be published)

7) K. Mima et al, Proceedings of Spring College for Fusion, Triest, Italy, 1981

8) K. Estabrook and W. L. Kruer; Phys. Rev. Lett. 40, 42 (1978)

9) T. Raven et al, Research Rep. ILE Osaka univ. 8104p (1981)

10) T. Mochizuki, Japanese Jour. Appl. Phys. 19, L 645 (1980), Appl. Phys. Lett. 37, 602 (1980)

11) T. Yabe, K. Mima et al, Phys. Rev. Lett. (to be published)

12) T. Yabe et al, Research Rept. ILE-8110p (1981) also published in Proc. of "Symmetry Aspect of Laser-Driven Implosion" May (1981), Washington D.C.

13) C. Yamanaka, 11th Anomalous Absorption Conf. 5-5, Montreal 1981, IEEE Inter. Conf. on Plasma Science, 1A4, Santa Fe 1981, Topical Meeting on Low Energy x-ray Diagnostics, Monterey 1981

14) T. Norimatsu, Jour. Vacu. Scie. Tech ICF Th-10 (to be published)

15) K. Yamada et al, Research Rep. ILE Osaka Univ. 8111p (1981)

16) H. Azechi et al, Japanese Jour. Appl. Phys. 20 L477 (1981)

17) C. Yamanaka et al, Nuclear Fusion Supplement IAEA-CN-35/F5,

147 (1977)

18) S. Ido et al, presented at the 8th International Conference on Plasma Physics and Controlled Nuclear Fusion Research, Brussels (1980), IAEA-CN-38/E-3 and ILE-8009P (1980)

19) S. Ido et al, presented at the 11th Symposium on Fusion Technology, Oxford (1980)

20) Annual Progress Report on Laser Fusion Program, p. 193, Institute of Laser Engineering, Osaka University, ILE-APR-78 (1978)

21) Report of System Design of ICF Reactor, Institute of Laser Engineering, Osaka University (1979) (in Japanese)

22) C. Yamanaka et al, 'Conceptual Design of 1240 MW_{th} Laser Fusion Reactor in ILE OSAKA', ILE-7913p (1979)

23) T. Ozaki et al, ILE 8120p (1981)

24) T. Ozaki et al, ILE 8108p (1981)

25) S. Miyamoto et al, ILE 8102P (1981)

26) K. Imasaki et al, ILE 8112p (1981)

27) S. Miyamoto et al, ILE 8118p (1981)

Figure Caption

Fig. 1 Block diagram of control system of GEKKO MII system.

Fig. 2 GEKKO MII glass laser system

Fig. 3 LEKKO VIII CO_2 laser system (a) Layout of laser system
(b) Laser beam pass system

Fig. 4 Staging of LEKKO VIII

Fig. 5 Simulation results of system performance and experimental data

Fig. 6 Absorption properties of laser light at different wave length

Fig. 7 Absorption and conversion of laser light by gold foil

Fig. 8 Radiation conversion of various laser intensities by gold foil

Fig. 9 Temperature distribution at rear surface of gold foil target irradiated by CO_2 laser

Fig. 10 1D hydrodynamic simulation of cold and hot electron pressure, cold electron temperature and Mach numbers at a time 0.255 nsec after the CO_2 laser input of 10^{15} w/cm^2

Fig. 11 Intensity dependences of ablation pressure for 10.6 μm and 1.06 μm lasers.

(—•—•—) for λ_L = 10.6 μm and hot electron driven ablation.

(———) for λ_L = 1.06 μm and conventional ablation.

(•••••) for λ_L = 1.06 μm and hot electron.

(• ×) are experimental data points

Fig. 12 Mixing of multi-layer target measured by a probe laser

Fig. 13 Uniformity of different focusing conditions measured by x-ray back light framing

Fig. 14 Schematic diagrams of hot electron and cold electron circulation and particle velocity distributions.

Fig. 15 Y-direction spatial profiles of hot electron density fluctuation ( ) and B field amlitude ( ). Broken line is the theoretical result for B field amplitude. Lh is hot electron range

Fig. 16 Double shell target

ig. 17 X-ray framing shadowgraphy of two wave lengths

Fig. 18 Double shell target implosion:

(a) Uniform compresssion at 1.5×10^{15} w/cm^2,

(b) Nonuniform compression at 4.4×10^{14} w/cm^2.

Fig. 19 Double foil target acceleration with inlet hole

Fig. 20 Responce of double foil target, simulation and experiment

Fig. 21 Cannon ball pellet

Fig. 22 1-D simulation of "Cannon ball pellet" scheme

Fig. 23 The schematic picture of Reiden IV

Fig. 24 The voltage waveforms of each section and simulated data

Fig. 25 Typical waveforms of diode voltage, current and impedance

Fig. 26 Typical voltage and current relation of diode

I_{FF}: focused flow model

I_{CL}: Child-Langmuir model

Fig. 27 Beam particle orbit with and without foil of 0.5 μm in thickness. The currents detected at shadow box are also indicated in upper trace

Fig. 28 Images of α particles via $^{11}B(p, \alpha)2\alpha$ reaction

Fig. 29 Threshold of the laser plasma channel formation

Fig. 30 Maximum angles of transported beam particles with each particle energy

Fig. 31 Ablation pressure and scaling by LIB

Table 1

LASER SYSTEMS AT ILE OSAKA

Facilities / Parameter	G-II	G-IV	GM-II	G-XII	L-II	L-VIII
Beam Number x Diameter(cm)	2x8	4x11	2x20	12x35	2x22	8x27
Output (TW)	$^{0.4}/_{0.1ns}$	$^{2}/_{0.1ns}$	$^{7.0}/_{0.1ns}$	$^{40}/_{0.1ns}$	$^{1}/_{1ns}$	$^{10}/_{1ns}$
Output (kJ)	$^{0.1}/_{0.8ns}$	$^{1}/_{1ns}$	$^{3}/_{1ns}$	$^{20}/_{1ns}$	$^{1}/_{1ns}$	$^{10}/_{1ns}$
Focusable Power (W/cm^2)	2×10^{16}	5×10^{17}	1×10^{18}		3×10^{14}	3×10^{15}
Prepulse Ratio & A.S.E. (mJ)	10^{-6} < 1	10^{-8} < 1	10^{-8} < 0.01	10^{-5} < 0.1	5×10^{-6} < 2	10^{-8} < 0.1
Shot per Month	200	100	60		80	100

Table 2

ALIGNMENT ACCURACY AND CONVERGING TIME

		Accuracy	Time Required
Beam Alignment	Pre Amp Chain	0.15 mm	1-2 min
Beam Alignment	Main Amp Chain	0.3-1.0 mm	1-2 min
Pinhole Alignment (Spatial Filter)		10 μm	3-4 min
Target Positioning	Coarse	20 μm	4 min
	Fine	4 μm	4 min

Table 3

1 Comparison of various parameters for the DFH target and the single foil target.

Target	Au 150μm^ϕ	Al 100μm^ϕ	Single Foil(C_3H_6)$_n$
Transmittance	80±8 %	67±7 %	——
η_{nb}	91±9 %	83±12%	——
$\eta_{ab}^{Au,Al}$	17±7 %	7.3±4.6%	——
η_{ab}	74±15 %	76±17%	5.2±3.5%
η_H	60 %	33 %	12 %
$\int P\,dl$	3200 g/cm·s	2200 g/cm·s	76 g/cm·s

Table 4

PARAMETERS OF LASER FUSION REACTOR CONCEPT

(A)	LASER	GAS PHASE (CO_2 etc.)	
		NUMBER OF BEAMS	8
		OUTPUT ENERGY	1 ∿ 5 MJ
		SHOT CYCLE	1 Hz
		PEAK POWER DENSITY	200 TW
		PULSE DURATION	100 nsec
		EFFICIENCY	10 %
(B)	PELLET	MULTI-SHELL	
		FUEL DT	
		RADIUS	∿ 3mm
(C)	OUTPUT POWER		1240 MW (THERMAL)
			496 MW (GROSS ELECTRIC)
			426 MW (NET ELECTRIC)
(D)	REACTOR VESSEL WITH MAGNETICALLY GUIDED INNER Li FLOW		
		SUS CONTAINER	R = 5.64 m (SPHERICAL)
		CAVITY	R ∿ 5.00 m
		INNER Li FLOW	d ∿ 0.64 m

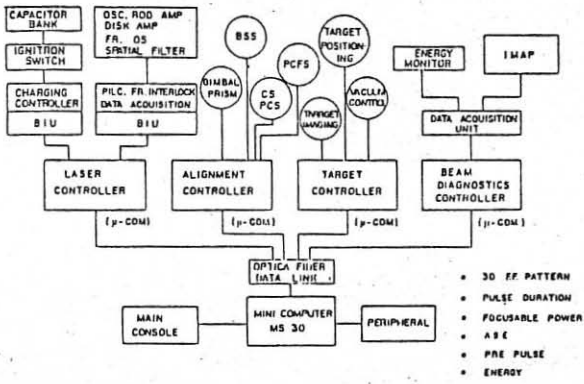
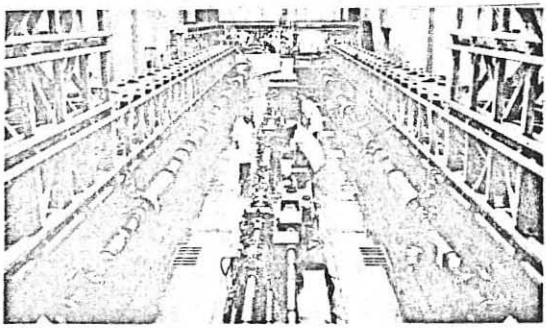


Fig.1

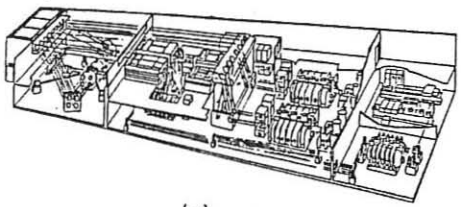
LASER BAY



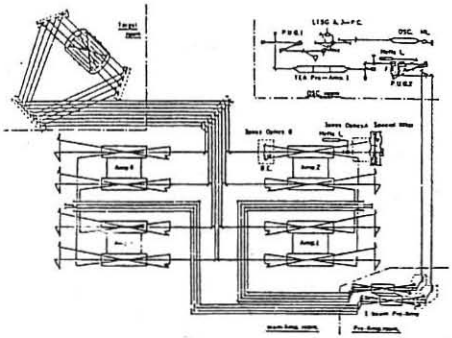
TARGET CHAMBER



Fig.2



(a)



(b)

Fig.3

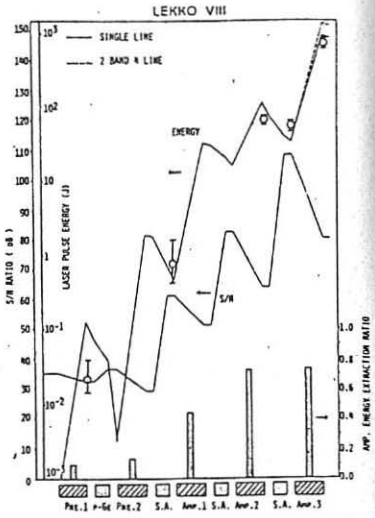


Fig.5

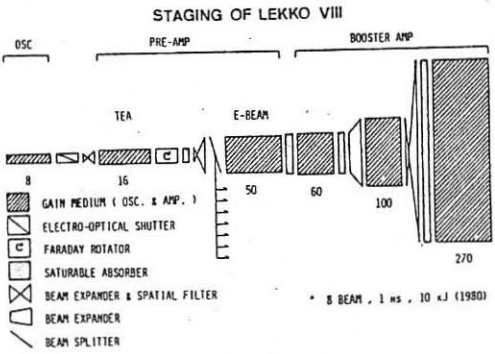


Fig.4

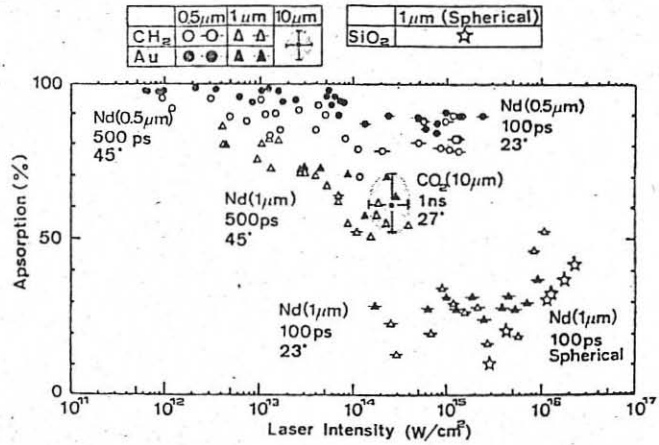


Fig.6

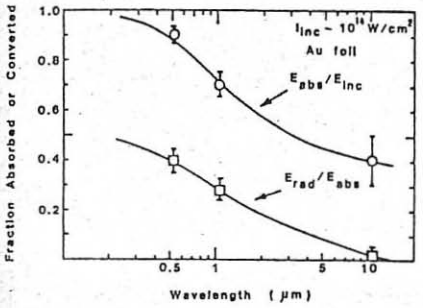


Fig.7

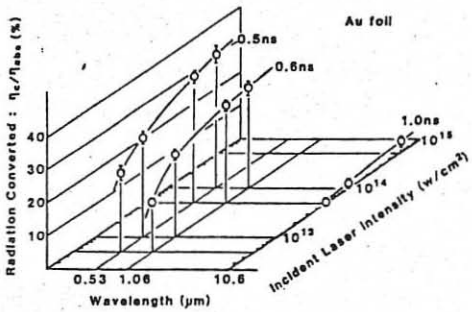


Fig.8

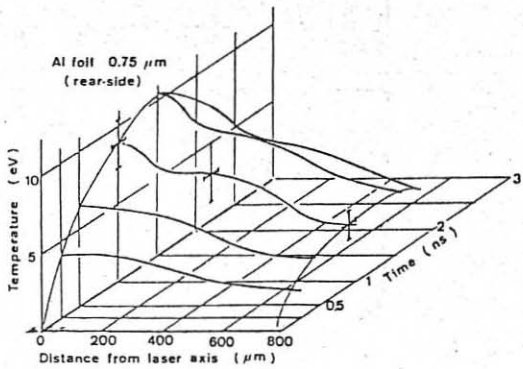


Fig.9

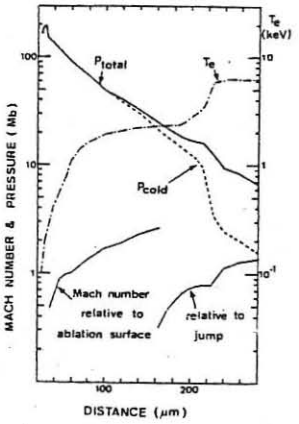
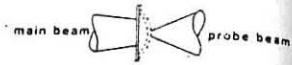


Fig.10



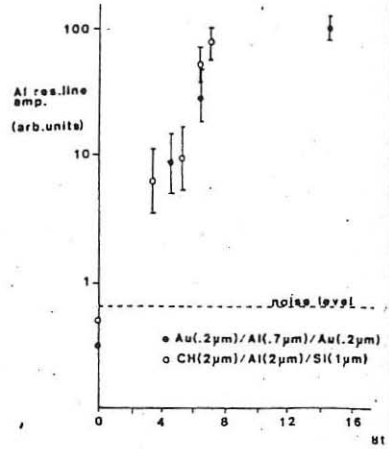


Fig.12

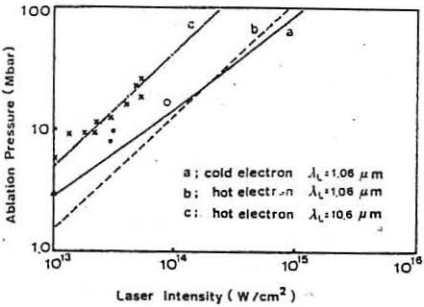


Fig.11

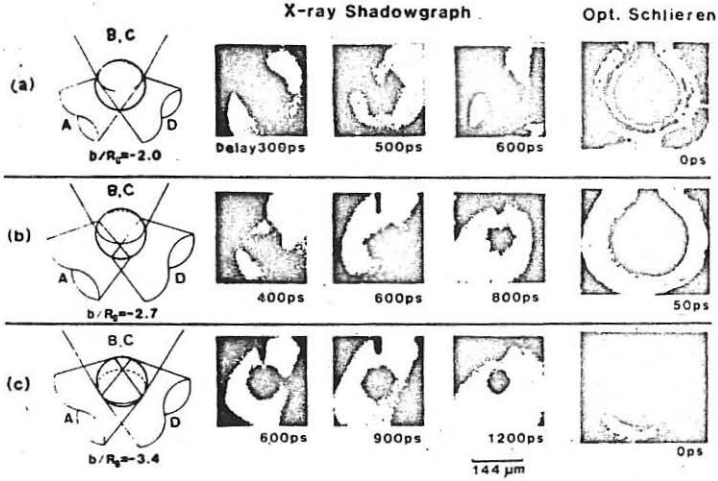


Fig.13

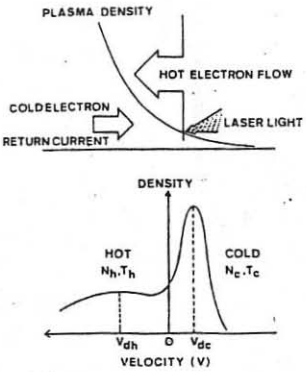


Fig.14

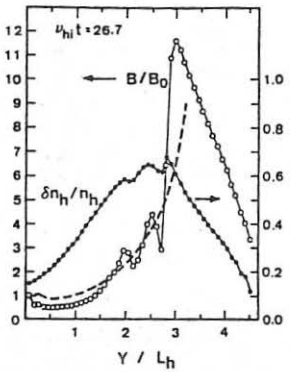


Fig.15

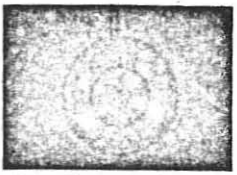


Fig.16

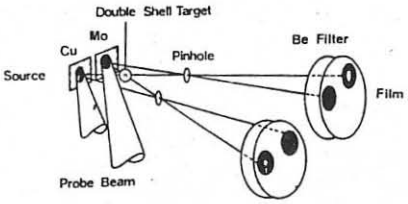


Fig.17

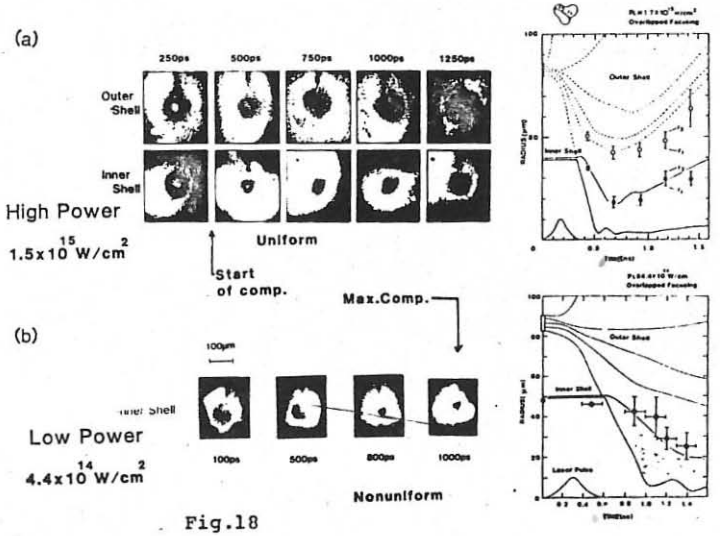


Fig.18

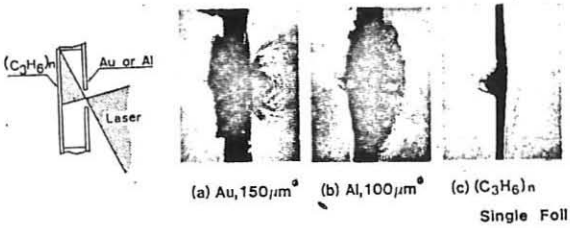


Fig.19

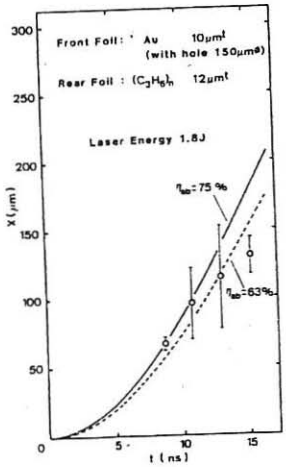


Fig.20

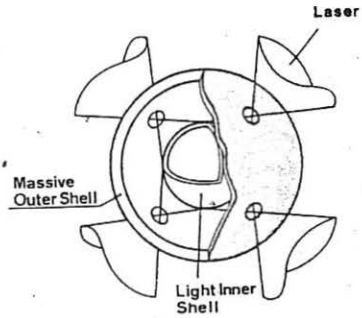


Fig.21

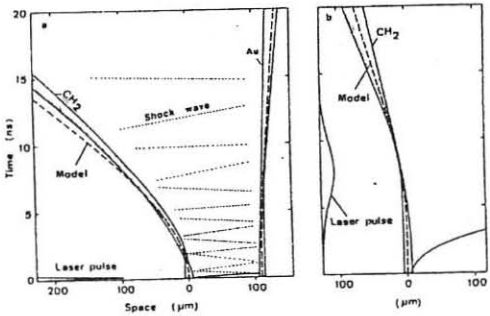


Fig.22

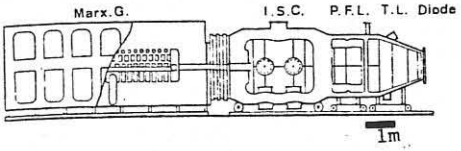


Fig.23

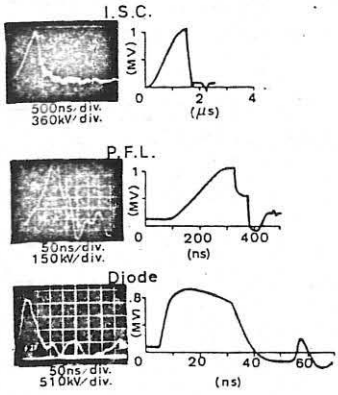


Fig.24

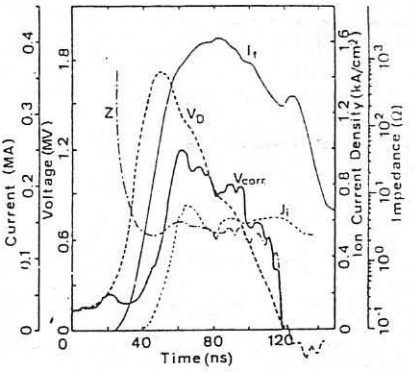


Fig.25

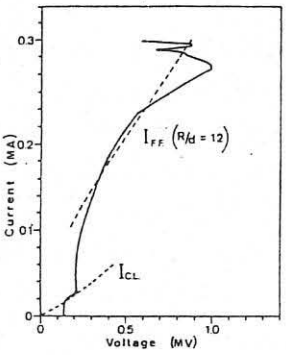


Fig.26

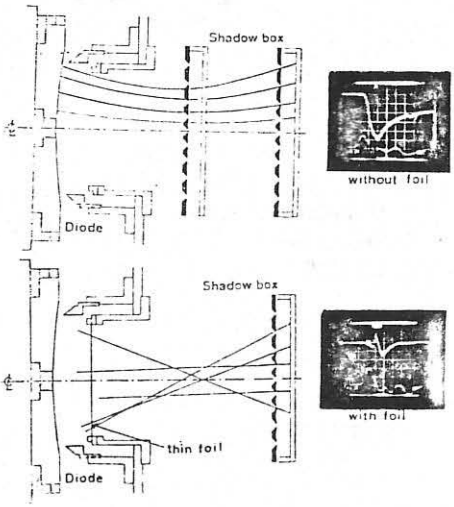


Fig.27

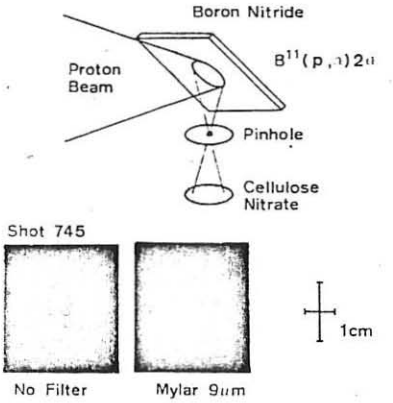


Fig.28

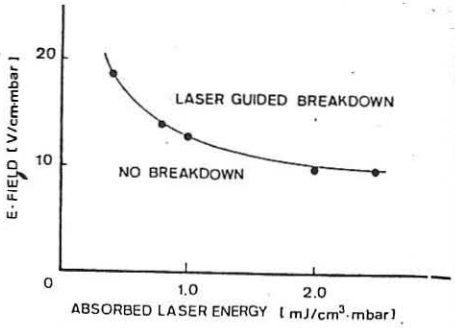


Fig.29

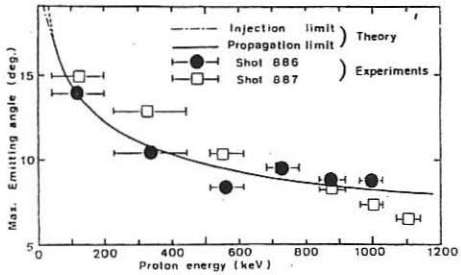


Fig.30

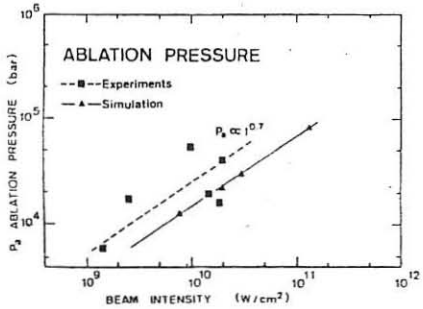


Fig.31

INERTIAL FUSION RESEARCH USING PULSED POWER DRIVERS

G. Yonas
Sandia National Laboratories
Albuquerque, New Mexico 87185 USA

Introduction

Inertial fusion research is focusing its attention on the central issue of demonstrating DT fuel ignition. Glass lasers are being efficiently frequency converted to produce green and blue light in order to allow target implosion studies with demonstrated low levels of electron preheat. CO_2 laser target interaction studies are employing vacuum insulation to inhibit the transport of hot electrons.(1) In both cases, achieving the needed level of beam intensity is straightforward and progress is being made in dealing with energy coupling issues. Given continued success with these lasers in the efficient absorption of energy and the symmetric stable implosion of a small fuel mass, then scientific breakeven is still likely to require the construction of a 1 MJ, ~100 TW laser. The cost of such a laser would be at least several hundred million dollars based on today's technology.

Pulsed power devices developed initially as relativistic electron beam accelerators have been converted with only minor modifications and negligible additional energy losses into light ion beam accelerators and imploding foil drivers. These devices can produce output energies and power levels at substantially lower cost than with lasers thus making MJ ignition experiments a tenable objective within funding constraints. Sandia National Laboratories is presently constructing, for the Department of Energy, the PBFA-II device which is to operate as either a multi-megajoule foil implosion driver or an ion beam accelerator. Preliminary experiments are underway on several prototype accelerators at Sandia as

well as PBFA-I which began operation in 1980. Additional research on beam focusing and transport is underway at the Naval Research Laboratory and Cornell University. The primary question under investigation here is just the opposite of the case for lasers. We believe that energy coupling will be straightforward but we have yet to demonstrate adequate temporal and spatial convergence of power onto a few mm radius target. This step must precede the study of the ultimate questions of implosion hydrodynamics which will become the subject of study on PBFA-II. In preparation for these ignition experiments as well as for precursor target experiments on PBFA-I beginning next year, diagnostic techniques are being prepared and utilized in beam diagnostic and demonstration experiments at low power levels. We review here the status of our efforts in power concentration and diagnostic development.

Power Concentration

Sandia's decision to change its emphasis from electron beams to light ions and magnetically imploding foils (liners) was made in 1979. At that time, the progress which had been made in the scaling of both approaches, taken together with target design calculations that showed substantially higher energy requirements for electrons than for the other approaches, justified this program decision. We now believe that a 100 TW, 1-2 MJ ion beam or imploding foil device will suffice for ignition experiments. This optimism is based to some extent on our reliance on a final stage of pulse shortening. We believe this power concentration step can be used to make up for other losses in delivering the power to a target. For light ions this last stage of power concentration can be achieved by ramping the output voltage pulse in order to bunch the beam by a factor of 2-3 as it propagates to the target. For imploding foils, the electromagnetic energy

delivered to the vacuum diode can be efficiently converted to foil kinetic energy during the foil implosion phase and the output energy can be extracted as thermal x-rays during the roughly five times shorter stagnation phase. In both cases we expect to be able to deliver ~100 TW to the target.

Light ion beam focusing can be carried out by extracting a beam from a diode and by ballistically focusing it in a force neutralized manner over a distance of several tens of cm. A target can be placed at this focal point or a beam transport channel can be introduced to allow multiple beam target irradiation with substantial stand off between the target and the diodes. Development of intense ion beam diodes has progressed rapidly over the last five years.(2) All light ion diodes being considered for inertial fusion applications utilize a magnetic field tangential to the anode in order to increase the path of the electrons and thus greatly increase the ratio of the ion to electron current. Beam focusing research has concentrated on methods to satisfy the following requirements:

1. Produce a dense, stable, high purity, and spatially controlled anode plasma to provide the source of an ion beam of low divergence and high current density.
2. Create near the anode an electron cloud that can act as a stable virtual cathode without contributing to excessive electron leakage to the anode or producing electrostatic or magnetic perturbations of the ion beam.
3. Provide electrons to charge and current neutralize the beam in transit to the target without the introduction of additional sources of divergence.

Because these ion beams are non-relativistic, charge neutralization must be practically perfect in order to avoid rapid beam blow up.[3] Charge neutralization can be provided by neutralization in a background plasma or by electron introduction from nearby materials. If this necessary neutralization is accomplished, then the beam focusing can still be no better than that determined by its power brightness, β, where $\beta = J_D V/\theta^2$. Here J_D, V, and θ are the beam current density, accelerating potential, and divergence at the diode.

Target ignition will require achieving energy densities of 20 MJ/g in a 10 ns pulse with an ion range, R, equivalent to that of a 3 MeV proton.[4] Thus R ~ 10 mg/cm^2 and heavier ions at higher energies such 12 MeV He or 64 MeV C will also be suitable.[5] Thus we require a beam intensity of ~20 TW/cm^2 at the target. The focused beam intensity is given by the product of the beam bunching factor, the beam brightness, and the fraction of the solid angle subtended by the diode surrounding the target. A bunching factor of two to three can be achieved with an increasing diode impedance, a power waveform as shown in Fig 1, and a drift distance of 50 cm.[6] Thus, with a solid angle fraction of .3, β (ignition) must be ~30 TW/cm^2. Proton experiments at Cornell,[7] NRL,[8] and Sandia[9] have demonstrated β values of 2-4 TW/cm^2 using three rather different magnetically insulated ion diodes operating at roughly 1 MV. Thus an order of magnitude increases in brightness is needed.

The present understanding of the causes of beam divergence is too limited to allow for scaling relations to be developed with confidence. Studies are underway to reduce the divergence angle, increase the ion current density, and to increase the diode voltage. Studies at Sandia and Cornell are aimed at producing uniform, several thousand cm^2, greater than

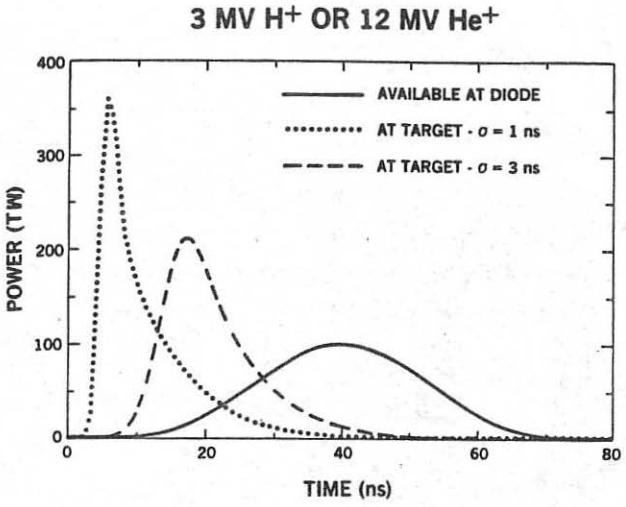


Figure 1. Calculated power concentration for the Ampfion diode on PBFA-II and a focal length of 50 cm for two values of module jitter, σ

$10^{15}/cm^3$ density plasma sources using surface flashover anodes, arrays of actively driven arc gaps, and multiple plasma gun injectors. Both flashover sources and plasma guns provide adequate densities but are subject to large scale non-uniformities which are dependent on geometrical effects, local electric fields, and diode voltage prepulse. Spark gap arrays produce well controlled plasmas but have thus far fallen an order of magnitude short of the needed density.(10) It has also been found that present spark gaps produce a large neutral gas component which results in a rapid decrease in the diode impedance and inefficient power transfer.(9) Optical techniques such as interferometry and spectroscopy are being used to study

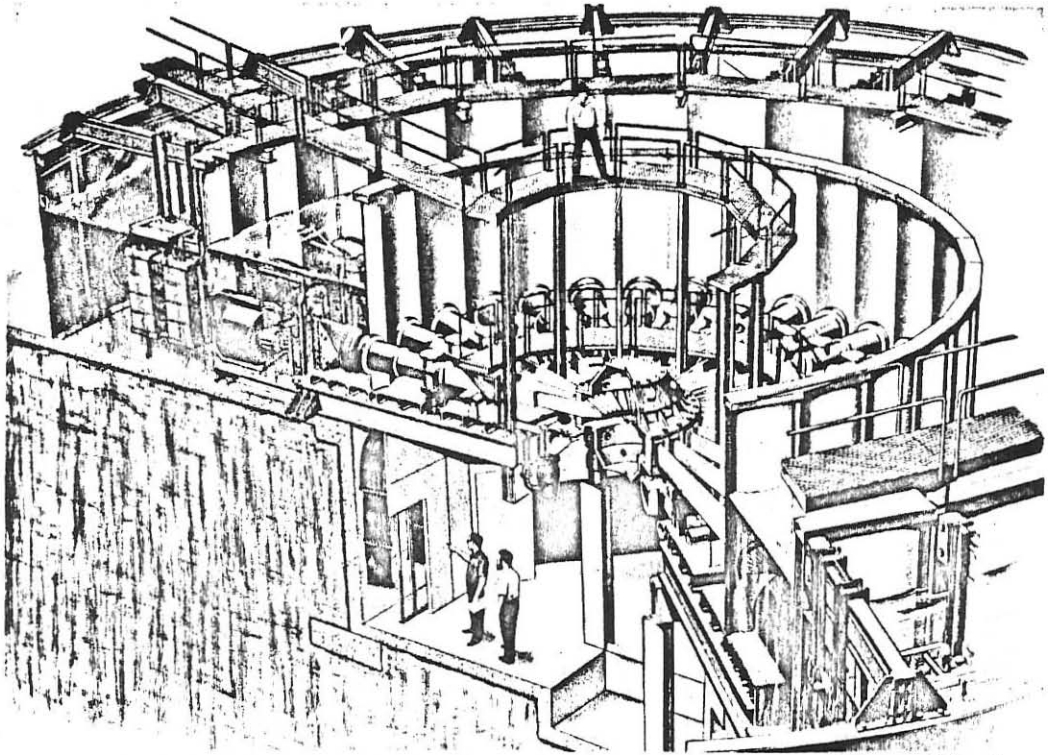


Figure 2. Particle Beam Fusion Accelerator, PBFA-I, showing polarity inverting transition in water pulse forming section. Note, 36 MITL's terminating within 50 cm of central axis.

these anode plasmas and new methods for driving arcs at higher power levels and controlling the initiation of uniform flashover are under investigation.[10] Attempts to increase the ion current density by the use of small area, low impedance diodes are underway also but there is some preliminary evidence of filamentation instabilities that result in additional beam divergence.[8]

It is thus clear from the studies to date that the most promising avenue to achieving higher power brightness is to increase the accelerating voltage and ion mass.[2,3,11] If beam divergence is caused by inhomogeneities in the anode plasma, then β should increase as V^2 while holding the ion current density constant. Under other assumptions of sources of divergence and impedance control, the scaling may be less than quadratic with voltage.[12] Nevertheless, if an appropriate plasma source providing He^{+1} or C^{+4} can be provided, then an operating voltage of 10-15 MV would be appropriate and should provide the necessary β with some margin.

Diode scaling experiments are underway using PBFA-I[13], (Fig. 2, in in the 2-4 MV range and are planned for the 2-16 MV range using PBFA-II. PBFA-I was orignally designed and constructed to operate as an electron beam accelerator with individual beams extracted from each of the 36 modules operating with a negative output terminal. In order to operate as an ion beam accelerator, we had to reverse the polarity and connect all of the individual module outputs to a single diode. Polarity inversion was carried out in the water insulated pulse forming section and the magnetically insulated transmission lines (MITL's) were connected to a common "current manifold" near the diode (Fig. 3).[14] In another experiment, two pairs of alternate negative and positive 2 MV transmission lines were connected in series to produce a 4 MV output (Fig. 4).[15]

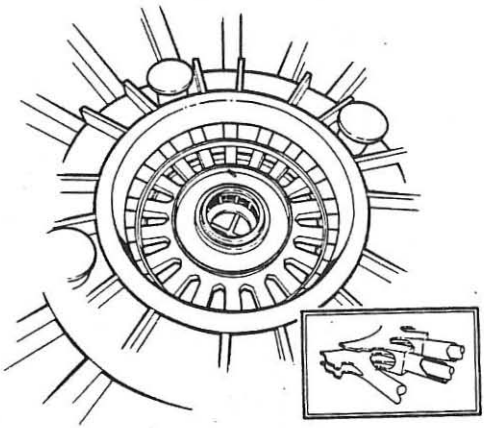


Figure 3. PBFA current manifold used to deliver power from 18 positively charged MITL's to a single diode.

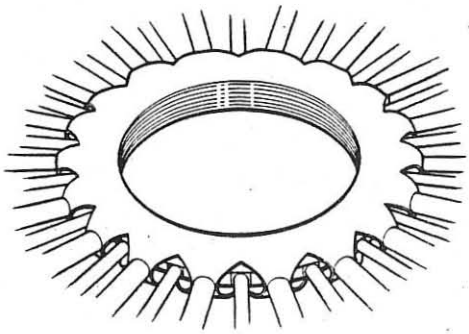


Figure 4. The method for series connection of positive and negative MITL's on PBFA to produce a 4 MV output.

These reconnections of terawatt transmission lines were made at electrical stress of ~2 x 10^6 V/cm and indicate the versatility of using magnetic insulation techniques in power delivery to various experiments via MITL's.

Diode experiments have begun on PBFA-I with 18 lines connected to a single diode based on the Ampfion concept of C. W. Mendel (Fig. 5).[16] This diode uses a self excited, distributed field coil that provides a spatially uniform magnetic field for electron suppression. The Ampfion concept involves a pre-injected plasma with an accelerating sheath which opens up during the power pulse. The sheath dynamics are controlled by magnetic pressure and by anode plasma erosion as ions are extracted.

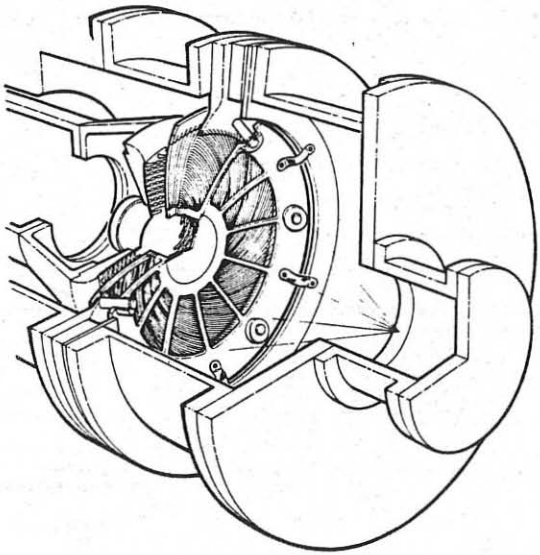


Figure 5. The Ampfion diode as tested on a single module of PBFA.

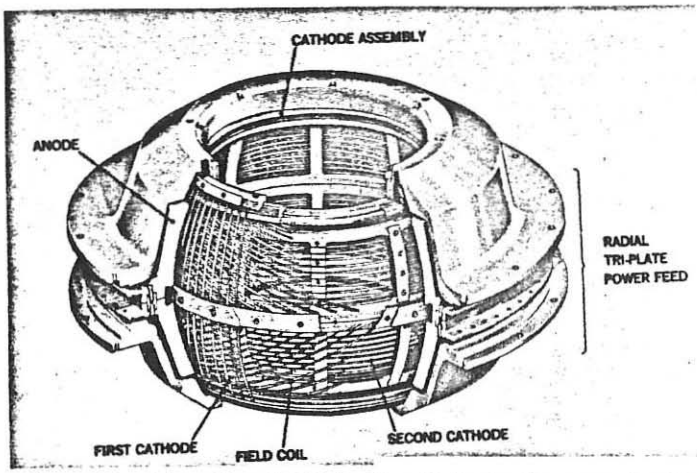


Figure 6A. Schematic of PBFA Ampfion diode showing current path.

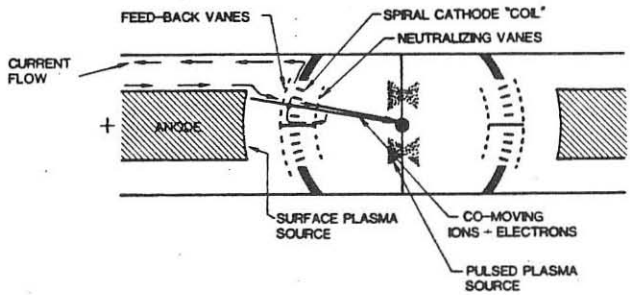


Figure 6B. Artists concept of Ampfion Diode as installed in PBFA-I.

This approach should allow us to both pre-select the proper ion specie in order to benefit from higher voltages and to achieve beam bunching from th increasing impedance and thus voltage during the power pulse. At the present, the Ampfion diode has been tested on a <1 TW accelerator, Hydramite, and has demonstrated 1° local beam divergence, good magnetic insulation, and sheath motion as predicted.(11) PBFA-I tests on the Ampfion diode (Fig. 6A, B) are underway using a flashover plasma source.(17) This diode should permit us to extend our target experiments to the 5 TW/cm^2 level and verify the basis for the diode concept to be used on PBFA-II. The present status of ion diode development is summarized in Fig. 7.(3)

SUMMARY OF ION DIODE DEVELOPMENT

ACCELERATOR AND LABORATORY	DIODE TYPE	V (MV)	I (kA)	J_D (KA/cm2)	θ (°)	$\beta = J_0\ V/\theta^2$ TW/cm^2
NEPTUNE CORNELL U.	APPLIED B PLANAR	0.6 - 0.8	70 - 110	0.25	0.4	~4
HYDRAMITE SANDIA	AMPFION	1.7	200	0.29	$\lesssim$1	~2
PROTO I SANDIA	APPLIED B RADIAL	0.8 - 1.4	360	~3.0	3.5	~1
GAMBLE II N.R.L.	PINCH REFLEX	1.2	600	25	~5	~4
PITHON PHYS. INT.	PINCH REFLEX	2.0	1000	10	?	?.
PROTO II SANDIA	APPLIED B RADIAL	1 - 1.7	1000 - 2000	5 - 10	•	•
PBFA I SANDIA	AMPFION	1 - 2	•	•	•	•

* EXPERIMENT CONTINUING AS OF 9/81

Figure 7. Summary of ion diode development.

PBFA II, (Fig. 8) which will consist of 36, 3 TW modules, is in final design and will begin construction of 1982. It will have a basic operating point of 4 MV but will utilize our ability to connect MITL's in both parallel and series to provide a wide range of operating conditions. A new laboratory building to house PBFA-II is under construction adjacent to the existing PBFA-I facility and we plan to continue operation of PBFA-I until PBFA-II becomes available in 1985.

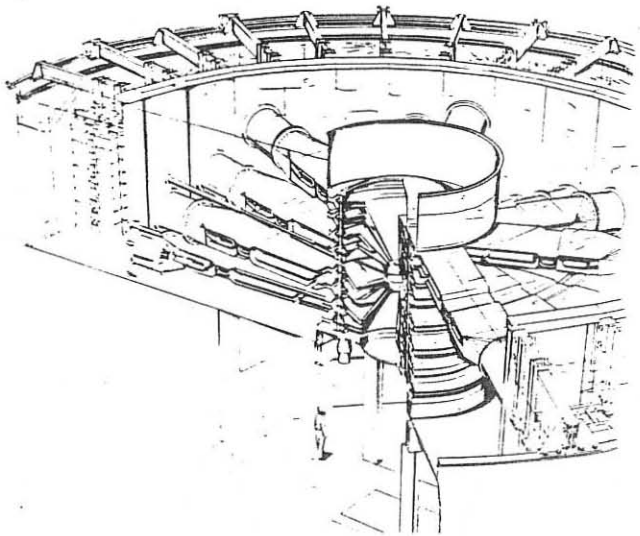


Figure 8. Artists concept of the 36 module PBFA-II.

The wide range of PBFA-II operating conditions was chosen not only to provide an opportunity to study the focusing and deposition of several ion species, but also to explore the magnetically imploded foil approach to ignition scaling. An extensive series of scaling experiments are underway on the Proto II accelerator where we have found that the thermal x-ray output from a stagnated foil scales with the square of the foil current up to

the 5 TW level.[18] In addition, the implosion appears to be sufficiently stable so that a 10 ns radiation pulse is produced in agreement with stability analysis.[19] In order to extend the experiments on Proto II to 10 TW, a low inductance diode employing magnetically inhibited flashover of the water-vacuum interface will be developed. If continuing scaling studies on Proto II are successful, then this approach is likely to be employed on PBFA-II.

Both of the approaches to ignition described above would result in damage to nearby diode components. This would be undesirable in future high gain experiments and is certainly unacceptable for any repetitive pulse applications. For this reason, studies of beam transport in preformed channels are underway. These channels have been produced by a capacitor discharge with wire and laser initiation over 50 cm[20] and in a wall confined geometry over distances up to 500 cm.[21] Under conditions where the channel is MHD stable, efficient and nonperturbing transport is observed. However, if the channel is kink unstable at too high a current or too low a background pressure, then transport efficiency is seriously reduced.[20] Present projections for reactor conditions[22] indicate that we should be able to choose appropriate beam and channel conditions to obtain efficient transport over several meters.[20,23-24] Another interesting concept is to allow the beam to self pinch in a background gas without the aid of a predischarge thus greatly simplifying reactor concepts.[25-26] This idea will require beams of very high brightness since the self pinching force is likely to be small and this approach will await further improvements in beam divergence before testing can begin.

Diagnostics and Target Experiments

Target experiments have emphasized the determination of incident beam parameters and the development of diagnostics for future fusion experi-

ments. A lower bound on the beam current can be obtained with magnetic probes when the drift conditions inhibit current neutralization. Nuclear reactions which produce prompt γ-rays from protons on Li or F can be detected by photonuclear activation of copper, and the neutron pulse time history can be measured with scintillator photomultiplier detectors.(27) In this way we have measured ~350 kA of protons incident of a 1.9 cm diameter target on the Proto I accelerator in agreement with magnetic probe measurements. Smaller cylindrical targets have been used in a measurement of proton range. The brightness temperature of the inner surface of a .6 cm base diameter thin wall conical aluminum target was measured using a triplet array of x-ray diodes. By varying the wall thickness it was possible to determine the incident fluence to be .5 TW/cm^2 with classical proton deposition (Fig. 9)(28) A four frame pulsed ruby laser holographic

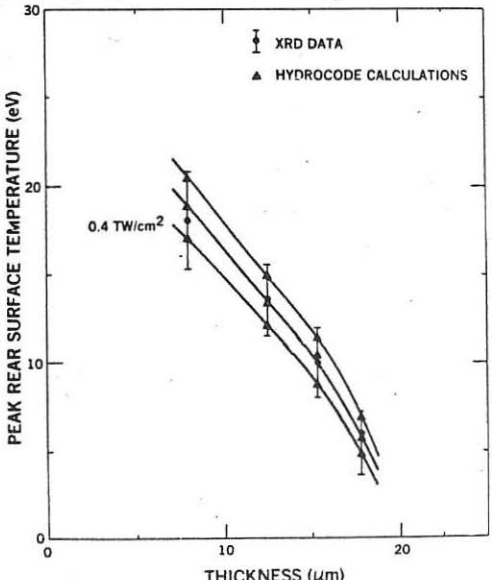


Figure 9. Rear surface temperature of a .6 cm base diameter conical aluminum target as a function of wall thickness and comparison with hydrocode calculation.

interferometer has been used to monitor the motion of the inner surface of a similar target.[29] Both a simple rocket model analysis as well as a hydrodynamic code treatment indicated a fluence of ~.6 TW/cm^2 and a range of 15 μm (Fig. 10) which correlates well with the inner surface temperature measurement.

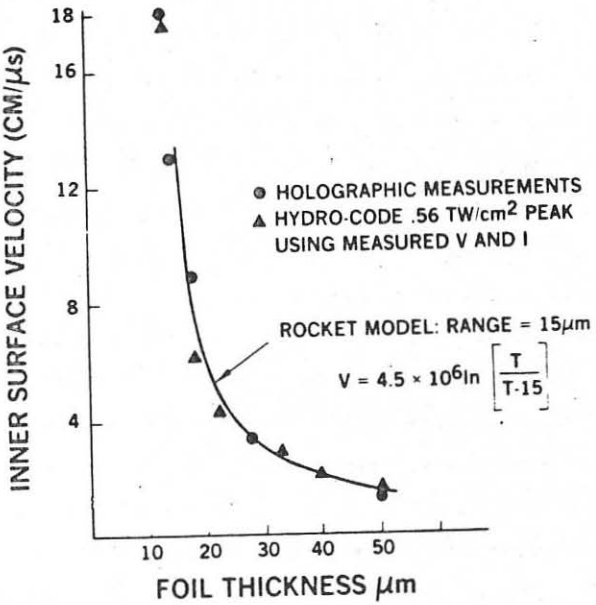


Figure 10. Rear surface velocity of a .6 cm diameter cylindrical aluminum target as a function of wall thickness and comparison with rocket model and hydrocode calculation.

Optical, x-ray and nuclear diagnostics should suffice to determine beam conditions, but the essential aspects of implosion and ignition will require neutron detection and x-ray shadowgraphy. Heavily shielded scintillator photomultipliers are used for neutron time of flight and neutron yield is measured via copper activation. Using these techniques we have measured, with exploding pusher targets, neutrons produced by recoil energies imparted to tritons or deuterons by incident protons. These energetic fuel ions produce a potentially misleading background level.[30] Because of asymmetry and defocusing effects we believe that fluence levels of at least 1.0 TW/cm^2 will be needed for light ion driven exploding pusher experiments.[31] The value of these experiments is primarily for diagnostic development. It is of more consequence, however, to be able to begin the study of ablative implosions.

Implosion hydrodynamics can be studied using flash x-ray shadowgraphs by backlighting the target with a pulsed, point source of x-rays.[32] The apparatus consists of an array of three 600 kV electron accelerators, each with a 3 ns pulse duration, and three cameras with direct recording of the implosion onto film with a 2.6X magnification (Fig. 11). The x-ray sources are synchronized with the ion beam pulse and the interframe time can be varied over several nanoseconds. Radiographs of spherical and cylindrical targets which are ablatively accelerated show details of both the target outer and inner surfaces. In one experiment, a 3 mm diameter, 16.5 μm thickness, cylindrical tungsten target was ablatively imploded at a velocity of ~1 cm/μsec indicating a beam fluence of .5 TW/cm^2. This technique should be useful in studying the critical issue of mixing of the pusher material with the fuel.

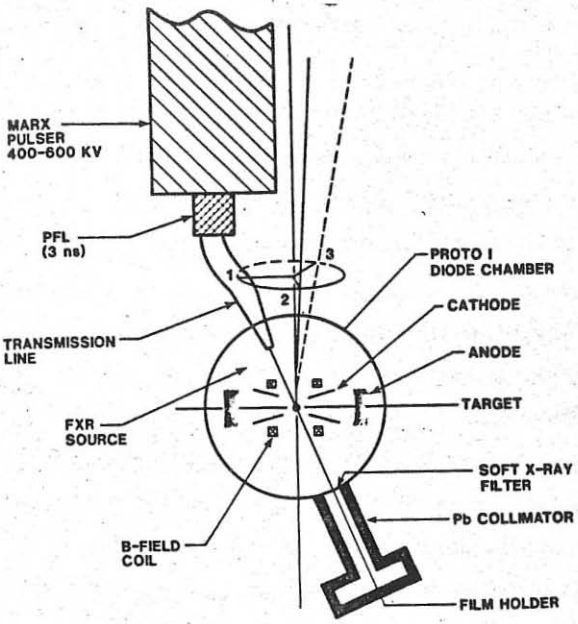


Figure 11. Apparatus for three-frame x-ray backlighting and recording of implosion of ion beam ablatively driven target.

Conclusion

Light ion beam focusing and stability of imploding foils are being studied using a series of pulsed power devices with a goal of ignition scaling experiments on PBFA-II in 1986. The critical issues are to demonstrate an order of magnitude increase in beam brightness with increasing accelerating voltage and ion mass, and to scale the implosions of cylindrical foils to the 100 TW drive level. Diagnostic techiques are being developed in order to allow us to investigate the fundamental issue of implosion hydrodynamics and ignition scaling.

Acknowledgment

I would like to thank several members of the Sandia Particle beam Fusion group for the use of much unpublished data.

Max-Planck-Institut für Plasmaphysik
8046 Garching bei München

REFERENCES

(1) S. Rockwood, Los Alamos National Laboratory, Private communication, and K. Lee et. al. Nuclear Fusion, 19, 1447 (1979).

(2) S. Humphries, Nuclear Fusion, 20, 1549 (1980).

(3) C. L. Olson, Sandia National Laboratories, to be published, Journal of Fusion Energy.

(4) G. Allshouse and S. Slutz, Sandia National Laboratories, Private communication.

(5) T. Melhorn and M. Widner, Sandia National Laboratories, to be published in Comments in Plasma Physics and Controlled Fusion.

(6) D. Seidel, Sandia National Laboratories, Private communication.

(7) H. Bluhm, et. al., "Intense Ion Beam Source Development Experiments," presented at 4th International Topical Conference on High-Power Electron and Ion-Beam Research and Technology, Palaiseau, France, June 29-July 3, 1981.

(8) G. Cooperstein, et. al., "Light Ion Production and Focusing with Pinch-Reflex Diodes," ibid.

(9) C. Mendel, "Ion Filtering in Ampfion Diodes," 1981 IEEE International Conference on Plasma Science, Santa Fe, NM, May 18-20, 1981.

(10) G. McClure, Sandia National Laboratories, Private communication.

(11) G. Kuswa, J. P. Quintenz, E. J. T. Burns, "Scalability of Light Ion Beams to Reach Fusion Conditions", ibid. Ref. 7.

(12) P. A. Miller and J. P. Quintenz, Sandia National Laboratories, Private communication.

(13) J. P. VanDevender, G. W. Barr, D. H. McDaniel, S. A. Goldstein, "PBFA-I: Pulsed Power Driver for Inertial Confinement Fusion,"

ibid. Ref. 7.

(14) T. Crow and G. Peterson, Particle Beam Fusion Progress Report, SAND 81-1459. January - June, 1981.

(15) B. N. Turman and P. J. Skogmo, ibid. Ref. 14

(16) C. W. Mendel, "Theory of Ampfion Class Ion Diodes," ibid. Ref. 7.

(17) P. A. Miller, Sandia National Laboratories, Private communication.

(18) D. H. McDaniel, Sandia National Laboratories, Private communication.

(19) T. W. Hussey and D. H. McDaniel, "Implosion Stability and Limitations on Hollow Plasma Liners," to be published in Comments in Plasma Physics and Controlled Fusion.

(20) J. Olsen and R. J. Leeper, to be published.

(21) F. C. Sandel, et. al., "Experimental Studies of Intense Light-Ion Beam Transport," ibid. Ref. 7

(22) D. L. Cook, M. A. Sweeney, M. T. Buttram, and K. R. Prestwich, Sandia National Laboratories; G. A. Moses, R. R. Peterson, E. G. Lovell, and R. L. Englestad, University of Wisconsin, "Light Ion Driven Inertial Fusion Reactor Concepts," 4th International Topical Meeting on Technology of Controlled Nuclear Fusion, Valley Forge, PA. October 14-17, 1980.

(23) J. R. Freeman, L. Baker, and D. L. Cook, "Plasma Channels for Intense Ion Beam Transport: Theory," ibid. Ref. 7.

(24) D. Mosher, D. G. Colombant, S. A. Goldstein and P. F. Ottinger, "System Requirements for Light-Ion ICF," ibid. Ref. 7.

(25) J. R. Freeman, Sandia National Laboratories, Private communication.

(26) S. A. Goldstein, et. al., "Ion Beam Handling in Magnetized Plasmas," ibid. Ref. 7.

(27) J. Golden, R. A. Mahaffey, J. A. Pasour, F. C. Young and C. A. Kapetanakis, Rev. Sci. Instr. 49, 1384 (1978) and R. J. Leeper,

E. J. T. Burns, D. J. Johnson and W. M. McMurtry, Proceed. of Workshop on Meas. of Elect. Quantities in Pulsed Power Systems, (1981).

(28) E. J. T. Burns and A. V. Farnsworth, ibid. Ref. 14.

(29) F. C. Perry and M. M. Widner, ibid. Ref. 14.

(30) R. J. Leeper, T. A. Melhorn and S. A. Slutz, ibid. Ref. 14.

(31) A. V. Farnsworth, ibid. Ref. 14

(32) J. Chang, ibid. Ref. 14.

CONTRIBUTED PAPERS
NOT INCLUDED IN VOL. I

THE ANALYTICAL SOLUTION AND MAXIMUM β FOR THE EQUILIBRIUM OF A FAT TOKAMAK WITH CIRCULAR CROSS-SECTION

L. J. Pan, F. L. Tang and K. C. Zhuo
Institute of Mechanics, Academia Sinica
Beijing/PRC

Abstract: The equilibrium of a fat tokamak with circular cross-section is treated analytically to order ϵ^3, by the method of expansion in powers of the aspect ratio ϵ, based on the fundamental equations in[1], consequently maximum $\langle\beta\rangle$ is obtained with restriction that no negative pressure appears.

Introduction

The MHD equilibrium and stabilities of plasma with rectangular cross-section for the homogeneous case were analytically treated by Maschke, [1] Herrnegger[2], Oshiyama and Fukutam[3], et al. and several other exact analytical solutions exist. But, to the best knowledge of these authors, the equilibrium of a fat tokamak with circular cross-section has not yet been treated analytically; by the way, an analysis by Mercier and Luc[4] for the tokamak with small cross-section was carried out to order ϵ for a special "linear" case, where $\epsilon = a/R_0$, a is the radius of cross-section and R_0 the distance of the center from the axis, namely the Z-axis in cylindrical coordinates (R, ϕ, Z). The purpose of this paper is to work out the solutions for a general "linear case" up to order ϵ^3 by a method of expansion in powers of ϵ so that the results may be accurate enough for a fat tokamak. In this way, the fundamental equation and some results given in[1] will be used and only a slightly different notation is introduced. A straightforward but rather lengthy calculation leads to the required solutions for poloidal flux function and pressure in terms of Bessel functions. Conse-

quently, a maximum $\langle\beta^*\rangle$ may be obtained by long integrations over the plasma volume of the equations for flux functions, pressure and current density. Where $\langle F\rangle$ is defined as $\int_v F d\tau / V$, and V is the volume of plasma.

Recapitulation of Equilibrium Equation

The ideal MHD equilibrium equation of plasma with circular cross-section given in[4] for the so-called "linear" case will be used here as the fundamental equation:

$$\left.\begin{aligned} L\psi &= -\left\{m_1 + \frac{P_1 \epsilon\rho\cos\theta}{2}(\epsilon\rho\cos\theta - 2) + \left[m_1 + \epsilon\rho\cos\theta(\epsilon\rho\cos\theta - 2)P_2\right](m_1 G + P_1 H)\right\} \\ &= -2(1-\epsilon\rho\cos\theta)^2 \eta / \langle\eta\rangle \end{aligned}\right\} (1)$$

where $a^2 L = \frac{1-\epsilon\rho\cos\theta}{\rho}\left[\frac{\partial}{\partial\rho}\left(\frac{\rho}{1-\epsilon\rho\cos\theta}\frac{\partial}{\partial\rho}\right) + \frac{1}{\rho}\frac{\partial}{\partial\theta}\left(\frac{1}{1-\epsilon\rho\cos\theta}\frac{\partial}{\partial\theta}\right)\right]$

and (ρ, θ) defined in Fig. 1 are polar coordinates with origin at the center of the circular cross-section; ψ is a normalized poloidal flux function with definitions: $\psi = \frac{\psi^*}{f_b a^2 \langle\eta\rangle}$ and reduced current density $\eta = \frac{R_0^3 J_\phi}{2 f_b R}$ here ψ^*, J_ϕ and f_b are poloidal flux function, toroidal current density, and the RB_ϕ at plasma boundary respectively.

Defining two functions G and H by the expressions:

$$\left.\begin{aligned} \left[L + m_2 + P_2 \epsilon\rho\cos\theta(\epsilon\rho\cos\theta - 2)\right] G &= -1 \\ \left[L + m_2 + P_2 \epsilon\rho\cos\theta(\epsilon\rho\cos\theta - 2)\right] H &= -\epsilon\rho\cos\theta(\epsilon\rho\cos\theta - 2)/2 \end{aligned}\right\} (2)$$

with the boundary condition $G = H = 0$ at $\rho = 1$, then one finds the solution of this problem is $\psi = m_1 G + \epsilon P_1 H$. P_2 is a parameter related to pressure profile with definition $\beta^* = \frac{2PR_0^2}{f_b^2\langle\eta\rangle\epsilon^2} = P_1\psi + P_2\psi^2$ (3) and m_2 another parameter related to current density profile with the relation $f/f_b + \epsilon^2\langle\eta\rangle^2\beta^* = 1 + \epsilon^2\langle\eta\rangle^2(2m_1\psi + m_2\psi^2)$ (4)

Integrations over the plasma volume of (1) and β^* lead to two important relations $\alpha_1 m_1 + \alpha_3 P_1 + 1 = 0$, and $\alpha_3 m_1 P_1 + \alpha_4 m_1^2 + \alpha_5 P_1^2 = \langle\beta^*\rangle$ where $\alpha_1, \alpha_2 \ldots$ are functions of m_1, m_2, P_1, P_2, ϵ and some volume average quantities. Give α_1, as an example, $\alpha_1 = \frac{1}{2}\left[\langle\frac{R_0}{R}\rangle + m_2\langle\epsilon\frac{R_0^2}{R^2}\rangle + \frac{2\epsilon P_2}{R}\langle H\frac{R_0^2}{R^2}\rangle\right]$, $\alpha_2, \alpha_3 \ldots$ are shown in 5

Solution

Since equation (1) contains $\epsilon\rho\cos\theta$ and ϵ, which are usually small, the solution of this problem may be obtained by "double

expansion", first in powers of $\epsilon\rho\cos\theta$, and then in powers of ϵ. Assuming $G = \sum_{n=0}^{n} G_n(\rho,\epsilon)\epsilon^n\cos^n\theta$, one gets the differential equations for G_0, G_1...respectively from equation (1) by expansion in powers of $\epsilon\rho\cos\theta$. Again, in a similar way, assuming $G_i = \sum_{m=0}^{n} G_i^{(2m)}(\rho)\epsilon^{2m}$ one obtains the differential equations for $G_i^{(0)}$, $G_i^{(2)}$...; for examples: ϵ^0 order $L_0 G_0^{(0)} = 1/\mu^2$, ϵ order $L_1 G_1^{(0)} = -\xi G_0^{(0)}/\mu + 2\alpha\xi G_0^{(0)}/\mu$ with boundary conditions $G_0^{(0)}(\mu) = G_1^{(0)}(\mu) = 0$ where $\xi = \sqrt{m_2}\rho = \mu\rho$ and $\alpha = \beta_2/m_2$. Give some of the solutions just for examples: $G_0^{(0)} = \left(\frac{J_0}{J_0(\mu)} - 1\right)/\mu^2$

$$\mu^3 G_1^{(0)} = -\frac{\xi J_0}{2J_0(\mu)} + \left[\left(\frac{\alpha\xi^2}{2J_0(\mu)} + \mu(1+4\alpha)/2J_1(\mu) - \alpha\mu^2/2J_0(\mu)\right)J_1 - 2\alpha\xi\right]$$

Maximum $\langle\beta^*\rangle$

Having the solutions shown above, one is ready to find $\langle\beta^*\rangle$ from (3) and (4) with the restriction $\frac{\partial\langle\beta^*\rangle}{\partial\rho}\Big|_{\rho=1,\theta=\pi} = 0$ for avoiding the appearance of negative pressure of the external side of plasma. Finally $\langle\beta^*\rangle$ is obtained as a function of μ, α and ϵ. The conditions $\partial\langle\beta^*\rangle/\partial\mu = 0$ and $\partial\langle\beta^*\rangle/\partial\alpha = 0$ give $\langle\beta^*\rangle_{MAX}$, ϵ is considered as a given constant.

Conclusions

Fig. 2 shows that $\langle\beta^*\rangle_{max}$ decreases with increasing ϵ and the $1/\epsilon$ order solution is accurate enough for small ϵ; the higher order solutions give about 20% correction for larger ϵ, say 0.3.

Fig. 5 shows the apperance of reversal current density in the neighborhood of the external side of plasma. Such a current density profile may not be realistic; one may find a new $\langle\beta^*\rangle_{max}$ with conditions $\frac{\partial}{\partial\mu}\langle\beta^*\rangle + \lambda\frac{\partial}{\partial\mu}\left(\eta\Big|_{\substack{\rho=0\\ \theta=\pi}}\right) = 0$, $\frac{\partial}{\partial\alpha}\langle\beta^*\rangle + \lambda\frac{\partial}{\partial\alpha}\left(\eta\Big|_{\substack{\rho=1\\ \theta=\pi}}\right) = 0$ and $\eta\Big|_{\substack{\rho=1\\ \theta=\pi}} = 0$ where λ is a Lagrange multiplier, used for avoiding reversal current density. The numerical calculation for new $\langle\beta^*\rangle_{max}$ is given in [5] The analytical solutions in this paper may be used for studying the properties of instabilities.

References

(1) E. K. Maschke, Plasma Physics 15, p. 535 (1973)

(2) F. Herrnegger, Proceedings of V European Conference on Controlled Fusion and Plasma Physics, Grenoble Aug. Vol. 1, p. 26 (1972)

(3) H. Oshiyama, Y. Fukutom, Nuclear Fusion, 14, p. 793 (1974)

(4) C. Mercier and Luc, Lectures in Plasma Physics

(5) L. J. Pan, F. L. Tang and K. C. Zhuo

The Equilibrium and Maximum β of Plasma with Circular Cross-Section (in Chinese, to be published).

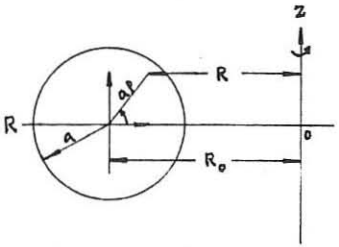


Fig. 1. Coordinates

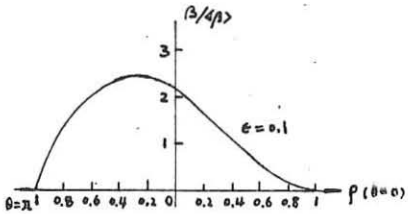


Fig. 4 $\beta/\langle\beta\rangle$ profile

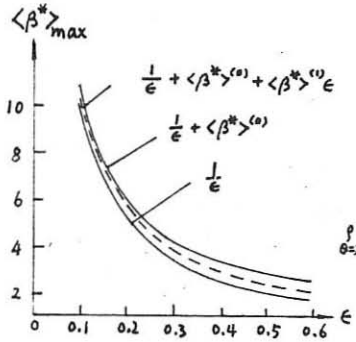


Fig. 2 The effect of higher solution on $\langle\beta^*\rangle_{max}$

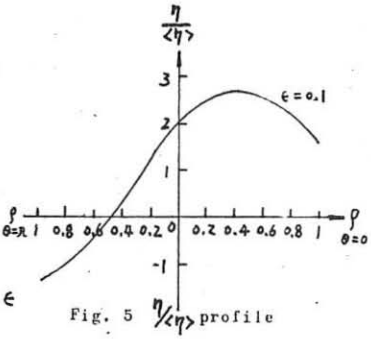


Fig. 5 $\eta/\langle\eta\rangle$ profile

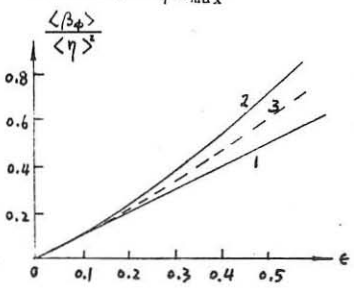


Fig. 3 The effect of higher solution on $\langle\beta_\phi\rangle/\langle\eta\rangle^2$

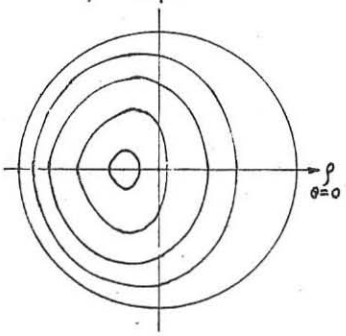


Fig. 6 Flux function

KELVIN-HELMHOLTZ INSTABILITY IN TOKAMAKS

Xu Fu Chen Le-Shan
(Institute of Mechanics, Academia Sinica)
and Xu Cui-Wei
(Department of Mathematics, Peking University)
Beijing, The People's Republic of China

One of the main problems in tokamaks is plasma heating. Neutral beam heating has made considerable stride recently, the ion temperature $T_i = 6.5\text{kev} = 7 * 10^7$ K has been obtained in PLT. But toroidal plasma rotational velocities up to 10^7 cm/sec due to an unbalanced injector system has been observed in the experiment[10]. S.Suckewer et al.[1] had reported the results of measurements for the radial distribution of the rotational velocities in May 1979.

Does a new MHD instability arise from the plasma rotation with velocity shear in PLT ? Lau-Liu[5] had discussed this problem in May 1980. They used the slab geometry and concluded that, the velocity shear alone could not produce an MHD instability which qualitatively changed the initially laminar state of the plasma when flow velocity was less than twice the Alfvén speed.

A metal limiter is adopted in PLT. The minor radius =40 cm, and a distance of 10 cm is there between the high temperature plasma and the conducting wall. The density of plasma is actually very low in this region, which may be regarded as a vacuum region. With this region taken into account, we discuss the MHD instability with velocity shear again. We except that some new MHD instabilities such as Rayleigh-Taylor instability and Kelvin-Helmholtz instability etc. may appear. Only the Kelvin-Helmholtz instability that is the instability of the plasma with velocity shear bounded by vacuum region is discussed in this paper.

We adopt the slab geometry which is the same as the Lau-Liu's model. See Fig.1. We suppose

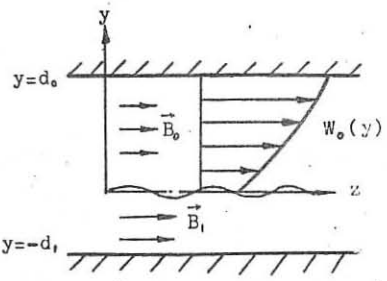
1. The velocities of plasma are $W_0(y)$, there are experimental data for the values[2] and there is shear.

2. The plasma is ideal, the solid wall is an ideal conductor.

3. The plasma is incompressible, ρ = const.

4. The uniform magnetic fields $\vec{B}_0, \vec{B}_1$ in the flow direction are present in the plasma region and the vacuum region respectively.

FIGURE 1



The mathematical formulation is to solve equation

$$\frac{d}{d\bar{y}}\left\{\left[(\Omega_0+W(\bar{y}))^2-1\right]\frac{d\bar{B}}{d\bar{y}}\right\}-k_0^2\left[(\Omega_0+W(\bar{y}))^2-1\right]\bar{B}=0$$

with the boundary conditions:

$$\bar{y}=1,\quad \bar{B}=0$$

$$y=0,\quad \frac{d\bar{B}}{d\bar{y}}\Big/\bar{B}=-\frac{k_0\cosh k_0}{\sinh k_0}\frac{a}{(\Omega_0+W(0))^2-1}$$

where

$$\bar{y}=y/d_0,\quad \bar{B}=B_{0x}/B_0,\quad W=W_0/v_{0A},$$

$$\Omega_0=\omega/k_x v_{0A},\quad k_0=k_x d_0,\quad \bar{B}_1=B_1/B_0,$$

$$a=d_1/d_0,\quad v_{0A}=B_0/\sqrt{4\pi\rho_0},$$

and Ω_0, the eigenvalues.

Only a special velocity distribution is discussed, i.e.

$$W(\bar{y})=r+s\,\bar{y},$$

where r, s are two constants. Let $\Omega_1=\Omega_0+r$. We use series expansion, suppose

$$\bar{B}(\bar{y})=\sum b_n \bar{y}^n.$$

After substituting this expression into the differential equation and eliminating b_0, b_1 from boundary condition, we obtain a dispersion relation.

It can be seen from Fig.2, when s= 1.8, 1.0, 0.3 which satisfies the sufficient condition for stability

$$s \equiv v_{0A}/v_{0s} < 2$$

indicated by Lau-Liu[3]; there exists an unstable region of wave numbers in the right hand side of $k_0=0$ owing to the presence of a vacuum region. But instability growth rates

decay rapidly as k_0 increases.

FIGURE 2

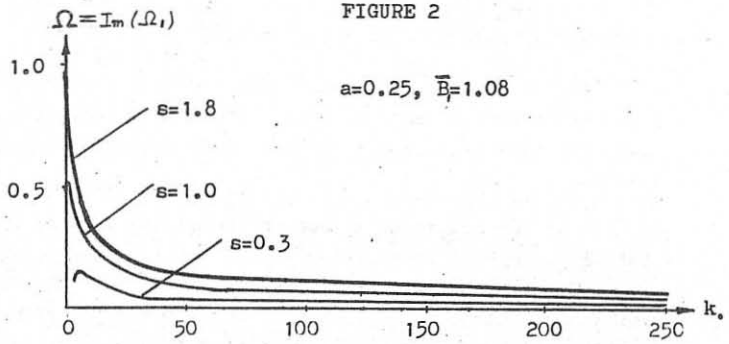


Table 1 gives $\Omega(k_0)$ for $a = 0.25$, $\bar{B}_1 = 1.08$ and $s = 0.1, 0.01, 0.0025$.

TABLE 1

Ω \ k_0 / s	0	1	2	5	10	20	100	200	250
0.1	0	0	0	0	0.049	0.046	0.024	0.017	0.015
0.01	0	0	0	0	0	0	0.0048	0.0046	0.0043
0.0025	0	0	0	0	0	0	0	0	0

We conclude that,

1. When the vacuum region is taken into account , the plasma may be unstable even if the sufficient condition for stability indicated by Lau-Liu [3] is fulfilled. In fact, there exists a vacuum region in PLT, so the conclusion about the effect of velocity shear on MHD stability must be modified.

2. The flowing plasma with uniform velocity distribution , i.e., when the velocity shear is absent, is stable.

3. When s decreases to 0.01, the minimum wave number of instability becomes larger, the maximum growth rates of instability are much lower, the plasma with velocity shear

displays a stable trend. When $s \lesssim 0.0025$, the plasma is nearly stable, therefore the computation coincides with the experimental data in PLT approximately.

4. The rotating plasma bounded by a vacuum region is MHD stable when we can make s small. Thus it is necessary to study the distributions of physical quantities in flowing plasma.

As to the nonlinear effect on the growth rate of instability, we have been studied it in the same configuration with the gravitational field taken into account. The problem is solved by singular perturbation method, and the results will be presented in the near future.

REFERENCES

1. Eubank,H. et al., Plasma Physics and Controlled Nuclear Fusion Research, 1,(1979) IAEA, 167.
2. Suckewer,S. et al., PPPL-1542, Uc-20d, (1979) 1.
3. Lau,Y.Y.and Liu,C.S., Phys. Fluids, 23, (1980) 939.

OPEN TRAP WITH min B AND $\beta = 1$

I.K.Konkashbayev, I.S.Landman, F.R.Ulinich
The Kurchatov Institute of Atomic Energy, Moscow, 1981

Certain success has been recently achieved in the constructing of plasma guns (plasma parameters in clots are: density $n \sim 10^{15} cm^{-3}$, braking temperature of ions $T_i \sim 1$ kev, a number of particles $N \sim 10^{20}$, impulse duration $\tau_{imp} \sim 10^{-5} s$ [1]). It allows the possibility of injector employment for thermonuclear experiment to be considered. In this report the scheme, including the collision of injected clots of plasma followed by their confinement in open trap with $\beta=1$, is being considered. The report is to consider the confinement of plasma, resulted in collision in a MGD--stable trap of the theta-pinch type device with cusps on its ends. The main part concerns a theoretical consideration of the two basic problems connected with plasma confinement, that is energy flux confinement through cusps and the question on cusps width.

Energy losses through cusps are due to electrons flow to the wall. At worst, when electrons freely reach the wall, their thermal flux is (m_i/m_e) times the ion thermal flux. This circumstance should have made any conception, based on cusp configuration, hopeless. However there is a solution of the electron heat flux decreasing problem [5], which consists of sudden expansion of plasma flow, leaking from trap, between the cusp and the wall. In such a "bell mouth" there appear electrons trapped between a mirror in the cusp region and a falling space potential of the bell

mouth created by trapped electrons themselves. As a result, a cloud of negative charge, which doesn't let electrons pass to the wall, is formed between the cusp and the wall. The trapping potential in a relatively small bell mouth (~1m) approaches an ambipolar value, and the heat flux becomes 10 times lesser.

In recent years new experimental results on cusps width, through which plasma leaks to the vacuum chamber wall [2,4], have been obtained on cusp configurations. The effective cusp width appeared to be equal approximately $2(r_{Hi}r_{He})^{1/2}$. The principle of cusp width calculation consists in using two mechanisms: these are diffusion of plasma into the boundary sheath and the particle losses from it along the field lines through cusps. For a sufficiently sharp boundary with thickness $\delta \ll r_{Hi}$, diffusive electron flux will be $j_e^{(+)} \sim \tau_{He}^2 n/\tau_e \delta$, a speed of departure per area unit $j_e^{(-)} \sim n \tau_{\tau_e} \delta \exp(-e\varphi_{amb}/T_e)/L$. From the condition $j_e^{(+)} = j_e^{(-)}$:

$$\delta \sim \tau_{Hi} \sqrt{\frac{L}{\lambda}} \left(\frac{m_e}{m_i}\right)^{1/4},$$

where λ is a free pass, L is a system length. Accounting of electrons, which go away without diffusion, leads to limitation of δ from below by value $4\tau_{Hi}\left(\frac{m_e}{m_i}\right)^{1/3} \ll \tau_{Hi}$ at $\frac{L}{\lambda} < \left(\frac{m_e}{m_i}\right)^{1/3}$.

On the foundation of these results it is supposed to obtain the following parameters of plasma confinement in experiment with collision of two blobs injected. At plasma energy 200 kj, density $10^{17}cm^{-3}$, pinch radius 6cm, length 1m temperature 1 kev in two limit cases it is obtained

a) $\delta = r_{Hi}$, without bell mouth: $n\tau = 4 \cdot 10^{12} cm^{-3}s$ (particles), $(n\tau)^{\varepsilon} = 5 \cdot 10^{11}$ (energy), $T_e = 350$ ev, $T_i = 1$ kev, a number

of neutrons $N_n = 2 \cdot 5 \cdot 10^8$.

b) $\delta = (r_{Hi} r_{He})^{1/2}$; with bell mouth: $n\tau = 3 \cdot 10^{13}$, $(n\tau)^{\epsilon} = 5 \cdot 10^{12}$; $T_e = 1$ kev, $T_i = 1$ kev, $N_n = 2.5 \cdot 10^9$.

One of the questions on this system is that of about permissible value of the inner magnetic field, the sheath width being still not too great. In case, the inner magnetic field is of close type configuration, the above obtained results are correct. If all the magnetic flux passes through cusps, it should lead to increasing of effective cusp width. Then the conservation of δ at the $(r_{He} r_{Hi})^{1/2}$ will be $2\pi R \delta H_o > \pi R^2 H_{in}$, from this follows $H_{in}/H_o < 2\delta/R$. It is a rigid constraint ($H_{in} \lesssim 1\%$). However the number factor is of great importance in this case, due to which the sheath width is approximately 5 times more than δ, as the calculations indicate. That is why a rather less rigid constraint $r_{Hi}(H_{in}) > R$ is more practical. At $r_{Hi}(H_{in}) < R$ the trap becomes adiabatical of Mirnov-Ryutov gasodynamic type [6], but with more great magnetic mirrors. From calculations the influence of inner feld at $r_{Hi}(H_{in}) \lesssim R$ is not large, and lifetime of particles decreases with H_{in}^{-1} rather slowly.

For powerful systems ($n\tau \gtrsim 10^{14} cm^{-3} s$) there appears a problem of α-particles using for selfheating of plasma to decrease its initial energy. In this case the configuration of baseball type, which is the system with slowly changed ellipse-like cross section should have the principal advantage because the α-particles acquire additional (adiabatical) motion integrals. But calculations show that

conservation of these integrals is bad because of resonances between the transversal motion frequencies.

Thus the system considered satisfies all the basic requirements made of prototype of thermonuclear reactor with magnetic confinement, from viewpoint of simplicity, energetics and MGD stability.

REFERENCES

1. Skvortsov Y.V., Umrikhin N.M. The Theses of the Report at the 3rd International Conference on Plasma Injectors, Minsk, 1975
2. Kitsunezaki A., Tanimoto M., Sekiguchi T., Phys. Fluids, 17, 1895 (1974)
3. Hershkowitz N., Leung K.N., Romesser T. Phys. Rev. Lett., 35, 277 (1975)
4. Hershkowitz N., Smith J.R., Kosima H. Phys. Fluids, 22, 122 (1979)
5. Konkashbayev I.K., Landman I.S., Ulinich F.R. JETP, 74, 956 (1978)
6. Mirnov V.V., Ryutov D.D. Gasodynamical Trap. Problems of Atomic Science and Technics. Series: Thermonuclear Synthesis, 1980, No.1 (5)

CURRENT CHANNEL FORMING PROCESSES AND ENERGY RELEASE IN THE DIODE OF THE "ANGARA-I" HIGH CURRENT ACCELERATOR

I.P.Afonin, M.V.Babykin, K.A. Baigarin, N.U. Barinov, A.V. Bartov, P.P. Gavrin, A.V. Gubarev, V.V. Gorev, V.I. Mizhiritskiy, V.N. Kiselev

I.V. Kurchatov Atomic Energy Institute, Moscow, USSR.

In "Angara-1" experiments [1] the interaction of focused beam (100-200 kA, 1 MV, power density 10^{13} W/cm^2) with the 10-20 m-thick gold or platinum foils, imitating an outer shell of termonuclear target, was investigated. Due to action of beam magnetic field the electrons undergo an enhanced ("anomalous") stopping in the foil plasma, and energy deposition in the foil material to an end of current pulse increases several times compare to classical stopping. Foil temperature, defined by vaccuum ultraviolet radiation, reached 30-40 eV. Thus, it became possible to investigate the metal foil heating in real scale of temperature and energy deposition needed for ignition of the pulse thermonuclear reaction. To increase the foil temperature up to 70-100 eV, when the effective heating and implosion of target up to thermonuclear temperatures is expected, it is necessary to get the further increasing of power flux density and the total accelerator energy release. The latter was, however, difficult because there was in our earlier experiments a current arising delay (~30 ns) relative to the voltage pulse, and, accordingly, reduced power growth rate at the start of process. It seems to be determined by duration of forming the plasmas on the cathode surface acting as the plasma electron emission sources [2].

On the other hand, in experiments on Triton, Mirage (Kurchatov Inst.) and others, with the prepulse, the current arising delay was small enough. In this work, to optimize the condition of the accelerator energy release, we tried to decrease the current arising delay by adding the fast prepulse with a variable amplitude and duration,

the latter being less than the main pulse duration, to prevent too early short-circuiting of the diode with the plasma produced by prepulse itself.

It was reached by placing into the inner electrode of transmission line the metal, various in length, cylindrical inserts. The insert contacted with the inner electrode of forming line near to sharpening switch connecting the forming and transmission lines. The displacement currents flowing through capacity between the insert and inner transmission line electrode and then through the transmission line produce in the latter the voltage pulse. This pulse occures before the main pulse, duration being equal to the time interval from the arising of pulse in forming line to the breakdown of the sharpening switch. It is possible to change the prepulse by varying the insert length, duration being constant, or by varying the pressure and sort of gas in the sharpening switch, when duration as well as amplitude of prepulse is increased or decreased. In our experiments the prepulse reached ~30% of the main pulse.

The influence of the prepulse on diode characteristics - impedance Z, total current I, and power calculated as $I(V-L\frac{dI}{dt})$, where L is the diode inductance, was investigated. The transmission line had the characteristic impedance 1,5Ω at the input and 0,8Ω at the output. In the case of prepulse with the level $\geqslant$ 20% the current starts approximately 30 nsec earlier than in abscence of it. It means that to the moment of the main pulse arising (beginning of fast growth of V, Fig. 1) there is a considerable emission from the cathode. In these conditions we have the more rapid power growth, curve P, and increasing of the half-width of P (75 nsec instead of 50 nsec without prepulse), i.e., the adding of the prepulse provides the increasing of the total energy release throughout pulse duration. The time dependence of diode impedance, Z, and other characteristics of current channel are considerably influenced by movement of the dense plasma layers from the cathode and anode towards each other. It results in the

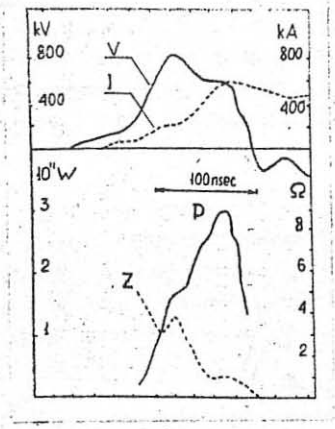


Fig. 1. Time dependence of the diode impedance and power release calculated by oscillograms of current and voltage, in presence of prepulse.

decreasing of impedance and improving of the matching of diode and transmission line at the initial and middle parts of process, and, on the other hand, in the short- circuiting of diode at the next part, when these layers join and all the diode gap is filled with dense plasma. With the adding of prepulse we have the more smooth fall of the diode impedance at the top of voltage pulse, that increases the total energy release throughout pulse duration.

To investigate features of the plasma layers movement in diode the image converter streak camera photographs, perpendicular to the diode axis, were taken. The photographs (Fig. 2) show that in the case of prepulse the anode plasma light occurs 20-30 nsec earlier, in accordance with the earlier current arising.

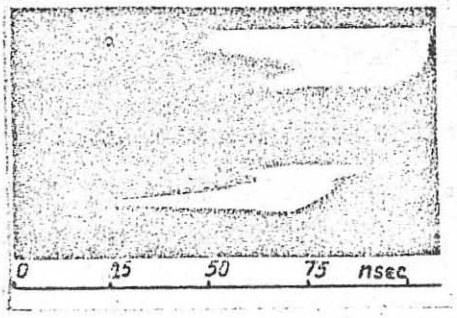


Fig. 2. Lighting from diode gap without (a) and with (b) prepulse.

In this series of experiments the power $\sim 3 \cdot 10^{11}$ W, 2-2,5 times more than

without prepulse, was obtained (Fig. 3), the total energy release during the pulse being up to 16 kJ. However, it is still remained the task of obtaining the optimal current focusing conditions at this voltage pulse shape, to reach the maximum energy deposition and anode foil temperature.

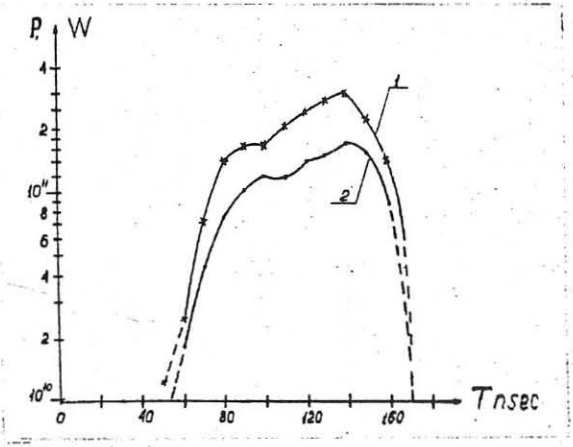


Fig. 3. Power released in the diode of "Angara-1" with (1) and without (2) prepulse.

References

I. И.П. Афонин и др. Доклады Всесоюзной конференции по инженерным проблемам термоядерных реакторов, т. II, с. 104, Ленинград, 1977.

2. M.V. Babykin et al. Proc. 3rd Intern. Top. Conf. on High Power Electron and Ion Beam Res. and Techn. v. II, p. 499, Novosib. 1979.

LIGHT-PRESSURE EFFECTS ON ION SPECTRA IN TWO-ION LASER PLASMAS

J.L. Montañés and J.R. Sanmartín
E.T.S.Ingenieros Aeronáuticos
Universidad Politécnica de Madrid, Madrid-3, Spain

In plasmas produced by high-power lasers, the electron temperature T_e may be so high that the ion temperature trail well behind (slow relaxation), and T_e be spatially uniform (large heat conductivity). Then a simple, often used, model, having initially $n=n_o$ ($x<0$), $n=0$ ($x>0$), involves ion continuity, and ion and electron momentum equations

$$\frac{Dn}{Dt} + n\frac{\partial v}{\partial x} = 0 \quad , \qquad \frac{D}{Dt} \equiv \frac{\partial}{\partial t} + v\frac{\partial}{\partial x} \quad , \tag{1}$$

$$mn\frac{Dv}{Dt} = neZE \quad , \qquad 0 = -\frac{\partial P_e}{\partial x} - n_e e E \tag{2}$$

where n, v, m, Z refer to ions, E is the charge separation field, and we take $n_e=Zn$. If electrons are Maxwellian ($P_e=n_e kT_e$), and T_e=const, we obtain

$$\frac{d\ln n}{d\eta} = -\frac{1}{M}\left(1+\frac{dM}{d\eta}\right) \quad , \qquad (M^2-1)\left(1+\frac{dM}{d\eta}\right) = 0 \quad , \tag{3}$$

where $\eta=x/c_s t$, $M=v/c_s-\eta$ and $c_s^2 = kT_e/m$. Solutions to (3) are $dM/d\eta=-1$ (v=const, n=const) and M=1. The solution then is

$$M=1 \quad (v=c_s + x/t), \quad n=n_o \exp(-v/c_s) \, , \quad \text{for } \eta>-1$$

(isothermal rarefaction wave) [1]. The number of ions in the interval v, v+δv is $\delta N \propto n\delta x \propto n\delta\eta$, and the ion velocity spectrum is then

$$\frac{dN}{dv} = C\frac{n}{dv/d\eta} \propto \frac{n}{1+dM/d\eta} \quad (C \equiv \text{const}) \; ; \tag{4}$$

here,

$$\frac{dN}{dv} \propto \exp(-v/c_s) \, ,$$

a well known result [1].

In some experiments where two species with different Z/m ratio (H^+, C^{6+} in Ref. 1) are involved, dN/dv for that one with larger Z/m presents

a large peak superposed to the exponential decay law. It may be shown that using a two- temperature electron population (which explains the shape of the current registered by a remote collector in certain cases [2]), does not lead to a peak in dN/dv, as required. On the other hand, it is clear from (4) that if a spatial region exists where v=const$\equiv v_o$, dN/dv will present a peak around v_o. In this respect it should be noted that Gurevich et al. [3] claimed that when two species 1,2 exist, where $Z_1/m_1 > Z_2/m_2$ say, n_2 vanishes at some point and a plateau (n_1=const) appears, where v_1=const. Let us consider the two-species case; the continuity equations read

$$\frac{d \ln n_j}{d\eta} = -\frac{1}{M_j}\left(1+\frac{dM_j}{d\eta}\right) \quad , \qquad (j=1,2) \qquad (5)$$

while the momentum equations (using $n_e=\Sigma n_j Z_j$) additionally yield

$$\frac{M_2}{\bar{c}_2^2}\left(1+\frac{dM_2}{d\eta}\right) = \frac{M_1}{\bar{c}_1^2}\left(1+\frac{dM_1}{d\eta}\right) \quad , \qquad (6)$$

$$\Sigma \frac{Z_j n_j}{m_j}\left(1+\frac{dM_j}{d\eta}\right)\left(\frac{M_j^2}{\bar{c}_j^2}-1\right) = 0 \qquad (7)$$

where $\bar{c}_j^2 = c_j^2/c_s^2$, $c_j^2 = Z_j kT_e/m_j$. Unless $d \ln n_j/d\eta \equiv 1 + dM_j/d\eta \equiv 0$, from (6) and (7) there results [3]

$$\Sigma n_j Z_j \left(\frac{\bar{c}_j^2}{M_j^2}-1\right) = 0 \; . \qquad (8)$$

From (5), (6) and (8) we finally get

$$\frac{dM_2}{dM_1} = \frac{M_2(\bar{c}_1^2 M_2 - \bar{c}_2^2 M_1)(M_1^2 - 3\bar{c}_1^2) + \bar{c}_2^2 M_1 (M_2 - M_1)(M_1^2 - \bar{c}_1^2)}{M_1(\bar{c}_2^2 M_1 - \bar{c}_1^2 M_2)(M_2^2 - 3\bar{c}_2^2) + \bar{c}_1^2 M_2 (M_1 - M_2)(M_2^2 - \bar{c}_2^2)} \cdot \frac{M_2^2 - \bar{c}_2^2}{M_1^2 - \bar{c}_1^2} \qquad (9)$$

The figure shows the singular points E (degenerated node), S (saddle) and N (node) of Eq. (9) in the nonshaded regions where the solution must remain [see Eq. (8)]; making the disturbance front to occur at η=-1, we have there M_j=1, and from (8), $c_s^2 = kT_e(\Sigma Z_j n_{jo} Z_j/m_j)(\Sigma Z_j n_{jo})^{-1}$. The solution to (9) starts at point I, crosses E, turns around [near S for $Z_2 n_{2o} >> Z_1 n_{1o}$], and finally reaches N, where

$$M_1 \equiv (v/c_1 - x/c_1 t)c_1/c_s = \bar{c}_1 \equiv c_1/c_s \quad ,$$

and, from (8), n_2=0 (at some point η_N). Since 1 is the only species from

there on, no plateau appears [see the discussion following (3)] (in opposition to [3]), the solution being of the type

$$v_1 = c_1 + x/t, \quad n_1 = n_1(n_N)\ \exp\{[v_1(n_N) - v_1]/c_1\}, \quad \text{for } n > n_N .$$

Gurevich et al. [4] claimed that a nearly-flat range observed in experimental ion spectra provide support for the n-profile plateau predicted in [3]; as pointed out above however, a plateau leads, contrariwise, to a peak in dN/dv.

It appears that light-pressure is the cause of the peak in Ref. 1. When the light-to-thermal pressure ratio is not small (~ 3 in Ref. 1), a plateau develops in the overdense region of a one-species plasma with T_e=const, in order to satisfy some appropiate conditions in the thin layer around critical density [5]; if T_e grows slowly with time, a near-plateau develops leading to a peak in dN/dv. However, the area under that peak is too small:

$$\int_{v>v_o} \frac{dN}{dv}\, dv = \int C\, n\, dn = -C \int d(nM) = C\, n M \Big|_{v_o} , \qquad (10)$$

where the continuity equation and Eq. (4) have been used; for T_e=const, (10) gives $C\,n(v_o)$, which equals an area of width $\Delta v = c_s$ and height $dN/dv\big|_{v_o}$

$$\left.\frac{dN}{dv}\right|_{v_o} \times \Delta v = Cn \Big/ \left.\frac{dv}{dn}\right|_{v_o} \times c_s = C\, n(v_o)$$

much less than that observed. Moreover the above discussion makes no distinction between plasmas with ions of equal (D^+, C^{6+} in Ref. 1) and different (H^+, C^{6+}) values of Z/m, whereas results for D^+ in Ref 1 show no peak comparable to that for H^+. [The reasoning around Eq. (10) also shows that finite Debye effects [1] cannot explain the large peak in dN/dv for H^+].

Nonetheless, consider light-pressure for one species, when T_e decreases with time; then an isothermal shock appears, to adjust the plasma to conditions in the critical layer [5], carrying the flow from values ahead n_a, v_a (supersonic) to $n_b > n_a$, v_b (subsonic) $< v_a$. Clearly, a large peak in dN/dv will appear around v_b: Now, for two species with different Z/m ratio, and T_e=const (or even slowly increasing), the dominant, lowest Z/m, species will be supersonic in a broad flow region ($M_1 > \bar{c}_1$ in between points E and N of the figure), and light-pressure will produce a shock

leading again to a peak in dN/dv for that species. An estimate of the peak area for H^+ in Ref. 1 is in reasonable agreement with the observed data.

ACKNOWLEDGMENT

This work was supported by the Junta de Energía Nuclear of Sapin.

REFERENCES

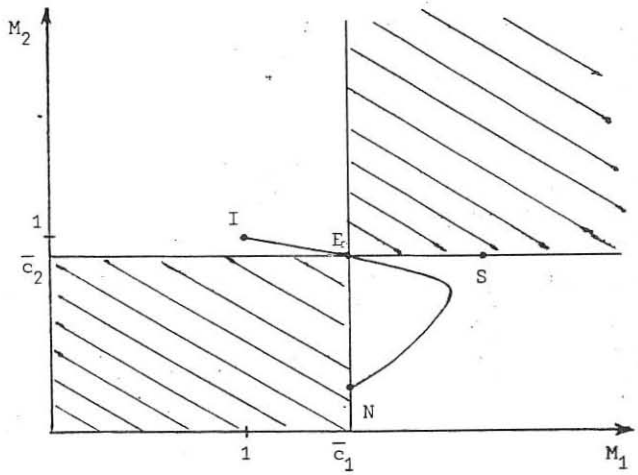
[1] E.L. Lindman, Journal de Physique, Fasc. 12, C-6, Third International Congress Waves and Instabilities in Plasmas, Palaiseau, France (1977).

[2] L.M. Wickens and J.E. Allen, J. Plasma Phys. 22, 167 (1979)

[3] A. Gurevich et al., Zh. Eksp. Teor. Fiz. 63, 561 (1972). [Sov. Phys. JETP 36, 274 (1973)].

[4] A. Gurevich et al., Phys. Rev. Lett. 42, 769 (1979).

[5] J.R. Sanmartín and J.L. Montañés, Phys. Fluids 21, 1957 (1980).



ONE DIMENSIONAL SIMULATION OF COLLECTIVE ION ACCELERATION BY A RELATIVISTIC ELECTRON BEAM

W. Hintze

Zentralinstitut für Elektronenphysik, Akademie der Wissenschaften der DDR, DDR-1080 Berlin, GDR

One-dimensional simulation of relativistic electron beam injection into two different neutral gas configurations (homogeneous filling of the drift space and gas cloud near the injection plane) was performed, mainly in order to study collective ion acceleration. In both cases, no deep-well acceleration to more than the electron energy was found. In the first case, the electric field region associated with the virtual cathode moves through the gas, thereby leading to maximum ion energy of four times the electron energy. In the second case, the electric field region remains at the downstream end of the gas cloud and a continuous charge neutral ion beam with approximately the injected energy is created.

Introduction

There has been considerable effort, both in experiment and theory, to investigate collective ion acceleration by linear intense relativistic electron beams (cf. the recent reviews /1/ and /2/).

The experiments may be divided into two different groups: First these using homogeneous gas filling in the drift tube thereby providing a volume source of ions and secondly those using a localized ion source near the injection plane (dielectric anode, gas cloud, etc.).

In the first type of experiment a moving potential well associated with the beamfront was identified as the main acceleration mechanism. Details are, however, still controversal: One basic assumption of the Olson theory /2/, viz. the deep-well acceleration to 2-3 times the electron energy is rejected by the Alexander theory /3/. Another problem is that the large energy multiplication factor of up to 15 observed in experiment is difficult to explain in a purely electrostatic beam head model.

In the second type of experiment as yet no satisfactory theory exists. Recently, thorough experimental investigations have been carried out using a dielectric anode /4/ or a metal anode and a gas cloud (or a laser induced

plasma source) near the anode /5/. We have carried out computer simulations of both types of experiment in order to explore what one dimensional electrostatic models can be expected to yield.

The Code

Details of the code are described in /6/. Electrons are injected at x=0 with velocity $v_0=\beta_0 c$ into a drift space extending to x=L the ends of which are grounded ($\varphi=0$). The drift space is filled with a gas in the region $0 \le x \le \Delta$ which is ionized by the beam with an ionization frequency proportional to the pressure p. Secondary electrons are either kept (strong magnetic field B_0) or are neglected as long as the potential was negative ($B_0=0$, fast radial escape). Small mass ratios of M/m=20 or 80 were used. We have used the following units: length $d_0=(I_A/4\pi J)^{1/2}$ (J - injected current density, $I_A=17\beta_0*(\gamma_0-1)\,kA$, γ_0 - relativistic factor of the injected electrons), time $t_0=d_0/v_0=\omega_b^{-1}(\gamma_0-1)^{1/2}/\beta_0$ (ω_b = beam plasma frequency), potential $\varphi_0=mc^2(\gamma_0-1)/e$, density n_b (density of the injected electrons).

Results

The case of homogeneous gas filling ($\Delta=L$) was discussed in some detail in /6/. Therefore we cite only the main results. The system evolves in three stages (i) stopped beam (ii) moving beam front (iii) beam plasma interaction. A deep potential well of depth $\varphi \simeq -2{,}2$ was observed in the beginning of stage (i), but it vanishes rapidly and no ions (even our very light ions) are accelerated to more than the injected energy (the ion velocity is then $v=v^*=[2m(\gamma_0-1)/M]^{1/2}/\beta_0$). The beamfront (region of both a strong electric field and reflection of electrons) moving with a velocity $\simeq v^*$ in stage (ii) accelerates some of the ions to $2v^*$, i.e. a short ion pulse with up to four times the injected energy is generated. No higher energies have been observed in any run. In stage (iii) some indication of the beam plasma instability behind the beamfront was seen.

A typical run (2107/5) of the gas-cloud-injection case (γ_0=5.5, M/m=80, L=10, p=0.2, Δ =1, B_0=0, zero risetime of the beam) is shown in the figure. From this and other runs the overall picture of the ion acceleration in the one-dimensional case is as follows. In the first stage (virtually vacuum injection) the virtual cathode (VC) forms (T=5). In the second stage (T=10) ions are created by ionization of the gas cloud. The ions are accelerated by an electric field which is located at the downstream end of the gas cloud to an energy equal to the injected energy (velocity V^* = 0.366 in the figure).
This region may be termed virtual ion diode (VID) with the anode beeing the downstream end of the gas cloud, the cathode beeing the virtual cathode and the ion source beeing the ionized gas cloud. Thus the second stage is that of VID formation.
In the third stage (T=15, 20, 25) a continuous ion beam with velocity V^* is generated because, in contrast to the case of a homogeneous gas filling, the VID does not move but remains stationary. The ion beam is charge neutral with the density beeing approximately that of the injected electron beam. The neutralizing electrons have a broad velocity spectrum from $V=0$ up to $V \simeq V_0$. There is no electric field associated with the ion beam head. The density of charged partides accumulating in the gas cloud region increases rapidly, the potential becomes positive and most of the slow ions are expelled backwards through the plane x=0.
The results obtained here are in agreement with the simulation of Taylor /8/ but do not confirm the recent theoretical considerations of the Maryland group /7/.

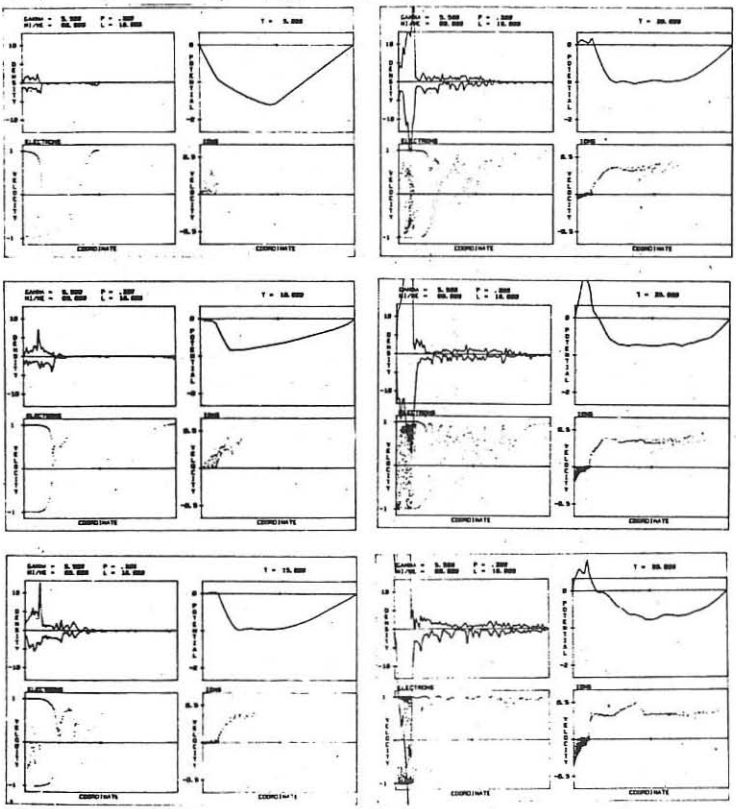
Acknowledgement

I wish to thank Prof. K.F.Alexander for valuable discussions.

References

/1/ Alexander,K.F., Hintze,W., ZIE-preprint 80-6 Academy of Sci. GDR, Berlin 1980
/2/ Olson, C.L., Schumacher,U., Collective Ion Acceleration, Springer Tracts in Mod.Phys. 84, 1979

/3/ Alexander K.F. et al ZhETF 67 (1974) 567
/4/ Adler R., Nation J.A., Serlin V., Phys.Fluids 24 (1981)2,347
/5/ Destler W.W., Floyd L.E., Cremer J.T., Parsons C.R., Reiser M., 4th Int. Topical Conf. High Power Electron and Ion Beam Res. and Technol., June 29-July 3, 1981, Palaiseau, France, paper 4A2 (and refs. therein)
/6/ Hintze, W., ibid, paper 4A5
/7/ Striffler C.D., Mayergoyz I., Grossmann J.M., ibid, paper 4P13
/8/ Taylor P.L., J.Appl.Phys. 51 (1980) 22



Time sequence of a typical run of REB injection into a gas cloud (parameters see text). Shown are particle densities (upper left, ions positive, electrons negative), potential (upper right) and phase space of electrons (lower left) and ions (lower right).

EFFECTS OF VELOCITY SPACE LOSS-REGIONS ON THE ALPHA PARTICLE DISTRIBUTION FUNCTION AND COLLISIONAL ALPHA PARTICLE LOSSES IN TOKAMAK REACTORS

By

M. Lisak, D. Anderson, H. Hamnén, M. Tendler*
and H. Wilhelmsson

Institute for Electromagnetic Field Theory and
EURATOM-FUSION, Research (EUR-NE), Chalmers University of Technology,
S-412 96 Göteborg, Sweden

*Royal Institute of Technology, S-100 44 Stockholm 70, Sweden

ABSTRACT: The steady-state distribution function for alpha particles in the presence of loss regions in velocity space is derived in an analytical form on the basis of the Fokker-Planck equation. The particle loss and the associated energy loss of alpha particles are estimated for parameters characteristic of a tokamak reactor.

1. Introduction

In a magnetized plasma the motion of the high-energy products of fusion reactions, i.e. the 3.52 MeV-alpha particles is controlled by the confining magnetic field. For alpha particles in tokamaks, particle excursions along drift orbits may be so large, that a significant number of them intersect the chamber walls [1-3]. The presence of the corresponding loss regions in velocity space may have important effects on alpha particle containment properties. During the slowing down process the alpha particles may pitch-angle-scatter into the loss regions and thus increase the alpha losses [4-6]. In the present paper, we determine the velocity distribution for the alpha particles in the presence of the velocity space loss region taking into account slowing down and pitch angle scattering due to Coulomb collisions. The result obtained may provide valuable information not only for determining the energy deposition profiles (cf [1]), but also in evaluating the current generated by the alpha particle losses (cf [7]), and furthermore for use in connection with fast alpha particle diagnostics. Here, we make use of the derived distribution function for estimating the particle loss and the associated energy loss of alpha particles due to scattering into the loss region.

2. Solution of the Fokker-Planck equation in presence of the loss region

We consider a situation where each thermonuclear reaction produces alpha particles with an almost mono-energetic and isotropic velocity distribution. However, an anisotropy develops as a concequence of the direct particle drift-losses discussed previously. The Coulomb interactions between the alpha particles and the plasma bulk particles tend to change the constants of motion of the alpha particles through slowing-down and pitch angle scattering. As a result of the pitch angle scattering the velocity vector of the alpha particles may eventually enter the loss-region and those particles will be lost from the system. We assume a Maxwellian background plasma consisting of electrons and 50%-50% DT-ions. The macroscopic electric field giving rise to a plasma potential field, [2], is neglected. Under these conditions the behaviour of the distribution function of the high-energy alpha particles can be described by the Boltzmann equation with a Fokker-Planck collision operator [8] . Neglecting the presence of trapped particles and performing the bounce averages the steady-state form of the Fokker-Planck equation becomes [5]

$$\frac{1}{v^2}\frac{\partial}{\partial v}\left[(v^3+v_c^3)f\right]+\kappa\frac{v_c^3}{v^3}\frac{\partial}{\partial\chi}\left[(1-\chi^2)\frac{\partial f}{\partial\chi}\right]-\beta(v)f+\tau_s S(v,\chi)=0 \qquad (1)$$

where $\chi\equiv v_{\parallel}/v$, $v_c^3=(3\sqrt{\pi}\, m_e\,[Z]/4m_p)^{1/3}\, v_e$ is the critical velocity at which electrons and ions contribute equaly to the slowing-down, $\kappa=m_p<Z>/2\, m_\alpha[Z]$, $<Z>=\sum_i (n_i Z_i^2)/n_e$, $[Z]\equiv(\sum_i n_i Z_i^2\frac{m_p}{m_i})/n_e$, m_p is the proton mass, v_e is the thermal velocity of electron, τ_s is the Spitzer slowing-down time, and $\beta(v)$ is a parameter taking into account effects which can be described by an isotropic damping in velocity space. The distribution function the source $S(v,\chi)$ of alpha particles formed as a result of thermonuclear reactions can be approximated as [9,10]

$$S(v,\chi)=\frac{n_i}{\tau_f\, 4\pi v_\alpha^2}\,\delta(v-v_\alpha)\sum_{j=1,2}\eta[(-1)^j(\chi-\chi_j(v))] \qquad (2)$$

where $\eta(x)$ is the step function, $\chi_{1,2}(v)$ are the boundaries of the loss region, and $\tau_f=4/(n_i<\sigma v>)$ is the characteristic time of alpha particle generation.

In the presence of the loss region the distribution function f has to satisfy $f\equiv 0$ inside the loss region. Thus the boundary conditions are $f(v,\chi_j(v))=0$, $j=1,2$. According to the simplified representation of the loss region in Fig. 1, the boundary χ_1 may be assumed as velocity independent, i.e. $\chi_1(v)=$const. while χ_2 is still a function of v ("moving boundary"). The part of the loss region which has to be considered depends on a relation between v_α and v_{90^o}, v_{180^o}, and v_s (see Fig. 1). The case of interest which we will consider without loss of generality is when $v_s<v_\alpha<v_{180^o}$. We introduce the following transformations

$$\Psi=(v^3+v_c^3)\exp\left[\int_v^{v_\alpha}\frac{\beta(v')v'^2}{(v'^3+v_c^3)}\,dv'\right]f(v,\chi)\,,\quad t=\frac{\kappa}{3}\ln\left[\frac{1+(v_c/v)^3}{1+(v_c/v_a)^3}\right]. \qquad (3)$$

Then, Eq. (1) reduces to a form similar to the well known "heat conduction" equation

$$\frac{\partial\psi}{\partial t}=\frac{\partial}{\partial\chi}\left[(1-\chi^2)\frac{\partial\psi}{\partial\chi}\right]+F(\chi,t);\quad F(\chi,t)=\frac{n\,\tau_s}{4\pi\tau_f}\,\delta(t)\sum_{j=1,2}\eta[(-1)^j(\chi-\chi_{jo})] \qquad (4)$$

where $\chi_{jo}\equiv\chi_j(v_\alpha)=\chi_j(t=0)$. Assuming $\chi_1(t)=\chi_{10}=$const, the previously mentioned boundary conditions become $\psi(t,\chi_{10})=0$, $\psi(t,\chi_2(t))=0$.

It can be verified that the values of t which are physically interesting in the presence of the loss region ($0<t<t_s$) satisfy $t\ll 1$. Thus, an approximate treatment of Eq. (4) for small values of t is motivated. Using the method of short time asymptotic expansions of solutions of parabolic equations, [11], the leading term in the asymptotic expansion of the Green's function for Eq. (4) is given by ($|\chi|<1$)

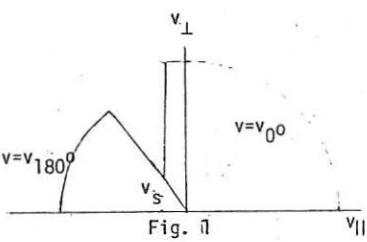


Fig. 1

$$G(t,\chi,\zeta)\simeq(4\pi t)^{-1/2}[(1-\chi^2)(1-\zeta^2)]^{-1/4}\exp\left[-\frac{1}{4t}(\arcsin\chi-\right.$$
$$\left.-\arcsin\zeta)^2\right]+O(t^{1/2})\exp\left[-\frac{1}{4t}(\arcsin\chi-\arcsin\zeta)^2\right] \qquad (5)$$

Assuming now a simplified representation of the boundary $\chi_2(t)$ in the form $\chi_2(t)=\sin(-\beta_1 t+\beta_2)$, where $\beta_1=(\arcsin\chi_{20}-\arcsin\chi_{10})/t_s$, and $\beta_2=\arcsin\chi_{20}$, the solution of the Fokker-Planck equation (1) in the presence of the loss region is given by

$$f(v,\chi) = \frac{n_i \tau_s}{4\pi\tau_f} \frac{\exp[-\int_v^{v_\alpha} \frac{\alpha\beta(v')v'^2 dv'}{v'^3+v_c^3}]}{(v^3+v_c^3)} \cdot$$

$$\begin{cases} \text{erf}\left(\frac{\arcsin\chi_{10}-\arcsin\chi}{2\sqrt{t}}\right), & \text{for } -1<\chi\leq\chi_{10}, \\ \text{erf}\left(\frac{\arcsin\chi-\arcsin\chi_{20}}{2\sqrt{t}}\right)+\Lambda(t,\chi), & \text{for } \chi_2(t)\leq\chi<1, \end{cases} \qquad (6)$$

where

$$\Lambda(t,\chi) = \frac{1}{2}[1 - e^{\Delta\beta_1} + \text{erf}(\frac{\beta_1\sqrt{t}}{2} - \frac{\Delta}{2\sqrt{t}}) + e^{\Delta\beta_1}\cdot\text{erf}(\frac{\beta_1\sqrt{t}}{2} + \frac{\Delta}{2\sqrt{t}}], \qquad (7)$$

with $\Delta=\arcsin\chi+\beta_1 t-\beta_2$, and erf(x) is the error function. The result (6)-(7) represents a generalization of the alpha particle distribution function considered in [9,10]. The new feature is the effect of pitch-angle scattering on the distribution function in the presence of the loss region. Other possible loss mechanisms are represented through the parameter $\beta(v)$.

3. Particle and energy losses

Using the derived distribution function we will now evaluate the particle and associated energy losses of alpha particles which scatter into the It can be shown that for $\beta(v)=0$, the particle loss fraction, L, and the associated energy loss fraction, Q, of alpha particles produced at some radius $r=r_B$ are given by

$$L \simeq [(1-\chi_{10}^2)\frac{t_s}{\pi}]^{1/2} + \frac{1}{2}(1-\chi_{20}^2)^{1/2}[\frac{1}{\beta_1}\text{erf } Z - \frac{\beta_1 t_s}{2}\text{erfc } Z + (\frac{t_s}{\pi})^{1/2}\exp(-Z^2)], \qquad (8)$$

and

$$Q \simeq (\frac{\kappa v_c^3}{3\pi v_\alpha^3})^{1/2}[(1-\chi_{10}^2)^{1/2}F(\rho,0) + (1-\chi_{20}^2)^{1/2}F(\rho,k)], \qquad (9)$$

where $Z = \beta_1\sqrt{t}/2$, $\rho=(3v_\alpha^3 t_s/\kappa v_c^3)^{1/2}$, $k = \frac{\beta_1}{2}(\kappa v_c^3/3v_\alpha^3)^{1/2}$, and for $v_c^3 \ll v_s^3$

$$F(\rho,k) = \int_0^\rho \frac{dz}{(1+z^2)^{2/3}}[e^{-k^2z^2} - \pi^{1/2}kz\,\text{erf}(kz)]. \qquad (10)$$

The total particle and energy loss fraction corresponding to particles produced in the whole region $0\leq r\leq a$ are defined by

$$\bar{L} = (\int_0^a \frac{n_i}{\tau_f} L 2\pi r dr)/(\int_0^a \frac{n_i}{\tau_f} 2\pi r dr), \quad \bar{Q} = (\int_0^a \frac{n_i}{\tau_f} Q\, 2\pi r\, dr)/(\int_0^a \frac{n_i}{\tau_f} 2\pi r\, dr) \qquad (11)$$

It is clear that the direct losses and consequently also the scattering losses of alpha particles exist only for $r>r_*$, where r is the point at which the velocity corresponding to the loss region vertex v_s is equal to the production velocity v_α. For both flat and parabolic current distribution profiles r_* is determined by

$$0.52\, AI_{MA}(1-\rho_*^2) \simeq [(1+\frac{\rho_*}{A})(3\rho_*+1)]^{1/2} + [(1+\frac{1}{A})(3+\rho_*)]^{1/2} \qquad (12)$$

where $\rho=r/a$. At $r=a$ the functions $L(r)$ and $Q(r)$ tend to zero because at this point all alpha particles produced are lost directly. Then we take approximately

$$\frac{L}{L_m} = \frac{Q}{Q_m} \simeq \frac{4}{(1-\rho_*)^2}\,[-\rho^2+(1+\rho_*)\rho-\rho_*] \qquad (13)$$

where L_m and Q_m are values of L and Q calculated at $\rho_m=(1+\rho_*)/2$. Assuming for simplicity a system with constant ion temperature profile $T_i(r) = T_e(r) = \text{const}$, and a parabolic density profile $n_i(r)=n_{io}[1-(r/a)^2]$, we obtain from (11) and (13)

$$\frac{\bar{L}}{L_m} = \frac{\bar{Q}}{Q_m} \simeq [\frac{64}{35}\,(1+\rho^*)-(1-\rho_*^2)^4 - 4\rho_*(1+\rho_*)(1-\rho_*^2+\frac{3}{5}\,\rho_*^4-\frac{1}{7}\,\rho_*^6)]/(1-\rho_*)^2 \qquad (14)$$

We will now compare the above analysis with the results of Ref. [6] where the containment properties of alpha particles during the slowing down and including the pitch angle scattering have been studied by using Monte-Carlo calculations. Taking the tokamak parameters $R_0=4.9$m, $a=1.5$m, $q=2.5$, $I=3.7$ MA, and assuming a flat current distribution profile we find from (12) that $\rho_*=0.25$ which is exactly the value obtained in [6]. For a pure DT plasma we obtain $L\simeq 1.8\%$ and $Q\simeq 1.5\%$ for $T_e=8$ keV and $\bar{L}\simeq 4.5\%$ and $Q\approx 4\%$ for $T_e = 20$ keV. This should be added to the initial losses $L_d=Q_d\simeq 19\%$. In Ref. [6] only $T_e=8$ keV has been consided and it has been found that for a pure DT plasma the scattering loss of alpha particles is about 1% and the direct loss amounts to 18% which is in a good agreement with our results. It has also been shown in [6] that if high-Z impurities exist in the plasma the scattering loss of the alpha particles increases proportionally to $\langle Z\rangle$. The increase in the alpha particle scattering loss for a plasma contaminated by impurities can also be seen from (8)-(10). However, the analytical results show that the particle loss fraction L scales as $L\sim\sqrt{\kappa}\sim\sqrt{\langle Z\rangle}$, which is in contradiction with the result of Ref. [6].

References

[1] Stringer, T.E., Plasma Phys. 16 (1974) 651.

[2] McAlees, D.G., Alpha Particle Energetics and Neutral Beam Heating in Tokamak Plasmas, Preprint ORNL-TM-4661, Oak Ridge (1974).

[3] Kolesnichenko, Ya. I., Fursa, A.D. Yavorskij, V.A., (Sov. J. Plasma Phys. 2 (1977)506), Fiz. Plazmy 2 (1976) 911.

[4] Rome, J.A., McAlees, D.G., Callen, J.D., Flower, R.H., Nucl. Fusion 16 (1976) 55.

[5] Tsuji, H., Katsurai, M., Sekiguchi, T., Nucl. Fusion 16 (1976) 287.

[6] Ohnishi, M., AO, N., Wakabayashi, J., Nucl. Fusion 18 (1978) 859.

[7] Koleshnichenko, Ya. I., Reznik, S.N., Yavorskij, V.A., Nucl. Fusion 20 (1980) 1041.

[8] Hazeltine, R.D., Plasma Phys. 15 (1973) 77.

[9] Koleshnichenko, Ya. I., Nucl. Fusion 15 (1975) 35.

[10] Kolesnichenko, Ya. I., Nucl. Fusion 20 (1980) 727.

[11] Cohen, J.K., Hagin, F.G., Keller, J.B., J. Math. Anal. Appl. 38 (1972) 82.

Los Alamos Compact Toroid (CT) Research on the Field-Reversed Configuration (FRC) and Spheromak-type, Magnetized-gun-generated CTs

R. R. Bartsch, W. T. Armstrong, J. C. Cochrane, I. Henins, H. W. Hoida, T. R. Jarboe, R. K. Linford, J. Lipson, J. Marshall, K. F. McKenna, D. A. Platts, D. Rej, A. R. Sherwood, E. G. Sherwood, R. E. Siemon, M. Tuszewski, and B. Wright

Los Alamos National Laboratory, Los Alamos, New Mexico USA

I. Field-Reversed Configuration

Recent experimental work on FRC's in field-reversed theta pinches at Los Alamos has been directed toward the understanding of transport and stability properties which influence the scaling of FRC's to the size and lifetimes required for a fusion reactor.[1,2] The transverse dimensions of the FRC (in elongated equilibria) have been analytically and experimentally determined to have an important influence on stability and transport,[3,4] and in general the radial extent of the FRC should be as large as possible with respect to coil radius and the ion gyroradius. The scaling of experimental results on the presently operating machines (FRX-A and FRX-B) to the next larger machine, FRX-C, which is approximately two times the size of FRX-B in length and diameter, is discussed below (See Table I).

Experimental and theoretical work have indicated that the stable period, before the particle-loss induced rotation spins up the FRC to the onset of the n=2 rotational instability,[5] scales as R^2/ρ_i where R is the major radius of the CT and ρ_i is the ion gyro-radius. Data from FRX-A and FRX-B have demonstrated this scaling over a wide range of ρ_i and a 30% variation in R.[6] Numerical transport studies have been based on diffusion of particles across the separatrix due to the lower hybrid drift instability.[4]

A semi-empirical method has been developed to extrapolate the experimental results of FRX-B work[7] and has been applied to the design of FRX-C. The model uses dimensionless empirical constants, x_h to scale the implosion heating phase, x_f (equal to ϕ_i/ϕ_o-ratio of trapped flux to initial flux) for the trapped flux fraction, x_B as the ratio of bias field to a maximum value first identified by Green and Newton,[8] and x_p as the fraction of the initial particles contained in the formed equilibrium. From FRX-B data, the values of these constants are fixed to 0.06, 0.13, 0.75, and 0.35, respectively. For a given device and fill pressure P_o, the model predicts the temperature ($T_e + T_i$), density, external confining field (B), ratio of major

TABLE I. FRX-C, SCALING-EXPERIMENT PARAMETERS

Parameters	FRX-B	FRX-C
Coil diameter	25 cm	45 cm
Coil length	100 cm	200 cm
Discharge tube i.d.	20 cm	40 cm
Source voltage	40 kV	110 kV
B-field swing	16 kG	16 kG
1/4 period time	2.6 μs	5 μs
Crowbar time	150 μs	300 μs
Bank energy	62 kJ	510 kJ
Bias Field (max)	3.5 KG	5 kG

radius R to ion gyro-radius ρ_i and the plasma dimensions (x_s = ratio of separatrix radius to coil radius and $z_s = L_{plasma}/L_{coil}$) for an elongated 2-D equilibrium. The electrical and mechanical parameters of FRX-C are given by comparison to those of FRX-B in Table I. The larger loop voltage (110 kV vs 45 kV for FRX-B) and bank energy are required to obtain adequate temperature over a wide range of P_o and enough adiabatic compression to contain the plasma within the coil length. A dual feed was chosen to achieve the effective 110 kV voltage on the theta-pinch coil with the same Scyllac spark-gap technology used on FRX-B. The first operation of FRX-C is scheduled for May 1981.

Plotted in Fig. 1 are predictions of FRX-C parameters based on the previously described formation model and the device parameters corresponding to the case of Table I. One observes from Fig. 1 that the expected values for x_s are in the same range (0.4 to 0.5) as for the FRX-B experiment, which reflects the fact that the same fraction of trapped flux ($\phi_i/\phi_o \sim 0.13$) has been assumed in both cases. Larger values of x_s would be achieved if one can increase the final value of ϕ_i/ϕ_o. A substantial increase in the range of ρ_i is achievable in FRX-C by comparison with FRX-B. Even larger values of R/ρ_i could be achieved if the trapped flux fraction exceeds the value of 0.13 assumed in these calculations. As seen from Table I, the larger coil diameter (and, therefore, larger R at fixed x_s) should allow substantial extension of the FRC confinement scaling with R/ρ_i and also test the possible stability limits as the ratio of plasma size to ion gyro-radius increases.

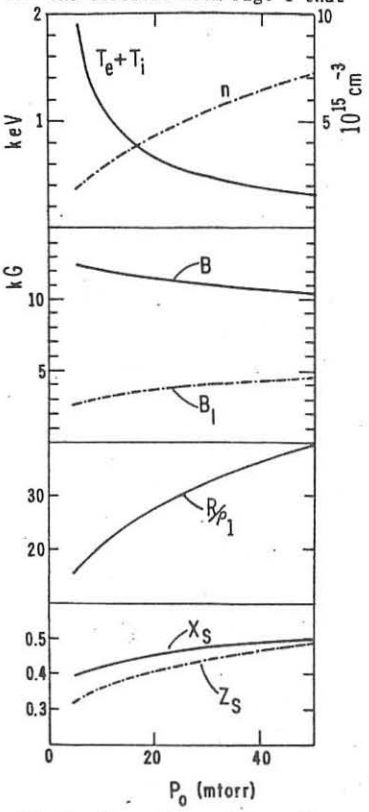


Fig. 1. Formation model predictions for FRX-C as a function of fill pressure, P_o.

II. Spheromak Configuration

In the CTX experiment we have been studying compact toroids containing toroidal magnetic field, which are generated with a magnetized coaxial plasma gun. When the gun is fired, the highly conductive plasma emerging in the axial direction stretches radial field lines present at the muzzle of the gun. These elongated field lines reconnect behind the plasma forming the closed poloidal field of the CT, with the magnetic field generated by the gun current becoming the embedded toroidal field.

Spheromak-like CTs produced in this manner have been trapped in prolate and oblate cylindrically symmetric metallic flux conservers. The plasma and magnetic field properties are studied using magnetic probes, pressure probes, interferometry, Thomson scattering, and spectroscopy.

In earlier experiments[9] these CTs were injected into and stopped within a simple, stainless steel, right-circular, cylindrical flux conserver. In some cases the CT stopped with its axis parallel to the common axis of the source and flux conserver, and then it rotated (tilted) until its axis was orthogonal to the axis of the flux conserver. In most cases the stopped CT, when first observed, was already partially tilted. Details of this work are reported elsewhere.[9]

In an attempt to stabilize this tilting of the CTs we have generated CTs in other flux conservers having oblate regions incorporated into their geometry. The plasma is injected through a 0.34-m diameter entrance cylinder into a confining region having typically a diameter of about 90 cm. Geometries have been found in which the tilting no longer occurs and the configuration is stable throughout its lifetime.[10]

With the elimination of the complication of tilting, three distinct time scales emerge. The first (~ 1 μs) is the time required to fill the flux conserver with magnetic field and plasma. The second (~ 15 μs) is the time for the decay of the fields in the entrance cylinder. We interpret this decay as being due to field line reconnection which is completed in about 30-50 μs. The third time (~ 150 μs) is the characteristic time for the decay of the fields in the flux conserver measured after reconnection has occurred.

Some properties of the CT plasma have been measured in a typical oblate geometry without external guide field. The density is about 2×10^{14} cm^{-3} (with ± 20% fluctuations for the first 100 μs), and it decays with a time constant a little longer than that of the magnetic field. Spectroscopic data are taken with a 5-channel polychromator, a monochromator, and a spectrograph. Nickel, chromium, and iron impurities have been identified, presumably originating from the gun electrodes, and copper from the flux conserver is also seen. Thomson scattering is used to measure the electron temperature at a position 5 cm from the midplane of the confinement region and at a radius equal to two-thirds of that of the confinement region. There is a large shot-to-shot variation of the temperature and density at this position, especially early in time. On shots where the density is high enough to get good scattering signal, the plasma appears to be fairly cool (T_e ~ 10 eV) after the reconnection (t > 50 μs). At the earliest measured time (30 μs), temperatures in the range 10-30 eV have been measured. Piezoelectric pressure probe data show a rapid pressure drop early in time and are consistent with the Thomson scattering temperature measurements. The time histories of impurity lines such as OIV are also consistent with the Thomson scattering measurements.

A "snipper coil" has been installed on the entrance region of the flux conserver to speed up the magnetic field reconnection in the entrance region by the application of a fast rising external field. The snipper coil has a quarter period of about 3.5 μs, and it is crowbarred near its current peak. When the snipper coil is energized the reconnection time is found to be three times faster than if it is not energized, and two times faster than observed in the earlier con-

figuration with a solid-conductor entrance cylinder. Making straightforward comparisons of cases when the snipper coil was energized with cases when it was not is rather difficult because of shot-to-shot variations in the temperature, but in general no significant change is observed in the average temperature (in the time range of 30 μs to 150 μs) or the lifetime.

In the CTX experiment we have demonstrated the production of Spheromak-type CT's using a magnetized coaxial gun, observed the instability of these CTs to a gross tilting mode, and found geometries of close-fitting flux conservers which stabilize this mode. The main concern at present is the low temperature of the resulting CT. Investigations are underway to see if CTs formed in the present manner are hot when first produced. Further studies are underway or contemplated to determine the importance of energy losses by impurity radiation and by electron thermal conduction along field lines before the reconnection process leading to a separated CT becomes completed.

REFERENCES

1. W. T. Armstrong, et al., Phys. Fluids (to be published).
2. A. G. Es'kov, R. Kh. Kurtmullaev, A. I. Malutin, V. N. Semenov, submitted to meeting of the IAEA Technical Committee on Critical Analysis of Alternative Fusion Concepts, Erice, Italy, March 23-27, 1981.
3. A. G. Es'kov, et al., in Plasma Physics and Controlled Nuclear Fusion Research (Proc. 7th Int. Conf. Innsbruck, 1978) Vol. 2, IAEA, Vienna (1979) 187.
4. S. Hamasaki and N. A. Krall, Conference Record IEEE International Conference on Plasma Science (Montreal) 5E10 (1979).
5. D. C. Barnes and C. E. Seyler, in Proceedings of the U.S.-Japan Joint Symposium on Compact Toruses and Energetic Particle Injection (Princeton, 1979), p. 110.
6. J. Lipson, et al., Appl. Physics Lett. (to be published).
7. R. E. Siemon and R. R. Bartsch, Third Symposium on Physics and Technology of Compact Toroids in the Magnetic Fusion Energy Program, Los Alamos 1980, Los Alamos National Laboratory report LA-8700-C (1981), 172.
8. T. S. Green and A. A. Newton, Phys. Fluids 9, 1386 (1966).
9. T. R. Jarboe, et al., "The Motion of a Compact Toroid Inside a Cylindrical Flux Conserver," Phys. Rev. Lett. 45, 1264 (1980).
10. I. Henins, et al., Third Symposium on Physics and Technology of Compact Toroids in the Magnetic Fusion Energy Program, Los Alamos 1980, Los Alamos National Laboratory report LA-8700-C (1981), 101.

ELECTROSTATIC WAVES IN A PLASMA STREAM INSTABILITY : MODIFIED LANDAU DAMPING AND STREAMING ION ACOUSTIC MODE.

JIN. MOHANTY,
DEPARTMENT OF PHYSICS,
RAVENSHAW COLLEGE, CUTTACK 753003
INDIA

ABSTRACT :

The relativistic Boltzman-Vlasov equation is solved linearly for a collisionless plasma stream yielding dispersion results for various limits of temperature. The classical Landau damping term is modified for streaming propagation at $KT_j \gg 1$, but $M_j/K^2KT \neq 1$. Fusion instability for ion accoustic mode is established.

INTRODUCTION :

While conventional analysis of fusion plasma in Tokamak, Stellarator and similar other devices of confinement in magnetic field and Mirror types of fusion are in progress (Kadomtsev and Pogutse, 1971; Porkolab, 1974 b; and Sundarum & Sen, 1977 etc.), attainment of fusion temperature necessitating thermal conditions for nuclear fusion is of paramount importance in an unmagnetised relativistic beam plasma, as it reveals the fusion instability especially in reaction chambers and similar other devices where streaming or drift of plasma is prominent. The thermonuclear fusion aspect in such a beam (REB expts) has not been analytically investigated or nummerically simulated, although in recent times physics of High current ion and electron beams have been amply studied (Sudan, 1980; Ryutov, 1980) along with Tandem Mirror experiments (Logan, 1980). Following the electro-

magnetic waves and instability (Mohanty, 1980) in low density two component beam plasma stream using an unapproximated Maxwellian distribution function, we present here the investigations of instability for electrostatic waves in a relativistic plasma stream with a net streaming velocity ($V_o < C$) and the relevant dispersion for nonrelativistic limits of temperature.

Basic Equation :

The current density $J_\alpha(k,w)$ can be expressed in terms of distribution function by

$$J_\alpha(R,W) = \sum_{j=+,-} jec \int \frac{dp\, p_\alpha f_j(R,p,\omega)}{(p_j^2 + m_j^2c^2)^{1/2}}$$

where $$f_j(k,p,w) = (2\pi)^4 \int_{-\infty}^{+\infty} f_j(r,p,t)\, exp\left[-i(k\cdot r - \omega t)\right] dr\, dt.$$

$f_j(r,p,t)$ obeys the relativistic Boltzman-Vlasov equation. Linearising by conventional way and solving the equation, one obtains the longitudinal component of the Lindhard tensor (K_1 or K_{33}) (Misra, 1975, Misra and Mohanty, 1980).

$$K_{33} \text{ or } K_L = \sum_{j=+,-} 2\pi i \pi^2 n_o e^2 c \int_0^\infty \int_{-1}^{+1} \frac{p_j^2\, dx'\, x'^2\, dp_j}{B - x'} \frac{df_{oj}}{dp_j}$$

where $x' = \cos\theta$, $B = \dfrac{\omega(p_j^2 + m_j^2c^2)}{c p_j k}$, $\omega = \omega_R - i\gamma$, $\gamma < 0$.

We have used $$f_{oj} = \sum_{j=+,-} \frac{Z_j\, exp\left[-Z_j\left\{(1 + p_j^2/m_j^2c^2)^{1/2} - \dfrac{V_o \cdot p_j}{m_j c^2}\right\}\right]}{4\pi m_j^3 c^3 \gamma_o^2 K_2(Z_j/\gamma_o)}$$

(Buti, 1963, 1972)

and

$$\mathrm{Re}\, k_L(R,w) = \sum_{j=+,-} \frac{Z_j\, \omega_{oj}^2\, y^2}{8\gamma_o^2\, K_2(Z_j/\gamma_o)kc} \left(1 + \frac{2\omega}{\alpha Z_j CRy} + \frac{2\omega^2}{\alpha^2 Z_j^2 c^2 k^2 y^2}\right)$$

$$\exp\left[-\alpha Z_j (1+y^2)^{1/2}\right].$$

$\mathrm{Im}K_L$ is obtained by evaluating a series of Integrals in terms of $K_n(\alpha Z_j)$. Nonrelativistic Temperature limit and plasma stream s Classical Landau Damping with streaming Coefficient. Using the generalised dispersion relation and solving the $\mathrm{Im}K_L$ expression analytically and employing the relevant expression, we arrive at the following dispersion relation for nonrelativistic streaming propagation of two component plasma.

$$W = \sum_{j=+,-} \omega_{oj}^2 \left[\frac{m_j w}{k^2 KT_j} + \frac{1}{\omega} + \frac{m_j V_o}{k^2 KT_j}\right]$$

For vanishing V_o and $k^2 KT_j \gg 1$, no streaming dispersion results are recovered.

The Landau damping term is further modified for the above propagation conditions and for streaming velocity in the following manner.

$$\gamma = \sum_{j=+,-} \frac{m_j}{k^2 KT_j} (1+V_o) \left(\frac{\pi}{8}\right)^{1/2} \frac{\omega_{oj}}{(kL)^3} \exp\left[-\frac{1}{2(kL)^2}\right]$$

where L is the phenomenal Debye length and W_{oj} is the local plasma frequencies of the species. For $V_o \to o$ and $\frac{M_j}{k^2 KT_j} \simeq 1$ non streaming conditions are retained. The phenomenal damping or absorption of waves by particle is further diminished owing to the streaming propagation than in the absence of it. Obviously the ionic damping is comparatively smaller than that of electron

species. Results of Bohm and Gross (1949), Landau (1946), Buti (1962,63) are inherent in it. Since electron temperature is 10^8K for relativistic limit or fusion, one has to use the separate approximations qualitatively; but for ion Temp. $T_j = 10^8$K, these dispersion results and damping are valid for fusion in the nonrelativistic limit. Ions become relativistic at 10^{13}K only.

References :

1. Bohm, D. and Gross E.P., 1949, Phy.Review, 75, 1851.

2. Buti, B., 1962, Phys.Fluids, 5, 1, 1963 a,b, Phys.Fluids, 6, 89 and 100. Phys.Rev., A, Vol.5, No.3, 1558.

3. Landau, L.D. (1946), J.Phys., USSR, 10, 25.

4. Logan B.G., 1980 (April), Proceedings of Int.Conf. on Plasma Nagoya.

5. Misra, P., 1975, J.of Plasma Physics, England, Vol.14, Part 3, pp.529-541.

6. Misra, P. and Mohanty, J.N., J.of Plasma Physics, England (April 1980) Vol.24, Part 3, pp.409-420.

7. Mohanty J.N. (1980) (April), Proc. of Int.Conf. on Plasma Nagoya.

8. Mohanty J.N. (1981), Tobe published, J.of Plasma Physics, England

9. Porkolab M, 1974a, Princeton Univ.Report MATT, 1069.

10. Ryutov, D.D., 1980, Proc. of Int.Conf. on Plasma Nagoya.

11. Sudan R.N., 1980, Proc. of Int.Conf. on Plasma Nagoya.

12. Sundarum, A.K. and Sen, A. J.of Plasma Physics, (1977), Vol.17, Part 1, pp.41-50.

13. Kadmotsev, B.B. and Pogutse, C.P., 1971, Nucl.Fusion, 11, 67.

SUPPLEMENTS TO CONTRIBUTED PAPERS IN VOL. I

ELECTRON CYCLOTRON HEATING IN FT-I TOKAMAK ABOVE CRITICAL PLASMA DENSITY (supplement)

D.G.Bulyginsky, V.E.Golant, S.G.Goncharov, V.K.Gusev, M.M.Larionov, L.S.Levin, G.T.Razdobarin, A.I.Smirnov, N.V.Shustova.
A.F.Ioffe Physical-Technical Institute, Leningrad,USSR.

Electron cyclotron heating (ECRH) using the microwave power input by an extraordinary wave launching from the stronger magnetic field side of a torus is described in the main paper of the same title presented at this conference. An essential heating was observed in a wide density range. First results of laser measurements of $T_e(r)$, $n_e(r)$ profiles are presented now. The gyrotron generator (f = 29,17 GHz, P=50-60kW, 2 ms) was used for ECRH. Critical density ($\omega = \omega_p$) for frequency used is $n_{cr}=1{,}06.10^{13}cm^{-3}$. Data are obtained at some line-averaged densities $\bar{n}$: $0{,}6.10^{13}$ cm^{-3}, $1{,}1.10^{13}cm^{-3}$, $1{,}4.10^{13}cm^{-3}$. Corresponding densities at the discharge axis are: $n_o = 1n_{cr}$, $n_o = 1{,}8n_{cr}$, $n_o = 2{,}4n_{cr}$. Discharge current of 30 - 34 kA provides ohmic heating (OH) power P_{oh} = 55 - 80 kW. Using $T_e(r)$, $n_e(r)$ profiles, total energy contents W_e and mean diamagnetic effect of a plasma electrons $\overline{nT}$ were calculated in OH and ECRH.

Fig.1 and fig.2 present T_e, n_e profiles in the case $n_o = 1n_{cr}$. Toroidal field B_o is 10,6 kGs and 9,7 kGs (position of ECR zone is +0,5cm and -4cm from the axis). W, ΔW, $\overline{nT}$, $\Delta\overline{nT}$ are shown also.

Fig.3 and fig.4 present the profiles for $n_o=1{,}8\ n_{cr}$ and $n_o=2{,}4\ n_{cr}$, $B_o=9{,}7$ kGs in both cases.

$\Delta\overline{nT}$ during ECRH is $(1{,}7 - 3).10^{14}eV.cm^{-3}$ at all densities. So, laser data confirm the diamagnetic measurements. Relative increase $\Delta nT/nT$ varies from 0,43 to 0,30 as the density rises from 1 n_{cr} to 2,4 n_{cr}. Optical measurements show no increase of impurity concentration during ECRH, but the effective charge of ions Z_{eff}, calculated using $T_e(r)$

profiles and conductivity measurements, is 1,0 - 1,3 in OH and 1,1 - 1,8 during ECRH. This apparent increase of Z_{eff} may result from the generation of trapped electrons by the heating wave. The efficiency η of ECRH in comparison with OH was obtained using the equation:

$$\frac{W + \Delta W}{W} = \frac{\eta P + P'_{OH}}{P_{OH}}$$

P'_{OH} - power of OH during ECRH, $P'_{OH} < P_{OH}$ due to the loop voltage drop during ECRH. T_e, n_e profiles Fig. 1 - 4 give us $\eta = 0,6 - 0,7$ in all cases.

So, ECRH produced by the extraordinary wave launched from the stronger magnetic field side remains efficient even in the rather dense plasma, $n_o=(1 - 2,4)\ n_{cr}$. However, as the density increases, the zone of maximal rise of T_e moves to the periphery, and the profile of T_e becomes broader during ECRH. This result corresponds to the numerical calculation of wave damping, if the cyclotron absorbtion and the linear transformation of a wave is taken into account.

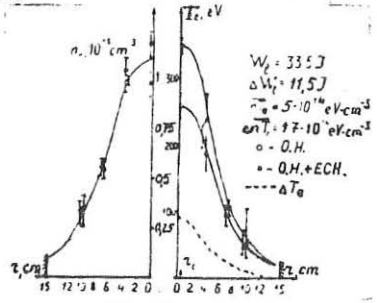


Fig.I

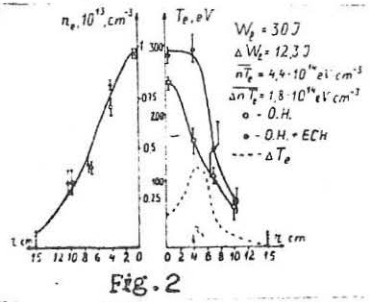


Fig.2

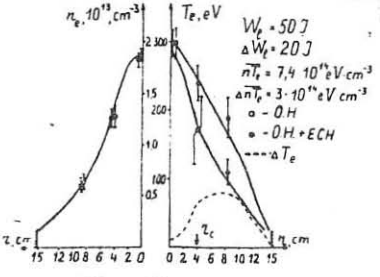


Fig. 3

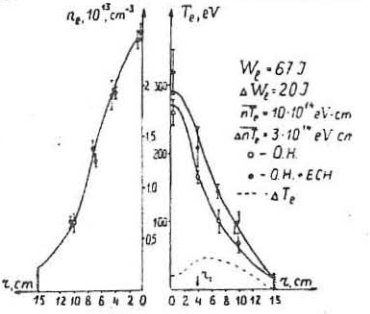


Fig. 4

Postcompression period investigation in Tuman2A - a tokamak with magnetic compression.

S.G.Goncharov, V.K.Gusev, V.A.Ipatov, S.G.Kalmykov, S.I.Lashkul, B.M.Lipin, Yu.V.Petrov, G.T.Razdobarin, V.V.Rozhdestvenskiy, A.I.Smirnov, I.D.Shpritz.
(Physical-Technical Institute, Leningrad, USSR)

This work is a development of that published in the 1st volume of the Conference. Here we study the relaxation of compressed plasma state. To realize this toroidal field B_T was kept during 2 ms at the highest value after 2-fold compression during Δt_c=0.5 ms. A "slow" compression with Δt_c=1.8 ms was available also. Initial, precompression plasma parameters were close to those described earlier: I_p=13kA, B_T=8kG, $n_e(0)=2.2\times10^{13}$ cm^{-3}, $T_e(0)$=130eV, τ_{eE}=0.33ms, Z_{eff}=1.2, radiation losses were 20÷30% from ohmic heating power.

Fig.1 and 2 show space-temporal evolution of T_e and n_e (Thomson scattering and microwave interferometric data) for both cases of compression. For the "slow" compression one can see a charakteristic "stop" in density (see fig.2) and current channel compression at 0.6÷0.7ms after the beginning. Supposing a diffusion rate to be equal to magnetic compression one for this moment it is possible to estimate averaged over the cross section coefficients of plasma and current density diffusion. This latest one may be estimated from inductive effects at the "fast" compression also. Experimental values are $\overline{D_\perp}=(8\div10)\times10^3$ cm^2/s whereas the classic one $\overline{D_\perp^{cl}} = c^2/4\pi\overline{\sigma}$ varies from 13×10^3 cm^2/s up to 6×10^3 cm^2/s during the compression. The particle diffusion coefficient is $\overline{D_p}=6\times10^3$ cm^2/s and the particle life time is τ_p=2÷4 ms. Particle balance based on relative hydrogen L_α-line intensity measurements yields the increase in τ_p for both cases of compression equally by factor 1.5÷2 (see fig.3,4). The electron energy life time evolution is shown in fig.3. too.

The results for the moment of maximum compression confirm data of the previous work. The energy confinement improves 2.5÷3 times during the "fast" compression and then drops slowly. Perhaps it follows the relaxation of plasma parameters n_e, T_e and the postcompression expansion of the current profile - a heat source profile. Comparing "fast" and "slow" compression data one can see that the influence of B_T on τ_{eE} is negligible whereas the particle confinement depens on B_T probably.

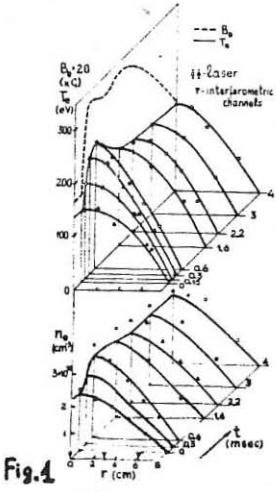


Fig.1

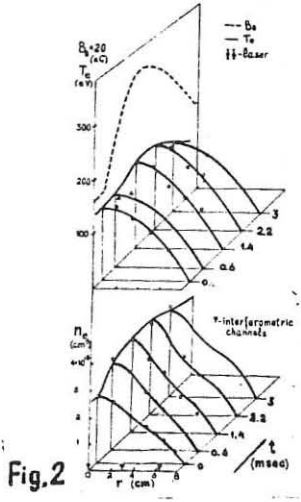


Fig.2

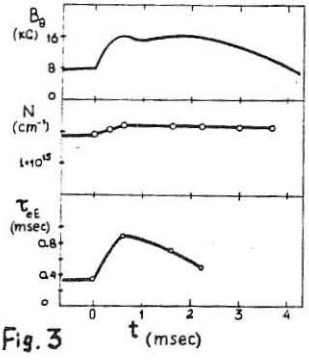


Fig. 3

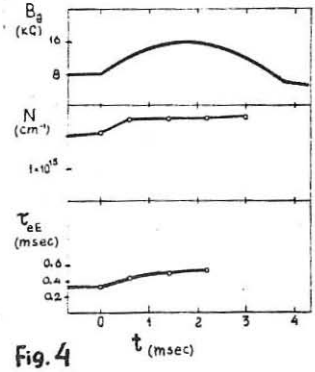


Fig. 4

POST - DEADLINE PAPERS

PLASMA EXPERIMENTS ON T-7 SUPERCONDUCTING TOKAMAK

A.A.Bagdasarov, M.Yu.Cherkashin, V.F.Denisov, Yu.V.Gvozdkov, V.V.Hilil, P.P.Hvostenko, D.P.Ivanov, N.V.Ivanov, A.M.Kakurin, A.Ya.Kislov, V.A.Kochin, P.E.Kovrov, Yu.S.Maksimov, V.A.Mihailichenko, B.A.Stavisskii.

I.V.Kurchatov Institute of Atomic Energy,
Institute of Control Problems, Moscow, USSR.

The permanent physical experiments on T-7 tokamak are in progress from 1980. T-7 is the first tokamak with superconducting toroidal magnetic field coils. The discharge chamber major and minor radii are R=122cm and b=35cm. The toroidal field $B_{\parallel}$ is up to 3T. The discharge current I_p is up to 400kA. Two carbon rail limiters can be placed at a distance of a=20-31cm from the chamer axis. The usual chamber wall temperature during plasma experiments is minus several tens degrees centigrade. By present time three experimental campaigns, about two months long every, have been performed. The total amount of the pulses exceed 6000. The discharge regimes with $B_{\parallel}$=1,6-2,3T and I_p= 100-300kA have been investigated.

The discharge conditions. The most detail measurements have been carried out for hydrogen discharges with $B_{\parallel}$=1.9T, I_p=160-210kA, $q(a)$=2.4-3.2. The average electron density was $\bar{n}_e = (1-5)\cdot 10^{13}\,cm^{-3}$. The typical oscillograms of discharge parameters are given in Fig.1. The discharge voltage was U_p=1.1-1.8 V in the mentioned

density interval. The part of radiation losses, obtained from bolometric measurements, P_r / P_{oH} =30%. The variation of energy confinement time, obtained from plasma diamagnetism, with density is given in Fig.2 in comparison with the [1,2] results. The electron temperature T_e was obtained from soft X-ray emission in the energy interval from 2.5 to 8 keV. The typical emission spectrum and T_e radial distribution are given in Fig.3,4. The results of ion temperature measurements, obtained with five channel charge exchange analyzer, are plotted in Fig.4. The Z_{eff} value was determined from visible ($\lambda = 5230 \pm 3$ Å) and soft X-ray bremsstrahlung. The results, calculated in assumption that $n_e(r) = n_{eo}(1 - r^2/a^2)$, are given in Fig.4. The Z_{eff} value, calculated from plasma conductivity was 1.2.

The discharge initial stages. The analysis of the experimental data showed that at presence of a small perpendicular magnetic field ($B_\perp \approx 10^{-3} B_\parallel$) there are two stages of the discharge development. At first, when the current is small, the discharge arises along the helical line of magnetic force between the opposite parts of the limiter. The slope of the dependence $\frac{I_L}{I_p}(B_\perp)$ coincides with $dI_L/dI_p = \pi R B_\perp / a B_\parallel$ (see Fig.5), where I_L is the current to a part of the limiter. The discharge delay t_f can be described in terms of Townsend's model (Fig.7). At the second stage, when the current field exceeds the perpendicular field, the rotational transform arises and a toroidal electrodeless discharge is formed.

The effect of quadrupole field. The perpendicular quadrupole magnetic field was deliberately excited with the help of one of the four sections of the T-7 control coils. The average amplitude of the quadrupole field over the torus was ~10 G. The quadrupole field turned out to produce standing m=2 perturbation of poloidal magnetic field, abolish the running perturbation of the same space stucture and widen plasma density and electron temperature radial profiles (see Fig.6). The experiment indicated the possibility of the T-7 quadrupole coils application for the m=2 perturbation control.

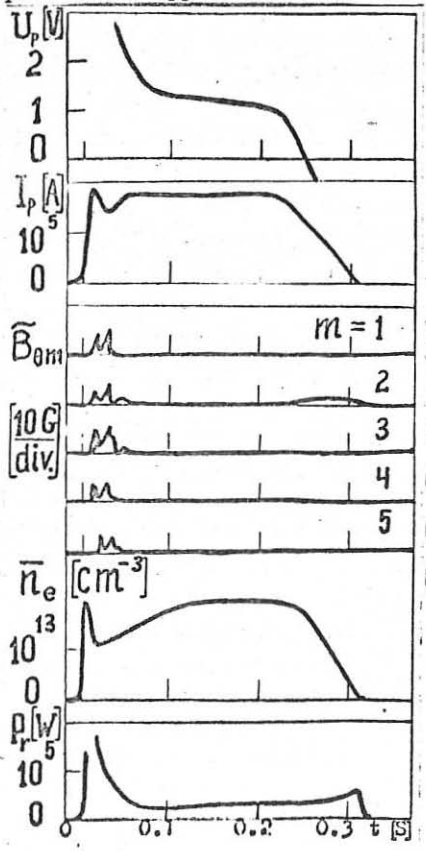


Fig. 1

REFERENCES

1. D.L.Jassby et al., Nucl. Fusion, 16, 1045, 1976.
2. В.Г.Мережкин, В.С.Муховатов. Письма в ЖЭТФ, т. 33, 463, 1981.

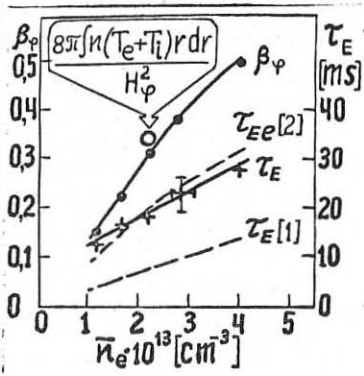


Fig. 2

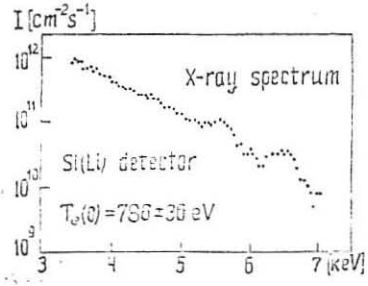


Fig. 3

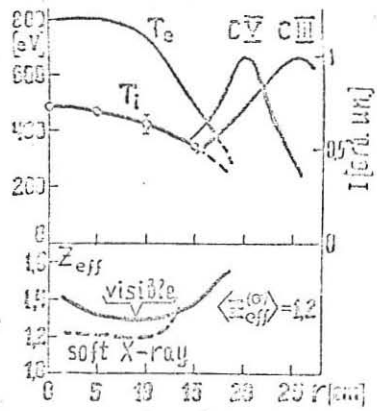


Fig. 4

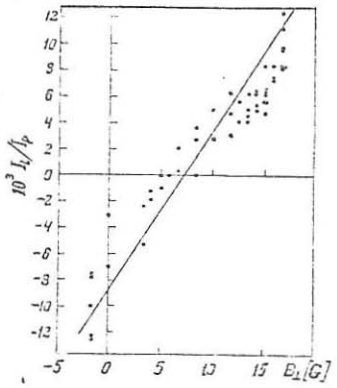


Fig. 5

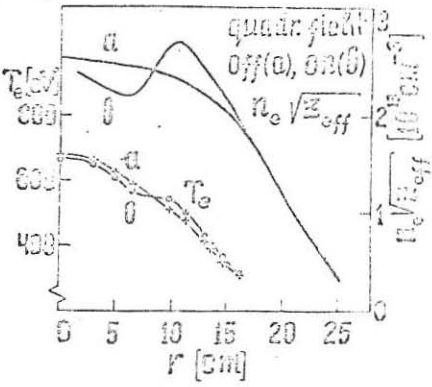


Fig. 6

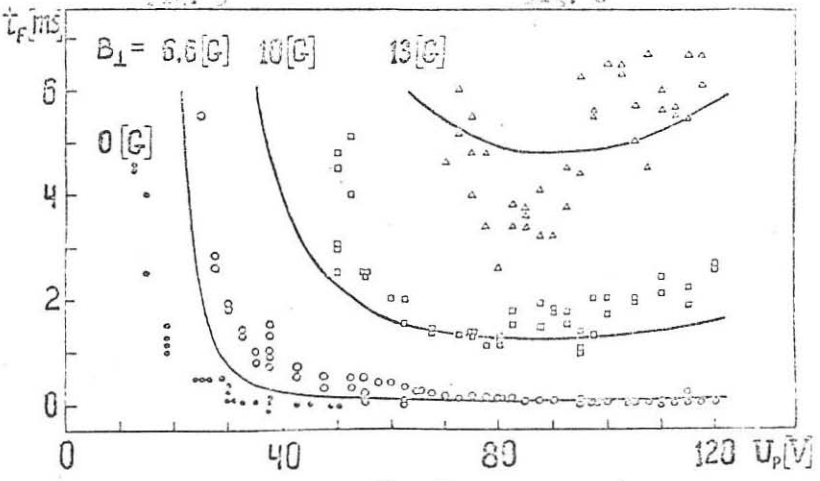


Fig. 7

PLASMA POTENTIAL AND ITS VARIATION WITH ECRH ON THE TM-4 TOKAMAK

A.V.Gorshkov, V.I.Poznyak, K.A.Razumova,
V.V.Sannikov, Yu.A.Sokolov

I.V.Kurchatov Institute of Atomic Energy, USSR

I.S.Bondarenko, L.I.Krupnik, I.S.Nedzelskii

Charkov Physical Technical Institute, USSR

The leading role of any plasma component in the diffusion losses determines the value and polarity of plasma potential. Considering neoclassical theory, electron diffusion is defined to give the rate of plasma particle losses, and the ion losses determine the polarity of plasma potential, the latter is negative in the plasma core.

The experiments show anomalously large values of the electron thermal conductivity and plasma diffusion /1/. Anomalous electron losses could influence the value and polarity of the plasma potential. Different behaviour of plasma losses is possible to expect in such case. An experiment is of interest when the dominant losses are mainly contributed by ions or electrons to understand the mechanism of plasma confinement. Plasma potential measurements must be necessary performed in such experiments.

Space potential in the plasma core corresponded to the dominant ion losses in the experiments on the ST and FT-1 /2,3/, while it corresponded to electron losses in the T-10 experiments /4/. All these measurements were performed at Joule heating. An experiment notably influencing one of the components /electrons or ions/ is needed to determine parametric scalings of the tokamak particle losses.

The measurement of space potential was performed on the TM-4 tokamak in experiment with ECRH. The heavy-ion (Cs^+) beam probe was used to measure the local values of plasma potential.

Radial profiles of the plasma potential were ob-

tained in two regimes: I regime: H_z = 14 kOe, I = 26 kA, $\bar{n}_e$ = 1.2÷ 1.5 . $10^{13}cm^{-3}$, $T_e(0)$ = 700 eV, $T_i(0)$ = 150 eV, II regime: H_z = 14.5 kOe, I = 24.5 kA, $\bar{n}_e$ = $3.10^{13}cm^{-3}$, $T_e(0)$ = 250 eV, $T_i(0)$ = 180 eV.

ERCH of plasma was performed in the first regime. Sawtooth oscillations are typical for the second regime /5/. Negative values of plasma potential were measured in both regimes, and these were equal to several hundreds electronvolts.The polarity of potential shows dominant ion losses. The value of plasma potential increases when passing to the periphery, becoming positive near the plasma column edge (Fig.1).

Passing to the high density regime when the inner disruption instability occured did not notably change the value and polarity of the plasma potential, although it was possible to expect the enhaucement of electron losses /6/. Such losses could change the value of plasma potential.

Electron heating experiments were performed on the II harmonic of ECF. The applied gyrotron had such characteristics as 3.6 mm wavelength, up to 150 kW power and 6 ms pulse duration. Notable decrease (25-30%) of plasma density (Fig.2) and the dominant electron heating are typical in the discussed case. We may consider T_i value remaining constant while heating due to the large difference in the values of the electron and ion temperatures, although no direct T_i measurements were performed ($T_i(0)$ was calculated according to Artsimovich formula). Notable increase of electron temperature happens with ECRH in the plasma core (Fig.3) simultaneously with the increase of the particle losses.

No plasma potential variation was observed with ECRH in the plasma core, and a slight increase was observed in the periphery within the energy resolution of measurements (Fig.2e).

So, ions determine plasma potential but the electron component obviously determines the rate of particle los-

ses in the discussed case. Electron transport depends on electron temperature or/and its gradient, causing the increase of particle losses with the growth of electron temperature. Such conclusion is true concerning plasma core, where the maximum variation of T_e is measured.

Considering all these facts we cannot yet exclude other mechnisms causing particle losses with ECRH. In particular, peripheral plasma parameters' variation may cause notable changes in the particle balance of the whole plasma column.

References

1. A.Gondhalekar et al.,in Plasma Physics and Controlled Nuclear Fusion Res. 1978 (Proceedings 7th Inter.Conf., Innsbruck, 1978), v.1, IAEA, Vienna (1979) 199.
2. F.C.Jobes, J.C.Hosea, 6th European Conf. on Contr. Fusion and Plasma Physics, Moscow, v.1, 199 (1973).
3. A.P.Zhilinsky, et al. 10th European Conf. on Controlled Fusion and Plasma Physics, Moscow, v.1, paper A-3a (1981).
4. S.M.Egorov et al., 10th European Conference on Contr. Fusion and Plasma Physics, Moscow, v.1, Paper A-3b (1981).
5. V.I.Bygarya et al., 10th European Conf. on Contr. Fusion and Plasma Physics, Moscow, v.1, Paper A-15 (1981).
6. G.Fussmann et al. Proceedings 7th Intern.Conf. Innsbruck, 1978, v.1, IAEA Vienna (1979) 401.

Figure Captions

Fig.1. Radial profile of the plasma potential
o—o - I regime
X—X - II regime

Fig.2 Plasma parameters oscillograms in regime with the ECRH pulse.
Cs^{++}ion current is given in Fig.2e for different values of the analysing grid potential.

Fig.3 Radial electron temperature profile.
X—X with ECRH.
o—o without ECRH.

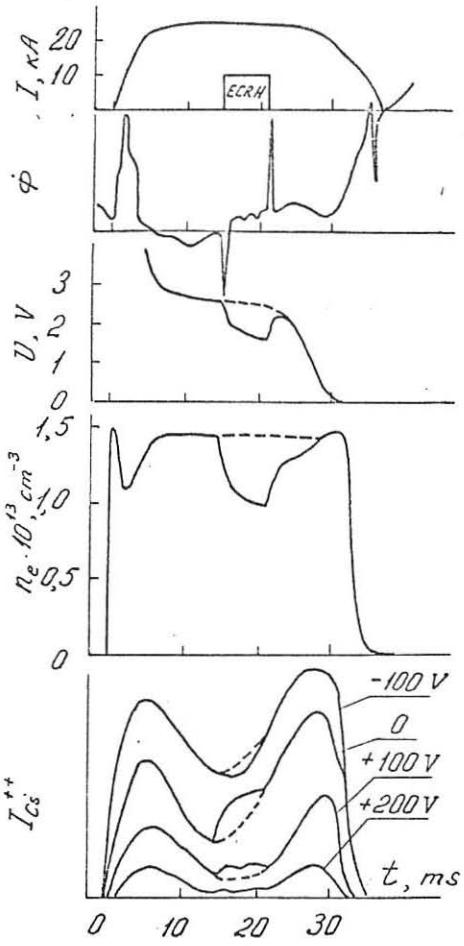


Fig. 2

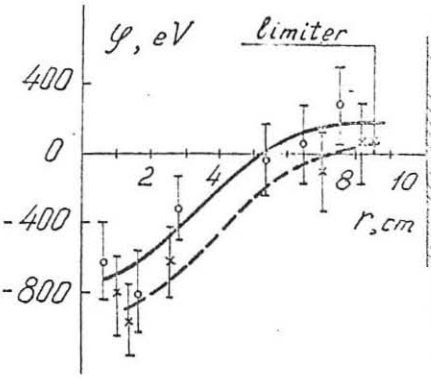


Fig. 1

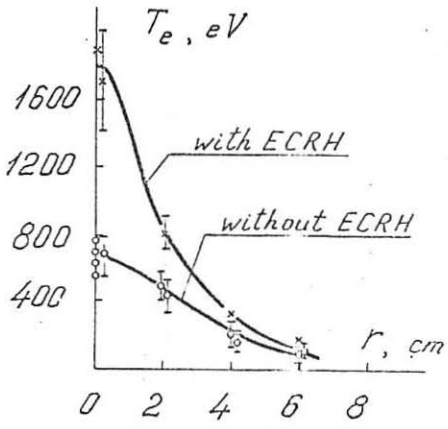


Fig. 3

TEARING MODE TIME EVOLUTION IN T-7 TOKAMAK

M.Yu. Cherkashin, A.N. Chudnovski, Yu.V. Gvozdkov, N.V. Ivanov, A.M. Kakurin

I.V. Kurchatov Institute of Atomic Energy

Institute of Control Problems, Moscow, USSR

Much attention is attracted now by the investigations of nonlinear tearing mode in tokamak plasma [I - 3]. This attention is caused by the fact that tearing mode forms magnetic islands and therefore affects energy and particle confinement, changes current profile and takes part in disruptive instability. The dependence of magnetic island width on the current profile was calculated in [I, 3]. The Rutherford regime of tearing mode time evolution was derived in [I].

In this work the reciprocal effect of the magnetic island and current profile is calculated numerically, plasma energy and particle balance taken into account. The energy and particle balance numerical code [4] is supplemented with the island width W nonlinear evolution equations:

$$\frac{dW}{dt} = \frac{\gamma}{2} W$$

if $W < \varepsilon$ and

$$\frac{dW}{dt} = \Delta' \omega_R a^2$$

if $W > \varepsilon$ (Rutherford regime).

In these equations $\omega_R = \eta / 2\pi a^2$ is the reciprocal skin time and ε is the so-called tearing width. The increase of transport coefficients over magnetic island is simulated by forming constant radial distributions of current and plasma densities as well as electron and ion temperatures inside the island. In equations (I) and (2)

$$\gamma = \left[\left(\frac{2ma^3}{g} \frac{d\mu}{dr} \right)^2 \Delta'^4 \omega_R^3 \omega_H^2 \right]^{1/5} \operatorname{sign} \Delta', \quad (3)$$

$$\Delta' = \frac{\Psi'(r_s + \frac{W}{2}) - \Psi'(r_s - \frac{W}{2})}{\Psi(r_s)} \quad (4)$$

depend on W. The values of γ and Δ' are determined from the solution of the linearized $\vec{B} \times \mathrm{rot}\, \vec{B} = 0$ equation in the cylindrical geometry in tirms of poloidal flux function Ψ. In (3) and (4) $\omega_H = B_z / \sqrt{4\pi\rho} R$ is the reciprocal Alfven time, $\mu = 1/q$ - reciprocal safety factor, m - the poloidal mode number, r_s - the rational magnetic surface radius.

The time evolution of $m = 2$ magnetic island and the amplitude of corresponding poloidal magnetic field perturbation at the chamber wall radius, calculated for the T-7 tokamak conditions, are given in Fig. I. The plasma minor radius interval, occupied by the island, is darkened. The T-7 experimental time traces of the

amplitudes of three space harmonics of poloidal field perturbation are given in Fig. 2. The comparison of Fig. I and Fig. 2 shows a good agreement between theoretical and experimental curves $\widetilde{B}_\theta(t)$ for $m = 2$ harmonic. The main peculiarities of the mode time evolution are two: the shape of separate pulse with pulse duration of some tens of milliseconds and arising sometimes oscillations of island width and poloidal field perturbation amplitude. The fact that the island width time dependence has the character of separate pulse shows a sort of tearing mode self stabilisation caused by the variation of the current profile due to the increased plasma transport over the magnetic island. The flattening of current profile in the vicinity of the rational magnetic surface usually stabilise tearing instability [5]. In some conditions the double time delay due to finite velocities of both the island width variations and current density diffusion outside the island can excite the island width oscillations [6].

The current profile variations due to the skin effect give a dependence of the perturbation amplitude on the discharge current time derivative (Fig. 3). The island disappears when the current increases quite rapidly and appears again as soon as the current begin to decrease.

The authors thank Yu.N. Dnestrovski and G.V. Pereversev for useful discussions and help with the energy balance numerical code.

REFERENCES

I. P.H.Rutherford. Phys. Fluids, I6, I903 (I973).

2. R.B.White, D.A.Monticello, M.N.Rosenbluth, B.V.Waddell. Phys. Fluids, 20, 800 (I977).

3. B.Carreras, B.V.Waddell, H.R.Hicks. Nucl. Fusion, I9, I423 (I979).

4.Ю.Н.Днестровский,Д.П.Костомаров. В кн. Вычислительные методы в физике плазмы. "МИР" М.I974,стр.483.

5. Furth H.P. et al. Phys. Fluids, I973, I6, I054

6. Ivanov N.V., Kakurin A.M., 9th Europ. conf. on Controlled Fusion and Plasma Physics, Oxford, I979, v.I, p.I55.

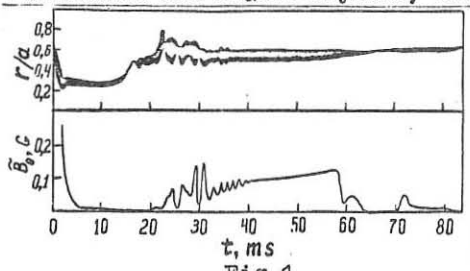


Fig.1

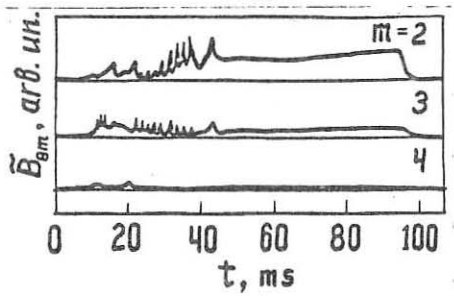


Fig.2

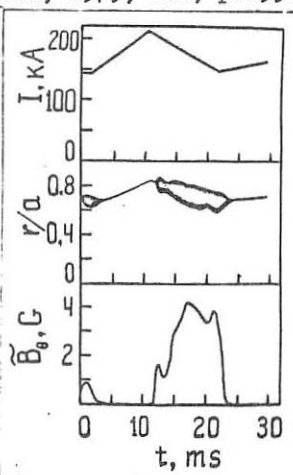


Fig.3

ANOMALOUS PLASMA DIFFUSION IN TOKAMAK

V.V.Parail, O.P.Pogutse

I.V.Kurchatov Institute of Atomic Energy,
Moscow, USSR

Equations for anomalous plasma diffusion due to interaction of ions with oscillations, localized in the vicinity of rational surfaces, are given in the paper.

In the recent experiments /1-3/ it has been shown that the plasma diffusion in a tokamak is an anomalous one and the diffusion coefficient, D, and that of electron heat conduction, χ_e are inversely proportional to the plasma density. This shows the possible similarity between both processes which result in the anomalities mentioned. One should remember that the modern theory allows to explain without contradictions the experimental value of anomalous electron heat conduction by the mechnism of resonance electron interaction with the flute-like instability localized in the vicinity of rational surfaces. In /4/ it has been shown that in the regime with strong turbulency, when $\tilde{n}/n_e \sim (k_\perp a)^{-1}$ ($\tilde{n}$ is the density perturbation in a field of the wave), the anomalous electron heat conduction coefficient becomes independent of the energy density oscillations and reaches an asymtotic value determined by the relationship $\chi_e = A \frac{c^2}{\omega_{pe}^2} \frac{V_{Te}}{qR} \varepsilon^2$ /4/ where, A is a numerical factor.

We would like to remind that the oscillations which are in resonance with the electron component only have been considered in /4/. Such oscillations cannot result in an anomalous diffusion of plasma as a whole. As it is always happened in such cases, an anomalous departure of electrons results in the emergence of a radial electric field with positive potential φ . This field produces a potential barrier which prevents the departure of electrons from plasma. An anomalous electron heat conductivity remains at the previous level in this case. In this paper, an anomalous diffusion coefficient for plasma as a whole will be obtained in the frames of the theoretical ideas described in /4/.

First of all, one should find the radial electric field E_r. Using the results /4/, one can write a kinetic equation for electrons in which their resonance interaction with oscillations is taken into account:

$$\frac{\partial f_e}{\partial t} = \frac{1}{r}\frac{\partial}{\partial r} r \frac{c^2}{\omega_{pe}^2} \varepsilon^2 \sum_{\omega} \omega^2 \delta\left(\omega - \frac{v_{\parallel}}{qR}\right) \frac{\partial f_e}{\partial r} \qquad (1)$$

where, $\varepsilon = r/R$. Let's consider the distribution function for electrons in the velocity space to be a Maxwellian one:

$$f_e = \frac{n_e(r)}{(\sqrt{\pi} v_{Te}(r))^3} \exp\left\{ - \frac{e\varphi(r)}{T_e(r)} - \frac{E}{T_e(r)} \right\}$$

where $E = \frac{mv^2}{2} - e\varphi$ is the integral of motion. Let's integrate the equation (1) for $d\vec{v}$ with weights I and $mv^2/2$:

$$\frac{\partial n_e}{\partial t} = \frac{1}{r}\frac{\partial}{\partial r} r \frac{1}{\sqrt{\pi}} \frac{c^2}{\omega_{pe}^2} \frac{v_{Te}}{qR} \varepsilon^2 \left[\frac{\partial n_e}{\partial r} + \frac{1}{2}\frac{n_e}{T_e}\frac{\partial T_e}{\partial r} - \frac{e n_e}{T_e}\frac{\partial \varphi}{\partial r} \right] \qquad (2)$$

$$\frac{3}{2}\frac{\partial}{\partial t} n_e T_e = \frac{1}{r}\frac{\partial}{\partial r} r \frac{2}{\sqrt{\pi}} \frac{c^2}{\omega_{pe}^2} \frac{v_{Te}}{qR} \varepsilon^2 \left[\frac{\partial n_e}{\partial r} + \frac{3}{2}\frac{n_e}{T_e}\frac{\partial T_e}{\partial r} - \frac{e n_e}{T_e}\frac{\partial \varphi}{\partial r} \right] \qquad (3)$$

One will obtain the value of radial electric field, E_r and the anomalous electron heat conductivity coefficient, if assumes that the electron flux $n_e v_r$ equals zero (validity of this assumption is shown below):

$$e\frac{\partial \varphi}{\partial r} = -eE_r = \frac{T_e}{n_e}\left(\frac{\partial n_e}{\partial r} + \frac{1}{2}\frac{n_e}{T_e}\frac{\partial T_e}{\partial r} \right) \qquad (4)$$

$$\chi_e = \frac{2}{\sqrt{\pi}} \frac{c^2}{\omega_{pe}^2} \frac{v_{Te}}{qR} \varepsilon^2 \qquad (5)$$

One should take into account the oscillations interecting with ions to obtain an equation which describes an anomalous diffusion of plasma as a whole. Let's consider that in the regime with strong turbulency, a wide spectrum of oscillations is excited, the frequency $\omega \sim \frac{v_{Ti}}{qR}$ included. Then, according to a scheme completely similar to that described in /4/, one can obtain a kinetic equation for the ionic distribution function:

$$\frac{\partial f_i}{\partial t} = \frac{1}{r}\frac{\partial}{\partial r} r \sum_{\omega, k_\perp} \frac{\omega^2}{k_\perp^2} \left| \frac{k_\perp^2}{k_\perp^2 + \frac{\omega^2}{c^2}\varepsilon_l} \right|^2 \varepsilon^2 \delta\left(\omega - \vec{k}_\perp \vec{v}_\perp - \frac{v_{\parallel}}{qR}\right) \frac{\partial f_i}{\partial r} \qquad (6)$$

In the derivation of (6), it is considered that the oscillations localized in the vicinity of resonance surfaces have been excited in plasma. In that case, the longitudinal component of the wave vector $k_{\parallel}$ is determined as $k_{\parallel} \simeq \frac{k_{\perp}\Delta r}{qR} S + \frac{k_{\perp}(\Delta r)^2}{qR}\frac{dS}{dr}$ where $S = \frac{r}{q}\frac{dq}{dr}$ is the term describing the magnetic shear. In the regime with strong turbulency, according to /4/, $\Delta r(t) \sim k_{\perp}^{-1}\sin\omega t$ and $\overline{k_{\parallel}}$ averaged in time is equal $\overline{k_{\parallel}} \simeq \frac{1}{k_{\perp}qR}\frac{dS}{dr} \ll (qR)^{-1}$. Therefore, the main contribution in δ-function (see(6)) is done by the effect of toroidicity which result in the following dependence of the transport coefficients: $\chi_e \sim \varepsilon^2$. In the equation (6), ε_l is the longitudinal component of dielectric permittivity in plasma which takes into account that the particles are frozen into the magnetic field of long-wave oscillations (see /4/): $\varepsilon_l \simeq \frac{\omega_{pe}^2}{\omega^2}\left(\frac{\omega^2}{\omega^2 + k_{\perp}^2 v_{Te}^2} + \sqrt{\varepsilon}\right)$. The general term of the series for $k_{\perp}$ in the right-hand side of the equation (6) reaches the maximum at $k_{\perp}^2 \simeq \frac{\omega^2}{c^2}\varepsilon_l$. Therefore, in the limit case $\sqrt{\varepsilon} > \frac{\omega^2}{\omega^2 + k_{\parallel}^2 v_{Te}^2}$

$$\frac{\partial f_i}{\partial t} = \frac{1}{r}\frac{\partial}{\partial r} r \sum_{\omega} \omega^2 \frac{c^2}{\omega_{pe}^2} \varepsilon^{3/2} \delta(\omega - v_{\parallel}/qR) \frac{\partial f_i}{\partial r} \qquad (7)$$

In the opposite limit case, the multiplier $\varepsilon^{3/2}$ in (7) is substituted by ε^2. Let's consider the distribution function be a Maxwellian one. Then, as in derivation of (2), (3) f_i depends on the integral of motion $E_i = \frac{M_i v^2}{2} + e_i \varphi$ where the potential φ is determined by the relationship (4), e_i is the charge of ion. Integrating (7) by velocities with weights I and $\frac{M_i v^2}{2}$, one obtains the equations which describe an anomalous diffusion and heat conduction for the ions of α = = type:

$$\frac{\partial n_\alpha}{\partial t} = \frac{1}{r}\frac{\partial}{\partial r} r D_\alpha \left[\frac{\partial n_\alpha}{\partial r} + \frac{T_e}{T_\alpha}\frac{z_\alpha n_\alpha}{n_e}\frac{\partial n_e}{\partial r} + \frac{1}{2}\frac{n_\alpha}{T_\alpha}\frac{\partial T_\alpha}{\partial r} + \frac{1}{2}\frac{z_\alpha n_\alpha}{T_\alpha}\frac{\partial T_e}{\partial r}\right] \qquad (8)$$

$$\frac{3}{2} n_\alpha \frac{\partial T_\alpha}{\partial t} = \frac{1}{r}\frac{\partial}{\partial r} r n_\alpha \chi_\alpha \frac{\partial T_\alpha}{\partial r}$$

where

$$D_\alpha = \frac{\chi_e}{2\sqrt{\varepsilon}}\sqrt{\frac{T_\alpha m}{T_e M_\alpha}} = \frac{c^2}{\omega_{pe}^2}\frac{v_{T\alpha}}{\sqrt{\pi} qR}\varepsilon^{3/2}\,; \quad \chi_\alpha = 2D_\alpha \qquad (9)$$

First of all, note that the diffusion coefficient for ions is found to be much smaller($(\frac{T_i m}{T_e M_i})^{1/2}$ times) than the diffusion coefficient for electrons, when the radial electric field is not taken into account. Due to this, the electric field can can be found according to the scheme described above.

From the relationships obtained it follows that the presence of the flute-like instability localized in the vicinity of the rational surfaces results in the emergence of anomalous diffusion, thermodiffusion and heat conduction of the bulk ions and of the impurities. In this case, the transport coefficients are inversely proportional to the plasma density. This effect is observed in the experiments. One should also note that the modern theory gives the diffusion and electron heat conduction coefficients within the accuracy range up to an unknown numerical factor. But one should hope that the ratio χ_e / D is determined with higher accuracy.

In conclusion the authors wish to thank academician B.B.Kadomtsev for helpful discussions.

References

1. E.Apgar, B.Coppi et al. In Plasma Phys. and Contr. Nucl. Fus. Res. (Pros. 6th Int. Conf. Berchfesgaden, 1976), v.1, p.247.
2. V.M.Leonov et al. Paper to the 10th European Conference on Contr.Fusion and Plasma Physics, Moscow, 1981.
3. V.G.Merezhkin, V.S.Mukhovatov. Pis'ma Zh.Ehksp. Teor. Fiz. 33, 463 (1981).
4. V.V.Parail, O.P.Pogutse. Pis'ma Zh.Ehksp. Teor. Fiz. 32, 408 (1980).

LOSSES OF HOT INJECTED IONS THROUGH MULTIPLE CHARGE EXCHANGE IN TOKAMAK

Yu.N.Dnestrovskii

I.V.Kurchatov Institute of Atomic Energy
Moscow, USSR

Abstract. An equation for the energy transfer from hot ions to plasma through multiple charge exchange is given for a flat model. The problem is reduced to a spatial diffusion and velocity transfer equation in approximation of high optical thickness. Some estimations of losses in modern tokamaks are made. The maximum neutral beam power which can be deposited in plasma is found. This power rises with an increase in size of a plasma ($\sim a^4R$) and its density ($\sim n^4$). Therefore, the multiple charge exchange will not be significant in large tokamaks.

1. Substitute the plasma column by a flat layer in a region $-a < x < a$. Let $f(x,v,t)$ be a distribution function for hot ions, f_N^+ and f_N^- are distribution functions for hot neutrals with positive and negative velocities v_x. Let's assume the density of hot ions be small in comparison with the density of the main plasma component $n(x,t)$, and the density of hot neutrals be small in comparison with the density of thermal neutrals $N(x,t)$. In this approximation the kinetic equation for f has the form

$$\frac{\partial f}{\partial t} + v_{iN} f = \nu_{Ni}\left(f_N^+ + f_N^-\right) + L[f] + P \qquad (1)$$

where $\nu_{iN} = \sigma_{cx} v N$, $\nu_{Ni} \simeq \left(\sigma_{cx} v + \sigma_{ii} v + \sigma_{ie} v_e\right) n \equiv \sigma v n$

$\sigma_{cx}, \sigma_{ii}, \sigma_{ie}$ are the cross-sections of charge exchange and ionization by ions and electrons. At sufficiently high velocities $v \sim v_0$ $v_i \ll v_0 \ll v_e$ (v_0 is the velocity of injected particles, $v_{i,e}$ is the thermal velocity of ions or electrons) /1/:

$$L[f] = \frac{v_0^3}{\tau} \frac{1}{v^2} \frac{\partial}{\partial v}\left(\beta f\right), \quad \beta = \frac{m}{m_i}\beta_i + \frac{m}{m_e}\beta_e \qquad (2)$$

$\beta_i \approx 1$, $\beta_e \approx \frac{4}{3\sqrt{\pi}}\left(v/v_e\right)^3$, $\tau = \frac{m^2 v_0^3}{4\pi z^2 e^4 n L}$. In (1)

$P = \frac{\delta(v-v_0)}{4\pi v_0^2}\frac{\Gamma_\beta^{tz}}{V}\Phi(x)$ (3)

$\Phi(x)$ is a deposition function, $\frac{2}{a^2}\int_0^a \Phi(z) z\,dz = 1$, Γ_β^{tz} is a fraction of the beam particle flux captured within plasma, V is a plasma volume. For a source (3) the equation (1) can be reduced to a homogeneous one with an inhomogeneous boundary condition at $v = v_0$.

Let's assume that at the charge-exchange of hot ions with thermal neutrals the hot neutrals with equiprobable velocities $v_x = \pm v/\sqrt{3}$ are produced. In this case, the equations for f_N^+ and f_N^- are written as

$$\pm v/\sqrt{3}\,\frac{\partial f_N^\pm}{\partial x} + \nu_{Ni} f_N^\pm = \frac{1}{2}\nu_{iN} f \qquad (4)$$

The solution of (4) has the form

$$f_N^\pm = \pm\frac{\sqrt{3}}{2v}\int_{\mp a}^{v} \exp\left[\mp\int_\xi^x \alpha\,dx'\right] f \nu_{iN}\,d\xi \qquad (5)$$

where $\alpha = \frac{\sqrt{3}}{v}\nu_{iN}$. Substituting (5) into (1), one obtains an integrodifferential equation in f:

$$\frac{\partial f}{\partial t} + \nu_{iN} f = \frac{\alpha}{2}\int_{-a}^{a} \exp\left(-\left|\int_\xi^x \alpha\,dx'\right|\right) f \nu_{iN}\,d\xi + L[f] + P$$

2. Let's consider some limit cases. (1) A small optical plasma thickness $\lambda = \alpha a = \sqrt{3}\,n\sigma a \ll 1$. In this case, the first term on the right-hand side of the equation (1) disappears (see /1/).

(2) Large optical plasma thickness

$$\lambda \gg 1 \qquad (6)$$

In this case, the solution (5) can be expanded in term of the parameter $1/\lambda$. As a result, in a stationary case one has

$$\frac{a^2}{\lambda^2}\frac{\partial^2}{\partial x^2}\left(\nu_{iN} f\right) + \frac{v_0^3}{\tau}\frac{1}{v^2}\frac{\partial}{\partial v}\left(\beta f\right) = 0 \qquad (7)$$

$$f(x, v_0) = \frac{\Phi\tau\,\Gamma_\beta^{tz}}{4\pi v_0^3 \beta_0 V}, \quad f(\mp a, v) = 0, \quad \beta_0 = \beta(v_0)$$

3. Let's neglect the dependence of the atomic process rate coefficients on the velocity and assume $\sigma_{cx} v = S^0_{cx} = \text{const}$, $\sigma v = S^0 = \text{const}$. In this case, $\lambda = \lambda_0 v_0 / v$, $\lambda_0 = \sqrt{3}\, n \frac{S^0}{v_0} a$, $\nu_{iN} = N S^0$. The equation (7) can be solved by the method of separation of variables. The main fraction of the solution is determined by the first term of the expansion. Therefore, the condition for small losses can be written as

$$\psi \equiv \mu_1 \int_0^{v_0} \frac{\xi^4 d\xi}{6 v_0^5} < 1 \qquad (8)$$

where μ_1 is the first eigenvalue of the problem $\left(\frac{d}{dx^2} + \mu \lambda_0^2 / (a^2 \tau \nu_{iN})\right) X = 0$, $X(\mp a) = 0$. For the reasonable profiles of plasma and thermal neutral densities one obtains

$$\psi = 0.7 \frac{N v_0^2 \tau}{3 n^2 S^0 a^2 \beta_0} < 1 \qquad (9)$$

It is possible to find the condition on the highest power adopted by plasma from (9)

$$Q_\beta (\text{MW}) < 350 \frac{\hat{n}^3 (S^0)^2 S_i a V \beta_0}{S^0_{cx} \tau \phi(0)} (1 - \psi_w) \qquad (10)$$

Here $\hat{n}$ is the plasma density in $10^{13}\,\text{cm}^{-3}$, ψ_w is obtained from (9) substituting N by N_w, N_w is the thermal neutral density due to fluxes from the walls, $N = N_\beta + N_w$, $N_\beta = S^0_{cx} \Gamma_\beta \phi / (S^0 S_i n V)$ is the thermal neutral density, born by the beam, $S_i = \sigma_{ii} v_i + \sigma_{ie} v_e$.

For T-11 $a = 20$ cm, $\mathcal{E}_0 = 20$ keV, $n = 5 \cdot 10^{13}\,\text{cm}^{-3}$, $N_w \sim 4 \cdot 10^8\,\text{cm}^{-3}$, $\tau/\tau_{iN} = N/3 \cdot 10^8$. In the case $Q_\beta = 0.6$ MW $N_\beta = 4 \cdot 10^8\,\text{cm}^{-3}$, $\psi \approx 1$, $\lambda_0^2 \approx 3$, so the losses are large and defined mainly by the multiple charge-exchange, For ISX-B $a = 27$ cm, $\mathcal{E}_0 = 40$ keV, $n = 5 \cdot 10^{13}\,\text{cm}^{-3}$, $\tau/\tau_{iN} = N/10^8$. In the case $Q_\beta = 2.5$ MW, $N_\beta = 2 \cdot 10^8\,\text{cm}^{-3}$, $\psi \approx 0.8$, $\lambda_0^2 \approx 2$, so the losses

through the simple and multiple charge-exchanges could be the same. In this case, one needs to solve the full integrodifferential equation.

References

1. Grishanov N.V., Dnestrovskij Yu.N., Karetkina N.V., Kostomarov D.P., Fisika Plasmi, 2, N 2, 1976, p.260.

COMPRESSION OF PLASMA JETS ($\beta=1$) IN A CONIC LINER AND THEIR COLLISION

V.V.Gavrilov, N.V.Goryacheva, I.V.Ilyushin, V.N.Liashenko, Yu.V. Skvortsov, V.M.Strunnikov, S.S.Tserevitinov, N.S.Shkvarina

I.V.Kurchatov Institute of Atomic Energy, Moscow, USSR

The 10-fold adiabatic compression of a dense plasma jet with $\beta=1$ in a conic liner has been experimentally obtained. Plasma with $n=2\div3\cdot10^{16}$ cm^{-3} and $\theta_i=1\div1.5$ keV has been obtained at the collision of such jets.

The plasma filling and confinement scheme, with $\beta=1$, in a mirror trap mith minimum B are described and based theoretically in paper [1]. The trap consists of a linear part with passive liner filled with the field and spindle casp traps at the ends. The type MK-200 accelerators are used for filling the trap with plasma. It has been shown that the Lawson criterion can be reached in the system with characteristic length $L\approx10$m, with the energy W=50÷100 MJ stored in plasma, with the circular slit width in the spindle casp traps not greater than the ion Larmor radius, $r_{i\omega}$, and the ignition of a subcritical hybrid reactor with U^{238} can be provided at $W\approx10$ MJ [2]. The modern accelerators with efficiency $\eta\approx30\%$ produce plasma jets with the energy 150-200 kJ. An effective thermalization due to Coulomb interactions and due to development of instabilities has been observed at the collision of such jets within the cylindrical liners.

For a trap with B_{min}, $\tau_c''=G\tau_\theta''$, where $G=2.65\cdot10^{-9}\sqrt{N(1+\frac{\theta_e}{\theta_i})}$. Here, τ_c'', τ_θ'' is a confinement time for particles in the trap and in the θ-pinch respective to the end-losses, N, cm^{-2}, is the linear plasma density, θ_e and θ_i are electron and ion temperatures. The spindle casp fields seem to be expedient only when $G\gg1$. Attention to the dependence $G=f(\sqrt{N})$ was first given by A.Zhitlukhin and V.Sidnev. Let R and r be radii (in cm) of the liner and of the plasma column; $\Delta r=R-r$; B_0 is an initial magnetic field inside the liner (Gs). Then, $\tau/\tau_{i\omega}=6G$; $\Delta\tau/\tau_{i\omega}=4.4\cdot10^{-3}B_0R/\sqrt{\theta_i}(1+\frac{r}{R})$ $\Delta\tau/\tau=7.4\cdot10^{-4}B_0R/G\sqrt{\theta_i}(1+\frac{r}{R})$ and, at last, $n\tau=2\cdot10^{6}GnL/\sqrt{\theta_i}$, cm^{-3}s, $W=3.4\cdot10^{-2}G^2L\theta_i$, J. The values G, L and θ_i are mainly dependent on the injector,

while η depends on the additional external devices.

Operation of the pulsed valves, which provide the initial dose of a gas in the accelerator (I in Fig.1), was forced in this experiment in comparison with [4], a rise in η was provided by a radial plasma compression at the jet motion along the conic liner (2). The cone cross-section area became 10-fold less along 287cm. The inlet diameter is 24.6cm, the cone outlets were matched with the cylindrical liner (6,8), 300cm long, 8cm in diameter, inside which the collision between two jets was provided. The magnetic flux under vacuum conditions inside the liners with the front rise time from 3 ms up to 16 ms was produced with a set of solenoids (3,9) and remained unchanged during the interaction with plasma. It that case, the flux was strictly conserved along the cone axis and it was slightly changed along the central part. At the cone outlet B_o=18 kG, in a symmetry plane B_o =21 kG.

Under adiabatic plasma streaming with β=1 in a conic liner at $B_o(z) \cdot R^2(z)$=const and N=const, the plasma compression coefficient $K=P_2/P_1$ depends on a decrease in the pipe cross-section, $m=S_1/S_2$, in the following way: $B_{e1}/B_{o1}=1-K^{1/\gamma-0.5}/1-m^{-1} \cdot K^{1/\gamma}$. Here, B_{e1} is the magnetic insulation field at the initial cross-section. P_1 and P_2 are transversal plasma pressures at the initial cross-section and at the final one.

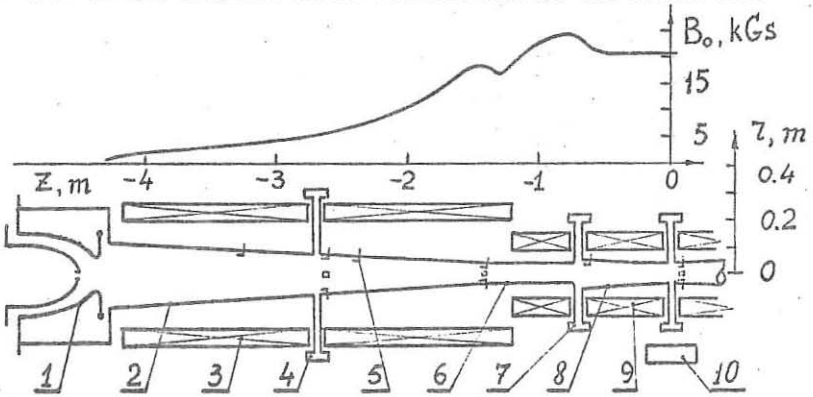


Fig.1. 1-accelerator; 2-conic liner; 3,9-solenoids; 4-port (interferometer); 5-magnetic probes; 6-liner; 7-port (interferometer, X-rays, visible lines); 8-central liner; 10-neutron detectors.

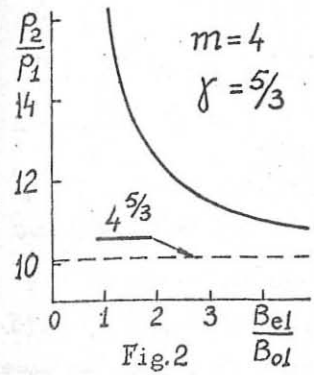


Fig.2

This dependence for m=4, γ=5/3 is shown in Fig.2 where an increase in B_0 at each cross-section, when B_e/B_0 the magnetic fild exceeds the degree of compression. The hydrogen plasma jets were produced in the experiment by the accelerator at its voltage U= =12 and 25 kV, when the energy stored in the condenser bank was equal 50 and 225 kJ, the energy of ions in the jet $\mathcal{E}_i$=0,2 and 2.5 keV. The jets in their motion became longer and at the cone outlet the jet heads turned to be separate clusters. Duration of the diamagnetic signals produced by these clusters does not exceed 1.5÷2 μs at U=25 kV. At that time, the field strength in the gap between plasma and the liner was raised from B_{02}=18 kG to B_{e2}=31 kG that gives $\beta \gtrsim 0.95$ in accordance with the field measurements inside plasma. The process of compression was studied in a narrow part of the cone, for which m=4. $K=12$, measered in the experiment; $\gamma = \ell g K / \ell g (r_1/r_2)^2$ coincides with γ=5/3. The plasma output pressure P =2.5.10^{19} eVcm^{-3}, that allows to expect n_2=(4÷8).10^{16}cm^{-3}, i.e. G=3÷4, when n_1=(1÷2).10^{16}cm^{-3} and the value of K is taken into account. The expected sum $(\theta_e+\theta_i)_2 \sim$300÷600eV is completely determined by ions as the measurements of the ratio between the line intensities C^{IV}/C111 gave $\theta_e \gtrsim$20 eV. $\Delta\gamma/\gamma_{i\omega}$-ratio in the adiabatic process has a weak dependence on the radius. In the experiment, $\Delta\gamma/\gamma_{i\omega}$=10 and 30 when U=25kV and 12kV, and this ratio is not changed along the cone within the error bars.

The complete jet separation during its flight was not observed in the operation with deuterium, K-values were less than the expected ones by a factor 0.6. The experimental results obtained in the central liner(8) at U=20 and 25kV without a collision(S) and with a collision(C) are given in comparison with [4] (R=15cm) in Table 1. The subcripts P, R, J designate the measurements made with probes, X-ray foils and with the neutron sensitive elements. Out of this Table one can see-that n was increased by 1.5 orders of magnitude

U kV			$v\times10^{-7}$ cm·s^{-1}	$n\times10^{-15}$ cm^{-3}	ℓ cm	$N\times10^{-17}$ cm^{-2}	G	$\frac{\Delta\tau}{\tau_{i\omega}}$	$\sum_{e,i}\theta^{\rho}$ keV	θ_e^{R} keV	θ_i^{τ} keV	$\tau_{0.1}^{\tau}$ μs	$\tau_{0.1}^{\rho}$ μs	τ_{ii} μs	λ_{ii} m
20	S		4	30	2	4	1.1	12	0.6						
		[4]	6	1	3.5	0.4	0.7	11.5	1	0.025	1				
	C			30	2.9	8	2.5	10	0.95	0.2	0.7	12	16	3	1
		[4]		0,8	7	1.4	1	7			2.2	15	40	600	300
25	S		5.5	20	1.4	1.25	0.95	11.5	0.8	0.1	0.65		1.5		
	C			15	2.5	3	1.5	9	1.7	0.2	1.5	10	20	17	7,5

in comparison with [4], N in the jet was increased by the order of magnitude. An effective thermalization of ions was observed at the collision of jets. It is confirmed by the 3÷5-fold rise in the signal from the magnetic probe. This rise is equal to $\Delta B=B_e-B_0$; the time of its existence, τ^{ρ}, also rises by order of magnitude. In the absence of thermalization, in accordance with the relationship $\frac{\Delta B_e}{\Delta B_S}=(4\chi)^{1/\gamma}\left(B_{eS}/B_{eO}\right)^{\frac{\gamma-2}{\gamma}}$, this ratio would have not greater than a 1.5-fold rise only. Here $\chi=\left(\frac{1}{3}\varepsilon_i+\frac{1}{2}\theta_S\right)/\theta_S$. The contribution of electrons into pressure is negligibly small. The times τ^{ρ} and τ^{τ} after interaction are found to be of the expected order or greater (i.e. $\tau''=\frac{2L}{v}$ as well as $\tau_{BOH}^{\perp}$). The neutron yield at the intersection of jets was $8\cdot10^{8}$ (up to $1.5\cdot10^{9}$) and $1.5\cdot10^{8}$ at U=25 kV and at 20 kV, and their intensity $J=2\cdot10^{14}s^{-1}$ and $2.5\cdot10^{13}s^{-1}$, respectively. Their origin can be dependent on the target effect at the encounter of the beams as well as on the radiation of the maxwellian plasma or (at 25 kV) of that with monoenergetic spectrum. But the first mechanism can be neglected in 2 us after the beginning of the signal arrival.

References: 1. V.M.Alipchenkov et al. Preprint IAE-2753, M (1976). 2. I.K.Konkashbaev, L.P.Feoktistov. Preprint IAE-3253/8, M, (1980). 3. V.M.Alipchenkov et al. Pr.IAE 2751, M (1976). 4. V.M.Alipchenkov et al. IAEA, Brussels (1980), p.CH-38/Z-3.

PLASMA FOCUS STUDIES AT ENERGIES UP TO 250KJ

V.I.Krauz, R.G.Salukvadze, E.Yu.Khautiev
Sukhumi Institute of Physics and Technology
of the State Committee on Utilization of Atomic
Energy, Sukhumi, USSR.

ABSTRACT. The chief parameters of the power supply for the KPF-3 device and the discharge system design features are described and preliminary experimental results are given.

The power supply for the KPF-3 device consists of four condenser bank compartments, with the total energy, W_{max}=250 kJ at V_{max}=40 kV. Energy values may range from 25 to 250 kJ as a result of change in capacitance and in the initial voltage too.

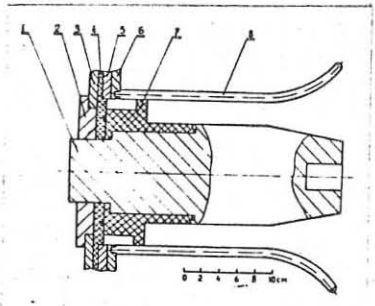


FIG.1

Fig.1 shows a schematic of the coaxial plasma accelerator used as a discharge system. The inner electrode (1) is connected to the collector plate (3) by means of a flange (2). Another plate (5) is used to be connected to the outer electrode which consists of 24 pins and a flange (6). Both electrodes are made of copper and are shaped as it is

shown in Fig.1. The accelerator insulator (7) is of china, while that of collector is made of Teflon.

Plasma focus investigations are carried out within the energy range from 25 kJ to 150 kJ. Stable neutron regimes are obtained for the whole range. The peak neutron output of 1.2 10^{11} n/discharge is produced at W=140kJ. The accelerator used is most optimally matched with the power supply at W=100 kJ.

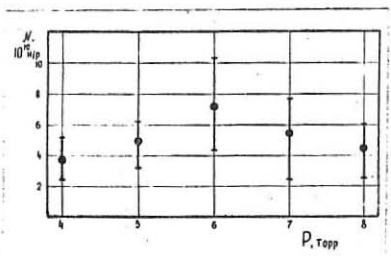


FIG.2

Fig.2 shows the neutron output (W=100 kJ) versus the initial pressure of deuterium in the vacuum chamber. Neutron output values are shown averaged over 10 discharges under stationary initial conditions and scatters are indicated for each of the series. For P_o=6 Torr the peak neutron output amounts to 10^{11} neutrons per discharge.

Discharge dynamic characteristics are defined by analyzing the traces of the total discharge current in the circuit and its derivative and by photorecording from the discharge chamber ends. The radial compression phase of the current layer behind the inner electrode end starts after 3 μs from the discharge beginning. Fig.3 shows the traces for the current I, dI/dt and for the neutron pulse recorded by a recorder placed 4 metres away. The pictures were taken for the discharge

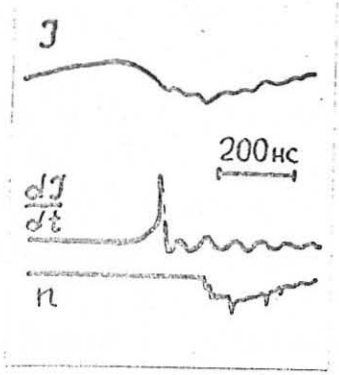


FIG.3

at W=144 kJ ($N=10^{11}$ n/discharge). The compression region geometry is well illustrated in soft X-ray time-integrated photoes (9μm and 18μm Al) and in spectrograph traces of the discharge within the visible range taken under the conditions when an axial region extending over 20 mm from the anode end is projected to the spectrograph entrance slit (Fig.4). In both cases pictures were taken normal to the discharge system axis. A complicated structure of the soft X-ray emission is well seen. This structure is ~40 mm in length, its lateral dimensions being ~ 4 mm.



FIG.4

The region with intense continuum radiation within the wavelength range from 2600 Å to 6200 Å has larger lateral dimensions, ~ 20 mm. Spectrograph traces of majority of discharges show two or more continuum

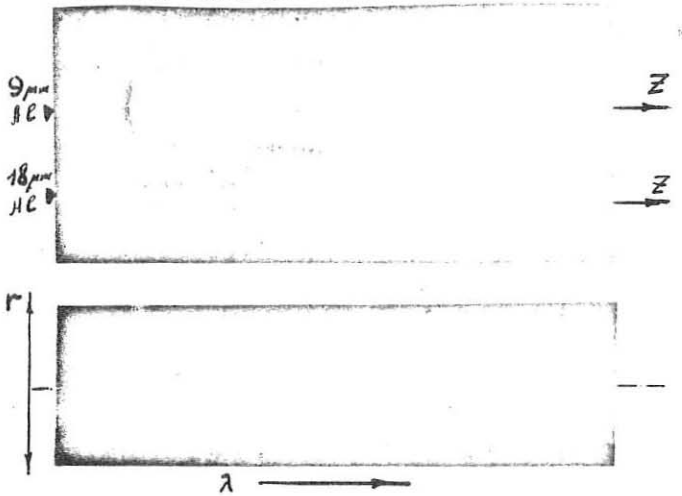
intensity lines indicating several dense regions formed within the cumulation zone.

Hard X-rays ($\gtrsim$ 100keV) of the electrons accelerated in the plasma focus and bombarding the anode, are emitted by the central region of the inner electrode being ~ 10 mm in diameter.

Extending the energy storage range for the KPF-3 device, it is proposed to carry out parametric measurements of ion beams generated in the plasma focus which are responsible for the chief part in the neutron output. Combined plasma focus systems [I]will be explored as well in order to intensify beam generation processes in plasma focus by means of an auxiliary additional discharge.

REFERENCES

1. E.Yu.Khautiev, V.I.Kraus. Plasma Focus in a Three-Electrode System. Proceedings of the IY All-Union Conference on Plasma Accelerators and Ion Injectors. Moscow, 1978, p.99-100.



ULTRA-HIGH DENSITY PLASMA EXPERIMENTS: MHD SIMULATIONS

J. H. Brownell, I. R. Lindemuth, T. A. Oliphant, D. L. Weiss
Thermonuclear Applications Group
Applied Theoretical Physics Division
Los Alamos National Laboratory
Los Alamos, NM 85545 U.S.A.

ABSTRACT

High density, laser-initiated, gas-embedded Z-pinch experiments which are being performed at Los Alamos are being treated computationally using a two-dimensional magnetohydrodynamic computer code. All aspects of the experiment are modeled including the laser-optics system, the Marx-bank/transmission line, electron avalanching, and the experimental diagnostics. Experimental observations have been reproduced very well. The plasma produced in the experiments has $n_e > 10^{20}/cm^3$, T=200eV, and $n_e\tau > 2x10^{13}$ s/cm^3.

Advances in pulsed power technology have made it possible to build a new type of plasma device, a laser-initiated, gas-embedded Z-pinch in which the plasma is primarily ohmically heated[1]. A device characterized by an energy of 70kJ and a peak charge voltage of 600kV has produced a plasma with $n_e > 2x10^{20}/cm^3$, T=200eV and $n_e\tau > 2x10^{13}$ s/cm^3; two-dimensional magnetohydrodynamic(MHD) computer calculations have reproduced the experimental observations to a very satisfactory degree[2]. In this paper we describe our computational model, computed results, and predictions.

Our computations model all aspects of the experiment. A voltage is applied across the electrode gap, an initiating laser is discharged along the axis, and current flows between the electrodes to create a hot, dense plasma column. In the computations a laser-optics package computes the temporal and spatial evolution of the laser profile in the discharge chamber. A Marx-bank/transmission-line package computes the temporal evolution of the self-consistent voltage across the discharge chamber. An electron avalanche model uses a non-linear Ohm's law to compute the spatially and temporally dependent electric field and the resulting non-uniform increase in electron density. When current flows, two-dimensional MHD calculations determine the spatial and temporal evolution of the plasma density, plasma temperature, plasma velocity, and magnetic field profiles. The MHD

model includes thermal conduction, resistive diffusion, radiation, dissociation, and ionization in addition to the Lorentz JxB force in a fluid description of the plasma. The charged-particle transport coefficients are "classical" and the atomic processes are based on local thermodynamic equilibrium(LTE). An extensive post-processor computes spectra from infra-red to x-ray frequencies, temperatures based on x-ray absorption by two different thicknesses of aluminum foil, and Schlieren shadowgrams, all of which can be compared directly to experimental data.

The plasma is formed in a chamber containing 3atm of H_2 between electrodes spaced 10cm apart. A current channel is formed from the pulse of a 5 J neodymium-glass laser which is focussed along the symmetry axis and which is fired near the peak of the voltage across the electrodes($\approx$400kV). The current rises to 250kA in 200ns.

According to our computations the laser initiation is very non-uniform and hence the initiation process is a complex two-dimensional one involving virtual electrode formation and streamer propagation. However, our two-dimensional calculations indicate that the plasma column is remarkably one-dimensional for greater than 75ns. Typical radial profiles are shown in Fig. 1; the mass density profile shows a shock wave propagating into the neutral embedding gas. Later in time an m=0 instability occurs in the computations when the central column expansion is stopped by the magnetic force. Even after the occurrence of the m=0 instability the computations reproduce the experimentally observed Schlieren shadowgrams(Fig. 2), "two-foil x-ray" temperatures(Fig. 3), and visible light measurements where the computed non-uniform source rate and corresponding plasma reabsorption are taken into account(Fig. 4). The computed shadowgram diameter of Fig. 2 corresponds to the front of the outward moving shock wave shown in Fig. 1; the actual current carrying channel is significantly smaller in diameter than the shadowgram and has a diameter of less than 1.5mm at 200ns. After an initial rapid rise the temperature reaches a plateau (Fig. 3) even though the current continues to rise.

According to the computations this is due to mass accretion into the column from the embedding gas, a two-dimensional effect caused by enhanced coupling of energy from the hot core to the outside as a result of the m=0 instability and by continued electron avalanching in the embedding gas.

Our MHD code has been used to scope out other possible modes of operation. These modes include operating at higher voltages, reducing and increasing the fill pressure, and using narrower, more intense laser beams. Our computations predict that higher fill pressures or narrower laser beams can lead to significantly higher temperatures although the m=0 instability may limit performance.

Our computations have been useful in the interpretation of experimental data and in the prediction of new experiments and the computed results appear to verify our initiation and MHD models. Questions remain to be answered on the nature of the instabilities and their effect on limiting the ultimate plasma temperature.

References

[1]R. S. Pease, Proc. Phys. Soc. B 70, 11(1957); D. A. Tidman, App. Phys. Lett. 20,23(1972); M. G. Haines, Proc. Phys. Soc. 76, 250(1960).

[2]L. A. Jones, K. H. Finken, A. Dangor, E. Kallne, S. Singer, I. R. Lindemuth, J. H. Brownell, T. A. Oliphant, App. Phys. Lett. 38, 522(1981); I. R. Lindemuth, J. H. Brownell, T. A. Oliphant, D. L. Weiss, submitted for publication in J. Appl. Phys.(1981).

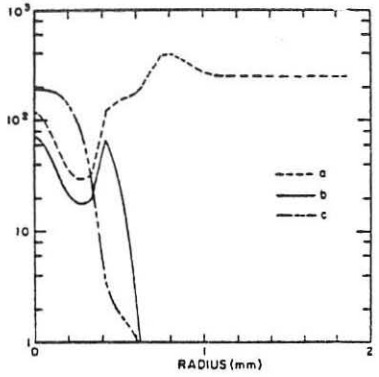


Fig. 1

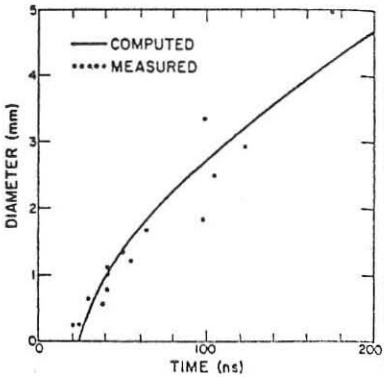


Fig. 2

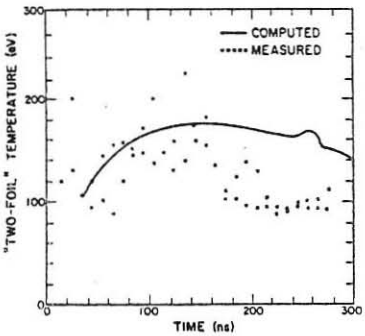


Fig. 3

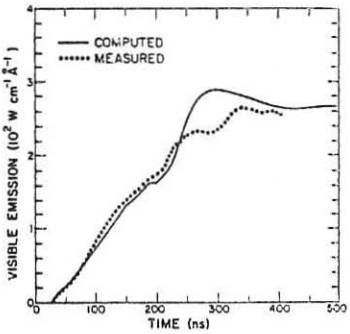


Fig. 4

Fig. 1. Typical Radial Profiles at 75ns: (a) Mass Density-10^{-3}kg/m^3; (b) Electron Number Density-10^{18}/cm^3; (c) Temperature-eV.

Fig. 2. Computed and Measured Schlieren Shadowgram Diameter.

Fig. 3. Computed and Measured "Two-Foil x-ray" Temperature.

Fig. 4. Computed and Measured Visible Emission at 4000 angstroms.

FIRST EXPERIMENTS ON ION-CYCLOTRON PLASMA HEATING ON L-2 STELLARATOR

Batyuk V.A., Grebenshchikov, S.E., Kovan I.A.[x], Meshcheryakov A.I., Moroz P.E., Sbitnikova I.S., Sukhodl'sky V.N., Khudolleev A.V., [xx] Spiegel I.S.

Lebedev institute on Physics, Academy of Science of the USSR

Results of first experiments on ion cyclotron heating of plasma in L-2 stellarator [1] (R = 100 cm, a_p = 11,5 cm, l = 2) are presented. Heating was investigated for deuterium plasma with a small fraction hydrogen (5 to 9%). Plasma was obtained by ohmic heating with gas puffing. Plasma parameters before ICRH pulse are the following: $\bar{n}_e = 1.5 \pm 2.5 \cdot 10^{13}$ cm^{-3}, Te(o) = 300-400 eV, T_i(o) = 65-85 eV, P_{OH} = 80-90 kW. The exciting antenna fabricated as stainless still nearly half-turn (angular size θ = 207°) coil (crosssection 25x3 mm^2) halfloop with double electrostatic screen was placed inside the vacuum vessel out of separatrix (Fig.1). Fast magneto-auqustic waves at the second harmonic of deuterium ion cyclotron frequency (f = 21.7 MHz) were excited.

Experiments of this kind were carried up to now on tokamak devices (see, e.g. [2-5]). In a tokamak magnetic surfaces B = const are circular, their centers coinsiding with the torus major axis. Stellarator magnetic field structure is much more complicated. Fig.2 shows two cross sections of B=const surfaces in two toroidal azimuthes. Solid lines - in the azimuth of the antenna (separatrix in also shown), dashed lines - at Δz = 11 cm. It is seen that two domains exist where cyclotron resonant conditions are agreed.

High frequency power was feeded through two 3/4-wave lines from the push-pull generator. The maximal voltage between antenna ends and vacuum vessel was up to 12 kV in this experiment.

High frequency probes situated in different points along the torus registed oscillation excited in plasma. When ion cyclotron resonant conditions were met, the ponounced absorbtion of high frequency power were observed (damping length

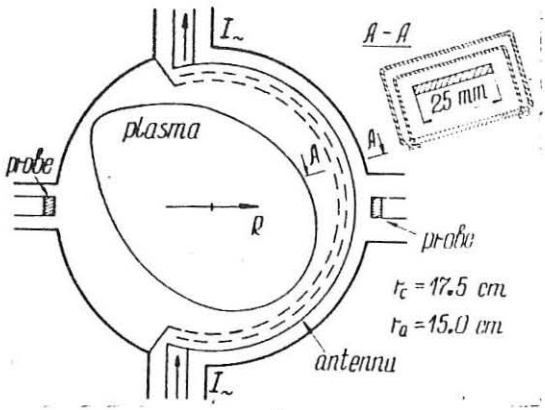


Fig. 1

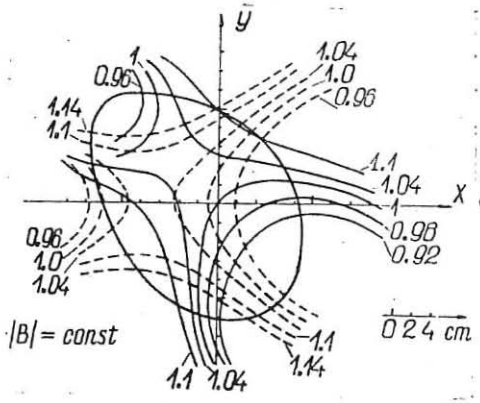


Fig. 2

ℓ < 1 m). The maximal high frequency power absorbed in plasma was 50-60 kw in this experiments. The antenna impedance was about 0.5-1 Ohm. Heating pulse duration - 3 to 4 msec. Ion temperature was measured with 5-channel charge-exchange particle analyzer with magnetic mass separation. When resonant conditions were met at B=14.2-15 kOe strong heating of hydrogen component was observed. Fig.3 shows energy spectra of hydrogen atoms for OH and ICRH measured through central chord. In the second case spectrum has a pronounced non-maxwellian character. Ion quasi-temperature varies from 150 ev for low energies to 4 keV at energy range of 5 to 7 keV. Fig.4 shows characteristic deuterium spectra. Bulk deuterium temperature was derived from the spectrum slope for energies from 200 to 800 ev. For energies higher than deuterium distribution almost always was observed to be non-maxwellina. Deuterium heating in coulomb collisions with hydrogen atoms appears to be accompanied with direct heating in high frequency field. As a result of ICR-heating deuterium temperature was rised up to T_i = 100 - 120 eV; ΔT_i usually equals to 30-50 eV. The heating efficiency was about 1 ev/kw for $\bar{n}_e = 2.10^{13}$ cm^{-3}. Maximal heating was observed for the center of plasma colomn, though it's profile is more flat than for OH (fig.5).

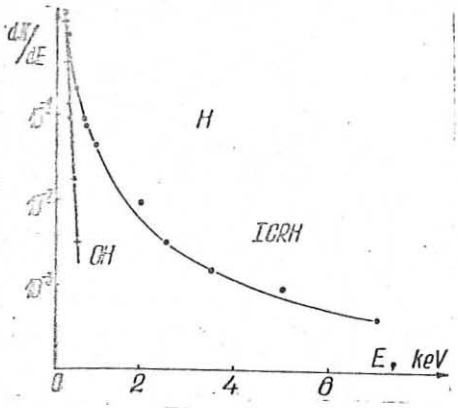


Fig. 3

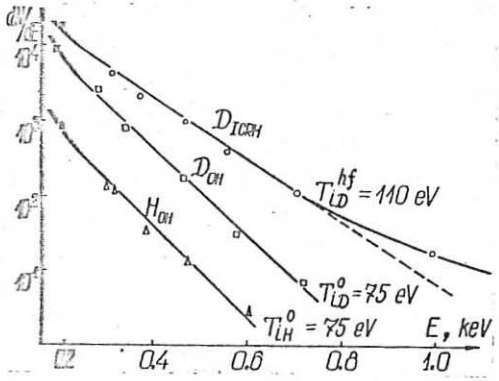


Fig. 4

Typical example of ion temperature time evolution is shown in fig.6. Ion temperature grows during high-frequency pulse and decays with characteristic time about 1 msec. Though average plasma density has never grown more than 10-15%, impurity flux from walls (particulary Fe) was observed to increase, that implied to increase of resistance and radiative losses. In order to eliminate influence of these effects on the discharge parameters, the heating pulse duration was restricted at 3-4 msec.

Thus, first experiments on IC RH in L-2 stellarator has indicated rather high efficiency of plasma heating in complicated magnetic field configuration for relatively low level of input power $P_{EF} < P_{OH}$. Value of input power was resticted by both weak coupling between plasma and antenna because of geometry (elliptic plasma, circular loop) and isolation of feeders. Along with classical mechanism of energy transfer from hydrogen to deuterium, direct heating of deuterim appears to play role, that leads to high energy tail in deuterium spectrum.

References

1. Akulina D.K., Andryukhina E.D., Berezhetsky M.S. et al. Plasma Phys. and Contr. Nucl. Fus. Res., IAEA, Vienna,

v.I, p.115, 1977.
2. Ivanov N.V., Kovan I.A., Los' E.V. JETP Lett. 14, 138, 9 1971.
3. TFR Group, 9th Europ. Conf. on Contr. Fus. and Plasma Phys., Oxford, 1979, p.355.
4. J.Hosea, D.Boyd, N.Bretz et al. 8th Int. Conf. on Plasma Phys. and Contr. Nucl. Fus. Res., Brussels 1980, IAEA-CN-38/D-5-1.
5. H.Kimura, K.Odajima, S.Iizuke et al. ibid. IAEA-CN-38/D-5-2.

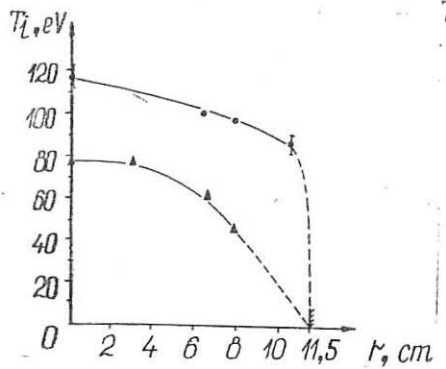


Fig. 5

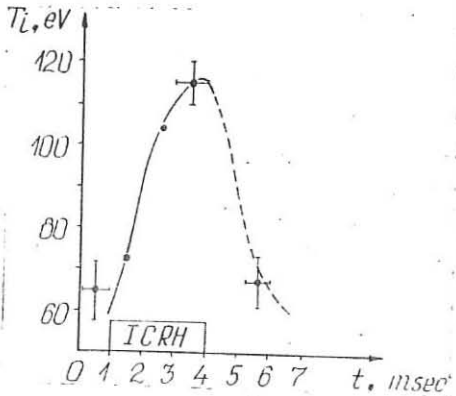


Fig. 6

x Kurchatov Institute of Atomic Energy.
xx Ioffe Physical-Technical Institute.

PRELIMINARY RESULTS FROM THE OHTE EXPERIMENT

T. Ohkawa, R. R. Goforth, G. L. Jackson, R. J. La Haye
M. J. Schaffer and P. L. Taylor

General Atomic Company, United States

1. Introduction

OHTE [1] is a new high shear toroidal pinch configuration with helical symmetry and pitch reversal, consisting of helical windings added around a reversed field pinch (RFP). Like the RFP [2], OHTE is stabilized primarily by shear, a conducting shell and pitch reversal. The helical field acts primarily near the plasma boundary and produces a translational transform in a direction chosen to augment the pitch reversal. As a result, reversal can be obtained theoretically with little or no plasma current in the cold, resistive edge region. The calculated reversal is also found to be less sensitive to the plasma current profile than similar RFPs. The OHTE plasma is bounded by a separatrix which behaves theoretically as a magnetic limiter, and open field lines just outside the separatrix might also permit some line tying stabilization to take place. The OHTE Confinement Test Experiment, which was built to test these concepts experimentally, has been in operation since late February, and preliminary results, obtained primarily with RFP plasmas, are reported.

Minimum energy OHTE states, constrained by the conservation of magnetic helicity $K = \int \vec{A}\cdot\vec{B}\, dV$ as first suggested by Taylor [3], are like axisymmetric RFPs and must satisfy $\mu_o\vec{J} = \mu\vec{B}$ with μ a constant. $\vec{A}$ is the magnetic vector potential and the other symbols have their usual mks meanings. Such states are readily found analytically for plasmas enclosed by straight, helically modulated conducting boundaries [1]. Experimental RFP plasmas tend to relax by instabilities toward Taylor's ideal state, and if the magnetic field line pitch $P = qR$ is monotonic and reversed, they become more quiet as they do so [2]. Similar behavior is anticipated for OHTEs.

Taylor states require large plasma currents out to the boundary. However, transport processes tend to cool the edge, peak the current on axis and may also overheat the plasma to excessive pressure in the interior. Internal turbulence associated with the latter two phenomena may be tolerable provided the turbulent core is surrounded by an effective confinement layer, but the cooling increases $d(\vec{j}\cdot\vec{B}/B^2)/dr$ and decreases shear, both of which favor resistive tearing. In terms of Taylor's theory, transport pushes a steady state, driven discharge to a

Max-Planck-Institut für Plasmaphysik

higher energy state, from which it is then continuously relaxing, dissipating plasma free energy to maintain adequate current in the resistive boundary plasma (plasma dynamo). This process may govern the the energy confinement.

Without a strong plasma dynamo, steady state reversal is impossible in axisymmetric systems. Using classical parallel and perpendicular resistivity and an anomalous, constant κ cross field thermal conductivity in a 1-D time independent transport code, the pitch increases monotonically because current is small near the cold edge. The force-free paramagnetic model [4] is misleading in this respect, because it ignores the inevitable temperature gradient. Monotonically decreasing P(r) are obtained if an electric field E_α parallel to B is added to represent the dynamo, provided E_α exceeds about twice the axial electric field and is peaked at 70-80% of the plasma radius. Translational transform in OHTE can augment the pitch by up to 20% of the central pitch [5]. The transform significantly reduces the dynamo requirement and substantially increases shear at the edge.

II. Preliminary Experimental Results

The OHTE experimental apparatus was described in [6]. It has a major radius of 1.24 m, a stainless steel bellows vacuum chamber with a 187-mm minimum inner radius, a 15-mm thick aluminum conducting shell of inner radius 199 mm, and an $\ell = 3$, $n = 16$ helical winding (H-coil) with a 45° average pitch angle, which provides both the desired toroidal and helical fields. Plasma current is driven by a multiple stage capacitor bank through an air core induction coil. Toroidal flux is conserved by the conducting shell, and only the self-reversal mode of operation is possible. RFP discharges have been made using toroidal electric from 25 to 100 V/m, abnormally low for RFPs, and RFP setup takes 0.3 to 1.0 ms. Volt-second consumption up to the time of reversal is presented as a function of initial toroidal field in Fig. 1. Although there is some voltage dependence, the main result is that above about 0.1 tesla most of the V·sec can be accounted for by the theoretical plasma inductance. Therefore, slow self-reversed RFP formation is not excessively lossy, except at low fields. Similar data from other RFPs of different minor radii would be desirable to resolve whether toroidal flux or field is the critical variable.

OHTE plasmas are produced by establishing the desired toroidal and helical fields through the conducting shell before the discharge is initiated. The gas breaks down easily in this initial stellarator-like field. However, helical field yields decreased rate of current rise, and increased apparent plasma resistance during setup, which is evident in Fig. 1. With the existing capacitor bank, reversed OHTEs have been made only up to 0.03 tesla toroidal field and 110 kA plasma current. All magnetic signals and the positions of the helical swaths of light seen in time-resolved imaging photographs are consistent with the expected OHTE configurations. Impurity light is usually somewhat less in OHTE shots.

Both RFP and OHTE discharges in the OHTE device inevitably follow an F - Θ trajectory ($F \equiv B_t(b)/\langle B_t \rangle$, $\Theta \equiv B_p(b)/\langle B_t \rangle$, b = shell radius) well to the right of Taylor's prediction, which is much too large to explain by finite β. It can be modeled by a Bessel function model (BFM) plasma of radius a surrounded by vacuum with a/b ≈ 0.7. See Fig. 2. Recent magnetic probe measurements in low current pinches, Fig. 3, confirm the a/b inferred from (F,Θ) and show in addition that the B profiles are a little more peaked than the BFM. The axisymmetric B component profiles in OHTEs are very similar.

A preliminary RFP scaling has been performed. Plasma resistance was measured when d(LI)/dt was small, while density was calculated from visible continuum emission and remained roughly constant. Magnetic fluctuations were measured between the liner and shell (liner cutoff frequency ≈ 50 kHz). The Spitzer temperature increases approximately in proportion to toroidal plasma current, while the fluctuation level is consistent with $\tilde{B}/B_0 \sim S^{-1/2}$ where $S = \tau_{resistive}/\tau_{Alfven}$. See Fig. 4. This latter was predicted theoretically at Culham [7] and, if correct, is a favorable scaling for fusion.

Acknowledgment

Work supported by Phillips Petroleum Co. and General Atomic Co. under Joint Research & Development Agmt. (GA Reference No. 01341).

References

1. T. Ohkawa, M. Chu, C. Chu and M. Schaffer, Nucl. Fusion 20 (1981) 1464.
2. H. A. B. Bodin and A. A. Newton, Nucl. Fusion 20 (1980) 1255.
3. J. B. Taylor, Phys. Rev. Lett. 33 (1974) 1139.
4. B. B. Kadomtsev, Nucl. Fusion Supplement, Part 3 (1962) 969.
5. C. Chu, M. J. Schaffer, R. J. La Haye and T. Ohkawa, General Atomic Company Report GA-A16336 (1981), to be published in Trans. on Plasma Sci. (1981).

6. F. A. Puhn and G. L. Jackson (Proc. Technol. Controlled Nuclear Fusion, King of Prussia, PA, 1980, Natl. Tech. Info. Service, 1981) III, 871.
7. P. G. Carolan et al. (IAEA Innsbruck Conference, 1978) 23.

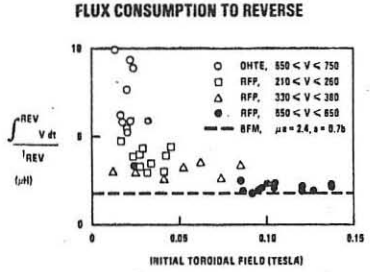


Fig. 1

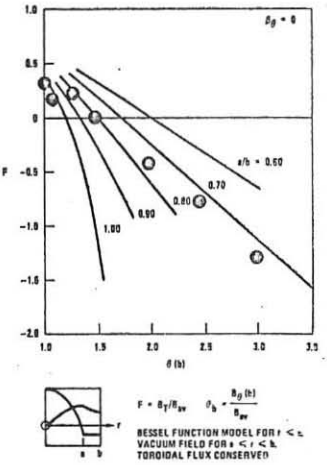


Fig. 2

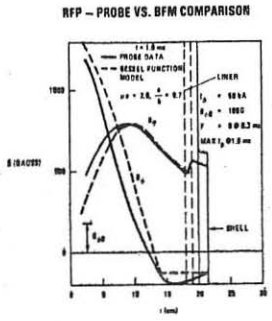


Fig. 3

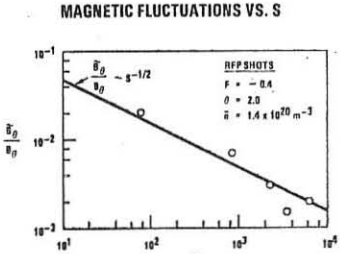


Fig. 4

PRELIMINARY EXPERIMENTS IN THE HEATING SPHERICAL TARGETS AT "DELFIN-1"

N.G.Basov, A.E.Danilov, Yu.A.Mikhailov, G.V.Sklizkov, S.I.Fedotov

Lebedev Physical Institute of Academy of Science of the USSR

Moscow, USSR

The installation "Delfin-1" has been planed for heating and compression of thermonuclear targets in ablative regime /1/ at a level of the absorbed energy of 1÷2 kJ. The scheme of the installation is shown in Fig.1. The basic part of it is powerfull Nd-laser, which designed to generate 3÷4 kJ during 0,5÷5 ns in six composed beams (CB). The laser construction is based on a principle of suxcessive-parallel amplification /2,3/. 108 elementary beams with an aperture of 40 mm each are formed at the output.

From the output of the laser all the beams are directed into the focusing system consisting of the elements, shown in Fig.2. The effective focal length of the system is 787 mm. F-number is 1/2,4.

The target chamber is a metallic spherical ball with windows for laser radiation, diagnostics, target supporting, vacuum guide and other auxiliary units. The target alignment unit makes it possible to tune a target at a given point with the accuracy of 1 μm along all three coordinates. The accuracy of the target pointing is 10

Basic parameters of the radiation at some points of the system have been measured experimentally, mainly,

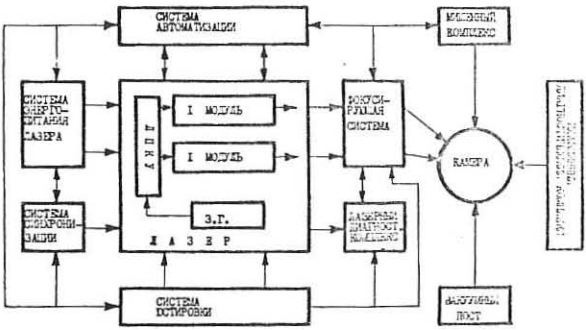


Fig. 1. The scheme of "Delfin-1."

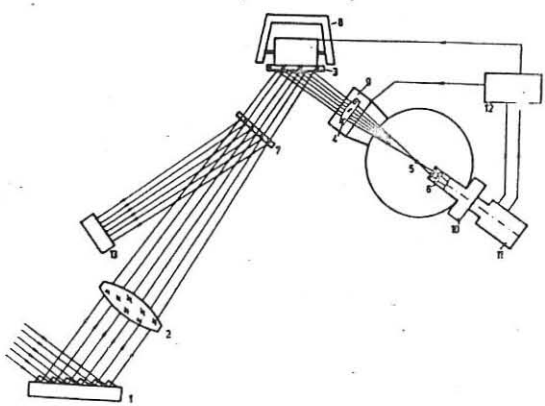


Fig. 2. 1,3 - mirrors; 2,4 - lenses; 5 - test target; 6-12 - tuning units; 13 - calorimeter.

for the purpose of improvement and development of the laser itself, the focusing system and the target arrangement.

The mean energy of the output radiation was 250 J and the total energy of all six CB was $\sim 1,5$ kJ for the considered preliminary shots. The energy at the target surface was of 700 J, i.e. 50% of output energy of the laser. The energy losses in the beam transport system and in the focusing system consist of the following: 25% due to fresnel losses, 10÷15% due to the losses on diaphragms and 10÷15% of the energy is lost in transportation of CB to the target chamber.

The divergency of CB which is $2\alpha \approx 3,5 \cdot 10^{-4}$ rad, makes it possible to heat spherical targets with a diameter of 300 μm.

The energy contrast ratio determined in one elementary beam is more than 10^6.

The experiments on shell target heating have been perfomed for three target materials (polysterene, glass, copper) having different Z-number. The energy coming onto the target surface varied from 400 to 700 J.

The investigation of heating effectiveness has been conducted mainly by means of X-ray diagnostic methods. These are as follows: crystal spectrometer with high spatial and spectrum resolution, three sevenframe obscure-cameras with ultimate resolution of 10 μm, four channel high f-number crystal microscope with spectral selection, and image converter tube combined with a fast plastic stintillator.

The energy balance has been measured with a system

of calorimeters placed both in the beams and inside the chamber, and with the shock wave method /2/.

The efficiency of absorption of the laser radiation in plasma was ~70%, which corresponds to 500 J absorbed for 700 J incident energy. Thus, total efficiency of laser-target system was 0,35.

Other important parameter for the laser-target system is the efficiency of concentration of laser radiation onto the target. This parameter results in uniformity of the target surface luminousity that is partly distribution of temperature in the corona. These data were obtained by observing spectral and spatial distribution of X-ray radiation from the heated corona. The experiments have demonstrated high enough uniformity of heating, and the value of temperature of 800÷1000 ev at flux density of 10^{14} w/cm^2.

REFERENCES

1. N.G.Basov a.o. JETP, 1980, 78, 1, 420-430.
2. N.G.Basov a.o. JETP, 1972, 62, 203-212.
3. N.G.Basov a.o. in the book "Laser Interaction and Related Plasma Phenomena", Plenum Press, 1977, 4A, 15-42.

PINCHING OF A LASER PLASMA IN A HIGH-CURRENT ACCELERATOR DIODE

S.M.Zakharov, G.V.Ivanenkov, A.A.Kolomensky,
S.A.Pikuz, A.I.Samokhin
P.N.Lebedev Physical Institute, USSR Acad. of Sci.,
Moscow, II7924, USSR

Recently, high current accelerators have been used succesfully as a source of energy for high-speed plasma Z-pinching /I,2,3,4/. Here we present a new method of plasma creation in a high-current accelerator diode.

The experiments were carried out in the vacuum diode of the accelerator "Don" /200 KV, I00 kA, 60 ns/ /5/. The scheme of the experiment is shown in Fig.I. The neodymium glass laser emission /5 J, 30 ns/ was focussed onto an Al-cathode surface through a hole in the anode. The Al-plasma served as the compression object. Processes occuring in the diode were studied by means of five-frame exposure, Q-switched, ruby-laser interferometry and shadow-photography systems /5/. Pin-hole cameras were used to obtain the X-ray image of compressed plasma. The pin-hole camera had four apertures covered with filters consisting of various foils. The cut-off energy of the filters was from 1.5 to 9 keV for different apertures. Highly resolved spectral lines were obtained from the quartz cryastal spectrograph. Two-dimensional resolved, soft X-ray spectral line emission images /Fig.2d/ were obtained by means of a KAP-crystal spectrograph.

The target unloading process is seen in the first

frame of the interferogram /Fig.2b/. The electron plasma density is about 10^{15}-10^{16} cm^{-3} at that instant.(Filling of the diode with plasma have been occured at about one microsecond before the beginning of diode current). The region that is transparent to ruby laser light is seen in the second frame. It has a diameter of about 5 mm.

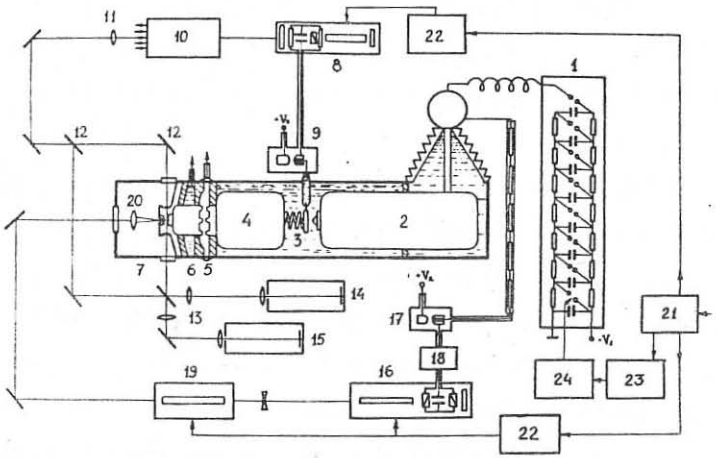


Fig.I. Schematic diogram of the apparatus. a) Accelerator (I-7); b) interferometry and shadow-photography systems (8-I5); c) Nd-glass laser (I6-I9); d) focussing lens (20); e) controlling apparatus (9,I7,2I-23).

The interferometric fringes are blurred at the boundary of the pinch due to the high velocity of the plasma. An instant close to the time of plasma pinching is seen in the third frame both in shadow and interferometric photos. /Fig.2a, Fig.2b/. Pinch disintegration and intence plasma formation at the cathode and anode are seen in the fourth frame.

The plasma colomn is also seen in the pin-hole images /Fig.2c/. The "hardness" of the radiation from the compressed plasma region did not exeed 3.5 keV. Regions radiating quanta of 2 keV energy do not reach the anode, but terminate a few millimeters from it. 9 keV X-ray radiation from the anode cone is also seen in the pin-hole images and it is due to electron bombardment of the anode.

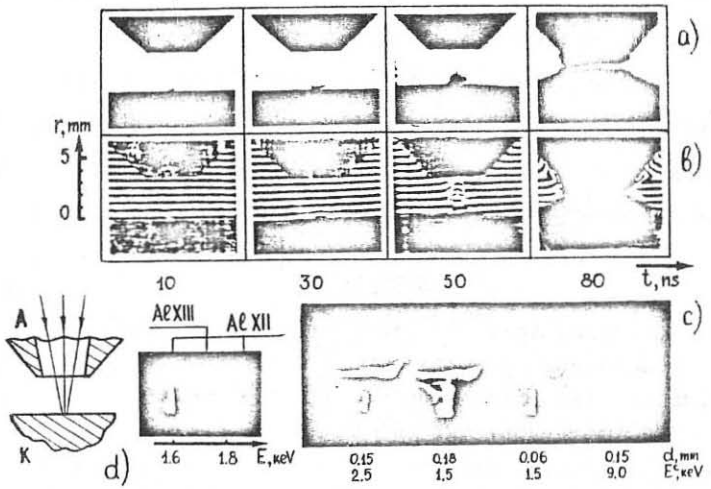


Fig.2. a) Shadow photos of the pinch; b) interferograms; c) soft X-ray pin-hole images; d) soft X-ray spectra.

X-ray spectral lines corresponding to spectra of multicharged Al-ions were observed /Fig.2d/. Plasma parameters were determined by X-ray spectral methods /6/. The change of relative intensities of spectral lines along the plasma column corresponds to an increase of temperature from 200 eV to I keV as the anode is approached. The radiation region of He-like ions has a transversal dimen-

sion of 0.3 mm. "Hot" plasma emission of H-like ions exists in a region having a transversal dimension of about 0.1 mm. The relative intensities of resonance and intercombination lines of He-like ions indicate that the plasma density in the pinch is not less than 10^{20} cm^{-3}. The rate of plasma pinching was estimated from the Doppler broading of the spectral lines, measured by the quartz crystal spectrograph and from the interferograms. It turned out $(1-5)\cdot 10^{7}$ cm^{-3}.

On the whole, the experiments showed that laser plasma pinching in a high-current accelerator diode is efficient as a source of high temperature dense plasma and as a source of multicharged ions and soft X-ray radiation.

REFERENCES

1. P.G.Burkhalter, J.D.Davis, J.Rauch, W.Clark, G.Dahlbacka, R.Schneider, J.Appl.Phys., 50, 705 (1979).
2. C.Stallings, K.Childers, I.Roth, R.Schneider, Appl. Phys.Lett., 35, 524 (1979).
3. S.M.Zakharov, A.A.Kolomensky, S.A.Pikuz, V.M.Romanova, A.I.Samokhin, Pisma v ZhTF, 6, 1223 (1980).
4. S.M.Zakharov, A.A.Kolomensky, S.A.Pikuz, A.I.Samokhin, Pisma v ZhTF, 6, 1135 (1980).
5. S.M.Zakharov et al., in Proceedings of the 14th International Congress on High Speed Photography and Photonics, USSR, Moscow, 1980.
6. V.A.Boiko, A.V.Vinogradov, S.A.Pikuz, I.Yu.Skobelev, A.Ya.Faenov, "Rentgenovskaya Spectroskopiya Lasernoy Plazmy", VINITI, M., 1980.

GENERATION OF A DENSE HOT PLASMA BY FAST COMPRESSION OF SHELLS

R.B.Baksht, B.M.Kovalchuk, V.V.Loskutov, A.V.Luchinsky, G.A.Mesyats

Inst. of High-Current Electr.,Siberian Branch of the USSR AS, USSR

The method of gas compression by an exploding shell /1-3/ is attractive due to the possibility to obtain a high efficiency of the energy transfer into a liner and DT-gas (50 p.c. and 2-5 p.c., respectively). In this work our computational and experimental investigations on perspectiveness of the method developed over the last years are presented. The calculations were conducted according to the one-dimensional magnetohydrodynamical code in a single-temperature approximation /4/.In Fig.1 the behaviour of the liner inner radius and the DT-mixture temperature in a compression phase at 30 MJ initial energy content in storage and 30 MA total current is presented. The calculated neutron yield of the system was of $6 \cdot 10^{17}$. To provide scaling on the basic of the calculations an experimental text of the assumptions contained in them is necessary that may be carried out on machines with much lower energy content than it is necessary for the fusion. Such experiments are supposed to conduct in three stages at current levels through the liner of 400 kA, 1÷2 MA, and 5 MA. At present, on the machine SNOP-I (I_{max}= 400 kA, $di/dt = 6 \cdot 10^{12}$ A/s), we are carrying out the experiments on the elucidation of correctness of a choice of the equation of state and the electric conductance for the

plasma generated as a result of the metal liner explosion. In this case we have used the following circumstance. A process of exploded wire discharge (EWD) is described by the same set of MHD equations as a liner implosion and its subsequent compression. Therefore, by conducting experiments on EWD one can obtain required information. We have carried out experiments and MHD calculations at EWD of copper conductors in vacuum and water /5/. Presented in Fig.2 are the current and voltage oscillograms that have been calculated and experimentally obtained for explosion in water of Cu wire. It is seen that a discrepancy between the calculated and experimental data is small. Note that the results of the calculations turned out to be rather sensitive to the description of the conductance of copper in the range of states at T=10 eV and $\rho = 10^{-2} g/cm^3$ (curve "a" and "b" in Fig.2). When investigating on EWD in vacuum for three typical waveforms and amplitude values of current through the conductor there were calculated by the MHD--code the time dependences of plasma internal energy, density and electron temperature for copper conductors used in the experiment. As distinct from the EWD-in-water calculations, the time dependence of current was taken directly from experimental traces (Fig.3). The calculation results indicate that as internal energy of plasma and its peak temperature are essentially dependent on amplitude and form of a current pulse. Therefore, a measurement of any macroscopic characteristic

that are proportional to Te are rather informative. In our opinion, such a characteristic is the plasma radiation in the wave length range of 1÷40 Å. Shown in Fig.3 are the traces of current and soft X-radiation that corresponds to the three calculated current regimes (Fig.4). It is seen that the initiation of X-radiation coinside in time with a moment of the abrupt rise of internal plasma energy. The amplitude of X-radiation is maximum for the regime 1 in which the internal plasma energy is significantly higher and the conductor expansion velocity appreciable smaller than for the regimes 2 and 3.(see Fig.4). Thus, the experiments have allowed to refine the calculation method and confirmed the correctness of usage of the conductance obtained on the basis of the Thomas-Fermi model with quantum corrections in the specified range of states /6/. Calculations show that at currents of 1-2 MA the appearance of thermonuclear neutrons at level of 10^8 neutron/pulse is possible. The experiments carried out presently on the "Modul" mashine (1-2 MA, 10^{13}A/s) /7/ will be rather representative and allow to proceed to experiments on the "Snop-3" machine with a store of energy about 1 MJ. It is planning to produce current pulse of amplitude 4-5 MA on the "Snop-3" machine in 1982. The calculations show that on the "Snop-3" machine it will be possible to come right up to the equality of energy deposited in gas and energy released as a result of the fusion.

References: 1. P.J.Turchi, W.L.Baker. J. of Appl. Phys. 44(11), 1973. 2. D.H.Daniel, et al. BAPS, 23, 822, 1978. 3. Д.Д.Бакулин и др. Изв.Вузов,Физика,12,1979. С.Г.Али-

ханов и др. Письма в ЖТФ,5,22,1979. 4.В.И.Афонин и др. ЖТФ,№1,1979. 5.Р.Б.Бакшт и др. Письма в ЖТФ,6,18,1980. 6.Н.Н.Калиткин, Л.В.Кузьмина. Препринт ИПМ АН СССР,М., 1975. 7.Новости УТС в СССР,№2,1979.

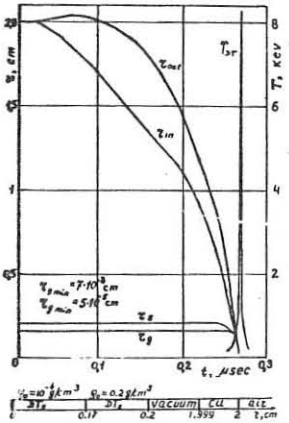


Fig.1. Average gas temperature and radius versus time for liner fusion. W_c=21 MJ, U_o=2 MV, R_o=7.5 $\cdot 10^{-3}$ OM. Subscripts g and s refer to gas and solid state, respectively.

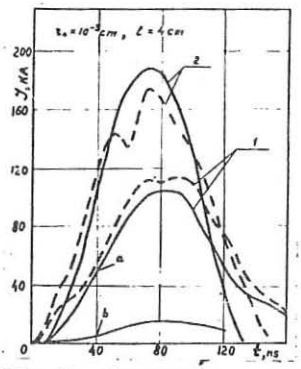


Fig.2. Current versus time for EWD in water (1) and for short circuit of the generator (2). - - - experiment, —— MHD calculation. Average charge of ion obtained from Thomas-Fermi Theory (a) and from Saha equation (b).

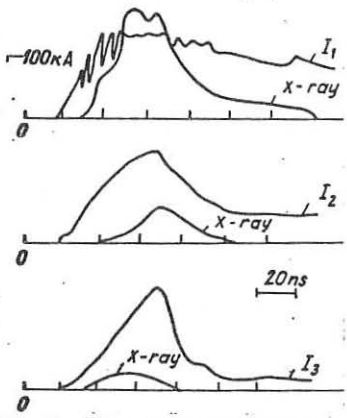


Fig.3. The traces of current and X-ray ($\lambda < 28$ Å) for three regimes.

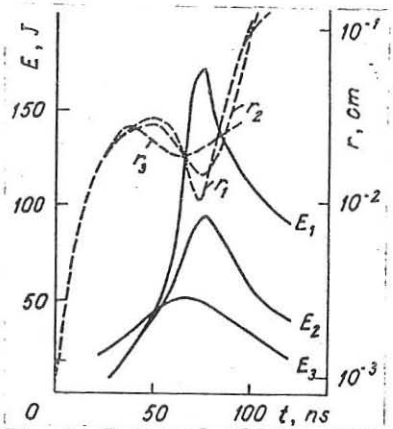


Fig.4. Internal plasma energy and radius of wire versus time. The curves 1,2,3 correspond to the current traces of Fig.3.

ABSORPTION EFFICIENCY OF POWERFUL LASER RADIATION OF VARIED DURATION AT WAVELENGTHS 350 nm - 1 um IN PLASMA WITH DIFFERENT z

A.A.Andreev, V.I.Bayanov, V.I.Kryzhanovsky, V.N.Krylov, A.A.Mack, V.A.Serebryakov, N.A.Solovyov, A.N.Shatsev

The State Optical Institute, USSR

When selecting the parameters of laser radiation for heating and compressing spherical targets, the problems of absorption and scattering of light in a plasma receive primary emphasis. The value of the absorption coefficient depends on many factors including a flux density, wavelength and duration of heating pulse as well as a target material. In this paper the results of the investigation of interaction of powerful laser radiation with planar and spherical targets irradiated by laser pulses with the parameters varied over a wide range are described.

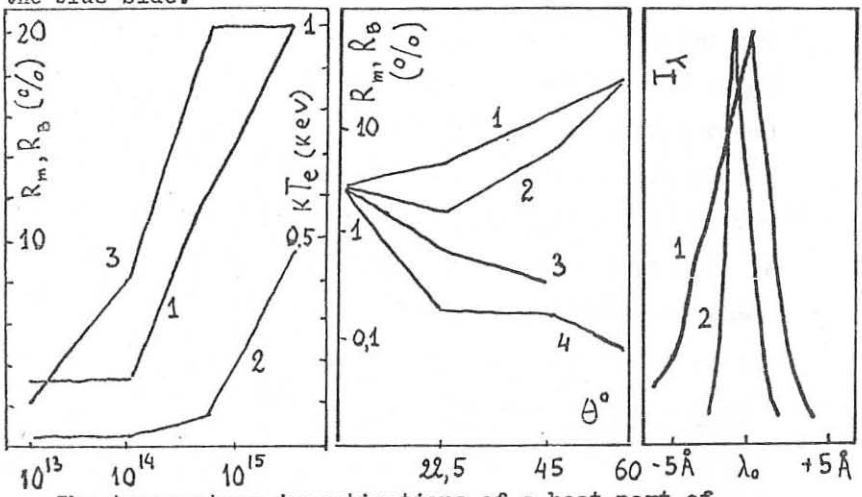
In our experiments we used a Nd-laser which comprised a driving oscillator with a controlled duration of pulse from 0.2 ns to 2 ns and five amplifying cascades. The diameter of a terminal amplifier was 60 mm. Application of the vacuum space filters and a retransmission system made it possible lasing with E = 2 J and the divergence of radiation 2×10^{-4} rad.[1]. Nonlinear crystals transformed ratiation to the second and third harmonics at the output of the system with efficiency about 80%[2].

A major part of our experiments was carried out by means of massive planar targets with inclined incident radiation upon the plasma in order to separate two compo-

nents in the scattered radiation, i.e. mirror and backward. The conducted experiments enable us to clarify a number of peculiarities in the nature of interaction of laser radiation with a high-temperature plasma.

Mirror and backward reflection at λ = 1.06 um increases sharply with flux densities above 10^{14} W/cm^2 (Fig.1, where curve 1 is the coefficient of mirror reflection, curve 2 is the coefficient of backward reflection). The absorption of laser radiation increases with shortening wavelength and decreasing flux density of heating radiation as well as with increasing z of the target material. At λ = 1.06 um, q = 5×10^{14} W/cm^2 and polyethylene target the absorption is 70%, at λ = 0.53um it reaches 80%. The directional diagram of the scattered mirror radiation is a function of the ratio between the flux density of incident radiation and the diameter of the focal spot at the target. When the flux density and the geometry of lighting are fixed it expands as one passes to longer wavelengths. A low-intensity corona appears around the main peak of mirror reflection with increasing flux density. Backward and mirror reflection depends on a polarization plane of incident radiation and has lower magnitudes for p-polarized radiation (Fig.2, where curve 1 is the coefficient of mirror reflection versus an angle of incidence for s-polarized radiation, curve 2 is R_m, p is polarization, curve 3 is the coefficient of backward reflection for s-polarization, curve 4 is R_b, p is polarization, λ = 1.06 um, q = 10^{13} W/cm^2).

The investigations of the spectra of backward and mirror scattered radiation showed that they are appreciably broadened compared to the spectrum of incident radiation, the spectrum broadening of backward scattered light being markedly more than that of the spectrum of a mirror component (Fig.3, where curve 1 is the spectrum of backscattering, curve 2 is the spectrum of a mirror component, the wavelength of incident radiation λ_0= 0.53 um, the width of the spectrum $\Delta\lambda_0$ = 0.5 um, $q = 5 \times 10^{14}$ W/cm^2). The spectrum of the backward scattered component is broadened to the red side with increasing flux density of incident radiation. With increasing angle of radiation incidence to the target the spectrum is broadened to both sides, however longwave broadening is more than that to the shortwave side. When passing from the single-pulse radiation of the target to double-pulse (τ = 0.5 ns, Δt = 2 ns) the spectrum is shifted to the blue side.



The temperature investigations of a heat part of

electronic distribution showed its increase to a flux density $\sim 5 \times 10^4$ W/cm^2 followed by saturation at ~1 keV level (Fig.1, curve 3). Studies on the line Roentgen spectrum demonstrated a relationship between the ionization composition of plasma and the flux density as well as the pulse duration of heating radiation.

Investigations with a planar target showed that in explanation of the processes taking place in plasma one should proceed from the assumption of joint action of the braking gear of absorption, linear transformation and nonlinear processes, the main of which are stimulated Brillouin scattering and absorption near the point $n_c/4$ [3]. Strong backscattering at $q > 10^{14}$ W/cm^2 is adequately described with a convective model of stimulated Brillouin scattering[4].

Studies on laser light scattering by a spherical microtarget were conducted as well. The envelope glass target of 100 um in diameter and with 2um thick wall was irradiated at $\lambda = 1.06$ um. Radiation was focused behind the target so that the diameters of the radiation spot and target coincided. The pulse duration was 5 ns, and the flux density on the target was 2×10^{14} W/cm^2. The investigations showed that at the angle of radiation convergence to the target equal to 34°, approximately 70% reflected energy is scattered behind the target in a cone of vertex angle about 70°.

1.K.Sh.Mustaev, V.A.Serebryakov, V.E.Yashin. Pisma Zhurn. Tekhnich.Fiz., 6, 856-859, 1980.
2.V.D.Volosov, V.N.Krylov, V.A.Serebryakov, D.V.Sokolov. Pisma Zhurn. Experim.Teor.Fiz., 19, 38-71, 1974.
3. O.G.Baikov, V.I.Bayanov, A.A.Mack, R.N.Medvedev, V.A.Serebryakov, N.A.Solovyov, ibid., 29, 44-47, 1979.
4.A.A.Andreev, A.N.Shatsev.Fiz.Plasmy, 6, 1032, 1980.

ANALYSIS OF FUSION PERFORMANCE BY INERTIAL CONFINEMENT: EFFECTS OF PRESSURE IONIZATION AND ELECTRON CONDUCTION ON THE IGNITION OF DT FUSION IN HOLLOW-SHELLS BY ISENTROPIC IMPLOSIONS.

G. Leira, M. Perlado, R. Luqui, C. Ahnert, J.M. Aragonés, J.M. Martinez-Val, J.L. Ocaña, G. Velarde.

JUNTA DE ENERGIA NUCLEAR AND UNIVERSIDAD POLITECNICA DE MADRID (SPAIN)

ABSTRACT

The problem of ignition by isentropic implosions of DT hollow-shells as studied by Kidder[1], results in an ideal "spark" condition, where, after void closure, less than 10% of the fuel at the center is heated above 5 keV, at low density, while the bulk of the fuel keeps cool but compressed to very high densities. Afterwards, fusion burn is achieved by propagation of the ignition by alpha transport, electron conduction and radiation transport, in decreasing order of contribution.

We have obtained the Kidder results using the same initial configuration and pressure boundary condition, with the equation of state for a completely ionized ideal gas ($\gamma=5/3$) and the electronic heat conductivity given by the classical model of Spitzer[2]. But, when we introduce the effects of pressure ionization and degeneracy of electrons, the ideal "spark" condition for ignition becomes smoothed and delayed in a significant amount. The models developed for these effects and the results obtained, are discussed in this paper.

1. PRESSURE IONIZATION

The ionization model is derived from the Saha equations[3], modified by adding a term to include the increase in free energy due to the effect of the finite size of the gas particles, condidered as a mixture of interacting hard spheres. Following Lebowitz et al.,[4] the increases of free energy and pressure are given by:

$$F_e = \frac{3KT}{\pi\rho}\left[-2\xi_0\ln(1-\xi_3)+6\xi_1\xi_2(1-\xi_3)^{-1}+3\xi_2^3(1-\xi_3)^{-2}\right] \qquad (1)$$

$$P_e = \frac{K\,T}{\pi}\left[6\xi_0\xi_3(1-\xi_3)^{-1}+18\xi_1\xi_2(1-\xi_3)^{-2}+18\xi_2^3(1-\xi_3)^{-3}\right] \qquad (2)$$

where, $\xi_0 = \frac{1}{6}\pi\sum_i(\frac{Ni}{V})$; $\xi_n = \frac{1}{6}\pi\sum_i(\frac{Ni}{V})\,2R_i)^n$ (3)

It follows that in the Saha equations for a mixture of ions, m and m+1, and electrons, the ionization potentitals should be corrected:

$$\frac{\Delta I}{KT} = \ln(1-\xi_3) + 6\xi_3(1-\xi_3)^{-1}(R_m - R_{m+1}) + \left[12\xi_1(1-\xi_3)^{-1} + 18\xi_2^2(1-\xi_3)^{-2}\right](R_m^2-R_{m+1}^2) + \frac{4}{3}\pi\frac{Pte}{KT}(R_m^3 - R_{m+1}^3) \qquad (4)$$

where: R_m, R_{m+1} are ionic radii, and Pte is the total pressure of the mixture. For elements with $Z>1$ with mean ionic charge $\bar{Z}<Z-1$, the equations simplify to

$$P_e = KT\rho N_0 \xi_3 (1-\xi_3)^{-1} \left[\bar{Z}+1+3(1-\xi_3)^{-2}\right] \quad (5)$$

$$\frac{\Delta I}{KT} = \frac{4}{3}\pi\rho N_0 (1-\xi_3)^{-1} \left[\bar{Z} + 1 + 3(1-\xi_3)^{-2}\right] (R_m^3 - R_{m+1}^3) \quad (6)$$

For $\bar{Z}$ Z-1, since R_m=R and R_{m+1}=0, it is obtained:

$$P_e = KT\rho N_0 \xi_3 (1-\xi_3)^{-1} \left[\bar{Z}+1+3(1-\xi_3)^{-1}(Z-\bar{Z})\right] \quad (7)$$

$$\frac{\Delta I}{KT} = \ln(1-\xi_3) + \frac{4}{3}\pi\rho R^3 (1-\xi_3)^{-1}\{\bar{Z}+1+(Z-\bar{Z})\left[6+\frac{3}{2}\xi_3(1-\xi_3)^{-2}(5-3\xi_3)\right]\} \quad (8)$$

Figure 1 shows the mean charge of Aluminum as a function of pressure and temperature as calculated by introducing eqs. (5) to (8) into our equations of state, described in refs. 5 and 6. In figure 2 we can see the same function with the old EOS, without pressure ionization effects.

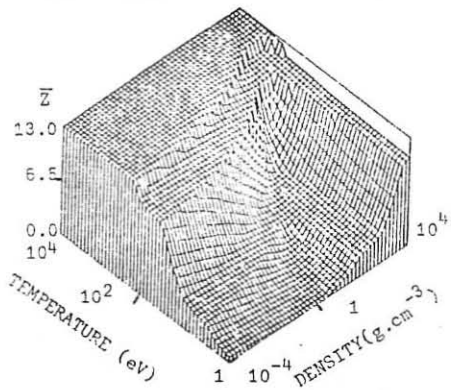


Figure 1.- Mean charge of Al, including pressure ionization.

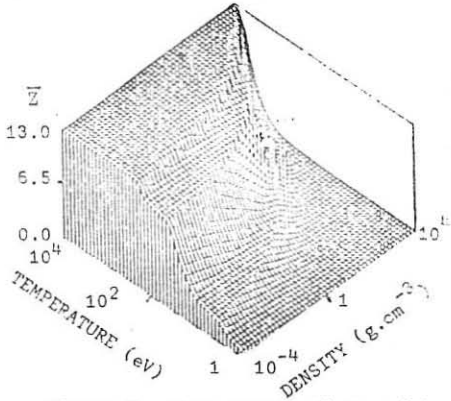


Figure 2.- Mean charge of Al, without pressure ionization.

2. DEGENERACY CORRECTIONS TO ELECTRON CONTRIBUTION IN EOS.

For the plasma conditions in inertial confinement fusion, the electron gas is in the intermediate region of partial degeneracy. Accordingly, the electronic contributions to the thermodynamic functions, are modified in our EOS[5,6], introducing a modified free-electron partition function from Kerley[7]:

$$q_e = \left(\frac{1+by+0.2636y^2}{0.2636\, y^2}\right)^{3/4} \quad ; \quad \begin{matrix} b = 0{,}4242 \text{ (DT)} \\ b = 0.7173 \text{ (heavier)} \end{matrix} \quad ; \quad y = \frac{h^2}{2\pi m_e KT}\left(\frac{n_e\rho}{2}\right)^{2/3} \quad (9)$$

We obtain:

$$F_e = -N_e KT \ln q_e + E_I \; ; \; E_I = \sum_L N_L A(\bar{Z}_L) \text{ (ionization energy)} \quad (10)$$

$$\left.\begin{matrix} P_e = \bar{Z}\, N_0\, KT\, F(y) \\ E_e = \frac{3}{2}\bar{Z}\, N_0\, KT\, F(y) \end{matrix}\right\} \; ; \; F(y) = \frac{1+\frac{b}{2}y}{1+by+0.2636\, y^2} \quad (11)$$

3. DEGENERACY CORRECTION TO ELECTRON HEAT CONDUCTION

This mechanism of electron heat conduction is ussually less efficient than radiative transfer, but in a very dense plasma the conductivity increases with increasing degeneracy. Following Clayton[8], we obtain for the equivalent conductive opacity:

$$K_e \begin{cases} 16.0\ \sqrt{T}\ \bar{Z}\ \dfrac{H}{\rho} & \text{(weak degeneracy)}; \quad H(v) = \dfrac{1}{2}\ln\dfrac{2}{1-\cos\theta_0(v)} \\ 17.25\ \dfrac{A\ H\ T^2}{\bar{\rho}^{\,2}} & \text{(strong degeneracy)} \\ 2.6\times10^{5}\ \dfrac{\bar{Z}^2\ H\ e^{\alpha}}{FTA} & \text{(intermediate degeneracy)} \end{cases} \tag{12}$$

Where the degeneracy parameter α should be reduced by the continuum depression, $\theta_0(v)$ is the small impact angle that characterizes the cutoff due to shielding, and F is a function of α tabulated by Cox[9].

In the Kidder problem of DT[1], a simple review of the degeneracy criterium (Clayton[8]) provides the density range of degeneracy for different temperatures:

$$\bar{Z}\ 6.276\times10^{-4}T^{3/2} \begin{array}{ll} T = 6.81\ \text{keV}; & \rho>5\ \text{g.cm}^{-3} \\ T = 2.61\ \text{keV}; & \rho>2\ \text{g.cm}^{-3} \\ T = 1.00\ \text{keV}; & \rho>0.6\ \text{g.cm}^{-3} \end{array} \tag{13}$$

where $\alpha>4$ is considered as the condition for non-degeneracy. It is then concluded that in this problem the range of densities with non-degeneracy effects is only a part of the total range of densities in the implosion process.

4. CALCULATIONS WITH DIFFERENT MODELS

The problem of ingnition studied by Kidder[1] is used as a reference to benchmark the theoretical and numerical models of implosions in DT hollow shells. Using our computer code NORMA[5,6], which solves the equations of conservation of mass, momentum and energy in one-dimensional Lagrangian coordinates for spherical geometry, coupling the thermal diffusion to the hydrodynamic movement and using the analytical EOS of Thompson and Lauson[10], with developments to include DT mixtures[6], we have performed some applications in the past[11,12] for different cuasi--isentropic implosions of solid spheres.

As shown in lines labeled(1)in figures 3 and 4 we reproduce within 1% the results of Kidder[1], when we use in our program NORMA an ideal gas EOS for DT and an electronic heat conduction given by the Spitzer classical model[2], without electron degeneracy effects. When we include in NORMA the effects of pressure ionization, and electron degeneracy in - EOS and in heat conduction, we obtain the results of lines labeled(2) in figures 3 and 4 for the same Kidder's problem, at the time - (37.88 ns) where the maximum temperature is obtained at the center.

The most relevant conclusions from both results are:

a) The maximum temperature at the center is 4.97 keV, lower than the - Kidder result (6.20 keV).

b) The density and pression in the center at that time are 255 $g.cm^{-3}$ and 0.99 Tbar, higher than those of Kidder (147 $g.cm^{-3}$ and 0.77 Tbar).

c) The time to ignition of 37.884 ns is larger than that of Kidder (37.819 ns) and hence the compression energy, 64.762 kJ, is larger (63 kJ), although the ratios between kinetic and internal energy are nearly the same.

Henceforth, the overall conclusion is that the effects of pressure ionization and electron degeneracy are significant for the dense and hot plasma at ignition in inertial confinement fusion. The "spark" configuration is also achieved with isentropic implosions of DT hollowshells, but with lower temperatures and higher densities at the spark. The radiation heat transport will smooth further the spark configuration and it will be included in our future calculations.

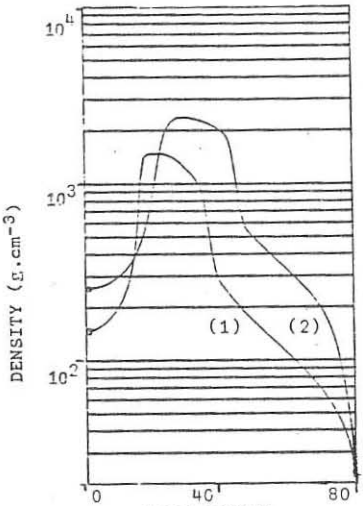


Figure 3.

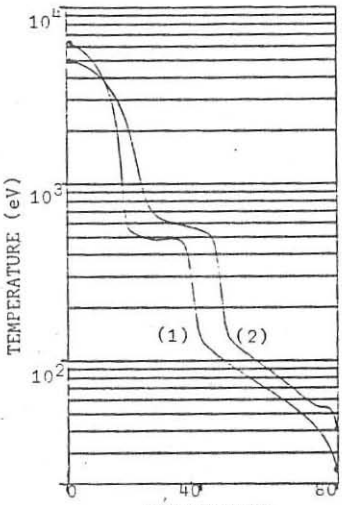


Figure 4.

REFERERENCES:

1. KIDDER, R.E., Nucl. Fusion, 19, 2 (1979)
2. SPITZER, L., "Physics of Fully Ionized Gases", Interscience (1962)
3. ZEL'DOVICH, YA. B. et al., "Physics of Shock Waves and High Temperature Hydrodynamic Phenomena", Academic Press (1966)
4. LEBOWITZ, J.L. et al., J. Chem. Phys., 43, 774 (1965)
5. VELARDE, G. et al., Atomkernenergie, 32, 58 (1978)
6. VELARDE, G. et al., Atomkernenergie, 35, 40 (1980)
7. KERLEY, G.I., LA-4776, Los Alamos Scientific Lab. (1972)
8. CLAYTON, D.D., "Principles of Stellar Evolution and Nucleosynthesis", McGraw-Hill (1968)
9. COX, A., "Stellar Absorption Coefficients and Opacities", in L.H. Aller and D.B. Mclaughlin (Eds.) "Stellar Structure", the Univ. of Chicago - Press(1965)
10. THOMPSON, S.L. and LAUSON, H.S., SC-RR-710713, Sandia Lab. (1972)
11. VELARDE, G. et al., Atomkernenergie 36, 213 (1980)
12. VELARDE, G. et al., Trans. Am. Nucl. Soc. 36, 208 (1981)

EFFECTIVE MULTISTAGE ABLATION

A.A. Filyukov
Keldysch Institute
of Applied Mathematics

A.A. Vedenov
Kurchatov Institute
of Atomic Energy

Moscow, USSR

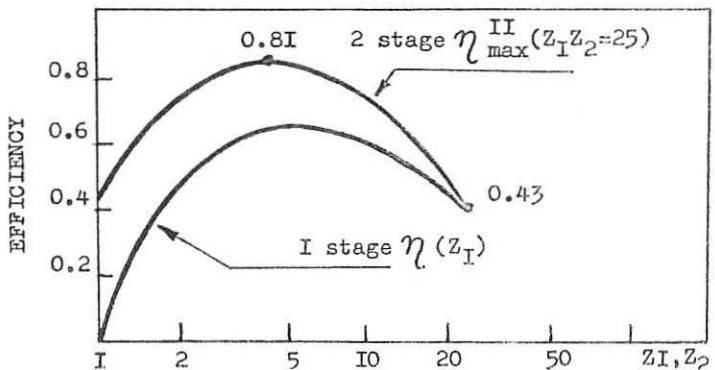
The method of short wave tailoring proposed few years ago[I]as indicate numerical simulations of target compressions and burning under the illumination by the sequence of impulses with increasing frequency [2,3] is realy a possible alternative to[4]the known method of power tailoring and possesses some potential advantages in the physical sense as well as for realization. If one uses wave tailoring - no problems exist with decoupling at the latest stages of illumination [5,6]. The coupling efficiency increases, fast ions and electrons dissapear, the limit of electron transport becomes insignificant. One has a relative free possibility to choose the appropriare rate of deepening the critical zone of absorption into the dense region of corona, advance it into the external layers of accelerated shells, and ablation of compressed matter is theoretically non excluded. The most essential present cause defining the practical interest of wave tailoring is certainly the possibility to decrease by a quantity of one order the least necessary radiation energy to achieve the given gain factor and to decrease the power of illumination.

The physical reasons determining high economy of energy consumption at the acceleration by the ablation with radiation of increasing frequency consist of following factors:

the rise of mechanical acceleration efficiency, the reduction of heat conductivity losses into corona, the decrease of absorption on the way to the critical region.

The mechanical efficiency of acceleration at the expense of mass ejection with constant exhaust velocity U is defined by $\eta^{I}=\ln^2 Z/(Z-I)$, where Z - Tsiolkovski number, the ratio of initial and final masses, the latter accelerated to the velocity $V=U\ln Z$. One reaches maximum value $\eta = 0.65$ if $Z = 5$.

The acceleration efficiency can be essentially increased by utilization of several acceleration stages with increasing exhaust velocities. The usage of twostage acceleration with different constant exhaust velocities U_I and U_2 and corresponding final stage masses M_I and M_2 guarantees the efficiency $\eta^{II} = (I + X)^2/[(Z_2/\eta_I) + (X^2/\eta_2)]$ at exhaust velocities ratio defined by $X = U_2\ln Z_2(U_I\ln Z_I)^{-1}$. At the optimal choice of this quantity the efficiency attains $\eta^{II}_{max} = (\eta_I/Z_2) + \eta_2$. Evidently the three-stage acceleration variant allows to ensure at least the efficiency $\eta^{III}_{max} = (\eta_I/Z_2Z_3) + (\eta_2/Z_3) + \eta_3$ which after the choice of stages $Z_I = 7.6$, $Z_2=Z_3=3.3$ achieves value $\eta^{III}_{max} = 0.87$ for the acceleration of the final mass of the third stage constituting 0.012 of the initial one. The corresponding effi-



ciency of the one-stage acceleration in this case is equal to 0.24. Such essential efficiency increase is reached because of minimization of exhaust kinetic energy on each acceleration stage in the reference frame connected with the start. This is a result of appropriate choice of the exhaust velocities ratio , correlated with the velocity of accelerated masses. In the numerical target ablation experiments under frequency tailoring we often observed the effect of decelereted disassembly in the laboratory frame after the switch in of frequencies of irradiation. Here the critical densities corresponding to the above mentioned frequencies were connected with the accelerated masses of the target. Analysis of the spherical corona model developed in [7] shows possibility to account efficiency increase under frequency tailoring by optimizing some functional from the unique parameter of this model α that the authors considered as a constant. From similarity relations of the spherical corona model obtained by the authors of [8] who had taken into account the electron conductivity limit one implies also the possibility to change the effective exhaust velocity at the expense of increasing irradiation frequency that leads, as the final result, to the increase of acceleration efficiency as well.

Efficiency increase at the multistage ablation may be used not only for the spherical implosion but also at long base acceleration in impact fusion. In this case the frequency tailoring allows to ensure radiative penetration with the higher frequency into more dense layers of the corona at the expense of preliminary corona heating by more longwave radiation.

Light ion usage for the aim of ablation and for the acceleration of shells and their fragments in inertial fusion can be organized under multistage acceleration as well at the expense of different ion ranges determined by their charge, mass and energy. It indicates sufficient generality of multistage ablation approach to the problem of increasing acceleration efficiency which does not reduce to the frequency tailoring and represents the general and evedently central problem of inertial fusion.

References

I. A.A. Filyukov, A.A. Vedenov. Paper presented at XII Europ. conf. on laser interaction with matter.,Moscow, I978

2. A.A. Filyukov, P.P. Volosevich. Preprint Inst.Appl. Math., N II7, I980.

3. A.A. Filyukov, P.P. Volosevich. Paper presented at X Europ. conf. on nuclear fusion and plasma physics, Moscow, I98I

4. J.Nuckolls, L. Wood et al. In "Problems of laser fusion", Moscow, Atomizdat, I976.

5. R. Kidder, J. Zink, Nucl.Fusion, I2,325, I972.

6. J. Nuckolls. In: "Laser Interaction". Ed. Schwarz,Hora,I974

7. Yu. Afanasiev et al. Preprint FIAN, N 30, I980.

8. C.E. Max, C.Mc Kee, W. Mead, Physics of Fluids, v.23,8, I620, I980.

ABLATIVE ACCELERATION OF DOUBLE-LAYER TARGETS.

Yu.A. Bondarenko, I.N.Burdonsky, V.V.Gavrilov,
A.Yu.Gol'tsov, E.V.Zhuzhukalo, N.G.Kovalsky, A.N.Kolomijsky,
L.S.Mkhitar'yan, A.F.Nastoyashchy, M.I.Pergament,
A.D.Rozhkov, V.V.Simonov, A.I.Yaroslavsky

I.V.Kurchatov Institute of Atomic Energy
USSR

Efficiency of thin double-layer targets acceleration, heat transport in the plasma corona, ablation rate and effects of the irradiation inhomogenity have been experimentally investigated. Experiments were performed by using one beam of the Nd-glass laser facility "Mishen" [2] (λ = 1,06 μm, τ =3 ns, E=100 ÷ 300 J). The small fraction of the main laser beam after pulse shortening (to 0,5 ns) and frequency doubling was used for interferometer illumination. Laser pulses were focused by two component objective onto various foil targets. The half-energy focal spot diameter was 250 μm, yielding an incident flux of 10^{13} ÷ 10^{14} W/cm^2. In a number of experiments the output laser beam was divided into two near equal parts propagating under slightly different angles and resulting in two separate spots on the target surface with their centers spacing either 250 μm or 500 μm. (Fig.1. Microdensitometer traces of the irradiation intensity distributions on the target surface: a) Δx =500 μm; b)Δx =250 μm). The appropriate measurements were accomplished with a wide variety of diagnostics. The data was taken with a five-frame interferometer (a frame exposure of 0,5 ns); X-ray pinhole cameras and calorimeters; infrared, visible and X-ray spectrographs. Comparision of experimental data with

results of the two-dimensional hydrodynamic calculations [1] has been widly used.

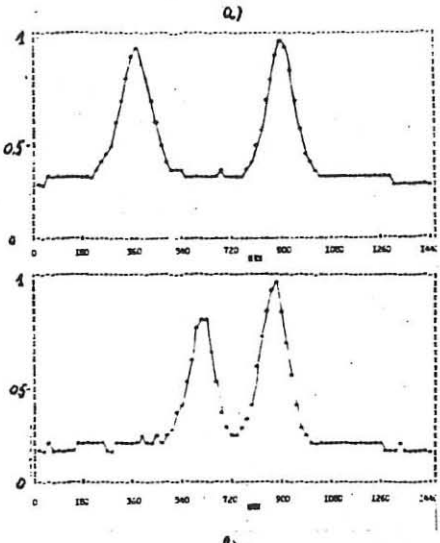


Fig. 1.

Intensity distributions on the target are not overlapped in the two beam illumination experiments both for 250 μm and 500 μm spacing. (Fig. 1). Distributions of X-ray sources in front of the aluminium (Al) and mylar ($C_{10}H_8O_4$) targets ripit the corresponding illumination intensity profiles as one can see in Fig. 2 (Al target, E=100J, a)Δx =500 μm, b)Δx =250 μm) and Fig. 3 (mylar target, E=80J,

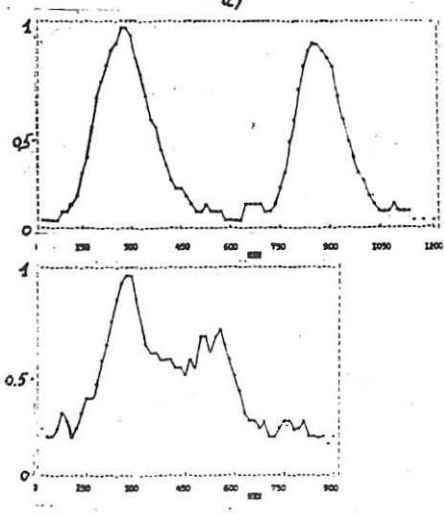


Fig. 2.

a)Δx =500 μm, b)Δx =250 μm). The similar experimental data led the authors of [3,4] to the conclusion about anomalous inhibition of lateral heat transport. But they did not take into account the plasma hydrodynamic motion in their analysis. At the same time the simple estimates performed for the experimental conditions under

consideration show the energy losses from the absorption zones due to hydrodynamic motion and thermal conductivity to be nearly equal. Temperature of the plasma near the critical density surface would be lower in the regions between illuminated areas without any assumptions about conductivity restriction. It seems of course to be more important to know temperature and pressure distributions at the ablation surface than near critical one. In this respect the interferometric patterns given in Fig.4 are representative. The frames with interferometric patterns presented in Fig.4 shown the dynamic of Al target rear part material acceleration. The 6 μm Al foils was irradiated with two laser beams (E ≈ 100 J). Two distinctly separated parts are seen to be accelerated in the case of 500 μm distance between the irradiated area centers (Fig.4a). But, if this distance equals 250 μm the accelerated part of the target material moves as a whole (Fig.4b). It seems likely that with $\Delta x = 250$ μm the temperature distribution was sufficently homogeneous ower the solid target surface. It follows

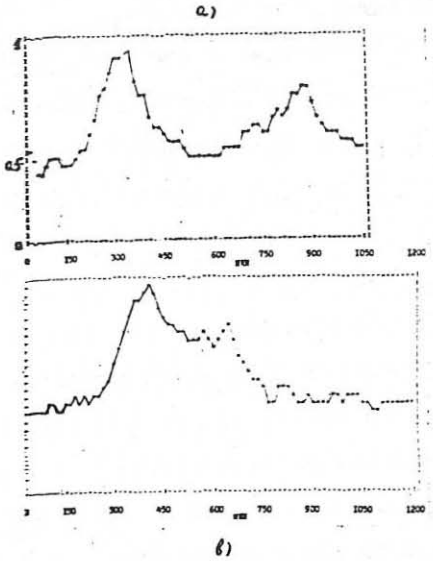


Fig.3

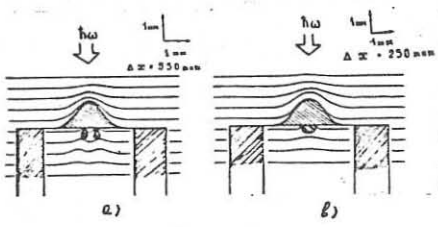


Fig.4.

from X-ray measurements carried out for the double-layer targets that 3,5±0,5 μm of mylar and 2,0±0,3 μm of aluminium burn out at an energy of 150J during the laser pulse.

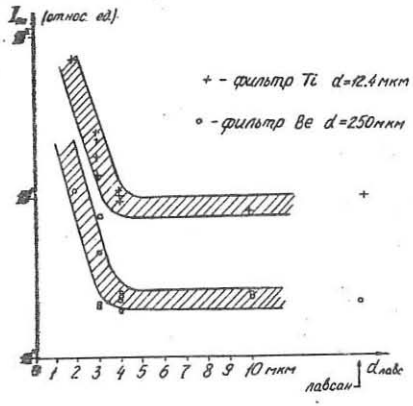


Fig.5.

Dependence of X-ray intensity on the mylar ablator thickness for the double-layer (mylar+Al) target is presented in Fig.5. (E=150J). The same values result from the two-dimensional hydrodynamic computations using the cla - ssical transport coefficients. Hydrodynamic efficiency of the target acceleration estimated from the experimental data was about 5%.

References

1. Д.А. Бондаренко, И.Н.Бурдонский и др. ЖЭТФ, т.81,1 (7), 1981

2. V.V.Belousov, V.L.Borzenko at al, IAEA-200, Technology of inertial confinement experiments, Vienna, 1977, p.241-243

3. W.L.Kruer, Comments Plasma Phys.and Controll Fusion, 5,3, 1979, p. 69-78

4. B.H.Ripin, C.M.Armstrong at al, NRL Memorandum Report, 3890, 1978

IRRADIATION OF MICROSPHERES WITH THE 2 Tw IODINE LASER

Zaretskii AI, Kirillov GA, Kozmez S.B. Kochemasov GG, Muzugov VM, Suhaz
I.V.Kurchatov Institute of Atomic Energy, Moscow, USSR

Abstract

Power of the iodine laser Iskra IY was raised to 2 Tw by pulse shortening without loss in energy. Irradiating microspheres filled with DT gas, neutron yield of $\sim 10^5$ in the "exploding pusher" mode was first obtained with the iodine laser.

Glass microspheres of 150-170 μm in diameter and 1 μm wall thickness filled with 10-40 atm of DT-gas were irradiated with the one-channel 1.315 μm iodine laser Iskra IY /1/. In the first experiments the laser energy of 500 J was delivered into the target chamber. To achieve high neutron yield with such energy the "exploding pusher" mode is preferable /2/. Its realization is possible if temperature of fast electrons is sufficiently high $\gtrsim$10 kev which requires flux densities of $\gtrsim 10^{15}$ w/cm^2 on the microsphere's surface. To get such flux densities for given powers and microsphere's dimensions the pulse length of $\lesssim$ 0.3 ns is required.

Pulse shortening was fulfilled by steepening the wavefront of the master oscillator as well as by choosing operating conditions of the amplifying stages of the

iodine laser. As a result the output pulse length $\tau_{0.5} = 0.3 \pm 0.05$ ns was attained which agrees with the results of calculations.

It is essential that unlike the neodymium lasers the output energy of the system did not practically decrease at pulse shortening from 1 to 0.25 ns.

To prevent self-excitation of the system MO-amplifying stages-target optical isolators in the form of bismuth films, deposited on a glass substrate, and saturable shutters, based on dyes, were used. It made possible to receive the output beam energy contrast $K_E = 10^7$ and power contrast $K_P = 2 \times 10^6$.

For spherical illumination of the target the 270 mm output beam was divided by splitting plates into four beams, which were focused on a glass microsphere with a 10-20 μ m accuracy by parabolic mirrors with F = 270 mm. The output beam divergence was $(1-2) \times 10^{-4}$ radn at the energy level of 80%. To achieve more homogeneous illumination the microsphere was arranged in the plane where the spot size was 200 μm.

Energy balance was defined by specially designed calorimeters. In a test in which the highest neutron yield ($N \simeq 1.5 \times 10^5$ neutron/pulse) was registered the energy delivered into the chamber, the incident energy , and the absorbed energy were 480 J, 280 J, and 50 J , respectively. The flux density incident on the target was 10^{15} w/cm^2. The continuous X-ray spectrum measured

by filter method is presented in Fig.I. Temperatures corresponding to soft and hard spectrum were $T \simeq 1$ kev and $T_h \simeq 9$ kev. The value of coronal temperature near the critical surface defined by line spectrum (relative intensities of resonance lines of He$^+$ and H-like ions of silicon) was 0.8 kev.

X-ray image of a target, obtained with a pinhole camera, permitted to determine approximately (ref.Fig.2) DT volume compression of 30.

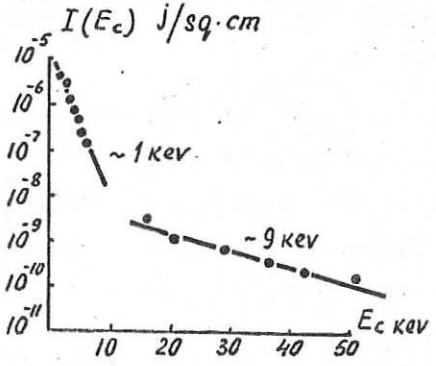


Fig.1.

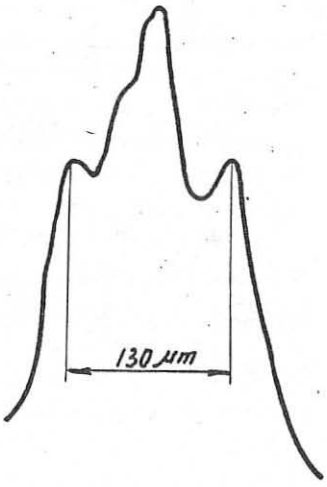


Fig.2.

Measured neutron yield is shown in Fig.3, where Ordinate is measured neutron yield, Abcissa is calculated neutron yield. The last was defined using semiempirical model /2/, which agrees with the results of experiments conducted in "exploding pusher" mode in Lawrence Livermore Laboratory, USA, and presented in the same figure.

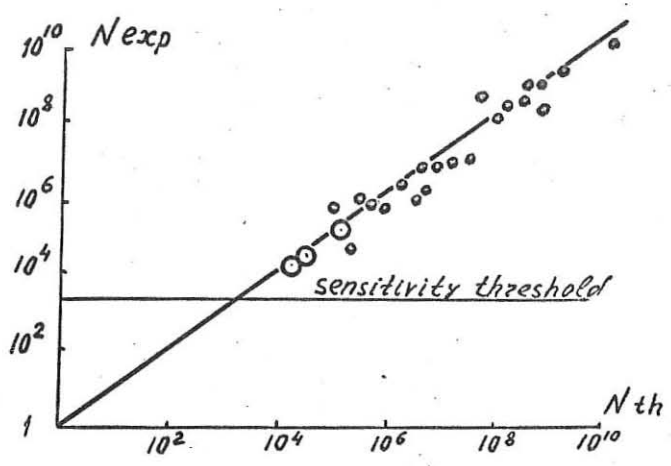


Fig.3. O - Experiments on Iskra IY.

• - Livermore data.

One can see that our results agree well with the experimental data of Lawrence Livermore Laboratory. The measured temperature of fast electrons (9 kev) shows that using glass microspheres of a given thickness we also realized the "exploding pusher" mode.

REFERENCES

1 S.B.Kormer, Izv.Akad. Nauk SSSR 44, 2002 (1980).

2 E.K.Storm et al , Phys.Rev.Lett., 40, 1570 (1978).

TANDEM MIRROR REACTOR CALCULATIONS WITH RESPECT TO AXIAL NONUNIFORMITY OF ELECTRON TEMPERATURE

Kuznetsov M.G.
Institute of High Temperatures AS USSR
Skovoroda A.A.
Kurchatov Institute of Atomic Energy

Tandem mirror reactor concept was studied first in [1,2,3] under the assumption of electron temperature axial constancy. However, 2XIIB experiments have shown this temperature to vary significantly along the trap axis under conditions when the electron meen-free-path was greater than its longitudinal size.

Electron temperature variation can considerably improve reactor parameters; this has been distinctly demonstrated by the calculations of a "thermal barrier" sheme [4], where special methods of creating the axial nonuniformity of electron temperature were proposed.

Present work deals with the classical tandem mirror reactor (without a thermal barrier) calculations considering a probable existence of natural axial nonuniformity of electron temperature. The interest to this problem has been caused by principle difficulties of a thermal barrier design, as well as by hopes to improve the classical tendem mirror parameters.

The ability of obtaining high electron temperature in plugs is based on the existence of an electron population trapped in the potential well and oscillating along the field lines only within the plug bounds. They exchange energy with a passing electron population oscillating along the hole trap. Although the characteristic exchange time is small (of the order of magnitude the electron-electron collision time) its finiteness and high nonuniform heating power level (electrons are heated mainly in plugs and cooled in the solenoid) make the temperature "cut off" possible.

Passing electrons (their density n_0 is equal to the solenoid electron density) leave the trap under collisi-

ons in a time τ_0 or are "captured" in the potential well transfering to the trapped electron population in a time τ_1. On the other hand, trapped electrons (their density $n_2 \simeq n_1 - n_0$, where n_1 is the total electron density in plugs) collisionly leave the plugs transfering to the passing electron population in a time τ_2. Values of τ_0 and τ_2 can be expressed by formulars derived in [5,6]. Under the assumption of sufficiently high potentials and small plug size compared to solenoid length one can write down the following approximate correlations:

$$\tau_0 \simeq \tau_{ee}(n_0, T_{e0}) f(R_0) \frac{\Phi_1}{T_{e0}} \exp\left(\frac{\Phi_1}{T_{e0}}\right); \quad \tau_2 \simeq \tau_{ea}(n_1, T_{e1}) f(R_2) \frac{\Phi_2}{T_{e1}} \exp\left(\frac{\Phi_2}{T_{e1}}\right).$$

Here $\tau_{ea}(n, T_e)$ -electron-electron collision time; T_{e0}, T_{e1}- electron temperatures; Φ_1, Φ_2 - potential barriers for passing and trapped electrons; R_0, R_2 - mirror ratios for solenoid and plug, $f(R) = \sqrt{\pi}/4 \, \frac{2R+1}{2R} \ln(4R+2)$.

We evaluate the time τ_1 with the help of balance equations derived in the limit of zero losses ($\tau_0 = \infty$) and sources of particles and energy, implying that the system remains in the thermodynamic equilibrium with constant axial temperature and Boltzmann correlation ($\Phi_2 = T_e \ln \frac{n_1}{n_0}$) is satisfied. From the condition ($\frac{n_2}{\tau_2} = \frac{n_0}{\tau_1}$) we obtain the following expression for τ_1 :

$$\tau_1 = \tau_{ea}(n_2, T_e) f(R_2) \frac{\Phi_2}{T_e}.$$

The above expression keeps its general form when naturally substituting T_e for T_{e0}.

With the help of characteristic times obtained one can write down particle and energy balance equations that lead to the following correlations neglecting heat exchange without particle exchange between the passing and trapped electrons:

$$\Phi_2 = T_{e1} \ln \frac{n_1}{n_0} \left(\frac{T_{ea}}{T_{e1}}\right)^{1/2},$$

$$\frac{\Delta T_e}{T_{e0}} = \frac{T_{e1} - T_{e0}}{T_{e0}} \simeq \frac{P \tau_{ea}(n_2, T_{e0})}{n_0 T_{e0}} f(R_2) \frac{\Phi_2}{T_{e0}},$$

where P represents the value of external plug electron heating specific power.

Additional balance equations derived were used in further reactor calculations conducted according the sheme [3]. The results were compared for elucidation

of the tendencies of modifications included.

When heating electrons by neutral injection $P \simeq \frac{E_i n_2}{\tau_E}$, where E_i - injection energy, τ_E - hot ion-electron cooling time, and $\frac{\Delta T_e}{T_{e0}} \simeq 10 \frac{m_e}{m_i} \frac{E_i}{T_{e0}} < 1$, where m_e, m_i - electron and ion masses. This temperature difference is seen to be small being determined mainly by the $\frac{E_i}{T_{e0}}$ ratio, i.e. by the solenoid electron cooling rate. Calculations have shown, that the introduction of some artificial electron cooling increases the $\frac{\Delta T_e}{T_{e0}}$ ratio, while ion heating by confined alphas decreases it greatly and in this case the consideration of electron temperature nonuniformity is practically superfluous.

Th· electron-cyclotron heating in plugs is natural to be put into consideration; in this case the value of P, generally speaking, is independent of plasma parameters. The employment of such external heating source can substantially increase the $\frac{\Delta T_e}{T_{e0}}$ ratio thus improving the reactor parameters, but only at the HF power level of the order neutral injection power.

Table 1 shows the comparative results of the reactor calculations conducted under various assumptions. Reactor parameters represented are not optimal but only illustrative.

Note that the employment of a thermal barrier with potential Φ_3 enhances the temperature jump: $\Delta T_e^b \simeq \Delta T_e \cdot e^{\frac{\Phi_3}{T_{e0}}}$, where ΔT_e is the temperature difference in the absence of a barrier. This enhancement is substantial, however, when $\frac{\Phi_3}{T_{e0}} > 1$. Such high barrier design would meet a number of principle difficulties. In the case, when $\frac{\Phi_3}{T_{e0}} \simeq 1$, a reactor with a thermal barrier is not much better then without it. Thus, consideration of the axial nonuniformity is important when using sufficiently powerful sources of an external plug electron heating. The requirements to the injector and magnetic system are simultaneously decreased.

Table 1

Parameters of tandem mirror reactor

N	Parameters	$T_{e\perp} = T_{e\parallel}$ α-heating [3]	$T_{e\perp} \neq T_{e\parallel}$ α-heating	$T_{e\perp} \neq T_{e\parallel}$ without α-heating HF-heating
1.	Fusion power, MW	780	780	780
2.	Injection power, MW	160	160	35
3.	HF-heating power, MW	0	0	70
4.	Power amplification factor Q (with respect to trapping efficiency of a neutral beam)	3,8	4,2	5,4
5.	Injection energy, keV	1500	1500	500
6.	Max.magnetic field, T	14	14	14
7.	Solenoid density, $10^{13} cm^{-3}$	4,0	4,0	4,0
8.	Plug average density, $10^{13} cm^{-3}$	19,0	19,0	7,6
9.	Solenoid ion temperature, keV	31	59	21
10.	Solenoid electron temperature, keV	33	48	27
11.	Plug electron temperature, keV	33	56	93
12.	Potential barrier, keV	100	160	95

References

1. G.I.Dimov, V.V.Zakaidakov, M.E.Kishenevskii, Fiz. Plazmy 2 (1976), 597.
2. T.K.Fowler, B.G.Logan. Comments on Plasma Physics and Controlled Fusion, 2, 167 (1977).
3. U.V.Gribov, V.A.Chujanov, G.E.Shatalov. "Fusion-Fission", Second Soviet-American Seminar, 1978, Moscow.
4. D.E.Baldwin, B.G.Logan, T.K.Fowler, UCID-18156, 1979.
5. V.P.Pastukhov, Nuclear Fusion, 14, 3, 1974.
6. R.M.Cohen, M.E.Rensink, T.A.Cutler, A.A.Mirin, Nuclear Fusion, 18, 1229 (1978).

Modelling of the Single-Null Divertor of INTOR: Plasma Exhaust and Gas Pumping

M F A Harrison, P J Harbour and E S Hotston
Culham Laboratory, Abingdon, Oxon, OX14 3DB, UK
(Euratom/UKAEA Fusion Association)

1. Introduction

Properties of the single null divertor of INTOR are considered in relationship to the transport, parallel to the magnetic field, of plasma particles and energy in the toroidal scrape-off region and the poloidal divertor chamber. It is assumed that plasma transport is collisional and is equally distributed to the inner and outer targets, that only gas produced in the outer divertor can be pumped from INTOR and so the flow to the pumps must equal the flow entering the outer divertor. The efflux of neutral gas to the pumps is produced by plasma impact at the divertor target but is attenuated by ionisation in the divertor plasma. The model used is analytical[1,2], permitting the sensitivity to variation in physical parameters to be readily identified. Plasma transport is considered only in one dimension parallel to the field which in INTOR is almost parallel to the tungsten divertor target. The gas flow analysis is also one-dimensional but in the direction normal to the target.

2. The Model

Input specifications taken for INTOR are the power, $Q^{(tot)}$ transported to each channel of the divertor, (ie $2Q^{(tot)} \approx 75$MW for the standard condition), the plasma density $n_s = 5 \times 10^{19} m^{-3}$ in the scrape-off region, and the helium exhaust rate $\Gamma^{(o)}_{He,pump} = 2 \times 10^{20}$ atoms s^{-1} for 620 MW fusion power. The topology of INTOR is such that A_n, the cross sectional area of the diverted magnetic flux, is given by

$$A_n = 2\pi a\bar{\Delta}/q_{local} = 0.35m^2 \quad , \tag{1}$$

where a is the minor radius, $\bar{\Delta}$ is taken to be 0.14m and the safety factor, q_{local}, is about 3 in the divertor chamber.

The procedure adopted is shown schematically in Figs. 1 and 2. The power, Q_t, carried to the target by a flow, Γ_t, of particles at temperature T_t, is given by,

$$Q_t = \Gamma_t Y(T_t) = A_n n_t M_t C_{s,t} Y(T_t) \quad , \tag{2}$$

where $n_t, C_{s,t}$ are the plasma density and ion sound speed at the target and the corresponding value of the Mach number, M, is $M_t = 1$. The term $Y(T_t)$ in Eq. (2) represents the energy transported by ion pairs of each atomic species J(i.e. D^+, T^+, He^{2+} and tungsten) and is

$$Y(T_t) = \sum_J Y(T_t)_J = \sum_J [(1 - R_{E,t})(2kT_i + ZeU) + \chi_i + 2ZkT_e/(1-\gamma)]_J \quad , \tag{3}$$

where $R_{E,t}$ is the energy reflection coefficient at the target, Z the ion charge state, U the potential of the sheath plus pre-sheath, χ_i the ionisation energy and γ, the coefficient for secondary electron emission, is taken to be zero for INTOR.

The energy balance within the divertor is given by,

$$Q^{(tot)} = \sum_J [Q_t + Q^{(r)} + Q^{(o)}]_J \quad . \tag{4}$$

Here the radiated power, $Q^{(r)}$, is estimated for DT by,

$$Q^{(r)}_{DT} = \Gamma_{DT,t} E^{(r)}_{DT} = \Gamma_{DT,t}[(16.4 + 210/T_t)_{eV}] \quad , \tag{5}$$

which is derived using the total energy required to produce one ion pair in atomic hydrogen. $Q^{(r)}$ for helium and tungsten is by scaling from $Q^{(r)}_{DT}$. The energy deposited upon the wall of the divertor chamber by neutral particles of species J [$Q^{(o)}_J$ in Eq. (4)] is given by

$$Q^{(o)}_J = [(1 - R_{E,wall})E^{(o)}_{wall}\Gamma^{(o)}_{wall}]_J \quad , \tag{6}$$

where $E^{(o)}_{J,wall}$, the mean energy per particle, is evaluated for fast atoms directly back-scattered from the target, for charge exchange atoms from the plasma and for particles thermalised by previous wall collisions. $E^{(o)}_{J,wall}$ therefore depends on plasma temperature and sheath potential, on R_E at target and wall, on associated values of the particle reflection coefficient R_N and on $\bar{P}$ and R_p, which are defined below. The flow of neutral species J to the wall, $\Gamma^{(o)}_{J,wall}$ in Eq. (6), is related to that at the target, $\Gamma_{J,t}$ by

$$\Gamma^{(o)}_{J,wall} = [\Gamma_t \bar{P}(1 + R_p)]_J \quad . \tag{7}$$

Here $\bar{P}$ (evaluated for D^+, T^+ by a random walk model [3]) is the probability that fast and slow atomic species formed at the target can escape through the wedge-shaped plasma (shown in Fig. 2) of effective thickness ℓ and reach the walls. The factor R_p in Eq. (7) allows for charge exchange in the plasma of those particles returning from the wall.

Within the toroidal scrape-off region, the maximum temperature T_s is derived from the heat flux equation with $T = T_t$ at the target:

$$-(K_o T^{2.5})dT/dz = \alpha Q^{(tot)}/A_\parallel, \text{ [with } dT/dz = 0, T = T_s \text{ when } z = 0] \; . \tag{8}$$

Here $K_o T^{2.5}$ is the parallel thermal conductivity, z is the distance along the field line, and α is a power distribution factor. Within the scrape-off plasma where $z \leq \pi Rq$, $\alpha = z/\pi Rq$, but within the divertor plasma $\alpha = 1$. The density n_s is related to that at the target by:

$$n_s T_s = nT(1 + M^2) = n_t T_t (1 + M_t^2) = 2 n_t T_t . \tag{9}$$

The efficiency, g, for pumping gas from the divertor chamber is determined by the total conductances, S_D, of the ducts and the total speed of the vacuum pumps, S_p. The exhaust flow of particles of species J is thus given by

$$\Gamma^{(o)}_{J,pump} = (\Gamma_t \bar{P}\, g)_J \quad . \tag{10}$$

The vacuum pumping requirement is established when $\Gamma_{He,t}/\Gamma_{DT,t} = n_{He,t}/n_{DT,t} \approx 0.05$.

3. Results

In the analysis, T_t is an independent variable and its value consistent with the INTOR specification is determined by the condition that n_s, given by Eq. (9), is $5 \times 10^{19} m^{-3}$. Results for the standard conditions of INTOR are shown in Fig. 3 and variation of the operating point with exhaust power in Fig. 4. Also shown in Fig. 3 is $\Gamma^{(o)}_{W,t}$ which is the flow of tungsten sputtered from each divertor target. The dependence of $(n_{He}/n_{DT})_t$ upon the combination of duct conductance and vacuum pump speed (twelve ducts and pumps) is shown in Fig. 5. Details of the modelling and results can be found in Ref. 4 and in contributions to the INTOR Workshops [5].

4. References

1. Harrison M F A, Harbour P J, Hotston E S et al, Culham Report CLM-R211, 1981.
2. Morgan J G, Harbour PJ, Fusion Technology 1980, 2 (1981) 1187 (Pergamon).
3. Hotston E S, Models for Transport of Fuel Atoms Across a Scrape-off Layer (1981) to be published.
4. Harrison, M F A, Harbour P J, Hotston E S, IAEA Divertor Workshop, Garching 1981.
5. INTOR Workshop (session 4 - 7), European Contributions. Euratom reference numbers: EUR-FU-BRU/XII 501(80/EDV60, 80/EDV80, 81/EDV10 and 81/EDV20).

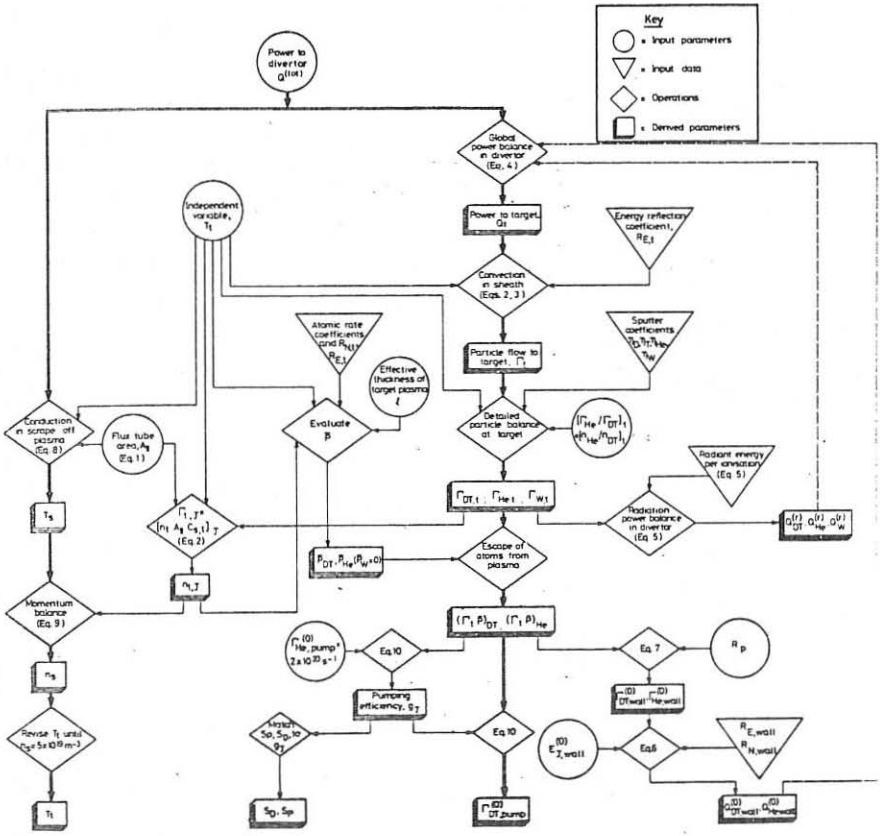


Fig. 1 A simplified schematic representation of the procedure used to derive parameters for the single-null divertor of INTOR.

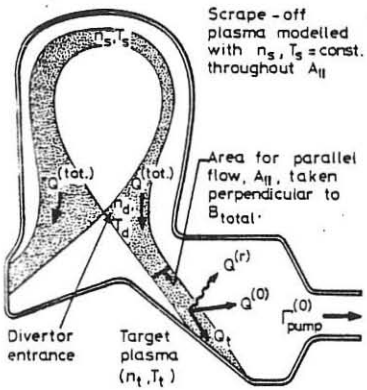


Fig. 2 Schematic diagram of INTOR in the plane of the minor cross-section showing key parameters of the exhaust.

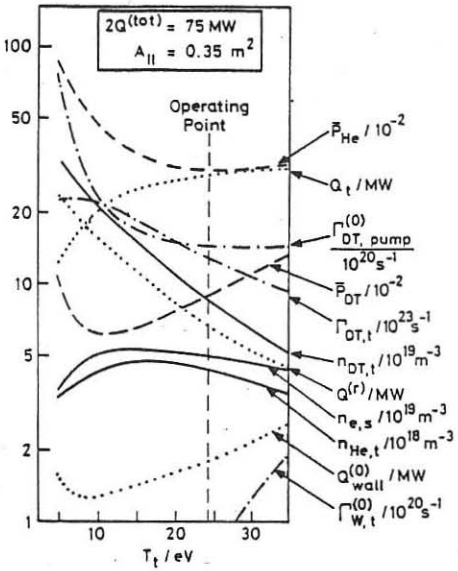


Fig. 3 Data for INTOR plotted as a function of plasma temperature close to the target. The operating conditions are shown for $n_{e,s}$ = 5 x 10^{19} m^{-3} and $(n_{He}/n_{DT})_t$ = 0.05.

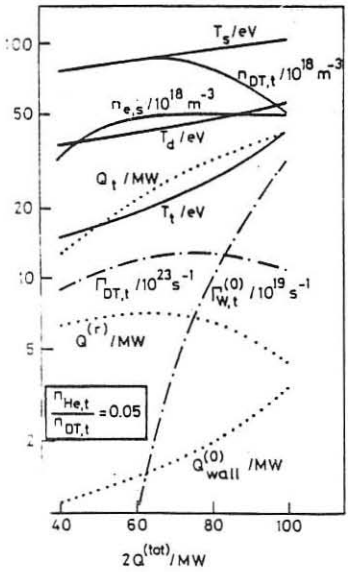


Fig. 4 Variation of operating conditions with exhaust power.

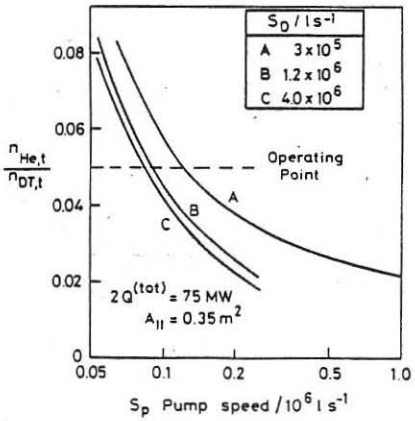


Fig. 5 Dependence of $(n_{He}/n_{DT})_t$ upon the combination of duct conductance, S_D, and vacuum pump speed, S_p (i.e. the total for 12 ducts and pumps.

ICRF HEATING OF A TWO-ION CURRENTLESS PLASMA IN THE URAGAN-2 STELLARATOR

O.M.Shvets, S.S.Kalinichenko, A.I.Lysoivan, N.I.Nazarov, A.S.Slavny, K.N.Stepanov, V.F.Tarasenko

Institute of Physics & Technology, the Ukrainian Academy of Sciences, Kharkov 310108, USSR

Introduction. Ion-cyclotron resonance (ICR) proved highly efficient in minority heating when Alfven waves (AW) [1] were utilized. This report presents some results on heating with AW's (or ICW's) of the hydrogen currentless plasma containing deuterium ions in a small quantity (up to 10%) under the conditions of both ICR's: $\omega \approx \omega_{cD}$ and $\omega \approx \omega_{cH}$. The experiments were performed in the Uragan-2 race track stellarator [2] ($\bar{a} \approx 7.0$ cm, R= 110 cm, L= 1035 cm, $\ell = 3$, $B_0 \sim 20$ KG, $\iota \sim 0.9$). Under the resonance conditions $\omega \approx \omega_{cD}$ the mean hydrogen ion energy was $T_{iH} \sim 1$keV with the density level $\bar{n}_e \sim 10^{12}$cm^{-3} and under the resonance conditions $\omega \approx \omega_{cH}$ the mean plasma ion energy was $T_{iH} \sim 400\,eV$ for hydrogen and $T_{iD} \sim 300\,eV$ for deuterium at the density level $\bar{n}_e \sim 2 \cdot 10^{12}$cm^{-3}. Plasma was produced and heated with rf-power input around $P_{RF} \sim$ 300kW at f=10 MHz. The overspeeded rate of energy exchange between the ion components cannot be accounted for by the Coulomb collisions, although it may have something to do with shortlength plasma instabilities in the ICW field. The employing of two rf-generators (one for plasma production, $f_1 \approx$ 10 MHz, $P_1 \sim 300$kW and the other for plasma heating, $f_2 \approx 20$MHz, $P_2 \sim 1$MW) ensured the ion heating up to $T_{iH} \gtrsim 300$eV at $\bar{n}_e \gtrsim 10^{13}$cm^{-3} with the pulsing of the generators being time separated. Any overlapping of the rf-pulses was found to cause an abrupt weakening of the ion heating.

Results & Discussion. During the first leg of our experiment the rf-power source was connected to the frame type antenna that operated within a broad spectrum of spatial longwave harmonics of the rf-field radiated ($\lambda_z \approx 1000 \div 100$ cm). Under the conditions of the AW resonance excitation the plasma density was $\bar{n}_e \sim (4 \div 10) \cdot 10^{12}$cm^{-3} across the broad sweep of longitudinal magnetic field strength, to include ICR regions for both hydrogen and deuterium ions, $\Omega_H = \frac{\omega}{\omega_{cH}} \approx 1 \div 0.4$. The re-

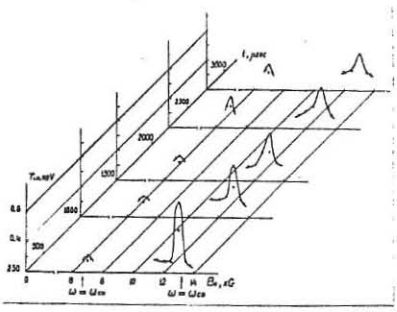
lative concentration amount of deuterium ions in the hydrogen plasma did not exceed $\frac{n_D}{n_H} \sim 0.1$. Plasma ions were observed to heat up a good deal when the magnetic field strength was $B_0 \sim 7$kG and $B_0 \sim 13$kG which is pretty close to the cyclotron values for protons and deuterons(Fig.1). The energy spectra of hydrogen and deuteron ions as measured in the ICR regions for both types of ions differed substantially from the Maxwellian ones (Fig.2). As compared to protons the deuteron energy spectra are characterized by possession of a higher energy tail during the heating in the resonance $\omega \approx \omega_{cD}$. However, the study of energy spectra time dependence for ions of those types reveals that the proton average energy $T_{\perp H}$ in both ICR's is higher than the deuteron one $T_{\perp D}$ during the entire course of heating as it is (Fig.1). The energy exchange time between deuterons and protons ($\tau_{exch.} < 100\ \mu s$) could not be explained by the Coulomb collisions between them (at $n_e \sim 4 \cdot 10^{12} cm^{-3}$ and $T_{\perp D} \gtrsim 300eV$ $\tau_{exch.} \ll \tau_c \sim 4\ ms$). The wave field amplitude in plasma under the ICR resonance conditions was $\tilde{H}_z \sim 150e$. With such rf-field strengths in plasma the assigned velocity of deuterons in their cyclotron resonance region $u_\perp = \frac{k_\perp c \tilde{A}_\perp}{4\pi n_e e} \sim 5 \cdot 10^7 \frac{cm}{s}$ rises above the plasma ion thermal velocity v_{Ti}. In accordance with the theory [3,4] the small scale beam type instabilities that can be excited under those conditions originate from the relative ion-ion oscillations. These instabilities have a characteristic increment γ and a frequency ω of the order ω_{pi} while their wavelengths are $\lambda_\perp \sim u_\perp / \omega_{pi}$. At the condition $u_\perp \lesssim v_{Ti}$ the parametric ion-cyclotron instabilities get excited [5,6]. The resulting plasma particle scatter on the instability-induced electric field pulsation brings about the turbulent heating of plasma the rate of which can be determined through the level of turbulence. The level of turbulence is especially great in case of ion-ion instabilities. The heating of both ion components in plasma can be associated with either the Cerenkov and cyclotron plasmon absorption-emission or with the finite instability correlation time for the conditions of strong turbulence otherwise known as the stochastic heating [7].

The second leg of our experiment included the heating of a dense ($\bar{n}_e \geq 10^{13}\,cm^{-3}$) two-ion plasma, the two generators in simultaneous operation at different frequencies. One generator paired with a frame type antenna ($\lambda_z \approx 1000 \div 100$ cm) was used for plasma production under the conditions of the AW excitation ($\Omega_{1H} \approx 0.44$). To heat the plasma up with IC waves in the magnetic fields $B_0 \sim 15$kG ($\Omega_{2H} \approx 0.83$) was the functional purpose of the other generator. The rf-power from this generator was fed to plasma via a slot antenna [2] which had a compact harmonics spectrum of the rf-field radiated ($\lambda_z \approx 80 \div 30$ cm). At these conditions the plasma ions were heated most effectively only upon switching on the second generator after the termination of a pulse from the first one(Fig.3). The function of proton distribution to energies remained close to the Maxwellian one throughout the entire heating period (Fig.4). A noticeably reduced efficiency of plasma ion heating was observed when both generators were in simultaneous operation. The afore-mentioned small scale instability build-up in the priorly produced plasma may well have something to do with this phenomenon. This state of plasma is characterized by both a higher effective collision frequency ν_{eff} of charged particles and a higher rate of their diffusion across the magnetic field with a possible result of lower plasma heating effectiveness [8].

Acknowledgements. The authors are indebted to the engineering and technical staffs of the Uragan-2 stellarator and the rf-generator installations for their expert handling of the technicalities involved.

References.

1. A.G.Dicky et al. Proc.6 Inter.Conf.on Plasma Phys. and Contr. Nucl.Fusion Research, v.2, p.129 (Vienna 1977).
2. S.S.Kalinichenko et al. Proc. 9 Europ.Conf. on Contr.Fusion and Plasma Phys., v.1, p.19 (Oxford 1979).
3. L.I.Grigor'eva et al. Proc. 4 Inter.Conf. on Plasma Phys. and Contr.Nucl.Fusion Research, v.3, p.573 (Vienna 1971).
4. V.L.Sizonenko, K.N.Stepanov. Pys'ma v ZhETF, 8, 592 (1968).
5. A.B.Kitsenko et al. ZhTF, 43, 1425, 1437 (1973).
6. A.B.Kitsenko, K.N.Stepanov. ZhETF, 64, 1606, (1975).
7. O.M.Shvets et al.Fyzika Plazmy y Problemy UTS, Naukova Dumka, 1971, No1, p.86.
8. O.M.Shvets, L.V.Dubovoy. Izvestia AN SSSR, 24, No 8, 1013 (1960).



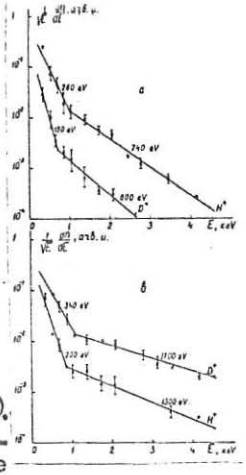


Fig.1. The ion $T_{\perp H}$(o) and deuterium $T_{\perp D}$ (x) mean ion energy dependence on the longitudinal magnetic field B_o magnitude during the rf-pulse (τ_{RF}=4.3ms).

Fig.2. The measurements of energy spectra for protons and deuterons under the ICR conditions:

a) B_o = 7kG, t = 2.0ms;

b) B_o = 13kG, t = 0.1 ms.

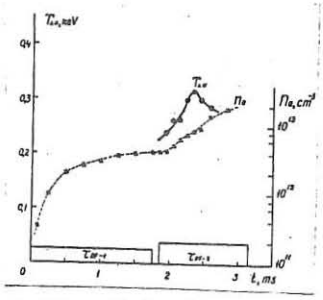


Fig.3. Time behavior of the as-produced two-ion plasma $\bar{n}_e$ density and hydrogen $T_{\perp H}$ ion temperature with both rf-generators in operation.

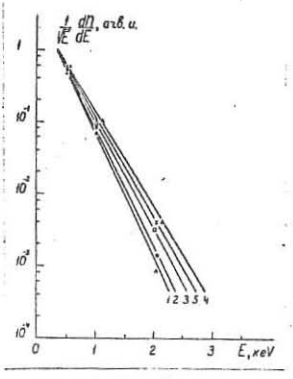


Fig.4. The hydrogen ion energy spectra behavior during the second generator pulse: 1 – $T_{\perp H}$≈240eV, t= 0.1 ms; 2 – $T_{\perp H}$≈270eV, t = 0.3 ms; 3 – $T_{\perp H}$≈300eV, t = 0.4 ms; 4 – $T_{\perp H}$≈330eV, t = 0.5 ms; 5 – $T_{\perp H}$≈290 eV, t = 0.75 ms.

DRAG CURRENTS PROFILES FORMATION AND DIFFUSION CONTROL BY HF FIELDS IN A STEADY-STATE TOKAMAK

A.G. Elfimov, K.G. Komoshvilli, V.P. Minenko, V.P. Sidorov

Sukhumi Institute of Physics and Technology, Sukhumi, USSR

The idea of creating a steady-state tokamak on the non-inductive current drive basis, suggested in [1], attracts even greater attention nowadays.

Experimental and theoretical efforts on drag currents [2] generation by travelling HF waves, undertaken for various wave modes and frequency ranges, prove the existence of power efficient physical mechanism, being able to sustain the stationary toroidal current. The calculations made for the Alfven wave electron heating ($k_\parallel c_A(0) < \Omega < \omega_{HL}$) show that power efficiency of drag current generation, determined by the expression

$$\eta = \langle I \rangle (A) / P(W) = 10 \frac{\sqrt{\frac{m_i}{m_p}}}{\lambda Z_{eff}} \cdot \frac{\sqrt{n_{13}^*}\, T_e^{3/2}(keV)}{\langle n_{13} \rangle R(m) H(T)}, \quad (I),$$

is large enough. Here $n_{13}^*, \langle n_{13} \rangle$ - resonant and average profile density values in $10^{13} cm^{-3}$.

It should be mentioned that the main contribution to the power, absorbed by electrons $W/nT = \sqrt{\frac{\pi}{2}}\left(\nu_{ee} + \frac{3\pi}{4}\nu_{ei}\right)\left(\frac{c_A}{V_{Te}}\right)^2 \sqrt{\frac{\sqrt{2}eE_z^0}{k_z m_e V_{Te}^2}}$ from the monochromatic Alfven wave with non-linear distortion of the electron distribution function for $\nu_{ei} < \sqrt{k_z eE_z^0/m_e}$ is made by "semi-trapped" particles having $|v - c_A|^2 \geq \sqrt{2}eE_z^0/k_z m_e$ [3]. In this case, in despite of [4], drag current, proportional to the square root of the wave amplitude value, is generated $\langle j \rangle = \sqrt{\frac{\pi}{2}}\left(\frac{\nu_{ee}}{\nu_{ei}} + \frac{3\pi}{4}\right)\sqrt{\sqrt{2}eE_z^0/k_z m_e V_{Te}^2}\; n_e e c_A$.

Alfven waves application enables to form specified steady-state currents profiles, which improves the MHD plasma stability and permits transport process control. The resonant surface in the Alfven wave case represents a torus of a certain absorption length (Fig.I). The required profile of the steady-state current can be formed by combinations of several monochromatic waves. The current is dis-

tributed corresponding to the density of the power absorbed according to $\langle j \rangle = \frac{e}{m_e \nu_{ei}} \sum_s \frac{k_{zs}}{\Omega_s} W_s$. The absorbed power radial distribution was found after numerical solution of differential equations sytem for Alfven range fields with parabolic profiles of density and temperature, as suggested in [5].

The data for calculations ($k_z a = 1,5$; $k_z c_A(0)/\omega_{Hi} = 0,07$; $\mathrm{Re}(\varepsilon_{zz}/\varepsilon_1) = 4,6 \cdot 10^4$; $m=2$; $\mu = 0,3$ - quasilinear attenuation coefficient of Landau damping) were $a=1,5$cm, $T_e = 5$keV. The resonant surface was located on different radii: $0.1 \leq x_{res} \leq 0.9$ its position being determined by the generator frequency choice: $x_{res} = \sqrt{1 - k_z^2 c_A^2(0)/\Omega^2}$. Figs.1a and b represent characteristic absorbed power profiles for two resonant surface positions: $x_{res} = 0,8$ ($\Omega = 1.1 \cdot 10^8$ s^{-1}) and $x_{res} = 0,355$ ($\Omega = 7.5 \cdot 10^7$ s^{-1}); Fig.1c shows the absorbed power profile for the sum of three waves of $\Omega_1 = 7,36\ 10^7 s^{-1}$, $\Omega_2 = 7,55\ 10^7 s^{-1}$, $\Omega_3 = 7,8\ 10^7 s^{-1}$ having the weight 2; 1 and 0,67, respectively.

By friction of plasma components toroidal current induces longitudinal ion movement in a torus. Nevertheless, the speed of the movement is limited by friction on supertrapped ions and ion neoclassical viscosity.

The estimation in terms of untrapped particles momentum balance gives:

$$\frac{2}{m_i n \nu_{ii} \sqrt{\delta}} \hat{L} v_i^u + v_i^u = v_i^s - 2 \frac{m_e \nu_{ei}}{m_i \nu_{ii}} \left[\frac{u_o}{\sqrt{\delta}} + (1 - \sqrt{\delta})(v_i^s - v_e^s) \right] . \qquad (2)$$

Here u and s correspond to the untrapped and supertrapped particles, $\hat{L}$ - viscosity operator, u_o -current velocity, δ -ripple ratio. The neoclassical viscosity in a real tokamak is low, as compared to the friction of the untrapped ions on the local trapped ones, and practically $|v_i^u / u_o| \ll 1$. Besides toroidal, the helical wave generates poloidal drag current, the latter contributing to plasma confinement along the small radius. The set of movement and continuity equations gives:

$$\frac{\partial n}{\partial t} = \frac{1}{r} \frac{\partial}{\partial r} r \frac{D_\perp}{T_\Sigma} \left(\frac{\partial P}{\partial r} + 16 \frac{T_\Sigma}{T_e} \frac{D_B}{D_\perp} \langle f_\varphi^e \rangle \right) . \qquad (3)$$

Here $D_\perp$ and D_B -transverse and Bohm diffusion coefficients,

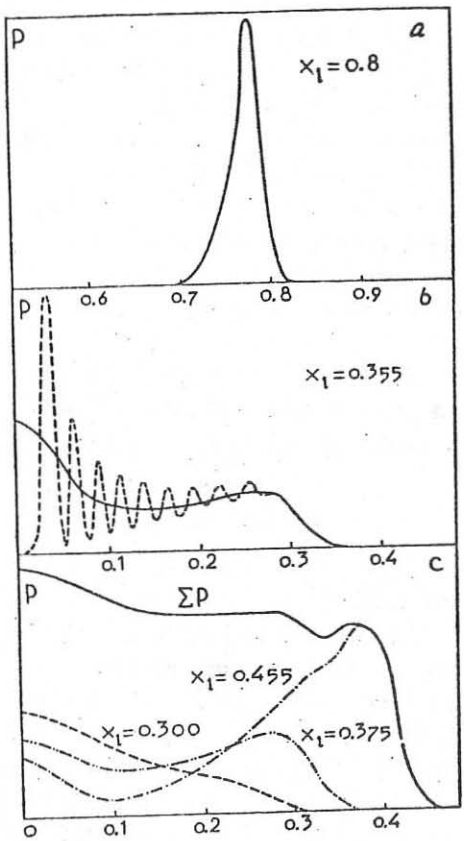


Fig. I

Fig.Ia,b. Absorbed power and current profiles for the following resonant surface positions: $x_{res} = 0,8$; $x_{res} = 0,355$.

Fig. Ic. Absorbed power and current profiles, formed by the superposition of three waves: $\Omega_1 = 7,36\ 10^7 s^{-1}$, $\Omega_2 = 7,55\ 10^7 s^{-1}$, $\Omega_3 = 7,8\ 10^7 s^{-1}$.

$\langle f_\varphi^e \rangle$ poloidal drag force. As can be seen, there exists a stationary distribution of plasma with

$$P(r) = P(0) - \int_0^r 16 \frac{T_\Sigma}{T_e} \frac{D_B}{D_\perp} \langle f_\varphi^e \rangle dr .$$

At the initial stage after $\langle f_\varphi^e \rangle$ switching, one can achieve an essentially greater, as compared to the diffusion, velocity of density evolution: $\frac{\partial n}{\partial t} \sim \frac{D_B}{r r'} \langle f_\varphi^e \rangle$.

With proper rotation direction and large enough HF amplitude, switching of $\langle f_\varphi^e \rangle$ results in plasma compression.

Hence, it is shown that using of HF fields of Alfven range one can generate specified drag currents, which would essentially improve plasma stability, its radial diffusion, which meets the demands of a steady-state tokamak existence and control.

The authors would like to express thier gratitude to A.G. Kirov and V.V. Parail for useful discussions and A.G. Dmitrenko for carrying out the necessary computation.

REFERENCES

I. D.F.H. Wort. Plasma Physics, 3, 258 (I97I).

2. R.A. Demirkhanov, Yu.S. Khodyrev, N.I. Leontjev. Nuclear Fusion Suppl., Part I, 259 (I962).

V.P. Sidorov, T.R. Soldatenkov. ZhTF, I0, I749 (I965).

R.A. Demirkhanov, A.G. Kirov, L.F. Ruchko, A.V. Sukachev. Pisma v ZhETF, 33, 3I (I98I).

3. V.E. Zakharov, V.I. Kariman. ZhETF, 43, 2, 490 (I962).

4. A. Hasegawa. Nucl.Fusion, 20, No9, II58 (I980).

5. A.G. Elfimov. Preprint SFTI-5, Sukhumi (I980).

MAIN FEATURES OF THE "KEDR" RF DEVICE AND FIRST RESULTS ON ICRF PLASMA HEATING IN T-10 TOKAMAK

A.V. Longinov, I.M. Arkatov, D.V. Berezov, E.I. Kolosenko, E.D. Kramskoj, G.A. Miroshnichenko, G.Ya. Nizhnik, S.P. Pozdnyshev, B.I. Smerdov, K.N. Stepanov, A.A. Chmyga
Kharkov Institute of Physics & Technology, Ukrainian Academy of Sciences, Kharkov, USSR

V.S. Strelkov, V.V. Alikayev, V.L. Vdovin, A.V. Chesnokov, N.V. Shapotkovsky
I.V. Kurchatov Institute of Atomic Energy, Moscow, USSR

Recent advantages [1] on ICRF heating in tokamaks by means of the fast magnetosonic waves involving the cyclotron resonance for minority ions [2] (see the first experiments [3,4]), the mode conversion [5] and the 2nd harmonic resonance are due to the development of loop type antennas [1] as well as to the realization of the regimes in which the toroidal mode resonances overlap [6] .

To make the next step, i.e. to heat the plasma up to the temperatures T =2-10 keV it is necessary to construct powerful RF sources (P = 5-10 MW, $\tau_{RF} \gtrsim$ 0.1 s, f = 40-80 MHz) and to solve the more difficult problem of coupling the RF power to the plasma.

In this report the basic data on the "Kedr" device for RF heating and the results of the first experiments on ICRF plasma heating in T-10 are presented.

"Kedr" device. The device consists of a powerful RF generator, an antenna array and auxiliary systems [7] . The generator is made according to the two-stage scheme (master oscillator-amplifier), the operating frequency range being f =30-50 MHz. The power achieved in the test pro-

cess amounted to P =7 MW at τ_{RF} =50 msec. The radiating surface of the antenna is made with a system of parallel conductors located at the angle α =30° to the magnetic field (Fig.1). The transmission line feeds the inner ends of the conductors, the outer ends being conductively coupled to the liner.

The antenna is supplied with the e.s. shield and the protecting diaphragms. Low impedance and the large area of the radiating surface (70x52 cm^2) allow one to diminish essentially the RF potential on the antenna elements and to increase therefore the RF power coupled to the plasma (according to the calculations $P \sim 5$ MW). The investigation of the antenna performed in the weak signal regime under the tokamak operating pulse conditions revealed a sufficiently good coupling between the antenna and the plasma. The coupled impedance due to the radiation of RF energy into the plasma is 5 times more than the impedance due to the proper losses in the antenna elements. Under the same conditions the possibility of the antenna operation in the toroidal mode resonance overlapping regimes was shown even at low plasma densities ($\bar{n}_e \lesssim 10^{13} cm^{-3}$). In the short pulse regimes ($\tau_{RF} \sim 0.1$ msec) the coupling of the large power ($P \sim 1$ MW) to the plasma was made which pointed to no effects that may impede its further increase. ICRF heating experiments. These experiments were preceded by a short time ageing of the antenna performed while operating with the operating pulse (gas - hydrogen, P = 100-150 kW, $\tau_{RF} \lesssim 350$ ms). This ageing time was also used for the rough tuning of the matching and frequency

tuning systems. The main parameters of the operating pulses were as follows: B_t =30.3 kG, I_p =360 kA, $q \approx 2.5$, a_p= 30 cm, f =47.6 MHz. RF heating was made in the deuterium plasma with the 12% component of hydrogen.

The experiments were performed in two regimes. In the first regime the essential growth of the plasma density during the RF pulse is observed, the density approaching a stationary value only at the end of the pulse (Fig.2a). The neutron flux is increased during the RF pulse (see Fig.2b). The proton temperature measured by the charge-exchange method is established on the 900 eV level during 20 ms and it changes weakly during the RF pulse whereas the deuteron temperature calculated from the neutron flux measurements rises during the whole pulse from 560 to 680 eV. (The electron-ion collisions are important in this regime and the increase in T_D is associated in part with the density $\bar{n}_e$ increase).

The second regime (Fig.3) is characterized by considerably smaller electron densities at the beginning of the RF pulse, $\bar{n}_{e_0} = 6 \cdot 10^{12} cm^{-3}$. The energy lifetime τ_E^D increases and the RF power exceeds considerably the power transferred from electrons to deuterons. During the RF pulse does not achieve a stationary value. At the end of the RF pulse T_D =0.95keV and ΔT_D=0.5 keV.

Taking into account that $T_e \approx T_D$ at the end of the RF pulse τ_E^D may be estimated using the rate of temperature decay at the moment of switching off the RF pulse $\tau_E^D \approx 220$ ms. That value agrees with the neoclassical value in the region of weak collisions. However this value exceeds conside-

rably the estimate τ_E^D(9) due to fast deuteron drift trapped by the toroidal magnetic field ripples. This allows one to hope to achieve bigger T_D values on coupling more RF power to T-10 plasma comparing with the values T_{Dmax} estimated on accounting for the superbanana ion thermoconductivity.

REFERENCES

1. Equipe T.F.R. 8th Intern.Conf.(Brussels,1980) Rep.IAEA-CN-38/D-3; J.C.Hosea et al.,ibid.,Rep.IAEA-CN-38/D-5-1; H.Kimura et al..ibid.,Rep.IAEA-CN-38/D-5-2.
2. А.В. Лонгинов, а.с. № 342560/Пр.21.01.1971/БИ, №5, 1975.
3. Н.В. Иванов и др. Письма в ЖЭТФ,24,349,1976.
4. В.И. Вдовин и др. Письма в ЖЭТФ,24,410,1976.
5. R. Klima et al.,Nuclear Fusion,15,1157,1975.
6. A.V. Longinov et al.Proc.7th Intern.Conf.(Innsbruck,1978), v.3, IAEA,Vienna,1979,p.583.
7. А.В. Лонгинов и др.Тезисы докл.II Всесоюзн.конф.по инж. проб.термояд.реакторов/Ленинград,1981/,с.156,169.
8. А.В. Лонгинов, а.с.762613/Пр.4.07.1979/БИ, №19,1981.
9. T.E.Stringer. Theory for Toroidal Plasma, Int.School of Plasma Physics, Varenna,1971.

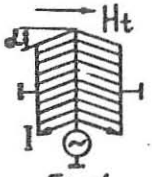


Fig.1

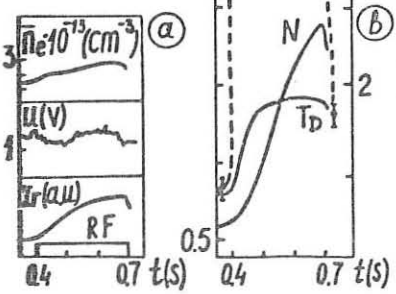


Fig.2. P=90±30kW, τ_{RF}=0.3 s

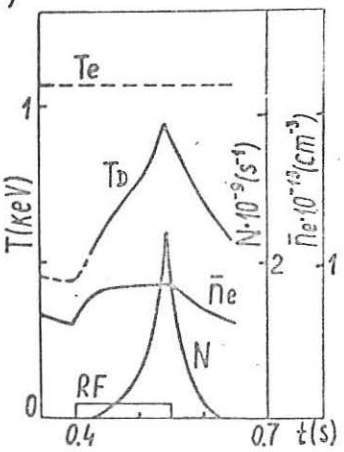


Fig.3. P=140±50kW, τ_{RF}=0.15s

OPTIMIZATION OF THE JOULE HEATING IN RFP PLASMAS

Buffa A., Costa S., Giudicotti L., Jacobson A.R.*, Nalesso G.F.,
Ortolani S., Scarin P.

Centro di Studio sui Gas Ionizzati
del Consiglio Nazionale delle Ricerche e dell'Università di Padova
(Associazione Euratom-CNR) - Padova (Italy)

INTRODUCTION Recent experiments [1,2] on the toroidal device Eta-Beta II have shown that a plasma regime characterized by reduced losses and improved confinement (quiescence) can be obtained when operating as a Reverse Field Pinch. Furthermore an optimum range for heating and confinement which depends on the ratio between the plasma current and the line density (I/N) has been evidenced. More recently other medium sized machines (TPE-IRM-Sakura Mura, ZT-40M-Los Alamos, HBTX1A-Culham) have confirmed this general behaviour and reinforced the interest on RFPs as potential fusion reactors.

In this paper a detailed study of the parameters influencing the regime of optimum heating, and results on plasma characteristics during the quiescent phase are presented.

EXPERIMENTAL RESULTS The setting up phase of both RFP and Stabilized Pinch discharges produced on Eta-Beta II has already been discussed [2] and the existence of an optimum range depending on the parameter I/N, where both τ_I (current decay time) and T_e reach the highest values, has been experimentally observed.

Recently a more systematic set of measurements has been carried out, varying, besides the filling density, also the plasma current peak in a wider range. From the collected data a clearer scaling of the maximum $\hat{\tau}_I$ and $\hat{T}_e$ and of the I/N at which these maxima occurs, has been derived. In figure 1, τ_I is drawn as a function of the ratio of the peak current and the filling line density (I/N) with $\hat{I}$ as a parameter and in figure 2 the same plot is shown for $T_e(0)$ measured by Thomson scattering on axis at the current peak.

The left part of these curves (i.e. for low values of I/N) is determined by increasing impurity radiation. This fact is confirmed by the measured total radiated energy (see for example figure 3) which presents an almost step like dependence on the filling pressure, and by the behaviour of the intensities of oxygen lines measured at various filling pressures. In fig. 4, as an example, the space and time integrated intensity of a line of OVI, V,

* On leave from Los Alamos Laboratory, N.M.

IV and III is drawn versus filling density. The observed shift toward lower ionization stages as the filling density increases is consistent with the measured increase of the total radiation and decrease of the electron temperature on axis. However we note that O VII lines are not observed, despite what one would expect from an average temperature $\geq$ 30 eV (consistent with Thomson scattering data) on the basis of a simple corona equilibrium. Calculations including charge-echange with neutrals (whose existance can be infered from the observed electron pump-out) can however explain these results. The importance of the impurity content for the heating of the plasma is evidenced also by considering that for the data shown in figure 2 an oxygen content of 1÷2% has been measured by adding known quantities of O_2 and comparing the line intensities. This method inevitably increases the amount of impurity present in the discharge, due to absorption of O_2 from the wall.

In fact, by comparing these results with those reported previously [2], ($\hat{T}_e \sim 80$ eV at $I/N \sim 1.3\ 10^{-14}$ A·m with $\hat{I}$ 250 KA), it can be observed besides a small shift of the optimum for T_e to higher values of I/N, a remarkable reduction of the maximum temperature achievable. This fact is interpreted assuming a reduced impurity content ($\lesssim$ 1%) for the old data, collected after a long series of cleaning discharges, and underlines the role of impurity radiation also in the optimum range. This amount of oxygen content can also explain the observed behaviour when considered in a 0-D plasma power balance [3] (figure 3).

While impurity radiation losses clearly explain the lower limit on I/N for optimum plasma heating, from figures 1 and 2 we see as the upper limit depends on the current itself. This behaviour may be interpreted assuming that the cooling of the discharge, at high values of I/N, is due to energy losses associated with instabilities, whose nature is however presently unknown, triggered when the streaming parameter $\xi = V_d/V_{th,e}$ becomes greater than a few percents. In this case a scaling of the I/N value corresponding to $\hat{\tau}_I$ and $\hat{T}_e$ with $\sqrt{T_e}$ can be easily derived and can indeed fit the experimental values shown in the figures. A spectral analysis of the magnetic field fluctuations, to try to identify the nature of the instabilities and the triggering mechanism is presently in progress. The average (rms) value of the fluctuations is < 1% in the optimum range and increase up to 3% as I/N increases.

Also the "quiescent phase" (QP) of RFP discharges has been studied in detail. Laser scattering measurements of $T_e(0)$ and $n_e(0)$ have been extended in time, but not yet till the end of the discharge because the plasma density

during QP is often below the limit of the sensitivity of the present scattering apparatus. The results, for a typical set of parameters are shown in figure 5 where also the line of sight density from an IR interferometer $\langle n_e \rangle$ (averaged over many shots) is reported for comparison. These results agree with the previously reported ones [2] and confirm the initial drop of the electron density (pump out) during the establishment of the configuration with the simultaneous rapid increase of the electron temperature, followed by the quiescent phase.

To measure the time and space behaviour of the magnetic field a set of magnetic coils has been inserted radially, in an equatorial plane, into the plasma. Unfortunately the probes drastically perturb the discharge, as can be seen in fig. 6. In fig. 7 a typical magnetic field configuration, during QP, is shown. The average β derived from these profiles, assuming pressure balance, is about 0.1. The β value derived from pressure balance is also consistent with the value on axis deduced from laser measurements of $T_e(0)$ and $n_e(0)$ (fig. 8) and assuming equal ion and electron temperatures. From the magnetic field measurements an estimate of the energy confinement time τ_E has been made assuming steady state. With the previously given value of β an average value of $\tau_E \simeq 30$ μs is derived. This value of τ_E represents obviously a lower bound for the standard discharges (i.e. without probes). A better estimate for the standard case can be derived taking into account the different decaying times of the two discharges and gives a value of $\tau_E \sim 100$ μs.

CONCLUSIONS New evidence of the existence of upper and lower limits on the ratio I/N to obtain the optimum plasma heating and confinement on Eta-Beta II is reported. The lower limit has been found to be related to excessive impurity radiation losses and this result has been confirmed by new measurements in the XUV region. The upper limit on I/N is set by transport losses associated with increasing fluctuations, and the results of Eta-Beta II support a dependence of this limit on the streaming parameter $v_d/v_{th,e}$.

Measurements of $T_e(0)$ and $n_e(0)$ have been extended in time and confirm the initial indications of an effective joule heating. Measurements of average β and energy confinement time indicate $\beta \sim 0.1 \div 0.2$ and τ_E in excess of 0.1 ms.

Acknoledgements We gratefully acknowledge the collaboration of L. Finesso and M. Guarino for the data acquisition and analysis system, the collaboration of G. Tondello on the XUV spectroscopy and the continuous technical assistance on the experiment of U. Alfieri, E. Baseggio, G. Bertocchi, I. Dalla Libera, G. Mella, I. Molon, A. Tamiazzo and S. Zago.

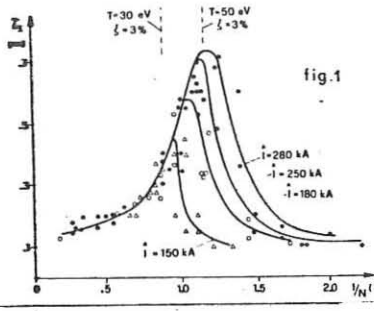


fig.1

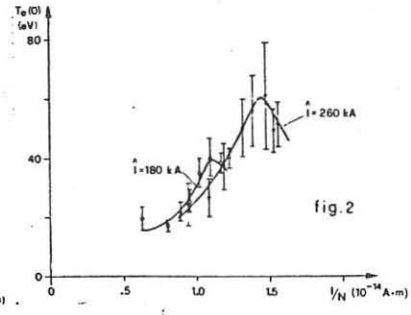


fig.2

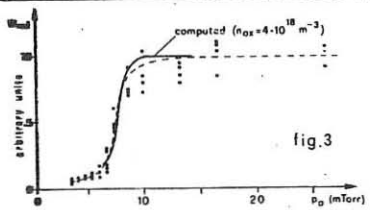


fig.3

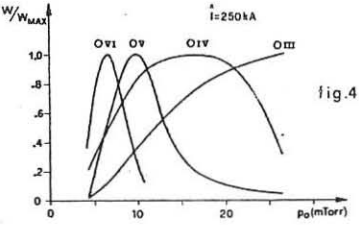


fig.4

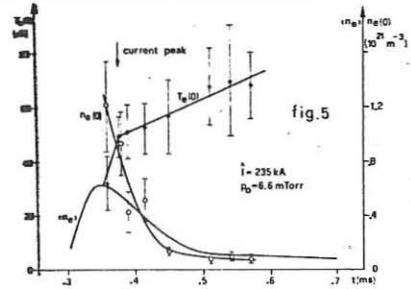


fig.5

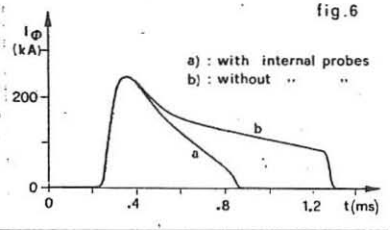


fig.6

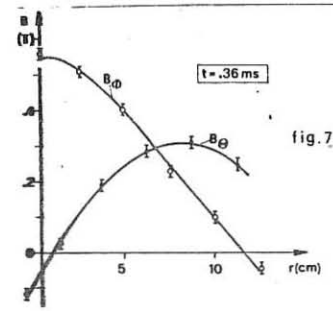


fig.7

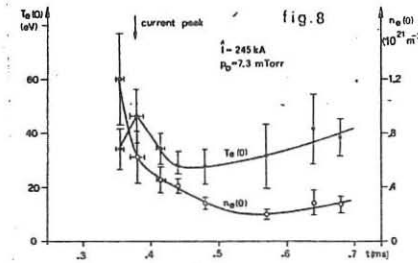


fig.8

REFERENCES

[1] Buffa A. et al.: 9th EPS Conf., vol. II, 544, Oxford (1979).

[2] Buffa A. et al.: 8th IAEA Conf., Bruxelles (1980), paper IAEA-CN-38/L1.

[3] Bagatin M. et al.: University of Padua Report, UPee 80/05, 1980.

RFP FORMATION AND VOLT SECOND CONSUMPTION WITH VARIOUS CURRENT RISE TIMES

Buffa A., Ortolani S.
Centro di Studio sui Gas Ionizzati
(Associazione Euratom-CNR) - Università di Padova (Italy)

INTRODUCTION - By changing the number of turns of the primary winding for the poloidal circuit (n_ϕ) and of the toroidal field inductor (n_θ), various characteristic times for the formation of Reversed Field Pinch (RFP) configuration have been obtained in the ETA-BETA II experiment. In this paper we discuss the flux consumption during the RFP formation as a function of the current rise time, and of the pinch parameter $\Theta=B_\theta(a)/\langle B_\phi\rangle$ (which varies mostly depending on the toroidal field programming). The results reported refer to a filling density of about $4\cdot10^{20}$ m^{-3} of deuterium which corresponds to the higher temperature and longer current pulses at about 200 kA [1].

DEPENDENCE ON FIELD PROGRAMMING (Θ) - A wide range of Θ values has been obtained by varying the toroidal field programming at the various current rise times. The volt second consumption is written as: $\int V_\phi(a)dt=L\,I_\phi+\int V_\phi(o)dt$; the inductance of the pinch has been measured by internal magnetic probes to be about 0.6 μH at $\Theta\simeq2$. We take this measured value of inductance and scale linearly with Θ. With the measured voltage and current we compute the quantity $K_\phi=\int V_\phi(a)dt/LI_\phi = 1+\int V_\phi(o)dt/LI_\phi$ at two characteristic times: t_1 corresponding to the end of the current rise phase when $dI_\phi/dt=0$; t_2 corresponding to the end of the applied toroidal voltage when the circuit is crow-barred ($V_\phi(a)=0$). In figure 1 the results obtained under various experimental conditions (see TABLE I) are plotted versus Θ. Even if the assumed linear scaling with Θ is somewhat arbitrary, the results reported in figure 1 clearly indicate a large increase of the flux loss during setting-up as Θ decreases to $\lesssim1$; i.e. for discharges in which a RFP is not formed at all (up to $t=t_2$) or not yet formed at $t=t_1$. To evidence the differences between "Self-Reversed Pinches" (SRP) and RFP's obtained by "aided reversal" [1], in figure 2 we have reported only the results obtained with the longer current rise time . When no field programming is applied a substantially larger flux loss is obtained as compared to the formation by "aided reversal", independently on the reached Θ value. An example of the variation of the applied volt second and of LI_ϕ during the formation phase is given in figure 3 for two RFP discharges and one Stabilized Pinch (SP). For a RFP it appears as the resistive flux loss ($\int V_\phi(o)dt$) increases during the rise of the current (up to t_1) and subsequently from t_1 to t_2 there is little variation. The field reversal is in these examples obtained shortly after t_1. The Stabilized Pinch case corresponds to a larger flux loss increasing up to t_2; in this case Θ is about constant between t_1 and t_2. The initial phase is then spent to produce the current at relatively low Θ values; in the second phase when a RFP configuration is formed, the plasma is detached from the wall, the confinement (expecially in the outer region) is improved and the heating takes place. This picture is substantiated by temperature and magnetic field profile measurements which will be discussed in the next section.

DEPENDENCE ON CURRENT RISE TIME - We now compare for given Θ values the results obtained with different current rise times (see figure 4). The shortest rise time considered (∿120 μs) corresponds to a little time difference between current peak and voltage crow-bar so that we refer only to t_2 for this case. Independently on Θ an almost linear dependence of K_ϕ with current rise time and or toroidal voltage quarter period is observed. For the three current rise times studied the on axis temperature has been measured by Thomson scattering at the two considered times (see figure 5) under similar programming conditions (i.e. Θ). When operating with the longer formation time , the temperature rises very slowly and at $t=t_1\simeq 350$ μs, when about 200 kA are reached, is still less than 20 eV, but subsequently it rises rapidly to about 70 eV at $t=t_2$. This behaviour supports quantitatively the fact that from t_1 to t_2 the flux loss is negligible as compared to the initial phase. In the intermediate case ($t_1\simeq 150$ μs; $t_2\simeq 270$ μs) the temperature at t_1 is already ∿30 eV and reaches also ∿70 eV at $t=t_2$. Finally with the shorter rise time the temperature is ∿45 eV at $t=t_1\simeq t_2$. From the temperature measurements on axis we can compute the resistive flux loss by writing: $\int V_\phi(o)dt = 2\pi R\int \eta(o)J(o)dt$, and assuming $J(o) = \langle J\rangle = I_\phi/\pi a^2$, and classical electrical resistivity. The resulting resistive flux loss are reported in figure 6. A large resistive loss (∿75% of the estimated poloidal flux) is obtained at the longer rise time. For comparison the resistive flux loss deduced as difference of the applied volt second and the estimated magnetic flux is also reported in figure 6. For simmetry in figure 4 the K_ϕ factor deduced from the temperature measurements is also reported. The two derivation based on independent evaluation are in fairly good agreement. A number of coils, equally spaced by 4 mm, have been inserted up to about 2.5 cm inside the liner inner convolution. In figures 7 and 8, for several shots, the measured profiles at t_1 and t_2 are reported corresponding to the longer current rise time operation and to measurements taken on the same discharge in which the temperature measurements have been made. We see from figure 7 as at t_1 the toroidal field is not yet reversed and substantial poloidal currents flow near the wall. At t_2 the RFP has been already formed and in the outer centimeter of the discharge there is little current flowing. Similarly in figure 8 we see as the poloidal field profiles are peaked near the wall at $t=t_1$ whereas at $t=t_2$ the peak of B_θ moves inward, where about the zero of the toroidal field is, indicating little toroidal current in the outer region after the configuration has been formed.

DISCUSSION - The assumed linear scaling of the magnetic flux with Θ is probably unrealistic far from Θ=2 where the flux has been measured. However the large increase of K_ϕ as Θ decreases to <1 is largely independent from the assumptions made and indicates clearly that the SP formation is more lossy than the RFP. In most of the cases discussed the field reversal is produced well before t_2 and this time may be regarded as the end of the formation of the RFP configuration. There is clear indication that the timing of the field reversal is important. Too early a field reversal does in fact cause a current shrinking because of poor trapping

of the internal toroidal field during the initial cold phase; a late reversal however (after t_2) causes a rapid current drop after peak, because the effect of the toroidal field programming is to increase Θ (i.e. the pinch inductance) and, since there is no more poloidal flux input, the current decreases. Associated with the current decrease there is a fast decrease of the density ("pump out") [1]. However an appropriate field programming has been achieved giving a correct current rise and a steadly current decay after peak, without any initial fast drop neither of the current nor of the electron density. The comparison between SRP and RFP indicates that field programming is very important and can indeed improve the spontaneous relaxation process of the pinch. However we point out that in ETA-BETA II there is a large toroidal flux reservoir outside the pinch so that self-reversal is difficult. Evidences have been discussed of the fact that in the slower setting-up studied, the flux loss is important during the current rise phase and subsequently, up to the end of the formation, there is little loss. Furthermore internal probe measurements at the plasma periphery indicate that untill field reversal is obtained the plasma is in close contact with the wall,with currents extending up to the metal liner, whereas when the RFP configuration is formed little current flows in the outer 1-2 centimeters. The initial phase is then spent to produce the current at relatively low Θ values. In the second phase field reversal should take place rapidly so to form a RFP, detach the plasma from the wall, and initiate the heating phase. With similar Θ values, there is a clear increase of the flux loss at the slower rise time. In the various cases roughly the same current is produced ($\sim$200 kA) with a larger expenditure of volt second at the longer rise time.

The question of how the obtained results apply to much larger future devices is a difficult one due to the small geometrical dimension of ETA-BETA II. However in comparing with the slowest envisaged setting-up for RFX [2], we notice that the obtained flux loss factor in ETA-BETA II (up to $\lesssim$2 with the longer rise times; in particular K_ϕ=1.5-1.75 from temperature measurements) is similar to that assumed in the design of RFX [2] and used to evaluate the plasma performance [3]. This assumption appears then reasonable because RFX (see Table II) will have similar electric field and a volume to surface ratio about 5 times larger than in ETA-BETA II. Operation is envisaged with comparable I/N values [1] (i.e. na^2 will be $\sim$10 times larger in RFX that in ETA-BETA II). A simple scaling calculation, based on operation with similar I/N and on the parameters of Table II, indicates that one should expect in RFX at the end of the formation phase temperatures of $\sim$200-350 eV as compared to 70 in ETA-BETA II. These values are consistent with more detailed performance calculations of RFX reported elsewhere [3]. A more complete study including the dependence on minor radius will be possible when further data from other intermediate RFP experiments will be available.

REFERENCES [1] Buffa A. et al., Optimization of the joule heating in RFP plasmas, this Conf.
Buffa A. et al., VIII IAEA Conf., Brussels, 1981, IAEA-CN38-L1 - Vol. II.
[2] The RFX Experiment Technical Proposal - RFX - R1 Report, 1981.
[3] Ragatin M., Ortolani S., University of Padova, Report UPee-81/05,1981.

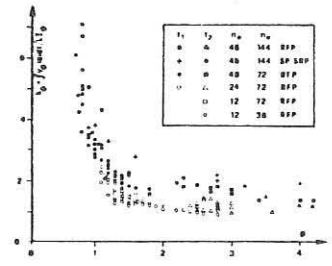


FIG 1

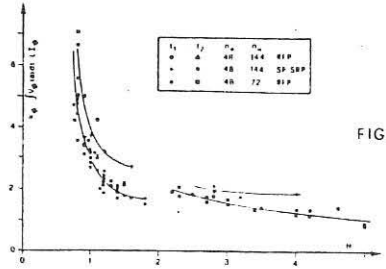


FIG 2

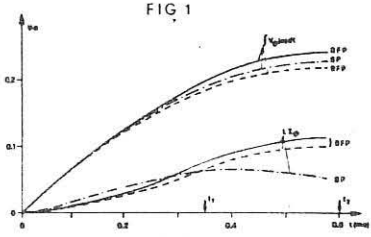


FIG 3

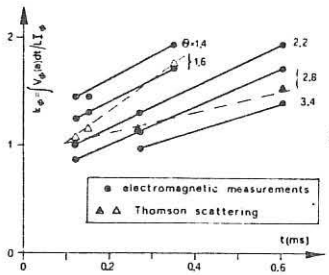


FIG 4

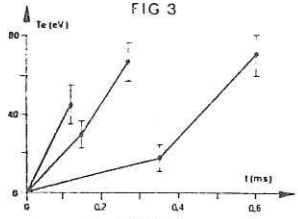


FIG 5

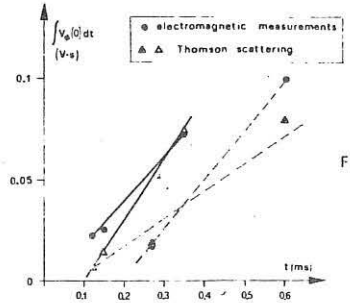


FIG 6

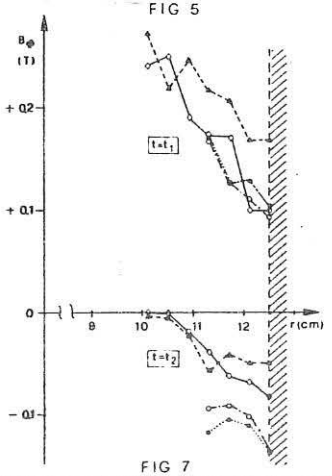


FIG 7

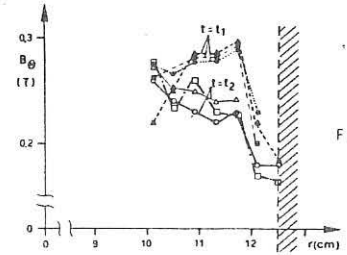


FIG 8

TABLE II

	$\bar{n}_e$(m^{-3})	a(m)	t_2(ms)	B(m^{-1})	n(m^{-3})	R(m)	$\bar{V}_\phi$(a)(kV)	$\bar{E}_i$(V/m)
RFX-BETA II	$2\cdot10^{19}$	.125	.6	210^{19}	410^{20}	>5	.5	125
RFX	2	.6	50	210^{20}	1.810^{20}	1.8	1	100

TABLE I

n_ϕ	n_θ	τ_1	$(T/4)_\phi=\tau_2$	$(T/4)_\theta$	$\bar{V}_\phi(a)$	$\bar{E}_\phi$
12	72	~100 μs	120 μs	200 μs	≤2 kV	≤500 V/m
24	72	~150	270	200	1	250
48	72	~350	600	200	0.5	125
48	144	~350	600	400	0.5	125
12	36	~100	120	100	≤2	≤500

EXPERIMENTAL INVESTIGATION OF STIMULATED CYCLOTRON MILLIMETER WAVELENGTH EMISSION OF RELATIVISTIC HIGH CURRENT ELECTRON BEAM

S.N.Voronkov, V.I.Krementsov, P.S.Strelkov, A.G.Shkvarunets.
Lebedev Physical Institute, Moscow, USSR.

The problem of producing helical trajectories of REB electrons is discussed. These beams allow to create the 25 MW, 7,5 mm gyrotron.

The gyrotron is the most effective device for production of high-power millimeter wavelength radiation [1]. The gyrotron is a microwave device based on the cyclotron maser interaction between an electromagnetic wave and an electron beam in which the individual electrons move along helical trajectories in the presence of an applied magnetic field.

The nonrelativistic electron beam for the ordinary gyrotron is created by the magnetron gun with the hot emission cathode in the temperature limitted regime. REB is created by the cold emission cathode in the space charge regime and therefore there is the problem of producing helical REB.

1. The device for producing helical trajectories of REB electrons is shown in Fig.1. The cathode (1) is placed inside the solenoid(2).The solenoid (2) serves at the same time as the anode. The anode-cathode voltage is equal to 350 kV and the voltage pulse duration is 30 ns. The electrons are injected only by the edge of the cathode [2] and after the diode they move to the nonadiabatic magnetic field region.Then electrons move to the region where the magnetic field increases adiabatically and finally they have inside the gyrotron resonator(3), $v_\perp \sim v_\parallel$. The beam current magnitude is varied by changing a few diaphragms (4) which have different numbers of 0.5-mm radial slits. The thickness of the annular beam after the diode is equal to 0.5 mm so the beam consists of a

number of small beams (0,5 mm x 0,5 mm) after the diaphragm. The electron beam parameters are measured by the method of luminosity photography of a thin dielectric film

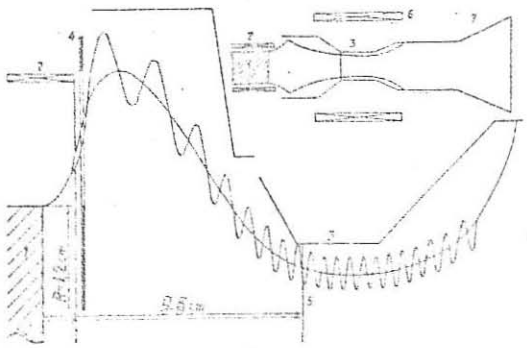


Fig.1.

when electrons pass through the film [3]. The metallized mylar film ((5) Fig.1) is located at the input of the gyrotron. The film serves at the same time as the resonator mirror. The photograph of the time integrated luminosity of the film is shown in Fig.2. The beam consists of 12 small beams in this case; the total current is 500 A. Each small beam of 0.5 mm x 0.5 mm cross-section after the diaphragm is transformed into a tube, the average diameter of the tube being equal to the average Larmor diameter of the electrons. The thickness of the circles in Fig.2 allows to estimate the dispersion of the angle of distribution ($25° < \alpha < 55°$).

2. Gyrotron. The gyrotron resonator (3) Fig.1) is calculated for generating the TE_{13} mode and a wavelength of 7.5 mm. The resonator has two longitudinal slots for selecting modes [4]. The beam is not injected near the slots (Fig.2). The electron beam terminates on the wall of the waveguide after the resonator and microwave power is emitted by the horn (7) Fig.1. The following experimental results were obtained. The dependence of microwave power on the magnetic field has a resonance form and $\Delta H / H_{opt} \sim 0.1$. The optimum value of magnetic field varies from 22 kG for 100 A up to 19 kG for 2 kA. This dependence can be explained by the decrease in electron energy for the high current due to a space charge accor-

ding to the resonance condition $\omega_H/\gamma \approx \omega_0$, where $\omega_H = eH_0/mc$, γ is the relativistic factor, ω_0 is the natural resonator frequency. The pulse duration of microwave power is equal to 20 ns. The wavelength was not measured exatly, 7 mm $< \lambda <$ 8 mm. We checked that the type of mode is TE_{13} indeed. The maximum electron efficiency of 6% was achieved of the beam current of 0,5 kA; microwave power is 11 MW. The maximum output of 25 MW was obtained at the current of 1,3 kA. The discharge in the air was registered after the horn (7) Fig.1. This fact confirms the measured level of the microwave power.

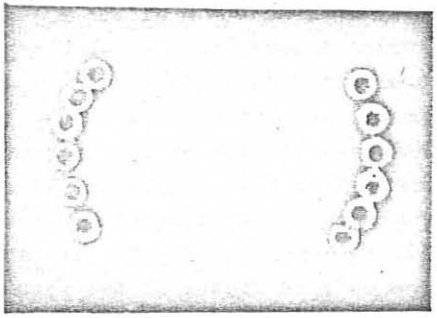


Fig.2.

These experimental results coincide with the theory. This question was discussed in our previous paper about a $\lambda = 3$ cm gyrotron [4]. But one experimental fact was not very clear in paper [4], namely, there was observed a strong dependence of microwave power on the ratio of the magnetic field in the gyrotron cavity to that in the diode. This ratio determines the beam radius and the angle between the electron velocity and the magnetic line in the gyrotron resonator. And, naturally, the electron-microwaves interaction depends on these parameters. But this experimental dependence was very strong

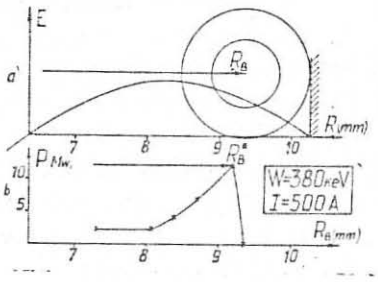


Fig.3.

and we suggested that this strong dependence was determined by the large change in the angular dispersion. Now, we measure the beam radius R_g, the angle α and the angular dispersion $\Delta\alpha$ when we change the ratio of magnetic field at the cavity to that of the cathode. New results are represented in Fig.3 Fig.3(a) shows the radial distribution of the microwave electric field and the typical size of the small beam in the gyrotron cavity. The strong dependence of microwave power on the beam radius is conserved, Fig.3b. As before, the microwave power decreases by a factor of two when $\Delta R_g / R_g \sim 7\%$. The average Larmor diameter of electrons does not change when the beam radius decreases from 9.3 mm to 8.1 mm. This dependence of microwave power on beam radius cannot, be explained by the change quality of beam.

Thus we have demonstrated the effectivity of gyrotrons for generating high-power millimeter wavelength microwaves. Most of the experimental results correspond to the theory. But the strong dependence of microwave power on the geometry of the magnetic field is not clear.

REFERENCES

1. Zaitsev, N.I., Pankratova, T.B., Petelin, M.I., Flyagin, V.A. in Radiotehnika i elektronika 19 1056(1974)
2. Gorshkova, M.A., Il'in, V.P., Nechaev, V.E., Sverhshnikov, V.M., Fuchs, M.I. JTP 50, 109 (1980)
3. Krementsov, V.I., Strelkov, P.S., Shkvarunets, A.G. JTP 50, 2469 (1980)
4. Ginzburg, N.S., Krementsov, V.I., Petelin, M.I., Strelkov, P. S., Shkvarunets, A.G. JTP, 49, 378 (1979)

EXPERIMENTAL INVESTIGATION OF STIMULATED MICROWAVE RADIATION OF HIGH POWER RELATIVISTIC ELECTRON BEAMS

A.N.Didenko, A.R.Borisov, A.G.Zherlitsin, A.V.Kozhevnikov, A.M.Lee, G.V.Melnikov, G.P.Fomenko, E.G.Furman. Yu.G.Shtein

Institute of Nuclear Physics, Tomsk, USSR

The generation of stimulated radiation of high power relativistic electron beam (REB) with 0,5÷1 MeV energy and current up to 13 kA was studied. The radiation of 20 MW power in the 7-13 cm band was produced due to pumping by sriral magnetic field of ondulator and of 6 MW in 3 cm band due to pumping by counterstreaming electromagnetic wave with 10 cm length. The influence of pumping field, longitudinal magnetic field, the length of interaction and REB's density on output power and the wave length of stimulated radiation was investigated.

The generators of microwave radiation using the phenomena of stimulated scattering of pumping wave on REB are being investigated in present time theoretically and experimentally very intensively. [1-3].

In this paper the results of REB stimulated radiation studies on high power generator Tonus and linear inductive accelerator (LIA) for magnetostatic and high power electromagnetic wave pumping are given. To get sufficiently intense scattered radiation the very big power of pumping electromagnetic wave is needed. Such a power in the 10 cm band was produced on the relativistic magnetron. The scheme of experimental set up is illustrated in fig.1.

For simultaneour producing of electron beam and high

power pumping microwaves the accelerator was operating with two loads switched in parallel to pulse forming line. The scattering of TH_{01} and TE_{11} types of waves on different values of magnetic field and pumping power levels was experimentaly investigated. The REB's current was 13 kA with 54 mm or 74 mm diameter and thickness 1÷2 mm. The fig. 2 illustrates the power of scattered radiation in (3±0,2) cm band v.s. the power of pumping wave for TH_{01} type (fig.2a) and TE_{11} (fig.2b) for different magnetic fields. For pumping by TH_{01} wave the power level of 1 GW in the region of niteraction was attained. Nevertheless the maximum power of radiation was not registered though the scattered ware power was comparable with the case of TH_{01} pumping.

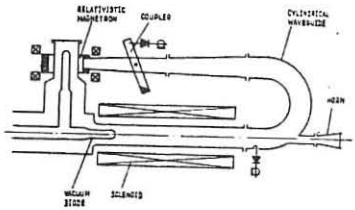


Fig.1.

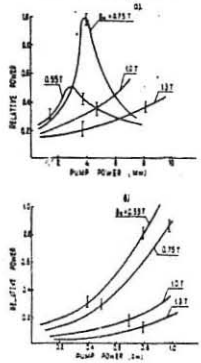


Fig.2.

Experiments with pumping by spiral ondulator were carried on generator Tonus with the REB of 6 kA current, (0,8÷0,9) MeV energy, 80 ns pulse duratuon and LIA with the REB of 0,5 kA current, (0,5÷0,8) MeV variable energy and 80 ns pulse duration. The REB drifted along the tube with inner diameter of 35 mm. The experimental REB's configuration were solid beams of 8 mm and 15 mm radiuses (for Tonus and LIA accordingly) and hollow beam with inner

radius of 8 mm and thickness of 2 mm for the last case. The investigations were carried on ondulators with helical current winding and l_0= 4 cm and 2.8 cm.

The value of generated power v.s. guiding magnetic field strength is given in fig.3. The maximums of power are related to the resonance condition of pumping wave and cyclotron frequency of electron revolwing for which the efficiency of beam wave interaction is increasing. The maximum of power on curve 4 is shifted in the region of higher B_z values in compison with the curve 1 ahich is allied with the shortening of ondulator period from l_0= 4 cm (curve 1) to l_0= 2.8 cm (curve 4). The both curves were obtained on Tonus generator for E = 0.8 MeV. In experiments on LIA the curves 2 (E≈0.8 MeV) and 3 (E≈0.5 MeV) for l_0= 4 cm were obtained. The experiments showed that in the case of REB's application the influence of REB plasma frequency on generated frequency $w_s = \frac{2\pi V/l_0 - w_b/\gamma}{1-\beta}$ is of great importance. Here the w_s - the generated frequency, V - the electron velocity, $\gamma = (1-\beta^2)^{-1/2}$, $\beta = V/c$, $w_0=(4\pi ne^2/\gamma m_0)^{1/2}$, n - REB density. This influence is evident by comparing the curves 1 and 2. In the first case w_b= 4,67.10^{10} c^{-1}, in the second - w_b = 0,74.10^{10} c^{-1}, the generated wave lengths 13 mm and 8 mm accordingly. The wave length changed in the same manner as in the Tonus experiments when

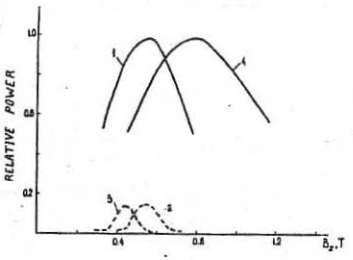


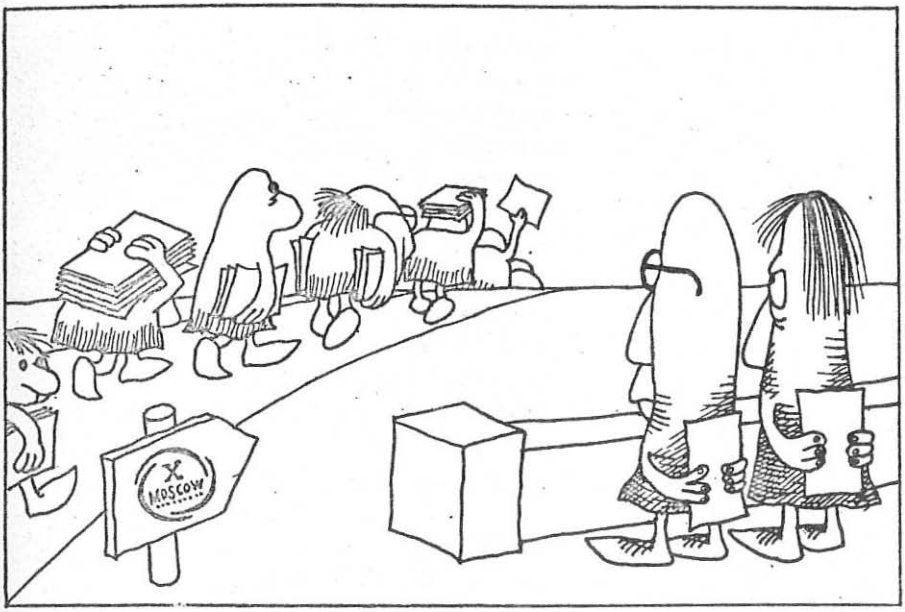
Fig.3.

the beam diameter changed. For solid beam the wave length was 8 mm, for hollow beam - 11 mm. The experiment was carried in ondulator with l_o= 2.8 cm, and constant net current 6 kA. The REB density is of considerable importance for the power of radiation: for w_b= 0,74.10^{10} c^{-1}, P = 100 kW (LIA), w_b = 4,67.10^{10} c^{-1}, P = .2 MW (Tonus, solid beam), w_b= 6,23.10^{10} c^{-1}, P = 20 MW (Tonus, hollow beam). So, experimentally it was prosed that REB density is of considerable importance for the frequency of generated radiation and its power.

REFERENCES

1. T.Kwan, J.M.Dawson, Phys.Fluids, 22, 1089, (1979).
2. P.G.Zhukov, V.S.Ivanov, M.S.Rabinovich, M.D.Rizer, A.A.Ruhadze,Zh.ETF , 76, 2065, (1979).
3. A.N.Didenko, A.G.Zherlitsin, A.V.Kozhevnikov, G.V.Melnikov, G.P.Fomenko, Yu.G.Shtein, Reports of AS USSR, 256, 5, 1106, (1981).
4. P.S.Efthimion, S.P.Schlesinger, Phys.Rev., A 16, 633, (1977).

AUTHOR INDEX



Afonin, I.P. 535
Ahnert, C. 623
Alikaev, V.V. 1, 655
Anderson, D. 547
Andreev, A.A. 619
Aragonés, J.M. 623
Arkatov, I.M. 655
Armstrong, W.T. 551
Arunasalam, V. 21
Babykin M.V. 535
Bagdasarov, A.A. 567
Baigarin, K.A. 535
Bakscht, R.B. 615
Barinov, N.U. 535
Bartsch, R.R. 551
Bartov, A.V. 535
Basov, N.G. 607
Batyuk, V.A. 599
Bayanov, V.I. 619
Bell, M. 1
Berezov, D.V. 655
Bitter, M. 21
Blanchard, W. 21
Bodin, H.A.B. 41
Bol, K. 21
Bondarenko, I.S. 571
Bondarenko, Yu.A. 631
Borchers, R.R. 107
Borisov, A.R. 671
Brau , K. 21
Brownell, J.H. 595
Buffa, A. 659, 663
Bulyginsky, D.G. 561
Burdonsky, I.N. 631
Chen Le-Shan, 527
Cherkashin, M.Yu. 567,575
Chesnokov, A.V. 655
Chistjakov, R.R. 177

Chmyga, A.A. 655
Chudnovski, A.N. 575
Cochrane, J.C. 557
Costa, S. 659
Danilov, A.E. 607
Davis, S. 21
Denisov, V.F. 567
Didenko, A.N. 671
Dimov, G.I. 81
Dnestrovskii, Yu.N. 583
Dylla, F. 21
Eubank, H. 21
Elfimov, A.G. 657
Fonck, R. 21
Fowler, T.K. 107
Furman, E.G. 671
Gaponov, A.V. 153
Gavrilov, V.V. 587, 631
Gavrin, P.P. 535
Geiger, G. 131
Giudicotti, L. 659
Goforth, R.R. 603
Golant, V.E. 651
Goldston, R. 21
Goncharov, S.G. 561, 563
Gorev, V.V. 535
Gorshkov, A.V. 571
Goryacheva, N.V. 587
Grebenshchikov, S.E. 599
Grek, B. 21
Gubarev, A.V. 535
Gusev, V.K. 561, 563
Gvozdkov, Yu.V. 567, 575
Hamnén, H. 547
Harbour, P.J. 643
Harrison, M.F.A. 643
Hawryluk, R. 21
Henins, J. 551
Hilil, V.V. 567

Hintze, W. 543
Hirschberg, J. 21
Horda, H.W. 551
Hotston, E.S. 643
Hugill, J. 21
Hvostenko, P.P. 567
Ilyushin, I.V. 587
Ioffe, M.S. 177
Ipatov, V.A. 563
Ivanenko, G.V. 611
Ivanov, D.P. 567
Ivanov, N.V. 567,575
Jackson, G.L. 603
Jacobson, A.R. 659
Jarboe, T.R. 557
Johnson, D. 21
Kaita, R. 21
Kakurin, A.M. 567, 575
Kalinichenko, S.S. 647
Kalmykov, S.G. 563
Kanaev, B.I. 177
Kapitza, P.L. 197
Kaye, S. 21
Keane, C. 21
Khautiev, E.Yu. 591
Khudollev, A.V. 599
Kirillov, G.A. 635
Kiselev, V.N. 535
Kislov, A.Ya. 567
Kochemasov, G.G. 635
Kochin, V.A 567
Kolomensky, A.A. 611
Kolomijsky, A.N. 631
Kolosenko, E.I. 655
Komoshvilli, K.G. 651
Konkashbayev,I.K. 531
Kormez, S.B. 635
Kovalchuk, B. M. 615
Kovalsky, N.G. 631

Kovan, I.A. 599
Kovrov, P.E. 567
Kozhevnikov, A.V. 671
Kozub, F. 21
Kramshoy, E.D. 655
Krauz, V.I. 591
Krementsov, V.I. 667
Krylov, V.N. 619
Kryzhanovsky, V.I. 619
Krupnik, L.I. 571
Kugel, H. 21
Kuznetsov, M.G. 639
LaHaye, R.J. 603
Landman, I.S. 531
Larionov, M.M. 561
Lashkul, S.I. 563
Lee, A.M. 671
Leira, G. 623
Levin, L.S. 561
Liashenko, V.N. 187
Lindemuth, I.R. 595
Linford, R.K. 557
Lipin, B.M. 563
Lipson, J. 557
Lisak, M. 547
Longinov, A.I. 655
Loskutov, V.V. 615
Luchinsky, A.V. 615
Luqui, R. 623
Lysoivan, A.I. 647
Mack, A.A. 619
Maksimov, Yu.S. 567
Manos, D. 21
Mansfield, D. 21
Marshall, J. 551
Martinez-Val, J.M. 623
McBride, T. 21
McCann, R. 21
McCune, D.21

McGuire, K.21
McKenna, K.F. 551
McNeill, D.21
Melnikov, G.V. 671
Meshcheryakov, A.I. 599
Mesyats, G.A. 615
Mihailichenko, V.A. 567
Mikhailov, Yu.A. 607
Milora, S. 21
Minenko, V.P. 651
Miroschnichenko, G.A. 655
Mizhiritskiy, V.I. 535
Mkhitar'yan, L.S. 631
Mohanty, J.N. 55
Montanés, J.L. 539
Moroz, P.E. 599
Murugov, V.M. 635
Nalesso, G.F. 659
Nastoyashchy, A.F. 631
Nazarov, N.I. 647
Nedzelskii, I.S. 571
Nizhnik, G.Ya. 655
Ocana, J.L. 623
Ohkawa, T. 603
Okabayashi, M. 21
Oliphant,T.A. 595
Ortolani, S. 659, 663
Owens, K. 21
Pan, L.J. 523
Parail, V.V. 579
Pastukhov, V.P. 177
Petelin, M.I. 153
Pergament, M.I. 631
Perlado, M. 623
Petrov, Yu. V. 563
Pikuz, S.A. 611
Potersky, V.V. 177
Platts, D.A. 551
Pogutse, O.P. 579

Ponomarev, L.I. 223
Pozdnyshev, S.P. 655
Poznyak, V.I. 567
Rager, J.P. 243
Razdobarin, G.T. 561, 563
Razumova, K.A. 571
Rej, D. 551
Reusch, M. 21
Rozhdestvenskiy, V.V. 563
Rozhkov, A.D. 631
Salukvadze, R.G. 591
Samokhin,A.I. 611
Sannikov, V.V. 571
Sanmartin, J.P. 539
Sauthoff, N. 21
Sbitnikova, I.S. 599
Scarin, P. 659
Schaffer, M.J. 603
Schilling, G. 21
Schmidt, G. 21
Serebnyakov, V.A. 619
Shapodkovsky, N.V. 655
Shafranov, V.D. 269
Shatsev, A.N. 619
Sherwood, A.R. 551
Sherwood, E.G. 551
Shkvarina, N.S. 587
Shkvarunets, G.A. 667
Shpritz I.D. 563
Shtein, Yu.G. 671
Shustova, N.V. 561
Shvets, O.M. 647
Sidorov, V.P. 651
Simenon, R.E. 551
Simonov, V.V. 631
Sklizkov, G.V. 603
Skovoroda, A.A. 639
Skvortsov,Yu.V. 587
Slavny, A.S. 647

Smerdov, B.I. 655
Smirnov, A.I. 561, 563
Sokolov, Yu.A. 571
Solovjov, N.A. 619
Spiegel, I.S. 599
Stavisskii, B.A. 567
Stepanov, K.N. 647, 655
Strachan, J. 21
Strelkov, P.S. 667
Strelkov, V.S. 327, 655
Strumnikov, V.M. 587
Suekewer, S. 21
Sukhodl'sky, V.N. 599
Sunka, P. 343
Suzuki, N. 307
Takahashi, H. 21
Tang, F.L. 523
Tarashenko, V.F. 647
Taylor, P.L. 603
Tendler, M. 547
Tenney, F. 21
Tserevitinov, S.S. 587
Tuszevski, M. 551
Uckan, N.A. 363
Ulinich, F.R. 531
Vdovin, V.L. 655
Vedenov, A.A. 627
Velarde, G. 623
Velikhov, E.P. 383
vonHalle, A. 21
Voronkov, S.N. 667
Weiss, D.L. 595
Wilhelmsson, H. 547
Williams, M. 21
Wolff, H. 445
Wright, B. 551
Xu Fu 527
Xu Cui-Wei 527

Yamanaka, C. 469
Yamazaki, K. 21
Yaroslavsky, A.I. 631
Yonas, G. 501
Yushmanov, E.E. 177
Zakharov, S.M. 611
Zaretski, A.I. 635
Zherlitsin, A.G. 671
Zhuo, K.C. 523
Zhuzhukalo, E.V. 631